GRUPPO NAZIONALE DI GEOFISICA
DELLA TERRA SOLIDA

Atti del 32° Convegno Nazionale

Trieste, 19-21 novembre 2013
Palazzo dei Congressi
della Stazione Marittima

Tema 1: Geodinamica

ISTITUTO NAZIONALE DI
OCEANOGRAFIA E DI
GEOFISICA SPERIMENTALE

GRUPPO NAZIONALE DI GEOFISICA DELLA TERRA SOLIDA

32° convegno nazionale

Trieste

19-21 novembre 2013

Stazione Marittima

ATTI

Tema 1: Geodinamica

ISTITUTO NAZIONALE DI
OCEANOGRAFIA E DI
GEOFISICA SPERIMENTALE

GRUPPO NAZIONALE DI GEOFISICA DELLA TERRA SOLIDA

32° Convegno Nazionale
Atti - Tema 1: Geodinamica

A cura di: D. Slejko, A. Rebez, A. Riggio, A. Argnani, E. Del Pezzo, P. Galli, R. Petrini, E. Serpelloni, S. Solarino

Con la collaborazione di: M. Bobbio, P. Giurco e L. Riosa

Copertina: M. Sedmach

Impaginazione e stampa:
Mosetti Tecniche Grafiche, Trieste

Finito di stampare nel mese di novembre 2013

ISBN 978-88-902101-9-8 collezione completa
ISBN 978-88-902101-6-7 questo volume

www2.ogs.trieste.it/gngts

Alla fine del film "Intrigo a Stoccolma" di Mark Robson, l'organizzatore del premio Nobel dice qualcosa come: "Mi preoccupo ogni anno per l'organizzazione del premio e poi tutto fila sempre liscio" nel frattempo, a sua insaputa, era successo tutto quello che ci si può aspettare in un film d'azione. Così per me è per il GNGTS, anche se è il sedicesimo anno che lo organizzo e nel passato "tutto è filato liscio", temo sempre in avvio che il convegno possa riuscire male, con pochi partecipanti e di scarso interesse. E quest'anno ce ne sarebbe ben stato motivo, visti i finanziamenti sempre scarsi per la ricerca e la concomitanza con altre manifestazioni geofisiche di respiro nazionale tenutesi recentemente.

Invece, anche quest'anno sembrerebbe (condizionale d'obbligo) che la partecipazione sarà nutrita, visto l'alto numero di note ricevute per la presentazione. Sarà merito della città di Trieste, che ospiterà quest'anno la manifestazione, che richiama numerosi partecipanti o saranno gli enigmi, che ogni terremoto propone, che invogliano i ricercatori al confronto, fatto sta che per tre giorni si parlerà di Geofisica e, anche se novità eclatanti non usciranno, conto che tanti ricercatori saranno un po' più ricchi di conoscenza.

Le prospettive, come dicevo, sembrano positive anche stavolta, con un numero di pre-iscritti che un mese prima del convegno ha già superato le 250 unità. Volente o nolente devo pensare al futuro e perciò a lasciare presto in altre mani l'organizzazione di questo convegno: chiudere in bellezza potrebbe essere una saggia soluzione.

La strutturazione del convegno su 3 temi, proposta negli ultimi anni, é stata mantenuta: ci sembra rispecchi le principali discipline geofisiche e risulta di semplice organizzazione. Le presentazioni sono state suddivise nei tre temi generali: Geodinamica, Caratterizzazione sismica del territorio e Geofisica Applicata, che sintetizzano i grandi filoni lungo i quali si articola la ricerca geofisica italiana. Ogni tema, poi, si sviluppa in tre sessioni specifiche con apertura sia alla componente geologica che a quella ingegneristica.

Anche quest'anno è stata fatta la scelta di raccogliere note estese (ma non troppo) a formare gli atti del convegno. Questa scelta, che in parte rinnega quanto si è scritto nel passato a favore dei riassunti estesi, è stata dettata dalla necessità di produrre un volume utilizzabile per la valutazione ufficiale dell'attività scientifica dei ricercatori e degli enti. Poteva essere una scelta azzardata con scarsa partecipazione, viste le recenti valutazioni ANVUR, che avrebbero potuto indirizzare soprattutto i giovani ricercatori a pubblicare su riviste con alto

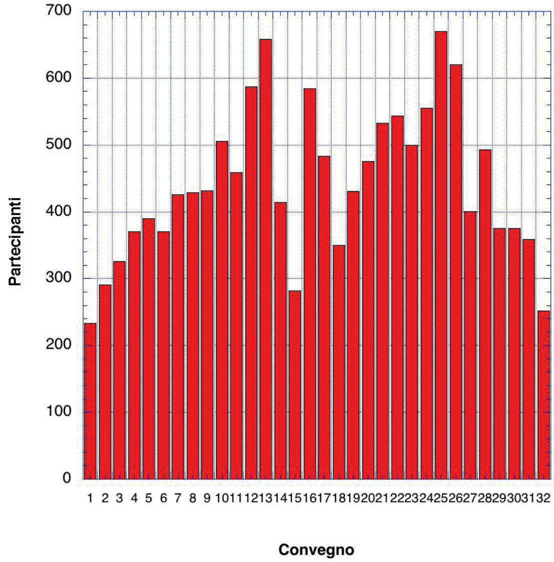

Fig. 1 – Numero di partecipanti ai convegni GNGTS. Il primo convegno si è tenuto nel 1981 e, in seguito, ha avuto cadenza annuale con l'eccezione del 1982. Il numero dei partecipanti all'ultimo convegno è aggiornato ad un mese prima dell'inizio del convegno stesso.

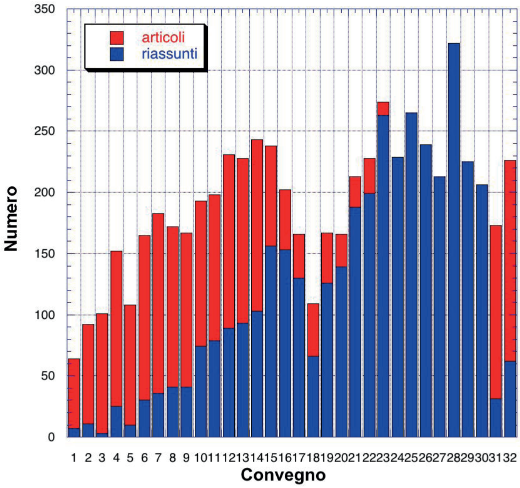

Fig. 2 – Numero di note presentate nei convegni GNGTS. Fino al 2004 è stato pubblicato il volume (dal 1997 sotto forma di CD-Rom) degli atti del convegno contenente in forma estesa le note presentate (barre rosse). In seguito, si è deciso di pubblicare soltanto il volume dei riassunti estesi (barre blu).

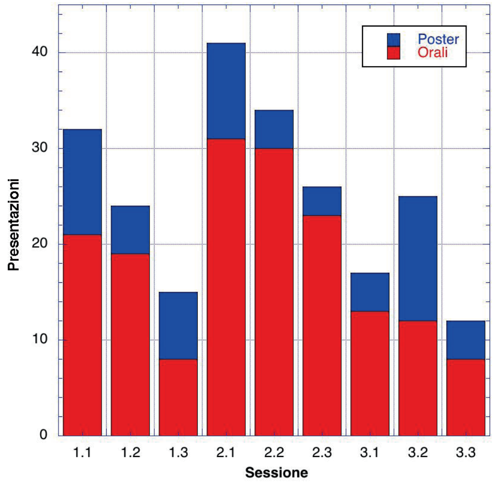

Fig. 3 – Numero di note presentate nelle varie sessioni del 32° convegno. Vengono indicate le comunicazioni orali con il colore rosso e quelle in forma di poster con il colore blu.

Impact Factor: bollino blu dell'eccellenza e panacea per la valutazione o solo parziale criterio speditivo di confronto senza garanzia di qualità? Invece il presente volume raccoglie ben 164 note, delle 226 che verranno presentate al convegno. Si tratta di una percentuale (73%) abbastanza alta che premia la scelta fatta. La produzione di atti di rilevanza scientifica ha determinato la necessità di avviare un processo di referaggio di tutti i testi. I convenor se ne sono fatti carico e, pertanto, risultano responsabili della qualità del materiale presentato. L'aumentata mole di materiale da stampare, rispetto a quella degli anni precedenti in cui venivano prodotti dei riassunti estesi, ha condizionato la scelta di suddividere gli atti in tre volumi, ciascuno dei quali raccoglie le note relative ad uno dei tre temi. Molte note (108) sono in lingua inglese: ciò permette una diffusione del presente volume anche all'estero. Delle 226 note in programma, ben 165 sono destinate alla presentazione orale.

Anche quest'anno alcune sessioni del convegno GNGTS (quelle di Geofisica Applicata) sono state organizzate in collaborazione con la Sezione Italiana EAGE-SEG, che realizza così il suo 13° Convegno Nazionale.

Una segnalazione degna di nota va all'Associazione Geofisica Licio Cernobori, che ha scelto anche quest'anno il convegno GNGTS quale sede per l'attribuzione del premio in memoria di un caro collega ed amico prematuramente scomparso anni or sono.

Un ringraziamento particolare va ai convenor (Dario Albarello, Andrea Argnani, Edoardo Del Pezzo, Mauro Dolce, Maurizio Fedi, Paolo Galli, Stefano Grimaz, Eugenio Loinger, Luca Martelli, Angelo Masi, Giuseppe Naso, Riccardo Petrini, Luigi Sambuelli, Giovanni Santarato, Enrico Serpelloni, Stefano Solarino, Umberta Tinivella e Aldo Vesnaver), che hanno proposto e organizzato le varie sessioni e hanno curato il referaggio dei testi, ed alla Segreteria Organizzativa (Muzio Bobbio, Paolo Giurco e Laura Riosa, oltre ad Alessandro Rebez e Anna Riggio, che firmano con me e con i convenor questi atti), che ha raccolto e preparato tutto il materiale qui stampato. Desidero ringraziare, infine e soprattutto, il Presidente dell'OGS, che ha accolto ancora una volta con entusiasmo e con generosità l'idea di finanziare il convegno GNGTS, nonostante le difficoltà economiche con cui tutti gli enti di ricerca devono scontrarsi.

Dario Slejko

"...cerco qualcosa: un briciolo di conoscenza in questo nostro piccolo grande pianeta.
E in me stesso..." L. C. 1989.

PREMIO DELL'ASSOCIAZIONE PER LA GEOFISICA "LICIO CERNOBORI" - 2013

L'**Associazione per la Geofisica Licio Cernobori – AGLC**, nata il 30 ottobre del 2000 per ricordare Licio Cernobori, geofisico prematuramente scomparso, ed il suo entusiasmo contagioso, ha come fine la promozione degli studi geofisici e soprattutto la formazione scientifica e la crescita dei più giovani.

Tale fine è stato perseguito attraverso l'elargizione di un premio di studio presso l'Università di Trieste, aperto anche a laureandi/laureati in Geofisica Applicata di altre università o strutture scientifiche coinvolte in progetti comuni con l'Ateneo di Trieste. Si ricordano i vincitori degli anni passati Giulio Paoli (2001), Sara Cisilin (2002), Marica Calabrese (2003), Manfredi Scozzi (2004), Ivan Gladich (2006), Manuela Zuliani (2006), Andreika Starec (2008), Sara Ferrante (2009).

Oltre all'attività didattica/divulgativa che i componenti dell'Associazione svolgono in diverse occasioni, sono stati finanziati negli anni diversi convegni, scuole, progetti, iniziative, in Italia e all'estero:

- Copie degli Atti del Convegno TRANSALP (Trieste, Febbraio 2003) per le biblioteche universitarie;
- Agevolazioni per gli studenti al Congresso: STRUCTURES IN THE CONTINENTAL CRUST AND GEOTHERMAL RESOURCES (Siena, 24-27 September 2003);
- Sovvenzione di uno studente, Alberto Gaudio dell'università di Urbino per la Scuola di Processing dati sismici marini (Trieste, ottobre 2004);
- Agevolazioni per studenti del terzo mondo alla partecipazione del Workshop IRIS-Orfeus "Understanding and managing information from seismological networks" (Palmanova (UD) 28 Febbraio – 6 marzo 2005);
- Finanziamento di € 400 Euro ad Andrejka Starec (2006), allora studentessa, per garantirle un altro mese presso il TNO (Paesi Bassi) a conclusione della sua borsa e consentirle la conclusione della tesi sullo stoccaggio geologico della CO_2, con la guida di Pascal Winthaegen e del chiar.mo Prof. Rinaldo Nicolich dell'Università di Trieste.
- Finanziamento annuale di € 400 per la partecipazione di un insegnante ai seminari GIFT per gli insegnanti delle scuole elementari e secondarie nell'ambito del convegno dell' European Geosciences Union - Geophysical Information for Teachers (GIFT): Giovanni Banchelli (2007), Pier Paolo Caputo (2008), Giovanni Aglialoro (2009), Francesco Gobbo (2010), Giulia Realdon (2011), Eva Godini (2012), Maria Barbera (2013).

Nell'occasione del decennale (2010) si è istituito un premio per i giovani relatori al Congresso annuale GNGTS, ripetuto nel 2011. Nel 2010 il premio di 2000,00 € è andato alla dottoressa **Marina Pastori**, per il lavoro "***Crustal fracturing field and presence of fluid as revealed by seismic anisotropy: case-histories from seismogenic areas in the Apennines",*** selezionato tra 40 lavori e 8 finalisti, nel 2011 al **dott. Edoardo Peronace**, per il lavoro "***Shallow geophysical imaging of the mt. Marzano fault zone; a kaleidoscopic view through ERT, GPR and HVSR analyses***", selezionato tra 38 lavori e 13 finalisti.

Dal 2012 il premio è stato suddiviso in tre premi di 700,00 €, uno per ciascuno dei Temi del convegno: *Geodinamica, Caratterizzazione sismica del territorio e Geofisica applicata*. I vincitori sono stati:

Lorenzo Bonini, per il lavoro: **"*Comprendere la gerarchia delle faglie attive per migliorare la caratterizzazione sismica del territorio: l'esempio del terremoto di L'Aquila del 2009 (Mw 6.3)*", Rocco Ditommaso,** per il lavoro **"*Risposta sismica delle strutture: dalla non stazionarietà alla non linearità apparente*", Gianluca Fiandaca,** per il lavoro **"*Time domain induced polarization: 2D inversion for spectral information*"**, selezionati tra 31 lavori presentati.

Quest'anno i lavori presentati sono 27. I riassunti e le presentazioni preliminari sono attualmente all'esame delle tre commissioni, che stanno lavorando per scegliere i tre vincitori, che verranno annunciati e premiati nel corso dell'Assemblea del Convegno (20 novembre 2013).

Per altre informazioni, per diventare socio e contribuire a continuare e migliorare le iniziative dell'Associazione per la Geofisica Licio Cernobori – AGLC, http://www2.units.it/cernobor/.

Il Presidente dell'Associazione
Marco Romanelli

Indice

Lectio Magistralis

THE CRUST IN ITALY FROM SEISMIC PROSPECTING AND ADDITIONAL INVESTIGATING TECHNIQUES

R. Nicolich
DIA, University of Trieste, Italy

The near-vertical reflection seismic method was the most appropriate exploration tool utilized in the crustal exploration of Italy and neighbouring Seas with the CROP (CROsta Profonda) project and with similar programs. The method, subsequent to the improvements in data acquisition and processing with increased dynamic range of digital data and more powerful processing software, provides signal easily interpreted in geological terms. To complete the information needed for major geological synthesis a combination of different geophysical investigating techniques were required and added. Significant the wide-angle refraction/reflection method (WAR/R), which yield propagation velocities at depth with greater accuracy. Both reflection and refraction techniques, separately used, supply results which are different in nature though complementary.

Examples of the current interpretation and the open debates about the structure and geodynamics of the crust of the Italian area will be presented with regard to: first, the definition of the seismic nature of the Moho discontinuity, in terms of its position, topography, smoothness and continuity; second, the lower crust contribution in the complexities of the collision mechanisms; third, the presence of decoupling levels within the subducting lithosphere or the intracrustal ones, related to the Neogenic evolution, an insight into the processes that built the geological structures of the upper crust; fourth, what to do and future improvements to crustal exploration.

Active seismic prospecting can give major information in the first 50-60 km of the lithosphere, with limited data quality in the collision zones where the utilization of the receiver functions analysis can help in the precise indication of the positions in the crust-mantle transitions of the colliding plates. The tectonic melange may dominate the thickened crust after collision, making difficult to isolate the different bodies because the physical differences are small. Larger depths are investigated by earthquake hypocentre distribution or by tomographic analysis of teleseismic events, outside of my presentation.

Of interest, the acquisition of wide-angle reflection fans, successfully employed for imaging the complex geometries of the M-interface on collision belts once information was available about an approximate position at depth of the target.

The study of the crust started in Italy with controlled source refraction profiles in the Western Alps in 1956, in replay to requests for international collaboration among the confining countries. Analog recorders were used, and the spacing between stations, the number of the acquired profiles, were related to the availability of instruments and operators (students) from different participating countries. Reliable results were obtained only on the gross changes in crustal thickness and on the main velocity structures, but the data quality increased as years go following the technological evolution (from the initial coffins to the Coca-Cola cans of ALP-2000).

The deep seismic soundings covered the whole Italian Peninsula with profiles integrated with other pertinent geophysical methods. This activity was concluded with the long N-S transect of the European GeoTraverse (EGT) program in 1986 (Ansorge *et al.*, 1992).

We returned to the Alpine chain with reflection seismics updated technologies in joint international multidisciplinary programs, exploring Western Alps in 1985-1986, first with a French-Italian joint venture (CROP-ECORS), followed by a co-operation with the Swiss NRP20 project in the Central Alps. The Eastern Alps were explored from 1999-2000 by partner institutions of Italy, Austria and Germany acquiring data along the TRANSALP profile. In the mean time the CROP venture programmed acquisitions across the Apenninic chain; Sicily was explored in 2009, but with different funding following the CROP-11 solution.

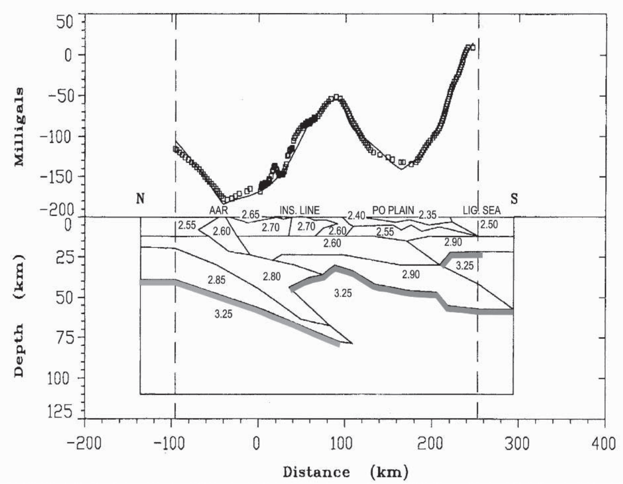

Fig. 1 – The gravimetric model (from Marson *et al.*, 1994) along the European GeoTraverse, crossing the Alps, the Po Plain and the Apennines, down to the Ligurian Sea. The model settles the European Moho at 60 km or more beneath the Po Plain with Adria Moho down-bended to about 40 km by the Apennines overthrust, Apennines here characterized by a vertical Moho uplift. Density values in gr/cm^3.

The deep exploration of the marine areas started in 1988 in the Provenzal Basin (again a CROP-ECORS joint venture) and after covered all the Italian neighbouring seas with CROP and with similar projects (ETNASEIS, SINBUS, PROFILES, IMERSE, ...).

The dynamite source was employed in several transects, but also heavy vibrators were used, for ex. in the narrow mountain valleys, but still adding explosive shots to aid imaging the deepest reflecting markers. The depth penetration of vibroseis signals is turned up to be particularly low in such areas where high-impedance rocks are exposed at the surface. The use of complementary wide-angle acquisitions continued about everywhere with in-line profiling or with fans or again designing cross-lines to enable 3D images extracted from a wide corridor centred on the main profile. The operative parameters employed in the acquisition were modified with the continuous improvements of the recording technologies and the gained experiences, varying the number of the active recording channels, the group intervals, the offsets; all parameters choice limited by the available funding.

The addition of the gravity information with the Bouguer anomalies can help to position the deep basins, the deep roots of the orogenies and of the high density bodies at shallow depths. Both the seismic and gravity interpretation take mutual advantage by iterative use of the two data sets and of the constraints posed to fulfill both observed data. The gravity field can be used to extend the interpretative models beyond the seismic profile and 3D gravity models have been presented to control the laterally variable crustal architecture. In Fig. 1 an example of a gravimetric model, which utilized the seismic information along a sector of the EGT transect from the internal crystalline massif in Switzerland to the Ligurian Sea, crossing the Milano belt, the western Po plain and the northern Apennine arc. The structural setting of the Adria domain results from the convergence of the plate margins producing a foreland-foredeep domain consumed by the advancing neighbouring chains with vertical offset of respective Moho's.

In Fig. 2 an example of wide-angle fan profiling, which were of primary importance for the interpretation of the deep interfaces disclosed in the reflection seismic sections of the CROP-ECORS project (Damotte *et al.*, 1990), revealing a dramatic imbrication of the upper mantle and crust. Organizing the sampling interval of reflectors along the cross sections and the shot-receivers distance in fan to have reflecting points around the critical distance corresponding to the common depth point of the near vertical reflection profile, the wavelet from the base of the crust is known to be very energetic and can be identified by the maximum amplitude signal. The root zone of the chain was outlined down to 55 km depth with the flaking of the lithosphere under the chain in the Briançonnais zone, while the hinterland Moho is raising stepwise from the Po plain up to about 13 km depth, the base of the outcropping rise known as the Ivrea lower crust body.

The exploration of the Alpine chain reached the peak with the TRANSALP transect, which utilized again multidisciplinary approaches: a) seismic multichannel acquisition with vibroseis and explosives, b) a 3D control of the deep structures utilizing a supplementary spread, c) wide-angle profiles, d) gravity measurements with compilation of a new map of cross-borders Bouguer anomalies covering NE-Italy, W-Austria and Bavaria, e) recording of seismological data with a permanent stations network.

Along TRANSALP profile the geophysical/geological models and the reflection seismic images with their well resolved small-scale heterogeneities (Lueschen *et al.*, 2006) have been extended on larger depths by teleseismic "receivers functions", P to S converted signals, illuminating the lithosphere from below which can give information on the main converter, the M-discontinuity, or on wide velocity gradient zone. An example is given in Kummerow *et al.* (2004), where the base of the crust and intracrustal structures in the Eastern Alps are recognized (Fig. 3), confirming the interpretation of the Transalp seismic sections (Castellarin *et al.*, 2006) with a south-dipping polarity of the Europe subducted mantle. It is not so immediate with the initially presented lower resolution teleseismic tomography procedures (Lippitsch *et al.*, 2003), probably with a poor control of the upper crust velocities and heterogeneities and construction of tomographic sections along direction where it is difficult to resolve the laterally variable structures (old, recent).

ALP 2002 experiment came again to WAR/R technique, but with many shots, several profiles and a large number of narrow spaced recording instruments, to complete the investigation of the Eastern Alps and Central Europe (Brückl *et al.*, 2010). The compression between Europe and the indenting Adria microplate generated the tectonic forces for the Dinaric orogeny, active from Cretaceous to Miocene, and for the extrusion and escape of the Eastern Alps towards the unconstrained Pannonian basin. Adria is moving towards north, obliquely thrusting

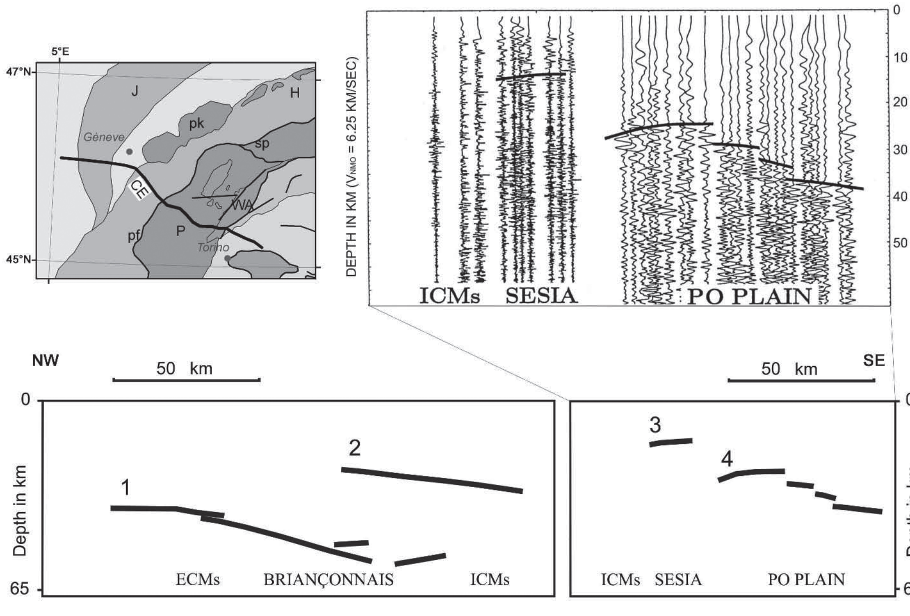

Fig. 2 – An example of the utilization of wide-angle fans with the crustal model and a stepwise M-discontinuity reflection images along a transect from the Po Plain to Gran Paradiso (from Thouvenot *et al.*, 1990, modified), intersecting Sesia-Lanzo zone and Canavese line, which marks the eastern limit of the chain (CE = seismic profile CROP-ECORS). Reflections are picked on the seismic section using a maximum amplitude criterion and traces correlation. ICMs = internal crystalline massif; ECMs= external crystalline massif. At the bottom the crustal scheme with main discontinuities across the whole Western Alpine chain: 1- European Moho, 2- Brianconnais Moho, 3 - base of the Ivrea body, 4- Adria Moho.

under the Pannonian fragment corresponding to the Dinaric chain. The upper crust is here characterized by the Dinaric thrusts (upper plate) moving westwards, opposed by the Istria massive Mesozoic shelf domain, the stable part of Adria that emerge from the Adriatic Sea. Europe is in the position of lower plate beneath Adria overthrust by a Pannonian fragment with vertical offsets of the respective Moho's, in the north; in front of the Adriatic coasts and beneath the Dinaric chain, the Moho surface seems to remain rather smooth and continuous from the foreland to the hinterland and down-bended towards the culmination of the Dinaric chain (Velebit mountains), suggesting that a major decoupling operates at or near the Moho between the Adria and Pannonian and the respective former mantle lithospheres (Šumanovac *et al.*, 2002). The lower crust of Adria probably plays a major role in the definition of the crust structure and evolution. The joint deep reflection seismic profiles with the WAR/R velocities could be the winning solution and give an answer to the role of the Adria indenter in a key area for crucial seismotectonic modelling.

The Adria collision with the Apennines developed from late Miocene to Quaternary. Unlike in the Alps, where a major lithosphere scale fault accounts for vertical offset of the Moho between the upper and lower plate, along the Apenninic chain facing the Adriatic Sea, the Moho surface remain rather smooth and nearly continuous, gently bended, from the foreland towards the Apennine chain and up to the hinterland mantle dome. A major decoupling is operating near the Moho and only the continental lithosphere of Adria seems to be currently involved in the subduction process presently active with a nearly south-eastward directed subduction plane, as proposed by Di Stefano *et al.* (2009) with earthquakes tomography analysis. These authors accept the upwelling of the asthenosphere and the related thermal softening of the crust on the Tyrrhenian side. Therefore the back-arc extension and the asthenosphere upwelling, in addition to the slab pull, constitute the major driving force in the Apennine-Adria collision.

The mobilized and uplifted asthenosphere, a not depleted mantle wedge, can be responsible of the lower crust lamination by magmatic intrusion. The mantle derived magmas releases heat at the base of the crust, induces anatexis in the overlying crustal rocks and produce granitoids melts, quickly migrating towards higher levels (Locardi and Nicolich, 2005). Wide-angle refraction/reflection acquisitions (Giese *et al.*, 1976) across the Tuscany Geothermal Province revealed a peculiar velocity structure with alternate velocity/density variations in the lower crust and a seismic waves propagation velocity not higher than 7.8 km/s, assigned to the Moho discontinuity. Crustal reflection seismic profiles give a well resolved image of the lower crust and of the brittle/ductile transition interval utilizing seismic attributes and the evaluation of strength (Accaino *et al.*, 2006).

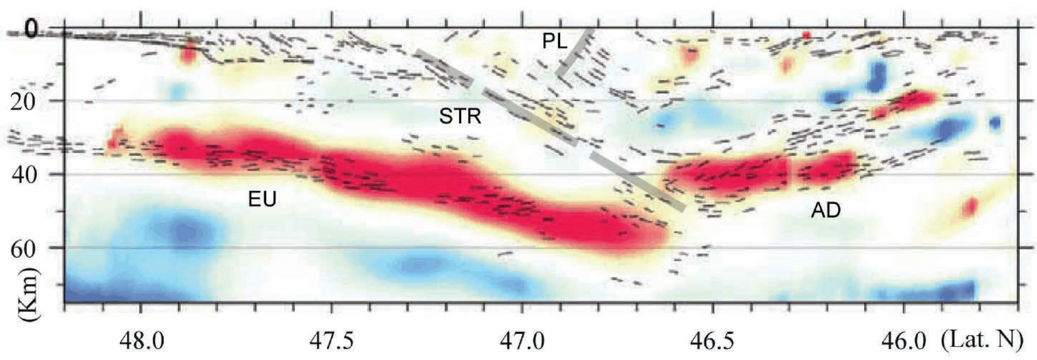

Fig. 3 – Receivers function and combined explosive and vibroseis depth migrated data line drawing along TRANSALP transect (from Lueschen *et al.*, 2006, modified). The presence of decoupling levels (the Sub Tauern Ramp: STR) within the subducted lithosphere poses an insight into the processes that built the geological structures of the upper crust. EU = Europe; AD = Adria; PL = Periadriatic Line.

The reprocessing of the CROP profiles in the region, let us to apply the wave equation datuming technique (Barison *et al*., 2011; Giustiniani *et al*., 2013) extracting information previously hidden by approximate static corrections and surface noise. From picked first arrivals, a tomography inversion created a near surface velocity model by iterative ray-tracing and travel time calculations. Then, the wave equation was applied to move shots and receivers to a given datum plane, removing time shifts related to topography and to near-surface velocity variations. Basically, WED is the process of upward or downward continuation of the wave-field between two arbitrarily-shaped surfaces; a process useful to attenuate ground roll, enhance higher frequencies, increase the resolution and improve the signal/noise ratio.

The new outputs show evidence of regional continuity of high amplitude horizons, a better fitting with the surface geological setting and with well data, resembling the local industry investigations; the results confirm the role of overpressured fluids, better define the tectonic setting as well as the contribution to the reflectivity of lithology and of hydrothermal fluids or thermo-metamorphic minerals.

The wave equation datuming is now applied to the SIRIPRO profile crossing central Sicily from the Tyrrhenian Sea to the Sicily Channel. This reprocessing requires large computers, parallel processors, because of the long listening times. The profile was acquired without additional complementary geophysical tools, like new wide-angle experiments, offshore-onshore continuation, … It shows the crustal flexure from the Hyblean foreland towards the Caltanisetta through, accompanied by crustal thinning: from an already thinned crust (around 30 km the Moho depth on coast of the Sicily Channel) to about 16-17 km thickness of the same interval beneath Caltanisetta. North of the collision zone the Maghrebides chain includes units of the African margin in a similar way to the crustal setting in the North-Algeria facing the Algerian basin. It is necessary to better resolve the structures of Maghrebides chain, north of the Caltanisetta through in the collision zone, where a Moho uplift is possible, as confirmed by the gravity anomalies and old deep refraction data. Again a bended continuous crust-mantle interface from hinterland to foreland is suggested, with delaminations and the decoupled mantle lithosphere still locally subducted and recycled in the asthenosphere, but more complex structures cannot be excluded. Moreover, contraction events are currently active at the toe of the North Sicilian margins, possibly accounting for the initiation of a new underthrusting/subduction zone along the southern margin of the Tyrrhenian basin, that will accomodate further convergence between Africa and Europe.

A crustal flexure has been observed moving from the Hyblean domain to the Ionian deep basin, where the crust-mantle transition interval is characterized by a curious high amplitude reflectors in the low frequency band (around 10 Hz). The crustal thinning from the Sicily channel to the Ionian basin across the Malta Escarpment is shown in reflection seismic profiles as well as the presence of a crustal transcurrent fault accounting for a major dextral lateral escape of the Calabria Block during the Plio-Quaternary opening of the Tyrrhenian Sea. The fault separates the eastward thinning continental crust from the deep Ionian domain, which crust is proposed as oceanic from many authors. The interpretation of the seismic data is still under debate and the presence of a wide oceanic domain or of an area still belonging to a distal portion of the North African continental margin cannot be confirmed or plainly denied. Following the exposed Tethian ophiolitic suture (in Albania, Western Greece, Crete, Western Turkey, …) the Tethian ocean has been already recycled within the asthenosphere. The Cretaceous rifting, presently recognized offshore Libia, is a possible origin of the thinning of the crust of a north African margin widely extended in the Ionian Sea with the presence of pull-apart basin up to oceanic openings; once more, the eclogitization of the upper mantle can account for the high velocities and high densities necessary to justify the positive Bouguer anomalies. The tectonic loading of the Africa foreland lithosphere by the Calabrian (and Aegean) arcs is not sufficient to account for the 4 km water depth in the Ionian abyssal plain. Other forces, like slab pull, lateral push of the asthenosphere upwelling in the Tyrrhenian and Aegean back-arcs are likely to account for the retreat of the deep mantle slabs and must therefore contribute to the decoupling operating close to the Moho. The decoupling of the crust is confirmed by the thrust-top pull-apart basins currently developing above the back-stop of the Hellenic Arc (Wardell *et al*., 2013; Barison and Nicolich, 2013).

The combined utilization of morphological analysis plus high resolution and deep penetration multichannel seismic jointly with OBS for wide-angle recordings and part of a permanent network of seismological station in connection with on land positioned recording points, is the optimum solution for the lithosphere exploration in subduction or collision zones. A first project was Etnaseis with marine and land synchronized operations (Laiglè *et al*., 2000). The SeaHellarc project followed these ideas studying the western continental margin of Peloponnesus. Thales project investigated the Lesser Antilles with European and French funding (Laiglè *et al*., 2013). This area was the target of a complete set of active and passive offshore seismic experiment: multichannel reflection seismic with air gun source organized in the Single Bubble mode, OBS WAR/R seismic profiles, OBS and land permanent seismological stations for earthquakes location, receiver functions analysis imaging the slab top and the LVL. The objective were the geometries of interplate boundary zone constrained from the subduction deformation front and the possible generation of mega-thrust earthquakes.

References

Accaino F., Nicolich R. and Tinivella U.; 2006: *Highlighting the crustal structure of the Tuscan Geothermal Province*. Boll. di Geof. teor. ed appl., **47**, 3, 425-445.

Ansorge L., Blundell D. and Mueller St.; 1992: *Europe's Lithosphere-Seismic Structure*. In: Blundell D., Freeman R. and Mueller St. (eds.) A Continent Revealed, The European Geotraverse. Cambridge University Press ISBN 0-521-42948X.

Brűckl E., Behm M., Decker K., Grad M., Guterch A., Keller GR. and Thybo H.; 2010: *Crustal structure and active tectonics in the Eastern Alps*. Tectonics, **29**, TC2011, doi:10.1029/2009TC002491, 1-17

Barison E., Brancatelli G., Nicolich R., Accaino F., Giustiniani M. and Tinivella U.; 2011: *Wave equation datuming to marine OBS data and to land high resolution seismic profiling*. J. Appl. Geophys., **73**, 267-277, doi: 10.1016/j.jappgeo 2011.01.009.

Barison E. and Nicolich R.; 2013: *Reflection seismic images from OBSs profiling across External Hellenides*. Boll. Geof. teor. appl., in press.

Castellarin A., Nicolich R., Fantoni R., Cantelli L., Sella M. and Selli L.; 2006*: Structure of the lithosphere beneath the Eastern Alps (southern sector of the Transalp transect)*. Tectonophysics, **414,** 1-4, 259-282.

Damotte B., Nicolich R., Cazes M. and Guellec S.; 1990: *Mise en oeuvre, traitment et présentation du profil plaine du Po-Massif Central*. In: Roure F *et al.* (eds.) Deep Structure of the Alps. Soc. Geol. de France, de Suisse, Ital., vol. spec. **1**: 65-76.

Di Stefano R., Kissling E., Chiarabba C., Amato A. and Giardini D.; 2000: *Shallow subduction beneath Italy: three-dimensional images of the Adriatic-European-Tyrrhenian lithosphere system based on high-quality P wave arrival times*. JGR, **114**, B05305, doi: 1029/2008JB005641.

Giese P., Wigger P., Morelli C. and Nicolich R.; 1981: *Seismische Studien zur Bestimmung der Krustenstruktur im Bereich der geothermischen Anomalie der Toskana*. EUR 7578, de MF: pp 1-108.

Giustiniani M., Nicolich R.and Tinivella U.; 2013: *The seismic image of the upper crust of the Tuscan geothermal province from CROP profiles*. Proceedings of Geoitalia 2013 - Session 12, Pisa.

Ismail Zadeh A.T., Nicolich R. and Cernobori, L.; 1998: *Modelling of geodynamic evolution of the Ionian Sea basin*. Computational Seismology and Geodynamic, **30**, 32-50.

Kummerow J. *et al*.; 2004: *A natural and controlled source seismic profile through the Eastern Alps: TRANSALP*. Earth Planet. Sci. Lett., **225**,115-129.

Laiglè M., Hirn A., Sapin M., Bécel A., Charvis P., Flueh E., Diaz J., Lebrun J.-F., Gesret A., Raffaele R., Galvé A., Evain M., Ruiz M., Kopp H., Bayrakci G., Weinzierl W., Hello Y., J.-C. Lèpine, Viodé J.-P., Sachpazi M., Gallart J., Kissling E. and Nicolich R.; 2013: *Seismic structure and activity of the north-central Lesser Antilles subduction zone from an integrated approach: Similarities with the Tohoku forearc*. Tectonophysics, **603**, 1-20.

Laiglè M., Hirn A., Sapin M., Lepine J.-C., Diaz J., Gallart J. and Nicolich R.; 2000: *Mt Etna dense-array local earthquake P and S tomography and implications for volcanic plumbing*. J. of Geophys. Res., B9, Solid Earth and Planets, **105**, 21.633-21.646.

Lippitsch R., Kissling E. and Ansorge J.; 2003: *Upper mantle structure beneath the Alpine orogen from high-resolution teleseismic tomography*. J. Geophys. Res., **108,** B8, 2376, ESE 5, 1-15.

Locardi E. and Nicolich R.; 2005: *Crust-Mantle structures and Neogene-Quaternary magmatism in Italy*. Boll. Geof. teor. appl., **46**, 2-3, 169-180.

Lueschen E., Borrini D. Gebrande H., Lammerer B., Millahn K. and Nicolich R.; 2006: *TRANSALP-deep crustal vibroseis and explosive seismic profiling in the Eastern Alps*. Tectonophysics, **414,**1-4, 9-38.

Marson I., Orlando L. and Stoka M.;1994: *Gravity model on the CROP profile*. In: Montrasio A. and Sciesa E. (eds.) Proceedings of Symp. "CROP-Alpi Centrali". Quaderni di Geodinamica Alpina e Quaternaria, vol. spec. **2**,161-169.

Thouvenot F., Senechal G., Hirn A. and Nicolich R.; 1990: *ECORS-CROP wide-angle reflection seismics: constraints on deep interfaces beneath the Alps*. In: F. Roure *et al.* (eds.) Deep Structure of the Alps. Soc. Geol. de France, de Suisse, Italiana, spec. vol. **1**: 97-106.

Šumanovac F., Orešković J., Grad M. and ALP 2002 W.G.; 2009: *Crustal structure at the contact of the Dinarides and Pannonian basin based on 2-D seismic and gravity interpretation of the Alp07 profile in the ALP 2002 experiment*. Geophys. J. int. **179**: 615-633.

Wardell N., Camera L., Mascle J., Nicolich R., Marchi M., Anagnostou C., Barison E. and SeaHellarc team; 2013: *The Peloponnesus Continental Margin from Zakynthos Island to Pylos area, Part 2: Structural framework from seismic reflection and morpho-bathymetric data*. Boll. Geof. teor. appl., in press.

Tema 1

Geodinamica

sessione 1.1

I terremoti e le loro faglie

Convenor: P. Galli e S. Solarino

THREE DIMENSIONAL SEISMIC IMAGING AND EARTHQUAKE LOCATIONS IN A COMPLEX, NORMAL FAULTING REGION OF SOUTHERN APENNINES (ITALY)

O. Amoroso[1*], A. Ascione[2], S. Mazzoli[2], J. Virieux[3], A. Zollo[1]
[1] Department of Physics, University 'Federico II', Naples, Italy
[2] Department of Earth Sciences, Environment and Georesources, University 'Federico II', Naples, Italy
[3] ISTerre, CNRS, Université de Grenoble I, France
** Now at Istituto Nazionale di Geofisica e Vulcanologia, Osservatorio Vesuviano, Naples, Italy*

Introduction. Delay time tomography based on local earthquakes can provide a detailed three-dimensional image of seismic velocity structure in areas which are expected to be affected by strong earthquakes. Refined earthquake locations in a reliable velocity model, allow to detect and characterize crustal structures, and embedded active faults with a high seismogenic potential (Eberhart-Philipps, 1993). On the other hand, the availability of a velocity model and the seismicity distribution allow to study the relationship between the geometry and mechanical behavior of a fault or faults system and the physical properties of the host environment (Michael and Eberhart-Phillips, 1991).

The accuracy of earthquake locations is strongly controlled by several factors, among which the geometry of the network, the number of available phases especially the capability of identifying both P and S phases, the accuracy of arrival time readings and the knowledge of the crustal structure (Pavlis, 1986). In addition, the use of 1D layered velocity models can introduce systematic errors in the estimation of P- and S-travel times due to the presence of large-scale three-dimensional heterogeneities in the propagation medium (Matrullo *et al.*, 2013). In order to reduce the effect of using a 1D velocity model, relative locations and double differences techniques can be used. With these apporaches, the effect of a poor knowledge of the structure can be cancelled out for two events, very close in space, recorded at the same station travel as they travel following nearly the same path except nearby the source zone (Waldhauser and Ellsworth, 2000). However, Michelini and Lomax (2004) emphasized that systematic errors on earthquake location using double-differences may also be caused if the velocity model is not accurate. In this respect, a joint inversion of hypocenter and velocity parameters could allow to overcome the simplistic assumptions of the location methods mentioned above. The methods used today for the joint tomographic inversion have made substantial progress with respect to the basic theory originally developed by Aki and Lee (1990). Recent methods include efficient techniques for 3D ray tracing calculation using the eikonal equation (Vidale, 1990) for first-arrival traveltimes estimation on a given finite-difference grid in which the precision of travel-time calculation can be significantly improved by a successive integration of the slowness along the ray (e.g, Latorre *et al.*, 2004).

High-resolution imaging of the sub-surface with local earthquake data requires the use of large and consistent data sets of first arrival times. The quality and resolution of the medium image depends not only on the source/receiver coverage of the target region but also on the accuracy of the travel time measurements. The common procedure of reading the arrival time of a phase (picking) involves the manual measurement of P- and S-arrival times on recordings of a single event at a time. Systematic errors can be introduced due to inadequate working procedures such as the interaction between the process of picking and the result of the location. The inconsistency of the data can remain unnoticed when the events are analyzed independently from each other, but it may clearly appear when performing a joint determination of the hypocentral and velocity model parameters and reducing the inconsistency would require a complete picking revision.

The knoweledge of the S-wave add important constraints to the earthquake location problem. The S-phase is important to derive physical parameters of the subsurfaces. The correct reading of the arrival times of these waves can be complicated by various factors, such as the superposition of the tail of the P-wave, the presence of converted waves generated at different interfaces, and the splitting of S-waves caused by seismic velocity anisotropy

(Crampin, 1977). The S-phase identification is approached by exploring the characteristic of an S-wave on three-components recording (3C) (Cichowicz, 1993). The product of different polarization filters applied to a 3C recording combines the major characteristics of an S-wave arrival into one single characteristic function (CF) (Diehl *et al.* 2009, Amoroso *et al.* 2012). Significant improvements in the quality of hypocentre location have been achieved through the use of correlation-based phase repicking (Satriano *et al.*, 2008). In particular, the technique of Rowe *et al.* (2002) is based on cross-correlation and clustering of similar waveforms.

In this study we have reconstructed a detailed three-dimensional image of the shallow crustal volume embedding the active normal fault system in the Campania–Lucania Apennines (southern Italy) which were causative of moderate to large earthquakes during the past centuries, e.g. the *Ms* 6.9, 1980 Irpinia earthquake. It is obtained by the joint inversion of P and S first arrival times from microearthquakes recorded by a dense, high dynamic range, multi-component seismic network recenty deployed in the area. We addressed the issues of data quality and the implementation of a reliable and robust tomographic inversion strategy in order to improve the resolution of the seismic image and accuracy on earthquake locations. As concerns the phase arrival time measurement, techniques based on polarization filtering and refined re-picking by waveform cross-correlation have been applied to enhance the accuracy of first P- and S-wave readings. Data inversion has been performed by using an iterative, linearized, delay-time 3D tomographic method for the joint determination of source location and medium velocity parameters.

We found that P- and S-wave velocity models follow the geological structure, with high Vp/Vs and low VpxVs values reflecting the occurrence of significant fluid accumulation within a ~15 km wide rock volume characterized by intense micro-seismicity. We suggest that significant concentration of background seismicity is controlled by high pore fluid pressure.

Data and processing techniques. The used dataset consists of 1311 events with 0.1≤ML ≤3.2, recorded in the period August, 2005- April, 2011 by a total of 42 stations owned and operated by the research consortium AMRA scarl Istituto Nazionale di Geofisica e Vulcanologia (INGV) (Fig. 1).

The P- and S- phases have been initially hand-picked on three-component ground velocity recordings. The seismic events were preliminary located in a 1D reference velocity model, recently developed for the area (De Matteis *et al.*, 2011), by using the NLLoc code, based on a probabilistic, non-linear, global-search Earthquake Location method in 3D media (Lomax *et al.*, 2000). For our analysis, a first data selection has been performed on the basis of the event location quality: only the events for which at least 5 P- and 2 S- picked arrival times were available, with an azimuthal gap smaller than 200 degrees and an RMS smaller than 0.5 s have been selected. The application of these selection criteria reduced the number of events to 634, to be used for further tomographic analysis.

For the analyzed dataset, we observed that co-localised events recorded by the same station, showed inconsistent S minus P times. This inconsistency may be due to changes in the signal to noise ratio or to the presence of multiple arrivals (due to near-surface wave type conversion or multi-path) in the S-wave arrival time windows, causing large uncertainties both on hypocentral location and on wave velocities variations in the subsurface. To overcome this problem, we first performed a specific analysis aimed at the optimal dentification and picking of S-phases, using a technique which combines the polarization analysis of single, three-components recordings (3C) of an event with the analysis of lateral waveform coherence across the network (Amoroso *et al.*, 2012). A new time series, called weighted characteristic function for the S phase (CFsw), is constructed upon the original three-component recordings that should enhance the polarization characteristics of the S-wave. For a given station, the 3C seismogram has been rotated into the ray coordinate system assuming the incidence angle as measured in a 0.3 sec window after the first-P arrival and the theoretical back-azimuth obtained from the preliminary earthquake location. Then the polarization attributes, e.g. the directivity, the rectilinearity, the ratio between transverse and total energy, have been computed. Finally, the CFsw time series is built, as the product, at each time along the seismogram, of three squared polarization attributes multiplied by a weighting function depending on the modulus of the radial components. The reading of the first S-arrival time was finally carried out on the CFsw functions and used for the subsequent analysis of refined re-picking.

The refined re-picking technique proposed by Rowe *et al.* (2002) has been applied to obtain highly accurate phase arrival time readings. The technique was applied to both the hand-picked first P- and S-phase arrival-times and to S-picks obtained from the polarization analysis. All waveforms from the analyzed seismic events have been preliminarily organized in common receiver gathers. For each pair of traces recorded at the same station, the waveform similarity is evaluated by using a cross-correlation function applied to a window bracketing the reference P- or S-picking. The choice of the appropriate time window length for the cross-correlation is assessed through preliminary tests, by studying the distribution of cross-correlation coefficients for variable window widths. The optimal time window corresponded to the window which allowed to have the largest number of waveform couples with a cross-correlation value greater than 0.5. This criterion leaded to the choice time window lengths of 0.5 and 1.0 seconds for the P- and S-phases, respectively. The waveform catalog is then divided in clusters, based on the similarity as assessed by the cross-correlation coefficient. The traces which are not classified according to the clustering criterion are discarded from the analysis and all the waveforms belonging to a cluster are cross-correlated again. At this step, the result is a table of time shifts that must be added or subtracted to all the waveforms belonging to the same cluster. The optimal pick adjustements are finally determined through an inversion method applied to the estimated delay times, using an iterative conjugate gradient technique (Aster and Rowe, 200; Rowe *et al.*, 2002). The uncertainty on refined picking measurements are therefore assigned as the standard deviation, after estimation via a Monte Carlo sampling technique (Tarantola, 2005).

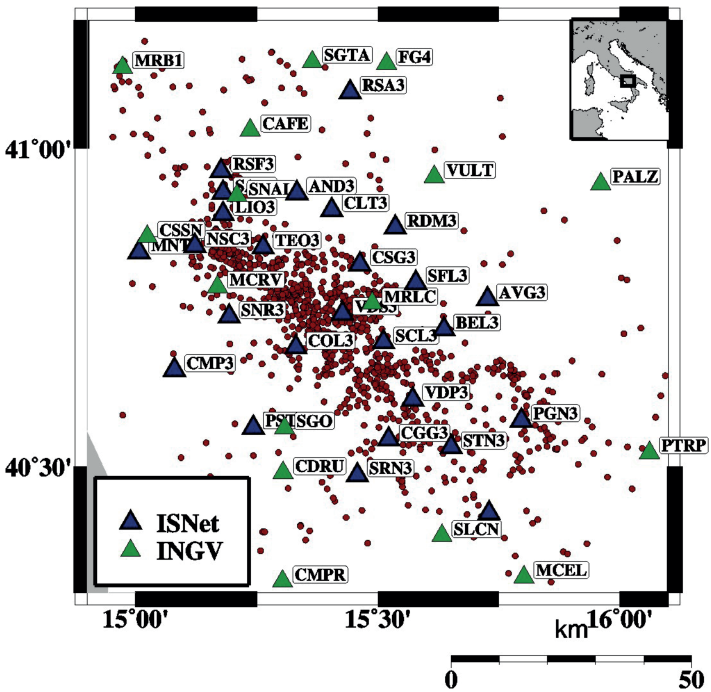

Fig. 1 – Epicentral map showing routine locations of the studied earthquakes. Triangles are INGV (in green) and ISNet (blue) stations.

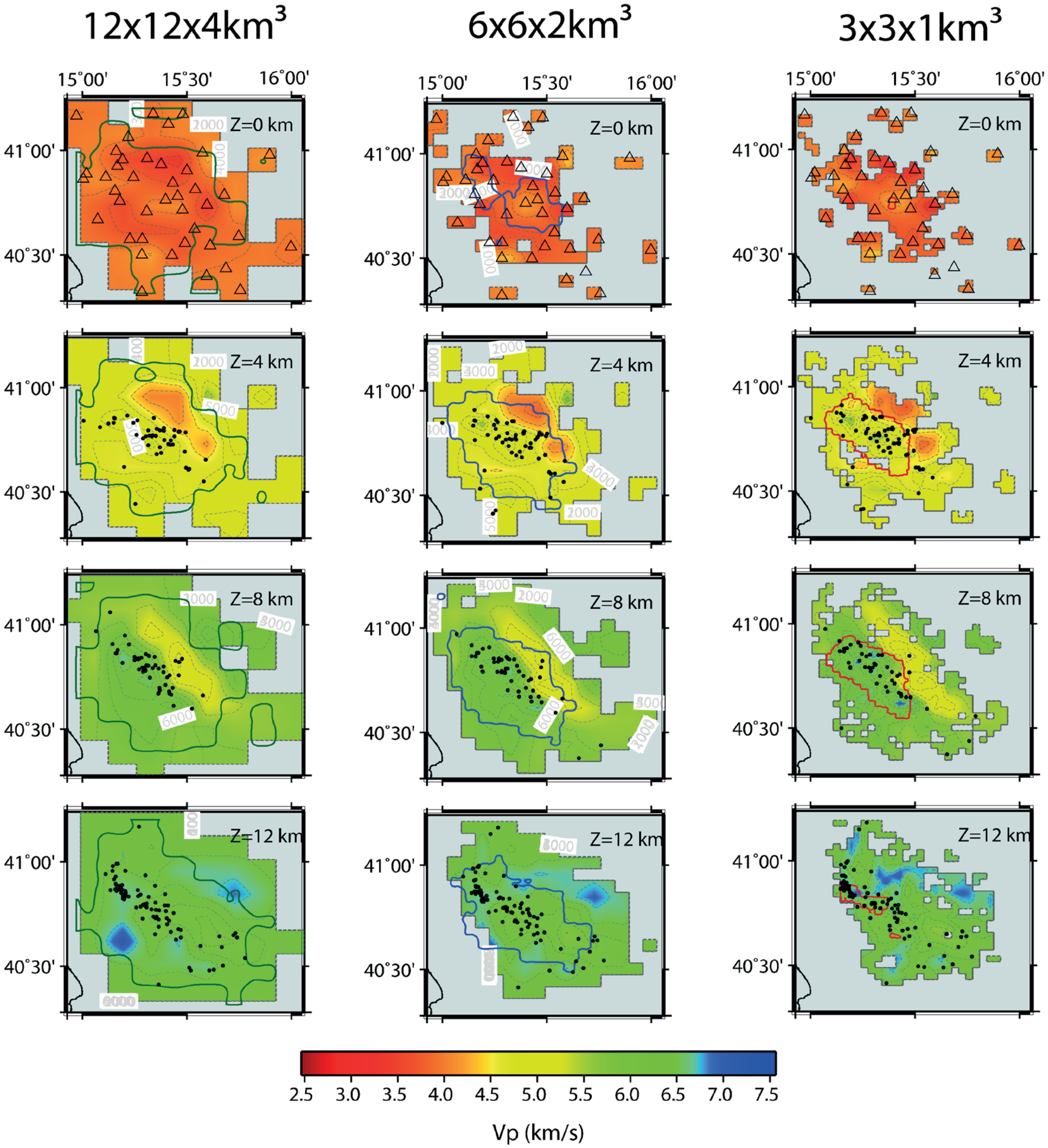

Fig. 2 – Map view of the P-wave tomographic model at each parametrization.

The tomographic method and inversion strategy. The method performs a simultaneous inversion of P- and S-arrival times to estimate the event location coordinates, origin times and P and S velocities at the nodes of a 3D discretized volume. The forward problem, e.g. the travel-time calculation, is solved by preliminary using the finite-difference solution of the eikonal equation and a re-calculation by integration of slowness along the ray path. This procedure makes the travel-time estimation less sensitive to the grid discretization. The inversion strategy is based on a multiscale approach (Chiao and Kuo, 2001) according to which a series of inversion runs are performed by progressively decreasing the velocity model grid spacing. At each step, the starting model is fixed at the one obtained in the previous step but using a larger grid size. This allowed to first estimate the large wavelength components of the velocity model and then to progressively introduce the smaller-scale components for the model reconstruction.

The complete procedure consisted of three different inversions in which the grid spacing was progressively shrinked from 12x12x4 km^3 to 3x3x1 km^3. The smallest grid space has been chosen based on the spatial resolution as inferred from specific checkerboard-type resolution tests. As a quantitative measure of the model resolution, the semblance between the true and recovered checkerboard anomalies has been computed which allowed to delineate the optimal resolved regions. For both the parameterizations 6x6x2 km^3 and 3x3x1 km^3, the minimum grid size used in our study, the extent of the resolved areas increases with depth according to the earthquakes location and the best resolution is obtained for depths ranging between 4 and 14 km for the first parameterization and 4-10 km for the latter (Fig. 2).

Results. Both the P- and S-wave velocity models indicate the presence of a strong lateral variation in the seismic velocity along a direction orthogonal to the Apeninic chain, in the 4-8 km depth range (Fig. 2). This variation defines two geological formation domains which are characterized by a relatively low (3.5-4.8 km/s) and high (5.2-6.5 km/s) P-velocity, respectively. The zone where the sharpest lateral transition occurs in the NE direction, is well correlated with the location of the NW-SE oriented, primary normal fault associated with the 1980, Ms 6.9 earthquake, which cuts at SW the outcrops of the carbonatic Campanian platform, and separates at NE the older Mesozoic limestone formations from the younger Pliocene-Quaternary basin deposits. The spatial distribution of seismicity delineates at south-west the possible border of the Irpinia master fault, while at northeast it shows a more diffused pattern due to the presence of a system of highly organized, sub-parallel normal faults as it has been inferred from the fault mechanisms and the coherent orientation of the tensional axes, consistently with a NE-SW dominant extensional stress regime (De Matteis *et al.* 2012).

We have extracted two 1D P-wave velocity models from the final 3D model obtained by using the 3x3x1km^3 parameterization, in correspondence of two deep wells (Fig. 3a). We note

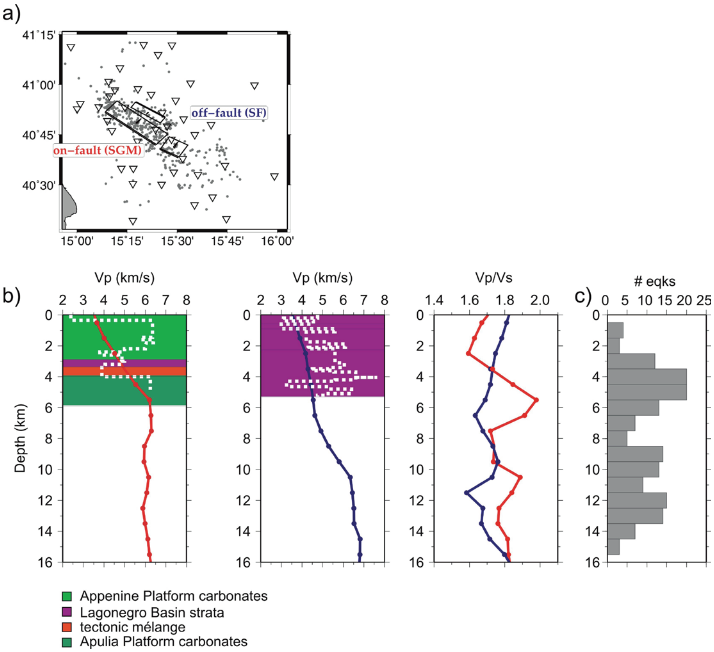

Fig. 3 – Earthquake locations and comparison of 1D borehole and tomography P-velocity models on- and off-fault zone. (a) Location of selected microearthquakes and stations used for the tomographic analysis. Sites of exploration wells San Gregorio Magno (SGM) and San Fele (SF) are also shown, together with trace of cross-section of Fig. 1B. (b) Comparison of the tomographic (continuous line) and sonic-log (dashed line) 1D P-velocity models at the borehole sites SGM and SF. (c) V_p/V_s ratio vs. depth measured at on-fault SGM (red line) and off-fault SF (blue) sites. (d) Histogram of number of events vs. depth for the earthquakes analyzed in this study.

that the P-wave velocities inferred from the tomographic analysis are generally consistent with the expected velocities of litho-stratigraphic units for the studied area, however the variation with depth is smoother due to the low number of earthquake sources sampling the shallow layers of the model and the chosen parameterization which does not allow one to resolve length scales less than 1 km in depth (Fig. 3b). The Vp/Vs ratio shows a large lateral and vertical variability within the investigated crustal volume. It ranges from a value of 1-7-1.8 at shallow depths and increases up to 2-2.2 between 5 km and 12 km depth in the volume where most of present microseismicity occurs. Such high values of the Vp/Vs ratio are a determinant for the fluid saturation state of shallow crust, rock formations as well as of their inner pore pressure condition.

The evidence for a predominant microearthquake activity confined within the highest Vp/Vs volume (Fig. 3c) and the combined interpretation of Vp/Vs ratio and Vp x Vs product confirms that in the explored low-magnitude earthquake range, fault lubrication processes occur and are driven by fluid pressurization along the fault zone, producing a substantial decrease of dynamic friction with a consequent increase in seismic radiation efficiency. These processes not only control the substantial concentration of background seismicity within a discrete, active fault-bounded block, but also the nucleation of large earthquakes such as the *Ms* 6.9, 1980 Irpinia earthquake through pore-pressure increase on fluid-filled cracks located within the damage zone volume surrounding the major active faults.

References

Aki, K. and W. Lee (1990). Determination of three-dimensional velocity anomalies under a seismic array using first p arrival times from local earthquakes, in a homogeneous initial model. *Journal Geophys. Res.*, 4381-99.

Amoroso, O., N. Maercklin, and A. Zollo (20123). S-wave identification by polarization filtering and waveform coherence analysis. *Bull. Seism. Soc. Am.,* Vol.102 No.2 doi:10.1785/0120110140.

Aster, R. and C. Rowe (2002, Jun). Automatic phase-pick refinement and similar event association in large seismic data sets. In *Advances in Seismic Event Location*, Volume 92, pp. 231-263. eds. C. Thurber and N. Rabinowitz. Kluwe, Amsterdam, 1993.

Chiao, L.-Y. and Kuo, B.-Y., 2001, Multiscale seismic tomography: *Geophysical Journal International, v.* 145(2), p. 517-527.

Cichowicz, A. (1993). An automatic s-phase picker. *Bull. Seism. Soc. Am. 83* (1), 180-189.

Crampin, S. (1977). A review of the effects of anisotropic layering on the propagation of seismic waves. Geophys J. R. ast. Soc. 49, 9-27.

De Matteis, R., E. Matrullo, T. A. Stabile, L. A. Rivera, and A. Zollo (2012). Fault delineation and regional stress direction from the analysis of background microseismicity in southern Apennines, Italy. *Bull. Seism. Soc. Am.*, doi: 10.1785/0120110225.

Diehl, T., N. Deichmann, E. Kissling, and S. Husen (2009). Automatic s-wave picker for local earthquake tomography. *Bulletin of the Seismological Society of America 99* (3), 1906.

Eberhart-Phillips, D. (1993). Local earthquake tomography: earthquake source regions *In Seismic Tomography: theory and practice* edited by H.M. Iyer and K. Hirahara- 1st ed. Published by Chapmann and Hall, 2-6 Boundary Row, London SE1 8HN.

Latorre, D., J. Virieux, T. Monfret, V. Monteiller, T. Vanorio, J.-L. Got, and H. Lyon-Caen (2004, Jan). A new seismic tomography of aigion area (gulf of corinth, greece) from the 1991 data set. *Geophys. J. Int. 159*, 1013-1031.

Lomax, A., J. Virieux, P. Volant, and B. Thierry (2000, Jun). Probabilistic earthquake location in 3d and layered models. in: Thurber c.h. and raibinowitz n. (eds.). *Advances in Seismic Event Location. Modern Approaches in Geophysics 18*, 101-134.

Matrullo E., R. De Matteis, C. Satriano, O. Amoroso and A. Zollo (2013**)**. An improved 1-D seismic velocity model for seismological studies in the Campania-Lucania region (Southern Italy). *Geophys. J. Int.* doi: 10.1093/gji/ggt224.

Michelini, A. and A. Lomax (2004, Apr). The effect of velocity structure errors on double-difference earthquake location. *Geophys. Res. Lett.*, 1-4.

Monteiller, V., J.-L. Got, J. Virieux, and P. Okubo (2005, Jan). An efficient algorithm for double-difference tomography and location in heterogeneous media, with an application to the kilauea volcano. *J. Geophys. Res. 110* (B12), 1-22.

Michael, A. J. and D. Eberhart-Phillips (1991). Relation among fault behavior, subsurface geology, and three-dimensional velocity models. *Science*, 651-654.

Pavlis, G. L. (1986). Appraising earthquake hypocenter location errors: a complete pratical approach for single-event locations. *Bull. Seism Soc. Am. 76*, 1699-1717.

Rowe, C., R. Aster, B. Brochers, and C. Young (2002). An automatic, adaptive algorithm for refining phase picks in large seismic data sets. *Bull. Seism. Soc. Am. 92*, 1660-1674.

Satriano C., A. Zollo and C. Rowe (2008). Iterative tomographic analysis based on automatic ref ined picking. Geophysical Prospecting, 56, 467–475, doi:10.1111/j.1365-2478.2008.00700.x.
Tarantola, A. and B. Valette (1987). Generalized nonlinear inverse problems solved using the least-squares criterion. *Rev. Geophys 20*, 219–232.
Vidale John E. (1990). Finite-difference calculation of traveltimes in three dimensions. Geophysics, Vol. 55, No. 5 pp 521-526.
Waldhauser, F. and W. L. Ellsworth (2000, Dec). A double-difference eartquake location algorithm: Method and application to the northern hayward fault, california. *Bulletin of the Seismological Society of America*, 1–16.

TRAVERTINES AS FAULT ACTIVITY INDICATORS: NEW DATA FROM THE SOUTHERN APENNINES

A. Ascione[1], A. Iannace[1], P. Imbriale[1], N. Santangelo[1], A. Santo[2]
[1]*Dipartimento di Scienze della Terra, dell'Ambiente e delle Risorse - DiSTAR, Università Federico II, Napoli, Italy*
[1,2]*Dipartimento di Ingegneria Idraulica, Geotecnica e Ambientale, Università Federico II, Napoli, Italy*

Introduction. It has been known since a long time that there is a worldwide association between travertines and tectonically active areas (Barnes *et al*., 1978). Furthermore, according to Hanckock *et al*. (1999), late Quaternary travertines can reveal much about areas that are experiencing active faulting. The linkage between travertines and active faults may be envisaged in the key role played by active faults in the transport, and rise, of hydrothermal fluids (Sibson, 1996). Several travertine deposits occur in proximity of either step-over zones (relay ramps) or lateral tips of fault zones, i.e. in settings in which complex strains can lead to the development of networks of intersecting tensional fissures that enhance the sub-surface flow of hydrothermal fluids (Hanckock *et al*., 1999).

Italy is the homeland of travertines. The western slope of the northern and central Apennines enclose several huge outcrops quarried since Roman time, which are the type localities of the rock. Such travertines punctuate the area affected by Quaternary volcanism and by the occurrence of hydrothermal springs (Chiodini *et al*., 2000; Minissale, 2004), and the role of deep-seated CO2 in their genesis is widely acknowledged (e.g., Brogi *et al*., 2012). By contrast, calcareous deposits in the southern Apennines, which may be texturally classified as tufa, have long been associated with cool meteoric waters (D'Argenio and Ferreri, 1988; Ford and Pedley, 1996; Golubic *et al*., 1993) discharging from the main aquifers of the region. Conversely, recent studies (Santo *et al*., 2011; Ascione *et al*., 2013a), based on comprehensive data sets including i) the regional scale distribution of the major (i.e. mappable on medium scale maps) tufa bodies, and of Quaternary extensional faults, ii) spring chemistry, and iii) petrographic and stable isotope ($d^{13}C$ and $d^{18}O$) analyses of tufa/travertine deposits, provided evidence that geologically significant continental carbonates of southern Italy are related to CO2-rich water rising along active extensional faults (Ascione *et al*., 2013a). As such large mappable travertine bodies may be considered as indicators of active tectonics, and hence they can be used to detect fault traces.

In this study, we examine the role of travertines as tools in the reconstruction of the tectonic history of a region. This is based on comparative analysis of Quaternary time-space distribution of both large travertine bodies and extensional fault activity.

Geological setting. The study region is the southern Apennines fold-and-thrust belt, which was formed from Miocene to Middle Pleistocene. Thrusting, with a general NE sense of transport, involved both ocean-derived units and deformed sedimentary successions of continental margin origin. These consist of carbonate platform/slope and pelagic basin successions, stratigraphically covered by Neogene foredeep and wedge-top basin sediments.

Extensional tectonics affected the internal portion of the chain since the late Miocene, with the formation of the Tyrrhenian back-arc basin (Sartori, 1990, 2003). Since Early Pleistocene times, extension in the southern Tyrrhenian basin affected the southern Apennines with the formation of large peri-Tyrrhenian grabens, bounded by both NW-SE and NE-SW trending extensional faults (e.g., Milia and Torrente, 1999; Caiazzo *et al*., 2006). Starting from the

Middle Pleistocene, the northern grabens (i.e. the modern Garigliano and Campana plains) were affected by intense volcanism (e.g. Brocchini *et al*., 2001; Rolandi *et al*., 2003). Following the ceasing of the orogenic transport in the early part of the Middle Pleistocene (at 0.7 Ma; Patacca and Scandone, 2001), the chain was affected by extensional tectonics (Cinque *et al*., 1993; Hippolyte *et al*., 1994). Dominantly extensional faults that postdate and dissect the thrust belt (e.g. Cello *et al*., 1982; Butler *et al*., 2004; Caiazzo *et al*., 2006) were also responsible for the formation of several, widespread intramontane basins. Extensional tectonics, which is driven by a NE-SW oriented extension direction, is currently active and controls the intense seismicity which affects the axial belt of the mountain chain (e.g. Cello *et al*., 1982; Hippolyte *et al*., 1994; Chiarabba *et al*., 2005; Macchiavelli *et al*., 2012). At the surface the pattern of active faults, i.e. of faults showing evidence of activity in the late Pleistocene-Holocene, is scattered and characterized by mainly NW-SE and E-W trending fault segments. Major extensional structures are around 10 km long, and characterized by cumulative offsets in the order of some hundreds of meters (e.g., Cinque *et al*., 2000; Caiazzo *et al*., 2006).

Time-space travertine distribution. The main travertine bodies (i.e. mappable on medium scale maps) of the Southern Apennines are all Quaternary in age. Such deposits were mapped and classified according to their age, i.e. those characterised by active encrustation were distinguished from continental carbonates of Late, Middle and Lower Pleistocene age (Fig. 1). Information constraining age of single travertine units was provided by stratigraphic evidence and/or local chrono-stratigraphical reconstructions. The map of Fig. 1 also shows the distribution of significant buried travertine bodies, which were detected based on both published and unpublished stratigraphic logs. The spatial distribution of travertine is markedly uneven, with

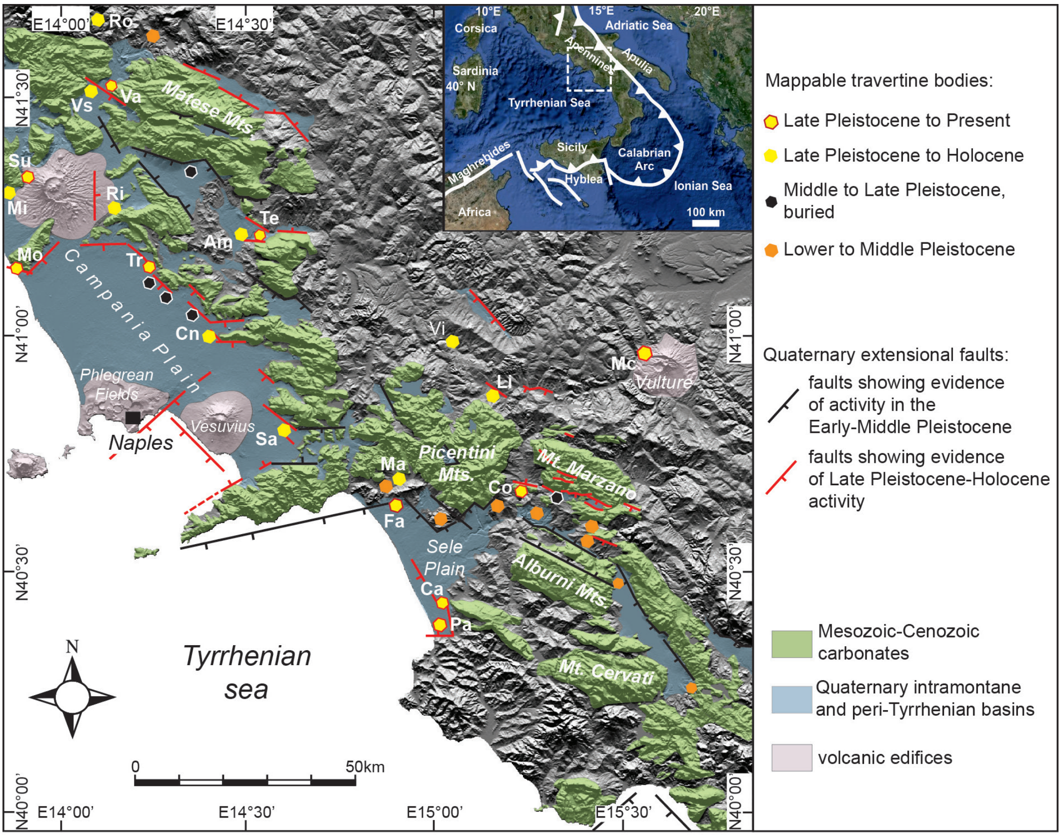

Fig. 1 – Distribution of mappable travertine bodies in the southern Apennines (after Ascione *et al.,* 2013, modified).

the main bodies being clustered along the boundaries of the main coastal and intramontane tectonic basins (Fig. 1).

In the Campania plain (Fig. 1), outcropping and buried travertine bodies follow the main faults which bound this coastal graben, and are located in the downthrown blocks. These faults, which have been responsible for the subsidence of the plain since Pleistocene times, show evidence of activity in the latest Pleistocene or Holocene (Brancaccio *et al*., 1991; Cinque *et al*., 2000; Irollo *et al*., 2005; Santangelo *et al*., 2010). Stratigraphical data point out that all outcropping travertines (which include currently depositing bodies, Fig. 2) are younger than the 39 ky old Ignimbrite Campana, which represents a major stratigraphical marker in the area (Rolandi *et al*., 2003). Conversely, all buried travertine bodies are older than the Ignimbrite Campana marker level. In some instances, the lowest drilled travertines may be related to the Middle Pleistocene based on their occurrence below shallow marine deposits correlated with the Last Interglacial (130 ka). Buried travertines are located in the subsurface of Triflisco, Caserta and Maddaloni, at depths ranging from 30 up to 300 m b.s.l., and have average thicknesses between 5 and 10 m. The thickest (50 m thick) layer is found in the neighbourhood of Maddaloni, at the depth of 300 m.

Fig. 2 – Late Pleistocene travertine at Contursi (a); historical travertine at Porta Marina Paestum (b); active encrustation at Triflisco (c).

In the Sele Plain coastal graben, which has been subject to subsidence from the Early to the Late Pleistocene (Amato *et al*., 1991; Brancaccio *et al*., 1991; Cinque and Romano 2009) deeply buried travertine bodies have not been detected to date. Outcropping units include Late Pleistocene and actively forming deposits, which occur in the northern (Pontecagnano-Faiano, Ma and Fa in Fig. 1; Anzalone *et al*., 2007) and southern (Capaccio and Paestum, respectively Ca and Pa in Fig. 1; D'Argenio *et al*., 1988; Amato *et a*l., 2012) parts of the Plain. Fossil deposits, which are related to the Lower and Middle Pleistocene (Brancaccio *et al*., 1987; Amato *et al*., 1991;), outcrop in the E-NE margin of the Plain. Such older travertines are either interlayered with alluvial deposits or occur as isolated bodies lying on the pre-Quaternary bedrock. These deposits outcrop in the footwall blocks of the faults bounding the late Quaternary depocentre uplifted up to some hundreds of metres above the Plain.

In the chain interiors, both fossil and currently forming travertine deposits are found either in the margins or/and within the main Quaternary continental basins, and in some instances are buried (Fig. 1). The oldest deposits, which are related to the Middle Pleistocene, are located to the NW of the Matese Mts. (Isernia basin; Brancaccio *et al*., 2000) and in the Bianco and Tanagro river valleys (Buccino *et al*., 1978; Amato *et al*., 1992; Ascione *et al*., 1992). The Middle Pleistocene travertines, which are generally interlayered with fluvial or lacustrine deposits, are deeply dissected and terraced and in some instances show evidence of deformation. Their thicknesses are in the order of some tens of meters.

Recent and actively forming travertines occur in the Late Pleistocene to Present alluvial plains in the Venafro (Vs and Va in Fig. 1), Telese (Te, Am) and Contursi (Co) areas (Fig. 1 and Fig. 2). These develop along faults/fault zones showing evidence of activity in the Late Pleistocene-Holocene (Galli and Naso, 2009; Ascione *et al*., 2013b), and may be considered as active faults.

Tab. 1 – Stable isotope data.

	Site	Sample label	$\delta^{18}O_{PDB}$ [‰]	$\delta^{13}C_{PDB}$ [‰]	Location Latitude	Longitude
Ro	Rocchetta al Volturno	Ro1	-8,05	1,51	41°38'19,064"N	14°4'19,186"E
Vs	Venafro Santa Cristina	Vs1]	-5,98	2,35	41°29'37,718"N	14°4'27,664"E
		Vs2]	-6,07	2,15		
		Vs3]	-6,40	0,23	41°29'12,951"N	14°5'17,898"E
		Vs4]	-6,16	-0,17		
Va	Venafro Terme di Agrippa	Va1]	-6,25	11,92	41°30'11,253"N	14°7'0,990"E
		Va2]	-6,22	12,56		
		Va3	-6,14	13,44	41°30'4,608"N	14°6'53,777"E
		Va4 #	-3,97	18,34	41°30'4,042"N	14°6'51,594"E
Su	Suio	Su1 #	-7,77	9,85	41°19'57,826"N	13°52'31,801"E
		Su2 #	-12,93	7,21	41°18'46,794"N	13°53'35,657"E
		Su3	-12,58	7,06	41°18'36,662"N	13°53'38,524"E
		Su4	-12,7	6,88	41°18'36,538"N	13°53'38,741"E
Mi	Minturno	Mi1	-4,2	6,26	41°18'36,538"N	13°53'38,741"E
Ri	Riardo	Ri1	-6,00	11,13	41°14'39,643"N	14°7'41,494"E
		Ri2	-6,39	10,05	41°14'39,130"N	14°7'40,283"E
Te	Telese	Te1]	-6,64	5,22	41°12'40,503"N	14°32'6,483"E
		Te2]	-7,23	9,45		
		Te3]	-7,40	8,74		
		Te4 #	-6,65	9,62	41°13'28,554"N	14°31'30,154"E
Am	Amorosi	Am1	-7,08	0,46	41°12'12,748"N	14°30'29,115"E
Mo	Mondragone	Mo1 #	-6,72	11,37	41°8'25,901"N	13°51'26,074"E
Sa	Sarno	Sa1	-5,86	3,57	40°48'9,405"N	14°37'41,851"E
Ma	Pontecagnano Malche	Ma1	-6,27	-4,33	40°41'31,354"N	14°53'23,251"E
		Ma2	-6,36	-5,71	40°41'30,428"N	14°53'23,456"E
Fa	Faiano	Fa1 #	-5,85	3,04	40°39'56,729"N	14°54'16,738"E
		Fa2 #	-5,33	4,02	40°39'56,613"N	14°54'16,625"E
Co	Contursi	Co1]	-6,79	10,45	40°40'22,237"N	15°14'46,427"E
		Co2]	-6,54	10,38		
		Co3]	-6,76	10,32		
		Co4	-6,59	10,32	40°40'21,280"N	15°14'46,822"E
		Co5 #	-6,78	10,28	40°40'29,374"N	15°14'47,861"E
		Co6 #	-6,88	9,11	40°40'21,280"N	15°14'46,822"E
		Co7	-10,77	6,78	40°41'21,416"N	15°14'55,222"E
Pa	Paestum	Pa1 #	-6,20	0,93	40°25'15,302"N	14°59'48,437"E
Ca	Capaccio	Ca1	-6,13	2,31	40°26'52,820"N	15°2'37,309"E
Vi	Villamaina	Vi1	-8,32	6,14	40°59'14,620"N	15°3'10,190"E
		Vi2	-8,23	4,41	40°59'17,450"N	15°3'9,840"E
Li	Lioni	Li1	-6,22	8,12	40°52'31,209"N	15°11'21,136"E
		Li2	-6,3	11,13	40°52'42,047"N	15°11'4,853"E
Mc	Monticchio Bagni	Mc1	-5,94	8,03	40°57'10,078"N	15°33'31,313"E
		Mc2 #	-8,07	7,89	40°57'1,936"N	15°35'16,709"E

sample from Present-day deposits
] samples from depositional successions

Discussion and concluding remarks. On the regional scale, the spatial distribution of large, mappable travertine bodies does not follow that of the major springs, discharging from the main aquifers of the study area, i.e. those hosted in the carbonate successions. Conversely, a striking spatial association between the late Pleistocene-Holocene deposits and the main (around 10 km in length, and with large offsets) extensional faults with coeval activity is observed (Fig. 1; Ascione *et al*., 2013a). All such recent travertines, as well as currently depositing ones, are characterised by positive carbon isotope ($d^{13}C$) values (Tab. 1), which indicate that their precipitation is driven by a supplementary –non-atmospheric– source of CO2. This would produce more aggressive water–rock interactions at depth, able to trigger –in favourable hydrogeological conditions– the production of geologically significant deposits (Ascione *et al*., 2013a). Overall evidence from the study area suggests that the additional CO2 source is provided by active faults, further pointing to the long evidenced major role of extensional fault zones, and particularly active faults, in the migration and degassing of deep-seated fluids in non-hydrothermal areas (Kerrich, 1986; Sibson, 2000; Toutain and Baubron, 1999; Cello *et al*., 2001; Ciotoli *et al*., 2007). Therefore in the southern Apennines, as well as in other tectonically active areas worldwide (e.g., Hancock *et al*., 1999), a link between conspicuous continental carbonate accumulation and active faults of regional relevance is evidenced. This implies that, independent from their facies (stiff travertines vs. porous tufa), large continental carbonate deposits may be considered as indicators of persistent fault activity.

Based on such evidence, the time-space distribution of the southern Apennines large travertine bodies may be considered as a tool for the reconstruction of the tectonic history of the region. Particularly it may provide information constraining both the location and age of activity of major extensional structures, i.e. of well-developed extensional faults, accumulating large offsets. Based on such assumption, the presence of uplifted travertine bodies in the margin of the Sele Plain coastal graben would suggest a seaward migration of both fault activity and main depocentral area over the Early to Middle Pleistocene time span, which is consistent with independent morphotectonic reconstructions (Brancaccio *et al*., 1987; Brancaccio *et al*., 1991; Amato *et al*., 1992) based on both surface and subsurface information. Similarly, migration of fault activity in the Alburni Mts. – Tanagro valley – Mt. Marzano area in the Middle to Late Pleistocene time span (Ascione *et al*., 2013b), is mirrored by a coeval shift in the travertine depositional loci. Conversely, the occurrence along the Campania Plain boundaries of superposed travertine layers progressively buried in the subsurface would suggest persistent activity of the faults bounding the Plain from the Middle Pleistocene to the Holocene, which is consistent with absence of uplifted Quaternary deposits along the boundaries of the Campania Plain.

All above evidence indicates that activation/deactivation of extensional faults is accompanied by a parallel activation/deactivation of associated phenomena, e.g. deep seated fluid advection and, in those areas in which soluble rocks are present (either outcropping or buried), dissolution and related carbonate precipitation. Furthermore it suggests that significant amounts of continental carbonates represent a record of fault activity, their ages helping constraining the age of faulting and faulting chronology.

References

Amato A., Ascione A., Cinque A., Lama A.; 1991: Morfoevoluzione, sedimentazione e tettonica recente dell'Alta Piana del Sele e delle sue valli tributarie (Campania). Geogr. Fis. Dinam. Quat., **14** (1), 5-16.

Amato, A., Cinque, A., Santangelo, N. and Santo, A., 1992., Il bordo meridionale del Monte Marzano e la valle del F. Bianco: geologia e geomorfologia: Studi Geologici Camerti, volume speciale (1992/1) 191-200.

Amato, V., Anzalone, E., Aucelli, P.P.C., D'Argenio, B., Ferreri, V., Rosskopf, C.M.; 2012: Sedimentology and depositional history of the travertines outcropping in the Poseidonia-Paestum archaeological area. Rendiconti Lincei 23, 37-44. doi:10.1007/s12210-011-0155-z.

Anzalone, E., Ferreri, V., Sprovieri, M. and D'Argenio, B.; 2007: Travertines as hydrologic archives: The case of the Pontecagnano deposits (southern Italy): Advances in Water Resources v. 30, p. 2159-2175.

Ascione, A., Cinque, A., Tozzi, M.; 1992: La Valle del Tanagro (Campania): una depressione strutturale ad evoluzione complessa. Studi Geologici Camerti, Spec. Vol. 1992/1, p. 209-219.

Ascione A., Iannace A., Imbriale P., Santangelo N., Santo A.; 2013a: Tufa and travertines of southern Italy: deep-seated, fault-related CO2 as the key control in precipitation. Terra Nova, doi: 10.1111/ter.12059.
Ascione A., Mazzoli S., Petrosino P., Valente E.; 2013b: A decoupled kinematic model for active normal faults: Insights from the 1980, MS = 6.9 Irpinia earthquake, southern Italy. Geol. Soc. Am. Bull., 125(7-8), 1239-1259.
Barnes, I., Irwin, W.P., White, D.E.; 1978: Global distribution of carbon-dioxide discharges and major zones of seismicity. United States Geological Survey, Water Resources Investigations 78-39, Open File report.
Brancaccio, L., Cinque, A., D'Angelo, G., Russo, F., Santangelo, N., Sgrosso, I.,; 1987: Evoluzione
tettonica e geomorfologica della Piana del Sele (Campania, Appennino meridionale). Geografia Fisica e Dinamica Quaternaria 10, 47-55.
Brancaccio, L., Cinque, A., Romano, P., Rosskopf, C., Russo, F., Santangelo, N., Santo, A.; 1991: Geomorphology and neotectonic evolution of a sector of the Tyrrhenian flank of the southern Apennines (Region of Naples, Italy). Zeit. für Geomorph., N.F., Suppl. Bd. 82, 47-58.
Brancaccio, L., Di Crescenzo, G., Rosskopf, C., Santangelo, N., and Scarciglia, F.; 2000: Carta geologica dei depositi quaternari e carta geomorfologica dell'alta valle del fiume Volturno (Molise, Italia meridionale). Note illustrative. Il Quaternario, v. 13(1/2), p. 81-94.
Brocchini, F., Principe, C., Castradori, D., Laurenzi, M.A., Goria, L.; 2001: Quaternary evolution of the southern sector of the Campanian Plain and early Somma–Vesuvius activity: Insights from the Trecase well. Mineral. Petrol., 73, 67-91.
Brogi, A., Capezzuoli, E., Buracchi, E., Branca, M.; 2012: Tectonic control on travertine and calcareous tufa deposition in a low-temperature geothermal system (Sarteano, Central Italy). J. Geol. Soc. London, 169, 461-476.
Buccino, G., D'Argenio, B., Ferreri, V., Brancaccio, L., Ferreri, M., Panichi, C., Stanzione, D.; 1978: I travertini della bassa valle del Tanagro (Campania). Studio geomorfologico, sedimentologico e geochimico. Boll. Soc. Geol. It., 97, 617-646.
Butler, R.W.H., Mazzoli, S., Corrado, S., De Donatis, M., Di Bucci, D., Gambini, R., Naso, G., Nicolai, C., Scrocca, D., Shiner, P., Zucconi, V.; 2004: Applying thick-skinned tectonic models to the Apennine thrust belt of Italy: Limitations and implications, *in* McClay, K.R., ed., Thrust Tectonics and Petroleum Systems: AAPG Memoires, 82, 647-667.
Caiazzo, C., Ascione, A., Cinque, A.; 2006: Late Tertiary–Quaternary tectonics of the Southern Apennines (Italy): New evidences from the Tyrrhenian slope. Tectonophysics, 421, 23-51.
Cello, G., Guerra, I., Tortorici, L., Turco, E., Scarpa, R.; 1982: Geometry of the neotectonic stress field in southern Italy: geological and seismological evidence. J. Struct. Geol., 4, 385-393.
Cello, G., Invernizzi, C., Mazzoli, S.,Tondi, E.; 2001: Fault properties and fluid flow patterns from Quaternary faults in the Apennines. Tectonophysics, 336, 63-78.
Chiarabba, C., Jovane, L., Di Stefano, R.; 2005: A new view of Italian seismicity using 20 years of instrumental recordings: Tectonophysics, v. 395, p. 251-268.
Chiodini, G., Frondini, F., Cardellini, C., Parello, F., Peruzzi, L.; 2000: Rate of diffuse carbon dioxide earth degassing estimated from carbon balance of regional aquifers: the case of Central Apennine (Italy). J. Geophys. Res., 105(B4), 8423–8434.
Cinque A., Romano P.; 2009; Note illustrative della carta Geologica d'Italia alla scala 1:50.000, Foglio 486 Foce Sele, Parte I. ISPRA e Regione Campania Eds, 82 pp.
Cinque, A., Ascione, A., Caiazzo, C.; 2000: Distribuzione spazio-temporale e caratterizzazione della fagliazione quaternaria in Appennino meridionale. In: Le ricerche del GNDT nel campo della pericolosità sismica (F. Galadini, C. Meletti and A. Rebez, eds) CNR – Gruppo Nazionale per la Difesa dai Terremoti – Roma, 203-218.
Cinque, A., Patacca, E., Scandone, P., Tozzi, M.; 1993: Quaternary kinematic evolution of the Southern Apennines. Relationships between surface geological features and deep lithospheric structures. Ann. Geofis., 36, 249–260.
Ciotoli, G., Lombardi, S., Annunziatellis, A.; 2007: Geostatistical analysis of soil gas data in a high seismic intermontane basin: Fucino Plain, central Italy. J. Geophys. Res., 112, B05407.
D'Argenio, B., Ferreri, V.; 1988: Ambienti deposizionali e litofacies dei travertini quaternari dell'Italia centro-meridionale. Mem. Soc. Geol. It., 41, 861–868.
Ford, T.D. and Pedley, H.M.; 1996: A review of tufa and travertine deposits of the world: Earth-Science Reviews v. 41, p. 117-175.
Galli, P.A.C., Naso, G.A.; 2009: Unmasking the 1349 earthquake source (southern Italy): paleoseismological and archaeoseismological indications from the Aquae Iuliae fault. J. Struct. Geol., 31, 128–149.
Golubic, S., Violante, C., Ferreri, V. and D'Argenio, B.; 1993: Algal control and early diagenesis in Quaternary travertine formation (Rocchetta a Volturno, Central Appennines). In: Studies on Fossil Benthic Algae. F. Barattolo *et al*. (eds). Bollettino Società Paleontologica Italiana volume speciale 1, Mucchi, Modena, p. 231-247.
Hancock, P.L., Chalmers, R.M.L., Altunel, E., Çakir, Z.; 1999: Travitonics: using travertines in active fault studies. J. Struct. Geol., 21, 903-916.
Hippolyte, J.-C., Angelier, J., Roure, F.; 1994: A major geodynamic change revealed by Quaternary stress patterns in the Southern Apennines (Italy): Tectonophysics, 230, 199-210.
Irollo G., Ascione A., Cinque A.; 2005: Segnalazione di attività olocenica lungo due fault zones dell'hinterland del Golfo di Napoli. 24° Convegno Gruppo Nazionale di Geofisica della Terra Solida (GNGTS), Roma 15-17 novembre 2005, 17-21.

Kerrich, R., 1986. Fluid infiltration into fault zones: chemical, isotopic and mechanical effects. Pure Appl. Geophys., 124, 225-268.
Macchiavelli, C., Mazzoli, S., Megna, A., Saggese, F., Santini, S., Vitale, S.; 2012: Applying the Multiple Inverse Method to the analysis of earthquake focal mechanism data: new insights into the active stress field of Italy and surrounding regions. Tectonophysics, 580, 124-149.
Milia, A., Torrente, M.M.; 1999: Tectonics and stratigraphic architecture of a peri-Tyrrhenian half-graben (Bay of Naples, Italy). Tectonophysics, 315, 301-318.
Minissale, A.; 2004: Origin, transport and discharge of CO2 in central Italy. Earth Sci. Rev., 66, 89-141.
Patacca, E., Scandone, P.; 2001: Late thrust propagation and sedimentary response in the thrust belt-foredeep system of the Southern Apennines (Pliocene-Pleistocene). In: Vai, G.B., Martini, I.P. (Eds.), Anatomy of a Mountain: the Apennines and Adjacent Mediterranean Basins. Chapman and Hall, London, p. 401-440.
Rolandi, G., Bellucci, F., Heizler, M.T., Belkin, H.E., De Vivo, B.; 2003: Tectonic controls on the genesis of ignimbrites from the Campanian Volcanic Zone, southern Italy. Mineral. Petrol., 79, 3-31.
Santangelo, N., Ciampo, G., Di Donato, V., Esposito, P., Petrosino, P., Romano, P., Russo Ermolli, E., Santo, A., Toscano, F., Villa, I.; 2010: Late Quaternary buried lagoons in the northern Campania plain (southern Italy): evolution of a coastal system under the influence of volcano-tectonics and eustatism. It. J. Geosci., 129/1, 156-175.
Santo, A., Ascione, A., Del Prete, S., Di Crescenzo, G., Santangelo, N.; 2011: Collapse sinkholes distribution in the carbonate massifs of central and southern Apennines. Acta Carsologica, 40/1, 95-112.
Sartori, R.; 1990: The main results of ODP Leg 107 in the frame of Neogene to Recent geology of the PeriTyrrhenian areas, *in* Kastens, A., Mascle, K.J., *et al*., eds., Proceedings of ODP, Scientific Results, 107, College Station, TX (Ocean Drilling Program), 715-730.
Sartori, R.; 2003: The Thyrrhenian backarc basin and subduction of the Ionian lithosphere: Episodes, 26, 217-221.
Sibson, R.H., 2000. Fluid involvement in normal faulting. Geodynamics, 29, 469-499.
Toutain, J.P., Baubron, J.C.; 1999: Gas geochemistry and seismotectonics: a review. Tectonophysics, 304, 1-27.

AN IN-DEPTH ANALYSIS OF SEISMIC EPISODES: THE EXAMPLE OF THE 2010 SAMPEYRE SWARM AND THE 2013 LUNIGIANA SEQUENCE

S. Barani, R. De Ferrari, G. Ferretti, M. Pasta, D. Scafidi, D. Spallarossa, C. Turino
DISTAV, Università degli Studi di Genova, Italy

Foreword and scope of work. The analysis of earthquake sequences and swarms provides useful hints to identify and characterize the seismogenic structures of an area, to investigate earthquake source properties, to study the propagation of seismic waves, and to investigate the recurrence of earthquakes. Accurate location methods, such as those based on the "master event" (e.g., Peppin *et al*., 1989; Joswig and Schulte-Theis, 1993; Cattaneo *et al*., 1999) or "double difference" (e.g., Waldhauser and Ellsworth, 2000; Zhixian *et al*., 2003; Yang *et al*., 2005) techniques, and seismogram cross-correlation are usual tools in these fields of research. For instance, seismogram cross-correlation has often been applied to identify distinct lineaments belonging to a fault system and to define clusters of dependent events (e.g., Shearer, 1998; Astiz *et al*., 2000). Similarly, the double-difference technique has been widely used to study fault structures and to investigate the spatial and temporal evolution of seismic sequences or swarms (e.g., Prejean *et al*., 2002; Schaff *et al*., 2002; Waldhauser and Ellsworth, 2002; Fukuyama *et al*., 2003). Note that these methods have been generally applied to analyze low-to-moderate magnitude seismicity episodes, including micro-seismicity events and aftershocks. Indeed, location of small earthquakes is one of the primary tools used by seismologists in order to constrain fault locations and orientations and to study the seismogenic process.

In this paper, we apply a comprehensive approach, including major techniques used to analyze sequences and swarm (i.e., waveform cross-correlation, double-difference location, and micro-event detection), to exhaustively investigate the Sampeyre swarm (left panel of Fig. 1), which occurred between October and November 2010 in the Southwestern Alps, and the recent Lunigiana sequence which started on June 21, 2013 in the Northern Apennines (Fig. 2).

Regarding the Sampeyre swarm, 550 earthquakes (the strongest one had a magnitude of 3.2) were recorded and localized by the Regional Seismic network of Northwestern Italy – RSNI (http://www.distav.unige.it/geofisica/) using standard monitoring procedures. Approximately 2800 micro-earthquakes were subsequently identified using an automatic detection algorithm based on the STA/LTA (short-term average/long-term average) triggering method (e.g., Withers *et al.*, 1998; Sharma *et al.*, 2010).

The Lunigiana sequence shocked an area comprised between the provinces of Lucca and Massa Carrara. The main shock, with local magnitude of 5.2, occurred near the municipalities of Minucciano (Lucca) and Casola in Lunigiana (Massa Carrara). More than 1800 aftershocks, with magnitude up to 4.4, were recorded by the RSNI network following the main shock.

The analysis of such seismic episodes is performed both to study the causative sources and to investigate possible changes in the scaling exponent (*b*-value) of the Gutenberg and Richter (1944) relationship within the rock volume involved during the events.

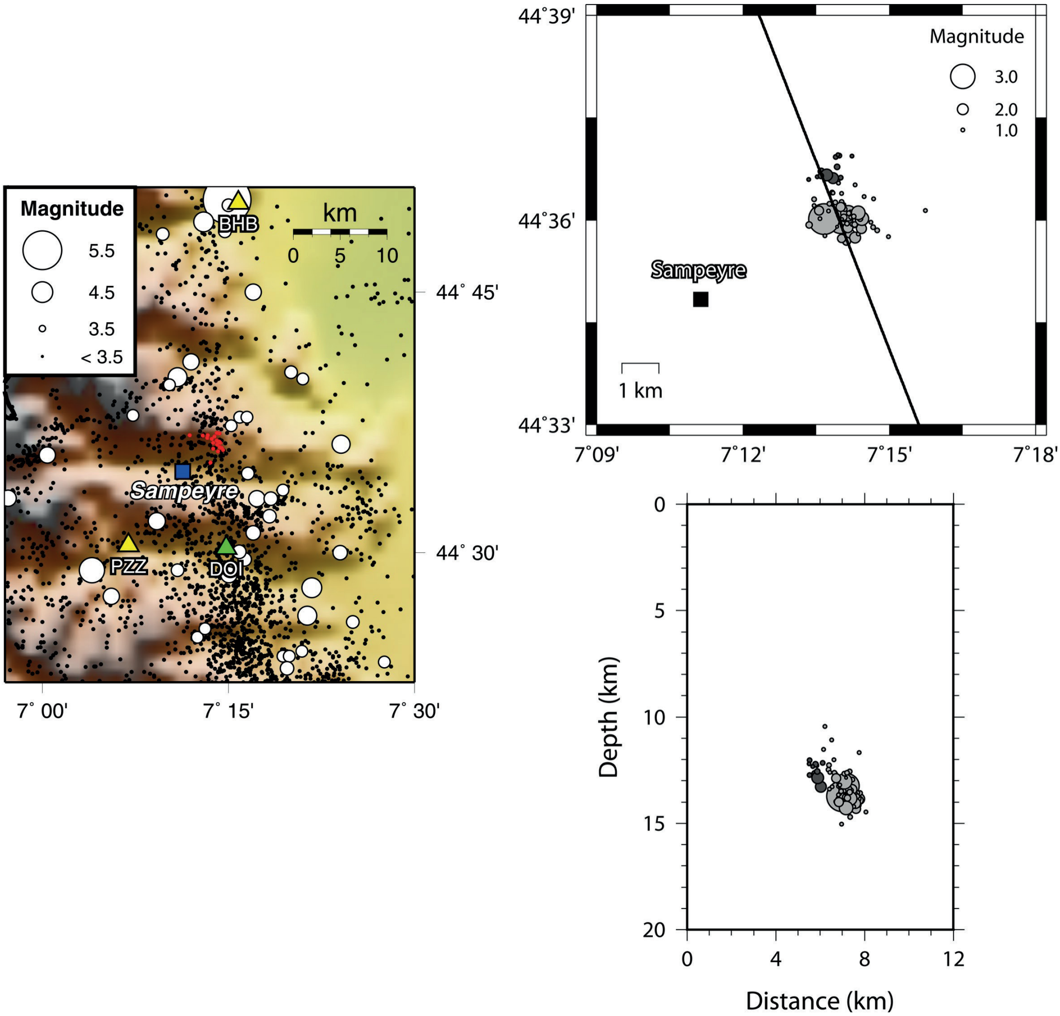

Fig. 1 – Left panel: distribution of the instrumental seismicity ($Ml \geq 2.0$) recorded by the RSNI network in the area surrounding the Sampeyre swarm; the events belonging to the investigated seismic crisis are displayed by red points. Right panels: seismicity distribution (top panel) and longitudinal cross section of hypocenters (bottom panel) after double-difference location. Light- and dark-gray circles indicate the events belonging to Family 1 and Family 2, respectively.

Area seismotectonics. Concerning seismotectonics, the Sampeyre area is located in the inner part of the Dora Maira crystalline massif, which corresponds to the northern Tethyan margin (part of the stretched European continental crust) exhumed during the collision of the Eurasia and Africa plates. The Dora-Maira massif is a large tectonic window that crops out as a broad half-dome. On the eastern side, it is delimited by steep faults and it is directly onlapped by Tertiary deposits of the Po basin (Wheeler, 1991; Michard *et al.*, 1993; Avigad *et al.*, 2003). On the western side, it structurally underlies the oceanic Penninic nappes, under which it subducted during the early Alpine events (Eoalpine stage). The Dora Maira massif is located near the border between the internal (Penninic zone, nearly corresponding with the axial sector of the Alpine chain) and external (eastern sector at the Po Plain border) sectors of the Western Alps where the tectonic regime changes from (prevalent) extension to compression.

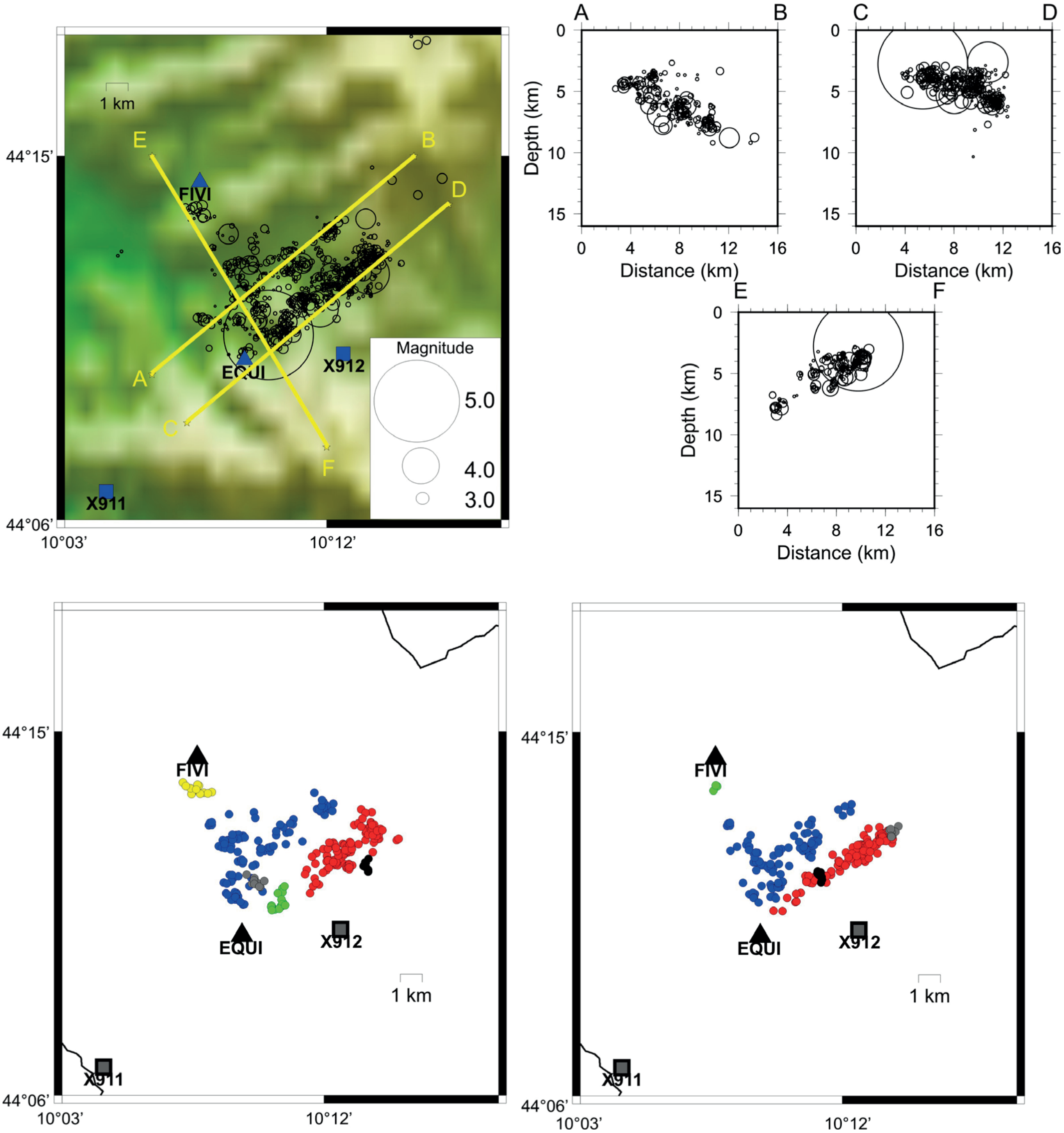

Fig. 2 – Top panels: seismicity distribution (left panel) and seismic cross-section (right panel) after double-difference location. Bottom panels: seismic families identified by EQUI (left panel) and FIVI (right panel) stations, respectively.

In this area, two distinct seismicity trends, one following the Penninic front to the west and one following the Austro-Alpine front to the east, converge delimiting an almost aseismic corridor (Giglia *et al.*, 1996). Following the large-scale zonation of Delacou *et al.* (2004) and Barani *et al.* (2010), the Dora Maira massif can be ascribed to the internal sector of the Western Alps, a continuous zone of extension characterized by low-to-moderate but relatively frequent earthquakes with hypocenters down to approximately 15-20km depth. Analyzing focal mechanism solutions and Global Positioning System (GPS) data shows that extension (i.e., *T*-axes) is virtually perpendicular to the structural trend of the Alps (e.g., Eva and Solarino, 1998; Calais *et al.*, 2002; Nocquet and Calais, 2003, 2004), following a radial pattern (e.g., Frechet, 1978; Nicolas *et al.*, 1990; Champagnac *et al.*, 2004; Delacou *et al.*, 2004). The focal mechanisms of the two major events of the swarm, which were computed by applying the first onset methodology through the FPFIT program (Reasenberg and Oppenheimer, 1985), agree with the regional seismotectonics, which, as stated above, is characterized by a prevalent extensional-transtensional regime. In particular, the orientation of the *T*-axis is in agreement with the direction of extension (approximately E-W) in this sector of the Alps.

Regarding the second seismic episode considered in this study, the Lunigiana-Garfagnana area represents the western border of the northern Apennines. This area is characterized by a complex structural setting which is related to the evolution of the northern Apennines, including three major episodes: 1) consumption of oceanic crust driven by a west-dipping slab, 2) post-collisional evolution, and 3) rotation of the Corsica-Sardinia block with opening of the Tyrrhenian sea (Cattaneo *et al.*, 1983; Ponziani *et al.*, 1995). The structures derived from these main events are related both to compressive and extensive forces. Compression, which is associated to the collision between Africa and Europe, is responsible for the emplacement of different tectonic units belonging to different paleogeographic domanis (the Liguride allochton formed by oceanic crust, the Tuscan unit, and the Umbria-Marche-Romagna unit) (Castaldini *et al.*, 1998). Extensional stresses are due to the roll-back of the subducting Adria-Ionian lithosphere (Negredo *et al.*, 1999), which created tectonic depressions such as the Lunigiana and Garfagnana basins (Bartolini and Bortolotti, 1971). The Lunigiana and Garfagnana basins are two NW-SE-striking asymmetric grabens, originated in the hanging wall of regional low-angle detachment faults, sloping gradually beneath the Apennine chain (Brozzetti *et al.*, 2007). The Lunigiana sequence took place between the Lunigiana and the Garfagnana basins, activating a fault system with anti-apenninic direction. The focal mechanism of the major event (Ml = 5.2), as derived from the INGV moment tensor solution database (http://ingvterremoti.wordpress.com/), shows a strike-slip rupture process confirming that the fault responsible of the main shock is NE-SW oriented.

Methodology. The waveform similarity analysis is used in this work to identify and characterize the seismogenic structures activated during the two seismic episodes. This technique is used to identify groups of events (i.e., earthquake families) characterized by similar locations, source mechanisms, and by similar propagation patterns. The waveform similarity analysis is performed on signals recorded along the vertical component by the seismic stations nearest to the area affected by the seismic events. More precisely, DOI and PZZ stations (Fig. 1) are considered for the Sampeyre swarm whereas EQUI and FIVI stations (Fig. 2) for the Lunigiana sequence. The cross-correlation analysis is performed on selected subsets of events with magnitude greater than or equal to 1.0, gap in azimuth coverage (i.e., maximum azimuthal distance between two nearby-distance seismic stations) less than or equal to 200°, horizontal and vertical location error less than 5 km. First, all waveforms are filtered by a band-pass filter to reduce the bias of noise and high frequency wiggles as well as minor waveform dissimilarities due to differences in magnitude, focal mechanisms, and small-scale heterogeneities. Then, seismogram cross-correlation is performed on pairs of signals including both the P-wave and S-wave onsets by using the normalized cross-correlation function (e.g., Augliera *et al.*, 1995; Cattaneo *et al.*, 1997, 1999). Multiplets are defined as groups of events with cross-correlation coefficient greater than a minimum threshold, defined by trial and error in order to recognize the minimum number of families that allows us to correctly reproduce the spatial distribution of earthquakes. In order to overcome possible dissimilarities between events differing from each other by more than one order of magnitude, the bridging technique, which is based on the Equivalence Class approach (Press *et al.*, 1988), is applied. Finally, differential times derived from earthquake cross-correlation (computed for all available station within 50km from the epicenters) are used in conjunction with travel-time differences from manually picked P- and S-phases to relocate the events using the double-difference (DD) algorithm "HypoDD" (Waldhauser and Ellsworth, 2000; Waldhauser, 2001). Results are discussed in the next section.

Results and discussion. The right panel of Fig. 1 shows the hypocenter distribution obtained after the relocation of the earthquakes belonging to the Sampeyre swarm. The figure indicates the existence of two nearby sources, recognized as two distinct families by the waveform similarity analysis; one (Family 1) is shallower and collects 12 events characterized by impulsive P-wave arrivals and one (Family 2) is slightly deeper and collects a larger number of earthquakes (72). As evident from the seismic cross section in the bottom panel of Fig. 1, both sources would present high-angle dipping planes directed towards S-SE, compatible with the geological setting of the area where a SE-dipping shear zone occurs in the lower part of the Maira Valley and along the southern side of the Varaita Valley (Balestro *et al.*, 1995).

In order to prove the hypothesis about the activation of two distinct sources, we compare the b-value of the Gutenberg and Richter (1944) relationship for the two earthquake families. To improve the completeness of the two data sets at lower magnitudes, an automatic procedure for detecting micro-seismicity is applied to the stream of waveforms recorded by DOI and PZZ stations. The procedure uses the STA/LTA triggering method with parameters (e.g., filter band, length of the STA and LTA windows, STA/LTA threshold) calibrated for the two stations on the grounds of the ambient noise and micro-earthquake duration. Specifically, the algorithm implements a coincidence system which detects a potential earthquake whether both DOI and PZZ signals exceed the STA/LTA threshold (= 3) within a common 10s window. Approximately 2800 micro-earthquakes are identified and then separated into distinct clusters via cross-correlation analysis. In particular, 40% of micro-earthquakes are joined into families: 280 of them (those characterized by a very impulsive P-wave arrival) are associated to Family 1 while 592 to Family 2. b-values are calculated by applying the maximum likelihood method proposed by Weichert (1980). A b-value equal to 0.98 (+/- 0.05) is obtained for Family 1 while a b = 0.81 (+/- 0.03) for Family 2. The two magnitude-frequency distributions are shown in Fig. 3. Comparing the b-values indicates that Family 1 and Family 2 are characterized by a different proportion of small and larger earthquakes, thus suggesting that they do not come from the same population. To verify this, the Utsu's p-test (Utsu, 1992) is applied. The test confirms our hypothesis that the 2010 Sampeyre swarm is the consequence of the activation of two distinct interacting fractures having different seismic productivity. Given the small difference

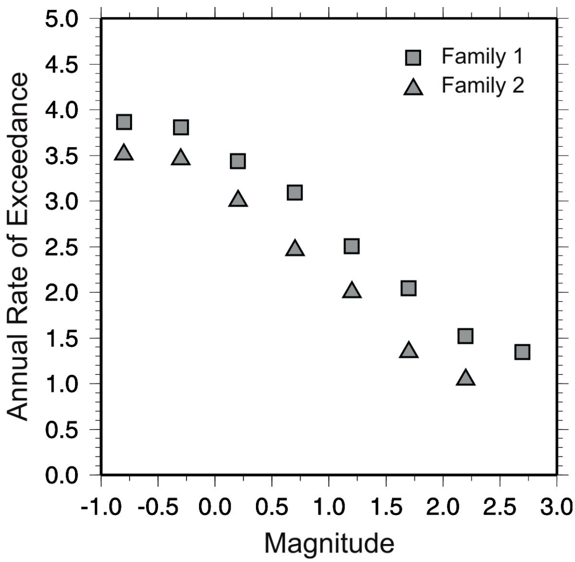

Fig. 3 – Cumulative magnitude-frequency distributions for Family 1 and Family 2.

in depth between the two earthquake families, fault heterogeneity, variation of rheological properties, and pore pressure variation appear reasonable causes for *b*-value variation observed in this application.

Fig. 2 (top panel) shows the preliminary results obtained for the Lunigiana sequence. The locations of the events obtained by using HypoDD indicate the existence of three different clusters. In particular, two of them could be associated to an anti-Apenninc system of faults oriented NE-SW, compatibly with the trend of the main shallow strike-slip faults linking the graben basins in the northern Apennines The third group of events, which is located near the FIVI station, seems to follow a NW-SE tectonic lineament (Apenninic direction). Looking at the NE-SW seismic cross-sections in Fig. 2, the anti-Apenninic sources present low-angle dipping planes, in accordance with the tectonic setting of the area. These observations are confirmed by the results of the waveform similarity analysis (Fig. 2, bottom panel), again showing the existence of different clusters of seismicity oriented both NE-SW and NW-SE. However, different families of earthquakes are identified along the same lineament. For instance, the southern NE-SW cluster appears to be characterized by three distinct families, indicating a very complex fault system.

Summarizing all previous observations, the work has strengthened the results of various research studies, many of which cited in the bibliography, about the capability of the methods applied here in characterizing the seismogenic process of an area. Seismismogram cross-correlation and double-difference relocation, which are here applied to areas with different seismotectonic settings, have been once more proved to be effective tools for the definition of the seismogenic structures in terms of location and orientation. These methods are of great importance to characterize surface fault lineaments but assume a greater importance in areas, such as those investigated here, where seismicity is triggered by deep structures with no clear geological evidences. Although limited to the case study of the Sampeyre swarm, our work has also pointed out that investigating changes of the *b*-value within the rock volume involved in the seismic process may help in identifying structural and rheological heterogeneities.

References

Astiz L., Shearer P. M. and Agnew D. C.; 2000: *Precise relocations and stress change calculations for the Upland earthquake sequence in Southern California*. J. Geophys. Res., **105**, pp. 2937-2953.

Augliera P., Cattaneo M., and Eva, C.; 1995: *Seismic multiplet analysis and its implication in seismotectonics*. Tectonophysics, **248**, pp. 219-234.

Avigad D., Chopin C. and Le Bayon R.; 2003: *Thrusting and extension in the southern Dora-Maira ultra-high-pressure massif (Western Alps): view from below the coesite-bearing unit*. J. Geol., **111**, pp. 57-70.

Balestro G., Cadoppi P., Di Martino L. and Sacchi R.; 1995: *Il settore meridionale del Massiccio Dora-Maira (Valli Maira e Varaita): inquadramento, carta geologica e guida a un'escursione*. In: Polino, R., Sacchi, R. (Eds.), Accademia Nazionale delle Scienze, Scritti e Documenti, **14**, pp. 501-529.

Barani. S., Scafidi D. and Eva C.; 2010: S*train rates in Northwestern Italy from spatially smoothed seismicity*. J. Geophys. Res., **115**, B07302, doi: 10.1029/2009JB006637.

Bartolini C. and Bortolotti V.; 1971: *Studi di geomorfologia e neotettonica, 1. I depositi continentali dell'Alta Garfagnana in relazione alla tettonica plio-pleistocenica*. Mem. Soc. Geol. It., **10**, pp. 203-245.

Brozzetti F., Boncio P., Di Naccio D., Lavecchia G., Tinari P., Torelli L., Bernini M., Eva E. and Solarino S.; 2007: *A Multidisciplinary approach to the seismotectonics of the Lunigiana and Garfagnana extensional basins (Northern Tuscany – Italy)*. Convegno in Memoria dei Prof. G. Giglia e A. Decandia: "Alps and Apennines: a natural laboratory for structural geology and geodynamics".

Calais E., Nocquet J.-M., Jouanne F. and Tardy M.; 2002: *Current strain regime in the Western Alps from continuous Global Positioning System Measurements, 1996-2001*. Geology **30**, 651-654.

Castaldini D., Genevois R., Panizza M., Puccinelli A., Berti M. and Simoni A.; 1998: *An integrated approach for analysing earthquake-indiced surface effects: a case study from the Northern Apennines, Italy*. J. Geodynamics, **26**, pp. 413-441.

Cattaneo M., Augliera P., Spallarossa D. and Eva C.; 1997: *Reconstruction of a seismogenetic structures by multiplet analysis: an example of Western Liguria, Italy*. Bull. Seism. Soc. Am., **87**, pp. 971-986.

Cattaneo M., Augliera P., Spallarossa D. and Lanza V.; 1999: *A waveform similarity approach to investigate seismicity patterns*. Natural Hazards, **19**, pp. 123-138.

Cattaneo M., Eva C., Giglia G. and Merlanti F.; 1983: *Seismic hazard in the Northwestern Apennines*. Pageoph., **121**, pp. 221-245.

Champagnac J.-D., Sue C., Delacou B. and Burkhard M.; 2004: *Brittle deformation in the inner NW Alps: from early orogen-parallel extrusion to late orogen-perpendicul collapse*. Terra Nova, **16**, pp. 232-242.

Delacou B., Sue C., Champagnac J.-D. and Burkhard M.; 2004: *Present-day geodynamics in the bend of the western and central Alps as constrained by earthquake analysis*. Geophys. J. Int., **158**, pp. 753-774.

Eva E. and Solarino S.; 1998: *Variations of stress directions in the Western Alpine Arc*. Gephys. J. Int., **135**, pp. 438-448.

Frechet J.; 1978: *Sismicité du Sud-Est de la France et une nouvelle méthode de zonage sismique*. Thesis, Université des Sciences Technologiques et Médicales, Grenoble, France.

Fukuyama E., Ellsworth W. L., Waldhauser F. and Kubo A.; 2003: *Detailed fault structure of the 2000 Western Tottori, Japan, earthquake sequence*. Bull. Seism. Soc. Am., **93**, pp. 1468-1478.

Giglia G., Capponi G., Crispini L. and Piazza M.; 1996: *Dynamics and seismotectonics of the West-Alpine arc*. Tectonophysics, **267**, pp. 143-175.

Gutenberg B. and Richter C. R.; 1944: *Frequency of earthquakes in California*. Bull. Seism. Soc. Am., **34**, pp. 185-188.

Joswig M. and Schulte-Theis H.; 1993: *Master-event correlations of weak local earthquakes by dynamic waveform matching*. Geophys. J. Int., **113**, pp. 562-574.

Michard A., Chopin C. and Henry C.; 1993: *Compression versus extension in the exhumation of the Dora-Maira coesite-bearing unit, Western Alps, Italy*. Tectonophysics, **221**, pp. 173-193.

Negredo A. M., Barba S. Carminati E., Sabadini R. and Giunchi C.; 1999: *Contribution of numeric dynamic modelling to the understanding of seismotectonic regime of the northern Apennines*. Tectonophysics, **315**, pp. 15-30.

Nicolas A., Polino R., Hirn A., Nicolich R., and ECORS – CROP Working Group; 1990: ECORS – CROP traverse and deep structure of the Western Alps: a synthesis. Mem. Soc. Geol. France, **156**, pp. 15-27.

Nocquet J.-M. and Calais E.; 2003: *Crustal velocity field of western Europe from permanent GPS array solutions, 1996-2001*. Geophys. J. Int., **152**, pp. 72-88.

Nocquet J.-M. and Calais E.; 2004: Geodetic measurement of crustal deformation in the Western Mediterranean and Europe. Pure and Applied Geophysics, **161**, pp. 661-681.

Peppin W. A., Honjas W., Somerville M. R. and Vetter U. R.; 1989: *Precise master-event locations of aftershocks of the 4 October 1978 Wheeler Crest earthquake sequence near Long Valley, California*. Bull. Seism. Soc. Am., **79**, pp. 67-76.

Ponziani F., De Franco R., Minelli G., Biella G., Federico C. and Pialli G.; 1995: *Crustal shortening and duplication of the Moho in the Northern Appenines: a view from seismic refraction data*. Tectonophysics, **252**, pp. 391-418.

Prejean S., Ellsworth W. L., Zoback M. and Waldhauser F.; 2002: *Fault structure and kinematics of the Long Valley Caldera region, California, revealed by high-accuracy earthquake hypocenters and focal mechanism stress inversions*. J. Geophys. Res., **107**, No. B12, 2355, doi:10.1029/2001JB001168.

Press W. H., Flannery P. B., Teukolsky S. A. and Wetterling W. T.; 1988: *Numerical Recipes in C, The art of Scientific computing*. Cambridge University Press, Cambridge, UK.

Reasenberg P. and Oppenheimer D. H.; 1985: *FPFIT, Fortran computer program for calculating and displaying earthquake fault-plane solutions*. U.S. Geological Survey Open File Rept. 85-739.

Schaff D. P., Bokelmann G. H. R., Beroza G. C., Waldhauser F. and Ellsworth W. L.; 2002: *High resolution image of Calaverals Fault seismicity*. J. Geophys. Res., **107**, No B9, 2186, doi 10.1029/2001JB000633.

Sharma B. K., Kumar A. and Murthy V. M.; 2010: *Evolution of seismic events detection algorithms*. J. Geol. Soc. India, **75**, pp.553-538.

Shearer P. M.; 1998: *Evidence from a cluster of small earthquakes for a fault at 18 km depth beneath Oak Ridge, Southern California*. Bull. Seism. Soc. Am., **88**, pp. 1327-1336.

Utsu T.; 1992: *On seismicity*, Report of the Joint Research Institute for Statistical Mathematics, Tokyo, pp. 139-157.

Waldhauser F. and Ellsworth W. L.; 2000: *A double-difference earthquake location algorithm: method and application to the Northern Hayward Fault, California*. Bull. Seism. Soc. Am., **90**, pp. 1353-1368.

Waldhauser F. and Ellsworth W. L.; 2002: *Fault structure and mechanics of the Hayward Fault, California, from double-difference earthquake locations*. J. Geophys. Res., **107**, No. B3, doi:10.1029/2000JB000084.

Waldhauser F.; 2001: *hypoDD – A program to compute double-difference hypocenter locations*. U.S. Geol. Survey Open File Report 01-113.

Weichert D. H.; 1980: *Estimation of the earthquake recurrence parameters for unequal observation periods for different magnitudes*. Bull. Seis. Soc. Am., **70**, pp. 1337-1346.

Wheeler J.; 1991: *Structural evolution of a subducted continental sliver: the northern Dora Maira massif, Italian Alps*. J. Geol. Soc. Lond., **148**, pp. 1101-1113.

Withers M., Aster R., Young C., Beiriger J., Harris M., Moore S. and Trujillo J.; 1998: *A comparison of selected trigger algorithms for automated global seismic phase and event detection*. Bull. Seism. Soc. Am., **88**, pp. 95-106.

Yang Z. X., Waldhauser F., Chen Y. T. and Richards P. G.; 2005: *Double-difference relocation of earthquakes in central-western China, 1992-1999*. J. Seismology, **9**, pp. 242-264.

Zhixian Y., Yuntai C., Yuejun Z. and Xiangwei Y.; 2003: *Accurate relocation of earthquakes in central-western China using the double difference earthquake location algorithm*. Science in China, **46**, pp. 181-188.

TOMOGRAFIE DI RESISTIVITÀ ELETTRICA ESEGUITE PER LO STUDIO DEI FENOMENI DI FAGLIAZIONE SUPERFICIALE PRESSO L'ABITATO DI SAN GREGORIO (L'AQUILA)

J. Bellanova[1], P. Boncio[2], P. Galli[3], B. Giaccio[4], V. Lapenna[1], E. Peronace[4], A. Perrone[1], B. Quadrio[4], S. Piscitelli[1]

[1] *CNR-IMAA, Tito (PZ), Italy*
[2] *Dipartimento di Scienze, Università degli Studi G. D'Annunzio di Chieti-Pescara, Italy*
[3] *Dipartimento Protezione Civile Nazionale, Rome, Italy*
[4] *CNR-IGAG, Monterotondo, Rome, Italy*

Introduzione. Il presente lavoro riporta i risultati relativi ad un'indagine geoelettrica svolta, nei pressi dell'abitato di San Gregorio (L'Aquila), dai ricercatori dell'Istituto di Metodologie per l'Analisi Ambientale del Consiglio Nazionale delle Ricerche (IMAA-CNR) di Tito (PZ), in collaborazione con ricercatori del Dipartimento di Protezione Civile (DPC) di Roma, dell'Università degli Studi G. D'Annunzio di Chieti-Pescara (Ud'A) e dell'Istituto di Geologia Ambientale e Geoingegneria del Consiglio Nazionale delle Ricerche (IGAG-CNR).

L'indagine geoelettrica, commissionata dal Dipartimento Ricostruzione ed Emergenza Sisma - Settore Emergenza Sisma e Ricostruzione Privata - Comune di L'Aquila, insieme a studi di tipo geologico-strutturale, sismotettonico e paleosismologico, condotti precedentemente nell'area di indagine (EMERGEO Working Group, 2009; Boncio *et al.*, 2010a; Galli *et al.*, 2010; WORKING GROUP SM-AQ, 2010; Boncio *et al.*, 2011; Giocoli *et al.*, 2011; Boncio *et al.*, 2012) era volta ad approfondire l'attività di ricerca sui fenomeni di fagliazione superficiale presso l'abitato di San Gregorio. In particolare, lo scopo dell'indagine geoelettrica era quello di fornire informazioni sull'eventuale presenza in profondità e sulla caratterizzazione geometrica di alcuni tratti sepolti della faglia di San Gregorio, da indagare successivamente tramite scavo di trincee paleosismologiche. Tale faglia fa parte del sistema di faglie normali Paganica-San Demetrio (PSDFS), che ha provocato nell'area aquilana il terremoto del 6 aprile 2009 (M_w = 6.3) (Galli *et al.*, 2010; Gruppo di Lavoro MS–AQ, 2010). La campagna di misure geoelettriche è consistita nella realizzazione di n. 6 Tomografie di Resistività Elettrica (ERT), eseguite lungo profili pianificati in accordo con i ricercatori del DPC, dell'Ud'A e dell'IGAG, sia nell'abitato di San Gregorio (L'Aquila) sia nel Comune di San Demetrio ne' Vestini (AQ) (Fig. 1).

Fig. 1- Area di studio con evidenziata l'ubicazione delle ERT (linee rosse).

Di seguito, si riportano un breve inquadramento geologico-sismotettonico dell'area investigata e i dettagli e l'esito dell'indagine geoelettrica.

Area di studio: assetto geologico e sismotettonico. L'area oggetto di studio è posta a sud-est della città de L'Aquila, all'interno della media valle dell'Aterno in Abruzzo, un bacino intramontano con direzione NW-SE, delimitato a ovest-sudovest dal massiccio dei M.ti D'Ocre e a nord-nordest dalla catena del Gran Sasso D'Italia.

Dal punto di vista geologico, in generale, i rilievi dell'area aquilana sono costituiti da depositi carbonatici e, in piccola parte, marnoso-arenacei meso-cenozoici. Nella Valle dell'Aterno affiorano, invece, depositi lacustri che formano una complessa sequenza deposizionale di unità limose e sabbioso-conglomeratiche, con frequenti variazioni laterali, soprastanti il substrato calcareo (Bosi e Bertini, 1970). I depositi più recenti (Olocene), che si rinvengono al di sopra dei terreni meso-cenozoici e Pleistocenici, sono invece costituiti da alluvioni ciottoloso-sabbiose e subordinatamente sabbioso-limose, da depositi detritici di versante, da depositi eluvio-colluviali con detriti immersi in matrice limoso-argillosa (Carta Geologica d'Italia in scala 1:50.000 – foglio 359 "L'Aquila").

Il 6 aprile 2009 tale area è stata colpita da un moderato terremoto (M_w = 6.3), provocato dal sistema di faglie normali Paganica-San Demetrio (PSDFS), costituito nel complesso da 5 segmenti di faglia, generalmente orientati N110°-140° secondo una geometria *en-échelon* con *step* destro, di circa 19 km di lunghezza (Galli *et al.*, 2010; Gruppo di Lavoro MS–AQ, 2010; Giocoli *et al.*, 2011).

In seguito all'evento principale del 6 aprile, lungo tale sistema di faglie sono stati osservati e rilevati fenomeni di fratturazione superficiale con rigetto verticale di ~ 15 cm.

In tale ambito, per approfondire l'attività di ricerca sui fenomeni di fagliazione superficiale presso l'abitato di San Gregorio e San Demetrio ne' Vestini, è stata condotta una indagine geolelettrica, mediante la tecnica della Tomografia di Resistività Elettrica, con lo scopo di fornire informazioni sull'eventuale presenza in profondità e sulla caratterizzazione geometrica di alcuni tratti sepolti della PSDFS, da indagare successivamente tramite scavo di trincee paleosismologiche.

Tomografia di Resistività Elettrica: acquisizione, elaborazione ed inversione dati. L'indagine geoelettrica, realizzata in questa campagna di misure, è stata eseguita mediante il georesistivimetro Syscal Junior (Iris Instruments), accoppiato ad un sistema di acquisizione multielettrodico (48 elettrodi). Lungo ogni profilo, i dati di resistività apparente sono stati acquisiti mediante la configurazione elettrodica Wenner-Schlumberger, che presenta una moderata risoluzione nell'individuare variazioni sia laterali che verticali di resistività, mediante 48 elettrodi con spaziatura variabile (da 1, 3 e 5 m), ottenendo differenti profondità di indagine (di circa 7, 20 e 35 m). Il processing dei dati di resistività apparente acquisiti è consistito essenzialmente, in una prima fase, nella rimozione di valori anomali (spikes or bad data points), mediante operazioni di filtraggio automatico e/o manuale per mezzo di software d'esercizio (Prosys II, Res2Dinv). Successivamente, è stata inserita la correzione topografica ad ogni profilo ERT. Infine, i dati di resistività apparente, dopo la fase di filtraggio e correzione topografica, sono stati invertiti mediante il software d'inversione Res2Dinv (Loke, 2001), al fine di ottenere le immagini 2D di resistività del sottosuolo. Nel processo d'inversione sono state necessarie almeno 3 iterazioni per il raggiungimento del *best fit* tra la pseudo sezione misurata e quella calcolata, ottenendo, in tal modo, immagini elettriche con *un RMS error* relativamente basso, variabile tra 1.6 e 8.4. Inoltre, per migliorare la fase di interpretazione e confronto diretto, tutti i modelli di resistività sono stati rappresentati con la stessa scala di valori di resistività elettrica, compresa tra i 15 e gli oltre 381 Ωm.

Risultati: San Gregorio (L'Aquila). La Fig. 2 riporta uno stralcio della Carta Geologico-Geomorfologica (scala 1:5000) dell'area di Paganica Teatro – Zona Industriale – Onna – San Gregorio con l'ubicazione delle ERT (linee rosse) (modificata da Boncio *et al.*, 2010b).

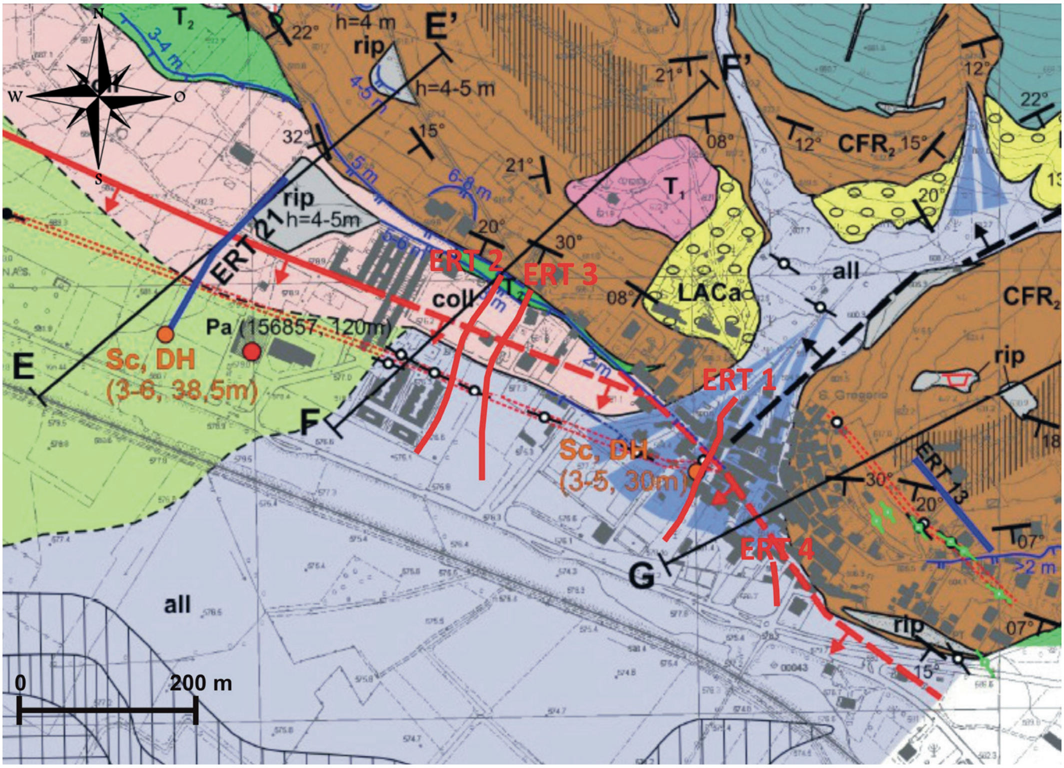

Fig. 2 – Stralcio della Carta Geologico-Geomorfologica (scala 1:5000) dell'area di Paganica Teatro – Zona Industriale – Onna - San Gregorio con l'ubicazione delle ERT (linee rosse) (modificata da Boncio *et al.*, 2010b).

La Fig. 3 mostra solo i modelli di resistività relativi alle ERT eseguite nell'abitato di San Gregorio (L'Aquila) (ERT 1, ERT 2 e ERT 3).

Nel complesso, le immagini elettriche mostrano un pattern di resistività caratterizzato da variazioni sia laterali che verticali, talora anche con forti gradienti.

In particolare, le tomografie ERT 1, ERT 2 e ERT 3, realizzate utilizzando una spaziatura interelettrodica di 5 m e raggiungendo, quindi, una maggior profondità di esplorazione (circa 35 m di profondità), mostrano quasi tutte la stessa distribuzione di resistività, caratterizzata da uno strato superficiale di materiale più conduttivo ($15 < \rho < 60\ \Omega m$), che poggia su materiale relativamente più resistivo ($\rho > 150\ \Omega m$). Il materiale conduttivo presenta, negli strati più superficiali (primi 10-15 m), una distribuzione disomogenea di nuclei relativamente più resistivi ($60 < \rho < 250\ \Omega m$).

In dettaglio, la ERT 1, eseguita all'interno del centro storico di San Gregorio in direzione NNE-SSW ed attraversante nel suo centro la Chiesa di San Gregorio Magno, mostra una stratificazione quasi piano-parallela a tre elettrostrati: il primo, con uno spessore massimo di circa 15 m, caratterizzato da una distribuzione disomogenea di nuclei relativamente resistivi; il secondo, compreso tra circa 15 m e 30 m dal piano campagna, da una prevalenza di materiale relativamente conduttivo; e il terzo, che occupa la parte profonda della ERT, caratterizzato da materiale resistivo.

Sulla base della Carta Geologico-Geomorfologica (cfr. Fig. 2) e della sezione geolitologica GG' (Boncio *et al.*, 2010b), riportata nell'ambito degli studi di Microzonazione sismica per la ricostruzione dell'area aquilana (WORKING GROUP SM-AQ, 2010) e passante in prossimità del profilo tomografico, è possibile associare al primo elettrostrato, relativamente resistivo, depositi di conoide alluvionale (ghiaie) (CON) e/o depositi alluvionali recenti ed attuali del Fiume Aterno (all); all'elettrostrato centrale, relativamente conduttivo, depositi fluviali e fluvio-lacustri (fl-lac), costituiti da un'alternanza di sabbie limose e limi argillosi; infine, allo strato relativamente resistivo posto in profondità si potrebbero associare depositi lacustri antichi (LACa2), ghiaie ben addensate e conglomerati, oppure il substrato calcareo (CFR_2).

Le ERT 2 e ERT 3, eseguite in direzione NNE-SSW, parallele e distanziate l'una dall'altra di circa 40-50 m, attraversano nel loro centro Via dei Filoni. Le immagini elettriche mostrano entrambe lo stesso pattern di resistività. In particolare, pur essendo contraddistinte dagli stessi valori di resistività della ERT 1, mostrano una diversa distribuzione geometrica dei tre elettrostrati già individuati e forti variazioni di resistività sia laterali che verticali. Infatti, lo strato più superficiale con nuclei relativamente resistivi occupa i primi 15 m di profondità della porzione SSW di entrambe le ERT; lo strato conduttivo intermedio, osservandolo dall'origine delle ERT fino a circa 200 m, tende a diminuire il suo spessore e ad affiorare al piano campagna; infine lo strato più resistivo, che occupava la porzione più profonda della ERT 1, si presenta con una forma a "*gradinata*" e occupa tutta la porzione NNE delle ERT, approfondendosi nella parte centrale delle stesse.

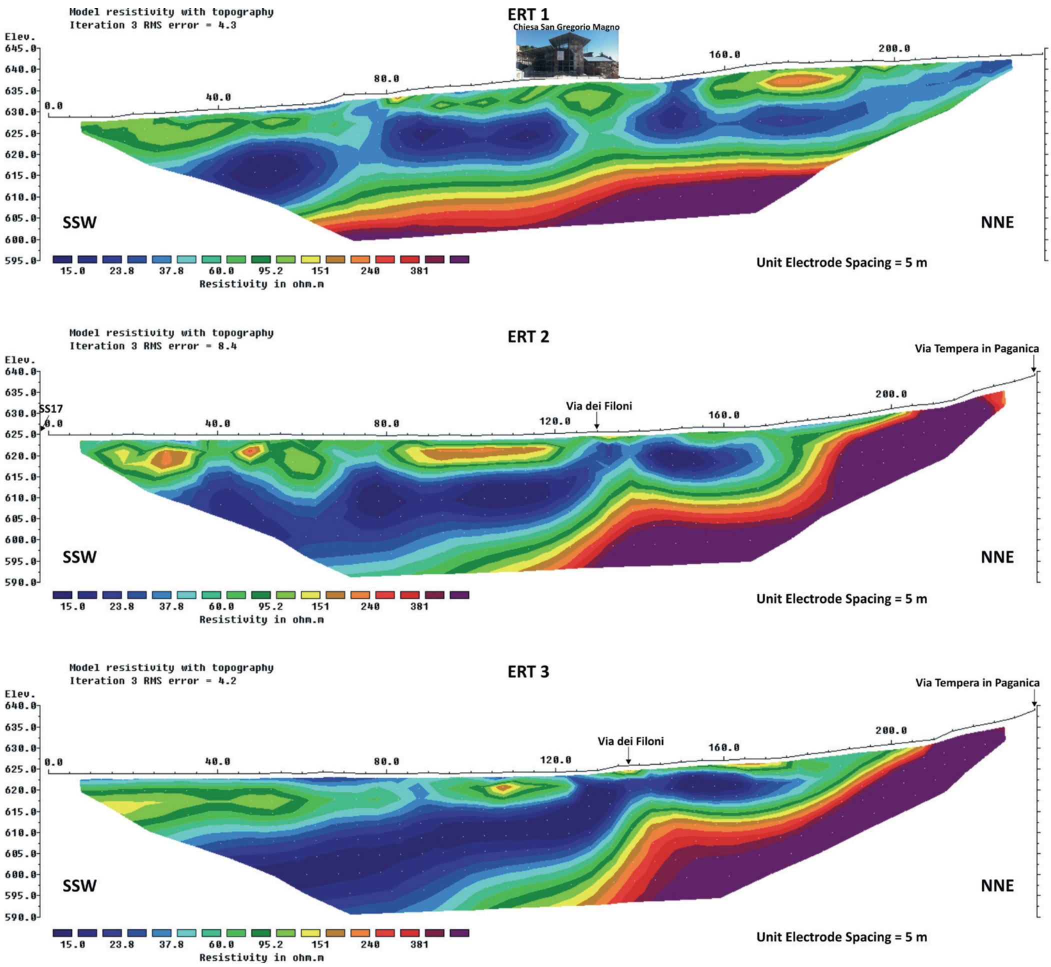

Fig. 3 – Modelli di resistività relativi alle ERT eseguite nell'abitato di San Gregorio (L'Aquila) (ERT 1, ERT 2 e ERT 3).

Sulla base della Carta Geologico-Geomorfologica (cfr. Fig. 2) e della sezione geolitologica FF'' (WORKING GROUP SM-AQ, 2010) passante in prossimità dei profili ERT, è possibile associare all'elettrostrato superficiale relativamente resistivo depositi eluvio-colluviali (coll.), nel settore NNE, e depositi alluvionali (all) e di conoide (CON), nel settore SSW. Al di sotto, l'elettrostrato centrale relativamente conduttivo potrebbe essere relativo alla presenza di depositi fluviali e fluvio-lacustri (fl-lac), costituiti da un'alternanza di sabbie limose e limi argillosi. Anche in questo caso, lo strato relativamente resistivo in profondità potrebbe essere associato o a depositi lacustri antichi (LACa2), ghiaie ben addensate e conglomerati, o al substrato calcareo (CFR_2). Degne di nota sono le forti variazioni laterali di resistività che potrebbero essere relative alla presenza di faglie (tratto sepolto della faglia di San Gregorio?).

Conclusioni. Il presente lavoro riporta i risultati relativi ad un'indagine geoelettrica svolta, nei pressi dell'abitato di San Gregorio (L'Aquila).

Lo scopo dell'indagine geoelettrica era quello di fornire informazioni sull'eventuale presenza in profondità e sulla caratterizzazione geometrica di alcuni tratti sepolti del sistema di faglie normali Paganica-San Demetrio (PSDFS), che ha provocato nell'area aquilana il terremoto del 6 aprile 2009 (M_w = 6.3), da indagare successivamente tramite scavo di trincee paleosismologiche.

Sei Tomografie di Resistività Elettrica (ERT) sono state eseguite nell'abitato di San Gregorio (L'Aquila) e San Demetrio ne' Vestini. Le ERT hanno mostrato dei pattern di resistività caratterizzati dalla presenza di variazioni sia orizzontali che verticali, associabili a contatti di natura litologico-stratigrafica e/o tettonici (possibile presenza di faglie), soprattutto nell'area di San Gregorio, utili per una corretta pianificazione di future indagini paleosismologiche.

È da sottolineare che l'analisi e l'interpretazione delle tomografie presentate in tale report è basata solo sulle caratteristiche elettriche dei terreni investigati e sulle evidenze di campagna. Ulteriori dati di tipo geologico, geofisico, idrogeologico, geognostico e paleosismologico potrebbero sicuramente migliorarne l'interpretazione.

Bibliografia

Boncio P., Pizzi A., Brozzetti F., Pomposo G., Lavecchia G., Di Naccio D., F. Ferrarini; 2010: Coseismic ground deformation of the 6 April 2009 L'Aquila earthquake (central Italy, Mw6.3). Geophysical Research Letters, Vol. 37, L06308, doi:10.1029/2010GL042807.

Boncio P., Pizzi A., Cavinato G.P., Cavuoto G., Giaccio B., Mancini M., Moscatelli M., Spadoni M. ;2010b: Carta Geologico-geomorfologica dell'area di Paganica Teatro – Zona industriale – Onna – San Gregorio, Microzonazione sismica dell'area aquilana, Macroarea 3, sito internet del Dipartimento della Protezione Civile, http://www.protezionecivile.it/cms/view.php?dir_pk=395&cms_pk=17356.

Boncio P., Pizzi A., Cavuoto G., Mancini M., Piacentini T., Miccadei E., Cavinato G.P., Piscitelli S., Giocoli A., Ferretti G., De Ferrari R., Gallipoli R., Mucciarelli M., Di Fiore V., Franceschini A., Pergalani F., Naso G., Working Group Macroarea 3; 2011: Geological and geophysical characterization of the Paganica-San Gregorio area after the April 6, 2009 L'Aquila earthquake (Mw 6.3, central Italy): implications for site response. Bollettino di Geofisica Teorica e Applicata, 52 (3), 491-512. doi: 10.4430/bgta0014.

Boncio P., Galli P., Naso G., Pizzi A.; 2012: Zoning Surface Rupture Hazard along Normal Faults: Insight from the 2009 Mw 6.3 L'Aquila, Central Italy, Earthquake and Other Global Earthquakes. Bulletin of the Seismological Society of America, 102 (3), 918-935. doi: 10.1785/0120100301.

Bosi C., Bertini T.; 1970: Geologia della Media Valle dell'Aterno. Memorie della Societa Geologica Italiana, Volume IX, 719-777.

EMERGEO Working Group; 2009: Evidence for surface rupture associated with the Mw 6.3 L'Aquila earthquake sequence of April 2009 (central Italy), Terra Nova, 22, 43–51, doi:10.1111/j.1365-3121.2009.00915.x.

Galli P., Giaccio B., Messina P.; 2010: The 2009 central Italy earthquake seen through 0.5 Myr-long tectonic history of the L'Aquila faults system, Quat. Sci. Rev. 29, 3768–3789, doi 10.1016/j.quascirev.2010.08.018.

Giocoli A., Galli P., Giaccio B., Lapenna V., Messina P., Peronace E., Romano G., Piscitelli S.; 2011: Electrical Resistivity Tomography across the Paganica-San Demetrio fault system (L'Aquila 2009 earthquake). Bollettino di Geofisica Teorica ed Applicata Vol. 52 (3), 457-469; DOI 10.4430/bgta0029.

Gruppo di Lavoro MS–AQ; 2010: Microzonazione sismica per la ricostruzione dell'area aquilana. Regione Abruzzo – Dipartimento della Protezione Civile, L'Aquila, 3 vol. e Cd-rom. http://www.protezionecivile.gov.it/jcms/it/view_pub.wp?contentId=PUB25330.

WORKING GROUP SM-AQ; 2010: Microzonazione sismica per la ricostruzione dell'area aquilana. Regione Abruzzo - Dipartimento della Protezione Civile, L'Aquila, 3 vol. e DVD-rom. http://www.protezionecivile.gov.it/jcms/it/view_pub.wp?contentId=PUB25330.

PALEOSEISMOLOGICAL INVESTIGATIONS ALONG THE SAN DEMETRIO NE' VESTINI FAULT (AQ)

A.M. Blumetti, P. Di Manna, E. Vittori, V. Comerci, L. Guerrieri
ISPRA, Geological Survey of Italy

Introduction and geological framework. In the months following the April 6th, 2009, Mw 6.3 L'Aquila earthquake, in the framework of a seismic microzonation, the Geological Survey of Italy (ISPRA) carried out a detailed geological and geomorphological survey of the San Demetrio ne' Vestini territorial municipality.

This village, severely damaged by the 2009 event, is located in the south-eastern part of the L'Aquila basin, a complex tectonic basin characterized by a system of northwest-southeast-trending tectonic depressions (total length about 30 kilometres) developed inside the inner sector of the Meso-Cenozoic orogenic belt of the Apennines, between the Gran Sasso and the Monti d'Ocre morphotectonic units (Fig. 1).

Active crustal extension in this zone is demonstrated by GPS observations, which reveal velocities across the Central Apennines in the order of 3 mm/yr (D'Agostino *et al.*, 2011), and confirmed by the large historical and instrumental seismicity occurred in the region. The geological evidence of active faulting is also widely recognised (Bagnaia *et al.*, 1992; Blumetti, 1995; Boncio *et al.*, 2004; Galadini and Galli, 2000; Roberts and Michetti, 2004; Blumetti and Guerrieri 2007; Galli *et al.*, 2010; Giaccio *et al.*, 2012; Blumetti *et al.*, 2013).

The San Demetrio area is located at the southern tip of the L'Aquila basin fault zone, which is characterized by the presence of *en echelon* and sub-parallel NW-SE trending fault segments. This is a typical structural setting at the transition between two primary fault zones (in this case between the L'Aquila Basin and Subequano Basin primary fault zones). Moreover in this area extension and faulting progressively migrated toward the inner part of the basin (Giaccio *et al.*, 2012; Blumetti *et al.*, 2013).

The territory of the San Demetrio municipality is crossed by 4 NW-SE trending fault segments that have displaced also Quaternary deposits (Fig. 1B; Bosi and Bertini, 1993). One of them, crossing the historical settlement of the village, was pointed out as a capable fault by Working Group MS–AQ, (2010). This fault (named San Demetrio fault) already identified as a possibly active fault by Bagnaia *et al.* (1992), does not crop out, but is "inferred" at the base of an up to 25 meters high fault scarp that displaces the flat surface of a recent alluvial terrace (Figs. 1 and 2).

This note summarizes the first results of paleoseismological investigations carried out by ISPRA along the San Demetrio fault, with the aim to i) characterize its capability in terms of seismic and surface faulting potential and ii) map the fault, and an appropriate setback area along it, where introduce specific land use restrictions, as requested by the Mayor of the San Demetrio ne' Vestini.

Paleoseismological analysis. In order to better locating the most suitable trenching site, a geophysical survey was performed, consisting of an ERT (Electrical Resistivity Tomography) profile and a seismic refraction tomography line. A previous ERT profile (Working Group MS–AQ, 2010), crossing the fault not far from the trench site, is reproduced in Fig. 2C.

The site selected for trenching is located north-west of the historical centre of the village (Fig. 1), where morphotectonic observations and geophysical data were consistently indicating the occurrence of a fault cutting up to the surface.

The detailed analysis of the stratigraphy exposed in the trench walls confirmed that the exposed fault is capable of producing surface ruptures (Fig. 3).

In fact, a major fault zone, 5 meters wide, characterized by four main (e.g. offsets larger than the trench wall height) synthetic faults and an antithetic structure, was found in the trench walls. Analysing the fault zone exposed in the eastern wall, at least two colluvial wedges were identified, *i.e.* Levels 4 and 10 in Fig. 3B. Level 4 is about 20 cm thick and is bounded downslope by a small antithetic fault. Moreover it is slightly displaced (just a few centimetres) by a tiny fracture that downward is linked to a major fault. This interpretation would imply two surface faulting events. Even if radiocarbon and OSL dating are still in progress, it is possible to refer these paleoearthquakes to the Holocene. In fact, the gravel layer sealing the faults (level 2 in Fig. 3B) appears to be very young, most likely historical due to its correlation with a nearby layer containing roman pottery (imperial age).

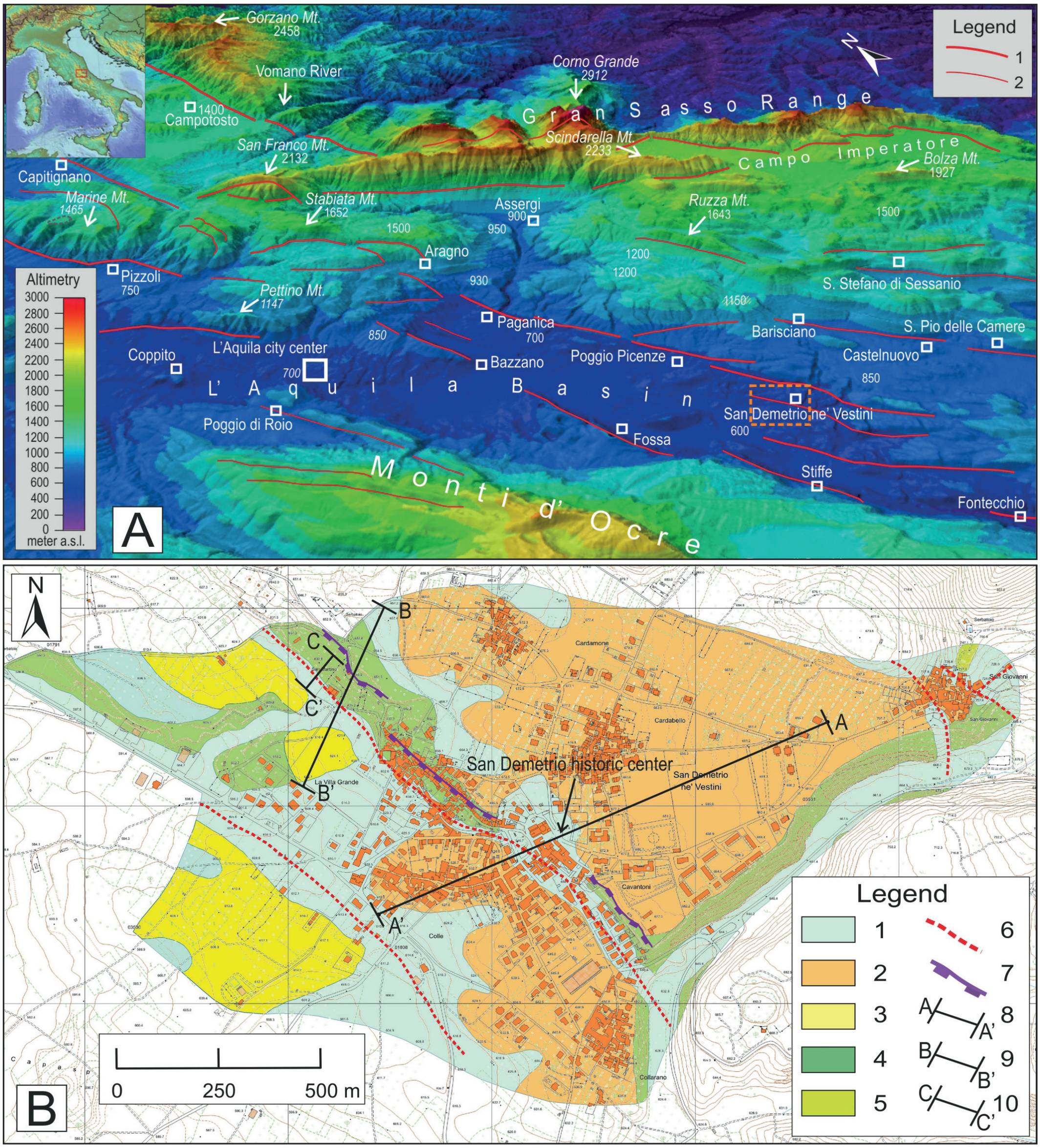

Fig. 1 – (A) Oblique view (based on a 20 m DTM) of the L'Aquila region with the net of capable faults. Legend: 1) primary fault; 2) secondary fault. (B) geological map of S. Demetrio ne' Vestini. Legend: 1) colluvial and debris deposits (Holocene); 2) alluvial fan gravels and sands (upper part of Middle Pleistocene); 3) sands (upper part of Middle Pleistocene); 4) fan delta conglomerates (Lower to Middle Pleistocene); 5) whitish silty lacustrine deposits (Lower to Middle Pleistocene); 6) capable fault (not outcropping); 7) fault scarp edge; 8) location of the cross section shown in Fig. 2B; 9) trace of the ERT profile shown in Fig. 2C; 10) trace of the paleoseismological trench. (modified after Working Group MS–AQ, 2010).

Level 3 is also involved in the deformation, and displaced of few centimetres only by the most recent event.

Level 10 is an about 50 cm thick colluvial wedge and is downthrown by a small synthetic fault linked in depth to a major fault. This small fault does not cut layers younger than level 10, so that it can be argued that it moved soon after the deposition of the colluvial wedge 10. This should indicate the occurrence of two additional older events, but occurred in a very short time, possibly in the same seismic sequence.

The presence of an antithetic fault located a few metres downslope the fault zone (not drawn in Fig. 3B, but visible in Fig. 3A) indicates the occurrence of a "gravity graben" during such older surface faulting events. Consequently, the amount of the coseismic offset related to the formation of colluvial wedge 10, and also the magnitude of the triggering event (using Wells and Coppersmith, 1994) cannot be evaluated. Nevertheless, such features, and in particular the

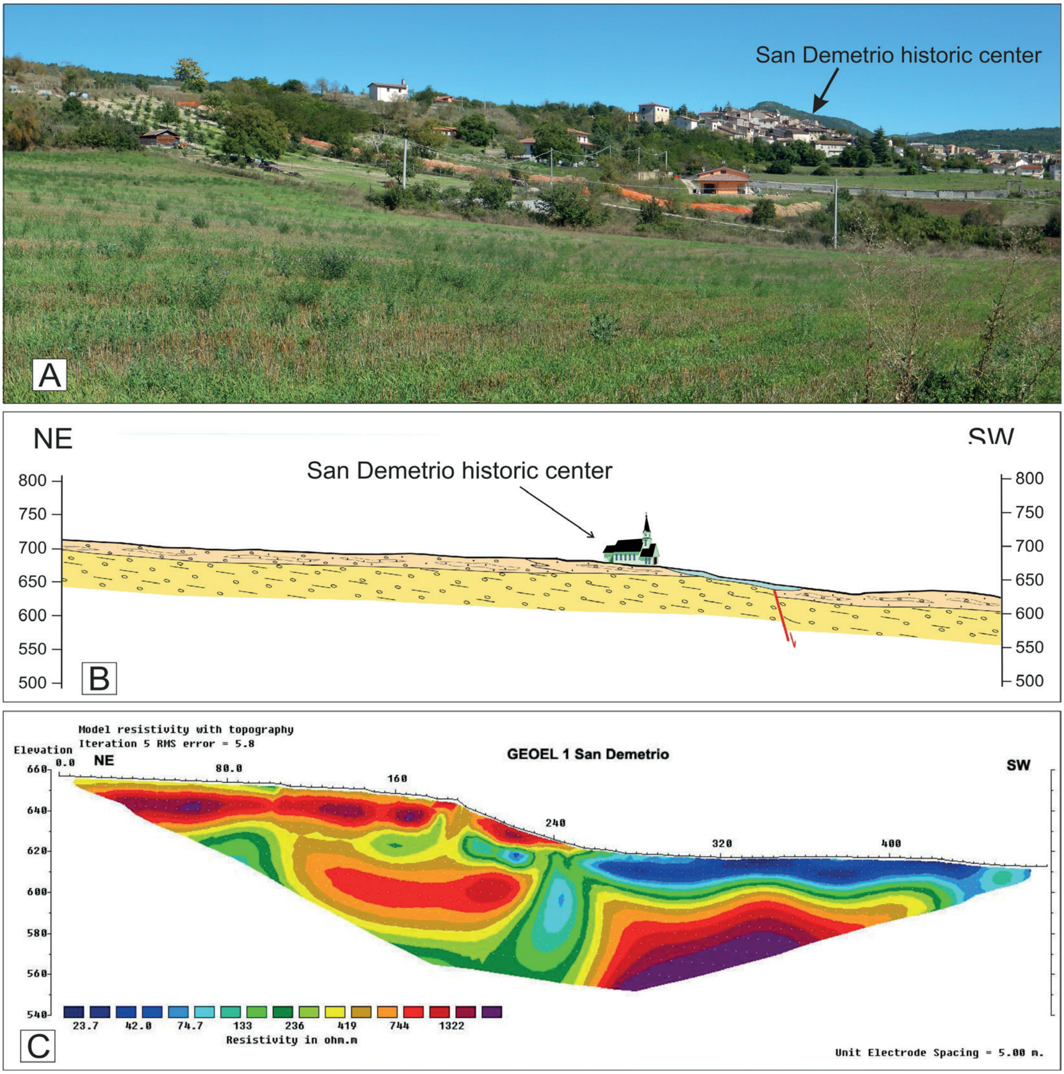

Fig. 2 – (A) Panoramic view of the fault scarp related to the Demetrio fault. The orange net marks the trench site. (B) Geological profile across the fault (location in Fig. 1). Legend: 1) fan delta conglomerates (Lower to Middle Pleistocene); 2) gravels and sands (upper part of Middle Pleistocene) (modified, after Working Group MS–AQ, 2010). (C) ERT profile across the San Demetrio fault (location in Fig. 1; after Working Group MS–AQ, 2010).

presence of such a wide and deep "gravity graben", suggest a magnitude value much larger than the 2009 earthquake (Mw=6.3).

Acknowledgements. The Authors wish to thank Valeria Eulilli, Fernando Ferri and Luca M. Puzzilli for providing the geophysical investigations, and Leonello Serva for his valuable suggestions in the paleoseismic interpretation of the stratigraphic log.

References

Bagnaia R., D'Epifanio A. and Sylos Labini S.; 1992: *Aquila and subaequan basins: an example of Quaternary evolution in Central Apennines, Italy.* Quaternaria Nova, **II**, 187-209 (preprint spec. number 1, 1-23- 989).

Bertini T. and Bosi C.; 1993; *La tettonica quaternaria nella conca di Fossa (L'Aquila).* Il Quaternario, **6**, 293-314.

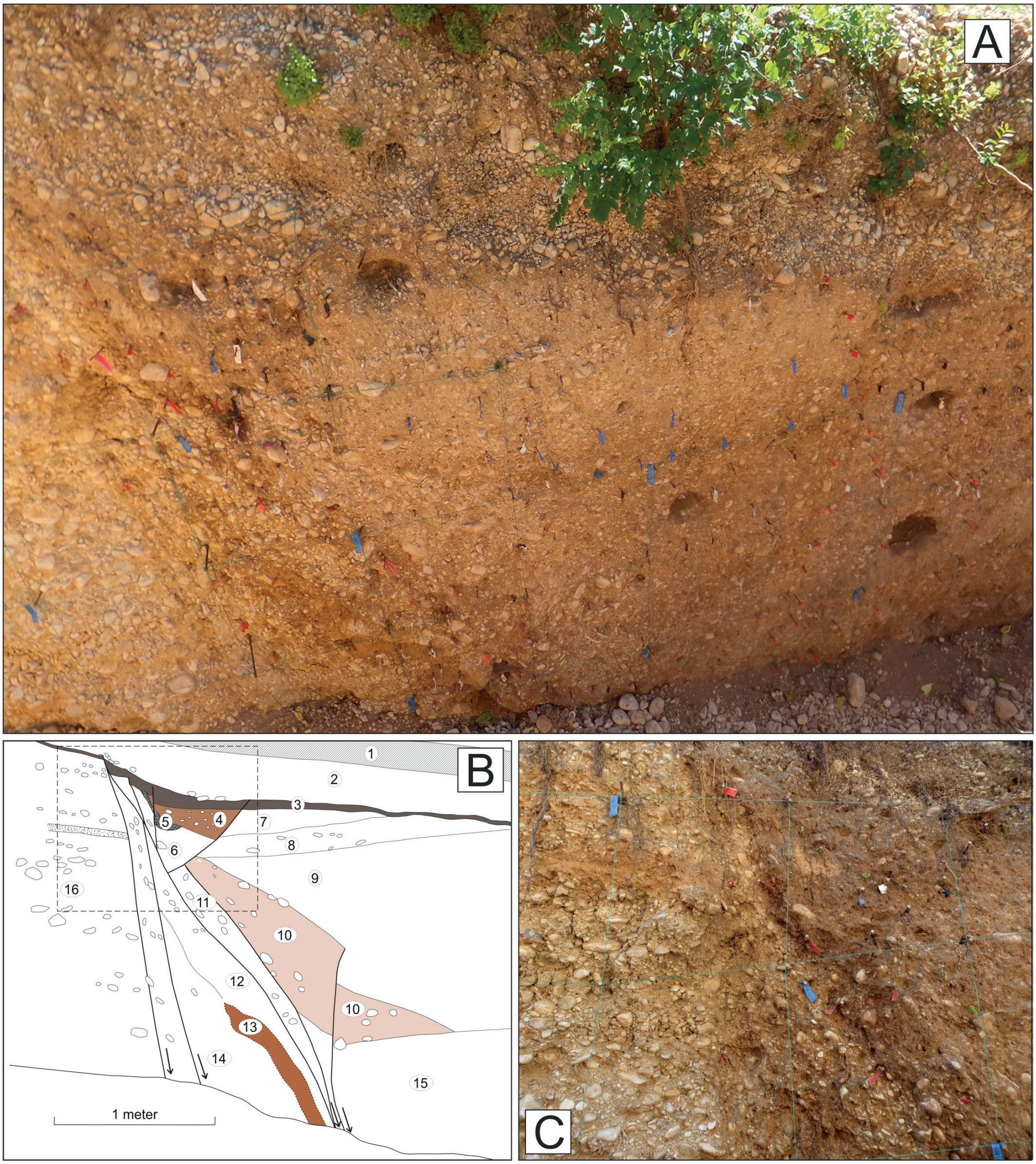

Fig. 3 – (A) View of the fault zone exposed in the eastern wall. (B) Stratigraphic sketch of the fault zone exposed in the eastern wall of the San Demetrio trench. Levels 4 and 10 are colluvial wedges. The dashed box locates Fig. 3C. (C) Close-up view of the upper colluvial wedges exposed in the eastern wall of the San Demetrio trench.

Blumetti A.M.; 1995: *Neotectonic investigations and evidence of paleoseismicity in the epicentral area of the January-February 1703 Central Italy earthquakes*, in Perspectives in Paleoseismology Leonello Serva (Editor), Bulletin of the American Association of Engineering Geologists, Special Volume n. **6**, Boston, 83-100.
Blumetti A.M. and Guerrieri L.; 2007: *Fault-generated mountain fronts and the identification of fault segments: implications for seismic hazard assessment*, Boll. Soc. Geol. It. (Ital.J.Geosci.), **126** (2) 307-322.
Blumetti, A.M., Guerrieri, L. and Vittori, E.; 2013: The primary role of the Paganica-San Demetrio fault system in the seismic landscape of the Middle Aterno Valley basin (central Apennines). Quaternary International, http://dx.doi.org/10.1016/j.quaint.2012.04.040.
Boncio P., Lavecchia G., and B. Pace; 2004: *Defining a model of 3D seismogenic sources for Seismic Hazard Assessment applications: the case of central Apennines (Italy)*, Journal of Seismology, **8** 407-425.
Cinti, F.R., Pantosti, D., De Martini, P.M., Pucci, S., Civico, R., Pierdominici, S., Cucci, L. Brunori C.A., Pinzi S. and Patera A.; 2011: *Evidence for surface faulting events along the Paganica fault prior to the April 6, 2009 L'Aquila earthquake (Central Italy).* Journal of Geophysical Research, **116**, B07308.
D'Agostino, N., Mantenuto, S., D'Anastasio, E., Giuliani, R., Mattone, M., Calcaterra, S., Gambino, P. and Bonci, L.; 2011: *Evidence for localized active extension in the central Apennines (Italy) from global positioning system observations.* Geology, **39**, 291-294.
Galadini, F. and Galli, P.; 2000: *Active tectonics in the central Apennines (Italy) e input data for seismic hazard assessment.* Natural Hazard, **22**, 225-270
Galli, P., Galadini, F. and Pantosti D.; 2008: *Twenty years of paleoseismology in Italy.* Earth Science Review, **88**, 89-117.
Galli, P., Giaccio, B. and Messina, P.; 2010: *The 2009 central Italy earthquake seen through 0.5 Myr-long tectonic history of the L'Aquila faults system.* Quaternary Science Reviews **29**, 3768-3789.
Galli, P.A.C., Giaccio, B., Messina, P., Peronace, E. and Zuppi, G.M.; 2011: *Palaeoseismology of the L'Aquila faults (Central Italy, 2009, Mw 6.3 earthquake): implications for active fault linkage.* Geophysical Journal International, **187**, 1119-1134.
Giaccio B., Galli P., Messina P., Peronace E, Scardia G., Sottili G., Sposato A, Chiarini E., Jicha B. and Silvestri S.; 2012: *Fault and basin depocentre migration over the last 2 Ma in the L'Aquila 2009 earthquake region, central Italian Apennines*, **56**, 69-88.
Moro M., Bosi V., Galadini F., Galli P., Giaccio B., Messina P., and Sposato A.; 2002: *Analisi paleosismologiche lungo la faglia del M. Marine (alta valle dell'Aterno): risultati preliminari*, Il Quaternario, **15**, 267-278.
Roberts, G.P. and A.M. Michetti; 2004*: Spatial and temporal variations in growth rates along active normal fault systems: An example from the Lazio– Abruzzo Apennines, central Italy*, J. Struct. Geol., **26**, 339-376, doi:10.1016/S0191-8141(03)00103-2.
Vittori E., Di Manna P., Blumetti A.M., Comerci V., Guerrieri L., Esposito E., Michetti A.M., Porfido S., Piccardi L., Roberts G., Berlusconi A., Livio F., Sileo G., Wilkinson, M., Mccaffrey, K., Phillips, R., Cowie, P. A.; 2011: *Surface faulting of the April 6, 2009, Mw 6.3 L'Aquila earthquake in Central Italy.* Bull. Seism. Soc. Am., **101**, 1507-1530, doi:10.1785/0120100140
Wells D.L. and Coppersmith K.J.; 1994: *Empirical relationship among magnitude, rupture length, rupture area, and surface displacement*. Bull. Seismol. Soc. Am., 84, 974-1002.
Working Group MS; 2008: *Indirizzi e criteri per la microzonazione sismica.* Conferenza delle Regioni e delle Province autonome - Dipartimento della protezione civile, Roma, 3 vol. + Dvd.
Working Group MS–AQ; 2010: *Microzonazione sismica per la ricostruzione dell'area aquilana*. Regione Abruzzo - Dipartimento della Protezione Civile, L'Aquila, 3 vol. + Cd-rom.

METODO DELTA-SIGMA E STUDIO DEL TERREMOTO DEL CILE DI MAGNITUDO 8.8 DEL 27 FEBBRAIO 2010

D. Caccamo[1], V. Pirrone[2], F.M. Barbieri[1], C. Laganà[1], C. Rubuano[1]
[1]*Dipartimento di Fisica e Scienze della Terra, Università di Messina*
[2]*Istituto di Istruzione Superiore IPSIA Barcellona Pozzo di Gotto (Me)*

Introduzione. In questo lavoro trattiamo, con il metodo Delta/Sigma, lo studio del terremoto crostale del Cile con magnitudo della mainshock $M_m = 8.8$, verificatosi il 27 febbraio 2010 lungo la costa tra il confine della regione del Maule e del Bio-Bio in Cile.

In Fig. 1a è rappresentata la mappa epicentrale della sequenza delle repliche. L'epicentro dell'evento è stato localizzato alla latitudine di 35.93°S e alla longitudine di 72.78°W; l'ipocentro è stato individuato ad una profondità di 35 km.

A partire dal 1960, questo è stato il più forte sisma a colpire il Cile causando il danneggiamento di circa 380.000 edifici, la morte di 523 persone e 24 dispersi. È stato lanciato anche un allarme tsunami sia per le coste del Cile che per tutte le coste pacifiche (USA e Canada escluse).

L'evento è dovuto alla convergenza verso est della placca di Nazca che va in subduzione alla placca sudamericana con una velocità di 7 m/secolo (Neic-usgs -banca dati http://neic.usgs.gov/neis/epic).

Il Metodo "Delta-Sigma", qui di seguito descritto, permette di trovare alcune anomalie nel decadimento temporale di una sequenza di repliche.

Fu il sismologo giapponese Fusakichi Omori che, prendendo in considerazione la sequenza sismica seguente al terremoto di Nobi del 1891, definì per primo la decrescenza del numero di repliche dopo un sisma importante con una formula empirica:

$$n(t)=1/t^p \qquad (1)$$

con n(t) = numero di repliche.

Questa legge (Omori, 1891) mette in evidenza la decrescita dell'attività secondo la (1), dove *t* si considera a partire dalla *mainshock* e *p* una costante compresa fra 1 e 1.4.

La serie temporale del numero di scosse per giorno di una sequenza sismica, dal punto di vista matematico, è considerata come somma di un contributo deterministico, che è dato dal decadimento della frequenza delle repliche secondo la legge di Omori modificata (Utsu, 1961) $n(t) = K(t+c)^{-p}$ e di uno stocastico, dovuto alle fluttuazioni casuali attorno al valor medio rappresentato dalla suddetta legge.

Il fenomeno del decadimento può essere modellato come un processo Poissoniano non stazionario (Page, 1968; Matsu'ura, 1986) mediante la formula di Omori modificata, proposta da Utsu (1961):

$$n(t) = K(t+c)^{-p} \qquad (2)$$

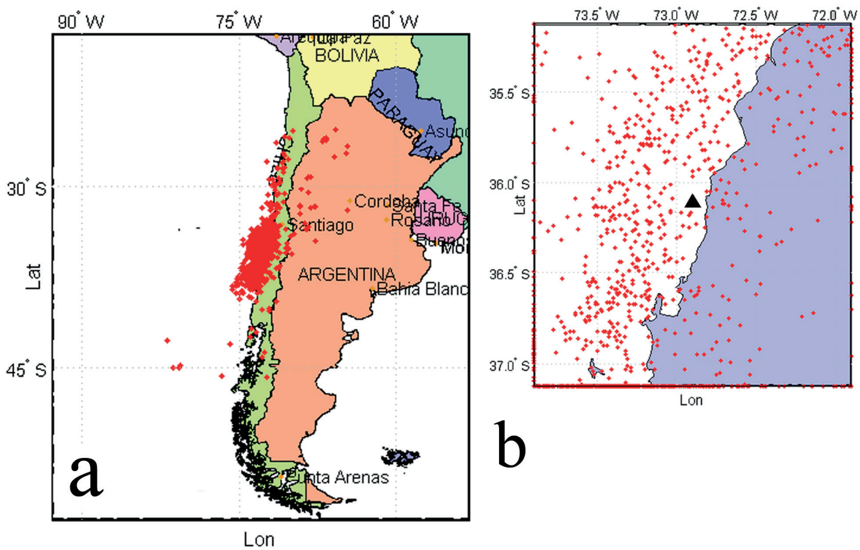

Fig. 1 – Con gli asterichi rossi è rappresentata la sequenza delle repliche, con il simbolo Δ (Fig. 1a) indichiamo l'ipocentro della mainshock relativa al terremoto del Cile del 27 febbraio 2010 con latitudine di 35.93°S, longitudine di 72.78°W e profondità 35 Km (Fig. 1b)

in cui *n(t)* è il numero di eventi per unità di tempo a partire dalla scossa principale, calcolato nell'intervallo di tempo Δt, il cui valor medio è $m = n(t) \cdot \Delta t$ e la deviazione standard $\sigma = \sqrt{n \cdot \Delta t}$. *K, c* e *p* sono costanti che dipendono dalle dimensioni del sisma e dalle caratteristiche geofisiche della zona in cui è avvenuta la scossa principale. Se si considera un campionamento delle repliche con Δt =1 giorno, allora il numero medio atteso di scosse per giorno sarà pari a $m = n(t)$, con una deviazione standard pari a $\sigma = \sqrt{n}$.

Elaborando i dati dei terremoti analizzati, abbiamo osservato che le fluttuazioni stocastiche attorno al valor medio $m = n(t)$ risultano pari al 99% circa entro un range di $\sigma \leq 2.5$, pertanto dette fluttuazioni hanno una probabilità di accadimento inferiore all'1% per valori di $\Delta/\sigma > 2.5$ (Caccamo *et al.*, 2005, 2007 a,b e c; Bussetti, 1983; D'Amico *et al.,* 2007).

Da quanto sopra detto i dati con:

$$\Delta = \left| n_{oss} - n_{calc} \right| > 2.5\sigma \tag{3}$$

$$\Delta/\sigma > 2.5 \tag{4}$$

vengono considerati anomalie presismiche, cioè precursori.

Si ricordi che il decadimento di repliche è un fenomeno discreto analizzato con una funzione che tende asintoticamente a 1, (Utsu *et al.,* 1995; Caccamo *et al.*, 2005, 2007 a,b,c; D'Amico *et al.*, 2010).

È possibile osservare delle anomalie nel decadimento, diversi giorni prima di una forte replica, anomalie che non sono necessariamente delle fluttuazioni di tipo casuale.

È importante precisare, da quanto si evince dalle statistiche sui dati delle sequenze, che gli eventi con $M > 5.5$ sono altamente frequenti entro i primi 10 giorni del decadimento per quei terremoti la cui magnitudo di mainshock supera i valori di 7.0 (Caccamo *et al.*, 2007 a,b,c), pertanto risulta superfluo fare un'analisi delle anomalie in detti giorni.

Data la generica serie completa di dati reali, con *d* durata della sequenza osservata $\{n_{oss}(t_j)\}$ e *j= 1....d*; se ipotizziamo che le anomalie si presentino diversi giorni prima dell'eventuale replica di magnitudo superiore a 5.5, inserendo nella estrapolazione della serie calcolata $\{n_{calc}(t_k)\}$ uno shift costante $s = 6$, evitiamo gli smorzamenti dovuti alle stesse nelle operazioni di fitting; ciò comporta una maggiore sensibilità del metodo Delta/Sigma nella loro individuazione.

Utilizzando la Omori(1) da noi modificata in:

$$n(t) = k \cdot t^{-p} + k_1 \tag{4}$$

otteniamo la serie completa di dati teorici $\{n_{calc}(t_k)\}$ (Caccamo *et al.*, 2002) ponendo:

- il pedice *k* pari a *k = a, a+1, a+2,...d,* con
- *a= h+s.*
- *h = 2 v,* dove *v =2* è il numero dei parametri k e p utilizzati nella (4), dove k è una costante che dipende dal numero totale degli eventi della sequenza e p è una costane che definisce il tasso di decadimento della sequenza di repliche,
- k_1 è la costante che tiene conto della sismicità di fondo, (tipica della sismicità di un'area) che poniamo uguale a 1.

Il programma di calcolo usato per l'analisi è Matlab, che ha anche la capacità di risolvere problemi che coinvolgono l'uso dei "minimi quadrati non lineari", e quindi è adatto per la (4), che è una legge di potenza.

I metodi utilizzati nel programma Delta/Sigma (Caccamo *et al.*, 2005, 2007 a,b e c; D'Amico *et al.*, 2010) sono di tipo iterativo e sono basati su algoritmi di ottimizzazione a larga scala, definiti come "metodo Newton" (Coleman e Li, 1994, 1996; Dennis, 1977). Ogni iterazione coinvolge la soluzione approssimata di un grande sistema lineare tramite il "metodo dei gradienti coniugati precondizionati" (Levenberg, 1944; Marquardt, 1963; More, 1977; Dennis, 1977; Coleman and Li, 1994, 1996). (Caccamo *et al.*, 2002, 2004, 2005, 2007 a,b e c; Bussetti, 1983, D'Amico *et al.*, 2007).

1) Per valutare la soglia di completezza dell'insieme di dati ottenuto, si usa il diagramma magnitudo-frequenza di Gutenberg-Richter dato dalla legge:

$$y = log_{10} N = a + b (M_m - M) \text{ (Gutenberg e Richter, 1954)}$$

dove M_m è la magnitudo della scossa principale, e i parametri *a* e *b* sono costanti.

Il parametro *a* si riferisce alla quantità di terremoti avvenuti in quella regione.

Del parametro *b*, tipicamente prossimo ad 1, col metodo Delta/Sigma se ne calcolano le variazioni temporali ed il suo errore, per ogni sequenza studiata.

La banca di dati, da noi principalmente utilizzata, per individuare la soglia di completezza, è quella dell'USGS, in quanto presenta dei formati compatibili con quelli utilizzati nel Delta/Sigma.

Va detto che gli studi da noi fatti, fino ad oggi, sulla previsione delle forti repliche ci hanno indotto a porre in tutte le misure, in modo rigoroso e perciò facilmente utilizzabile anche da altri ricercatori, come non accettabile una perdita di dati superiore al 10%, pertanto se $y = log_{10} N = a + b (Mm - M)$ rappresenta l'ordinata di un punto qualunque della retta nera (fit della Gutenberg-Richter, Fig. 2) e Y l'ordinata di un generico punto della linea rossa, si ha:

$$Y = y - 10\% \, y$$

Il criterio usato per stabilire la magnitudo di completezza minima M_c consiste, allora, nel calcolare la retta di regressione (linea nera, Fig. 2) per i terremoti di magnitudo $M \geq 4.0$ prendendo come magnitudo di soglia M_s il primo punto che cade al di sotto della retta parallela (linea rossa, Fig. 2; $M_s = 4.2$).

Se $M_c < 4$ si assume $M_c = M_{th} = 4$, (M_{th} magnitudo di completezza di soglia), in modo da effettuare il fit solo sui terremoti con magnitudo superiore a 4, perché detti eventi li riteniamo più completi in uno studio statistico delle previsioni. (Caccamo *et al.*, 2005, 2007 a, b, e c; D'Amico *et al.*, 2010)

Va, altresì detto che la durata temporale della sequenza è definita dall'espressione

$$d = n_1 + n_2,$$

dove *d* è l'ultimo termine della sequenza temporale, n_1 è il numero di scosse del primo giorno e n_2 il numero di giorni che seguono, dopo l' n_1, all'interno dei quali sono contenuti 10 giorni successivi che presentano zero repliche.

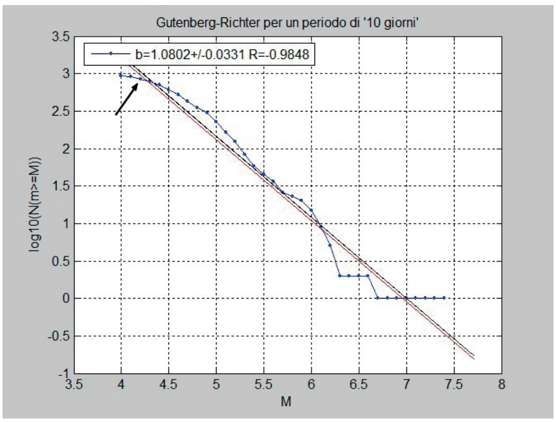

Fig. 2 – Diagramma di Gutenberg-Richter per i primi dieci giorni. A partire dalla magnitudo più bassa, il primo punto (indicato dalla freccia), più vicino e che sta al di sotto della retta rossa, rappresenta il minimo valore di magnitudo, per cui i dati si possono ritenere completi. In questo caso è $M_c = 4.2$.

2) Per individuare la sequenza sia nello spazio che nel tempo:
1. calcoliamo la dimensione dell'area coinvolta mediante la (Utsu, 1969):

$$\log_{10} L = 0.5 \cdot M_s - 1.8$$

con L lunghezza del segmento di faglia che ha subito la fratturazione ed M_S magnitudo dell'evento sismico responsabile di ciò;
2. acquisiamo i dati contenuti in un riquadro di lato 3L, con centro nell'epicentro della mainshock;
3. consideriamo un periodo di tempo pari ad un anno a partire dall'accadimento della mainshock;
4. calcoliamo il "baricentro" della sequenza, considerando solo i dati relativi ai primi 10 giorni, che sono rappresentativi dal punto di vista della completezza, perché la maggior parte delle repliche avviene proprio in questo periodo;

$$B_{LAT} = \frac{\sum_{i=1}^{n} Lat_i}{n} \; ; \; B_{LON} = \frac{\sum_{i=1}^{n} Lon_i}{n}$$

dove Lat_i è la latitudine e Lon_i la longitudine dell'epicentro dell'i-esima replica ed n è il numero di repliche con magnitudo $M \geq 4.0$.

Il termine "baricentro" non deve essere inteso nel senso fisico della parola, ma come un punto geometrico dato dalla media aritmetica delle latitudini e longitudini di tutti i terremoti della sequenza nei primi 10 giorni.

In questo lavoro vengono analizzate 1749 repliche.

Per questa scossa si è determinata una lunghezza di faglia L pari a 397.44 km.

Si è poi passati alla determinazione della magnitudo di completezza M_c, mediante la figura fornita dal programma (Fig. 2).

Nella nostra ricerca del valore della magnitudo di completezza M_c scegliamo il primo valore fuori dalla linea rossa, valore indicato dalla freccia nel grafico della Fig. 2., in questo caso pari a 4.2. Pertanto tutti gli eventi con M < 4.2, considerati non completi, vengono esclusi dall'indagine.

Verifica del metodo sul terremoto del Cile. Nella Fig. 3 sono analizzate, fra tutte le possibili repliche con M>5.5, solo quelle con M>6.0 e M>6.5.

Dalla Fig. 3a si evince come la sequenza decade inizialmente in maniera molto veloce, con dei picchi nel 13°, il 35°, 138°, 310°, 350° giorno, date in cui si registrano forti scosse, tutte con magnitudo superiore a 5.5.

In Fig. 3b viene riportato l'andamento del Delta/Sigma delle repliche con $M > 6$ dopo il decimo giorno fino a conclusione della sequenza stessa, indicando i giorni in cui questo parametro supera il valore 2.5.

Da notare come le anomalie $\Delta/\sigma > 2.5$ si presentino, ad eccezione di quella del 34° giorno (1 aprile 2010), sempre entro e non oltre dieci giorni prima di forti scosse ($M > 6$).

Dai grafici 3b e 3c si vede come i picchi $\Delta/\sigma > 2.5$ siano dei precursori, infatti:
1. Il precursore del 12° giorno (10 marzo 2010) e quello del 13° (11 marzo 2010) precedono le due repliche, una con M=6.9 e l'altra con M=7.0 avvenute entrambe il 13° giorno (11 marzo 2010);
2. Il precursore del 13° giorno (11 marzo 2010) anticipa le repliche una con $M = 6.2$ del 17° giorno (15 marzo 2010) l'altra con M=6.7 del 18° giorno. Nel grafico 3b si ha una anomalia Delta/Sigma il 34° giorno, non seguita da eventi con M>6 nei 10 giorni successivi; questo precursore registra nello stesso arco temporale, scosse con 5.5<M<6.0

3. I precursori del 65° ed del 66° giorno (2 e 3 maggio 2010) anticipano la scossa con M = 6.3 del 3 maggio 2010;
4. Il precursore del 137° giorno (13 luglio 2010), anticipa la scossa con M = 6.6 che avviene il 138° giorno (14 luglio 2010);
5. Il precursore del 309° giorno (1 gennaio 2011) anticipa la scossa con M = 7.2 del 310° giorno, del 2 gennaio 2011;
6. Il precursore del 349° giorno (10 febbraio 2011) anticipa 2 scosse una con M=6.9 (11 febbraio 2011) e l'altra con M = 6.1 (12 febbraio 2011);
7. Il precursore del 351° giorno (12 febbraio 2011) anticipa quella con M = 6.7 del 353° giorno (14 febbraio 2011).

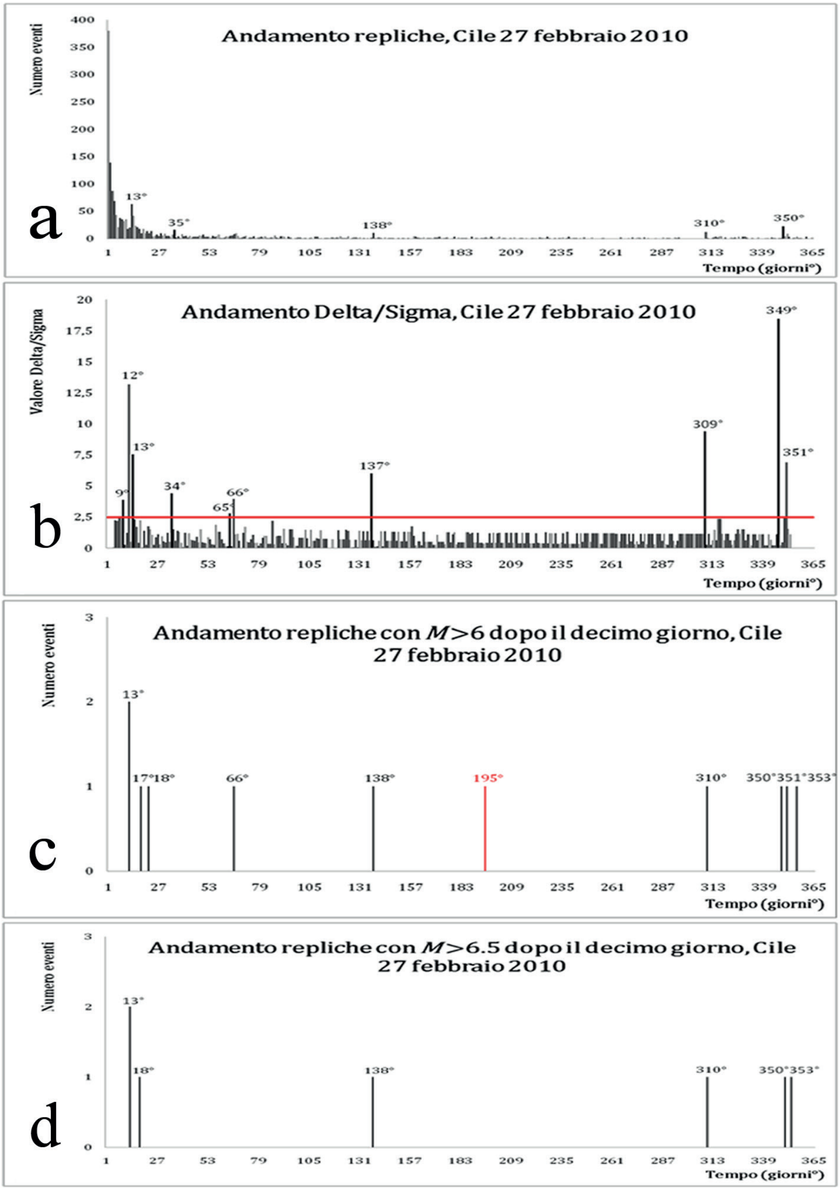

Fig. 3 – Distribuzione temporale: a) dell'intera sequenza; b) del Δ/σ; c) degli eventi con M > 6.0; d) degli eventi con M > 6.5.

Tra quelle con M> 6.0, la scossa di M= 6.2 del 195° giorno (9 settembre 2010) è l'unica a non essere preceduta, entro e non oltre i 10 giorni, da almeno un'anomalia del Delta/Sigma maggiore di 2.5.

Per la sequenza, con *M*>6, otteniamo 10 scosse previste, entro e non oltre 10 giorni, e una non prevista, con una percentuale di riuscita del 90.9%.

Analizzando in fine, la Fig. 3d, si osserva che le repliche con $M > 6.5$ sono 7 e tutte anticipate, entro e non oltre dieci giorni, da un'anomalia Delta/Sigma maggiore di 2.5; pertanto la percentuale di successi è del 100%.

Tab. 1 – Dati e risultati del metodo Delta/Sigma.

Magnitudo delle repliche indagate	Numero repliche dopo il 10° giorno dall'inizio della sequenza	numero repliche precedute, entro e non oltre i 10 giorni, da $\Delta/\sigma > 2.5$	Numero repliche non precedute, entro e non oltre i 10 giorni, da $\Delta/\sigma > 2.5$	Percentuale di riuscita del metodo Delta/ Sigma P Δ/σ
M>5.5	36	24	12	66.7%
M>5.6	29	20	9	69.0%
M>5.7	26	20	6	77.0%
M>5.8	22	17	5	77.2%
M>5.9	16	13	3	81.3%
M>6.0	11	10	1	90.9%
M>6.1	10	9	1	90.0%
M>6.2	8	8	0	100%
M>6.3	7	7	0	100%
M>6.4	7	7	0	100%
M>6.5	7	7	0	100%
M>6.6	6	6	0	100%
M>6.7	4	4	0	100%
M>6.8	4	4	0	100%
M>6.9	2	2	0	100%
M>7.0	1	1	0	100%

In conclusione, dalla Tab. 1 si evince che per 6 <M <6.1 il metodo ha una percentuale di riuscita del 90.9% su un discreto numero di eventi (10 su 11 per M>6.0, e 9 su 10 per M>6.1).

Per M>6.2, la riuscita del metodo è del 100%, in quanto le 8 scosse sono tutte previste.

Un buon risultato visto il numero di repliche.

Utilizzando lo stesso metodo, che proprio per la sua ripetitività possiamo considerare rigoroso, su terremoti che presentano le stesse caratteristiche di quello del Cile, quali quello del Giappone e quello del Perù, abbiamo osservato che per magnitudo superiori a 6.7 nel Giappone (mainshock M=9.0) e 6.4 nel Perù (mainshock M=8.4), i precursori danno previsioni di repliche pari al 100%.

Al momento stiamo studiando, con questo metodo, tutti quei terremoti che presentano le stesse caratteristiche di quelli sopra citati, e con repliche con magnitudo M>5.5.

Questa è la prima volta che presentiamo dati su terremoti la cui mainshock ha una magnitudo maggiore di 8.5.

Bibliografia

Bussetti G.; 1983. Esercitazioni pratiche di fisica. Libreria Editrice Universitaria Levrotto & Bella.

Caccamo D., Barbieri F. M., Laganà C., D'Amico S., Parrillo F., 2005. The temporal series of the New Guinea 29 April 1996 aftershock sequence, Physics of the Earth and Planetary Interiors, 153 (4), 175-180, doi:10.1016/j.pepi.2005.03.007.

Caccamo D., Barbieri F. M., Laganà C., D'Amico S., Parrillo F., 2007a. A study about the aftershock sequence of 27 December 2003 in Loyalty Islands. Boll. Geo. Teor. Appl., 48 (1), 53-63.
Caccamo D., D'Amico S., Parrillo F., Barbieri F. M., Laganà C., 2007c. Umbria-Marche sequence (central-Italy): a study about its aftershock sequence. Boll. Geo. Teor. Appl., 48, 385-398
Caccamo D., Parrillo F., D'Amico S., Barbieri F. M., Laganà C., 2007b. Seismic anomalies in the aftershock sequence of November 16, 2000 in Papua New Guinea, Izvestiya - Physics of the Solid Earth. 43, 662-668, doi:10.1134/S106935130708006X.
Coleman T. F.; Y. Li, 1994. On the convergence of reflective Newton methods for large-scale nonlinear minimization subject to bounds, Mathematical Programming, Vol. 67, N. 2, 189-224.
Coleman T. F.; Y. Li, 1996. An interior, trust region approach for nonlinear minimization subject to bounds, SIAM Journal on Optimization, Vol. 6, 418-445.
D'Amico S., Caccamo D., Parrillo F., Laganà C., Barbieri F., 2010. The 20th September 1999 Chi-Chi earthquake (Taiwan): a case of study for its aftershock seismic sequence. Izvestiya - Physics of the Solid Earth. 46, 4, 317-326, doi: 10.1134/S106935131004004X.
Dennis, J. E. Jr., 1977. Nonlinear Least Squares, State of the Art in Numerical Analysis, ed. D. Jacobs, Academic Press, 269-312.
Gutenberg B. & Richter, C.F., 1942. Earthquake Magnitude, intensity, energy and acceleration, Bull. Seism. Soc. Am., 32, 162-191.
Gutenberg, B. and Richter, C.F., 1954. Seismicity of the earth, Princenton University Press, Princenton, N. J. 310.
Gutenberg, B. and Richter, C.F., 1956. Magnitude and energy of earthquakes, Ann. Geopys., 9, 1.
Levenberg K., 1944. A method for the solution of certain problems in least squares, Quarterly Applied Math. 2, 164-168.
Marquardt D., 1963. An algorithm for least-squares estimation of nonlinear parameters, SIAM Journal Applied Math. Vol. 11, 431-441.
Matsu'ura R. S., 1986. Precursory quiescence and recovery of aftershock activities before some large aftershocks. Bulletin of the Earthquake Research Institute University of Tokyo, 61, 1-65.
More J. J., 1977. The Levenberg-Marquardt algorithm: implementation and theory, Numerical Analysis, ed. G. A. Watson, Lecture Notes in Mathematics 630, Springer Verlag, 105-116.
Page R., 1968. Aftershocks and microaftershocks of the great Alaska earthquake of 1964. Bull. Seism. Soc. America, 58, 1131-1168.
Udias A., 2001. Principles of seismology. Cambridge University Press.
Utsu T., 1961. A statistical study of the occurrence of aftershocks, Geophys. Magazine, 30, 521-605.
Utsu T., 1969. Aftershocks and earthquake statistics - source parameters which characterize an aftershock sequence and their interrelations, J. Phys. Earth, 43, 1-33.
Utsu T., Ogata Y., Matsu'ura R., 1995. The Centenary of the Omori Formula for a Decay Law of Aftershock Activity. J. Phys. Earth, 43, 1-33.

THE SIGNIFICANCE OF THE "HIDDEN" FAULTS OF THE EASTERN FLANK OF MT. ETNA AND THEIR SEISMOGENIC POTENTIAL: NEW GEOLOGICAL CONSTRAINTS

S. Catalano[1], G. Tortorici[1], A. Torrisi[2], G. Romagnoli[1], F. Pavano[1]
[1]Dipartimento di Scienze Biologiche, Geologiche e Ambientali – Sezione di Scienze della Terra, Università di Catania, Italy
[2]Regione Sicilia – Dipartimento Regionale di Protezione Civile – Servizio Regionale per la Provincia di Catania, Italy

Introduction. The main seismic events on the eastern flank of Mt. Etna, characterized by low to medium magnitude ($M \leq 5$; Azzaro *et al.*, 2009), are generally accompanied by the development of well-defined coseismic fracture zones. Their coincidence with the elongation of the mesoseismic areas, where most of the damages are confined, suggests interpreting the fractures as the emergence at surface of capable seismogenic structures (Azzaro, 1999; Barreca *et al.*, 2013). This hypothesis is fully demonstrated along the NNW-oriented tectonic alignments, where the historical coseismic fracturing matched oblique (dextral) normal faults, showing well defined Late Quaternary cumulative scarps (e.g. Timpa of Acireale and Moscarello; see inset in Fig. 1; Monaco *et al.*, 1997). On the contrary, discrete NW-SE oriented fracture zones cyclically form along alignments, where neither morphological nor geological cumulative displacements can be recognized. Even if their relation with rooted faults is obscure and mostly based on their cyclical coseismic renewal, these alignments have been interpreted as seismogenic "hidden" faults (e.g. Fiandaca Fault and S. Tecla Fault), responsible for part of the main local seismicity (Azzaro, 1999). The full understanding of the origin and nature of the coseismic fracturing associated with the hidden faults of Mt. Etna is, thus, a crucial topic in the seismic microzonation analyses to validate the location of seismogenic sources and assess their potential. In this paper we discuss the results of the geological and morphostructural investigation that has been performed across the Fiandaca, Santa Tecla and Santa Venerina hidden faults, in order to define their role in the active kinematic picture of the eastern flank of Mt.Etna.

Seismotettonic setting. The eastern flank of Mt. Etna is dissected by two distinct sets of active structures. The prominent NNW-oriented fault belt, representing the northern termination of the Ionian-Etnean Branch of the Siculo-Calabrian Rift Zone (inset in Fig. 1; Catalano *et al.*, 2008), consists of a half graben that includes the Acireale-S. Alfio master fault, the synthetic San Leonardello Fault and the antithetic Trepunti Fault. The epicenters of several main earthquakes (A.D. 1881; 1911; 1971) have been located at hangingwall of the rift zone (Monaco *et al.*, 1997; Azzaro, 1999; Azzaro *et al.*, 2009). On the footwall of this rift zone, discrete NW-oriented fracture systems, represented by the Fiandaca, Santa Tecla and Santa Venerina faults (ff, STF and SVF in Fig. 1; Barreca *et al.*, 2013), have been described as alignments that are usually affected by both diffuse aseismic creep (Azzaro, 1999; Monaco *et al.*, 2012) and coseismic remobilisation. The updated models on the active tectonics and the seismicity of Mt. Etna (Azzaro, 1999; Azzaro *et al.*, 2012; Barreca *et al.*, 2013) refer to the Fiandaca (A.D. 1894, 1984), S. Tecla (A.D. 1865, 1914) and SantaVenerina (A.D. 1879, 2002) faults some relevant seismic events, which have been otherwise attributed to the NNW oriented faults of the rift zone (Monaco *et al.*, 1997). The most recent episode of remobilization of a “hidden” fault has been referred to the 29th of October 2002 earthquake (Mm=4.1; Azzaro *et al.*, 2006), which was associated to the reactivation of an historical ground fracture zone (A.D. 1879), crossing through the village of Santa Venerina (SVF in Fig. 1; Azzaro *et al.*, 2006; Barreca *et al.*, 2013).

Stratigraphy of the eastern flank of Mt. Etna. Along the eastern flank of Mt. Etna, the volcanostratigraphic succession includes the products of all the stages of the etnean volcanism (Gillot *et al.*, 1994). The volcanic cover rests, as a whole, on marine deposits, consisting of a monotonous Early-Middle Pleistocene marly-clay succession (Di Stefano and Branca, 2002) that bears submarine tholeiitic lava horizons, ranging in age from 0.58 to 0.46 Ma (Gillot *et al.*, 1994). The marine succession is capped by subaerial transitional products from tholeiitic to alkaline, ranging in age from about 225 ka B.P. to 168 ka B.P. (Gillot *et al.*, 1994; Corsaro *et al.*, 2002). In a large area, going from Acireale to Giarre (inset in Fig. 1), a buried clastic wedge, which was exclusively detected by geophysical data (Cassinis *et al.*, 1970; La Delfa *et al.*, 2007), is interposed between the top of the marly clays and the outcropping etnean volcanic cover. The clastic deposits, here designed as Basal Clastic Wedge, fill a prominent triangular shaped tectonic depression, the Giarre Basin, which is bordered by two culminations of the Middle Pleistocene marly-clay substratum: the Acitrezza Ridge and the Nunziata High (inset in Fig. 1). The sequence of the alkaline products can be divided in four distinct units, which are separated by epiclastic deposits marking first order erosion surfaces. The oldest alkaline products, showing radiometric age from 140 ka to 132 ka (Gillot *et al.*, 1994; Branca *et al.*, 2007) have been grouped in the pre-Tyrrhenian alkaline lavas. These are unconformably covered by huge volumes of epiclastic deposits, here named Acireale Lahars that concealed the pre-existing volcanic topography, reaching a maximum thickness of about 150 m, in the area of Acireale. The Acireale Lahars shows distinctive reddish horizons that have been drilled in different sites of the southeastern flank of Mt. Etna, indicating a wide distribution beneath the recent volcanic covers, from Acireale to Santa Venerina. On top of the Timpa of Acireale, the Acireale Lahars are capped by coastal marine deposits that form the wide terrace of the 5.5 OIS (125 ka), extending towards the Acitrezza Ridge. The marine terrace is covered by alkaline lavas, ranging in age from 120 ka to 60 ka. These have been referred to the Tyrrhenian alkaline lavas, grouping the products of several spread edifices (Branca *et al.*, 2007). A major epiclastic horizon, here designed as Milo Formation, conceals the deeply entrenched erosion surface that models the Tyrrhenian alkaline lavas, in the whole northwestern sector of the Giarre Basin. The backbone of the modern stratovolcano is constituted by products, ranging in age from about 40 to 15 ka, while the recent volcanic covers consist of products emitted from the active feeding systems, in the last 15 ka (Gillot *et al.*, 1994; Branca *et al.*, 2007). A distinction between the Wurmian alkaline lavas and the Holocene lavas is here proposed on the basis of their position with respect to the deposits of the Chiancone alluvial fan (Calvari and Groppelli, 1996). The conglomerates of the "Chiancone" actually belong to two distinct sequences, separated by an erosional surface. The older sequence, confined in age in the last 15 ka (Guest *et al.*, 1984; Calvari and Groppelli, 1996), forms most of the alluvial fan that is unconformably draped by a thin horizon made up of the younger sequence, showing a radiometric age of 7.6 ka B.P. (Calvari and Groppelli, 1996).

Fiandaca Fault. The Fiandaca Fault represents a major tectonic alignment that controls the boundary between the Acitrezza Ridge and the Giarre Basin. The fault is marked by a dramatic offset of the top of the Middle Pleistocene marly-clay, from about – 500 m b.s.l. (Cassinis *et al.*, 1970), within the basin, to 210 m a.s.l., in the Acitrezza Ridge. The fault motion was also responsible for the emergence of the 460 ka-old tholeiitic pillow-lavas, which were emitted at a minimum depth of about 400 m b.s.l. (Corsaro and Cristofolini, 2000) and for the huge vertical displacement between the pre-Tyrrhenian alkaline lavas resting on the Acitrezza Ridge and those cropping out along the Timpa of Acireale (Fig. 1). On the downthrown sector of the fault, the Basal Clastic Wedge accumulated, with a thickness of about 400 m, comparable with the depth of deposition of the underlying marly clay. The fault is concealed by the marine terrace of the OIS 5.5 (125 ka), which crosses undisturbed the structure. It directly covers the batial marly clays of the Acitrezza Ridge, while it rests on subaerial volcanic succession, including the transitional basalts (225 ka) and the overriding 190 m-thick pre-Tyrrhenian alkaline lavas (140-132 ka), on the downthrown sector. Here, the thickness of the pre-Tyrrhenian sub-aerial products constrains a minimum apparent amplitude (>210 m) of the Tyrrhenian transgression (125 ka) that is at least 70 m wider than the actual absolute rise of the sea-level (136 m; Chappel and Shackleton, 1986).

The Fiandaca Fault is buried beneath the Tyrrhenian alkaline lavas and the overriding recent lava flows. However, its trace has been reconstructed taking into account the distribution of the outcrops of the Early-Middle Pleistocene marly-clays, representative for the extent of the upthrown sector, and the isopachs of the lava succession (Cassinis *et al.*, 1970), significant to discriminate the volcanic cover accumulated on the downthrown sector. The resulting fault trace matches the location of the historical coseismic fracture zones which has been referred to the Fiandaca "hidden" fault (Azzaro, 1999). The relations of the fault with the different stratigraphic units are illustrated along a NNE-SSW oriented cross-section (profile 1 in Fig. 1). The profile shows that the Tyrrhenian alkaline lavas and the overriding recent lava flows, being very thick on the top of the Basal Clastic wedge within the Giarre Basin and thinner on the Acitrezza Ridge, have obliterated a tectonic scarp that cumulated before the Tyrrhenian. Considering all the described geological constraints, we can conclude that the fault activity along the Fiandaca Fault was confined in the 460-125 ka interval, during which it accommodated the whole relative vertical motions along the southwestern margin of the Giarre Basin.

Santa Tecla Fault Zone. Adjacent to the Fiandaca Fault, the Santa Tecla Fault Zone (Fig. 1) consists of two main left-stepping NW-oriented segments. The southeastern segment, showing a length of about 6 km, splays from the Acireale Fault, to the north of Acireale. Along a short length of the fault, at its southeastern termination, a tectonic scarp as high as 160 m is exposed. Along the scarp, the fault offsets a volcanic succession that includes the pre-Tyrrhenian and the Tyrrhenian alkaline lavas. The scarp is clearly bypassed by the Holocene lava flows, that cross undisturbed the structure, obliterating every morphological evidence of the fault motion. The trace of the fault has been, thus, reconstructed following the trend of historical coseismic ground fractures (Azzaro, 1999). The northwestern segment, showing a length of 4 km, developed in the area of Zafferana. This segment is marked by a

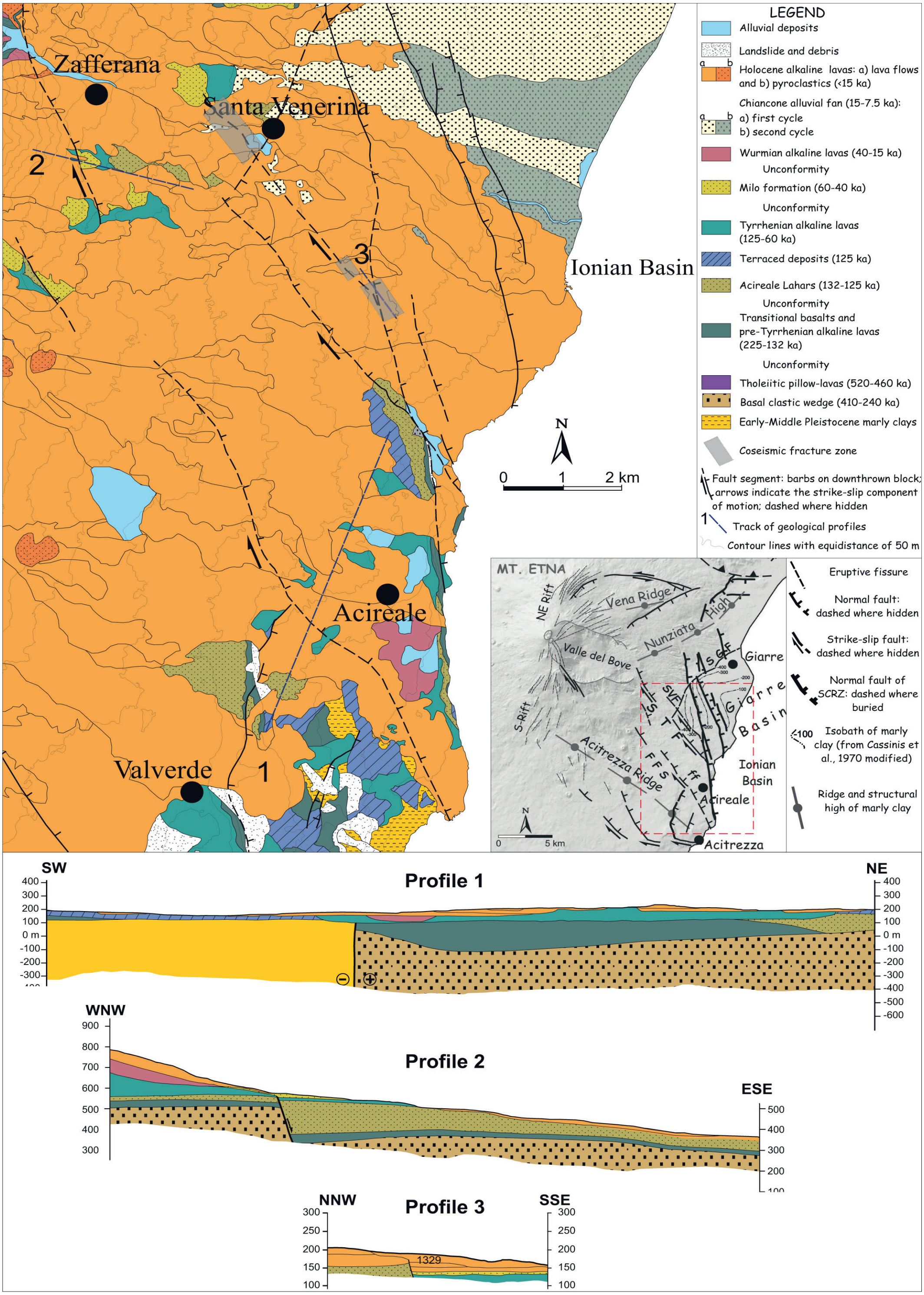

Fig. 1 – Geological map of the lower south-eastern flank of Mt. Etna (for location see dotted frame in the inset) and geological profiles across the ff, STF and the north termination of Acireale Fault. The inset shows the main tectonic features of the region.

cumulative scarp, which is completely draped by the Holocene lava flows. Along this segment, the stratigraphy of the volcanic products on the two sides of the structure is well exposed, providing several constraints for determining the age and the displacement-rate of the fault (Profile 2 in Fig. 1). The cross-section evidences that most of the total vertical displacement (180 m), corresponding to the offset of the top of the pre-Tyrrhenian alkaline lavas (> 125 ka), pre-dates the emplacement of the Tyrrhenian alkaline lavas of the Valle del Bove centers, showing radiometric age of about 93 ka (Branca *et al.*, 2007). They unconformably cover the Acireale Lahars (132-125 ka) that reach a maximum thickness of about 200 m on the hangingwall of the fault, while they are reduced to a few meters preserved by erosion in the footwall of the fault. The later vertical displacements affect the Tyrrhenian alkaline lavas and the deposits of the Milo Formation (60-40 ka). At the northern termination, the fault segment, as well as the southeastern segment, shows a 160 m-high tectonic scarp. Also in this case, the scarp offsets a volcanic succession that includes the pre-Tyrrhenian and the Tyrrhenian alkaline lavas, ranging in age from 128 to 93 ka. The tectonic scarp is by-passed by the 40 ka-old basal levels of the Wurmian alkaline lavas, that cross undisturbed the fault. The field evidence, collected along the entire Santa Tecla Fault Zone would constrain, thus, an activity of the fault that must be confined in the 125-40 ka.

Santa Venerina Fault. The Santa Venerina Fault was described by Azzaro (2004); Azzaro *et al.* (2009) as a NW-SE oriented, 5 km long seismogenic fault responsible for at least two main historical shocks (1879, Mm=4.3; 2002, Mm=4.1), associated with ground fracturing. Because of the absence of any surface evidence of the structure, the fault has been traced on the basis of the distribution of the coseismic ground fractures that are cyclically renewed. These outline an alignment that splays from the northern tip of the NNW-SSE oriented Acireale segment of the Acireale-S.Alfio fault (Azzaro *et al.*, 2009; 2012; Monaco *et al.*, 2010; Barreca *et al.*, 2013). The last episode of reactivaction of the Santa Venerina Fault, which occurred during the 2002 event, was characterized by the development of two distinct discrete fracture zones: the former originated at the southeastern end of the structure, in the localities of San Giovanni Bosco and Dagala Canne, the latter developed at the northeastern termination of the "hidden" fault, across the village of Santa Venerina (Fig. 2).

The southern fracture zone was composed of two distinct clusters of closely spaced N-S to N170° oriented fractures, ranging in length from few hundreds to about 500 m that flanked a discrete segment of the northern termination of the Acireale Fault. This latter, characterized by oblique (dextral) motion (Monaco *et al.*, 1997) clearly cut through very recent lava flows, forming a buried fault scarp by-passed by historical (1329) lavas (profile 3 in Fig. 1). The two clusters of coseismic fractures developed parallel to the main structure, on both the hangingwall and footwall of the fault, showing kinematics consistent with that of the major structure.

The northern fracture zone reactivated a length of 1 km of the termination of the "hidden" fault, along which closely spaced N10°-20° oriented fractures, ranging in length from 100 to 300 m, originated. The fracture zone crossing Santa Venerina has been investigated in detail through a grid of 9 cross-sections, based on integration of field data, from 1:5000 geological mapping, and several logs from bore-holes. The collected data provided sufficient information to outline a 3D geometry of the topography that have been concealed by the recent alkaline lava flows, related to the modern activity of Mt. Etna (< 15 ka; Recent Mongibello; Gillot *et al.*, 1994)(Fig. 2). In the 3D reconstruction, a sharp 20 m-high scarp marks the trace of a buried NE-SW normal fault, separating the western and eastern sectors of the village (profile 1 and 2 in Fig. 2). The shallow stratigraphic horizons characterising the hangingwall of the structure have been analysed by three aligned, 90 m-deep bore-holes (profile 2 in Fig. 2) that are aligned from the buried fault line towards the east. The borehole S1, located immediately to the south-east of the fault trace, crosses the fault, thus constraining the southeast-dipping geometry of the structure. The deeper portion of the log, related to the horizons uplifted in the footwall of the fault, is represented by the pre-Tyrrhenian alkaline lavas that rest on a paleosoil draping

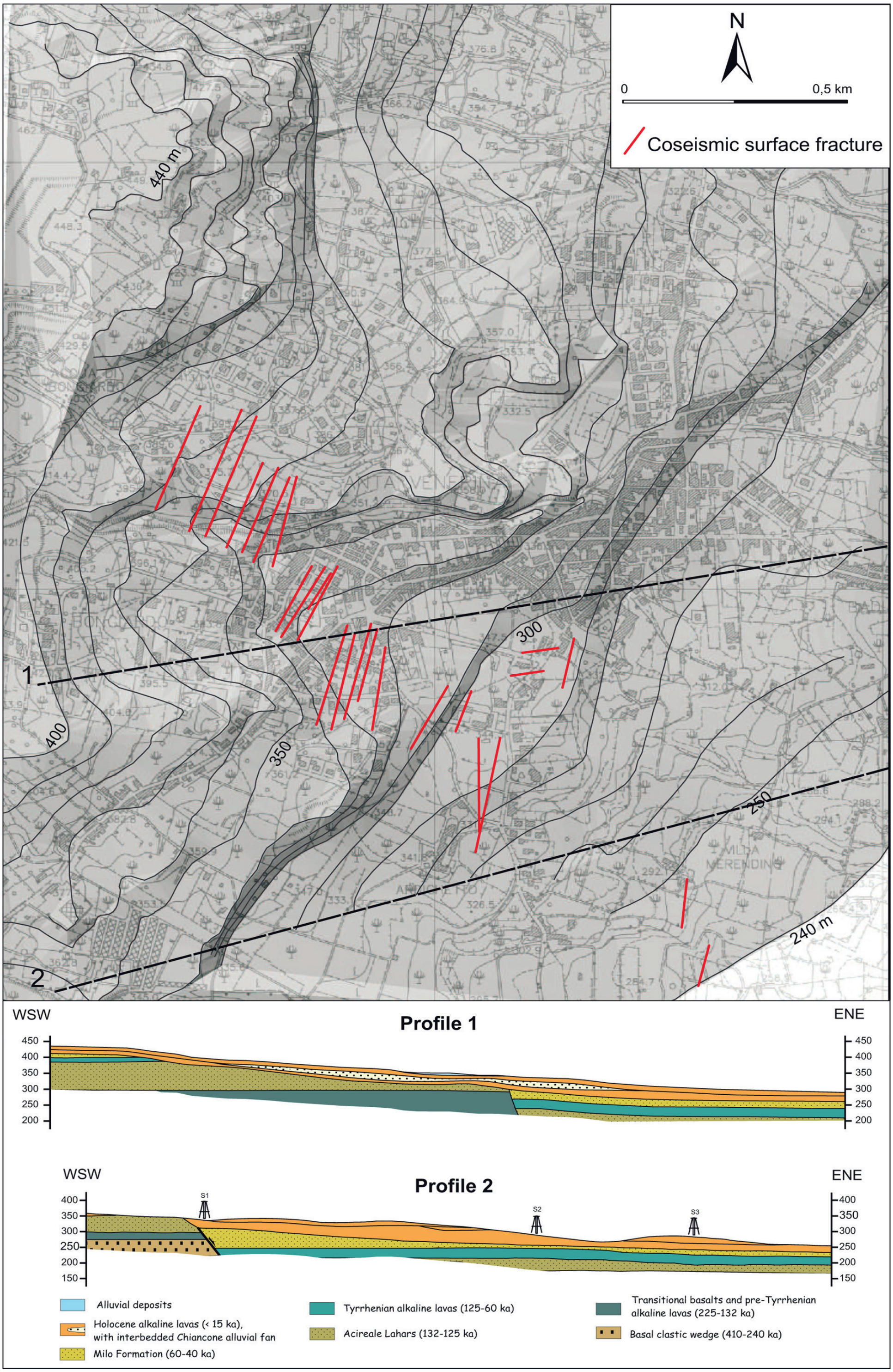

Fig. 2 – 3D model of the substratum of the Holocene lava flows in the surroundings of Santa Venerina and distribution of the coseismic ground fractures related to the seismic event of 2002. Two geological profiles across the SGF and the ground fracture zone are reported.

epiclastic deposits. These have been correlated with the top of Basal Clastic Wedge of the Giarre Basin that, in the hangingwall, has been detected by geophysical data (Cassinis *et al.*, 1970) at an elevation of about 150 m lower. The entire stratigraphic succession encountered in the boreholes S2 and S3, located more to the east, can be clearly referred to the volcanic succession that accumulated on the hangingwall of the fault, on top of the Basal Clastic Wedge. The stratigraphy and the geometry of the successions involved on both the footwall and the hangingwall of the fault, here designed as Santa Venerina-Giarre Fault (SGF in the inset of Fig. 1), are illustrated by the two cross-sections (Fig. 2). They show that the base of the Tyrrhenian alkaline lavas was vertically displaced by the fault for about 150 m and that the accommodation space due to motion along the SGF has been mainly filled with the Milo Formation that forms a wedge widening towards the fault. Finally, the structure appears to be bypassed by huge volumes of the volcanic products of the Recent Mongibello (< 15 ka) and the associated deposits of the two cycles of the Chiancone alluvial fan, which cross undisturbed the structure. The bore-hole data, combined with field information, thus suggest an age of the fault, starting from 125 ka B.P.. The end of the fault activity pre-dates the 15 ka and more probably was confined at the age of the top of the Milo Formation (40 ka). However, the buried fault played a major role in the evolution of the paleotopography reproduced in Fig. 2. The structure controlled the pre-15 ka river entrenchment that was confined at the footwall of the structure, while in the hangingwall was dominating the deposition. This topography has influenced the distribution of the volcanic products of the last 15 ka. In the western sectors of the village, where the coseismic fractures developed, the recent volcanic cover, alternating with several alluvial horizons, are channelized within WNW-oriented valleys that are modeled on a succession including the Acireale Lahars, the Tyrrhenian alkaline lavas and the Milo Formation (profile 1 in Fig. 2). The subsurface data, fitting well the surface evidence, show a clear continuity of the different stratigraphic units, which exclude the existence of a rooted fault beneath the surface co-seismc fracture zone. The data rather point out that the fracture zone affects the volcanic products and the alluvial deposits infilling the axis of a buried valley.

Discussion and conclusions. According to the new geological data on the eastern flank of Mt. Etna, the coseismic fracture zones that have been referred to "hidden" faults developed in almost two distinct conditions. The fracture zones aligned along the Fiandaca and the Santa Tecla faults are actually connected to buried tectonic structures. In both the cases, along the rooted faults, huge Late Quaternary vertical displacements can be recognised, even if the end of their activity can be referred to 125 and 40 ka B.P., respectively. This implies that there is no a direct connection between the active coseismic ground deformation with the long-term evolution of the two structures. This is also demonstrated by the evidence that the lava flows of the last 40 ka by-passed the two faults, obliterating their older morphological expression. Moreover, none new morphotectonic feature generated and cumulated on these recent volcanic products. The cyclical renewal of the active fracture zones, thus, did not produce an appreciable cumulative permanent ground deformation. On the other hand, the explanation of the active fracture zones developed along the Santa Venerina fault is even more problematic, as our data would exclude a connection between the ground deformation and a deep-seated NW-SE oriented fault. Paradoxically, the most unclear situation could provide the explanation for the genesis of the "hidden" faults at Mt. Etna. If the development of the coseismic fracture zones of the 2002 event is considered, we can distinguish along an apparent single NW-SE alignment, designed as Santa Venerina "hidden" fault, two distinct sets of structure. The former consists of the N170° fractures that, being developed in the San Giovanni Bosco area with the same trend and kinematics of the main Acireale Fault, can be referred to the remobilization of a discrete length of the major structure. The latter set of fractures, in the area of Santa Venerina, developed where the geological data inhibit to locate a rooted fault. A genesis of the fractures different from tectonics is also suggested by their unusual geometry that deviates from that of the modeled shear zones, because of the high angle orientation of the single fractures (N 10-20°) compared to the trend of their alignment (N 150°). The detailed subsurface investigation have evidenced that the ground fracture zone is aligned with the axis of a buried paleovalley, whose flanks represent sharp lateral discontinuities between an alternation of lavas and clastic deposits, infilling the valley, and the more homogeneous epiclastic sequences of the substratum. In this context, the coseismic fractures originated at almost right-angle to the valley orientation, being centred on its axis, and extend for a length which is consistent with the reconstructed width of the valley at depth. Finally, the fracture alignment abruptly interrupts at the mouth of the valley, which is controlled by a NE-SW oriented buried fault zone. The direct connection between their geometry and that of the buried valley strongly suggests interpreting the coseismic fracture zones of Santa Venerina as a site effect of the ground motion, determined by major lateral mechanical discontinuities of the substratum that likely produced a differential ground motion between the valley infilling and the surrounding terrains. As well, the active coseismic ground deformation along the Fiandaca and Santa Tecla faults, where cumulative features are absent, could be explained in terms of differential site response, due to the sharp lateral discontinuities of the rock mechanics on the opposite sides of the two major structures. The two faults, located at the southwestern border of the prominent Giarre Basin, can represent mechanical barrier along which the ground motion generated by seismic events located along the main seismogenic faults of the SCRZ, cutting through the Giarre Basin, concentrate their effects.

References

Azzaro R.; 1999: *Earthquake surface faulting at Mount Etna volcano (Sicily) and implications for active tectonics*. J. Geodyn., **28**, 193-213.

Azzaro R.; 2004: *Seismicity and active tectonics in the Etna region:constraints for a seismotectonic model*. In: Bonaccorso A., Calvari S., Coltelli M., Del Negro C. and Falsaperla S. (eds.), «Mt. Etna: volcano laboratory», American Geophysical Union, Geophysical Monograph, **143**, 205-220.

Azzaro R., Branca S., Gwinner K. and Coltelli M.; 2012: *The volcano-tectonic map of Etna volcano, 1:100.000 scale: an integrated approach based on a morphotectonic analysis from high-resolution DEM constrained by geologic, active faulting and seismotectonic data*. Ital. J. Geosci. (Boll. Soc. Geol. It.), **131**, No. 1, 153-170.

Azzaro R., D'Amico S., Mostaccio A., Scarfì L., and Tuvè T.; 2006: *Terremoti con effetti macrosismici in Sicilia orientale nel periodo Gennaio 2002 - Dicembre 2005*. Quad. di Geof., **41**, 1-60.

Azzaro R., D'Amico S., Mostaccio A., Scarfì L. and Tuvè T.; 2009: *Terremoti con effetti macrosismici in Sicilia orientale nel periodo Gennaio 2006 - Dicembre 2008*. Quaderni di Geofisica, **72**, 39 pp.

Barreca G., Bonforte A. and Neri M.; 2013: *A pilot GIS database of active faults of Mt. Etna (Sicily): A tool for integrated hazard evaluation*. J. Volcanol. Geotherm. Res., **251**, 170-186.

Branca S., Coltelli M., De Beni E. and Wijbrans J.; 2007: *Geological evolution of Mount Etna volcano (Italy) from earliest products until the first central volcanism (between 500 and 100 ka ago) inferred from geochronological and stratigraphic data*. Int J Earth Sci (Geol Rundsch) DOI 10.1007/s00531-006-0152-0

Calvari S. and Groppelli G.; 1996: *Relevance of the Chiancone Volcanoclastic deposit in the recent history of Etna volcano (Italy)*. J. Volcanol. Geotherm. Res., **71**, 239-258.

Cassinis R., Cosentino P., Ponzini G. S. and Riuscetti M.; 1970: *Contributo all'esplorazione geofisica lungo la costa etnea*. Atti del Convegno Internazionale sulle acque sotterranee, Palermo 6-8 dicembre 1970, 144-154.

Catalano S., De Guidi G., Monaco C., Tortorici G. and Tortorici L.; 2008: *Active faulting and seismicity along the Siculo-Calabrian rift zone*. Tectonophysics, **453**, 177-192.

Chappell J. and Shackleton N.J.; 1986: *Oxygen isotopes and sea level*. Nature, **324** (6093), 137-140.

Corsaro R.A. and Cristofolini R.; 2000: *Subaqueous volcanism in the Etnean area: Evidence for hydromagmatic activity and regional uplift inferred from the Castle Rock of Acicastello*. J. Volcanol. Geotherm. Res. **95** (1-4), 209-225.

Corsaro A.R., Neri M. and Pompilio M.; 2002: *Paleo-enviromental and volcano-tectonic evolution of the southeastern flank of Mt. Etna during the last 225 Ka inferred from the volcanic succession of the "Timpe", Acireale, Sicily*. J. Volcanol. Geotherm. Res., **113**, 289-306.

Di Stefano A. and Branca S.; 2002: *Long-term uplift rate of the volcano basement (southern Italy) based on biochronological data from Pleistocene sediments*. Terra Nova, **14**, 61–68.

Gillot P.Y., Kieffer G., and Romano R.; 1994: *The evolution of Mount Etna in the light of potassium-argon dating*. Acta Vulcanol., **5**, 81-87.

Guest J. E., Chester D.K. and Duncan A.M.; 1984: *The Valle del Bove, Mount Etna: its origin and relation to the stratigraphy and structure of the volcano*. J. Volcanol. Geotherm. Res., **21**, 1-23.

La Delfa S., Patanè G., Presti F., and Tringali G.; 2007: *Changing in crust mechanical behaviour due to raising magma: A fracturing model of SE flank of Mt. Etna (Sicily)*. Earth Planet. Sci. Lett., **256**, 493-509.

Monaco C., De Guidi G. and Ferlito C.; 2010: *The morphotectonic map of Mt. Etna*. Boll. Soc. Geol. It., **129** (3), 408-428

Monaco C., Tapponnier P., Tortorici L. and Gillot P.Y.; 1997: *Late Quaternary slip rates on the Acireale-Piedimonte normal faults and tectonic origin of Mt. Etna (Sicily)*. Earth Planet. Sci. Lett., **147**, 125-139.

GEOLOGICAL, SEISMOLOGICAL AND GEODETIC EVIDENCE OF ACTIVE THRUSTING AND FOLDING SOUTH OF MT. ETNA (EASTERN SICILY)

G. De Guidi[1], G. Barberi[2], G. Barreca[1], V. Bruno[2], F. Cultrera[1], S. Grassi[1], S. Imposa[1], M. Mattia[2], C. Monaco[1], L. Scarfì[2], S. Scudero[1]
[1]*Dipartimento di Scienze Biologiche, Geologiche e Ambientali, Sezione di Scienze della Terra, Università di Catania, Italy*
[2]*Istituto Nazionale di Geofisica e Vulcanologia, Osservatorio Etneo, Sezione di Catania, Italy*

Introduction. Mt. Etna volcano is located in eastern Sicily over the front of the collisional fold and thrust belt, where it is cut by the major Aeolian-Tindari-Malta Escarpment lithospheric boundary (Fig.1, Palano *et al.*, 2012). Accordingly, in the Mt. Etna area two distinct tectonic domains, characterized by compressive and tensional regimes, coexist (Cocina *et al.*, 1997; Monaco *et al.*, 2002). They are separated by a NNW-SSE trending boundary composed of en–echelon normal-dextral faults, roughly extending from the summit craters to the northern suburbs of Catania (Fig. 1a). The eastern sector is characterized by normal-oblique faults, related to WNW-ESE regional extension (Monaco *et al.*, 1997), and flank sliding phenomena (Azzaro *et al.*, 2013). Conversely, in the western sector, south of the volcanic edifice, contractional structures mostly occur. They are represented by a W-E trending fold belt that have deformed Pleistocene foredeep deposits in response of NNW-SSE oriented regional compression (Labaume *et al.*, 1990; Catalano *et al.*, 2011; Ristuccia *et al.*, 2013). According to Lavecchia *et al.* (2007) this area is part a unique regional-scale, deep crustal seismogenic structure (named Sicilian Basal Thrust) whose focal mechanisms are compatible with a nearly average N–S shortening and with some field evidence of active fold-and thrust deformation at the Sicilian chain front.

Seismological (Neri *et al.*, 2005), geodetic data (Mattia *et al.*, 2012) and stress in situ measurements (Ragg *et al.*, 1999) confirm the occurrence of a still active compressional regime south of Mt. Etna, accommodated by thrusting and folding. In particular, new interferometric data recorded in the last 20 years, depict a large anticline (named the "Catania anticline") aseismically uplifting at a rate of ~10 mm/yr in the northern outskirts of Catania (Lundgren *et al.*, 2004; Bonforte *et al.*, 2011). In order to verify if this aseismic frontal folding can be related to regional processes, characterized by convergence rates of about 5 mm/yr (Mattia *et al.*, 2012), in this work we have analyzed deep crustal seismicity, geological field information and morphometric data obtained by 2x2m grid resolution DEM. Moreover, to the aim of verifying if strain accumulation is presently occurring on the growing anticline, we surveyed some benchmarks of a GPS network of the Italian Military Geographical Institute (IGMI) realized in 1994 for cartographic and geodetic purposes.

Geological setting. The geodynamic setting of Eastern Sicily (Fig. 1a) is characterized by the Neogene-Quaternary flexure of the African- Pelagian continental paleo-margin beneath the SSE-verging chain, culminating in the south-eastern sectors of the island to form the Hyblean Plateau, the foreland domain (Ben Avraham *et al.*, 1990). Northwards, the Hyblean slab deepens under the chain, intersecting the Moho at a depth of about 30 km (Lavecchia *et al.*, 2007 and reference therein) between the northern coast of Sicily and Mt. Etna (Fig. 1b). In such a geodynamic context, the area between the southern edge of the Mt. Etna volcanic edifice and the Catania Plain represents the remnant of a foredeep domain, filled by Pliocene-Pleistocene sediments and volcanics, and by Holocene alluvial-coastal deposits (Longhitano and Colella, 2001). This sedimentary succession is mostly deformed by an asymmetric south-facing anticline, about 10 km long and ~W-E trending (the "Terreforti anticline", Monaco *et al.*,1997; Labaume *et al.*, 1990) and other minor folds (Catalano *et al.*, 2011). They have been interpreted as thrust propagation folds at the front of the chain, related to the lately migration of the thrust belt, as a response to the regional NNW-SSE compressive tectonic regime (Palano *et al.*, 2012). GPS velocity fields (Ferranti *et al.*, 2008; Mattia *et al.*, 2012), seismological (Lavecchia *et al.*, 2007) and interferometric synthetic aperture radar data (Lundgren *et al.*, 2004; Bonforte *et al*., 2011) suggest that contractional processes are still active and cause the growth of another large anticline (the "Catania anticline") in the north-western outskirts of the town. Fold structures outcropping south of Mt. Etna have also been interpreted as the result of the gravitational spreading of the volcanic edifice of Mt. Etna over the sedimentary substratum (Borgia *et al*., 2000; Solaro *et al*., 2011).

Since the Middle Pleistocene, contractional structures have coexisted with extensional tectonics, as suggested by the occurrence of a NNW-SSE striking oblique (normal-dextral)

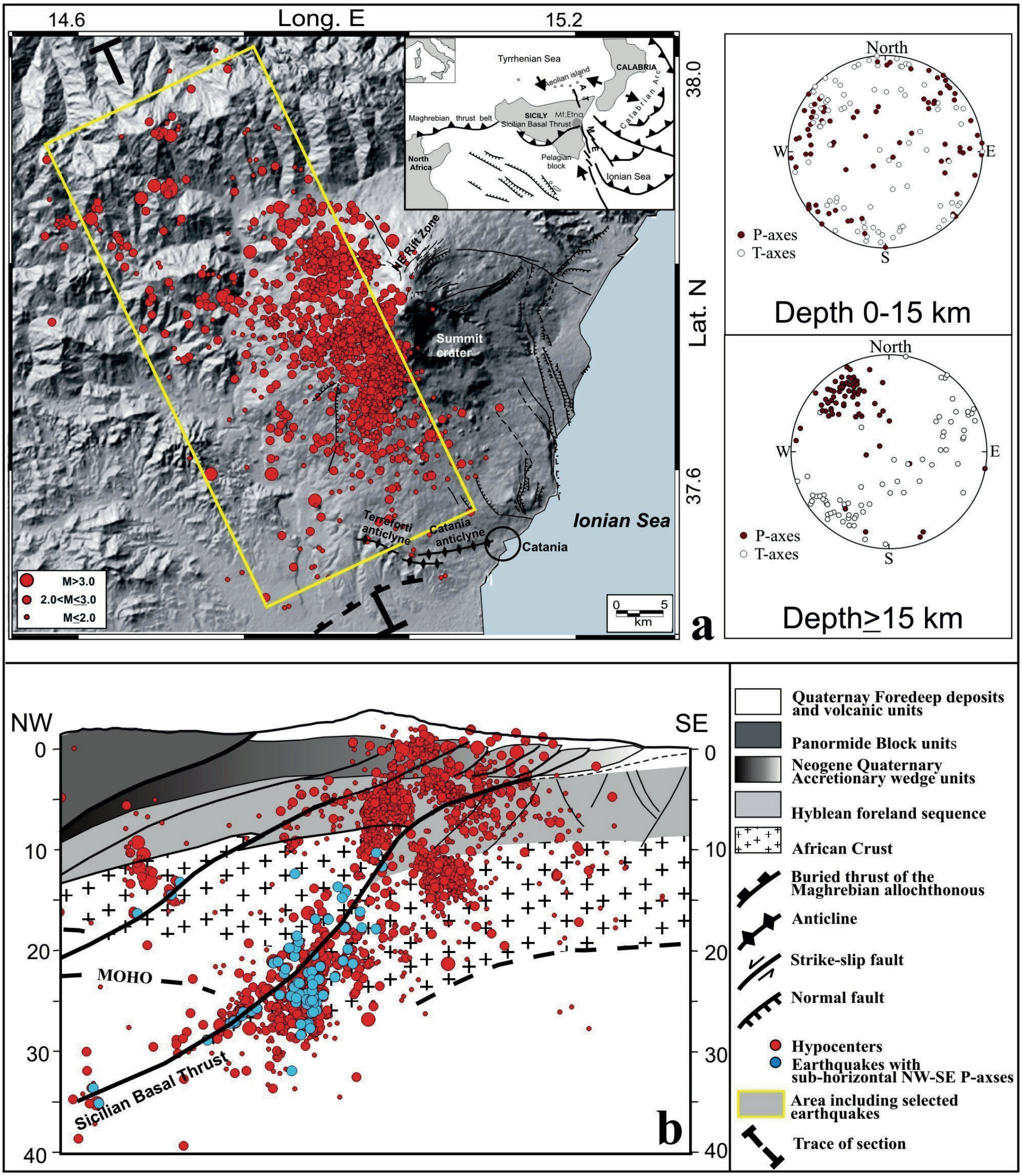

Fig. 1 – a) Quaternary seismotectonic map of Mt. Etna region and stereographic projections of the principal stress axes (P-axes). Earthquakes recorded during the period 1994-2012 are also reported (http://www.ct.ingv.it/ufs/analisti/catalogolist.php). b) Crustal section with projection of the hypocentral distribution and structural interpretation [Moho depth from Lavecchia *et al*., (2007) and references therein].

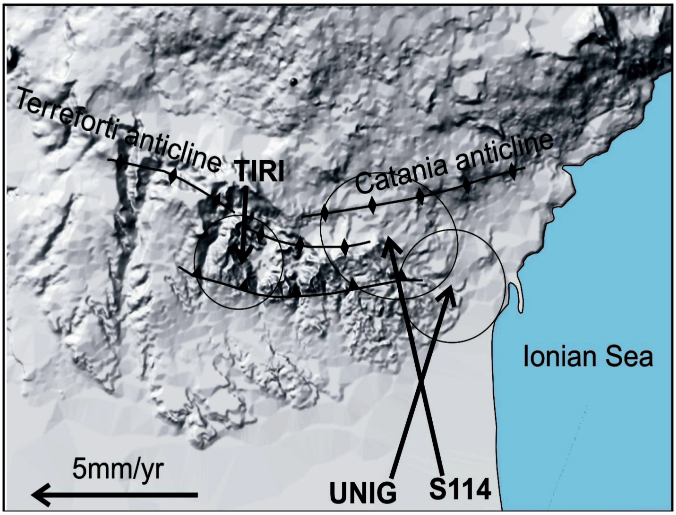

Fig. 2 – Velocity map (1994-2013) of the IGM GPS benchmarks.

fault system running offshore, sub-parallel to the Ionian coast, where it has reactivated the Malta Escarpment (Bianca *et al.*, 1999; Palano *et al.*, 2012). Accordingly, the overall orogenic belt along the eastern Sicily coastal sector has been affected by a rift-driven vigorous tectonic uplift, with rates progressively decreasing southwards from about 2 mm/yr to 1 mm/yr, that, combined with relative sea-level change, has caused the terracing of fluvial and coastal deposits (Ferranti *et al.*, 2006; Spampinato *et al.*, 2012; Ristuccia *et al.*, 2013).

Current tectonic activity is also responsible for the destructive historical earthquakes (M≥7) that occurred in south-eastern Sicily (e.g. 1169 AD, 1693 AD events, Boschi *et al.*, 1995). The location of seismogenic sources is a topic still widely debated: normal faults located along the Ionian offshore (see Bianca *et al.*, 1999 and references therein) and/or compressional structures located to the north and to the south of the Catania Plain, between the front of the chain and the northern margin of the Hyblean foreland (see DISS Working Group, 2010).

Seismicity. We analyzed distribution and kinematics of the earthquakes located in the southern and western sectors of Etna, between the chain, to the north, and the margin of the Hyblean Foreland, to the south (Fig. 1a). We excluded the events located in the eastern sector of the volcano to prevent that the shallow seismicity related to the extensional structures could complicate our analysis. About 2000 earthquakes, with a magnitude ranging between 1.0 and 4.3 and recorded by a local network between 1994 and 2012, were selected from the "*Catalogo dei terremoti della Sicilia Orientale - Calabria Meridionale. INGV, Catania*", (further details about the catalogue at: http://www.ct.ingv.it/ufs/analisti/catalogolist.php). More accurate hypocentres were obtained by relocating the events with advanced techniques, by using a 3D velocity model (from Chiarabba *et al.*, 2004; Patanè *et al.*, 2006) and the software tomoDDPS (Zhang *et al.*, 2009), that provide results with fewer uncertainties than those produced by the use of more simple algorithms. The distribution of earthquakes shows a clear trend of the seismic events to deepen from very shallow hypocenters in the area south of Etna, down to a depth of about 35 km to the NNW (Fig. 1b).

The analysis of the fault plane solutions (see also Scarfì *et al.*, 2013) indicate that the majority of the events are strike-slip or oblique type. Furthermore, a careful analysis of the direction of the principal stress axes (P-axes) reveals that at the shallower and intermediate levels (down to 5 and 10 km), the stress field is inevitably influenced by the deep magmatic system of the volcano, the greater is the proximity to crater area. At greater depths, the regional dynamics is the main driving force with the P-axes NW-SE oriented (Fig.1a).

Gps data. In 1992 the IGMI (Italian Military Geographical Institute - www.igmi.org) started the GPS measuring of a network made up of 1260-bechmarks, extended over the whole Italian area. We have reoccupied three IGMI benchmarks north and south the Catania Anticline (Figs. 1a and 2) in order to calculate the velocities map of some benchmarks very close to the alignment revealed by interferometric data. The GPS survey was carried out by using Leica GX1220 receivers and AR10 antennas, while instruments used by the IGM in

1994 were Trimble 4000 SSE receivers and Trimble compact with ground plane (model 22020-00) antennas. GPS data have been processed using the GAMIT/GLOBK software (Herring *et al.*, 2006) with IGS (International GNSS Service) precise ephemerides and Earth orientation parameters from the IERS (International Earth Rotation Service). We tied the measurements to an external global reference frame by including in our analysis the data from seven CGPS stations belonging to the IGS and EURA networks and operating since 1994 (GRAZ, HERS, JOZE, MADR, ZIMM). The quasi-observations were then combined with global solutions (IGS1, IGS2, EURA) provided by the Scripps Orbital and Permanent Array Center (SOPAC) at UC San Diego. The loosely constrained daily solutions were transformed into ITRF2005 (2005 International Terrestrial Reference Frame; Altamimi *et al.*, 2007) and then rotated into a fixed Eurasia frame.

Preliminarily, the Eurasian velocity field shows that the two GPS stations south of the anticline (UNIG, S114) move with velocities ranging from about 4 to 7 mm/yr along NNW to NNE directions, whereas the station located north of the structure (TIRI) move to the SSW with velocity of about 2 mm/yr (Fig. 2). This results are consistent with NNW-SSE vectors obtained by permanent stations (Mattia *et al.*, 2012), related to the Africa-Europe convergence process (with the exception of the TIRI benchmark that could be affected by the dynamics of the volcano).

Morphostructural data. New field surveys were performed with the aim to verify if ground deformation provided by satellite data agree with geological and morphological features. The Catania Anticline is located in a volcanic and strongly anthropized area. So, field evidence of active thrusting and folding is difficult to observe. However, preliminary results indicate that the differential ground motion provided by interferometric data (Lundgren *et al.*, 2004; Bonforte *et al.*, 2011) matches with the vertical deformation of the drainage network along the hinge of a large WSW-ENE trending anticline west of the urban area of Catania. Moreover, high resolution topographic profiles obtained by 2x2 m grid DEM show the occurrence of bulging coaxial with the hinge zone (Fig. 2).

Information on geometric relationships between the growing anticline and the underlying thrust is lacking. However, thrust-related anticlines can be described by three end-member geometries, depending on the relationships between thrusts and the overlying anticlines: fault-bend folding, fault-propagation folding and detachment folding (see Storti and Poblet, 1997 and references therein). Combining the 5-6 mm/yr shortening across the anticline with the 10 mm/yr of the corresponding uplift, the hypothetical slip on a unique shear surface would result on a >60° dipping plane. Such attitude is unrealistic for a thrust ramp, therefore we exclude fault-propagation folding or fault-bend folding models (Fig. 3). Conversely, kinematic models have shown how detachment fold model can account for uplift rate greater than shortening, in particular in the early stages of the anticline (Storti and Poblet, 1997). An incipient sub-horizontal detachment within the clayish foredeep deposits or at the top of the buried foreland sequence is clearly showed by seismic profiles (Torelli *et al.*, 1998).

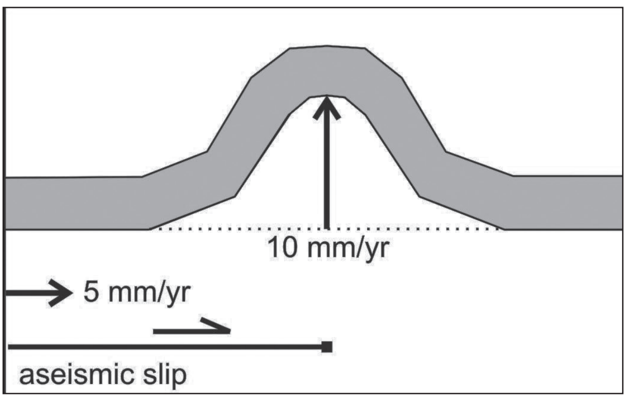

Fig. 3 – Kinematic model of detachment folding in the area south of Mt. Etna.

Discussion and conclusion. Geological and morphological analysis, compared with seismological and geodetic data, suggest that a compressive regime currently occurs in the western sector of Mt.

Etna, accommodated by aseismic folding at the front of the chain, south of the volcanic edifice, and seismogenic oblique thrusting at crustal depth under the northwestern sector of the volcano. Moreover, the NNW-SSE direction of the axis of compression obtained by seismological data is consistent with that suggested by geological and geodetic data.

In particular, a large WSW-ENE trending anticline is growing west of Catania (the Catania anticline). For its location, within a middle-late Pleistocene fold system, and growth rates, consistent with detachment fold models, we exclude that this structure have only developed in response to volcanic spreading, as proposed by previous authors. Moreover, the gentle slope of the southern flank of the volcano (5-6° on average) would not be a sufficient gradient to drive the process and, mainly, the steady deformation growth rate is in contrast with the episodic magmatic injections that are invoked as another promoting mechanism of the spreading. We therefore propose the occurrence of detachment folding at the chain front, as response of a shallow thrust migrating within the clayish foredeep deposits or at the top of the buried foreland sequence.

In conclusion, our analysis confirms that, besides the activity related to the volcanic feeding system, the seismic pattern under Mt. Etna edifice can be certainly related to the regional dynamics. The compressive stress is converted into elastic accumulation and then in earthquakes along the ramps to the rear of the chain, whereas along the frontal detachment it is accommodated by aseismic ductile deformation. In fact, despite the high rates of convergence, the seismicity is moderate at the front of the chain and the “seismic efficiency” of the Sicilian Basal Thrust is greater in correspondence of ramps at the rear, where strong earthquakes can occur.

Acknowledgement. This work was funded by a DPC-INGV 2012 grant, Project V3 “Multi-disciplinary analysis of the relationship between tectonic and volcanic activity” and by grant of University of Catania - PRA n. 20104001082 -.

References

Altamimi Z., Collilieux X., Legrand J., Garayt B., Boucher C. 2007. ITRF2005: A new release of the International Terrestrial Reference Frame based on time series of station positions and Earth Orientation Parameters. Journal of Geophysical Research, 112, B09401.

Azzaro R., Bonforte A., Branca S., Guglielmino F. 2013. Geometry and kinematics of the fault systems controlling the unstable flank of Etna volcano (Sicily). Journal of Volcanology and Geothermal Research, 251, 5-15.

Ben-Avraham Z., Boccaletti M., Cello G., Grasso M., Lentini F., Torelli L., Tortorici L. 1990. Principali domini strutturali originatisi dalla collisione neogenico-quaternaria nel Mediterraneo centrale. Memorie Società Geologica Italiana, 45, 453-462.

Bianca M., Monaco C., Tortorici L., Cernobori L. 1999. Quaternary normal faulting in southeastern Sicily (Italy): a seismic source for the 1693 large earthquake. Geophysical Journal International, 139, 370-394.

Bonforte A., Guglielmino F., Coltelli M., Ferretti A., Puglisi G. 2011. Structural assessment of Mount Etna volcano from Permanent Scatterers analysis. Geochemistry Geophysics Geosystems, 12, 19 pp. Q02002, doi:10.1029/2010GC003213.

Borgia A., Lanari R., Sansosti E., Tesauro M., Berardino P., Fornaro G., Neri M., Murray J.B. 2000. Actively growing anticlines beneath Catania from the distal motion of Mount Etna’s decollement measured by SAR interferometry and GPS. Geophysical Research Letters, 27(20), 3409-3412.

Boschi E., Ferrari G., Gasperini P., Guidoboni E., Smriglio, G., Valensise G. 1995. Catalogo dei forti terremoti in Italia dal 461 a.C. al 1980. ING-SGA, Bologna, 973 pp.

Catalano S., Torrisi S., Tortorici G., Romagnoli G. 2011. Active folding along a rift-flank: The Catania region case history (SE Sicily). Journal of Geodynamics, 51, 53-63.

Chiarabba C., De Gori P., Patane` D. 2004. The Mount Etna plumbing system: the contribution of seismic tomography. In Mt. Etna: Volcano Laboratory, A. Bonaccorso, S. Calvari, M. Coltelli, C. Del Negro, S. Falsaperla, Ed., Geophysical Monograph Series, American Geophysical Union, Washington, DC, vol. 143, pp. 191-204.

Cocina O., Neri G., Privitera E., Spampinato S. 1997. Stress tensor computation in the Mount Etna area and tectonic implications. Journal of Geodynamics, 23, 109-127.

DISS Working Group 2010. Database of Individual Seismogenic Sources (DISS), Version 3.1.1: A compilation of potential sources for earthquakes larger than M 5.5 in Italy and surrounding areas. http://diss.rm.ingv.it/diss/, © INGV 2010.

Ferranti L., Antonioli F., Mauz B., Amorosi A., Dai Pra G., Mastronuzzi G., Monaco C., Orrù P., Pappalardo M., Radtke U., Renda P., Romano P., Sansò P., Verrubbi V. 2006. Markers of the last interglacial sea level highstand along the coast of Italy: tectonic implications. Quaternary International, 145-146, 30-54.

Herring T.A., King R.W., McClusky S.C. 2010. Introduction to GAMIT/GLOBK, Release576 10.4, MIT, Cambridge, MA, 48pp.

Labaume P., Bousquet J. C., Lanzafame G., 1990. Early deformation at a submarine compressive front: the Quaternary Catania foredeep south of Mt. Etna, Sicily, Italy. Tectonophysics 177, 349-366.
Lavecchia G., Ferrarini F., De Nardis R., Visini F., Barbano M.S. 2007. Active thrusting as a possible seismogenic source in Sicily (Southern Italy): Some insights from integrated structural-kinematic and seismological data. Tectonophysics, 445, 145-167.
Longhitano S., Colella A. 2007. Geomorphology, sedimentology and recent evolution of the anthropogenically modified Simeto River delta system (eastern Sicily, Italy). Sedimentary Geology 194, 195-221.
Lundgren P., Casu F., Manzo M., Pepe A., Berardino P., Sansosti E., Lanari. R. 2004. Gravity and magma induced spreading of Mount Etna volcano revealed by satellite radar interferometry. Geophysical Research Letters 31, L04602, doi:10.1029/2003GL018736.
Mattia M., Bruno V., Cannavò F., Palano M. 2012. Evidences of a contractional pattern along the northern rim of the Hyblean Plateau (Sicily, Italy) from GPS data, Geologica Acta, 10, 1-9.
Monaco C., Tapponnier P., Tortorici L., Gillot P.Y. 1997. Late Quaternary slip rates on the Acireale-Piedimonte normal faults and tectonic origin of Mt. Etna (Sicily). Earth Planetary Science Letters, 147, 125-139.
Monaco C., Bianca M., Catalano S., De Guidi G., Tortorici L. 2002. Sudden change in the late Quaternary tectonic regime in eastern Sicily: evidences from geological and geomorphological features. Bollettino Società Geologica Italiana, 1, 901-913.
Neri G., Barberi G., Oliva G., Orecchio B. 2005. Spatial variations of seismogenic stress orientations in Sicily, south Italy. Physics of the Earth and Planetary Interiors, 148, 175-191.
Palano M., Ferranti L., Mattia M., Monaco C., Aloisi M., Bruno V., Cannavò F., Siligato G. 2012. GPS velocity and strain fields in Sicily and southern Calabria, Italy: updated geodetic constraints on tectonic block interaction in the central Mediterranean. Journal of Geophysical Research 117, 1-12.
Patanè D., Barberi G., Cocina O., De Gori P., Chiarabba C. 2006. Time-Resolved Seismic Tomography Detects Magma Intrusions at Mount Etna. Science, 313, 821-823.
Ragg S., Grasso M., Muller B. 1999. Patterns of tectonic stress in Sicily from borehole breakout observations and finite element modeling. Tectonics, 18 (4), 669-685.
Ristuccia G.M., Di Stefano A., Gueli A.M., Monaco C., Stella G.,Troja S.O. 2013. OSL chronology of Quaternary terraced deposits outcropping between Mt. Etna volcano and the Catania Plain (Sicily, southern Italy). Physics and Chemistry of the Earth, 63, 36-46.
Scarfì L., Messina A., Cassisi C. 2013. Sicily and Southern Calabria focal mechanism database: a valuable tool for the local and regional stress field determination. Annalas of Geophysics, 56, 1, D0109, doi:10.4401/ag-6109.
Solaro G., Acocella V., Pepe S., Ruch J., Neri M., Sansosti E. 2010. Anatomy of an unstable volcano from InSAR: Multiple processes affecting flank instability at Mt. Etna, 1994-2008. Journal of Geophysical Research, 115, B10405, doi:10.1029/2009JB000820.
Spampinato C., Scicchitano G., Ferranti L., Monaco C. 2012. Raised Holocene paleo-shorelines along the Capo Schisò coast, Taormina: New evidence of recent co-seismic deformation in northeastern Sicily (Italy). Journal of Geodynamics, 55, 18-31.
Torelli L., Grasso M., Mazzoldi G., Peis D. 1998. Plio–Quaternary tectonic evolution and structure of the Catania foredeep, the northern Hyblean Plateau and the Ionian shelf (SE Sicily). Tectonophysics, 298 209–221.
Zhang H., Thurber C., Bedrosian P. 2009. Joint inversion for Vp, Vs, and Vp/Vs at SAFOD, Parkfield, California, Geochemistry Geophysics Geosystems, 10:Q110032, doi:10.1029/2009GC002709.

FIRST PALEOSEISMIC RESULTS FROM THE MOUNT MORRONE FAULT (SULMONA, CENTRAL APENINNES)

P. Galli[1,2], B. Giaccio[2], P. Messina[2], E. Peronace[2], B. Quadrio[2], J. Bellanova[3], S. Piscitelli[3]
[1]*Dipartimento della Protezione Civile Nazionale, Roma*
[2]*CNR-IGAG, Roma*
[3]*CNR-IMAA, Potenza*

Introduction. At the end of the past century, Galadini and Galli (1999, 2000) claimed the existence of at least two parallel sets of seismogenetic fault systems running along the backbone of central Apennines. The western one has been responsible for all the main Mw>6.5 historical earthquakes, whereas they defined the eastern one as *silent* (i.e., no historical earthquake associated with), estimating an elapsed time since the last fault rupture longer than 1500 years. As historical and paleoseismological studies have demonstrated that this time often exceeds the average recurrence interval for Mw≥6.5 Apennine earthquakes (e.g. in Galli *et al.*, 2008), they concluded that future strong earthquakes might preferentially occur along faults of this eastern set.

The NW-SE trending Mount Morrone fault is one of these silent faults, affecting with its two splays the hillslope facing the intermontane Sulmona Plain (Fig. 1). Here Vittori *et al.* (1995) reported the displacement of Late Pleistocene alluvial fan sediments along the western fault splay, while Galadini and Galli (2000) showed the offset of Late Pleistocene slope deposits along the eastern splay, providing also an overall, long-term (1 Ma), vertical slip-rate of 0.5-0.66 mm/yr. Recently, Gori *et al.* (2010, 2011) published new robust evidence of Late Pleistocene fault activity which was also accompanied by large scale gravity deformations.

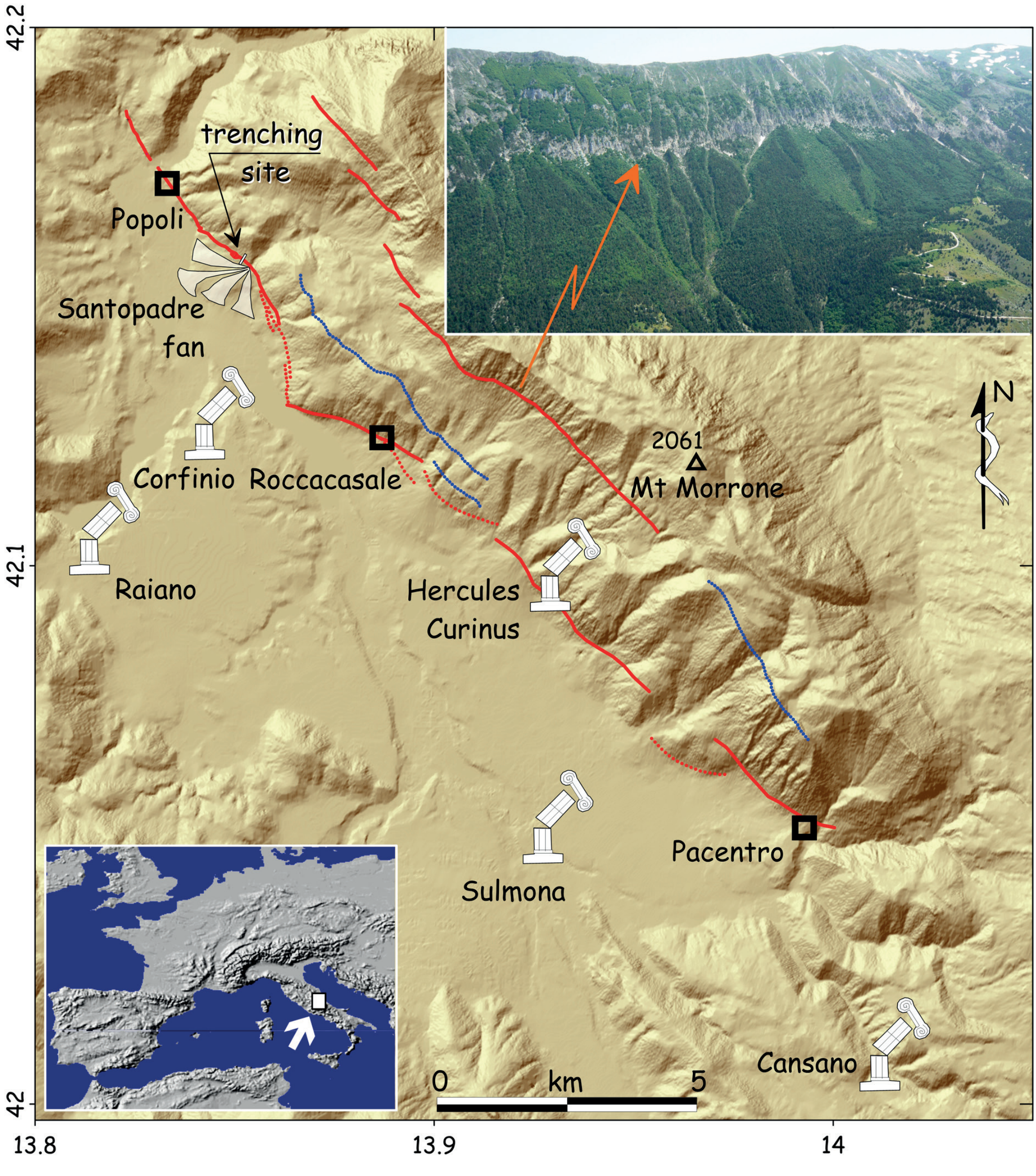

Fig. 1 – DEM of the Sulmona Plain. Red lines are the western basal splay, and the upper eastern (right inset) splay of the Mount Morrone fault system. In blue the trace of the trenches of the main, NE-dipping, deep seated gravity slides affecting the whole fault-slope. Collapsing columns indicate the site with archaeoseismic evidence for a 2nd century AD earthquakes (mod. from Galadini and Galli, 2001). Upper inset, aerial view looking east of the rock-fault scarp along the eastern fault splay.

On the other hand, neither important historical earthquakes nor moderate instrumental epicentres are known to be occurred within the Sulmona Plain or can be attributed to this fault system. The only indication of possible, local seismic activity is provided by the archaeoseismic investigations carried out by Galadini and Galli (2001), who hypothesized that a large magnitude event hit several settlements in the Sulmona Plain around the middle of 2nd century AD (Fig. 1; see also Ceccaroni *et al.*, 2009). According to these authors the earthquake was likely generated by the Mount Morrone fault rupture.

Notwithstanding all these indications, the lack of certain (i.e., directly dated through radiometric analyses) post Last Glacial Maximum (LGM)-Holocene deposits affected by the fault prevented any conclusive assessment regarding the recent activity of this structure. Therefore, in order to cast light on this debated issue, following aerial photo and LiDAR interpretation, geological field surveys, high-precision topographic levelling, and geoelectrical investigations (ERT), we have finally decide to open a first set of three paleoseismological trenches across the western basal fault.

The Mount Morrone fault system. The Mount Morrone fault system is expressed at surface by two main, discontinuous fault splays which roughly parallel the western slope of the massif, for a total length of 22 km (Fig. 1). The eastern one runs mainly at 1100-1200 m a.s.l., and it is evidenced by an impressive, up to 50-m-high rock fault scarp within the Jurassic limestone (upper inset in Fig. 1). In the hanging wall, it affects a thick sequence of slope debris which likely formed during the cold and arid phases of the LGM (Galadini and Galli, 2000). In turn, the western splay runs along the base of the foothill, roughly between 300-400 m a.s.l., from the northern outskirts of Popoli to the Pacentro village. In some sector of the slope the western fault is evidenced by a rock-fault scarp (e.g., Roccacasale strand), with an outcropping, smoothly polished plane (slickenside) carved in the carbonate footwall (e.g. in Boncio *et al.*, 2012). However, most of its surficial trace is buried below several, active and coalescing alluvial fans which mantle the whole piedmont of Mount Morrone. All together, these fans form an alluvial apron, the distal limb of which rests over the upper terrace of the Sulmona Plain (350-380 m a.s.l.). Several quarries opened in these fans allowed the observation of metre-scale displacements of the Late Pleistocene deposits, even if these always concerned secondary faults, i.e. N-S transfer faults between *en echelon* strands (Vittori *et al.*, 1995).

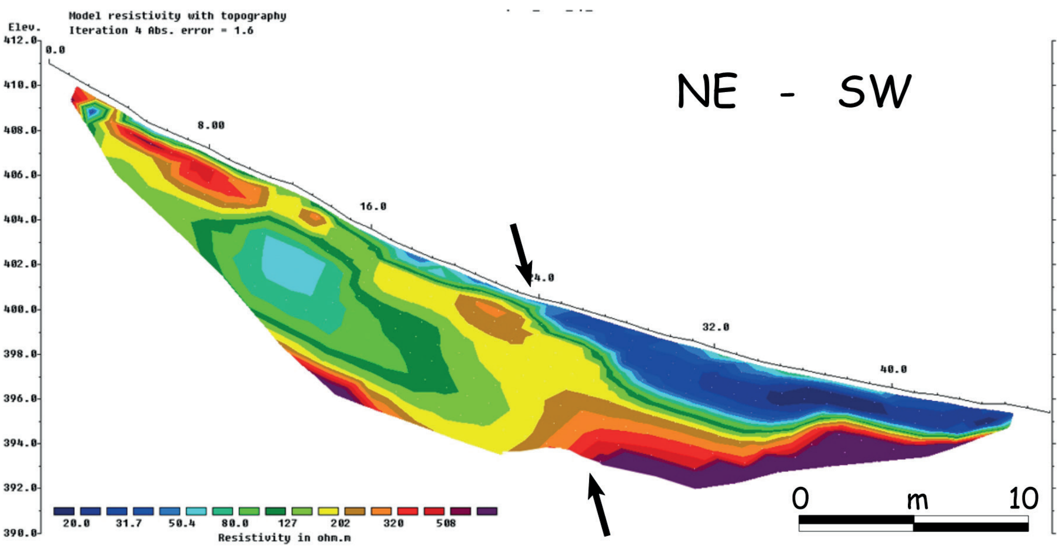

Fig. 2 – ERT profile across the northwestern, basal splay of the Mount Morrone fault system. Arrows indicate the possible fault position. Blue area match very low resistivity deposits, i.e. silty-clayey colluvia. Upper inset: view looking N of the slope where we have made ERT 1 and trench 1.

Paleoseismological trenches. In the northernmost sector of the Sulmona Plain, at the deeply entrenched mouth of the Malepasso Valley (ca. 400 m a.s.l.), the basal fault splay offsets by 12 m the apex of the Late Pleistocene Santopadre alluvial fan. This is a composite fan which formed at least during four different alluvial phases, each one linked to a different base level, with the younger terraces progressively carved into the older and higher ones. The youngest and still active phase forms a telescopic fan which opens in the present alluvial plain at ca. 250 m a.s.l. (i.e., the same elevation of the neighbour Sulmona Basin outlet, in Popoli), whereas the oldest and highest one has a top surface reaching ca. 400 m a.s.l. in the fault hanging wall. Its base level was reasonably the mentioned upper terrace of the Sulmona Plain (locally at 340 m a.s.l.), whereas the minimum age of its original top-surface can be inferred by the presence of an idiosyncratic tephra outcropping extensively up to 3-4 meters below this. Indeed, on the basis of the chemical, isotopic and textural feature (see also Giaccio *et al.*, 2007), the tephra can be associated to a well-known volcanic level spread all over the central Apennines, and attributed to the last explosive activity of the Albano Maar (Colli Albani volcanic district, Rome; 36±1 kyr, Freda *et al.*, 2006; Giaccio *et al.*, 2009).

Along the northern tail of the fan, where this joins and interfingers with the Colle Ferrano slope talus, the fault is revealed by a subdued scarp which is deeply reshaped, and retreated uphill by millennial agricultural works. We decided to open here the first three paleoseismological trenches, which have been preceded by one electrical resistivity tomography (ERT), and by several high precision topographic levelling.

The ERT survey was performed by means of a Syscal R2 (Iris Instruments) resistivity meter, coupled with a multielectrode acquisition system (48 electrodes), with a constant spacing of 1 m between adjacent electrodes. Along the profile, we applied different array configurations (Wenner-Schlumberger and Dipole-Dipole), obtaining an investigation depths of about 10 m. The apparent resistivity data were inverted using the RES2DINV software (Loke, 2001) to obtain the 2D resistivity images of the subsurface. The best result was obtained from the Wenner-Schlumberger data which have shown a higher signal-to-noise (s/n) ratio, a larger investigation depth and a better sensitivity pattern to both horizontal and vertical changes in the subsurface resistivity. Root Mean Squared (RMS) error was less than 2%, with resistivity values ranging from 20 to more than 508 Ωm (Fig. 2).

Around the middle of the NE-SW trending section, the ERT evidences a sharp lateral contact between terrains with different resistivity values. The whole SW side is characterized by a couple of layers with high (bottom, >300 ohm*m), and very low (top, <30 ohm*m) resistivity values, whereas the NE side has intermediate values (>50 ohm*m <400; Fig. 2). Both the sharp lateral contact (presumably the fault) and the presence of low resistivity deposits (reasonably matching with silty colluvia) in the supposed hanging wall, oriented here the opening of the first three trenches.

In the footwall, all the trenches unveiled clearly the upper sequence of the oldest Santopadre alluvial fan (left side of Fig. 3) which contains here a brownish pedogenized layer very rich in the volcanic minerals colluviated from the 36 ka Albano tephra layer. This immature paleosol is truncated by other few alluvial gravel layers - also with abundant reworked tephra minerals in the matrix - which are interfingered and progressively substituted upward by slope debris. All these units are faulted against different generation of reddish and brownish colluvia in the hangingwall (right side in Fig. 3), resting over a stiff alluvial sandy unit. The fault plane trends here N110°, dipping 65° southward.

The geometry of the faulted succession account for four rupture events, each one evidenced by colluvial wedges, tectonic wedge filled by scarp-derived deposits, secondary splays and fractures and warping of the sedimentary units.

The entire sedimentary succession has been chronologically constrained by eleven radiocarbon dating performed in the Beta Analytic Inc. laboratories through AMS analyses. Leaving aside the footwall deposits, which contain and surely postdate the reworked 36 ka Albano tephra layer, the hanging wall colluvia fall all inside the Holocene, from ca. 9 ka to Modern time.

By comparing and cross-matching the results obtained in the three trenches, we are able to constrain very well the age of the last surface rupture event which has occurred contemporary or slightly after 80-130 AD (1s calibrated age), and before 130-220 AD (1s calibrated age). In turn, due to a stratigraphical hiatus spanning between the High Middle Age (post 9th cent. AD) and the Modern Age (before 17th cent.), we cannot evaluate the entire coseismic surficial slip of this event. Therefore, the measured vertical offset of 0.4 m has to be regarded as a minimum estimate.

A previous event might be occurred considerably after 5 ka, but slightly before 4150-3980 BP (2s calibrated age). Before this, other two events have likely occurred post 9440-9140 BP, although we are not able to provide more precise interval.

In the whole, by considering the age of the colluvial units in the hanging wall, we can estimate a minimum vertical slip rate for this splay of 0.44 mm/yr during the Holocene. This value is in the same order of the one that can be calculated by measuring the vertical offset of the top surface of the oldest fan at the Malepasso Valley mouth, and also in other places along the foothill of Colle Ferrano, near our trenching site. Indeed, as we have measured a cumulated vertical offset of 11-12 m in several profiles across the main fault (see methodology in Galli *et al.*, 2013), plus other 3 m across a secondary splay in the hanging wall, if we do consider an age younger than 36 ka for the top-surface of the oldest fan, the minimum vertical slip rate is ca. 0.43 mm/yr.

From all the above it emerges that the Mount Morrone fault system ruptured the last time ca. 1850-1900 years ago, and again ca. 2000 years before. Then, it likely ruptured two more times between 5 kyr and 9 kyr BP. This would yield a rough, average recurrence time close to 2 kyr, which is also the elapsed time since the last earthquake.

As far as the last earthquake is concerned, it is worth noting that the very narrow time-span defined by the AMS dating of *post-quem*, *ad-quem*, and *ante-quem* terms in the trenches fits with the period (half of 2nd century AD) in which Galadini and Galli (2001) have placed the earthquake that destroyed the Roman Sulmo and the neighbouring settlements (i.e., Interpromium=San Clemente a Casauria; Hercules Curinus sanctuary; Cansano; Raiano;

Fig. 3 – View looking SE of trench 1 (net 1 m). The footwall (left side) is made up by well-organized gravels deposited during the final activity of the oldest cycle of the Santopadre alluvial fan (post 36 ky BP). The hanging wall (right side) hosts different generations of Late Holocene slope colluvia (9 ka to Present), beside colluvial and tectonic wedges. Note the fault plane, here striking N110°.

Corfinio; Fig. 1). Therefore, it seems realistic to conclude that such an earthquake was generated by the (at least) 22-km-long rupture of the Mount Morrone fault, with a rough energy release approximating a Mw 6.5 event, as suggested by the empirical relationship between Apennine fault length and magnitude (Galli *et al.*, 2008).

Considering the number of residents in the region, the vulnerability class of each building, and cross-matching these with the possible shaking effects in each locality (i.e., macroseismic site intensity attenuated from the epicentre), if an earthquake like this were to occur now on this fault, it would cause a very severe damage scenario, with thousands of collapses and inhabitants involved in the ruins, both in the Sulmona Plain and in the neighbouring zones.

Acknowledgments and notes. We are grateful to the municipality of Popoli, and in particular to Arch. F. Visconti, who provided us all the permissions and the facilities for excavating our trenches. We thank the members of the Marino's family who allowed the excavations in their olive grove. We also thank P. Boncio, F. Galadini and A. Pizzi who discussed with us the rupture-events inside the trenches. M. Quigley kindly reviewed the manuscript.
Damage scenario caused by the fault rupture derives from FaCES (Fault Controlled Earthquake Scenario; Galli *et al.*, 2002). The views and conclusions contained here are those of the authors, and should not be interpreted as necessarily representing official policies, either expressed or implied, of the Italian Government.

References

Boncio P., Galli P., Naso G., Pizzi A.; 2012. *Surface Fault Rupture Hazard along normal faults: insight from the 2009 L'Aquila earthquake (Mw 6.3, central Italy), observations from global normal faulting earthquakes and implications for earthquake fault zoning*. Bull. of the Seism. Soc. Am., **102**, 918-935.

Ceccaroni E., Ameri G., Gomez Capera A.A., Galadini F.; 2009: *The 2nd century AD earthquake in central Italy: archeoseismological data and seismological implications*. Nat Hazards, **50**, 335–359.

Freda C., Gaeta M., Karner D.B., Marra F., Renne P.R., Taddeucci J., Scarlato P., Christensen J., Dallai L.; 2006: *Eruptive history and petrologic evolution of the Albano multiple maar (Alban Hills, Central Italy)*. Bull. Volcanol., **68**, 567–591.

Galadini F., Galli, P.; 1999: *The Holocene paleoearthquakes on the 1915 Avezzano earthquake faults (central Italy): implications for active tectonics in Central Apennines*. Tectonophysics, **308**, 143-170.

Galadini F., Galli P.; 2000: *Active tectonics in the central Apennines (Italy) – Input data for seismic hazard assessment*. Natural Hazards, **22**, 202-223.

Galadini F., Galli P.; 2001: *Archaeoseismology in Italy: case studies and implications on long-term seismicity*. J. of Earthquake Engineering, **5**, 35-68.

Galli P., Orsini G., Bosi V., Di Pasquale G., Galadini F.; 2002: *Testing damage scenarios. From historical earthquakes to silent active faults*, Abstract EGS02-A-03979 of the European Geophys. Society XXVI General Assembly, NH4, Nice, France, 21-26 April 2002.

Galli P., Galadini, F., Pantosti, D.; 2008: *Twenty years of paleoseismology in Italy*. Earth Science Reviews, **88**, 89-117.

Galli P., Peronace E., Quadrio B., Esposito G.; 2013: *Earthquake fingerprints along fault scarps: A case study of the Irpinia 1980 earthquake fault (southern Apennines).* Geomorphology, http://dx.doi.org/10.1016/j.geomorph.2013.09.023, in press.

Giaccio B., Sposato A., Gaeta M., Marra F., Palladino D.M., Taddeucci J., Barbieri M., Messina P., Rolfo M.F.; 2007: *Mid-distal occurrences of the Albano Maar pyroclastic deposits and their relevance for reassessing the eruptive scenarios of the most recent activity at the Colli Albani Volcanic District, Central Italy*. Quat. Int., **171-172**,160-178.

Giaccio B., Marra F., Hajdas I., Karner D.B., Renne P.R., Sposato A.; 2009: *40Ar/39Ar and 14C geochronology of the Albano maar deposits: implications for defining the age and eruptive style of the most recent explosive activity at the Alban Hills volcanic district, Italy*. Journal of Volcanology and Geothermal Research, **185**, 203-213.

Gori S., Galadini F., Galli P., Giaccio B., Messina P., Sposato A., Falcucci E., Dramis F.; 2010: *Active normal faulting and large scale gravitational deformation: the case of the Mt. Morrone SW slopes (central Apennines, Italy)*. Rend. Online Soc. Geol. It., **11**, 23.

Gori S., Giaccio B., Galadini F., Falcucci E., Messina P., Sposato A., Dramis F.; 2011: *Active normal faulting along the Mt. Morrone south-western slopes (central Apennines, Italy)*. Int. J. Earth. Sci. (Geol. Rundsch.), **100**, 157-171.

Loke M.H.; 2001: *Tutorial: 2-D and 3-D electrical imaging surveys. I: Course notes for USGS workshop "2-D and 3-D inversion and modeling of surface and borehole resistivity data*". Storrs, CT, 13-16 March 2001.

Vittori E., Cavinato G.P., Miccadei E.; 1995: *Active faulting along the northeastern edge of the Sulmona basin, central Apennines, Italy*. In: Serva L., Slemmons B.D. (eds.), Perspective in paleoseismology. Special Publication-Association of Engineering Geologists, **6**, 115-126.

THE 2012 EMILIA SEQUENCE: APPLICATION OF AN AUTOMATIC PROCEDURE TO DETERMINE MOMENT MAGNITUDE

A. Gallo[1,2], G. Costa[2], P. Suhadolc[2]
[1]*AREA Science Park – Trieste, Italy*
[2]*Seismological Research and Monitoring Group, Department of Mathematics and Geosciences, University of Trieste, Italy*

On May 2012 a seismic sequence took place in the Emilia Romagna region, northern Italy. The two main-shocks on May 20 and May 29 with M_L=5.9 and M_L=5.8, respectively, were followed by several relevant aftershocks with M_L>4. Using a procedure implemented by the SeisRaM group of the Department of Mathematics and Geosciences of the University of Trieste, the seismic moment is estimated, as well as the moment magnitude and the corner frequency of the events recorded by strong motion instruments. The goals of this procedure are: the rapid determination of earthquake parameters and an interface to obtain a fast and reliable communication of the parameters related to the seismic events to the Civil Defense. We analyze a strong-motion dataset consisting of high-quality records (among which the two main events and several aftershocks with magnitudes ranging from 3 to 5) obtained by the National Strong Motion Network (RAN).

The RAN is distributed on the Italian territory to record earthquakes of medium and high intensity. It is managed by the Seismic Monitoring Service of the Territory within the Seismic and Volcanic Risks Office of the Civil Protection Department (DPC) in Rome (Gorini *et al.*, 2010; Zambonelli *et al.*, 2011). RAN has more than 500 digital stations equipped with a GSM modem or GPRS, connected to the RAN data capture Centre of Rome (*last update: 20 May 2011*). The Antelope® software (BRTT, Boulder) that collects and archives data, and the SeisRaM procedure to determine moment magnitude and all seismic source parameters in near real-time (Gallo *et al.*, 2013), is now installed also at DPC for managing and analyzing recorded data.

The SeisRaM procedure is extensively described in Gallo *et al.* (2013), but we recall here only the main aspects. Using spectral analysis, the seismic source parameters are calculated following Andrews (1986). The source model used is a simple ω^2 model proposed by Brune (1970, 1971). For the attenuation we use the Q frequency-depend attenuation factor (Console and Rovelli, 1981) and we assume a body-waves theory for the geometrical spreading. From the corrected amplitude spectra the corner frequency also the Brune low-frequency spectrum amplitude and the seismic moment are computed. Finally, the moment magnitude is determined according to the Kanamori (1979) formula. The procedure starts by taking the event location, Richter magnitude (Richter, 1935), P and S phases, signals and instrumental response from Antelope databases. We remove the average, trend, spike and instrumental response. We limit ourselves to events with epicentral distances up to the maximum of 70 km, in order to respect the assumption of the spherical geometrical decay. It is essential to determine the frequency range over which the observed spectral levels are significantly higher than noise. We select band pass corner frequencies using SNR. The minimum frequency corresponding to the first value for which SNR > 2.5, the maximum frequency the last value for which SNR > 5. Following Ottemoller and Havskov (2003), in the selected frequency window the SNR average must be everywhere larger than 1.5. This additional requirement that the average ratio between signal and noise spectral amplitude in the selected frequency range be above a threshold value, allows to choose the final frequency window and to avoid processing only noise. We apply a Butterworth band pass filter, and then we obtain accelerations, velocities and displacements from the derivative or the integral of the signal. We apply the Fast Fourier Transform (FFT) to obtain the signal spectra. Then we correct them for geometrical spreading and intrinsic attenuation to retrieve the source spectra. At the end we calculate seismic moment and moment magnitude and strong motion parameters like as PGA, PGV Arial and Housner intensity, and store these results in a database table. A report is also generated within 10 min from the event.

The Emilia 2012 seismic sequence was a great opportunity to validate our procedure. In Tab. 1 we report the results of the events with ML>5 in which the location, the local magnitude ML (Richter, 1935) calculated by Antelope® software, the moment magnitude, the seismic moment, the corner frequency estimation are reported. The error on our moment magnitude estimation represents the variance and is linked to the number of stations selected by the procedure inside the range of distance defined a priori (0-70 km).

Tab. 1 – List of the results regarding the events of the Emilia 2012 sequence. The location is automatically calculated by Antelope® software; M_L represents the Richter magnitude by Antelope® software; M_W,M_0, f_0 and eqR are the moment magnitude, the seismic moment, corner frequency and the equivalent radius calculated by our procedure in near-real time following Andrews (1986); ERR represents the variance linked to the number of stations used (USTA); STRESS DROP is estimated following Madariaga (1976).

LAT (°N)	LON (°E)	DEPTH (km)	DATA (mm/gg/aa)	TIME (hh:mm)	ML	Mw	ERR	Mo (Nm)	fo (Hz)	eqR (km)	usta	STRESS DROP (MPa)
44.92	11.23	8	5/20/2012	2:03	6.1	6.1	0.2	2.84E+18	0.3	4.5	13	1.65
44.90	11.14	11	5/20/2012	3:02	5.3	5.3	0.2	1.46E+17	0.5	2.7	12	0.42
44.83	11.46	8	5/20/2012	13:18	5.3	5.3	0.1	1.16E+17	0.5	2.7	11	0.29
44.92	11.10	4	5/29/2012	7:00	5.8	5.9	0.2	1.37E+18	0.3	4.2	25	1.16
44.92	10.99	5	5/29/2012	10:55	5.5	5.5	0.3	4.42E+17	0.4	3.5	23	0.70
44.92	11.00	8	6/03/2012	19:20	5.0	5.2	0.2	1.07E+17	0.6	2.4	25	0.58

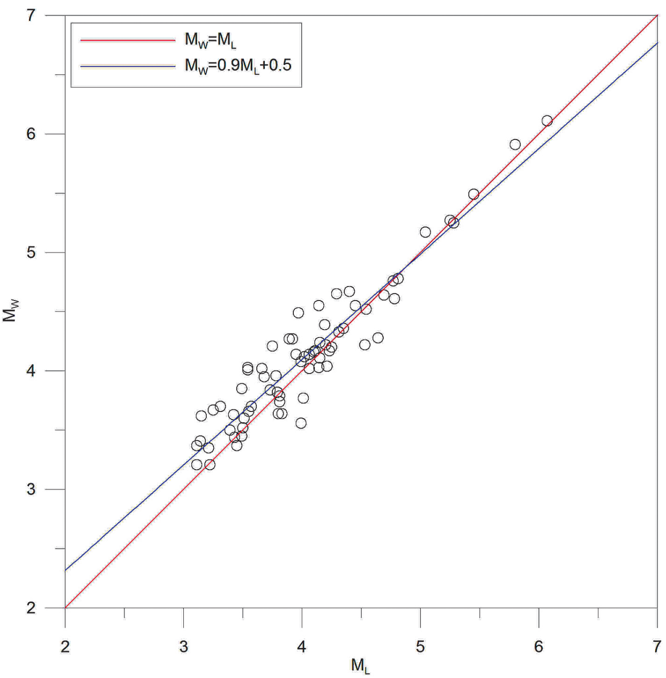

Fig. 1 – Comparison between the local magnitude as estimated by Antelope and the moment magnitude estimated by our procedure. The red line shows the bisector, the blue one the regression line.

In Fig. 1 we report Richter local magnitude versus moment magnitude estimates for all events used in this work. M_L generally underestimates the moment magnitude M_W by about 0.5 magnitude units, principally in the range $3 < M_L < 4.5$. A possible reason could be the site effect not yet taken into account by the procedure. A recent study (Castro *et al.*, 2013) shows important amplification variability between the sites located within the Po Plain. The area under study has a complex geological structure, so a more detailed analysis on the attenuation and spreading of waves will most probably also lead to improved estimates of seismic source parameters.

Fig. 2 shows corner frequency plotted versus seismic moment (on a log-log scale).

The corner frequency estimation appears quite stable. The relationship between seismic moment and corner frequency is approximately $M_0 \propto f_0^{-3.5}$. We calculate stress drop using the following equation (Madariaga, 1976):

$$\Delta\sigma = \frac{7}{16} \cdot M_0 \cdot \left(\frac{2\pi f_0}{2.34 \cdot \beta} \right)^3$$

The values range between 0.1 and 1.8 MPa (Fig. 3), which are within the bounds generally found for crustal earthquakes (10^4 Pa < Δσ < 10^8 Pa, e.g. Hanks, 1977; Kanamori, 1994). The obtained values of stress drop are within the range reported by several authors for the Emilia seismic sequence (Malagnini *et al.*, 2012; Castro *et al.*, 2013). We have also compared, wherever possible, our magnitude estimation with the ones obtained by other Authors (Malagnini *et al.*, 2012; Pondrelli *et al.* 2012; Saraò *et al.*, 2012; Scognamilio *et al.*, 2012). The agreement is quite fair especially for the major events (MW > 5). The differences for some values are due to different initial assumptions to compute moment magnitude, such as, e.g., velocity model, epicentral distance and frequency range. The results obtained represent an important validation for our real-time procedure proving that it is robust and reliable. This real-time automatic procedure is now routinely used at DMG and at the Department of Civil Defense (DPC) in Rome for a rapid determination of earthquake parameters.

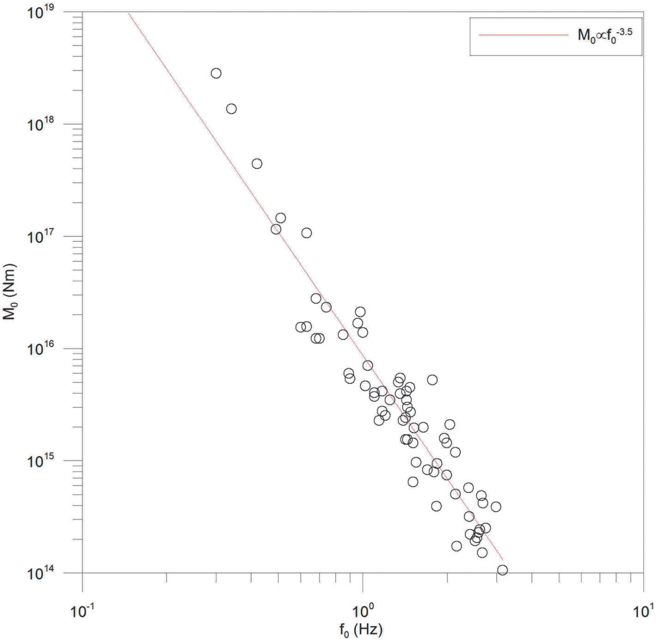

Fig. 2 – Corner frequency versus seismic moment. The relationship between seismic moment and corner frequency is approximately $M_0 \propto f_0^{-3.5}$.

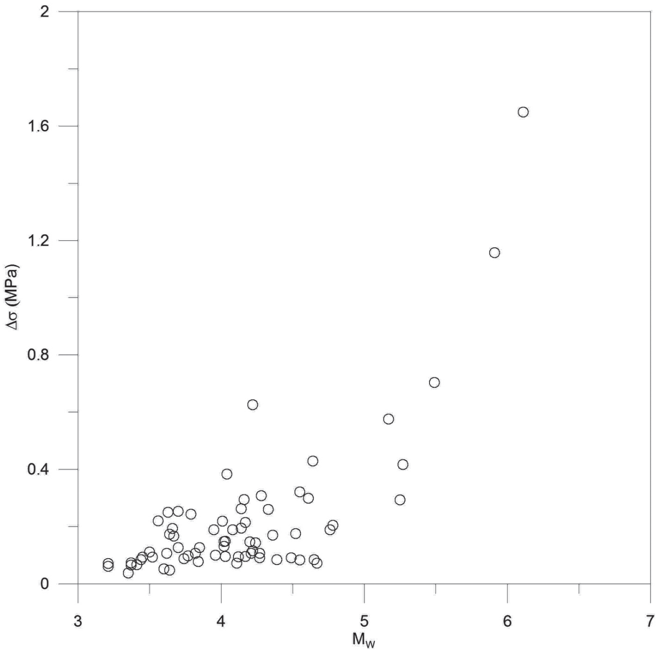

Fig. 3 – Stress drop values computed following Madariaga (1976).

Acknowledgements. We would like to thank the Italian Civil Protection for kindly providing us part of the seismic data used in this research. Part of his work was financially supported by the S.H.A.R.M. Project of the Area Science Park of Trieste: "Tomografia crostale per la valutazione e mitigazione del rischio sismico". This study was partially supported also by Project S1 of the Instituto Nazionale di Geofisica e Vulcanologia (INGV) (2012-2013): "Miglioramento delle conoscenze per la definizione del potenziale sismogenetico".

References
Andrews D.J.; 1986: *Objective determination of source parameters and similarity of earthquakes of different size*, in Earthquake Source Mechanics, S. Das, J. Boatwright, and C.H. Scholz, Editors, A.G.U. monograph 37, 259-267.
Brune J.; 1970: *Tectonic stress and spectra of seismic shear waves from earthquakes.* J. Geophys. Res., 75, No. 26, 4997-5009.
Brune J.; 1971: *Correction*. J. Geophys. Res., 76, No. 20, 5002.
Castro R.R., Pacor F., Puglia R., Ameri G., Letort J., Massa M., Luzi L.; 2013: *The 2012 May 20 and 29, Emilia earthquakes (Northern Italy) and the mail aftershocks: S-wave attenuation, accelerationsource functions and site effects*. Geophys. J. Int. doi: 10.1093/gji/ggt245.
Console R., Rovelli A.; 1981: *Attenuation parameters for Friuli region from strong-motion accelerogram spectra*. Bull. Seism. Soc. Am., 71, No. 6, 1981-1991.
Gallo A., Costa G., Suhadolc P.; 2013: *Near real-time moment magnitude estimation*. Submitted to Bull. Earth. Eng.
Gorini A., Nicoletti M., Marsan P., Bianconi R., De Nardis R., Filippi L., Marcucci S., Palma F., Zambonelli E.; 2010: *The Italian strong motion network*. Bull Earthquake Eng. doi: 10.1007/s10518-009-9141-6.
Hanks C.; 1977: *Earthquakes stress drops, ambient tectonic stresses and stresses that drive plate motions*. Pure Appl Geophys., 115, 441-458.
Hanks C., Kanamori H.; 1979: *A moment magnitude scale*. J. Geophys. Res., 84, 2348-2350.
Kanamori, H.; 1994: *Mechanics of earthquakes*. Ann. Rev. Earth Planet. Sci. 22, 207-237.
Madariaga R.; 1976: *Dynamics of an expanding circular fault*. Bull. Soc. Am.,66, No.3, 639-666.
Malagnini L., Hermann R.B., Munafò I., Buttinelli M., Anselmi M., Akinci A., Boschi E.; 2012: *The 2012 Ferrara seismic sequence: Regional crustal structure, earthquake sources, and seismic hazard*. Geophys. Res. Lett., 39, L19302, doi:10.1029/2012GL053214, 2012.
Ottemoller L., Havskov J.; 2003: *Moment magnitude determination for local and regional earthquakes based on source spectra*. Bull. Seism. Soc. Am., 93, No. 1, 203-214.
Pondrelli S., Salimbeni S., Perfetti P., Danecek P.; 2012: *Quick regional moment tensor solutions for the Emilia 2012 (northern Italy) seismic sequence*. Annals of Geophysics, 55, 4, doi: 10.4401/ag-6146.
Richter C.F.; 1935: *An instrumental earthquake magnitude scale*. Bull. Seism. Soc. Am., 25, 1-32.
Saraò A., Peruzza L.; 2012: *Fault-plane solutions from moment-tensor inversion and preliminary Coulomb stress analysis for the Emilia Plain*. Annals of Geophysics, 55, 4, doi: 10.4401/ag-6134.
Scognamiglio L., Margheriti L., Mariano Mele F., Tinti E., Bono A., De Gori P., Lauciani V., Lucente F.P., Mandiello A.G., Marcocci C., Mazza S., Pintore S., Quintiliani M.; 2012: *The 2012 Pianura Padana Emiliana seismic sequence: locations, moment tensors and magnitudes*. Annals of Geophysics, 55, 4, doi: 10.4401/ag-6159.
Zambonelli E., De Nardis R., Filippi L., Nicoletti M., Dolce M.; 2011: *Performance of the Italian strong motion network during the 2099, L'Aquila seismic sequence (central Italy)*. Bull. Earth. Engin., 2011, 9, No. 1, 39-65.

UNDERGROUND ARRAY RECORDINGS OF LOCAL AND REGIONAL EARTHQUAKES IN CENTRAL ITALY: A TOOL FOR TESTING EQUIPARTITION OF ENERGY IN A DIFFUSIVE WAVEFIELD

D. Galluzzo[1], M. La Rocca[1], L. Margerin[2], E. Del Pezzo[1], R. Scarpa[3]
[1]Istituto Nazionale di Geofisica e Vulcanologia - Osservatorio Vesuviano, Napoli, Italy
[2]Université de Tolouse, Tolouse, France
[3]Università degli Studi di Salerno, Salerno, Italy

Introduction. The scattering of seismic waves propagating in heterogeneous media is more complex than the scattering of other waves (electromagnetic, acoustic) due to the conversion from P to S and vice versa. The multiple scattering theory describes sufficiently well the energy decay along the earthquake coda. When the travel time is much greater than the mean free scattering time and the travel distance is much greater than the mean free scattering distance, the seismic wavefield is expected to be diffuse, as observed for electromagnetic and acoustic waves propagating through heterogeneous media. When a high number of waves of similar amplitude reach the observation point at the same time with different propagation directions and random phase, the resulting wavefield is said diffusive. The most relevant features of such wavefield are a small variation of amplitude with time and a low coherence. Regarding seismic waves, a wavefield is diffusive at a given frequency if in any chosen time window there are many P and S waves (and surface waves if the observation point is at or near the free surface) of comparable amplitude propagating with different random directions and random phases. A signal like that is expected to have a low coherence. Seismic noise usually has the characteristics of a diffusive wavefield.

The earthquake source radiates energy in a broad frequency range, therefore the wavelength of seismic waves involved in the scattering process cover a broad range of distance. Moreover, the scattering coefficient Qs has been observed dependent on the frequency in most of studied regions. For these reasons, a seismic wavefield may be diffusive at a given frequency but not at other frequencies. Higher frequency waves are expected to reach a diffusive regime before lower frequency waves. On the other hand, higher frequency signals attenuate faster than lower frequencies, therefore the late coda spectrum is dominated by low frequency energy. This means that diffusive wavefield of seismic waves may not be observed at any frequencies in the same time window along the late coda.

Theoretical arguments about the multiple scattering imply the energy equipartition of a diffusive wavefield. In a diffusive regime the available energy is equally distributed, in fixed average amounts, among all the possible states (Sanchez-Sesma *et al.*, 2011). Another way to state the equipartition principle is that the phase space is uniformly populated (Weaver, 1982). Regarding seismic waves, the properties of conversion from P to S and from S to P are such that at the equilibrium (diffusive regime) the following energy relation holds (Papanicolaou *et al.*, 1996; Hennino *et al.*, 2001):

$$\frac{E_S}{E_P} = 2\frac{\alpha^3}{\beta^3} \simeq 10 \qquad (1)$$

From this relation we expect S waves to be much more abundant than P waves along the earthquake coda. The few attempts to measure energy partition in the earthquake coda have given controversial results, mostly because separating P and S waves in a diffusive wavefield is impossible. The fact that most of seismic stations are installed at surface, or at most at few hundreds meters depth, and the strong heterogeneity that characterize the shallowest layers further contribute to the results uncertainty. In this paper we take advantage of a seismic array installed underground, at about 1.4 km depth, in the INFN Laboratory of Gran Sasso (Italy), from 2003 to 2010. The data from this array (named Underseis, hereafter UND) offer several advantages compared with typical surface single station recordings. First of all, the depth of 1.4 km makes negligible the contribution of surface waves for frequency greater than about 2 Hz. Second, the high number of stations in a small area permits to measure the spatial coherence of the wavefield. Third, the analysis by array methods gives an estimation of the propagation properties of the seismic wavefield. Fourth, site effects at the array stations are negligible because all stations are installed in the same geologic environment, constituted of hard rock limestone (Catalano *et al.*, 1984).

Methods of analysis. The coherence of the seismic wavefield among the array stations is estimated by applying the equation:

$$\gamma(\omega) = \sum_{i \neq j} \frac{|c_{ij}(\omega)|}{\sqrt{|c_{ii}(\omega)||c_{jj}(\omega)|}} \qquad (2)$$

(Foster and Guinzy, 1967), where *i* and *j* represent the stations, and c_{ij} is the smoothed cross spectral matrix defined as:

$$c_{ij}(\omega) = \sum_{k=-N}^{N} a_k F_i^*(\omega + k\Delta\omega) F_j(\omega + k\Delta\omega) \qquad (3)$$

Fi (ω) is the discrete Fourier transform of the *ith* signal, and *ak* are smoothing coefficients chosen in the range 0 – 1. It is noteworthy that without smoothing *cij*(ω) would be always equal to 1 (Bath, 1984). The coherence gives a measure of the signal similarity among the array stations as a function of frequency. It can be computed between two signal windows recorded at the same place but different times (time coherence), or between two signals recorded at the same time at different places (spatial coherence). In the first case the coherence measures the persistence of similarity in time, while in the second case it measures the persistence of similarity as the signal propagates from a place to another. The case of coherence between signals recorded at different places and different times is not of interest in seismology, and will not be deepened any more. On the contrary, we will focus our attention on the spatial coherence.

Many methods of analysis are available to study the propagation properties of the seismic wavefield, in both frequency and time domain. All of them, applied to time window sliding along the signal, furnish azimuth and apparent velocity of the most coherent signal. In this work we have applied the Beam Forming method (BF) in frequency domain, and the Semblance method (Semb) in time domain.

The partition of energy is evaluated in frequency domain by calculating power spectra of three component seismic signals as described by Nakahara and Margerin (2011). The energy partition ratio (PE_{hr} and PE_{ud} for horizontal and vertical components) and *H/V* spectral ratios on coda waves are calculated on 20 s time windows starting after twice S-wave travel time and are given by:

$$H/V = (N + E) / 2\,V \qquad (4)$$

$$PE_{hr} = (N^2 + E^2) / (N^2 + E^2 + V^2) \qquad (5)$$

$$PE_{ud} = V^2 / (N^2 + E^2 + V^2) \qquad (6)$$

where *E*, *N* and *V* are the amplitude spectra of east-west, north-south and vertical components of motion respectively.

Data analysis and results. UND array was composed of 20 short period three component seismic stations installed at an average distance of about 90 m for a maximum extension of about 0.5 km (Scarpa *et al.*, 2004; Saccorotti *et al.*, 2006; Formisano *et al.*, 2012). The wavelength well sampled in space by the array is in the range [0.1 km, 0.5 km], which corresponds to frequency in the range 10 Hz - 50 Hz for P waves, and 5.7 Hz - 30 Hz for S waves, assuming a P wave speed of 5 km/s. Since data were acquired at 100 sps, the intrinsic high frequency limit of our signals is 40 Hz. However, many stations were affected by local sources of noise, particularly important in many cases in the band 23 Hz – 40 Hz. Therefore we trust that our data set is suitable for measuring the spatial coherence in the 5 – 23 Hz range. At lower frequency we expect the signals be more coherent as the wavelength increases, even for diffusive regime and seismic noise, because the array extension is smaller than the signal wavelength.

We selected many local and regional earthquakes characterized by high signal to noise ratio (SNR). They were analyzed by applying array methods to many different frequency bands in the range 1 Hz – 20 Hz. Since the array consisted of three component stations, the array methods were applied to the three components independently. Beside the array analysis, the coherence of seismic signals among the array stations was computed on sliding window of length 10 s. Results have been plotted by colors versus time and frequency. Fig. 1 shows an example of this analysis for a regional earthquake. The spectrogram is also shown in the same picture to give a precise idea of the coda decay. The coherence is characterized by very high values (near 1) for signals at frequency lower than 1 Hz in the seismic noise and along the earthquake coda. For the P wave and its early coda the coherence takes the maximum at frequency in the range 2 – 18 Hz. On the contrary, for this earthquake the coherence of the S wave and early coda is very high only at frequency lower than 3 Hz. The very high coherence of any signals at low frequency is a consequence of the array extension, which is smaller than the signal wavelength for frequency lower than about 6 Hz (S wave). In other words, UND array is not appropriate to measure the spatial coherence of seismic waves at frequency smaller than about 3 Hz. This consideration is also independent from the window length. In fact, whatever the window length is, the low frequency signals will be always very similar to each

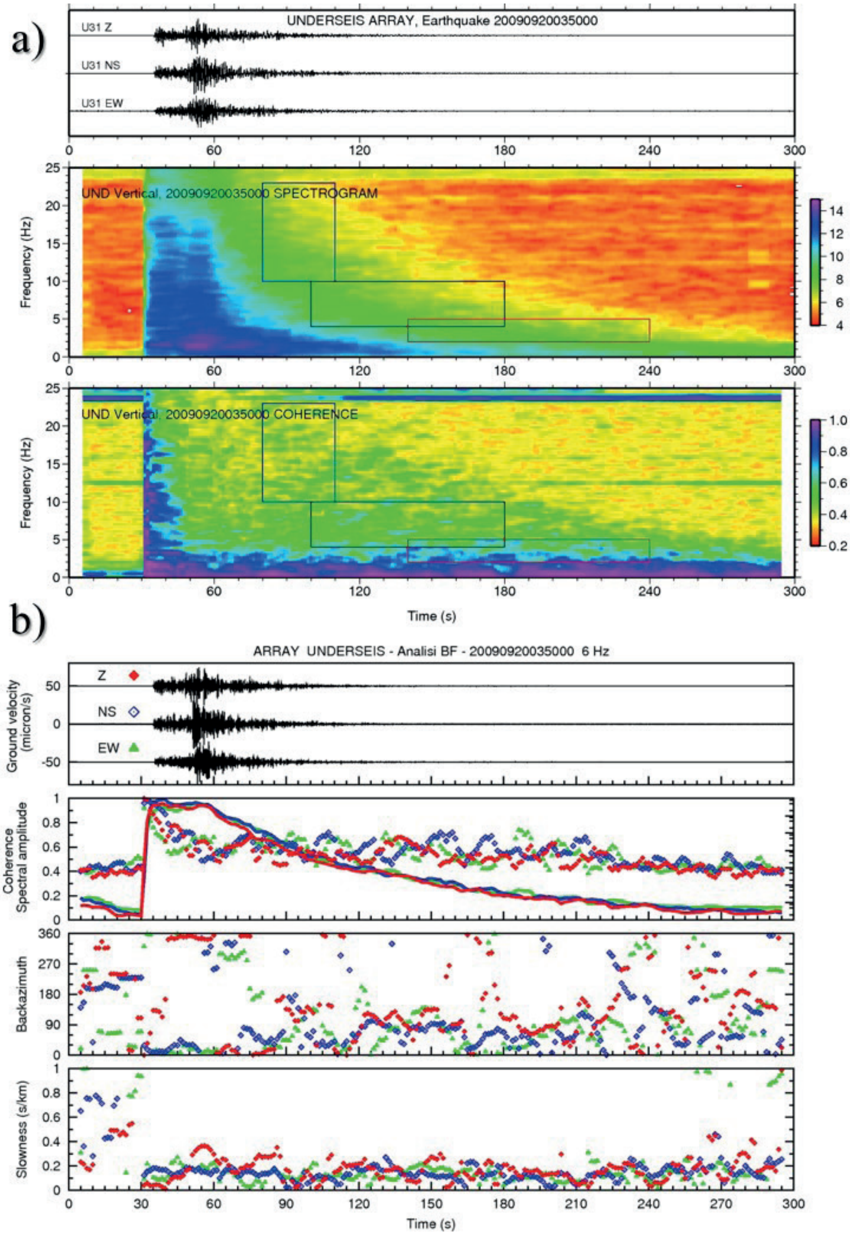

Fig. 1 – Regional earthquake 200909200350. a) Seismograms of one station, Spectrogram of the vertical component and Coherence among the array stations. b) Results of the array analysis with the Beam Forming method focused at 6 Hz: Coherence at 6 Hz, spectral amplitude, backazimuth and slowness. Different symbol and color refer to the three components of ground motion.

other at the array stations, independent of their origin (earthquake, body waves, coda waves, seismic noise) and their regime (diffusive or not). At frequency higher than 3 Hz the coherence varies greatly between seismic noise, earthquake body waves, and along the coda. In this range it is noteworthy the strong similarity between spectrogram and coherence patterns. The high coherence line between 23 and 25 Hz reveals a coherent noise produced inside the laboratory. Looking at the pictures of Fig. 1 we can choose the best windows along the coda for successive analysis. Our purpose is to verify the hypothesis that the late coda is composed by a diffuse wavefield. Our data set allows the investigation of this feature in the frequency range 5 – 23 Hz.

Results of BF analysis for the same regional earthquake are also shown in Fig. 1b by different symbol and color for the three components of ground motion. The second plot contains the coherence, shown by symbol and referred to the left axis, and the spectral amplitude, shown by lines and referred to the right axis (with log scale). The coherence shown here corresponds to the same values readable at frequency of 6 Hz in the coherence of the third plot of Fig. 1a. The spectral amplitude suggests that the earthquake coda at 6 Hz lasts until at least 240 s, perhaps more. Coherence returns to values comparable to the seismic noise preceding the earthquake at about the same time. Important indications about the end of coda come also from the values of backazimuth, that return comparable to the seismic noise after 220 s, and from the slowness, that suggests 250 s. From the earthquake onset (30 s) to 260 s the values of slowness are always smaller than 0.35 s/km, corresponding to 3 km/s of apparent velocity. This demonstrate that the earthquake seismic wavefield recorded at the underground array is composed only of body waves at the frequency of 6 Hz, as expected. The slowness distributions obtained from the analysis performed at different frequencies confirm that surface waves are negligible in the signals recorded at UND array for frequency greater than 3 Hz as also shown by La Rocca *et al.* (2013).

In a wavefield composed of only body waves in diffusive regime (far from the surface) the horizontal to vertical ratio (*H/V*) must be very near to 1. Similarly, the PE_{hr} should be very close to 0.67 (Hennino *et al.*, 2001). Therefore we have computed the *H/V* ratio and PE_{hr} along the coda of local and regional earthquakes. To perform the spectral analysis, the time window along the coda has been chosen looking at the values of coherence and spectral amplitude. We require low coherence and spectral amplitude at least 10 times that of the seismic noise preceding the earthquake. The low coherence is a condition required by the diffusive regime,

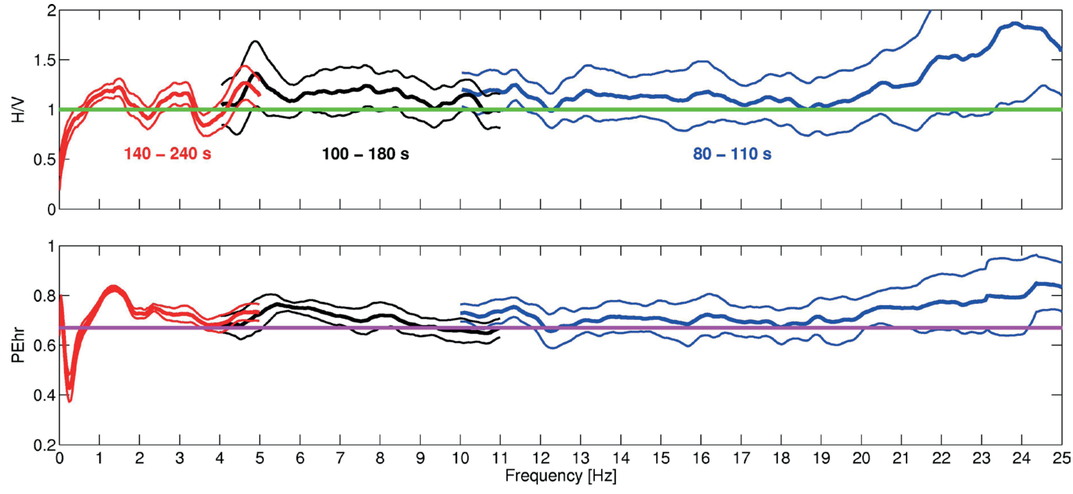

Fig. 2 – Energy partitioning ratio of two horizontal components PE_{hr} and Horizontal over Vertical amplitude ratio (H/V) versus frequency computed as the average among the array stations for the earthquake 200909200350. The different colors (red, black and blue) are referred to time and frequency limits (respectively [0-5], [5-10] and [10-22] Hz) shown by boxes in Fig. 1a. The green and magenta lines show the expected value for H/V ratio equal to unity (top) and equipartition in an homogeneous halfspace far from free surface (bottom) respectively.

while the high SNR condition is necessary to make negligible the effects of the many local sources of noise active in the underground laboratory. Looking at Fig. 1 we see immediately that there is not any windows along the coda where the two conditions are verified in the whole frequency range we are studying. Therefore it is necessary to split the frequency range in different intervals that will correspond to different time windows along the coda. The boxes in spectrogram and coherence of Fig. 1 shows as an example the time windows and their corresponding frequency intervals adopted for that earthquake. After have selected the time window, Fourier spectra are computed for each component of any stations over a 20 s sliding window with 50% overlapping. The spectral amplitude ratio *H/V* and spectral power amplitude ratio are computed as a function of frequency, and finally the mean and standard deviation among the array stations are computed. At this point we consider only the result in the frequency interval corresponding to the selected time-frequency window. The result for a regional earthquake is shown in Fig. 2. The spectral ratios in Fig. 2 show at least two distinct trends in two different frequency band of analysis:

- H/V is very close to unity (equal to 1.1 - 1.2) and PE_{hr} is equal to 0.67 within error bars in the high/medium frequency range (from 7 to 22 Hz) identified by blue and partly black lines;
- for the low frequency range (0-7 Hz, mostly in red), H/V depart from a constant value with oscillations around unity and PE_{hr} assumes values between 0.4 and 0.8.

The results for high frequencies band (7-22 Hz) is a clue of equipartioned coda in subsurface under the hypothesis of wavefield composed by body waves propagating in an homogeneous medium.

Further observations can be performed for low frequencies part of energy partition by simulating energy ratios and comparing them with the observed ones (Margerin *et al.*, 2009). By considering a reliable velocity and density model for the area under investigation (Capuano *et al.*, 1998; Chiarabba *et al.*, 2009), energy partition ratios have been simulated by applying a method based on a spectral decomposition of the elastic wave in a stratified half-space (Margerin, 2009). The energy ratios have been calculated at different depths (between 1 and 2 km) and for three different assumptions on the origin of coda waves: 1) coda composed of body waves incident from below the crust only; 2) coda composed of surface and guided waves in the crust only; 3) the coda is the sum of the two previous contributions. The best qualitative

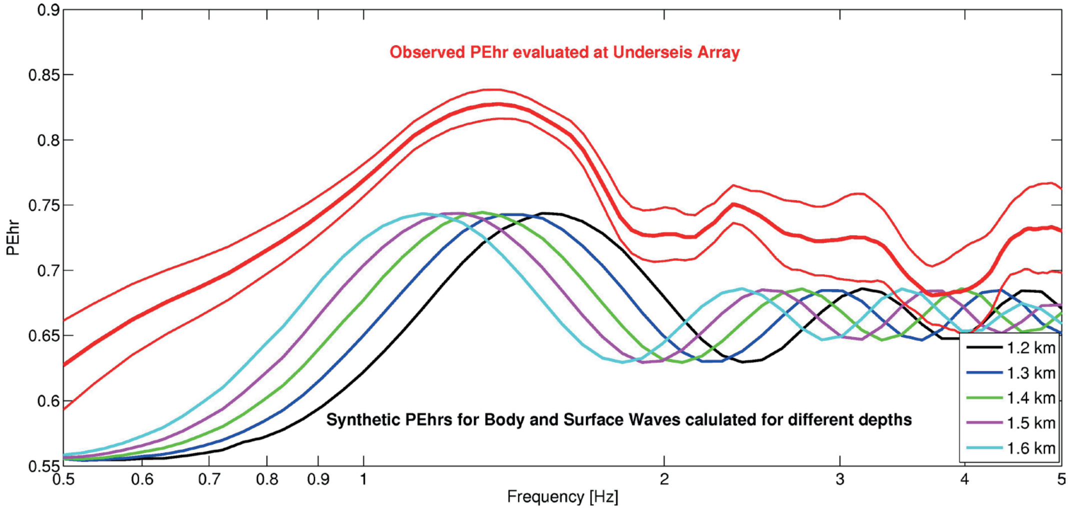

Fig. 3 – Observed (red line with error band) and simulated values of PE_{hr} (lines with other colors) obtained for different depths (see legend) and under the hypothesis of coda waves composed by surface and body waves. The best qualitative agreement is obtained for 1.4 km depth (green line).

agreement is obtained under the hypothesis n. 3 (body and surface waves) as shown in Fig. 3, where the red line with errors are the observed PE_{hr} while the curves with other colors show the simulations for different depths. The best agreement is obtained for 1.4 km depth which coincides with the depth from surface at which UND array was located.

Discussion and conclusion. The results of our analysis on observed coda waves (Coherence, propagation parameters, H/V ratio) indicate that the late coda of local and regional earthquakes recorded at about 1.4 km depth is composed of body waves in a diffusive regime for frequency greater than 3 Hz. As the lapse time increases along the coda the features of diffuse wavefield become more evident. This is particularly evident for regional earthquakes. For local earthquakes the observations are limited by the coda duration.

The energy equipartition in the late coda is inferred by the results of PE_{hr}. PE_{hr} has been calculated in different coda windows for different frequency bands in order to assure the conditions of diffuse wavefield (time windows starting after twice S-wave travel time, low coherence and spectral amplitude of coda waves higher than noise). For the frequency band 8-20 Hz the observed PE_{hr} is very close inside the errors to the expected value for equipartition in an homogeneous halfspace. However, a final proof of the energy equipartition would be achievable only by using a 3D underground array. That would allow for a complete separation of longitudinal and shear waves.

By considering a stratified halfspace we have simulated energy partition in the case of diffusive wavefiled and simulated and observed energy partition curves show a qualitative agreement in the frequency range 0.5 - 5 Hz under the hypothesis that coda are composed by surface and body waves. We believe that the main cause of discrepancy between observed and simulated results is due to the flat layer model that does not fit the area of Gran Sasso massif. In future simulations it will be necessary to include the local topography.

References

Bath M., 1974; 1974: *Spectral Analysis in Geophysics*. Elsevier (Holland).

Foster M. and Guinzy N.; 1967: *The coefficient of coherence: its estimation and use in geophysical data processing.* Geophysics, 32(4), 602–616. doi: 10.1190/1.1439878

Catalano G. P., Cavinato P. G., Salvini F., Tozzi M.; 1984: *Analisi strutturale nei laboratori dell'I.N.F.N.del Gran Sasso d'Italia*. Mem. Soc. Geol. It., 35, 647-655.

Capuano P., De Luca G., Di Sena F., Gasparini P., Scarpa R.; 1998: *The density of the rock covering Gran Sasso Laboratories in Central Apennines, Italy by underground gravity measurements*. Journal of Applied Geophysics, 39, 25-33.

Chiarabba C., AA. VV.; 2009: *The 2009 L'Aquila (central Italy) M_W6.3 earthquake: Main shock and aftershocks*. 2009, Geophysical Research Letters, vol. 36, doi:10.1029/2009GL039627.

Formisano L.A., La Rocca M., Del Pezzo E., Galluzzo D., Fischione C., Scarpa R. (2012), *Topography effects in the polarization of earthquake signals: a comparison between surface and deep recordings.* Bollettino di Geofisica Teorica e Applicata, vol. 53, n. 4., pp 471-484, doi: 10.4430/bgta0055.

Hennino R., Tregoures N., Shapiro N. M., Margerin L., Campillo M., van Tiggelen B. A., Weaver R. L.; 2004: *Observation of Equipartition of Seismic Waves*. Physical Review Letters, vol. 86, num. 15, 9 April 2001.

La Rocca M., Del Pezzo E., Galluzzo D., Scarpa R.; 2013: *Joint observation of coherent coda waves at surface and underground arrays*. Geophys. J. Int., Express Letter, doi:10.1093/gji/ggt111.

Margerin L.; 2009: *Generalized eigenfunctions of layered elastic media and application to diffuse fields.* J. acoust. Soc. Am., 125, 164-174.

Margerin L., Campillo M., Van Tiggelen B. A., Hennino R.; 2009: *Energy partition of seismic coda waves in layered media: theory and application to Pinyon Flats Observatory*. Geophys. J. Int., 177, 571-585.

Nakahara H., and Margerin L.; 2001: *Testing equipartition for S-wave coda using borehole records of local earthquakes.* Bull. Seismol. Soc. Am.,101, 2243-2251, 2011.

Sanchez-Sesma F. J., Rodriguez-Castellanos A., Perton M., Luzon F., Ortiz-Aleman C.; 2011: *Diffuse seismic waves and site effects*. J. Geophys. Eng., 8, 109-114.

Papanicolaou G. C., Ryzhik L. V., Keller J. B.; 1996: *Stability of the P-to-S Energy Ratio in the Diffusive Regime*. Bulletin of the Seismological Society of America, 86, n.4, 1107-115.

Weaver R.; 1982: *On diffuse waves in solid media*. J. Acoustic. Soc. Am., 71(6), June 1982.

Saccorotti G., Di Lieto B., Fischione C., Tronca F., Scarpa R.; 2006: *Performances of the UNDERground SEISmic array for the analysis of seismicity in Central Italy*. Annals of Geophysics, 49, 2006.

Scarpa R., Muscente R., Tronca F., Fischione C., Rotella P., Abril M., Alguacil G., De Cesare W., Martini M.; 2004: *UNDERSEIS: The underground seismic array*. Seism. Res. Lett. 75, 4, 493-504, 2004.

ATTENUATION TOMOGRAPHY OF FRIULI VENEZIA GIULIA ITALIAN REGION

S. Gentili, F. Gentile
Centro di Ricerche Sismologiche, Istituto Nazionale di Oceanografia e di Geofisica Sperimentale, Udine, Italy

Introduction. The Friuli Venezia Giulia Italian region and the western Slovenia are very peculiar from the tomographic point of view, due to the large lateral variation of velocity and Vp/Vs ratio, that is related to the high level of fracturing and, on the east, to the inhomogeneity of the medium. In this work we carry out for the first time the attenuation tomography of Friuli Venezia Giulia Italian region and western Slovenia. In particular, we analyze the 3D distribution of the frequency independent part of the S-waves quality factor, starting from a dataset of high frequency attenuation parameter k. The spectral decay parameter k was estimated using data from small-to-moderate earthquakes recorded by the NEI (northeastern Italy) seismic network managed by the National Institute of Oceanography and Experimental Geophysics (Istituto Nazionale di Oceanografia e Geofisica Sperimentale, OGS – http://www.crs.inogs.it/). The next section describes the relation between attenuation parameter and quality factor. In the following, the method adopted for k decay parameter estimate is described. Subsequently, the seismicity distribution (historical and instrumental) and details of the application of method tomographic inversion to Friuli Venezia Giulia region are shown. Finally, the obtained results are compared with both the previous k attenuation studies and the tomographic studies on Vp Vs velocities in the same area.

Attenuation parameter vs. quality factor. The attenuation of seismic waves which propagate through the Earth can strongly influence the ground motion recorded at a site thus modifying the energy content of the signal radiated from the source. The attenuation is modelled in literature either using the quality factor Q, a dimensionless parameter introduced to quantify the fractional energy (E) loss per cycle of oscillation as $Q = 2\, \pi\, E\, /\, \Delta E$ (Aki and Richards, 1980), or using the attenuation parameter k (e.g. Anderson and Hough, 1984).

The attenuation due to high frequency spectral decay of acceleration amplitude Fourier spectrum has been modelled as (Cormier 1982):

$$A(r,f) = A_0 e^{-\pi t^* f} \qquad (1)$$

A_0 depends on the source and the geometrical spreading and f is the frequency. In this model t^* is defined as :

$$t^* = \int_{path} \frac{1}{QV} dr \qquad (2)$$

where Q is the quality factor and V is the average velocity of the waves. Anderson and Hough (1984) modelled high frequency acceleration spectrum as:

$$A(r,f) = A_0 e^{-\pi k f} \qquad (3)$$

Hough and Anderson (1988) modelled k as:

$$k = \int_{path} \frac{1}{Q_I(z)V(z)} dr \qquad (4)$$

where Q_I is the frequency-independent part of Q, and Q is parameterized as:

$$Q(f)^{-1} = Q_D(f)^{-1} + Q_I^{-1} \qquad (5)$$

Q_D and Q_I are respectively the frequency dependent and independent part of Q. $Q_I(z)$ means that in their simplified model Q_I depends only on the depth (plane and parallel layers) but can be generalized. Hough and Anderson (1988) noted that the model they used for k^* is the same of Cormier (1982) with the difference that only frequency independent part of Q is considered. In the works on k estimation the term Q_D is generally considered (Anderson and Hough, 1984, Castro *et al.*, 1997, Franceschina *et al.,* 2006, Bressan *et al.*, 2007). Vice versa, when t^* is estimated for attenuation tomography inversion, the frequency dependent term is usually neglected (Rietbrock 2001, Haberland and Rietbrock 2001, Olsen *et al.*, 2003, Eberhart-Phillips *et al.*, 2005). The opportunity to considering or not the Q dependence on frequency is debated. The reason for neglecting it is the difficulty in the evaluation of this term for the whole area under study and/or the lower dependence of the quality factor on frequency for higher frequencies. The latter reason is debated. Several different authors analysed the area under study in this paper and estimated the frequency dependence of Q. Console and Rovelli (1981) obtained a dependence of $\sim f^{1.1}$ in the frequency range 0.1-10 Hz, Castro *et al.* (1996) obtained a dependence of $\sim f^{1.01}$ in the frequency range 0.4-25 Hz, Malagnini *et al.* (2002) obtained a dependence of $\sim f^{0.55}$ in the frequency range 0.5-14 Hz. Estimates of k in the study area of this paper were performed by Franceschina *et al.* (2006) and Bressan *et al.* (2007) considering a term Q_D=78 $f^{0.96}$ [according with Govoni *et al.* (1996) in the frequency range 1-25 Hz]. In a successive paper, Gentili and Franceschina (2011) considered the relation $Q_D(f)$ = 251 $f^{0.7}$ correspondingly to the total quality factor estimated for this area by Bianco *et al.* (2005) in the frequency range 0.5-16 Hz. In this work, for coherence with previous ones in the same area, we will not neglect the frequency dependence of Q. In particular, we will adopt Bianco *et al.* (2005) estimation, like Gentili and Franceschina (2011). Considering such correction does not affect too much the value of Q for small values of Q. For example, considering the value of Q_D at a frequency in the middle of our spectral window (Eberhart – Phillips *et al.*, 2005), say 15 Hz, for Q_I=20 we have Q=19.8. For very low attenuation, the effect of considering frequency dependence is larger: e.g. with Q_I=1000 we have Q=626. For coherence with previous papers notation, we will call the frequency independent part of the quality factor for S waves simply Q_S instead of Q_{IS}.

Attenuation parameter estimation. Assuming a negligible dependence of the geometrical spreading on frequency, we estimated the parameter by correcting the S-wave spectra for the frequency dependent part of the quality factor. Both the N-S and the E-W horizontal components of the signal were used. The S wave window was manually selected for both traces and the resulting data were tapered by a 5% cosine taper and padded with zeros before applying the FFT. The resulting spectra were smoothed by a sliding Hann window (Oppenheim and Schafer, 1999) of 0.5 Hz half-width. The spectral band adopted for the analysis was determined by selecting the part of the spectrum where a linear decay was clearly evident. In particular, we selected data in a frequency band $[f_1, f_2]$: f_2 is the frequency at which the noise level starts contaminating the signal and, in this study, ranged from 20 to 45 Hz. In order to determine f_1, accordingly with Gentili and Franceschina (2011), we estimated k values for increasing values of the minimum frequency, we plotted the obtained k as function of f and selected $k(f_1)$ values in an observed range of stability of this function by a visual inspection of each plot; f_1, generally depending on event size, ranged from 5 to 10 Hz. We adopted a threshold on the duration magnitude of analysed earthquakes of M_D>3 in order to ensure the validity of the condition $f_1 > f_C$, where f_c is the corner frequency. In fact, accordingly with previous analysis in this area (Bressan *et al.*, 2007) for M_D=3, $f_C \cong$ 4.6 Hz. In order to fit the amplitude spectrum, we used the least absolute residual method. This method minimizes the absolute difference of the residuals rather than the squared differences, thus decreasing the influence of outliers on results. The k values estimated from the two horizontal components of each record were averaged by computing the corresponding weighted mean and standard deviation. In order to increase the robustness of the method, the weights were chosen as the inverse of the error of each single fit.

Seismicity distribution and tectonics of the area. The area we analysed is sited in north-eastern Italy (Friuli Venezia Giulia region) and western Slovenia between the outer front of

Southern Alps and the Periadriatic lineament. It is included in a convergent margin zone between the Adria microplate and the Eurasian plate (see e.g. Castellarin *et al.*, 2006; Burrato *et al.*, 2008) and it is one of the most seismic active zones of Italy.

The area is sited at the tip of Adria plate. The progressive north-eastward pushing of African plate, respect to the Eurasian plate, generates an anticlockwise rotation of Adria microplate, which causes the present complex tectonic deformation (Mantovani *et al.*, 1996). Several tectonic phases in the region inherited and reactivated the main pre-existing faults and fragmented the crust into different tectonic domains corresponding to different seismotectonic zones (Bressan *et al.*, 2003). The eastern part of the region, in western Slovenia, is characterized by a strike-slip regime on Dinaric faults. The Friuli Italian region is characterized by thrust tectonic, mainly EW oriented and south verging in the centre and NE-SW-oriented and SE-verging thrust in the western part (Bressan *et al.*, 2003).

Fig. 1 shows both the historical and instrumental seismicity in the area. Brown squares correspond to earthquakes in CPTI04 catalogue (Gruppo di lavoro CPTI, 2004) from 1100 with intensity ≥IX. The other symbols correspond to instrumentally recorded seismicity. In particular, stars correspond to the events with magnitude ≥5 In the area. See figure caption for more details. Red symbols are the earthquakes used in this work. They are the 156 earthquakes

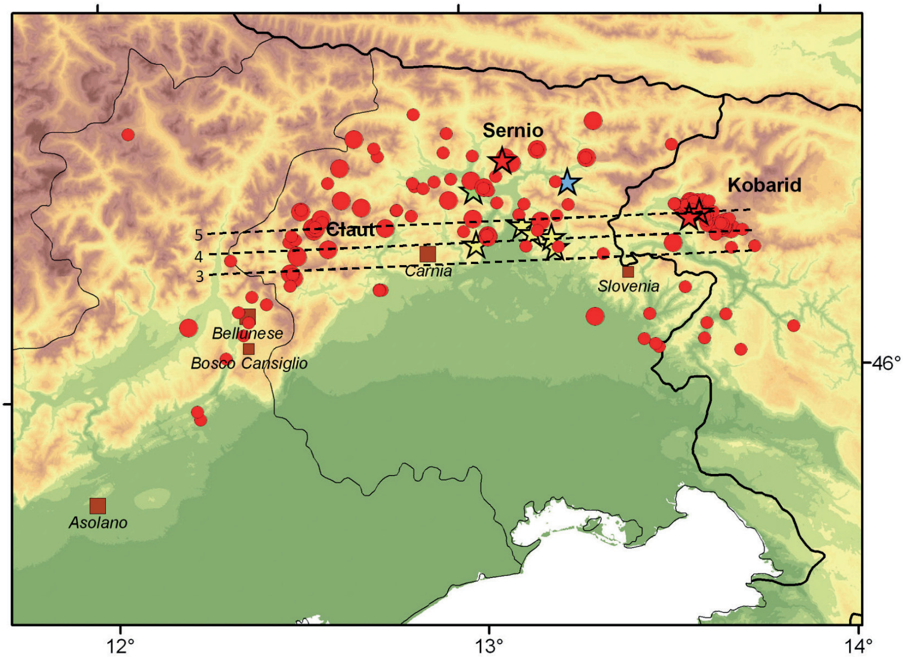

Fig. 1 – Seismicity in the area. Brown squares: historical seismicity (earthquakes with intensity ≥IX are shown with squares dimensions proportional to earthquake intensity). Red symbols: seismicity with magnitude >3 from 1994 to 2011. Stars: earthquakes with magnitude > 5. Yellow stars: 1976 swarm. Green star: 1977 Trasaghis earthquake. Blue star: 1979 Lusevera earthquake. Red stars: Kobarid and Sernio earthquakes. Dashed lines: Sections shown in Fig. 3.

with duration magnitude ≥ 3 recorded in the area from 1994 to 2011. In particular, a cluster of seismicity can be easily detected in the northeastern part in correspondence with the two Kobarid 1998 and 2004 seismic sequences. Smaller clusters of lower magnitude seismicity were recorded also after Sernio 2002 mainshock and during and in Claut region (for seismic sequences in the area see Gentili and Bressan, 2008). The instrumentally recorded seismicity roughly follows the historical earthquakes distribution.

Attenuation tomography in Friuli Venezia Giulia region. To invert the *k* data we used the same grid used by Bressan *et al.* (2012) in 3D tomographic inversion of velocity in the area. The grid extends 114 km in E-W direction and 55 km in N-S direction. The grid centre has latitude 46.33 N and longitude and 13.08 E. The W-E grid nodes are at X: -60, -50, -35, -25, -15, -7, 0, 7, 15, 25, 36, 45, 54 km; the S-N grid nodes are at Y: -35, -20, -10, -5, 0, 5, 10, 20 km; the Z nodes are at depth 0, 2, 4, 6, 8, 10, 12, 15, 22 km with a layer at negative 3 km depth to account for the Earth's topography. The X-axis is positive to the east, the Y-axis is positive to the north. The velocity of S waves in the medium is parameterized by assigning velocity values obtained in Bressan *et al.* (2012) paper at the nodes of the grid. Bressan *et al.* used 394 events from 1988 to 2004 with duration magnitude between 1.4 and 5.1 and performed an iterative simultaneous inversion of hypocentral parameters and 3D velocity structure with a damped least squares technique using a previous version of the code SIMULPS2000, i.e. SIMULPS12 (Evans *et al.* 1994). We used 156 events from 1994 to 2011 with duration magnitude between 3.0 and 5.7 for a total of 980 3-D records. The smaller number of earthquakes analyzed in this study is due on the constraints on the minimum magnitude we selected.

Like in tomographic applications in which velocity is inverted, an adequate starting model for the inverted parameter is important before attenuation tomographic inversion, due to the non-uniqueness of the solution of linearized inverse problem. A wrong starting model can lead to blunders and biases in the result. No previous knowledge for a valuation of the Q_s field in the Friuli area are available; so for finding the 1D starting crustal model a search heuristic was employed, that does not use linearization method. We adopted a genetic algorithm technique (Goldberg, 1989). In particular, the David L. Carroll GAFORTRAN code with MICRO-GA enabled (Carroll, 2001). A micropopulation of five individuals was utilized using as cost function the same SIMULPS2000 code minimizing the total weighted RMS; 600 generations were generated.

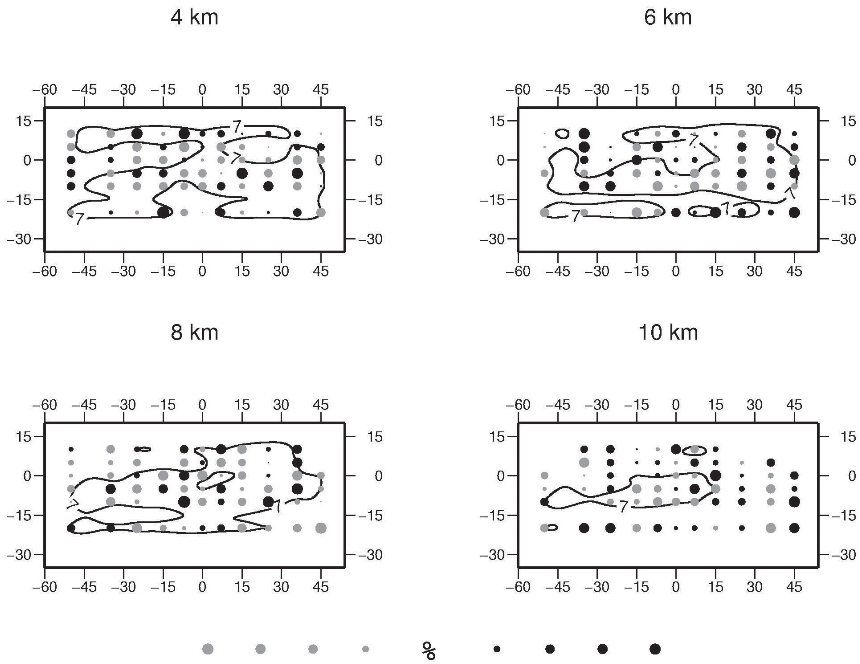

Fig. 2 – Checkerboard test for depth 4-10 km. Circle size correspond to the percentage difference respect to the mean value.

Starting from the previous 1D Q_s Earth model we performed the 3D inversion using the program SIMUL2000 (Thurber, 1993; Eberhart-Phillips, 1993, Thurber and Eberhart-Phillips, 1999), starting from the values of k. The code applies an iterative damped least squares method. In the inversion, as suggested in SIMUL2000 code, the earthquakes hypocenters and origin times were kept fixed. The Q_s crustal values are inverted using a damping value of 0.002, chosen evaluating the trade-off curve of the data variance versus model variance achieved after single iterations (Eberhart-Phillips, 1986, 1993).

Results. A refined estimate on the data reliability was performed through the comparison between the checkerboard test and a spread function test (Michelini and McEvilly, 1991).We performed the checkerboard test with a mean Q_s of 200 with variations of ±40%; we added to synthetic t^* a noise comparable to the residual level of real data. We choose such a value because it's near to the RMS obtained by the genetic run (Chen and Clayton, 2012). Fig. 2 shows the shows the checkerboard test, for depth 4-7 km, superimposed an isoline of the spread function S value of 7.

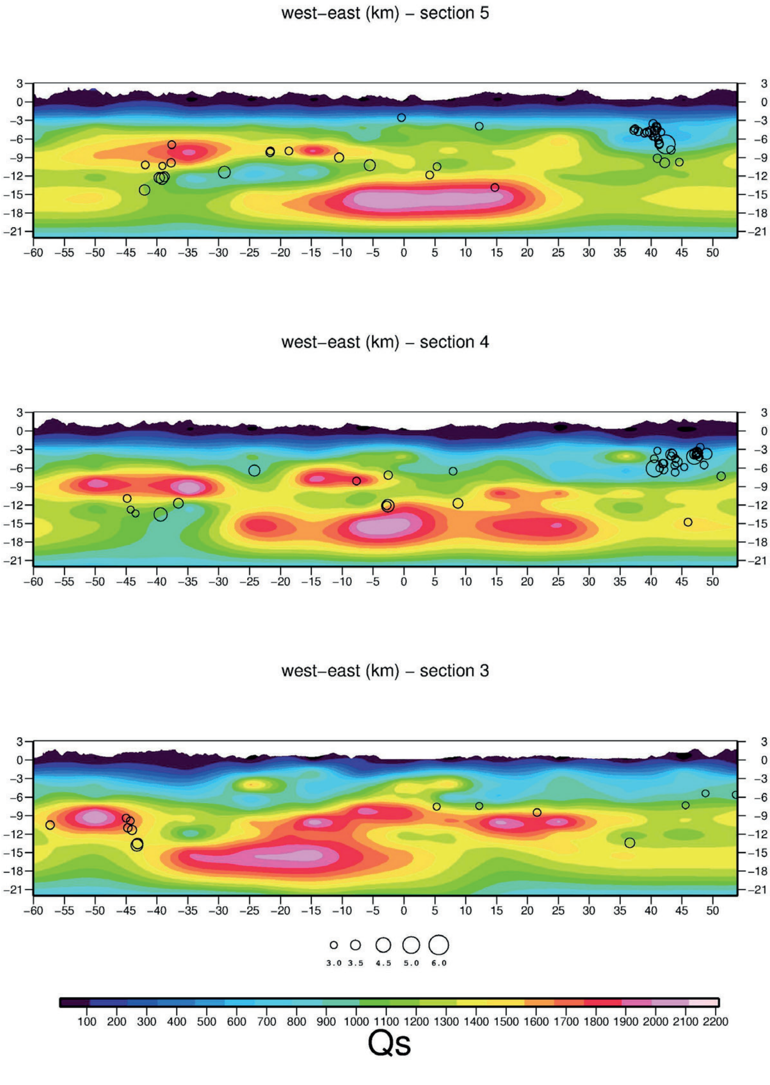

Fig.3 – Vertical cross sections 3-5 of the 3D Q_s distribution.

Fig. 3 shows the resulting Q_s for sections 3, 4, 5. The earthquakes are indicated as circles whose size corresponds to the magnitude. On the generic nth section characterized by y coordinate equal to y_n, the earthquakes corresponding to y in the range $[(y_{n-1}+y_n)/2, (y_n+y_{n+1})/2]$ are projected. A cluster of earthquakes can be detected in the rightmost area of sections 4 and 5, corresponding to the Kobarid sequences. In the same area, a large decrease of the value of Q_s, and therefore a larger attenuation, can be detected, in good agreement with the results by Gentili and Franceschina, 2011. Another cluster of seismicity can be detected in section 5 on the left, with a depth between 3 and 15 km. This seismicity belongs to the Claut area, where several low moderate magnitude earthquakes happened in the past (Gentili and Bressan, 2008). To the right of the cluster, there is on the top a region characterized by high values of Q_s (low attenuation) and on the bottom with low value of Q_s (high attenuation). Gentile *et al.* (2000) detected in the same region on the top an area of low V_p/V_s respect to the surrounding (1.76) and high V_p velocity (6.2). Considering their results, together with the high value of Q_s obtained in this paper, we hypothesize that it can correspond to un-fractured dolomitic limestones path, inside a more fractured one. On the bottom, Gentile *et al.* (2000) detect an area of V_p/V_s in the range 1.84-1.89. This region is interpreted by Gentile *et al.* (2000) as an highly fractured zone that corresponds to the Tramonti-But Chiarsò fault. This is compatible with our low attenuation results, even if the Q_s anomaly extends deeper than the V_p/V_s one and, unlike for the high V_p/V_s zone, does not reach the surface, but is interrupted by al low attenuation zone.

Both Bressan *et al.* (1992) and Gentile *et al.* (2000) detected an high P waves velocity body in the central part of the area with depth between 4 and 8 km. This is coherent with the detected high values of Q_s (1100-1500). The even higher values of Q_s at 15-18 km depth is not well resolved by both this work and by Bressan *et al.* (1992) and Gentile *et al.* (2000) works.

References

Aki K. and Richards, P.G.; 1980: *Quantitative Seismology, Theory and Methods*. Vol. 1, W.H. Freeman and Company, San Francisco, CA.

Anderson J.G. and Hough S.; 1984: *A model for the shape of Fourier amplitude spectrum of acceleration at high frequencies*. Bull. seism. Soc. Am., **74**, 1969-1994.

Bianco F., Del Pezzo E., Malagnini L., Di Luccio F. and Akinci A.; 2005: *Separation of depth-dependent intrinsic and scattering seismic attenuation in the northeastern sector of the Italian Peninsula*. Geophys. J. Int., **161**, 130-142.

Bressan G., Bragato P.L. and Venturini C.; 2003: *Stress and strain tensors based on focal mechanisms in the seismotectonic framework of the Friuli-Venezia Giulia region (Northeastern Italy)*. Bull. seism. Soc. Am., **93**, 1280-1297.

Bressan G., De Franco R. and Gentile F.; 1992: *Seismotectonic study of the Friuli (Italy) area based on tomographic inversion and geophysical data*. Tectonophysics, **207**, 383-400.

Bressan G., Gentile G.F., Tondi R., De Franco R. and Urban S.; 2012: *Sequential Integrated Inversion of tomographic images and gravity data: an application to the Friuli area (north-eastern Italy)*. Bollettino di Geofisica Teorica ed Applicata, **53**, 2, 191-212.

Bressan G., Kravanja S. and Franceschina G.; 2007: *Source parameters and stress release of seismic sequences occurred in the Friuli-Venezia Giulia region (Northeastern Italy) and in Western Slovenia*. Physics of the Earth and Planetary Interiors, **160**, 192-214.

Burrato P., Poli M.E., Vannoli P., Zanferrari A., Basili R. and Galadini F.; 2008: *Sources of Mw 5+ earthquakes in Northeastern Italy and Western Slovenia: an updated view based on geological and seismological evidence*. Tectonophysics, **453**, 157-176.

Carroll D. L.; 2001: GAFORTRAN. Genetic algorithm approach for parameter estimation. Urbana. http://cuaerospace.com/carroll/ga.html

Castellarin A., Vai G.B. and Cantelli L.; 2006: *The Alpine evolution of the Southern Alps around the Giudicarie faults: a late Cretaceous to early Eocene transfer zone*. Tectonophysics, **414**, 203-223.

Castro R.R., Pacor F. and Petrungaro C.; 1997: *Determination of S-wave energy release of earthquakes in the region of Friuli, Italy*. Geophys. J. Int., **128**, 399-408.

Castro R.R., Pacor F., Sala A. and Petrungaro C.; 1996: *S-wave attenuation and site effects in the region of Friuli, Italy*. J. Geophys. Res., **101**, 22355-22369.

Chen T. and Clayton R. W.; 2012: *Structure of central and southern Mexico from velocity and attenuation tomography*. J. Geophys. Res., **117**, B09302, doi:10.1029/2012J2IB009233.

Console R. and Rovelli A.; 1981: *Attenuation parameters for Friuli region from strong-motion accelerogram spectra*. Bull. seism. Soc. Am., **71**, 1981-1991.

Cormier V.; 1982: *The effect of attenuation on seismic body waves*. Bull. seism. Soc. Am., **72**, 6, S169-S200.

Eberhart-Phillips D.; 1986: *Three-dimensional velocity structure in Northern California Coast ranges from inversion of local earthquake arrival times*. Bull. seism. Soc. Am., **76**, 1025-1052.
Eberhart-Phillips D.; 1993: *Local earthquake tomography: Earthquake source regions*. in Seismic Tomography: Theory and Practice, edited by H.M. Iyer and K. Hirahara, Chapman and Hall, New York, pp. 613-643.
Eberhart-Phillips D., Reyners M., Chadwick M. and Chiu J.; 2005: *Crustal heterogeneity and subduction processes: 3-D Vp, Vp/Vs and Q in the southern North Island, New Zealand*. Geophys. J. Int., **162**, 270-288.
Evans J.R., Eberhart-Phillips D. and Thurber C.H.; 1994: *User's manual for SIMULPS12 for imaging Vp and Vp/Vs :A derivative of the "Thurber" tomographic inversion SIMUL3 for local earthquakes and explosions*. U.S.G.S., Open File Report, 94-931, 101 pp.
Franceschina G., Kravanja S. & Bressan G.; 2006: *Source parameters and scaling relationships in the Friuli-Venezia Giulia (Northeastern Italy) region*. Phys. Earth planet. Inter., **154**, 148-167.
Gentile G.F., Bressan G., Burlini L. and De Franco R.; 2000: *Three-dimensional VP and VP/VS models of the upper crust in the Friuli area (northeastern Italy).* Geophys. J. Int., **141**, 457-478
Gentili S. and Bressan G.; 2008: *The partitioning of radiated energy and the largest aftershock of seismic sequences occurred in the northeastern Italy and western Slovenia*. J. Seismol., **12**, 343-354.
Gentili S. and Franceschina G.; 2011: *High frequency attenuation of shear waves in the southeastern Alps and northern Dinarides*. Geophys. J. Int., **185**, 3, 1393-1416.
Goldberg, D.E. *Genetic Algorithms in Search, Optimization, and Machine Learning*, Addison-Wesley Publishing Company, INC.,1989, ISBN 0-201-15767-5.
Gruppo di lavoro CPTI, 2004. Catalogo Parametrico dei Terremoti Italiani, versione 2004 (CPTI04), INGV, Bologna, http://emidius.mi.ingv.it/CPTI04/.
Haberland C., Rietbrock A.; 2001: *Attenuation tomography in the western central Andes: A detailed insight into the structure of a magmatic arc*. J. Geophys. Res., **106**, B6, 11151-11167.
Hough S.E. and Anderson J.G.; 1988: *High frequency spectra observed at Anza, California: implications for Q structure*. Bull. seism. Soc. Am., **78**, 692-707.
Malagnini L., Akinci A., Herrmann R. B., Pino N.A. and Scognamiglio L.; 2002: *Characteristics of the ground notion in Northeastern Italy*. Bull. seism. Soc. Am., **92**, 2186-2204.
Mantovani E., Albarello D.,Tamburelli C. and Babbucci D.; 1996: *Evolution of the Tyrrhenian basin and surrounding regions as a result of the Africa-Eurasia convergence*. J. Geodyn., **21**, 35-72.
Michelini A. and McEvilly T.V.; 1991: *Seismological studies at Parkfield. Simultaneous inversion for velocity structure and hypocenters using cubic B-splines parametrization*. Bull. seism. Soc. Am., **81**, 2, 524-552.
Olsen K.B., Day S. M. and Bradley C.R.; 2003: *Estimation of Q for Long-Period (>2 sec) Waves in the Los Angeles Basin*. Bull. seism. Soc. Am., **93**, 2, 627-638.
Oppenheim A.V. and Schafer R.W.; 1999: *Discrete-Time Signal Processing*. Prentice-Hall, Upper Saddle River, NJ.
Rietbrock A.; 2001: *P wave attenuation structure in the fault area of the 1995 Kobe earthquake*, J. Geophys. Res., **106**, 4141-4154.
Thurber C.H.; 1993: *Local earthquake tomography: velocities and Vp/Vs – theory*, in Seismic Tomography – Theory and Practice, pp. 563-583, eds Iyier, H.M. & Hirahara, K., Chapman and Hall, London.
Thurber C.H., Eberhart-Phillips D.; 1999: *Local earthquake tomography with flexible gridding.* Computer and Geosciences, **25**, 809-818.

ACTIVE DEFORMATION ACROSS THE ZAGROS COLLISIONAL BELT AS DEDUCED FROM GEODETIC AND SEISMOLOGICAL OBSERVATIONS: PRELIMINARY RESULTS

P. Imprescia[1], M. Palano[2], A. Agnon[3], S. Gresta[4,5]
[1] *Istituto di Geologia Ambientale e Geoingegneria, Consiglio Nazionale delle Ricerche, Rome, Italy*
[2] *Istituto Nazionale di Geofisica e Vulcanologia, Osservatorio Etneo, Catania, Italy*
[3] *Institute of Earth Sciences, Hebrew University of Jerusalem, Israel*
[4] *Dipartimento di Scienze Biologiche, Geologiche e Ambientali, Università degli Studi di Catania, Italy*
[5] *Istituto Nazionale di Geofisica e Vulcanologia, Rome, Italy*

Introduction. The current tectonic setting of the Bitlis-Zagros Fold and Thrust Belt (BZFTB) is related to the complex convergent process between the Arabian and Eurasian plates which has been continuous since Late Cretaceous times after the closure of the Neo-Tethys Ocean, with a late episode of accentuated shortening during the Pliocene-Quaternary (e.g. Dewey *et al*., 1973; Numan, 1997; Abdulnaby *et al*., 2013). BZFTB is ca. 1200 km long and trends NW-SE between eastern Turkey, where it connects to the Anatolian mountain belt, and the Strait of Hormuz, where it connects to the Makran subduction zone (Fig. 1). It shows two main trends: the Bitlis EW trend, between the Arabian Plate and the Anatolian tectonic block, and the Zagros NW-SE trend, between the Arabian Plate and the Iranian tectonic block (Fig. 1).

Here we focused on the Zagros mountains which, longitudinally, is divided into two main geological domains: the North Zagros (hereinafter NZ) to the west and the Central Zagros (hereinafter CZ) to the east, separated by the NS-trending strike-slip Kazerun Fault System that cross-cuts the entire belt. NZ is considered as an high-taper wedge (ca. 2°) above a high-friction contact between the Phanerozoic cover and its Precambrian basement, whereas to the east, beneath CZ, the taper is lower (<1°) and pierced by diapirs of the infra-Cambrian Hormuz salt layer that lubricate the sole of the wedge (see Hessami *et al.*, 2006 and references therein).

Taking into account a large geodetic and seismological dataset, we investigated the pattern of the present-day crustal tectonic stress and strain-rate fields characterizing the Zagros. In particular, we compiled a database of fault plane solutions (FPSs) by merging data from public catalogues and literature. Subsequently, we divided the mapped area into 1°×1° squares and applied a stress inversion analysis to estimate the directions of maximum horizontal compressional stress in each square. In addition, we analyzed new GPS data coming from recent continuously operating stations, which were rigorously integrated with published velocities in order to provide a more complete picture of the crustal deformation along the Zagros. As a final step, we compared the horizontal directions of compressive stress (from seismological and geological observations) with those of the minimum contractional geodetic strain-rate.

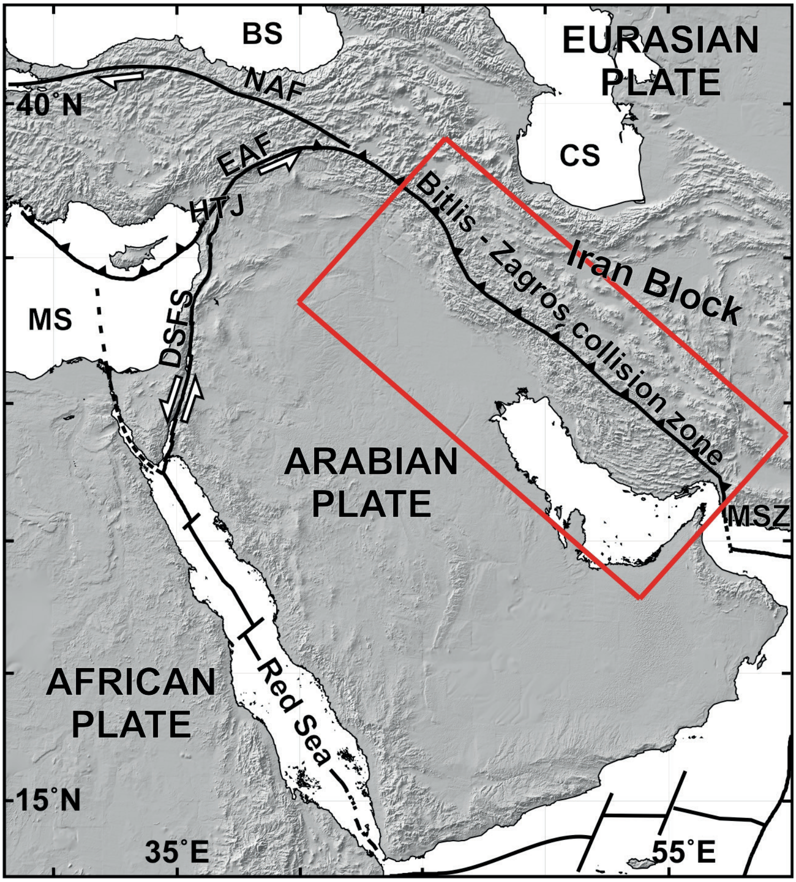

Fig. 1 – Regional plate tectonic setting of the study region and surrounding areas. Abbreviations are as follows: BS, Black Sea; CS, Caspian Sea; NAF; North Anatolian fault; ESF, East Anatolian fault; HTJ, Hatay triple junction; MS, Mediterranean Sea; DSFS, Dead Sea fault system; MSZ, Makran subduction zone. Red box is showing the study area.

Seismic data. Historical seismicity catalogues, probably incomplete due to political and social conditions in the area, reveal 5 events with M >7 before 1960 (Ambraseys and Jackson, 1998; Mirzaei *et al.*, 1997). Seismicity is anyway spread over the width of the Zagros (Fig. 2a), but it is characterized by moderate magnitude, generally less than 5. Instrumental catalogues are devoid of earthquakes with M ≥ 7 but only 6 events with $M_b \geq 6$.

Instrumental crustal seismicity (since 1960; M ≥ 2.5) registered on the investigated area is mainly distributed along the Zagros collisional belt, and defines elongated NW-SE-trending lineaments parallel to the fold axes (Fig. 2a). Seismicity decreases considerably toward the NW Arabia-Eurasia boundary line. In this gap, seismicity appears quite spread and earthquakes are little clustered. In the southern Iran and along Iran-Iraq southern boundary, seismic events show homogeneous behaviour in terms of magnitude and depth, which is generally confined in the first 35 km but most frequent between 10 and 25 km.

In order to study the pattern of seismic deformation and obtain a detailed map of stress orientations later, we have compiled a database of 387 fault plane solutions (with M ≥ 3) merging data from public catalogues and literature. We collected focal mechanisms from existing online and literature catalogues. In particular, we use the following on-line and free available moment tensor catalogues: Global Centroid Moment Tensor catalogue (Dziewonski *et al.*, 1981; Ekström *et al.*, 2012; GCMT; http://www.globalcmt.org); European-Mediterranean Regional Centroid Moment Tensor catalogue (Pondrelli *et al.*, 2002, 2004, 2007, 2011; RCMT; http://www.bo.ingv.it/RCMT/searchRCMT.html) and U.S. Geological Survey catalogue (USGS; http://earthquake.usgs.gov/earthquakes/eqarchives/sopar/).

To extend back in time the dataset and enlarge the magnitude range, we use published first-motion FPSs collected in the "Earthquake Mechanisms of the Mediterranean Area" database (EMMA; Vannucci and Gasperini, 2003, 2004; Imprescia, 2010; Vannucci *et al.*, 2010 and references therein) which contains in the last version (3.1) more than 12000 first-motion polarity FPSs of earthquakes from the Mediterranean area since 1905 and published until 2007. The final dataset count ca. 300 FPSs.

Focal mechanisms depict dominant reverse faulting and their nodal planes strike generally in a NW-SE direction which gradually changes toward EW approaching the south-east Persian Gulf (Fig. 2b). Nodal planes are parallel to regional structures and strikes behaviour follows folding directions of BZFTB, in accord with previous studies (e.g. Hatzfeld *et al.*, 2010). A significant fraction of reverse focal mechanisms are associated with hypocentral depth < 20 km, probably due to seismicity in the basement and not in the sedimentary succession (Berberian, 1995), and high dip angle, maybe related to reactivation of Mesozoic normal faulting (Jackson, 1980) inherited from the opening of the Tethys Ocean. The shortening is also accommodated by frequent strike-slip faulting processes, rupturing along the major tectonic structures.

In addition, we present a preliminary inversion of the state of stress in the investigated area by taking into account our dataset of earthquake focal mechanisms. For the stress inversion method, we adopted the Spatial And Temporal Stress Inversion (SATSI) program (Hardebeck and Michael, 2006) available from the USGS webpage. The SATSI method is a damped grid-search inversion for stress tensor orientation. The damping helps to decrease the artificial noise or isolated data singularities associated with stress field orientation inversion (Hardebeck and Michael, 2006). We divided the mapped area into 1°×1° squares, requiring a minimum of 10 earthquakes in each square to be included into the inversion procedure. The smoothed results, reported in Fig. 2c, well evidence a regional trend of the maximum horizontal compressional stress (Sh_{MAX}) which systematically changes from a NNE-SSW attitude, along NZ and the western sector of CZ, to a NS attitude on the eastern sector of CZ, maintaining always an orthogonal orientation with respect to the collisional mountain belt.

GPS data. Data acquired by continuous GPS sites installed across the Zagros collisional belt and freely availably on-line archives (i.e. SOPAC, UNAVCO, NGS) were processed by using the GAMIT/GLOBK software (Herring *et al.*, 2010) following the strategy reported

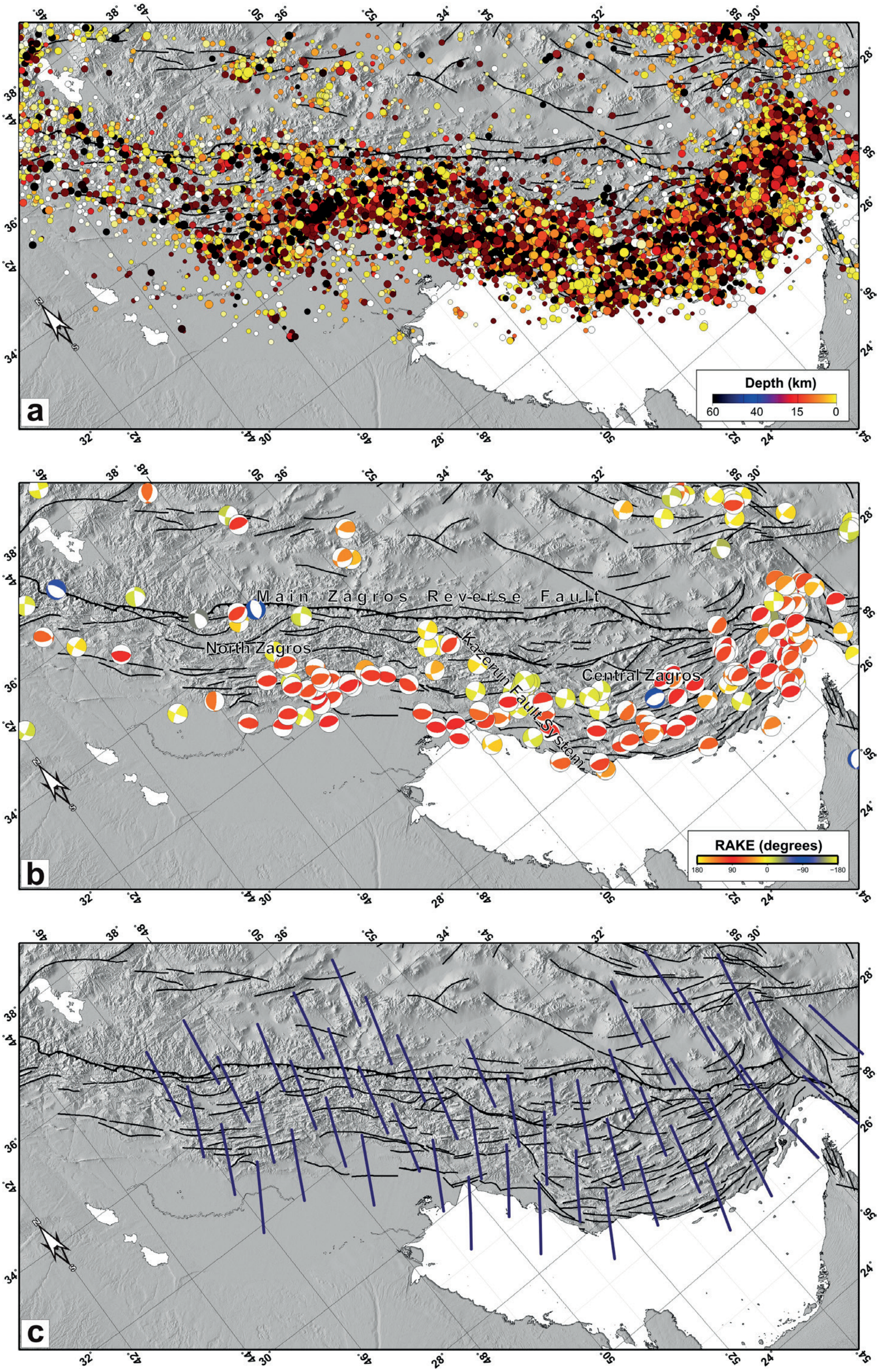

Fig. 2 – a) Instrumental crustal seismicity (M ≥ 2.5) occurring in the investigated area since 1960 (http://www.isc.ac.uk). b) Lower hemisphere, equal area projection for the 387 FPSs compiled for this study; FPSs are coloured according to rake: red indicates pure thrust faulting, blue is pure normal faulting, and yellow is strike-slip faulting. c) Sh_{MAX} pattern as obtained by preliminary inversion of the FPS dataset.

in Palano *et al.* (2012). To improve the overall configuration of the network and to tie the regional observations to an external global reference frame, data coming from 10 continuously operating IGS (International GNSS Service) stations were introduced in the processing. By using the GLOBK module, the regional observations are then combined, on a daily basis, with global solutions of the Scripps Orbital and Permanent Array Center (SOPAC) at University of California, San Diego (Bock *et al.*, 1997) and aligned to the ITRF2008 reference frame through a seven-parameter Helmert transformation (3 translations, 3 rotations and a scale factor). We then combined the corrected daily position estimates and their full covariance matrices to estimate a long-term average site velocity in the ITRF2008 reference frame.

Our GPS network shares some stations with the ones processed by Walpersdorf *et al.* (2006), Masson *et al.* (2007), Tavakoli *et al.* (2008), Djamour *et al.* (2011) allowing a rigorous integration by applying a Helmert transformation of the five estimated velocity fields. To adequately show the crustal deformation pattern over the investigated area, we rotate the final ITRF2008 GPS velocity solution into an Arabian fixed reference frame (Fig. 3a; Palano *et al.*, 2013). In addition, we compute the 2D strain-rate tensor over the studied area. In particular, as a first step, by taking into account the observed horizontal velocity field and associated

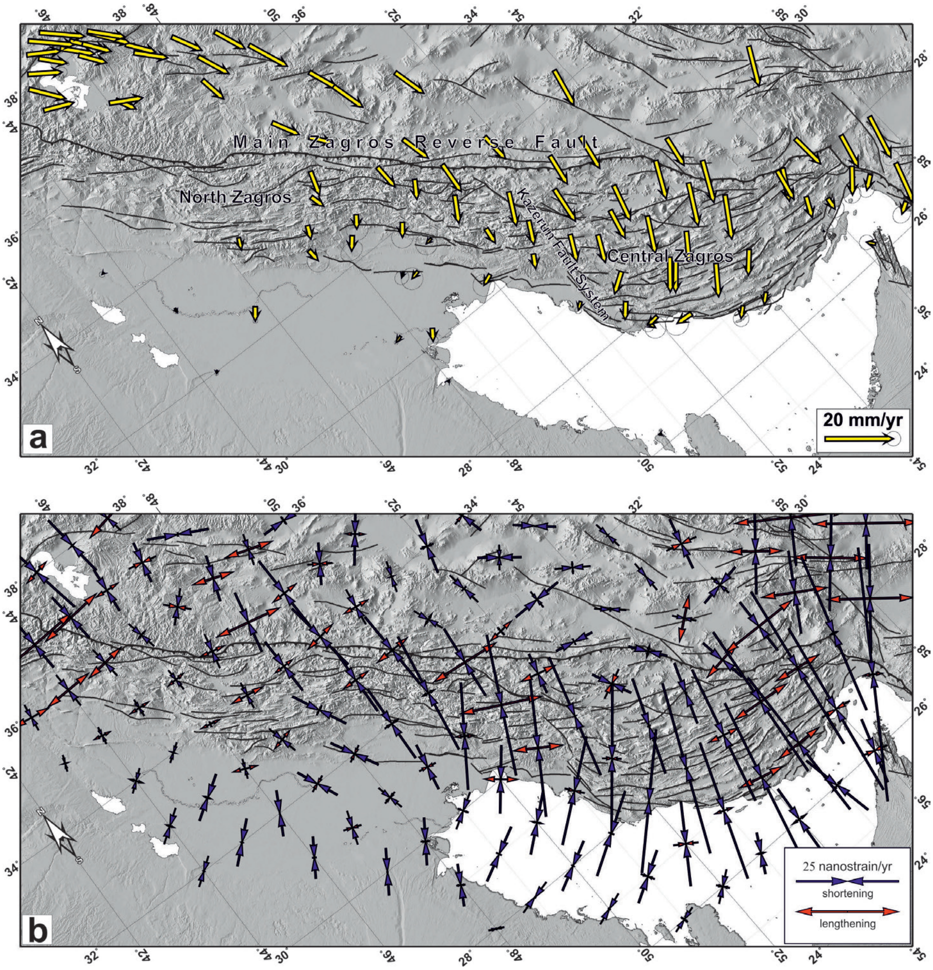

Fig. 3 – a) GPS velocities and 95% confidence ellipses in a fixed Arabian plate (see Palano *et al.*, 2013 for more details). b) geodetic strain-rate field: arrows represent the greatest extensional (red) and contractional (blue) horizontal strain-rates.

covariance information, we derived a continuous velocity gradient tensor on a regular 1° x 1° grid (whose nodes do not coincide with any of the GPS stations) using a "spline in tension" technique (Wessel and Bercovici, 1998). The tension is controlled by a factor T, where T=0 leads to a minimum curvature (natural bicubic spline), while T=1 leads to a maximum curvature, allowing for maxima and minima only at observation points; in our computations we set T=0.4. As a final step, we computed the average 2D strain-rate tensor as derivative of the velocities at the nodes of each grid cell. The estimated strain-rates are shown in Fig. 3b.

As shown in Fig. 3a, available GPS data do not cover with the same density the investigated area. In particular, while the southern part (i.e. Central Zagros; CZ) shows a regular station density across the collisional belt, the northern part (i.e. North Zagros; NZ) is sampled by few data, mainly concentrated along its NE and SW borders. Beside this limitation, the geodetic velocity field clearly depicts two main features. NZ is affected by a prevailing right-lateral shear mainly concentrated along the Main Zagros Reverse Fault (MZRF): stations located NE of MZRF move toward SW with rates of ~12 mm/yr while stations located across the collision belt move toward SE with rates of ~3 mm/yr. Southward, the velocity field depicts a spectacular rotation passing from a South-directed motion (rates of ~10-13 mm/yr) NE of MZRF to a SW-ward motion across CZ (rates of ~1-3 mm/yr). The 2D strain-rate map highlights better these main features (Fig. 3b). In particular, the maximum contractional horizontal strain-rate shows a fan-shaped feature across CZ maintaining always an orthogonal orientation with respect to the curvature of the collisional mountain belt; across this area a shortening up to ~50 nanostrain/yr can be recognized. Along NZ, the 2D strain-rate shows a complex pattern, probably due to the poor station density; on this area a general shortening up to ~25 nanostrain/yr is inferred.

Conclusive remarks. Based on the data presented here and discussed in the previous section, we may draw the following conclusions:

- A large amount of instrumental seismicity of the Zagros collisional belt ruptures a narrow belt located westward of MZRF. Seismicity appears mainly confined into the 10 and 25 km depth interval.
- Focal mechanism solutions show prevailing high-angle reverse faulting features with NW-SE strikes, parallel to the folding and well depicting the contractional nature of the mountain belt. Preliminary results about the state of stress of the area infer a Sh_{MAX} pattern showing trends always orthogonal with respect to the collisional mountain belt.
- GPS data indicate that NZ is affected by a prevailing right-lateral shear mainly concentrated along the Main Zagros Reverse Fault (MZRF), while across CZ the velocity field depicts a spectacular rotation coupled with a decrease of the velocity values. These patterns are well recognized on the 2D strain-rate field.
- A simple visual comparison of seismological stress and geodetic strain-rate directions shows that crust in the investigated area is contracting in the direction of maximum compression evidencing that, at this scale of observation, the release of elastic stress is at par with the tectonic loading of the crust.

References

Abdulnaby W., Mahdi H., Numan N., Al-Shukri H.; 2013: Seismotectonics of the Bitlis–Zagros Fold and Thrust Belt in Northern Iraq and Surrounding Regions from Moment Tensor Analysis. Pure and Applied Geophysics, doi:10.1007/s00024-013-0688-4.

Ambraseys N.N., Jackson J.A.; 1998: Faulting associated with historical and recent earthquakes in the Eastern Mediterranean region. Geophysical Journal International, 133, 390-406, doi:10.1046/j.1365-246X.1998.00508.x.

Berberian M.; 1995: Master 'blind' thrust faults hidden under the Zagros folds: active basement tectonics and surface morphotectonics. Tectonophysics, 241, 193-224.

Bock Y., Wdowinski S., Fang P., Zhang J., Behr J., Genrich J., Williams S., Agnew D., Wyatt F., Johnson H., Stark K., Oral B., Hudnut K., Dinardo S., Young W., Jackson D., Gurtner W.; 1997: Southern California Permanent GPS Geodetic Array: Continuous measurements of crustal deformation between the 1992 Landers and 1994 Northridge earthquakes. J. Geophys. Res., 102, 18,013-18,033.

Dewey J.F., Pitman W.C., Ryan W.B.F. and Bonnin J.; 1973: Plate tectonics and evolution of the alpine system. Bull. Geol. Soc. Am., 84, 3137-3180.

Djamour Y., Vernant P., Nankali H.R., Tavakoli F.; 2011: NW Iran-eastern Turkey present-day kinematics: Results from the Iranian permanent GPS network. Earth and Planetary Science Letters 307, 27-34, doi:10.1016/j.epsl.2011.04.029.

Dziewonski A.M., Chou T.A., Woodhouse J.H.; 1981: Determination of earthquake source parameters from waveform data for studies of global and regional seismicity. J. Geophys. Res., 86, 2825-2852, doi:10.1029/JB086iB04p02825.

Ekström G., Nettles M., Dziewonski A.M.; 2012: The global CMT project 2004-2010: Centroid-moment tensors for 13,017 earthquakes. Phys. Earth Planet. Inter., 200-201, 1-9, doi:10.1016/j.pepi.2012.04.002.

Hardebeck J.L., Michael A.J.; 2006: Damped regional-scale stress inversions: methodology and examples for southern California and the Coalinga aftershock sequence. J. Geophys. Res., 111, B11310, doi:10.1029/2005JB004144.

Hatzfeld D., Authemayou C., van der Beek P., Bellier O., Lavé J., Oveisi B, Tatar M., Tavakoli F., Walpersdorf A., Yamini-Fard F.; 2010: The kinematics of the Zagros Mountains (Iran) Geological Society, London, Special Publications, 330:19-42, doi:10.1144/SP330.3.

Herring T.A., King R.W., McClusky S.C.; 2010: Introduction to GAMIT/GLOBK, Release 10.4. Massachusetts Institute of Technology, Cambridge MA, 1-48.

Hessami K., Nilforoushan F., Talbot C.J.; 2006: Active deformation within the Zagros Mountains deduced from GPS measurements. Journal of the Geological Society, 163, 143-148, doi:10.1144/0016-764905-031.

Imprescia P.; 2010: Meccanismi focali di terremoti come strumento per la definizione della sismotettonica dell'area mediterranea. Ph.D. thesis, University of Catania.

Jackson J.A.; 1980: Reactivation of Basement Faults and Crustal Shortening in Orogenic Belt. Nature, 283, 343-346.

Masson F., Anvari M., Djamour Y., Walpersdorf A., Tavakoli F., Daignieres M., Nankali H., Van Gorp S.; 2007: Large-scale velocity field and strain tensor in Iran inferred from GPS measurements: new insight for the present-day deformation pattern within NE Iran. Geophysical J. International, 170, 436-440.

Mirzaei N., Gao M.T., Chen Y.T., Wang J.; 1997: A uniform catalog of earthquakes for hazard assessment in Iran. Acta Seismologica Sinica, 10, 6, 713-726.

Numan N.M.S.; 1997: A plate tectonic scenario for the phanerozoic succession in Iraq. Iraqi Geological Journal, 30, 85-119.

Palano M., Ferranti L., Monaco C., Mattia M., Aloisi M., Bruno V., Cannavò F., Siligato G.; 2012: GPS velocity and strain fields in Sicily and southern Calabria, Italy: Updated geodetic constraints on tectonic block interaction in the central Mediterranean. Journal of Geophysical Research, 117, B07401, http://dx.doi.org/10.1029/2012JB009254.

Palano M., Imprescia P., Gresta S.; 2013: Current stress and strain-rate fields across the Dead Sea Fault System: Constraints from seismological data and GPS observations. Earth and Planetary Science Letters, 369-370, 305-316, doi:10.1016/j.epsl.2013.03.043.

Pondrelli S., Morelli A., Ekström G., Mazza S., Boschi E., Dziewonski A.M.; 2002: European-Mediterranean regional centroid-moment tensors: 1997-2000. Phys. Earth Planet. Int., 130, 71-101.

Pondrelli S., Morelli A., Ekström G.; 2004: European-Mediterranean Regional Centroid Moment Tensor catalog: solutions for years 2001 and 2002. Phys. Earth Planet. Int., 145, 1-4, 127-147.

Pondrelli S., Salimbeni S., Morelli A., Ekström G., Boschi E.; 2007: European-Mediterranean Regional Centroid Moment Tensor catalog: Solutions for years 2003 and 2004. Phys. Earth Planet. Int., 164, 1-2, 90-112.

Pondrelli S., Salimbeni S., Morelli A., Ekström G., Postpischl L., Vannucci G., Boschi E.; 2011: European-Mediterranean Regional Centroid Moment Tensor Catalog: solutions for 2005-2008. Phys. Earth Planet. Int., 185, Issue 3-4, p. 74-81.

Tavakoli F., Walpersdorf A., Authemayou C., Nankali H.R., Hatzfeld D., Tatar M., Djamour Y., Nilforoushan F., Cotte N.; 2008: Distribution of the right-lateral strike-slip motion from the Main Recent Fault to the Kazerun Fault System (Zagros, Iran): Evidence from present-day GPS velocities. Earth and Planetary Science Letters, 275, 342-347.

Vannucci G., Gasperini P.; 2003: A database of revised fault plane solutions for Italy and surrounding regions. Computers & Geosciences, 29 (7), 903-909, doi:10.1016/S0098-3004(03)00094-3.

Vannucci G., Gasperini P.; 2004: The new release of the database of Earthquake Mechanisms of the Mediterranean Area (EMMA Version 2). Annals of Geophysics, 47 (1S), 307-334.

Vannucci G., Imprescia P., Gasperini P.; 2010: A new release (3.1) of the database of Earthquake Mechanisms of the Mediterranean Area (EMMA). European Seismological Commission 32nd General Assembly, September 6-10, Montpellier, France.

Walpersdorf A., Hatzfeld D., Nankali H., Tavakoli F., Nilforoushan F., Tatar M., Vernant P., Chéry J., Masson F.; 2006: Difference in the GPS deformation pattern of North and Central Zagros (Iran). Geophysical Journal International 167, 1077-1088.

Wessel P., Bercovici D.; 1998: Interpolation with splines in tension: a Green's function approach. Mathematical Geology. 30, 77-93.

DI ALCUNI TERREMOTI SCONOSCIUTI E POCO CONOSCIUTI DELL'ISOLA D'ISCHIA

F. Mastino
Free lance geologist, Roma

Si è intrapreso uno studio sulla sismicità dell'Isola d'Ischia con lo scopo di migliorare le conoscenze attuali, concentrando le ricerche sui forti terremoti poco conosciuti. È stata condotta all'uopo una ricerca bibliografica esclusivamente consultando testi stampati (articoli, libri e giornali) reperiti in biblioteche (in particolar modo nella Biblioteca Nazionale di Roma) e tramite internet consultando i testi nei siti dove è possibile leggerli e scaricarli in versione digitale (Google Books, Gallica ed altri). Questo studio può considersi come propedeutico alla consultazione di materiale documentale manoscritto presso archivi e biblioteche. Durante queste fase iniziale sono stati scoperte informazioni inedite che hanno permesso migliorare la conoscenza su alcuni terremoti ed in alcuni casi scoprire terremoti sconosciuti.

Parlando dei terremoti dell'Isola d'Ischia viene subito alla mente il disastroso terremoto del 1883 che causò la morte di 2333 persone (SSN, 1998). Tuttavia, oltre a questo, ve ne furono molti altri di minore intensità e meno disastrosi. Per molto tempo le conoscenze sulla sismicità di Ischia sono state ferme ai dati sintetizzati dal catalogo sismico del CNR-PFG (1985) nel quale, almeno per quanto concerne i forti terremoti dell'isola d'Ischia, si fa riferimento al catalogo di Baratta (1901). Nel tempo studi adeguati, soprattutto rivolti a revisionare i dati conosciuti, sono stati svolti sui forti terremoti del 1796, 1828 e 1883 (ING-SGA, 1995) e quelli del 1762, 1767, 1796 e 1828 (GNDT, 1995), ma apportando solo poche nuove conoscenze in termini di dati inediti.

Più recentemente Molin et alii (2008) hanno condotto uno studio su molti terremoti forti e minori presenti nel CPTI (Catalogo Parametrico dei Terremoti Italiani), mai revisionati in precedenza e le cui conoscenze avevano come riferimento il solo catalogo del CNR-PFG. In questo studio sono stati revisionati, per l'isola d'Ischia, i terremoti avvenuti negli anni 1557, 1841, 1863, 1867 e 1980. Gli autori per questi eventi apportano poche nuove informazioni a quello che già si conosceva, limitandosi a riportare solo in alcuni casi (1863, 1867 e 1980) notizie inedite tratte da giornali di scarsa importanza ai fini delle valutazione del campo macrosismico. Tuttavia, per il solo terremoto del 1980 questi dati migliorano la conoscenza di questo evento, i cui parametri erano riferiti solo a dati di tipo strumentale, senza notizie macrosismiche, mentre ora si conoscono anche gli effetti macrosismici. Per gli altri terremoti la revisione dei dati già conosciuti ha comunque apportato alcune modifiche in termini di valore delle intensità (vedi Tab. 1). Specificare. Sono sostanziali o secondarie?

Solo su due terremoti sono stati condotti studi ad hoc ed approfonditi. Il terremoto del 1883 è stato oggetto di una monografia da parte del Servizio Sismico Nazionale (1998), dove è stata condotta una ricerca su documenti d'archivio, giornali e libri a stampa, ricostruendo in modo dettagliato i danni verificatesi nelle varie località dell'isola. Lo stesso è avvenuto per il terremoto del 1275, conosciuto in bibliografia, ma che non era stato mai prima inserito nei cataloghi sismici in precedenza, pubblicato da Guidoboni e Comastri (2005) tramite un adeguato studio che ne ha, tra l'altro, determinato con precisione la data.

Tutti queste informazioni sono confluite e state inserite nel CPTI (versione 2011 aggiornata, Gruppo di lavoro CPTI); nella Tab. 1 si può vedere come sono evolute nel tempo le conoscenze sulla sismicità dell'Isola d'Ischia in termini di intensità massima risentita. In dettaglio, si nota che due terremoti riportati nel catalogo del CNR-PFG con una intensità pari a VII MCS (quelli del 1228 e del 1302), nel catalogo CPTI non sono presenti sin dalla prima versione del 1999, così come nelle versioni del precedente catalogo NT4.1.

Il terremoto del 1228 è ricordato in una cronaca medievale di Riccardo da San Germano (1937), maestro notaio del monastero di S. Germano vivente al momento dell'evento. Premettendo che non tutte le notizie da lui annotate sono vissute in prima persona, ma spesso alcuni fatti gli sono stati riferiti, la frase "… *Eodem mense Iulii Mons Iscle subversus est, et operuit in Casalibus sub eo degentes fere septigentos homines inter uiros et mulieres.* …" che

Data	CNR-PFG (1985)	GNDT (1997)	CPTI (1999)	Molin & alii (2008)	CPTI (2011)
1228/07/	VII	—	—	—	—
1275/11/02	—	—	—	—	VIII-IX
1302/02/	VII	—	—	—	—
1557	VII	VII	VII	**D**	—
1762/07/23	VII	**VI-VII**	VI-VII	—	VI-VII
1767	VII	**VI-VII**	VII-VIII	—	**D**
1796/03/18	IX	**VII-VIII**	VII-VIII	—	**VIII**
1828/02/02	IX	**VIII-IX**	**IX**	—	IX
1841/03/06	VII	VII	VII	**VI**	—
1863/01/30	VI-VII	VI-VII	VI-VII	**V**	—
1867/08/15	VI	VI	VI	**V-VI**	—
1881/03/04	VIII	VIII	VIII	—	**IX**
1883/07/28	IX	**X**	X	—	X
23/04/1980	—	—	—	V	—

Tab. 1 – Confronto dei cataloghi sismici. In grassetto sono riportati i parametri dei terremoti revisionati di volta in volta.

ricorda l'evento non è di immediata interpretazione e traduzione. Di fatto, la parola chiave subversus ha dato adito a diverse interpretazioni nel tempo.

Il primo autore che propone la possibile traduzione della frase è il Bonito (1691), nel suo eruditissimo testo sui terremoti, interpretando la notizia come una frana causata da terremoto. Altri autori interpretano in modo diverso la stessa frase riportata nella cronaca. Capecelatro (1724) la traduce parlando della formazioni di una voragine in cui sprofonda un monte e dei villaggi, mentre Camera (1842) la traduce parlando di un evento eruttivo. Mercalli (1885) è dell'idea che la frana sia stata causata da un terremoto, in quanto si sono innescati movimenti franosi in occasione di altri terremoti. Il Baratta (1901) riporta la conclusione del Mercalli. Sicuramente la notizia riportata nella cronaca non fa riferimento ad un'eruzione vulcanica, pur non essendo comunque chiaramente riconducibile ad un terremoto, ma più facilmente ad un evento franoso. Visto che l'isola d'Ischia è soggetta a frequenti fenomeni franosi, non solo innescati da terremoti, ma molto più spesso da eventi meteorici (Del Prete e Mele, 2006), si può pensare che la cancellazione dell'evento del catalogo possa essere legato alla sua origine non tettonica. Tuttavia, in studi recenti si continua a riportarlo come evento sismico, tanto che nella citata monografia del SSN (1998) gli viene anche assegnata un'intensità del IX-X MCS.

Nel 1302 sull'isola d'Ischia avviene l'eruzione vulcanica del Monte Arso, così come ricordato da diversi autori. Il catalogo del CNR-PFG riporta come fonte il Baratta, il quale a sua volta si rifà al Bonito che sembrerebbe riportare in modo integrale la notizia tratta da un libro di Paolo Regio (vescovo di Vico Equense tra il 1583 ed il 1607). Questi ricorda che il Pontano parla di questo evento nel "Trattato di Benea". Il fatto viene riportato con queste parole "… per l'horribile terremoto caddero a terra diversi nobili edifici …", non dando adito a dubbi riguarda la natura sismica dell'evento. Tuttavia, tutti gli altri autori non fanno riferimento ad alcun terremoto, ma solo all'eruzione vulcanica (si può vedere lo studio svolto da Buchner, 1986, dove vengono riportate le fonti principali), ne tanto meno si fa menzione di edifici distrutti. Ad oggi, non è stato ancora possibile consultare de visu il testo del Regio; ma, per quanto riguarda lo scritto di Giovanni Pontano, "Trattato di Benea", sicuramente egli fa riferimento al "De Bello Neapolitano". Di fatto, consultando l'edizione del 1509 (i.e., prima edizione a stampa del manoscritto del 1499), sull'intestazione di ogni pagina si trova scritto "DE BEL NEA", acronimo di "De Bello Neapolitano", che per errore può essere diventato "di Benea". In questa edizione però non si fa riferimento ad alcun terremoto, ma si riporta solo l'eruzione avvenuta sull'isola (vedi lib. VI). In conclusione si potrebbe pensare che Regio, non contemporaneo all'evento, abbia riportato l'eruzione del 1302 aggiungendovi di sua sponte il fatto del terremoto. In base a queste congetture si dovrebbe ritenere poco attendibile il Regio e quindi inesistente anche che il terremoto. Tuttavia, un recente studio condotto da Iacono (1996) sul libro VI del "De Bello Neapolitano", dove si parla di Ischia, parlando dell'eruzione si fa riferimento ad una postilla marginale, scritta in forma di appunto, contenuta nel codice autografo dell'ultima redazione del "De Bello Neapolitano" dove si menziona il terremoto. La frase latina, nella traduzione dell'autrice, restituisce così l'evento: "Il 15 gennaio della 15a indizione nell'anno del Signore 1302, di lunedì, durante un plenilunio vi fu un'eclissi di colore sanguigno. Successivamente il 18, a notte inoltrata, con un terremoto si verificò un'eruzione di lava infuocata". Questa postilla è stata cancellata dal curatore dell'edizione postuma, Pietro Summonte, con una serie di sbarrette per significare al proto che essa non doveva essere incorporata nel testo. L'autrice trae anche la conclusione che il Pontano abbia compiuto una ricerca su documenti coevi forse perduti. A questo punto si può pensare che il Regio abbia consultato tale manoscritto o altra versione manoscritta di questo testo, dove era riportata la notizia del terremoto che poi ha trascritto nel suo libro. Non è sbagliato, a questo ponto, riconsiderare la possibilità di reinserire questo evento nel catalogo dei terremoti.

Nell'attuale versione del catalogo CPTI (Gruppo di lavoro CPTI, 2011) non sono riportati, inoltre, i terremoti del 1557, 1841, 1863 e 1867, i quali sono invece presenti nel catalogo di AHEAD (2013). Per questi terremoti vedremo più avanti alcune possibili conclusioni.

Nella Tab. 1, dove sono riportati i forti terremoti al di sopra della soglia del danno (intensità ≥V-VI e magnitudo ≥4.0), si nota come dal terremoto del 1275 si passi a quello del 1557. Nel catalogo del CNR-PFG, dove sono riportate anche scosse di minore intensità, non vi è traccia di nessun altra scossa, neanche di bassa intensità. Quindi per 282 anni non si sa nulla dell'attività sismica dell'isola d'Ischia. Dal terremoto del 1557 si passa poi a quello del 1762; anche in questo caso, consultando il catalogo del CNR-PFG, non si trova riferimento a nessuna scossa neanche di bassa intensità. Per altri 205 anni non sappiamo nulla.

Per il XVIII secolo si ha contezza di tre forti scosse di terremoto (1762, 1767 e 1796) ma nessuna notizia relativa ad eventi di bassa intensità. Passando al XIX secolo, si conosce un numero doppio di forti scosse (1828, 1841, 1863, 1867, 1881 e 1883), mentre di scosse di bassa intensità, escludendo le repliche avvenute con i forti terremoti, se ne hanno undici, avvenute nell'arco di tutto il secolo. Se a queste ultime aggiungiamo quelle riportate da Mercalli (1885), e non presenti nel catalogo del CNR-PFG, arriviamo ad un totale di 17 scosse.

Analizzando questi dati si può giungere a due distinte conclusioni. In una si può pensare che l'attività sismica dell'isola d'Ischia sia andata crescendo nel tempo, culminando con il forte terremoto distruttivo del 1883, per poi decrescere e tornare ad una bassa attività sismica (per il XX ed inizio XXI secolo l'attività sismica è rappresentata solo da scosse di bassa intensità). D'altra parte, si può anche pensare che le lacune siano invece dovute ad una scarsa conoscenza di informazioni, riconducibile alla perdita della memoria storica di altre forti e minori scosse avvenute nell'isola negli archi di tempo considerati.

Nessuno finora ha intrapreso uno studio prendendo in considerazione la sismicità minore dell'isola. In passato, solo Alessio *et al.* (1996) accennano in pubblicazione un loro studio di revisione delle scosse principali e minori, studio che però non ha mai visto la luce.

Partendo non solo da queste considerazioni è stata intrapresa una ricerca sull'attività sismica di Ischia con lo scopo di migliorarne le conoscenze.

Ricordando le frasi di alcuni autori, possiamo subito affermare che qualcosa manca. Iasolino (1588) scrive "per, quasi, portentosi prodigi, incendi, terremoti, e altre cose simili, le quali nell'Isola, alcune volte, benché rare, appaiono", così come il d'Aloisio (1757) che scrive "…Da quel tempo [1301] in poi fino a giorni nostri non vi è memoria di altra accensione di fuochi sotterranei nell'Isola accaduta, sentendosi solamente di tempo in tempo qualche leggiero scotimento della terra …". Gli stessi Palmieri e Oglialoro (1884), facendo riferimento al periodo sismico del luglio 1880, scrivono "…Alcune di queste scosse furono avvertite a Casamicciola, ma con minore intensità, e le persone quivi convenute per l'uso delle acque furono consigliate a rimanersi, essendo le piccole scosse assai comuni nel paese, ma non pericolose. …". Infine, nel catalogo del CNR-PFG, per alcuni terremoti (1557, 1762, 1767, 1796 e 1867) si fa riferimento sempre alla stessa fonte (Baratta, 1901), mentre per due di questi terremoti (1557 e 1767), si hanno scarse informazioni: più avanti vedremo il perché.

Si è pensato quindi di condurre una ricerca su questi ed altri terremoti. Reperire informazioni sul terremoto del 1557 è risultato e risulta difficile. Di fatto, non si è mai scoperta la fonte originale da cui ha attinto la notizia D'Ascia (1867) nel redigere la sua storia sull'isola. La notizia riporta l'evento del crollo della chiesa parrocchiale di S. Vito, sita all'epoca a Campagnano. La difficoltà incontrata è dovuta al periodo storico, dove a scrivere non erano in molti e la stampa e la diffusione dei libri era molto limitata. In questo periodo la diffusione di notizie avveniva soprattutto con fogli manoscritti od a stampa (Avvisi) di tiratura molto limitata o tramite corrispondenze che avvenivano tra un regno ed i loro corrispondenti, così come il Vaticano veniva informato delle vicende delle varie chiese e parrocchie dai loro vescovi ed arcivescovi o avevano notizie degli altri regni dai nunzi apostolici. Considerando inoltre le varie vicissitudine in cui è passata l'isola d'Ischia nel XVI con guerre e scorribande di pirati, si può capire perché vi sia una carenza di notizie per questo periodo.


STORIA
DELL'ISOLA D'ISCHIA
DESCRITTA
DA
GIUSEPPE D'ASCIA
PARTE PRIMA
NAPOLI
STABILIMENTO TIPOGRAFICO DI GABRIELE ARGENIO
Vico de' SS. Filippo e Giacomo n. 26.
1867.

Fig. 1 – Frontespizio del libro di D'Ascia (1867), storia dell'isola d'Ischia, dove sono riportate le notizie sui terremoti del 1557 e del 1767, senza dare riferimenti delle fonti.

Per il terremoto del 1762 sono state reperite informazioni in alcune testate giornalistiche dell'epoca, sia nazionali che europee. Queste, comparate alle informazioni riportate dal Vanvitelli, aiutano a capire meglio il quadro dell'evento. Nel complesso, è possibile ricostruire che si è trattato di almeno tre scosse avvenute a distanza di pochi giorni una dall'altra. La prima molto lieve, la seconda più forte (V MCS) e la terza con danni associati, quali il crollo di una chiesa ed altri danni, senza comunque perdita di vite umane (VII MCS).

Per il terremoto avvenuto nel 1796, il primo a parlarne è stato De Rossi (1881) in un articolo sul terremoto del 1881, in cui dice di aver trovato rifermento a questo terremoto in un memoriale di una famiglia dell'isola d'Ischia e che avrebbe parlato di questo terremoto in modo più approfondito successivamente in un altro scritto. Cosa che non fece mai. Chi invece ne parlò in modo approfondito fu Mercalli (1884), senza tuttavia rivelare dove avesse attinto le informazioni. Tutti gli altri autori che riportano la notizia di questo terremoto fanno riferimento a questo lavoro, compreso Baratta (1901). Si sono dunque cercate informazioni consultando giornali dell'epoca ma lo spoglio ha dato esito negativo. Questa scossa sembra non aver lasciato traccia pur avendo causato la morte di 7 persone. Si ricorda che Breislak (1798) nell'estate del 1796 si trova a soggiornare a Lacco Ameno e pur girando tutta l'isola non accenna assolutamente a questo terremoto.

Per il terremoto del 1841 finora non sono state trovate informazioni inedite, a parte notizie in alcuni giornali e scritti. Sono stati invece trovati nuovi dati per la scossa del 1863, quale la traccia del risentimento a Capodimonte (Napoli), località per la quale non si conoscevano gli effetti, e dove sei minuti dopo la scossa si verificò anche una frana.

Per la scossa del 1867 sono state reperite informazioni che riportano danni al campanile della Chiesa parrocchiale che era situata in Piazza Maio (Casamicciola), oltre ad una notizia inedita sul risentimento a Lacco Ameno (almeno V MCS), altrimenti prima non nota.

È da notare che eseguendo la ricerca per gli eventi sopra citati sono stati trovati i riferimenti ad altre scosse sconosciute e mai considerate prima dai cataloghi sismici o studi scientifici.

Alcune di queste sono state menzionate in studi di carattere storico, ma mai prese in considerazione da quelli di sismologia storica.

Sono stati individuati 11 nuovi terremoti compresi nell'arco di tempo tra il 1631 ed il 1833 (vedi Tab. 2). La maggior parte di questi terremoti, pur essendo di bassa intensità, vanno comunque a colmare alcune lacune delle conoscenze sull'attività sismicità. Tra queste undici scosse quelle del 1635, 1768 e 1800 presentano effetti di maggiore intensità (**, vedere conclusioni). Per esempio, nel 1635, il terremoto causa la caduta di una torre di una chiesa (non ancora identificata) con la relativa morte di alcune persone. Da questi pochi e scarni dati si evince l'importanza di questo terremoto per i danni inferti.

Ancora, si è trovato il riferimento ad una scossa di terremoto avvenuta nel 1768 ad Ischia. La persona che ne fa menzione la riporta come una "considerevole" scossa, senza riportare ulteriori informazioni. La persona in questione, soggiornando in estate sull'isola qualche tempo dopo l'avvenimento, fa probabilmente riferimento alla scossa del 1767, a meno di non pensare che la scossa del 1767 sia in realtà avvenuta nel 1768. Di fatto, della scossa del 1767 si è sempre saputo poco; il primo a parlarne è il D'Ascia (1867) che fa riferimento al crollo di una chiesa al Rotaro, ma come per la scossa del 1557, l'autore non cita la fonte primaria da cui attinge questa notizia. Giornali dell'epoca attestano comunque che nel 1768 si è verificata una scossa, avvertita sino a Napoli e dintorni. Va verificato, quindi, se la scossa in questione è una nuova scossa o si tratta di quella del 1767.

Infine, per quanto concerne la scossa del 1800, per adesso si può dire soltanto che ci fu un terremoto ad Ischia, avvertito anche a Napoli con una certa "apprensione". Si può quindi pensare che il terremoto in questione possa aver causato danni ad Ischia, verosimilmente lievi.

DATA	AREA INTERESSATA	FONTE DI RIFERIMENTO
~~1228/07/~~	Isola d'Ischia	CNR-PFG (1985)
1302/01/18	Isola d'Ischia	Mastino (in preparazione)
~~1302/02/~~	Isola d'Ischia	CNR-PFG (1985)
1577	Isola d'Ischia	Tortora (1991)
1587	Isola d'Ischia	Tortora (1991)
?1622	Isola d'Ischia	Mastino (in preparazione)
1631	Isola d'Ischia	Mastino (in preparazione)
1635	Isola d'Ischia	Mastino (in preparazione)
1711/	Isola d'Ischia	Camassi & Caracciolo (1994)
1711/10	Isola d'Ischia	Camassi & Caracciolo (1994)
1731	Isola d'Ischia e di Procida	Mastino (in preparazione)
1762/07/	Isola d'Ischia	Mastino (in preparazione)
1762/07/14	Casamicciola	Mastino (in preparazione)
1800/12/31	Isola d'Ischia	Mastino (in preparazione)
?1806	Ischia	Mastino (in preparazione)
1812/09/	Casamicciola	Mercalli (1885)
1827	Isola d'Ischia	Mercalli (1885)
1830/06/26	Casamicciola	Mastino (in preparazione)
1833/11/27	Isola d'Ischia	Mastino (in preparazione)
1834	Isola d'Ischia	Mercalli (1885)
1863/01/30	Casamicciola	Mastino (in preparazione)
1864/10/30	Forio	Mercalli (1885)
1867/08/15	Casamicciola	Mastino (in preparazione)
1874/01/23	Casamicciola	Mercalli (1885)
1875/07/13	Casamicciola	Mercalli (1885)

Tab. 2 – Elenco riassuntivo delle scosse di cui si è fatto cenno. Le scosse barrate sono quelle da eliminare. Le scosse sottolineate sono quelle revisionate. Le scosse in grassetto sono sconosciute. Le altre sono scosse già conosciute, ma mai riportate in cataloghi sismici.

Oltre queste scosse sconosciute, si possono ricordare quelle riportate da Tortora (1991) avvenute negli anni 1577 e 1587, ma con informazioni scarne e non utili per valutare intensità e campo macrosismico. La stessa considerazione si può fare per il terremoto del 1711 riportato da Camassi e Caracciolo (1994), con notizie riprese dalla Gazzetta di Bologna.

In conclusione, la Tab. 2 elenca le scosse revisionate ed inedite menzionate in questa nota, evidenziando che l'attività sismica di Ischia avvenuta prima del XIX secolo è ancora poco conosciuta. I dati emersi dalla sola consultazione di testi a stampa permettono di ipotizzare che vi sia ancora molto da scoprire compulsando documenti originali in archivi e biblioteche. Ciò implica che l'isola d'Ischia ha avuto nel tempo un'attività sismica più frequente rispetto a quanto finora conosciuto.

Pensando agli sviluppi ed alla utilità che può avere questa ricerca, condotta senza l'appoggio di nessun istituto ed aiutato inizialmente solo da Diego Molin, spero di trovare il consenso da parte di qualcuno per continuarla, dedicandoci più tempo e poter mettere a frutto gli sforzi sinora conseguiti.

Bibliografia

AHEAD Working Group (2013). AHEAD, the European, distributed Archive of Historical Earthquake Data, doi:10.6092/INGV.IT-AHEAD. Consultabile alla pagina web http://www.emidius.eu/AHEAD/main/

Alessio G., Esposito E., Ferranti L., Mastrolorenzo G. & Porfido S. (1996). Correlazione tra sismicità ed elementi strutturali nell'Isola d'Ischia. Il Quaternario, 9 (1), 303-308.

Baratta M. (1901). I terremoti d'Italia. Saggio di Storia, Geografia e Bibliografia sismica italiana con 136 sismocartogrammi. Torino, Fratelli Bocca Editori, pp. 950 + errata corrige.

Bonito M. (1691). Terra tremante ovvero continuatione de' terremoti dalla creatione del mondo sino al tempo presente. Napoli, Parrino, pp. 822.

Breislak S. (1798). Topografia fisica della Campania di Scipione Breislak prof. di mineralogia del corpo reale d'artiglieria di sua maestà il re delle Due Sicilie dedicata a S. E. la signora contessa Skawronsky nata baronessa Strogonow dama di ritratto di S. M. Imp. delle russie e cav. dell'ordine di S. Caterina. Firenze, nella Stamperia di Antonio Brazzini, MDCCLXXXXLVIII, pp. XII+368.

Buchner G. (1986). Eruzioni vulcaniche e fenomeni vulcano-tettonici di età preistorica e storica nell'Isola d'Ischia. In: "Eruptions volcaniques, tremblements de terre et vie des hommes dans la Campanie Antique", Pubbl. n. 7 (Napoli, Centre J. Bérard), 145-188.

Camassi R. & Caracciolo C. (1994). The gazette "Bologna": an observer of European natural events in the early 18th century. In: Materials of the CEC Project "Review of historical seismicity in Europe", edited by Albini P. & Moroni A., vol. 2, 153-162.

Camera Matteo (1841-1860). Annali delle Due Sicilie dall'origine e fondazione della monarchia fino a tutto il regno dell'augusto sovrano Carlo III di Borbone. Napoli, dalla Stamperia del Fibreno, voll. 2, I (1841) – pp. LXIII+368, II (1860) – pp. 523.

Capecelatro Francesco (1724). Istoria della Città, e del Regno di Napoli detto di Cicilia da che pervenne sotto il dominio de i Re, di D. Francesco Capecelatro napoletano. In Napoli, per Gio: Andrea Benvenuto, MDCCXXIV, vol. I – pp. 389+index, vol. II – pp. 331+index.

CNR/PFG (Postpischl D. ed.) (1985). Catalogo dei terremoti italiani dall'anno 1000 al 1980. C.N.R., Progetto Finalizzato Geodinamica, Quad. Ric. Scient., n. 114-2B. Bologna, pp. 239.

D'Aloisio Gian-Andrea (1757). L'infermo istruito dal dottore D. Gian-Andrea d'Aloisio nel vero salutevole uso de' rimedj minerali dell'Isola d'Ischia, colle lettere critiche scientifiche ed erudite concernenti una tal'Opera del dottore D. Giuseppe Maria Verlicchi dedicata all'Eccellentissimi Signori eletti della fedelissima città di Napoli. Napoli, MDCCLVII. Nella Stamperia di Giuseppe di Domenico e Vincenzo Manfredi. Con licenza de' Superiori, pp. 16+488.

D'Ascia, Giuseppe (1867 [1985]). Storia dell'Isola d'Ischia. Nota introduttiva di Nino D'Ambra. Riedizione. Edizioni del Castello aragonese. Edizioni del Castello aragonese. [Bologna]: Analisi, 527 p. Ripr. dell'ed.: Napoli, Stab. tip. G. Arsenio, 1867.

De Rossi M.S. (1881). Intorno all'odierna fase dei terremoti in Italia e segnatamente sul terremoto in Casamicciola del 4 marzo 1881. Boll. Soc. Geogr. It., s. 2a, 6, 329-351.

Del Prete S. & Mele R. (2006). Il contributo delle informazioni storiche per la valutazione della propensione al dissesto nell'Isola d'Ischia (Campania). Rend. Soc. Geol. It., 2, nuova serie, pp. 29-47.

GNDT (1997). NT4.1 - un catalogo parametrico di terremoti di area italiana al di sopra della soglia del danno, a cura di R. Camassi e M. Stucchi. Rimini, Tipolitografia Garattoni, pp. XX+66+XVII.

GNDT Archivio Macrosismico (1995). Studi preliminari di terremoti attraverso i repertori sismologici. Archivio macrosismico del GNDT, Milano.

Gruppo di lavoro CPTI (1999). Catalogo parametrico dei terremoti italiani. Bologna, Editrice Compositori, pp. 88. [prima versione]

Gruppo di lavoro CPTI (2011). Catalogo parametrico dei terremoti italiani. Ultima versione aggiornata consultabile alla pagina web http://emidius.mi.ingv.it/CPTI11/

Guidoboni E. & Comastri A. (2005). Catalogue of earthquakes and tsunamis in the Mediterranean area from the 11th to the 15th century. Roma-Bologna, INGV-SGA, pp. 1037.

Iacono Antonietta (1996). La "Guerra d'Ischia" nel De Bello Neapolitano di G. Pontano. Quaderni dell'Accademia Pontaniana, n° 19. Napoli, Accademia Pontaniana, nelle Officine grafiche napoletane "Francesco Giannini & Figli S.p.A.", pp. 90.

Iasolino Giulio (1588). De' rimedi naturali che sono nell'isola di Pithecusa hoggi detta Ischia. Lacco Ameno d'Ischia, 2000. IMAGAENARIA, pp. XXVII+342.
ING-SGA (1995). Catalogo dei forti terremoti in Italia dal 461 a.C. al 1980. A cura di E. Boschi, G. Ferrari, P. Gasperini, E. Guidoboni, G. Smriglio & G. Valenzise, Istituto Naz. di Geofisica - SGA storia geofisica ambiente. Ozzano Emilia, pp. 973 con allegato CD-ROM 1.
Mastino F. (in preparazione). Catalogo dei terremoti dell'Isola d'Ischia.
Mercalli G., (1885). L'Isola d'Ischia ed il terremoto del 28 luglio 1883. Mem. R. Ist. Lombardo di Sc. e Lett., 15 (2) (6 della s. III), 99-154. Milano.
Molin D., Bernardini F., Camassi R., Caracciolo C.H., Castelli V., Ercolani E., Postpischl L. (2008). Materiali per un catalogo dei terremoti italiani: revisione della sismicità minore del territorio nazionale. Quaderni di Geofisica, 57, 78 pp. (CD-Rom, 1444 pp.)
Palmieri L. & Oglialoro A., 1884. Sul terremoto dell'isola d'Ischia della sera del 28 luglio 1883. Estratto Atti Acc. Sc. fis. e mat., s. 2a, 1(4), pp. 1-28.
Pontano Giovanni (1509). De Bello Neapolitano. Napoli, Mayr, pagine non numerate.
Riccardo da San Germano [Ryccardi de Sancto Germano] (1937). Cronica. In: Raccolta degli storici italiani dal cinquecento al millecinquecento ordinata da L.A. Muratori. N. ed. riveduta ampliata e corretta con la direzione di G. Carducci – V. Fiorini – P. Fedele, Tomo VII, P. II, pp. 1-219. R. Ist. Storico Italiano per il Medio Evo.
SSN - Servizio Sismico Nazionale (1998). Il terremoto del 28 luglio 1883 a Casamicciola nell'Isola d'Ischia. Istituto Poligrafico e Zecca dello Stato, Roma, pp. 333.
Tortora Alfonso (1991). Per una storia dei terremoti nella Campania del '500. In: Atti "Colloquio sulle scienze della terra in onore di Nicola Covelli" – Caiazzo 27 maggio 1989, a cura di Antonio Pozzuoli. Associazione Storica del Caiatino, vol. 8, pp. 67-73. Napoli, Arte Tipografica.

CHARACTERISTICS OF HIGH FREQUENCY GROUND MOTIONS IN THE MAULE REGION (CHILE), OBTAINED FROM AFTERSHOCKS OF THE 2010 M_W 8.8 EARTHQUAKE

I. Munafò[1], L. Malagnini[1], R. B. Herrmann[2]
[1] *Istituto Nazionale di Geofisica e Vulcanologia, Rome, Italy*
[2] *Saint Louis University, St. Louis, MO, United States*

Introduction. The M_w 8.8 Maule earthquake occurred about 3 km off the coast of the central Chile on 2010 February 27 at 03:34 local time (06:34 UTC) with intense shaking lasting for about three minutes and it was followed by thousands of aftershocks. The earthquake took place along the boundary between the Nazca and South American tectonic plates, at the location where the Nazca plate is subducting beneath the South America tectonic plate at a rate of about 74 mm/yr.

The subduction zone event caused severe ground shaking across a 660 km swath of the country and generated a tsunami that ravaged the coastline. Chile is located on a convergent plate boundary that generates maga-thrust earthquake since the Paleozoic era (500 million years ago). In fact, based on the historical record, the Chilean coast has suffered many mega-thrust earthquakes along this plate boundary, including the strongest earthquake ever measured (1960 Valdivia earthquake, M 9.5). The segment of the fault zone that ruptured in this earthquake was estimated to be over 700 km long with a displacement of almost 10 meters. It lays immediately north of the 1000 km segment that ruptured in the great earthquake of 1960.

This study uses a data set consisting of 172 aftershocks of the M_w 8.8 Maule earthquake recorded by more than 100 temporary broadband stations deployed between March 2010 and January 2011 (Fig. 1). Each of these earthquakes use the relocations performed for National Earthquake Information Center (NEIC) and is characterized by a well-constrained focal mechanism and moment magnitudes in the range M_w 3.7 to 6.2. The RMTs were determined using the WUS velocity model (Herrmann *et al.*, 2011). Most of these earthquakes are characterized by shallow, eastward-dipping, thrust-type focal mechanisms consistent with faulting at or near the plate interface.

The aim of this work is to quantitatively describe the high-frequency ground motion scaling in the Chile region for constraining the amplitude expected from future earthquakes in subduction zone. To accomplish this, regressions are performed with large data sets that cover a wide range of earthquake size and hypocentral distance to calibrate model-based predictions of excitation and propagation.

Data processing. We will use the same methodology (for more details see the papers below) for data processing and analysis as was successfully used in studies with data sets from Italy (Malagnini *et al.*, 2000a, 2002; Morasca *et al.*, 2006; Scognamiglio *et al.*, 2005), Central Europe (Malagnini *et al.*, 2000b; Bay *et al.*, 2003) and from Utah e Yellowstone (Jeon *et al.*, 2004).

In order to obtain the scaling relationships for the high-frequency ground motion in the Maule region (Chile), regressions are carried out from 172 regional aftershocks with magnitude ranging from $M_w \simeq 3.7$ to $M_w = 6.2$. The digital data are corrected for instrument response to ground and the peak ground velocities are measured in selected narrow-frequency bands, between 0.2 and 30 Hz.

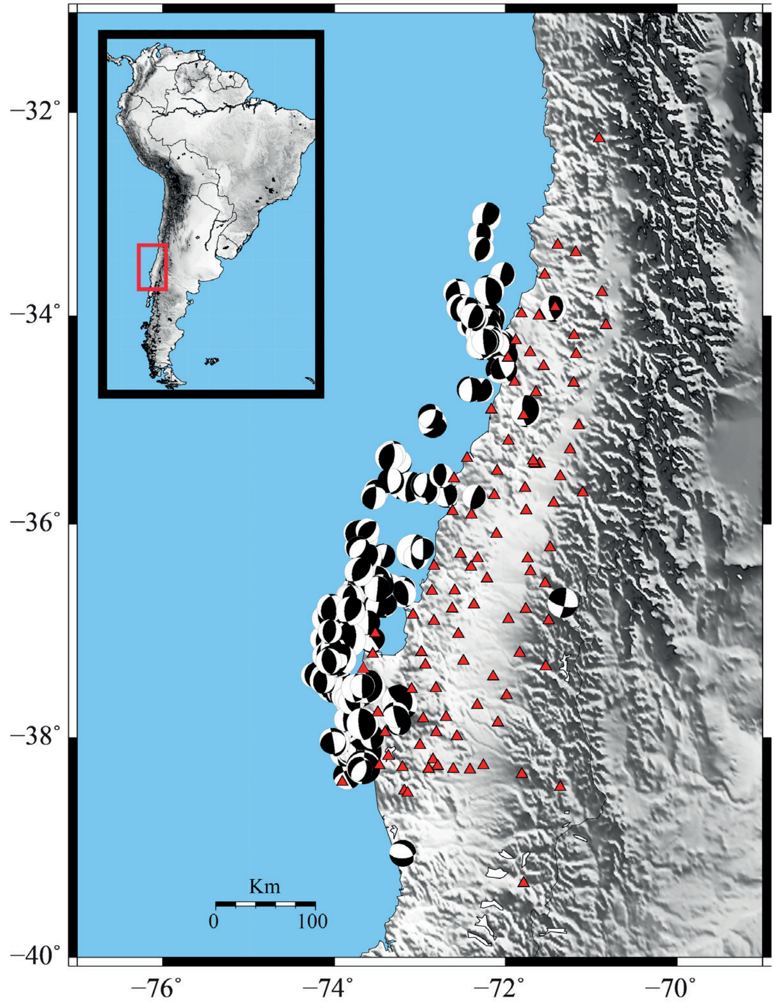

Fig. 1 – Map of the Maule region (Chile). Beach balls indicate the moment tensor solutions of all 172 aftershock in the range M_w 3.7 to 6.2. Red triangles indicate the positions of the broadband seismic stations used in this study.

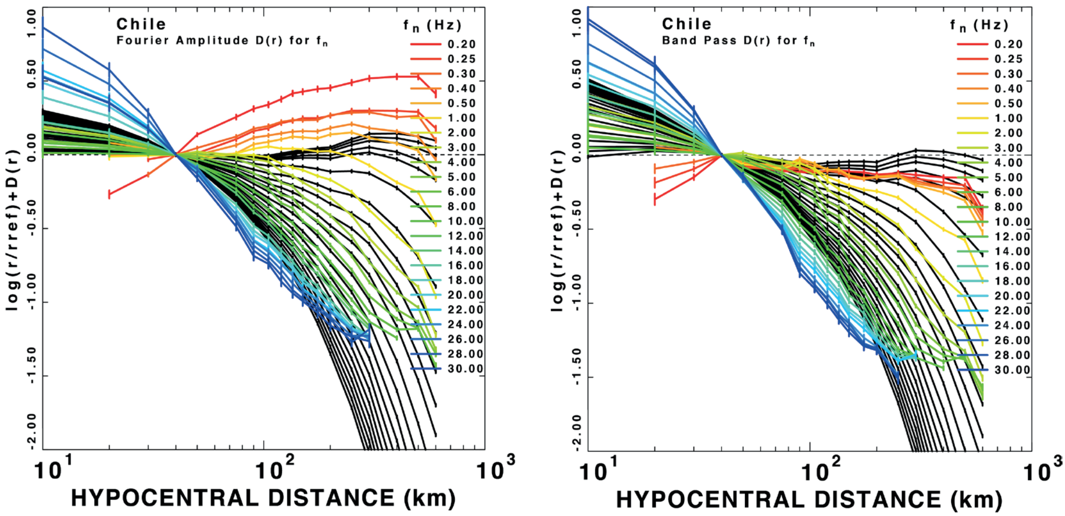

Fig. 2 – The regional attenuation functional D (*r, rref, f*) obtained for the Maule region from the regression on the peak amplitudes of the band-pass-filtered ground velocities (right) and of the Fourier spectral amplitudes (left) at the sampling frequencies of 0.20, 0.25, 0.30, 0.40, 0.50, 1.00, 2.00, 3.00, 4.00, 0.50, 1.00, 2.00, 3.00, 4.00, 5.00, 6.00, 8.00, 10.00, 12.00, 14.00, 16.00, 18.00, 20.00, 22.00, 24.00, 26.00, 28.00 and 30.00 Hz (color curves). The attenuation function is normalized to zero at the reference hypocentral distance of 40 km. The black curves in the background are from a attenuation model: geometrical spreadind 1/r from the source, out to 100 km, $r^{0.7}$ for larger distances; the anelastic attenuation used was the following: $Q(f)=200f^{0.5}$.

Ground motion attenuation with distance and the variation of excitation with magnitude are parameterized for this area to define a consistent model that describes both peak ground motion and Fourier spectra observations (Fig. 2). The regression results are plotted with color lines and the theoretical predictions as a solid black curves. Regression results for Fourier amplitude spectra and peak velocities are used to define a piecewise continuous geometrical spreading function, frequency dependent attenuation paramenter *Q (f)*, and a distance-dependent duration.

A general form for a predictive relationship for observed ground motion is written as:

$$\mathrm{AMP}\,(f, r) = \mathrm{EXC}\,(f, r_{\mathrm{ref}}) + \mathrm{SITE}\,(f) + \mathrm{D}\,(r, r_{\mathrm{ref}}, f) \qquad (1)$$

where AMP (f, r) represent the logarithm of peak amplitude of ground motion velocity on each filtered seismogram recorded at the hypocentral distance r, EXC (f, r_{ref}) is the excitation term for the ground motion at an arbitrary reference hypocentral distance r_{ref}, SITE (f) represents the distortion of the seismic spectra induced by the shallow geology at the recording site, D (r, r_{ref}, f) represents an estimate of the average crustal response for the region at the hypocentral distance r, at the frequency f. It is determined as a piecewise linear function (Yazd, 1993; Anderson and Lei, 1994; Harmsen, 1997), allowing to consider complex behavior of the regional attenuation.

The results of the analysis show that the regional attenuation of the ground motion can be modeled with a geometric spreading function with a 40-km crossover distance. A body-wave geometric spreading, $g\,(r) \sim r^{-1}$, is used at hypocentral distances (r < 100 km). Eq. (1) is solved in time domain, from multiple narrow band-pass signals.

Due to the constraints applied to the system prior to the regressions, the excitation term represents the expected peak ground motion at the reference distance, as it would be observed at a site representative of the average site response of the network. For reproducing $D\,(r, r_{\mathrm{ref}}, f)$ we use the crustal attenuation parameter

$$Q\,(f) = 200\,f^{0.5} \qquad (2)$$

The quality factor given in Eq. (2), and coupled with a simple $1/r$ geometrical spreading, is consistent with the results described by Garcia *et al.* (2004), who found: $Q\,(f) = 251\,f^{0.58}$.

Also two parameters are used to predict shapes and levels of the seismic spectra, the stress drop $\Delta\sigma$, and a high-frequency attenuation parameter $\kappa = 0.030$.

For example, comparisons can be done among different zone in which this kind of studies have been conducted. It has been found that the western Alps (Morasca *et al.*, 2006), eastern Alps (Malagnini *et al.*, 2002), Southern Appenines, central Italy (Malagnini *et al.*, 2000a), eastern Sicily (Scognaniglio *et al.*, 2005), Central Europe (Malagnini *et al.*, 2000b; Bay *et al.*, 2003), Utah e Yellowstone (Jeon *et al.*, 2004), and Chile region (this work) have different characteristics for the attenuation parameters because the combination of the geometrical spreading function and the parameter $Q\,(f)$ is strictly related to the crustal characteristics.

Fig. 3 compares the observed and predicted excitation of filtered velocity spectra obtained from the Chile region. The black lines indicate the regression result, and the red thick lines denote the theoretical excitations computed. After trying to fit using a costant stress drop, we then programmed a frequency dependent stress drop scaling

$$\Delta\sigma = M_0 f_c^{\,3} \qquad (3)$$

with the constrain that $M_0 f_c^{\,p}$ = costant. We found:

$$\log\Delta\sigma = (1\text{-}3/p)\,\log M_0 + \log\,(k^{-3/p}) \qquad (4)$$

where $\log M_0 = 1.5\,(M_w + 6.03)$.

By referring everything to D_{sref}=10 MPa and M_{wref} =3, we can compute stress drop that changes with M_w:

$$\log\Delta\sigma = (1\text{-}3/p)\,(M_w - M_{wref}) + \log\Delta\sigma_{\,ref} \qquad (5)$$

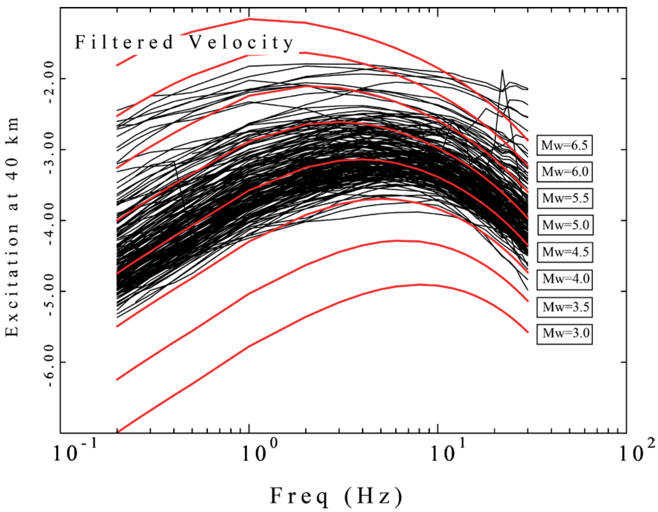

Fig. 3 – Filtered ground velocity excitation terms relative to the aftershocks recorded during the Maule seismic sequence in 2010 (black lines). Red thick lines indicate the theoretical prediction at the indicated levels of moment magnitude.

For this work we assume that p=4 and that $\Delta\sigma$ = 10 MPa at M_w=3. Tab. 1 provide the parameters of our working model.

An important goal of this research it will be represented by the study on source scaling. We will perform this task by using a technique based on the analysis of source spectral ratios. Numerous studies were published by Malagnini, Mayeda, and co-workers on all tectonic environments (normal, strike-slip, and reverse), but no data have yet been analyzed on subduction earthquakes; for this reason, the present data set is thus of special interest.

Conclusions. The prediction of the earthquake ground motion has always been of primary interest for seismologists and structural engineers. For engineering purposes it is necessary to describe the ground motion according to certain number of ground motion parameters such as: amplitude, frequency content and duration of the motion. However, it is necessary to use more than one of these parameters to adequately characterize the ground motion excited by a specific source, and observed at a specific site. In order to do that, we analyzed data set acquired by portable network installed to monitor the aftershocks of the Maule earthquake to validate the analysis procedure.

Tab. 1 – Parameters of our working model.

M_w	Δσ (MPa)
3.0	10
3.5	15.4
4.0	23.7
4.5	35.6
5.0	56.2
5.5	86.6
6.0	133.4
6.5	205.4

This study provides a unique opportunity to quantify high-frequency earthquake ground motion in a subduction zone due to the quality and quantity of observations in the frequency and distance range of 0.2-30 Hz and 40-500 km, respectively. The analysis was done using a two-step modeling procedure: 1) a regression is performed to characterize source duration and excitation, source-receiver distance dependence, and station site effects; 2) a point-source forward model is constructed in terms of geometrical spreading, observed duration, site effects, and source scaling, in order to match the regression results. This procedure may provides the necessary point source parameters for a stochastic finite-fault modeling of the ground motions for future large earthquakes in this subduction zone.

A proper description of ground motion scaling requires presenting enough information to duplicate the observations. This means that, until definitive information will be available on source scaling and absolute site effects, $Q(f)$ cannot be presented without also being coupled to $g(r)$ and κ.

Acknowledgements. We are grateful to IRIS for providing all the data used in this research. We would like to thank to Dr. Kendra L. Johnson for collecting the data set for the RMTs solutions. We thank Dr. Harley Benz for his comments about this work. Fig. 1 was produced using the Generic Mapping Tools (Wessel and Smith, 1995).

References

Anderson J.G. and Lei Y.; 1994: *Non-parametric description of peak acceleration as a function of magnitude, distance and site in Guerrero, Mexico.* Bull. Seism. Soc. Am., 84, 1003-1017.

Bay F., Fah D., Malagnini L. and Giardini D.; 2003: *Spectral shear-wave ground motion scaling for Switzerland.* Bull. Seism. Soc. Am., 93, 414-429.

García D., Singh S.K., Herráiz M., Pacheco J.F. and Ordaz M.; 2004: *Inslab earthquakes of central Mexico: Q, Source Spectra, and Stress Drop.* Bull. Seism. Soc. Am., 94, 789-802.

Harmsen S.; 1979: *Estimating the diminution of shear-wave amplitude with distance: application to the Los Angeles, California, urban area.* Bull. Seism. Soc. Am., 87, 888-903.

Herrmann R.B., Benz H. and Ammon C.J.; 2011: *Monitoring the Earthquake source process in North America.* Bull. Seism. Soc. Am., 101, 2609-2625, doi: 10.1785/0120110095.

Jeon Y.S. and Herrmann R.B.; 2004: *High-frequency ground-motion scaling in Utah and Yellostone.* Bull. Seism. Soc. Am., 94, 1644-1657.

Malagnini L., Herrmann R.B. and Di Bona M.; 2000a: *Ground motion scaling in the Apennines (Italy).* Bull. Seism. Soc. Am.,90, 1062-1081.

Malagnini L., Herrmann R.B. and Koch K.; 2000b: *Ground motion scaling in Central Europe.* Bull. Seism. Soc. Am.,90, 1052-1061.

Malagnini L., Akinci A., Herrmann R.B., Pino N.A. and Scognamiglio L.; 2002: *Characteristics of the ground motion in northeastern Italy.* Bull. Seism. Soc. Am., 92, 2186- 2204.

Morasca, P., Malagnini L., Akinci A., Spallarossa D. and Herrmann R.B.; 2006: *Ground motion scaling in the Western Alps,* J. Seismol., 10, 315-333.

Scognamiglio L., Malagnini L., Akinci A.; 2005: *Ground Motion scaling in Eastern Sicily (Italy).* Bull. Seism. Soc. Am., 95, 568-578.

Yadz M.R.S.; 1993: *Ground motion studies in the Southern Great Basin of Nevada and California.* Ph.D. Thesis, Saint Louis University.

FAULT ACTIVITY MEASUREMENTS FROM INSAR SPACE GEODESY: THE FUNDAMENTAL ROLE OF GEOLOGICAL CONSTRAINTS FOR CORRECT DATA INTERPRETATION AND ANALYTICAL FAULT MODELING

G. Pezzo

Istituto Nazionale di Geofisica e Vulcanologia, CNT, Roma, Italy

Introduction. In this study we present some examples of measurement and modeling of the earthquake cycle, in different tectonic domains; we discuss some common problems concerning geodetic data interpretation and fault modeling related to the availability of geological data at the surface and at depth.

The study of surface deformation is one of the most important topics to improve the knowledge of the deep mechanisms governing the seismic cycle itself and, eventually, improve the assessment of seismic hazard. To measure the crustal ground deformation associated to fault activity and to the earthquake-cycle we use DInSAR (Differential Interferometric Synthetic Aperture Radar) (Massonnet and Feigl, 1995), MAI (Multi Aperture Interferometry) (Scheiber and Moreira, 2000), (Bechor and Zebker, 2006) and multitemporal InSAR methods (Ferretti *et al.*, 2001; Berardino *et al.*, 2002; Hooper, 2007). Currently these techniques allow measuring short-term ground displacement with centimetric accuracy (DInSAR and MAI), and ground velocities with an accuracy of up to one millimeter per year over time periods of several years (Casu *et al.*, 2006). These levels of accuracy make interferometric methods suitable for the study of tectonic processes, typically affected by deformation rates ranging from millimeters to centimeters per year. Furthermore, these methods allow measurement of ground movements occurring on the different time scales of the earthquake cycle, from the nearly instantaneous deformation caused by seismic dislocations (Massonnet *et al.*, 1993), to the slow strains of the interseismic phase (Wright *et al.*, 2001).

Many conceptual, numerical, analytical and analog models of the earthquake cycle have been proposed to explain seismological, geological, geomorphological and geodetic data.

It is today accepted that the seismic cycle can be subdivided in three main different phases: interseismic, coseismic and postseismic (e.g. Scholz and Kato, 1978). Actually, the interseismic phase can be again subdivided into a purely interseismic step and a preseismic one, but the state of knowledge concerning the latter is still vague (e.g. Deng *et al.*, 1998).

The post-seismic deformation occurs soon after the seismic event and it can be subdivided in two phases, characterized by short and long-term deformation. The short-term deformation can usually be attributed to afterslip and/or pore pressure readjustments, which take place over periods ranging from a few hours to a few months after the earthquake. Deformation cannot be accurately measured by interferometric methodologies if the image sampling interval over the area is too long (several days or months).The long- term postseismic deformation is instead related to the viscoelastic relaxation that occurs in the lower crust and upper mantle, following several months or years (depending on the magnitude) after the earthquake (e.g. Segall, 2002). This kind of deformation, also called viscoelastic rebound, is difficult to be isolated using InSAR data, because: a) it is often characterized by ground velocities at the lower boundary of the InSAR measurement capability (<1 mm/yr); b) is spread over long distances and can be confused with long-wavelength InSAR error sources as well as with interseismic deformation. In this work we do not consider crustal deformation caused by the viscoelastic rebound because of the small magnitude of the considered earthquakes and the small length of the data time-series; we focus our attention on the interseismic, coseismic and postseismic (afterslip and/or pore pressure readjustments) phases.

From the geological point of view the earthquake cycle reveals itself through field evidence, such as abrupt offsets or diffuse deformation of lithological reference layers, fluvial or marine terraces, depositional or erosional landforms, faults escarpments, etc. The seismic cycle and the fault activity are also studied using paleo-seismological trenches, where geologists can measure and date stratigraphic layers to evaluate long term averages of strain rates and displacements. Starting from geological or paleoseismological field data, it is possible to evaluate the mean slip rate along a fault, and recognize the main seismic events (those which have ruptured the surface); these slip rates are usually averaged over a time span of thousands or tens of thousands of years (Pantosti *et al.*, 1993).

To study the seismic cycle in the long term (interseismic phase), we need to integrate geological and geodetic data, which entails integrating slip rates averaged over many seismic cycles, and present day ground velocity maps. To reconcile these different data we need to identify the sources responsible for the present day strain accumulation (and geodetic velocity), and possibly know the long term slip rate along them. In this way we can compare the geologic and the geodetic slip rates. The geodetic slip rate can only be obtained by appropriate modeling of the geodetic data; normal methods for interseismic geodetic data inversion neglect transient deformation processes and estimate slip rates by assuming slip on a fault to occur by steady creep only below a locking depth, in an elastic half-space, over the course of the earthquake cycle. On the other hand, for short-term studies of the earthquake cycle (co and post seismic phases), is very important to understand and identify the seismic sources and the interaction between each other. In fact, during a seismic crisis, typically several different data are available to the researchers concerning the hypocenters, preexisting geological and *ad hoc* field data, cinematic of the sources, magnitudes, punctual displacement data (GPS) and displacement fields (SAR); one of the main goals is to reconcile all of these data to define the seismic sources (geometries, kinematics and locations) and to investigate the relationship between the main sources and the static stress variations along the modeled fault planes (e.g. Pezzo *et al.*, 2013).

In this work, we present the results of the multitemporal InSAR-SBAS analysis (Berardino *et al.*, 2002) for the measurement of low interseismic ground velocities, in particular we study the interseismic deformation in the Gargano promontory (Southern Italy) and in the Doruneh region (Northern Iran) (Pezzo *et al.*, 2012). In both cases we focused our attention (i.e. the modeling) on the most prominent tectonic structures of the areas, the Mattinata Fault, for the

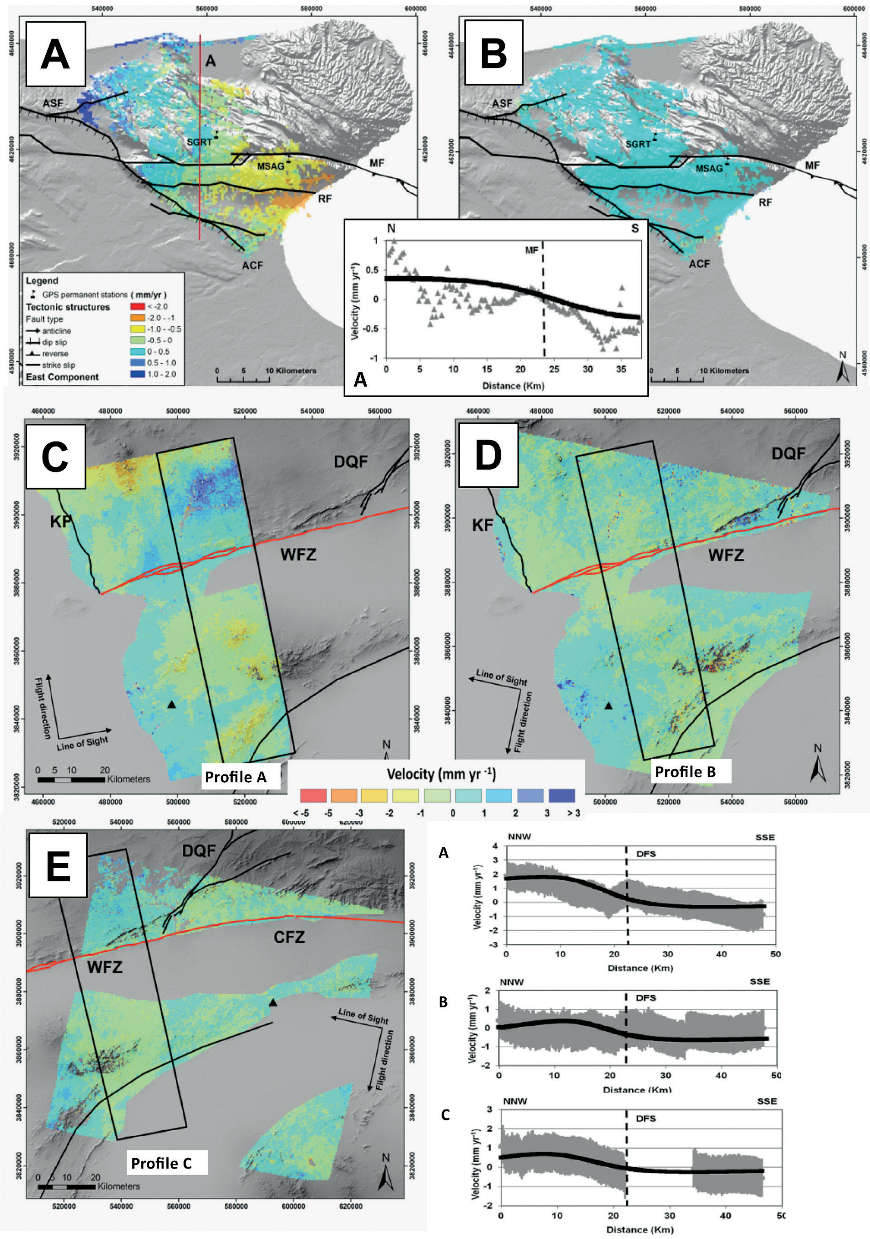

Fig. 1 – East (A) and up (B) components mean velocity maps of the Gargano area with main tectonic features. In panel A, the blue colors represent positive velocities (eastward) and in red the negative ones (westward). In panel B, the blue colors represent positive velocities (upward) and in red the negative ones (downward). Black flags represent the GPS permanent stations and the red line is the trace of the velocity profiles (2.5 km buffered) shown below. In panel C, D and E the mean LOS velocity maps from (C) ascending track 156, (D) descending track 206 and (E) descending track 435 (from Pezzo *et al.*, 2012). Positive velocity values (blue colors) indicate ground movement toward the satellite along the LOS direction (inclined 23hı from the vertical), negative ones (red colors) indicate the opposit. In red we show the DFS system trace; other faults in the region are in black. Black triangles indicate the reference point; black boxes mark the ~20 km buffered velocity profiles reported with the profile (A), (B) and (C), used in the data inversion; dashed black lines mark the intersection with the DFS trace. We show velocity error bars of 1 mmy^{-1}. All the maps are geo- referenced in UTM WGS84, Zone 40 N.

Gargano, and the Doruneh Fault System for Northern Iran. Both test sites are characterized by prevalent transcurrent tectonic regimes with low deformation rates (few mm per yr).

We also present some examples of coseismic studies in which the geological field data availability or absence played a fundamental role in the definition of the seismic sources: the 2012 Emilia seismic sequence and the 2008 Baluchistan (Central Pakistan) seismic swarm. For both interseismic and coseismic datasets we performed the data inversions using the elastic model of Okada (1985), with the aim to investigate its applicability in the general context of the study of the earthquake-cycle in different tectonic domains, analyzing the limits of the method and the contribution of surface and deep geological data.

Concerning the postseismic deformation, we present results concerning two strong earthquakes affecting the Italian peninsula in the last four years: the 2009 L'Aquila and the 2012 Emilia earthquakes. In this cases we show the fundamental role of geological field data concerning the survey of the afterslip ground faulting with respect to gravitational phenomena (for the L'Aquila event), and the survey of the hydrogeological dynamic and paleo-topography analysis of the epicentral area to discern the tectonic contributions to the ground deformation (for the Emilia events).

Results. *Ground deformation during the interseismic and preseismic phase.* We used multitemporal InSAR techniques for the measurement of low interseismic ground velocities, in particular we studied the interseismic deformation in the Gargano promontory (Southern Italy) and in the Doruneh region (Northern Iran).

The Gargano Promontory is an ENE-WSW oriented topographical and structural high representing a portion of the Apulian foreland extending into the Adriatic Sea. This area is characterized by active (instrumental and historical) seismicity that can originate strong earthquakes reaching intensities of XI MCS. The E-W Mattinata Fault (MF) has been frequently proposed as a natural candidate to represent the major seismogenic structure in the Gargano area; however the spatial distribution of the recorded seismicity does not concentrate along this structure. Using the SBAS multitemporal DInSAR technique (Berardino *et al.*, 2002) we analyzed a SAR dataset of 88 descending (from 1992 to 2010) and 46 ascending (from 1995 to 2008) ERS and ENVISAT images to retrieve high resolution, mean velocity maps of the Gargano area (Southern Italy). Combining ascending and descending line of sight velocity maps, we obtained the East and Up component velocity maps (Figs. 1A and 1B). The Up velocity component (Fig. 1B) shows no vertical movement in the inner Gargano, whereas, in the East velocity component (Fig. 1A), we identify a NW-SE oriented maximum gradient of about 0.03 mm yr^{1} per km in the inner Gargano, across the MF, in good agreement with GPS data and the main stress axis orientation. We also evaluate a deformation rate of about 40-50 nanostrains yr^{1} for the East component in the inner Gargano along E-W oriented velocity profile. These values are higher than the regional ones calculated using GPS, borehole or seismological punctual data. We modeled the MF using the elastic dislocation model proposed by Okada (1985). Our measurements are compatible with a right-lateral kinematics of MF with a slip rate of about 1.5 mm yr^{1} to a depth of 15 km, as shown by comparing observed and modeled velocity profile (Profile A of Fig. 1A). Our results confirm the slip rate values proposed by many authors, and the right-lateral geodynamical interpretation of the MF as a fundamental active junction in the dynamic equilibrium between the different motion of the Adria and Apulia microplates. We interpreted the interferometric signal and we inverted the SAR maps using the MF source parameters, subsequently evaluating the inversion goodness by comparing our results with bibliographic data. Without fundamental a priori information about the geometry of the fault, the hypocenter distribution and geological knowledge of the area, it would have been impossible to carry out a correct data interpretation and source modeling.

Concerning the Northern Iran site, we used the SBAS DInSAR analysis technique to estimate the interseismic deformation along the western part of the Doruneh fault system (DFS) (Pezzo *et al.*, 2012). We processed 90 ENVISAT images from four different frames from ascending and descending orbits (Figs. 1C, 1D and 1E). Using a simple dislocation approach we modeled 2-D velocity profiles obtaining a good fit to the observations (Profile A, B and C of Figs. 1C, 1D and 1E).Our model confirms the general left lateral kinematics of the DFS, but an additional important thrust component along the WFZ is necessary to fit the observations (rake angle of 34°±4°). The modeled rake angle results in the left-lateral component being about 2/3 of the slip rate, which is in agreement with the long-term record as reconstructed by structural and geomorphic observations. A steep fault dip to the North (~60°) is well constrained by the observations, and is in agreement with field observations on the Western and Central DFS. Our modeled slip rate of 5±1 mm yr^{-1} is the first quantitative estimate of strain accumulation for the Western DFS, corresponding to ~4 mm yr^{-1} of pure horizontal movement. In the long term, Fattahi *et al.* (2007) estimates ~2.4 mm yr^{-1} of left lateral slip rate on the central fault zone, by Infrared Stimulated Luminescence Dating (ISLD) of one Holocene alluvial fan. In our model, the anticorrelation between slip and rake indicates that some vertical component (rake > 0) is needed to explain the observations, otherwise the slip rates for pure strike slip fault would be unrealistic compared to the geological estimates. None of the latter are available forthe Quaternary uplift rate along the western fault zone (WFZ). Extrapolating the vertical component of our modeled slip rate (2.4±1 mm yr^{-1}) in the geological past does not seem to justify the relatively low relief across the WFZ (500-700 m), but a number of different factors, e.g. observation and/or model uncertainties, spatio-temporal slip rate variations, interaction with close tectonic structures could justify this discrepancy.

Based on a geologically determined average slip per event of 4.7 m, the recurrence interval along the Central DFS has been estimated to be ~2000 yr (Fattahi *et al.*, 2007). The slip rate we estimated for the WFZ would require a slip per event of ~10 m to obtain the same recurrence time. This is unrealistic, especially if we consider the field observations and the segmentation model by Farbod *et al.* (2011). Accepting a similar slip per event for the WFZ and the CFZ, including a conservative uncertainty estimate of 20%, we obtain a recurrence interval varying between 630 and 1400 yr. The lack of strong seismicity in the last 1500 yr along the WFZ may be due to the incompleteness of the historical seismic catalogues (Ambraseys and Melville 1982), and our results show that recurrence intervals below 1000 yr cannot be excluded.

Ground deformation during the Coseismic phase. Regarding the contribution of geological constrains to the interpretation and modeling of coseismic displacement SAR maps, we present two examples in which a priori geological information had a very different significance.

The first example concerns two earthquakes occurred in the Emilia region, Northern Italy, respectively on May 20th 2012, Ml 5.9, and May 29th, Ml 5.8, inverting COSMO-SkyMed and Radarsat-1 surface displacements and GPS observations (Fig. 2A) (Pezzo *et al.*, 2013). The Emilia seismic sequence filled a seismic gap existing at least since the year 1000 A.D. (Rovida *et al.*, 2011), and might therefore give important information on the mechanisms of strain accumulation and release in this area. Thus, some considerations can be made based on our results about the long-term strain accumulation. The location of the coseismic deformation measured by InSAR data corresponds to part of the Mirandola and Ferrara folds, located, under the Po alluvial plain. This evidence supports the long-term geomorphic analyses that attribute to the growth of the same folds the wide northward bend of the Po river course and the deviation of the Secchia and Panaro rivers (Burrato *et al.*, 2003). Both the 20 and 29 May 2012 sources were found to be well modeled by ~E-W, S-dipping thrust faults with a flat-ramp geometry (Figs. 2C and 2D), corresponding to the Mirandola and Ferrara thrusts. Furthermore, we identified a displacement pattern of ~10 cm towards the satellite sensors, not associated to any of the largest aftershocks (Fig. 2B). The pattern is temporally co-located or following the first event and preceding the second one. Spatially it is located halfway between the displacement fields of the two main events. We investigate some possible interpretations of our observations, favoring the hypothesis of a slip along the fault plane of the May 29th event, supported by the results of a Coloumb Failure Function analysis, which suggests an increasing

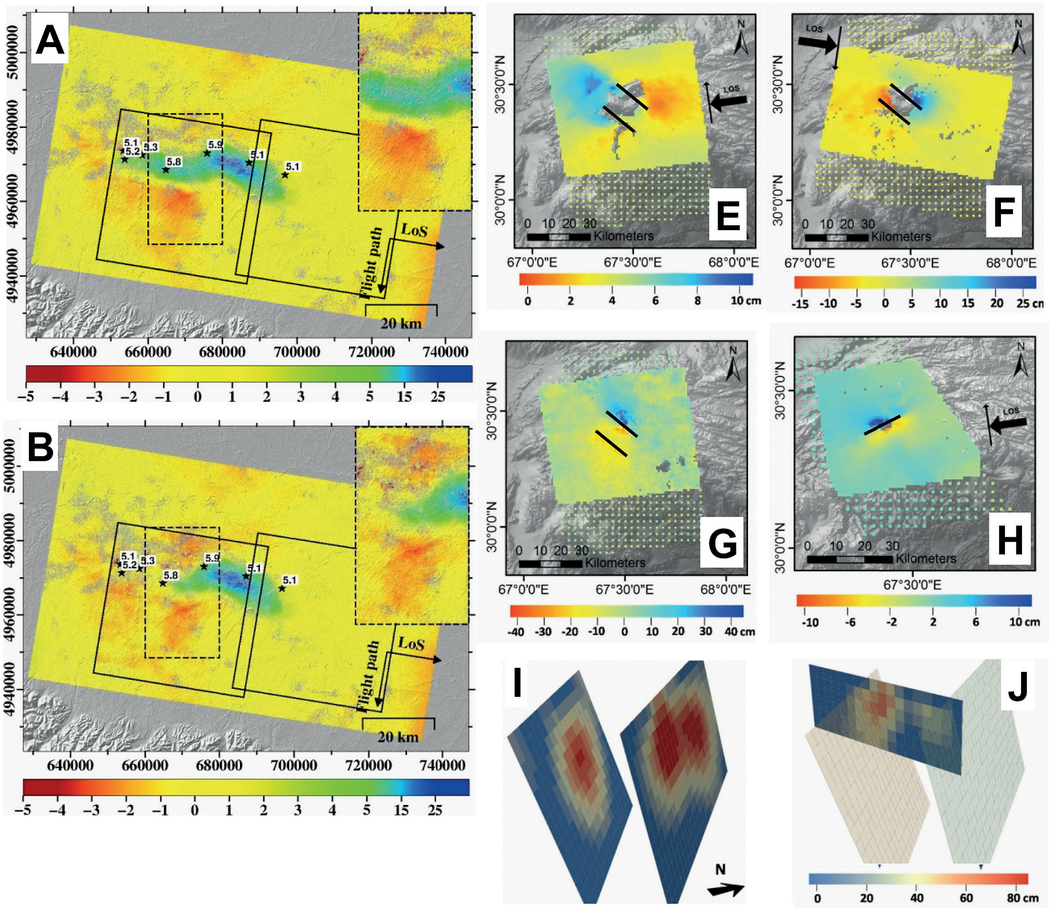

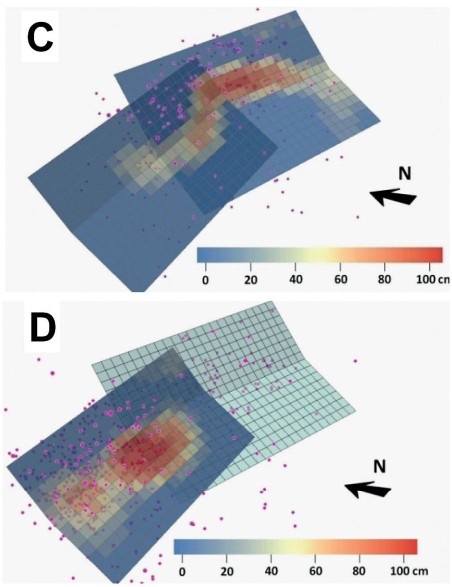

Fig. 2: (A) Cumulative displacement map spanning all main events of the sequence, obtained from the Radarsat-1 12 May–5 June interferogram. (B) Cumulative displacement from 12 to 27 May and 4 to 5 June, obtained by subtracting the COSMO-SkyMed 27 May–4 June displacement from the map shown in (A). Solid-line black rectangles indicate the footprint of the COSMO-SkyMed satellite image pairs. The insets in the top-right corners contain a zoom of the area enclosed by the dashed-line black rectangles. Arrows indicate the ground-projected line-of-sight (from ground to satellite) and the satellite flight path. (C) and (D) The slip distribution (1:5 î 1:5 km patches) along the 20 and 29 May sources, respectively. Purple spheres represent the hypocenter (http://iside.rm.ingv.it; ML >2) relative to the following time spans: (C) 17–28 May 2012 and (D) 29 May–11 June 2012 (from Pezzo *et al.*, 2013). Observed displacement maps from ENVISAT interferograms: (E) 06/05/2008-02/12/2008, (F) 04/03/2006-08/11/2008 and one MAI ENVISAT (G) 23/09/2008-02/12/2008 maps relating to the 28-28 October 2008 earthquakes. (H) Coseismic displacement map of the 09 December 2008 event from 02/12/2008-06/01/2009 interferogram. Satellite paths and line-of-sight (LOS) directions are shown in the boxes; black lines indicate the surface projections of the modeled faults. (I) and (J) the slip distribution (1.5 X 1.5 km patches) along the 28-29 October 2008 and 09 December sources, respectively. In panel B, in transparency the two mainshock fault planes

load on the May 29th fault plane, following the first mainshock. Two seismic sourceswere obtained using the fault plane parameters provided byseveral published geological studies in this area (e.g. Boccaletti *et al.*, 2010; Picotti and Pazzaglia, 2008). This information is essential in this area, since, due to the symmetric shape of the deformation pattern and its small N-S component, the North/South dipping fault ambiguity could not be solved by SAR and GPS data inversion alone.

The second example concerns the three largest events of the 2008 Baluchistan (western Pakistan) seismic sequence, namely two Mw 6.4 events only 11 hours apart and an Mw 5.7 event 40 days later. We used Synthetic Aperture Radar Differential Interferometry (DInSAR) (Figs. 2E, 2F and 2H) and Multi-Aperture Interferometry (MAI) (Fig. 2G) to constrain the sources of these events. Our InSAR surface displacement maps and subsequent modeling results suggest the sources of the two main earthquakes of the Baluchistan 2008 seismic sequence were two NW-SE oriented right-lateral strike-slip faults (Figs. 2I and 2J). The modeled fault planes are found to be almost vertical and quasi parallel to each other, forming an about 90° angle with an ENE-WSW oriented fault responsible for the largest aftershock; the latter is a vertical left-lateral strike slip fault located between the two main sources. Moreover, CFF analysis suggests that the second mainshock fault plane was not overloaded by the first mainshock in spite of the very brief lapse of time between the two events. On the contrary, the December aftershock fault plane was intensely loaded by the occurrence of the October mainshocks.

These results are insightful when interpreted in the tectonic context of the Quetta syntaxis. In fact, the latter is placed in crucial junction between two blocks characterized by opposite relative motion, namely the northward motion of the Kirthar range and the southward motion of the Sulaiman Lobe. The former can be considered the right block of the left-lateral strike-slip Chaman fault system, whereas the latter is considered a transpressive zone in the northwestern part of the Indian subcontinent (Yadav *et al.*, 2012), with a southward extrusion accommodated by the SE verging thrust fault surrounding the lobe itself and the left-lateral Kingri fault (Rowlands, 1978). In this complex tectonic context, our quasi parallel mainshock fault planes are in good agreement with a right-lateral shear zone located in the Quetta syntaxis. Moreover, the CFF suggests the October 28th and 29th earthquakes were two independent mainshocks characterized by a similar magnitude, mechanism and geometry. Conversely, concerning the December 9th aftershock, the stress increase along the fault plane due to the mainshocks suggests that it was likely triggered by the October earthquakes. Thus, at this scale, in the area included between the two mainshock fault planes, we can suppose a reorientation of the stress field due to the general right-lateral displacement of the blocks. Under this assumption, our observations, together with the modelled fault geometries, suggest that at a local scale this area could be affected by left-lateral shear zone, with a bookshelf type deformation, in a wider regional tectonic context of right-lateral shear zone, confirmed by our mainshock modelling.

This test case is characterized by the almost total absence of geological data at surface and at depth, as well as of any coseismic ground evidences of surface faulting. Constraints for source modeling are provided only by the abundance of SAR measurements (three independent motion components could be measured for the main events) and from seismology. In particular, the MAI technique was crucial in solving the fault plane ambiguity determined by moment tensors. Our results and hypothesis would however have to be confirmed by a field geological survey and a more accurate seismological study of the seismic sequence, as well as of stress readjustments and reorientations analysis during the seismic sequence evolution.

Ground deformation during the postseismic phase. The first postseismic deformation analysis we present concerns the well-known deformation following the Mw 6.3 L'Aquila earthquake occurred on 06/04/2009 (Lanari *et al.*, 2010; D'Agostino *et al.*, 2012).

We used 25 COSMO-SkyMed SAR images (beam 09 asc.) to obtain a postseismic deformation time series and mean velocity map (spanning12/04/2009 to 13/10/2009) (Fig. 3A).

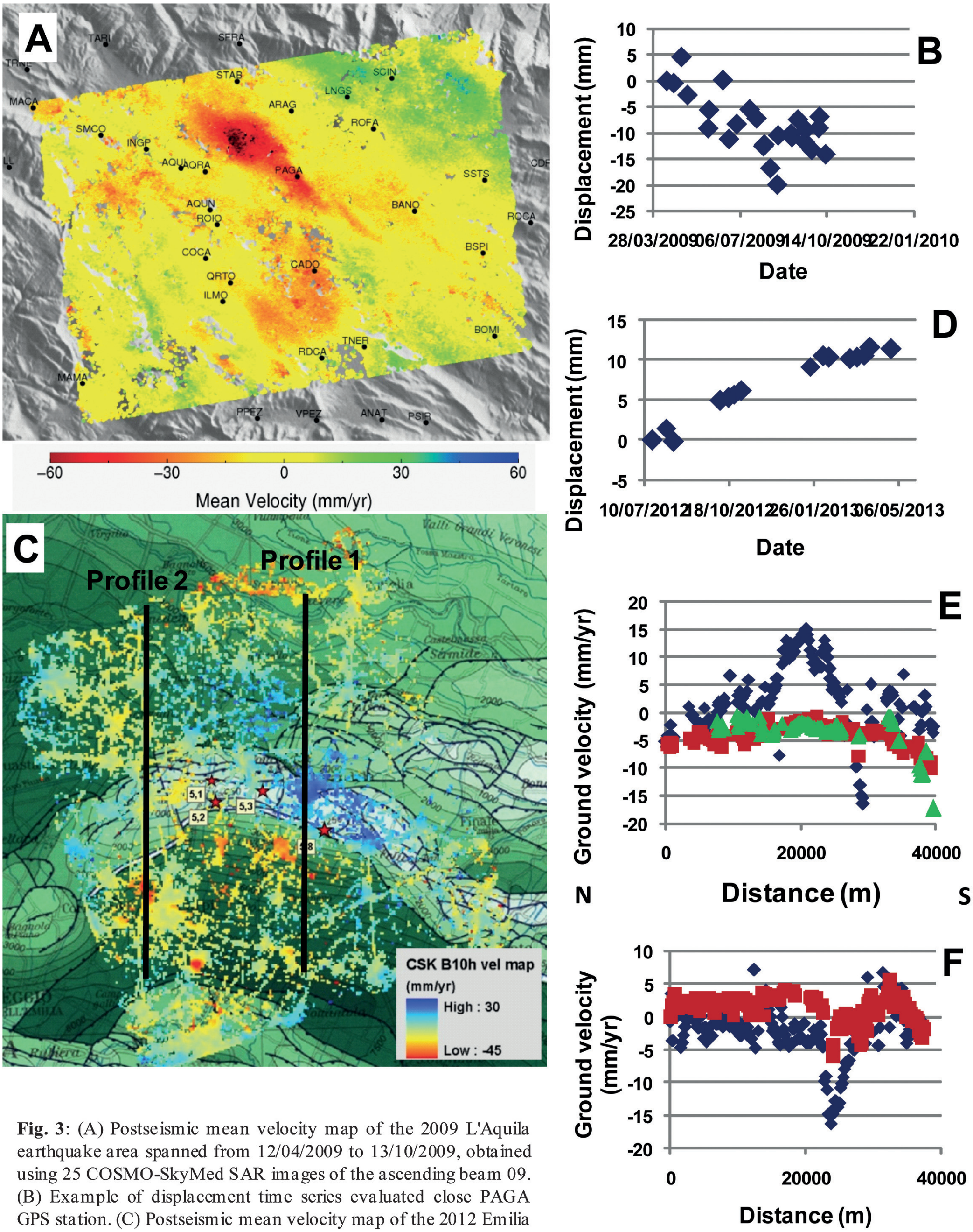

Fig. 3: (A) Postseismic mean velocity map of the 2009 L'Aquila earthquake area spanned from 12/04/2009 to 13/10/2009, obtained using 25 COSMO-SkyMed SAR images of the ascending beam 09. (B) Example of displacement time series evaluated close PAGA GPS station. (C) Postseismic mean velocity map of the 2012 Emilia seismic sequence area spanned from 20/07/2012 to 27/04/2013, obtained using 15 COSMO-SkyMed SAR images of the ascending beam b10h,superimposed to the Structural model of Italy (Bigi *et al*., 1983) In A and B, positive velocity values (blue colors) indicate ground movement toward the satellite along the LOS direction (inclined 23° from the vertical), negative ones (red colors) indicate the opposite. (D) Example of displacement time series evaluated in the maximum line of sight displacement. (E) and (F) N-S displacement profile calculated across the 20/05/2012 earthquake epicentral area (E) and far from the entire seismic sequence (F); blue rumbles are the postseismic displacement, whereas green triangles and red squares indicate the preseismic displacement obtained from ERS (from 30/09/1992 to 05/06/1999) and ENVISAT-ASAR images (from 15/01/2007 to 06/09/2010).

We also performed a correction of atmospheric effects correlated with topography, estimated from the SAR data itself in non-deforming areas. The time series analysis in the epicenter area show a typical exponential trend (Fig. 3B), so that we can mainly attribute the deformation pattern to the afterslip occurred along the 06/04/2009 earthquake fault plane. Based on ground based SAR interferometry, some authors have estimated the post seismic deformation along the fault plane trace to be of several centimeters (Wilkinson *et al.*, 2012, 2010); despite the actual difficulty in field identification of centimetric surface deformation, it appears fundamental, soon after a strong earthquake, to provide a temporally continuous field deformation survey to identify the co and postseismic deforming areas. On the other hand, in addition to the afterslip correlated pattern, the postseismic velocity map shows many other features related to gravity, like deep seated gravitational slope deformations (DSGSD). Thus, a correct interpretation of the postseismic velocity map cannot be carried out without a detailed field investigation. Furthermore, the latter is crucial to correctly interpret possible transient deformation patterns from one tectonic structure to another, as well as the evolution of the seismic sequence (e.g. Pezzo *et al.*, 2013).

As a second test-case, we present a post seismic multitemporal SAR analysis of the 2008 Emilia seismic sequence, in which 15 COSMO-SkyMed stripmap SAR images (Fig. 3C). Also in this case we observe a quasi-exponential afterslip deformation pattern in the epicentral area (Fig. 3D). In addition we detect a velocity pattern not directly attributable to the postseismic phenomena. In fact, local subsidence occurs due to fluid migration and compaction of the Po plain sediments. Moreover, there is a rough correspondence between the growth anticline and the positive (approach to the satellite) velocity values. Vice versa, negative velocity patterns correspond to the locations of the tectonic synclines. Furthermore, we observe a general agreement between the preseismic and postseismic, albeit for the afterslip pattern located in the epicentral area (Figs. 3E and 3F). Thus, only knowledge of the geological setting and active processes, at depth and at the surface, can provide a correct interpretation of all deformation features measured by InSAR space geodesy.

Acknowledgements. G. Pezzo was funded by the INGV-ASI MUSA project. The COSMO-SkyMed SAR data are copyright of the Italian Space Agency (ASI), and were provided by the Department of Civil Protection (DPC) in the framework of the ASI-INGV-Space-based Monitoring System for Seismic Risk Management (ASI-INGV SIGRIS) project. The ENVISAT ASAR data are copyrighted by the European Space Agency and were provided through CAT1 proposal 3769. Some figures were prepared using the public-domain GMT software (Wessel and Smith, 1998). The ASTER GDEM is a product of METI and NASA. The author thanks J.P. Merryman Boncori and C. Tolomei for their fundamental support in the SAR data processing; S. Atzori and A. Antonioli for their precious help for the data inversions and CFF analysis and S. Salvi for the fruitful geological discussions and comments.

References

Ambraseys, N.N. and C.P. Melville; 1982: *A History of Persian Earthquakes*. Cambridge University Press, Cambridge.

Bechor N.B.D. and H.A. Zebker;2006.*Measuring two-dimensional movements using a single InSAR pair*. Geophys. Res. Lett.,**33**, L16311, doi:10.1029/2006GL026883.

Berardino, P., G. Fornaro, R. Lanari and E. Sansosti; 2002:*A new algorithm for surface deformation monitoring based on small baseline differential interferograms*, IEEE Trans. Geosci. Remote Sensing, vol. 40, pp. 2375-2383.

Bigi, G., G. Bonardi, R. Catalano, D. Cosentino, F. Lentini, M. Parotto, R. Sartori, P. Scandone and E. Turco; (Editors; 1983); *Structural Model of Italy* 1:500,000, CNR Progetto Finalizzato Geodinamica.

Boccaletti, M., G. Corti, and L. Martelli; 2010:*Recent and active tectonics of the external zone of the Northern Apennines (Italy)*, Geol. Rundsch. Z. Allg. Geol. 100, 1331-1348, doi: 10.1007/s00531-010-0545-y.

Burrato, P., F. Ciucci and G. Valensise; 2003:*An inventory of river anomalies in the Po Plain, Northern Italy: evidence for active blind thrust faulting*. Ann. of Geophys. 46 (5), 865-882.

Casu, F., M. Manzo and R. Lanari; 2006:*A quantitative assessment of the SBAS algorithm performance for surface deformation retrieval from DInSAR data*, Remote Sens. Environ., 102, no. 3/4, 195-210.

D'Agostino, N., D. Cheloni, G. Fornaro, R. Giuliani, and D. Reale; 2012: *Space-time distribution of afterslip following the 2009 L'Aquila earthquake*, J. Geophys. Res., 117, B02402, doi:10.1029/2011JB008523.

Deng, J., M. Gurnis, H. Kanamori and E. Hauksson; 1998:*Viscoelastic flow in the lower crust after the 1992 Landers, California, earthquake*, Science, 282, 1689-1692.

Farbod, Y., O. Bellier, E. Shabanian, and M.R. Abbassi; 2011:*Geomorphic and structural variations along the Doruneh Fault System (central Iran)*,Tectonics, 30, TC6014, doi:10.1029/2011TC002889.

Fattahi, M., R.T. Walker, M.M. Khatib, A. Dolati and A. Bahroudi;(2007).*Slip-rate estimate and past earthquakes on the Doruneh fault, eastern Iran*. Geophys. J. Int., 168, 691-709
Ferretti, A., C. Prati and F. Rocca; 2001: *Permanent scatterers in SAR interferometry*. IEEE Trans. Geosci. and Remote Sens., 39(1):8 – 20.
Hooper, A.;2007: *StaMPS (Stanford Method for Persistent Scatterers) Manual, Version 2.2*.
Lanari, R., P. Berardino, M. Bonano, F. Casu, A. Manconi, M. Manunta, M. Manzo, A. Pepe, S. Pepe, E. Sansosti, G. Solaro, P. Tizzani and G. Zeni; 2010: *Surface displacements associated with the L'Aquila 2009 Mw 6.3 earthquake (central Italy): New evidence from SBAS-DInSAR time series analysis*, Geophys. Res. Lett., 37, L20309, doi:10.1029/2010GL044780.
Massonnet, D. and K.L. Feigl, 1995a.*Discrimination of geophysical phenomena in satellite radar interferograms*. Geophys. Res. Lett., 22 (12), 1,537-1,540.
Massonnet, D., M. Rossi, C. Carmona, F. Adragna, G. Peltzer, K. Feigl and T. Rabaute;1993:*The displacement field of the Landers earthquake mapped by radar interferometry*. Nature, 364, 138-142.
Okada, Y.; 1985:*Surface deformation due to shear and tensile faults in a half-space*. Bull. Seismol. Soc. Am., 75, 1135ñ1154.
Pantosti, D., D.P. Schwartz, G. Valensise; 1993:*Paleoseismology Along the 1980 Surface Rupture of the Irpinia Fault: Implications for Earthquake Recurrence in the Southern Apennines, Italy*. J. Geophys. Res., vol. 98, n. b4, pp. 6561-6577, doi:10.1029/92JB02277.
Pezzo, G., J.P. Merryman Boncori, C. Tolomei, S. Salvi, S. Atzori, A. Antonioli, E. Trasatti, F. Novali, E. Serpelloni, L. Candela and R. Giuliani; *Coseismic deformation and source modeling of the May 2012 Emilia (Northern Italy) earthquakes*. Seismological Research Letters, v. 84 no. 4 p. 645-655, 2013. doi: 10.1785/0220120171.
Pezzo, G., C. Tolomei, S. Atzori, S. Salvi, E. Shabanian, O. Bellier and Y. Farbod;2012:*New kinematic constraints of the western Doruneh fault, northeastern Iran, from interseismic deformation analysis*. Geophysical Journal International, 190: 622-628.doi: 10.1111/j.1365-246X.2012.05509.x
Picotti, V. and F. J. Pazzaglia; 2008: *A new active tectonic model for the construction of the Northern Apennines mountain front near Bologna (Italy)*, J. Geophys. Res. 113, no. B08412, doi: 10.1029/2007jb005307.
Rovida, A., R. Camassi, P. Gasperini and M. Stucchi; 2011: (eds.). CPTI11, *the 2011 version of the Parametric Catalogue of Italian Earthquakes*. Milano, Bologna, http://emidius.mi.ingv.it/CPTI.
Rowlands, D.; 1978: *The structure and seismicity of a portion of the southern Sulaiman Range*, Pakistan, Tectonophysics, 51, 41–56.doi:http://dx.doi.org/10.1016/0040-1951(78)90050-1
Scheiber R. and A. Moreira (2000). Coregistration of interferometric SAR images using spectral diversity, IEEE Trans. Geosc. Rem. Sens., **38** (5), 2179-2191, doi:10.1109/36.868876.
Scholz, C.H. and T. Kato;1978:*The behavior of a convergent plate boundary: crustal deformation in the south Kanto District, Japan*. J. Geophys. Res., 83, 783-791.
Segall, P.; 2002:*Integrating geologic and geodetic estimates of slip rate on the San Andreas fault system*, Int. Geol. Rev., 44, 62-82.
Wessel, P. and W.H.F. Smith;1998:*New, improved version of the generic mapping toolsreleased*. EOS, Transactions American Geophysical Union,79 (47), pp. 579.
Wilkinson, M.W., K.J.W. McCaffrey, G.P. Roberts, P.A. Cowie, R.J. Phillips, M. Degasperi, E. Vittori and A.M. Michetti; 2012: *Distribution and magnitude of post-seismic deformation of the 2009 L'Aquila earthquake (M6.3) surface rupture measured using repeat terrestrial laser scanning*. Geophysical Journal International, 189: 911-922.doi: 10.1111/j.1365-246X.2012.05418.x
Wilkinson, M.W., K.J.W. McCaffrey, G.P. Roberts, P.A. Cowie, R.J. Phillips, A.M. Michetti, E. Vittori, L. Guerrieri, A. M. Blumetti, A. Bubeck, A. Yates and G. Sileo; 2010: *Partitioned postseismic deformation associated with the 2009 Mw 6.3 L'Aquila earthquake surface rupture measured using a terrestrial laser scanner*, Geophys. Res. Lett., 37, L10309, doi:10.1029/2010GL043099.
Wright, T., B. Parsons and E. Fielding; 2001:*Measurement of interseismic strain accumulation across the North Anatolian Fault by satellite radar interferometry*, Geoph. Res. Lett., 28 (10), 2117-2120.
Yadav, R.B.S., V.K. Gahalaut, Sumer Chopra and Bin Shan; 2012:*Tectonic implications and seismicity triggering during the 2008 Baluchistan,Pakistan earthquake sequence*, Journal of Asian Earth Sciences 45, 167-178. doi: http://dx.doi.org/10.1016/j.jseaes.2011.10.003

MORPHOMETRIC ANALYSIS OF THE WESTERN ASPROMONTE MTS. (SOUTHERN CALABRIA, ITALY): EVIDENCE FOR ACTIVE TECTONICS

C. Pirrotta, M.S. Barbano, C. Monaco
Dipartimento di Scienze Biologiche, Geologiche e Ambientali, Università di Catania, Italy

Introduction. Fluvial network development and organisation are influenced not only by climatic and lithological factors but also by tectonic movements, such as regional uplift, subsidence and fault activity causing local landscape modification. Rivers are the most sensitive geomorphological elements capable to record recent tectonic activity, indeed when perturbed by landscape changes they leave their equilibrium state and lose their hierarchical organization. Then, rivers tend quickly to restore equilibrium producing anomalous segments and also create typical features such as fluvial capture, deflections, abandoned channels and so on. Thus, geomorphological and morphometric studies of fluvial network and associated hydrographic basin allow analysing landscape modifications and they can provide information about active tectonics. Numerical calculation of geomorphological indexes (Keller, 1986; Cox, 1994) applied to rivers can be a basic reconnaissance tool in order to determine the influence of faults on the hydrographic network and to identify areas with rapid tectonic deformation (Verrios *et al.*, 2004).

In southern Calabria, NE-SW to NNE-SSW striking and west-dipping normal faults dominate the neotectonic deformation scenario (Fig. 1). Our study focus on the evaluation of active tectonics in the Aspromonte Mts. area by geomorphological, morphometric and morphostructural analyses of two rivers and their basins: the Petrace Fiumara and the Catona Fiumara. These rivers run from the Aspromonte ridges towards the Tyrrhenian Sea and are intercepted by normal faults, whose activity has been recorded by drainage network.

Geological setting. The Aspromonte Mts. are located in the southern part of the Calabrian Arc which connects the Apennines and the Sicily orogenic belts (Fig. 1). The Calabrian Arc, which includes Calabria and the north-eastern side of Sicily, is a forearc terrain which was emplaced to the south-east during north-westerly subduction and roll-back of the subjacent Ionian slab (Malinverno and Ryan, 1986; Neri *et al.*, 2012). During the Late Pliocene-Quaternary, contractional structures of the hinterland part of the forearc were superseded by extensional faults which caused its fragmentation into structural highs and shallow marine sedimentary basins, including the Mesima and Gioia Tauro basins and the Messina Straits (Ghisetti and Vezzani, 1982). At present, an active swarm of normal faults runs along the Calabrian Arc and is associated with strong seismicity (Monaco and Tortorici, 2000). Current WNW-ESE-trending crustal extension is documented by focal mechanisms of earthquakes (CMT and RCMT Catalogues; Neri *et al.*, 2004), structural studies (Tortorici *et al.*, 1995; Jacques *et al.*, 2001; Ferranti *et al.*, 2007) and geodetic velocities (Mattia *et al.*, 2009; D'Agostino *et al.*, 2011). Since the Middle Pleistocene, extensional tectonics has been coupled with intense regional uplift which developed flights of marine terraces (Ferranti *et al.*, 2006 and references therein).

Active tectonics in the Calabrian Arc is attested by the uplift of the coast (Westaway, 1993; Ferranti *et al.*, 2007), by landscape imprint (Guarnieri and Pirrotta, 2008), structural evidence (e.g. Tortorici *et al.*, 1995; Jacques *et al.*, 2001; Aloisi *et al.*, 2012) and by the frequent occurrence of strong and moderate earthquakes (Rovida *et al.*, 2011). Southern Calabria was hit by disastrous earthquakes and long seismic sequences during historical times (1659, February-March 1783, 1894 and 1908 earthquakes), that caused thousands of fatalities and several secondary effects including tsunamis (Fig. 1). Although the dramatic impact of these earthquakes on the region, the association with their causative faults is still debated and they are often related to different seismogenic sources (e.g. Valensise and Pantosti, 1992; Jacques *et al.*, 2001; Galli and Bosi, 2002; Basili *et al.*, 2008; Aloisi *et al.*, 2012). The 1783 sequence (mainshock M ~ 7; Rovida *et al.*, 2011) changed the Aspromonte Mts. landscape triggering several landslides, liquefactions and ground fracturing. Long and continuous fractures, described by contemporary witnesses, were considered as the superficial expression of the seismogenic fault of the main shock, occurred the 5 February. This ground fracturing well fits with the Cittanova Fault (Fig. 1), a NE-SW trending, 30 km long, west-dipping extensional segment bounding the Aspromonte Mts. from the Gioia Tauro basin (Tortorici *et al.*, 1995; Jacques *et al.*, 2001; Galli and Bosi, 2002). Alternatively, this event has been attributed to a blind, east-dipping, low angle fault, located in the Gioia Tauro basin (Basili *et al.*, 2008 and references therein). Northwards, the Mesima Fault was associated with the 7 February 1783 earthquakes (Jacques *et al.*, 2001). Southwards, the Scilla Fault, located along the western coast of southern Aspromonte Mts. (Fig. 1), has been associated with the 6 February event (Jacques *et al.*, 2001). The northern segment of the Santa Eufemia Fault probably ruptured during the 1894 event (Galli and Bosi, 2002); finally the Santa Eufemia Fault and the Armo Fault, more to the south, could have slipped during the 1908 earthquake (Aloisi *et al.*, 2012).

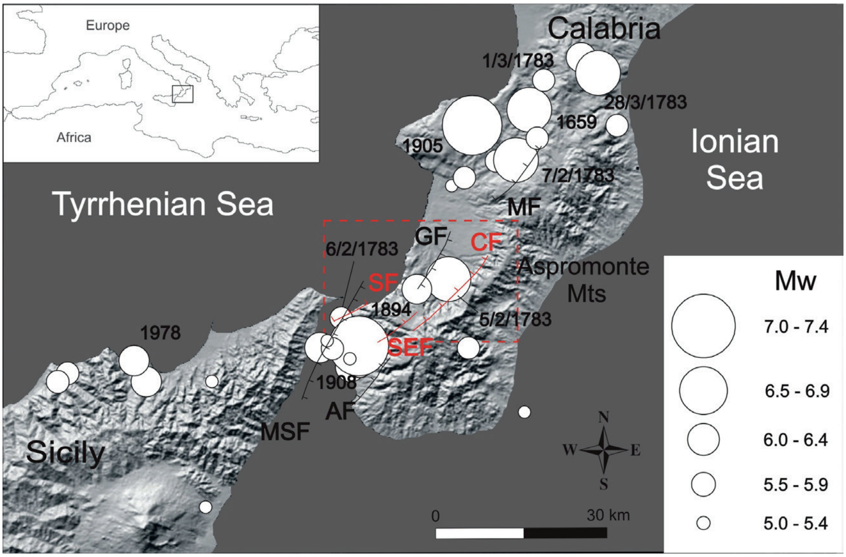

Fig. 1 – Seismotectonic map of Southern Calabria and north-eastern Sicily and main historical earthquakes; epicenters (filled circles) from the CPT11 catalogue (Rovida *et al.*, 2011). Faults associated with the most disastrous earthquakes are also shown: MF = Mesima Fault; CF = Cittanova Fault (Jacques *et al.*, 2001; Galli and Bosi, 2002); GF = Gioia Fault (Basili *et al.*, 2008); SF = Scilla Fault (Jacques *et al.*, 2001; Ferranti *et al.*, 2007); SEF = Santa Eufemia Fault; AF = Armo Fault (Aloisi *et al.*, 2012); MSF = east dipping Messina Strait Fault (Pino *et al.*, 2000; Basili *et al.*, 2008). Red rectangle is the inset of Fig. 2.

Geomorphological and morphometric analysis. We performed a geomorphological and morphometric study, both quantitative and qualitative, of the Petrace Fiumara and the Catona Fiumara in order to quantify the geomorphological evolution of the studied area and to individuate possible perturbation of the basins that can be due to active tectonics. The term “fiumara” is used to describe a particular typology of river, with limited length and elevated slope, characterized by deep valleys and torrential regime. These water courses typically flow in north-eastern Sicily and Calabria.

By using a photo-interpretation analysis (scale 1:10,000) we preliminary localized more accurately the Cittanova Fault, S. Eufemia Fault and Scilla Fault, and mapped the drainage geometry of the Petrace Fiumara and Catona Fiumara and their geomorphological elements.

The fluvial network hierarchy has been analysed according to Strahler (1957) ordering. Then, we calculated parameters describing the hierarchical maturity of the drainage and able to highlight anomalies ascribable to active tectonics. Bifurcation index (**R**) highlights possible hierarchical anomalies of the fluvial network providing information on the typology of the erosive processes and on the degree of evolution of the basin. Index **A** represents the number of anomalous fluvial segments. Hierarchical anomaly index (**Δa**) allows to better quantify drainage anomalies. First order flow density (**D1**) indicates possible areas suffering uplift due to dip slip movements. Also, we calculated some morphometric indexes indicating possible basin asymmetry (Asymmetry factor, **AF**; Transverse topography asymmetry, **T**) and basin differential uplift (Basin elongation Ratio, **Re**; hypsometric curve and Stream length-gradient index, **SL**). Finally, a morphostructural study allowed us to evaluate the relationship between the geometry of the hydrographic network and the trend of the tectonic structures.

Morphometric indexes are very sensitive to lithological change, thus each parameter has been punctually related to the rock type cropping out, classified on the basis of the erosion susceptibility (Fig. 2). **A** class includes the crystalline terrains of the metamorphic massif, that is the most resistant lithology. **B** class represents the terrains of Tortonian, Pliocene and Lower Pleistocene age, made of conglomerates, sandstones, sands and clays with mid/low resistance to the erosion. **C** class includes clays, sands and poorly cemented conglomerates of Pleistocene age and Holocene alluvial deposits. These terrains have low degree of strengthened and are easy to erosion. In some cases, the Catona Fiumara and Petrace Fiumara have been divided in sub-basins with the aim to examine in depth possible perturbation of their drainage.

Results. The basin of the Catona Fiumara is 67.47 km^2 wide; most of the drainage flows on the crystalline terrains of the metamorphic massif (A class) and on Pleistocene marine and continental deposits (C class), in the lower sector. Trunk stream flows towards NW and changes running towards SW in the final tract (Fig. 2). Fluvial network reaches the V hierarchical Strahler's order and shows parallel shape pattern and trellis pattern as it regards the I order branches.

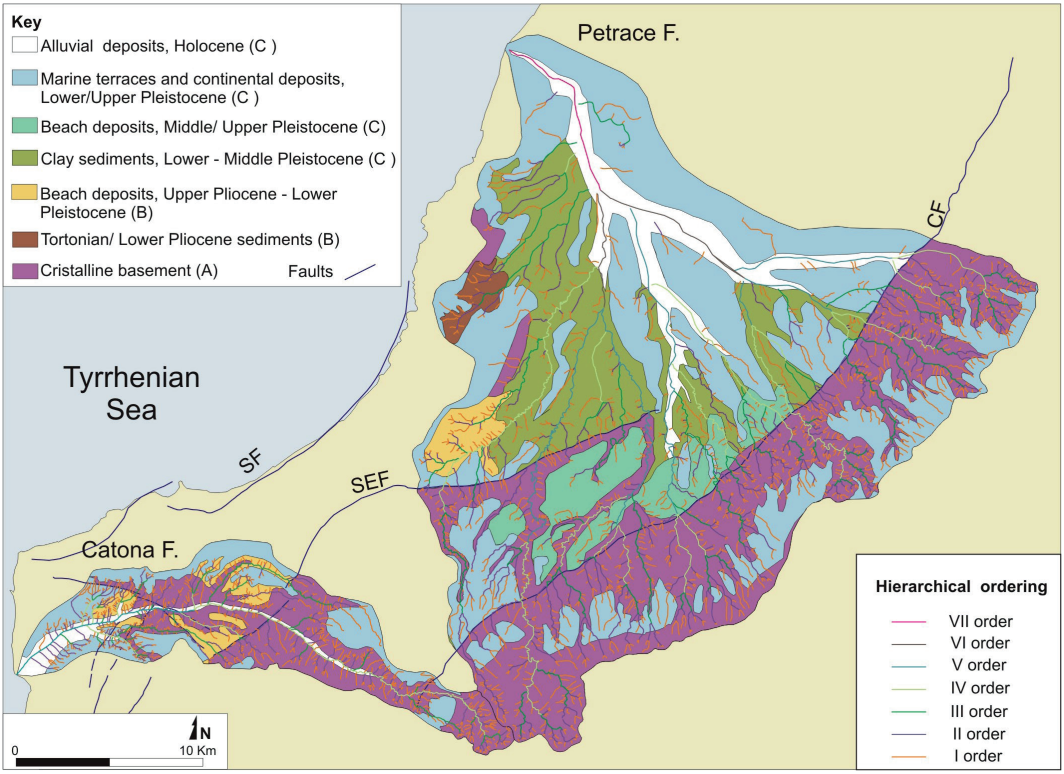

Fig. 2 – Sketch map of the Catona Fiumara and Petrace Fiumara. Drainage is divided into hierarchical orders according to Strahler (1957) ordering. Terrains are classified on the basis of their susceptibility to erosion.

The basin of the Petrace Fiumara is 258.29 km^2 wide, drainage flows on the metamorphic terrains (A class) in the upper part, on marine and continental deposits (Lower/Upper Pleistocene) and partially on clay sediments (Lower/Middle Pleistocene) (C class). Trunk channel runs towards N, in the final tract it changes flowing NW-ward. Fluvial network reaches the VII order and it shows a parallel pattern as it regards high order branches (from IV to VII) (Fig. 2).

For both the Petrace Fiumara and Catona Fiumara basins we observed several geomorphological elements interpreted as markers of perturbation due to active tectonics. Numerous fluvial branches are straight and aligned along the Santa Eufemia Fault as it regards the Catona Fiumara and along the Cittanova Fault for the Petrace Fiumara. Fluvial channels characterized by anomalous stretch and meandering branches are observed on the Santa Eufemia Fault and Cittanova Fault footwall. Deflected streams and alignments of branch deflections, fluvial captures and suspended valleys are evidence of recent modification of the analyzed fluvial networks (Fig. 2).

For both the studied rivers, hierarchical parameters indicate a poor organization of the fluvial network and the presence of uplifted and rejuvenated sectors. Indeed, the bifurcation index, **R**, reaches high values (Tab. 1) as it regards the segments with low order, I and II, that are the youngest fluvial segments more susceptible to active tectonics. Similarly, the anomaly parameter, **A**, indicates that there are numerous anomalous branches of I and II orders, particularly high value is detected for the first order of the Petrace Fiumara. Finally, **D1** parameter highlights a high density of I order segments with respect to the flowed area due to differential uplift of specific sectors.

Tab. 1 – Hierarchical parameters and morphometric indexes of the Catona Fiumara and Petrace Fiumara: see the text for the description. AF index for the Catona Fiumara was also calculated for its 10 sub-basins.

Catona Fiumara					Petrace Fiumara			
R1 1,3	**A1** 271	**Sub-basin**	**AF**	**T1** 0,46	**R1** 1,5	**A1** 536		**T1** 0,15
R2 2,7	**A2** 102	1	49,94	**T2** 0,14	**R2** 1,4	**A2** 94		**T2** 0,04
R3 0,8	**A3** 7	2	21,18	**T3** 0,03	**R3** 0,5	**A3** 9	**Δa** 1,69	**T3** 0,01
R4 0	**A4** 0	3	33,10	**T4** 0,12	**R4** 0,4	**A4** 2		**T4** 0,08
		4	73,53	**T5** 0,14	**R5** 0	**A5** 0	**D1** 6,26	**T5** 0,18
		5	73,53	**T6** 0,12	**R6** 0	**A6** 0		**T6** 0,32
Δa 0,96		6	52,90	**T7** 0,35			**Re** 0,69	**T7** 0,47
	Re 0,40	7	79,54	**T8** 0,10				**T8** 0,64
		8	78,58	**T9** 0,35				**T9** 0,69
D1 12,77		9	62,24	**T10** 0,21			**AF** 70,78	**T10** 0,77
		10	74,26					
		Catona F.	56,06					

AF index of the Catona Fiumara approaches to 50, indicating no asymmetry, thus this index has been evaluated for the 10 sub-basins. Results show that both the sub-basins on the left side and that on the right side of this fluvial basin are asymmetric due to the differential uplift of specific sectors. **Re** index highlights an elongated shape of the Catona Fiumara basin indicating an immature stage. Hypsometric curve and **SL** index evaluated for this river highlight uplifted and rejuvenated sectors where it meets the Santa Eufemia Fault and Cittanova Fault. Furthermore, hypsometric curves of the sub-basins 1, 8 and 10 evidence a localized uplift affecting the northern sector of the Catona Fiumara that lies on the Scilla Fault footwall (Fig. 3).

AF and **T** indexes of the Petrace Fiumara indicate that the basin is asymmetric and the trunk channel flows close to the left side of the watershed (Tab. 1). Hypsometric curve shows a mature stage of this river with a rejuvenated sector in proximity of the Cittanova Fault where **SL** index shows localized uplift.

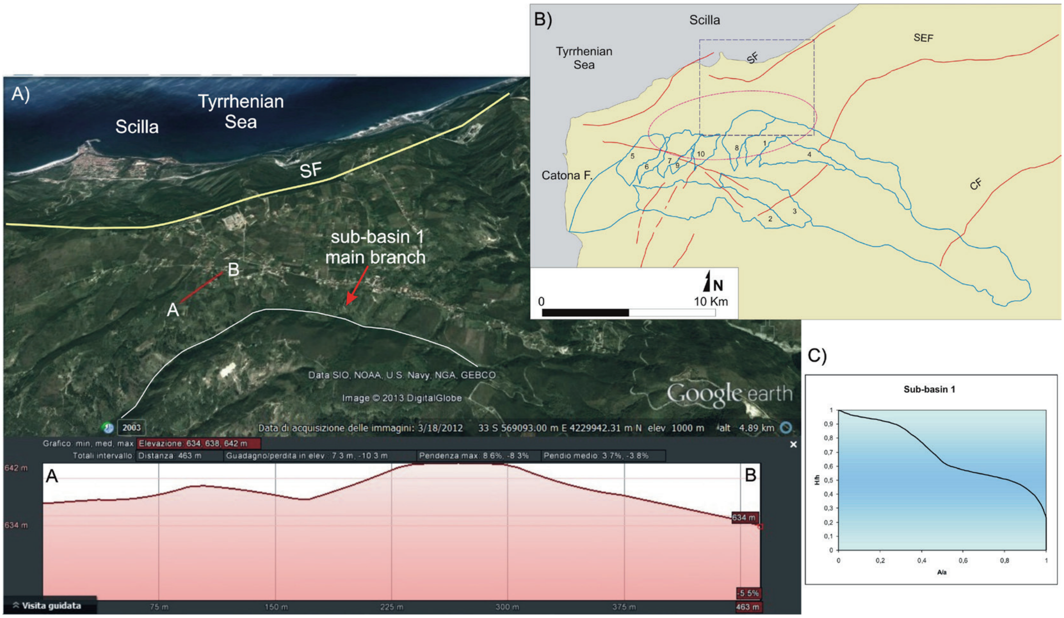

Fig. 3 – A) Google Earth image showing the track of the Scilla Fault (SF) and the rotation of the sub-basin 1 main branch because of capture; the topographic profile shows a suspended valley testifying the original northwestward drainage of the sub-basin 1 main branch; B) sketch map of the Catona Fiumara sub-basins, ellipse shows the uplifted sector due to the Scilla Fault activity, rectangle is the inset of A; C) Hypsometric curve of sub-basin 1 showing rejuvenated sectors on the footwall of the Scilla Fault (SF) and Santa Eufemia Fault (SEF).

Conclusions. Geomorphologycal and morphometrich analyses performed on the Catona Fiumara and Petrace Fiumara highlight that their drainage is perturbed by recent tectonic movements. In particular localized uplift causes rejuvenation of specific sectors where drainage is trying to restore equilibrium. The Petrace Fiumara evolution seems to be controlled principally by the Cittanova Fault whose recent activity produced a depocentre in the northern sector of the basin. The Catona Fiumara mainly suffers the activity of the Santa Eufemia Fault and Scilla Fault and also of the Cittanova Fault. In particular the counterclockwise rotation and the rejuvenation of part of the basin can be ascribed to the recent activity of the Scilla Fault, which caused local uplift and tilting. This is shown by the rotation of sub-basins 1 and 4 occurred through fluvial captures, as testified by several suspended valleys (Fig. 3). Our results contribute to constrain the seismotectonic setting of southern Calabria supporting the hypothesis that the normal faults intercepting the drainage network have Holocene activity and they can have slipped during recent earthquakes.

Acknowledgements. This work was funded by the Project MIUR-PRIN "Geodinamica attiva e recente dell'Arco Calabro e del complesso di accrezione nel Mar Ionio " (Resp. C. Monaco).

References

Aloisi M., Bruno V., Cannavò F., Ferranti L., Mattia M., Monaco C. and Palano M.; 2013: Are the source models of the M7.1 1908 Messina Straits earthquake reliable? Insights from a novel inversion and a sensitivity analysis of levelling data. Geophys. J. Int., 192 (3), 1025-104.

Basili R., Valensise G., Vannoli P., Burrato P., Fracassi U., Mariano S., Tiberti M.M. and Boschi E.; 2008: The Database of Individual Seismogenic Sources (DISS), version 3: summarizing 20 years of research on Italy's earthquake geology. Tectonophysics, 453, 20-43.

Cox R.T.; 1994: Analysis of drainage basin symmetry as a rapid technique to identify areas of possible Quaternary tilt-block tectonics: an example from the Mississippi Embayment. Geol. Soc. Amer. Bull. 106, 571-581.

D'Agostino N., D'Anastasio E., Gervasi A., Guerra I., Nedimović M. R., Seeber L. and Steckler M.; 2011: Forearc extension and slow rollback of the Calabrian Arc from GPS measurements, Geophys. Res. Lett., 38, L17304, doi:10.1029/2011GL048270.

Ferranti L., Antonioli F., Mauzc B., Amorosi A., Dai Pra G., Mastronuzzi G., Monaco C., Orrù P., Pappalardo M., Radtke U., Renda P., Romano P., Sansò P. and Verrubbi V.; 2006: Markers of the last interglacial sea level highstand along the coast of Italy: tectonic implications, Quat. Int., 145-146, 30-54.

Ferranti L., Monaco C., Antonioli F., Maschio L., Kershaw S. and Verrubbi V.; 2007: The contribution of regional uplift and coseismic slip to the vertical crustal motion in the Messina Straits, Southern Italy: evidence from raised Late Holocene shorelines, J. geophys. Res., 112 (B06401), doi:10.1029/2006JB004473.

Galli P. and Bosi V.; 2002: Paleoseismology along the Cittanova fault: implications for seismotectonics and earthquake recurrence in Calabria (southern Italy). J. Geophys. Res. 107, B2044.

Ghisetti F. and Vezzani L.; 1982: Different styles of deformation in the Calabrian Arc (southern Italy): implications for a seismotectonic zoning, Tectonophysics, 85, 149-165.

Guarnieri P. and Pirrotta C.; 2008: The response of drainage basins to the Late Quaternary Tectonics in the Sicilian side of the Messina Strait (NE-Sicily), Geomorphology, 95, 260-273.

Jacques E., Monaco C., Tapponier P., Tortorici L. and Winter T.; 2001: Faulting and earthquake triggering during the 1783 Calabria seismic sequence. Geophys. J. Int., 147, 499-516.Keller E.A.; 1986: Investigations of active tectonics: use of surgical earth processes. Panel on Active Tectonics. National Academy Press, Washington, D.C.

Malinverno A. and Ryan W.B.F.; 1986: Extension in the Tyrrhenian Sea and shortening in the Apennines as a result of arc migration driven by sinking of the lithosphere, Tectonics, 5, 227-245.

Mattia M., Palano M., Bruno V. and Cannavò F.; 2009: Crustal motion along the Calabro-Peloritano Arc as imaged by twelve years of measurements on a dense GPS network, Tectonophysics, 476, 528-537.

Monaco C. and Tortorici L.; 2000: Active faulting in the Calabrian arc and eastern Sicily, J. Geodyn., 29, 407-424.

Neri G., Barberi G., Oliva G. and Orecchio B.; 2004: Tectonic stress and seismogenic faulting in the area of the 1908 Messina earthquake, south Italy, Geophys. Res. Lett., 31, doi:10.1029/2004GL019742.

Neri G., Marotta A.M., Orecchio B., Presti D., Totaro C., Barzaghi R. and Borghi A.; 2012: How lithospheric subduction changes along the Calabrian Arc in southern Italy: geophysical evidences, Int. J. Earth Sci (Geol. Rundsch.), 101 (7), 1949-1969.

Pino N.A., Giardini D. and Boschi E.; 2000: The December 28, 1908, Messina Straits, southern Italy, earthquake: waveform modelling of regional seismograms. J. Geophys. Res. 105, B11, 25473-25492.

Rovida A., Camassi R., Gasperini P. and Stucchi M. (eds.); 2011: CPTI11, the 2011 version of the Parametric Catalogue of Italian Earthquakes. Milano, Bologna, http://emidius.mi.ingv.it/CPTI. DOI: 10.6092/INGV.IT-CPTI11

Strahler A.N; 1957: Quantitative analysis of watershed geomorphology", Transactions of the American Geophysical Union, 38 (6), 913-920.

Tortorici L., Monaco C., Tansi C. and Cocina O.; 1995: Recent and active tectonics in the Calabrian arc (southern Italy), Tectonophysics, 243, 37-55.

Valensise G. and Pantosti D.; 1992: A 125 Kyr-long geological record of seismic source repeatability: in the Messina Straits (southern Italy) and the 1908 earthquake. Terra Nova, 44, 472-483.

Verrios S., Zygouri V. and Kokkalas S.; 2004: Morphotectonic analysis in the Eliki Fault Zone (Gulf of Corinth, Greece). Bull. Geol. Soc. Greece 36, 1706-1715.

Westaway R.; 1993: Quaternary uplift of Southern Italy, J. geophys. Res., 98, 21 741-21 722.

NEW DATA ON THE POLLINO AND CASTROVILLARI FAULTS: FILLING THE GAP BETWEEN PALEOSEISMOLOGY AND HISTORICAL SEISMICITY

L. Alfonsi[3], A. Berlusconi[1], F. R. Cinti[2], R. Civico[2], P.M. De Martini[2], M.F. Ferrario[1], R. Gambillara[1], F. Livio[1], A.M. Michetti[1], D. Pantosti[2], S. Pinzi[2]
[1]*Università dell'Insubria, Como, Italy*
[2]*Istituto Nazionale di Geofisica e Vulcanologia (INGV) - Roma 1, Italy*
[3]*Istituto Nazionale di Geofisica e Vulcanologia (INGV) - Roma 2, Italy*

Introduction. The Pollino Range is the southernmost segment of the Southern Apennines at the boundary with the Calabrian Arc. Crustal extension characterized this region during the Quaternary creating a system of tectonic basins and is still active today as shown by geological and seismological data (e.g., Cinti *et al.*, 1997, 2002; Michetti *et al.*, 1997, 2000a; Fig. 1). Between June 2010 and 2012 the northern part of the Pollino foothills experienced a seismic swarm, culminating in a M = 5.0 event on night of the the October 25th, 2012 (ISIDe, 2012; Fig. 1a).

Several strong, Io = X MCS, earthquakes (e.g., Rovida *et al.* 2011) occurred to the N (e.g., 1857 Val D'Agri) and to the S (e.g., 1638 Valle del Crati) nevertheless no known historical seismic events of intensity greater than Io = VIII MCS originated in the Pollino area. The seismic catalogue only includes a seismic sequence interesting the region in the 1693; thus making this area one of the most obvious seismic gaps along the central and southern Apennines.

This apparent lack of historical seismicity can be caused by the long recurrence interval characterizing the seismogenic sources of this area and/or may be due to the loss of historical sources recording those events. For these reasons during the '90s two different research groups took the first steps in investigating the paleoseismology of two of the main faults of the area: the Pollino and the Castrovillari faults, respectively bordering to the south the Pollino Range and crosscutting the Castrovillari basin (Cinti *et al.*, 1997, 2002; Michetti *et al.*, 1997). Both the research projects testified Middle Pleistocene to Holocene faulting along these structures and, for both, recognized the occurrence of paleoearthquakes during historical times. Even if there was a general agreement about the occurrence and timing of the faults activity, coming from dating of the paleoearthquakes on both the structures, still exist some open questions about i.e. the possible linkage of the two structures, their deep geometry and recurrence interval.In order to solve some of these issues, in the framework of the of Project S1, DPC-INGV 2012-2013, we studied the Pollino and Castrovillari faults integrating on-fault field survey, paleoseismological analysis and geophysical data acquisition (GPR and ERT).

In particular, in recent years, the electrical imaging techniques have been largely applied in near-surface geophysics giving significant results to solve a wide range of geological problems, including the imaging and characterization of active faults (e.g., Caputo *et al.*, 2003).

The geophysical survey was acquired using a PASI® instrument, composed of a PC resistimeter, charged by a 12V–45A battery, 32 steel pikes for voltage measurement divided into two sets of 16 pikes each one and connected by two isolated cables and through two link-boxes to a booster.

The sections were acquired using Wenner, Wenner-Schlumberger or dipole-dipole arrays and spacing ranges between 2 and 5 according to the geometry and the estimated depth of the target. Sections were georeferenced through a GPS (horizontal accuracy: 4–6 m) and electrodes position was surveyed, for vertical topographic correction, with a Total Station (sub-cm accuracy). Signal has been processed using the Res2DinV software.

The Castrovillari fault. The Castrovillari fault (Fig. 1b) is located in the Castrovillari basin, at the foothills of the Pollino Range, and is composed of three main WSW-dipping normal-fault scarps. The scarps run for ca. 10 km across the Castrovillari basin.

Previous paleoseismological studies (Cinti *et al.* 1997, 2002) indicate that the most recent reactivation of this fault lies between 530 A.D. and 1100 A.D.

We selected two investigation sites along the Castrovillari fault: Cozzo S. Elia and Castrovillari site.

Cozzo S. Elia site. Cozzo S. Elia site is located on northern gently dipping slope of the Cozzo S. Elia hill; the fault strand is here expressed as a scarp smoothed by intense ploughing (Fig. 2a). Here we acquired a tomographic section (Wenner array; spacing 5 m) oriented ca. NE-SW and perpendicular to the scarp direction (Fig. 2b). The section displays a small resistivity range, spanning between 2 and 150 Ohm·m. This possibly reflects lateral changes in the presence of a relatively shallow water-table. The resistivity pattern depicted in the central part of the section is likely consistent with the presence of a fault showing a SW side downthrown of ca. 4-5 m. Resistivity absolute values are not referable to bedrock but the low values are typical of fine-grained sediments (fine sands, silts and clays), thus the inferred offset possibly occurs on recent soft deposits (i.e. fine grained alluvial cover).

Castrovillari site. The Castrovillari site (Fig. 1b) is located across a stream incision transverse to one of the southern scarps of the Castrovillari scarp system.

The fault is here expressed by a scarp that is built in fan delta deposits, characterized by thick packages of sand and silt, alternating with strongly cemented conglomerates and gravels. A fault zone (F1 in Fig. 2) outcrops at the modified edge of the valley in correspondence of the upper part of the scarp. The main fault trace (dipping N250/70) shows dip-slip displacement (SW-side down) of fan delta deposits. To the SW another fault (F2) crops out and puts in lateral contact conglomerates and sandy deposits of the fan delta sequence. We performed three tomographic sections, acquired within the valley floor perpendicularly to the fault trending and centered on the fault trace.

In order to detect both horizontally and vertically oriented subsurface structures, the sections were acquired with different configurations (i.e. dipole-dipole, Wenner and Wenner-Schlumberger) and spacing.

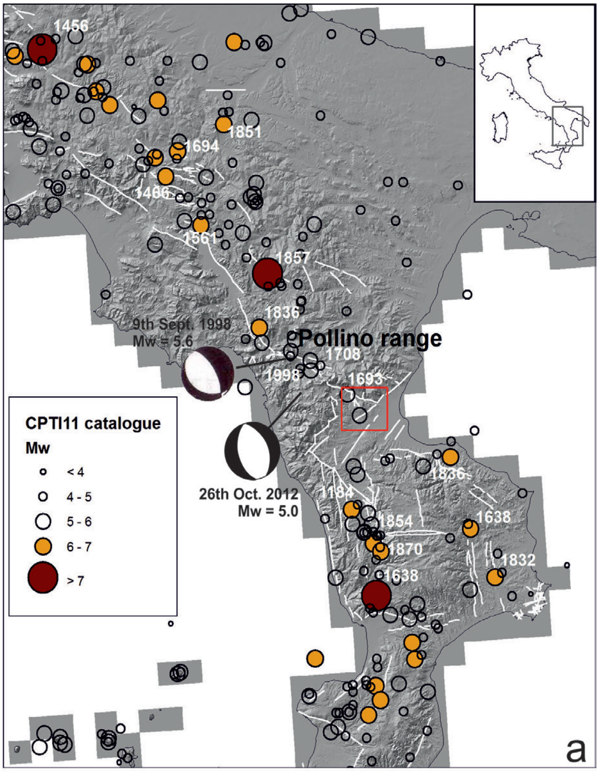

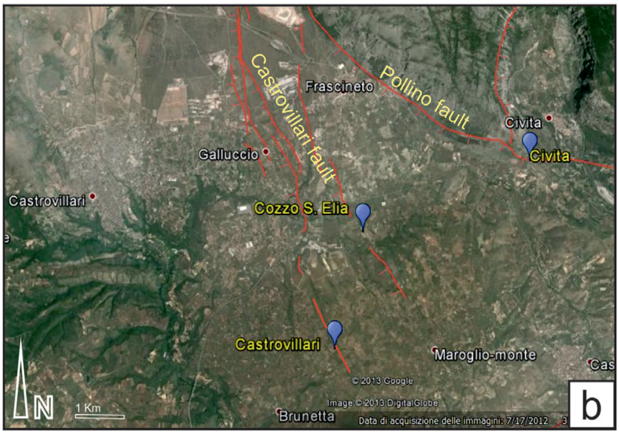

Fig. 1 – Regional seismotectonic framework for the Pollino region: a) main Quaternary faults (ITHACA database; e.g. Michetti *et al.* 2000a) and historical and instrumental seismicity from XI Sec. A.D. to 2006 (CPTI Catalogue, Rovida *et al.* 2011); b) GOOGLE™ image of the Castrovillari basin: Castrovillari and Pollino faults are indicated as well as the study sites.

Two sections, named Castrovillari A, were centered at the southward projection of the outcropping F1 fault trace. The 5 m spacing line allowed to investigate the subsurface down to 30 m; a more detailed line, reaching the depth of 12 m, was acquired using a 2 m spacing. Resistivity values range between less than 50 Ohm·m and more than 900 Ohm·m. The outcrop exposed by the road cut (Fig. 2e) shows a sequence of alternating conglomerates and sands that can be typically associated to high and relatively low resistivity values respectively. Abrupt lateral changes in the resistivity values can thus strongly suggest a tectonic contact between high impedance units. The 2 m spaced array provides a better resolution of the central sector, showing two different bands of low-resistivity: the first one between 32 and 40 meters and at a depth of 5-8 m, and another one between 40 and 60 meters and from surface to 5 m of depth. These two areas are clearly offset by another secondary discontinuity (F3) located in the footwall of the main fault.

The third line of the site, marked as Castrovillari B, runs some tens of meters SW of line A and was acquired to verify the presence of fault displacement (F2 fault) within recent fluvial deposits. In this area fine-grained material is present at the gully edge wall. Fig. 2d shows a 2 m spaced section reaching 14 m of depth. Resistivity values range between more than 45 Ohm·m and less than 400 Ohm·m. A high resistive zone is present in the eastern sector of the section, between the distance of 32 and 56 m, at a depth of 3-7 m. We associate this zone to gravel layers, coarser than the sandy and silty deposits, the latter typically characterized by smaller resistivity values. This tabular body is abruptly cut by a steep SW dipping plane (as better highlighted by the dipole-dipole array acquisition; not in figures) that can be interpreted as due to fault displacement. Offset cannot be not easily measured, even if from the dipole - dipole array a 5-6 m of vertical offset can be inferred.

F1 fault has been trenched for paleoseismological analyses. The stratigraphy is composed of a strongly cemented conglomerate, the oldest unit exposed, and a succession of alluvial and colluvial deposits (silt, clayey silt, conglomerate and gravel). The trench shows a fault zone composed by two main, 1 m spaced, 70° dipping fault traces displaying dip-slip displacement. The fault zone is aligned with the fault outcropping on the retreated valley edge and define a N 160°-165° oriented trace.

The analysis of the stratigraphic and structural setting allowed to recognize at least three distinct paleoearthquakes. Although uncertainties affect the values of offsets across the faults, due to channeling and slope deposition, slip per event is larger than 0.6 m (earthquake M>>6). Preliminary datings confirm the timing of the paleoearthquakes previously recognized by Cinti *et al.* (1997; 2002): best estimate around V-VI century A.D. (no later than X century). Although evidence are uncertain, the age of a possible younger earthquake is set between XIII and XV century A.D.

The Pollino fault. The Pollino fault (Fig. 1b) is a WNW-trending structure characterized by an impressive range front with more than 1400 m of relief. The fault hangingwall hosts the Castrovillari basin, whose sedimentary fill reaches its maximum thickness of about 600 m, filled in with upper Pliocene to lower Pleistocene marine rocks and about 300 m of middle Pleistocene to Holocene continental deposits. The field survey performed along the Pollino fault concentrated the efforts in the previously un-investigated eastern portion of the Pollino scarp. This latter is less studied than the western sector, where data on the fault activity, previously collected through paleoseismological investigations (Michetti *et al.*, 1997), indicate two probable paleo-events, dated respectively at VI – XII century A.D. and XIII – XV century A.D.

We selected the studied site as suitable for geological and subsurface investigations in order to acquire new data on the geometry of the fault and on its activity in time. We thus focused our analysis at the Civita site, along the Pollino scarp (Fig. 1b).

In this site we observed the outcropping fault plane of the Pollino fault along two walls of a dismissed quarry, orientated perpendicular to the fault trace. A wide zone of tectonic deformation composed of two main faults with relative slope changes at surface has been recognized on both walls of the quarry.

Two sections ca. SW-NE oriented, were acquired (Fig. 3a). "Cava Civita West" section (Fig. 3b) shows a wide variability of resistivity values: from 70-80 Ohm·m in the southern part, to more than 4000 Ohm·m in the northern part. The resistivity values increase also downward with depth. The zone of high resistivity in the northern sector of the section is consistent with the presence of sub-outcropping rock that tends to deepen towards the south. The low resistivity values in the southern part of the section are consistent with the presence of fine grained deposits. In the central part, the resistivity values of ca. 500 Ohm·m are related to

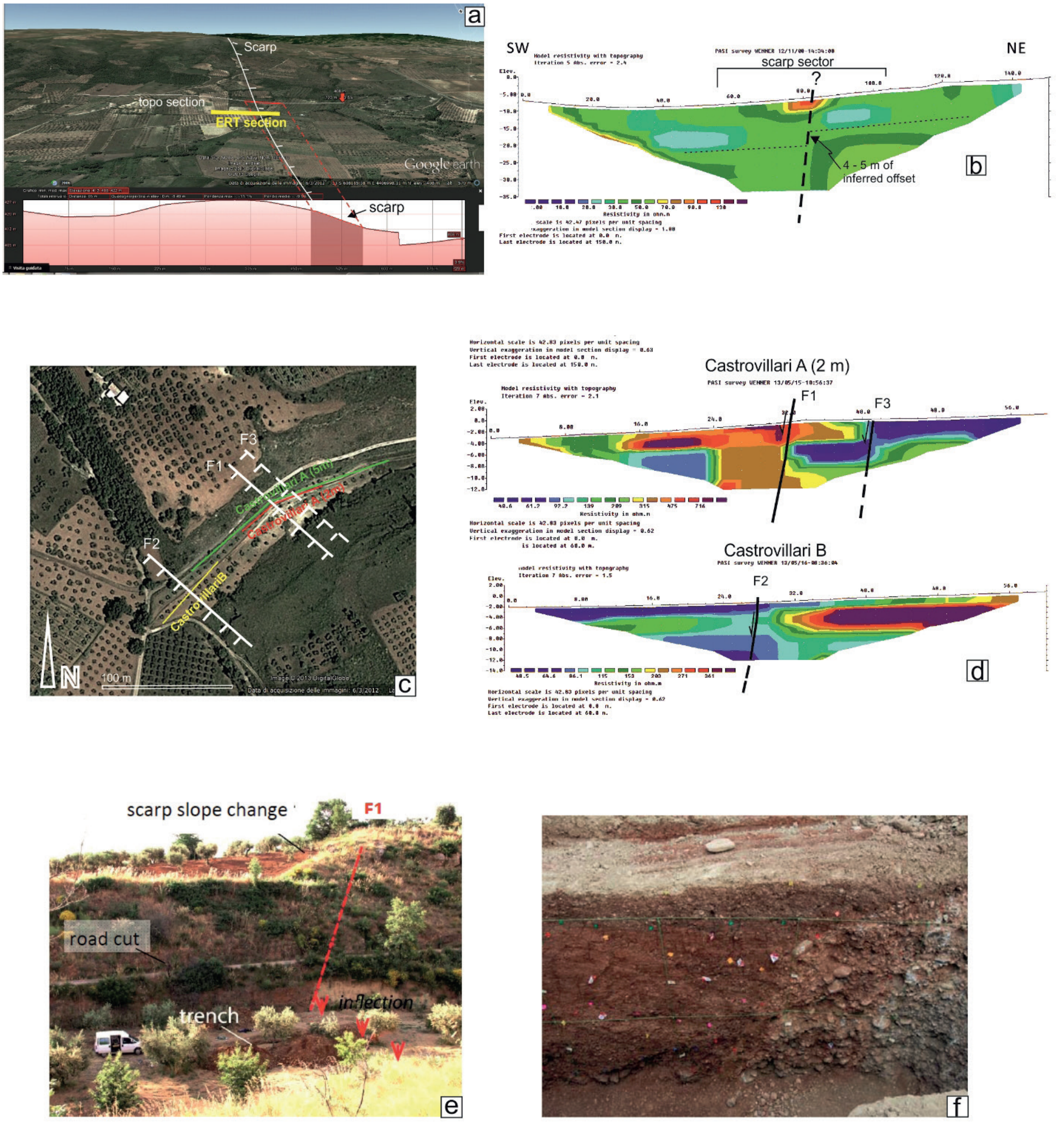

Fig. 2 – Geophysical and paleoseismological data acquired for the Castrovillari fault: a) 3D perspective from GOOGLE EARTH™ of the Cozzo S. Elia site: the Castrovillari fault scarp and the location of the ERT are reported; b) tomographic section of the Cozzo S. Elia site; c) location of the three tomographic lines acquired at the Castrovillari site; d) Castrovillari A and Castrovillari B tomographic lines; e) F1 N valley side with F1 fault highlighted and f) fault plane within the trench wall.

the presence of slope deposits and/or fractured rocks. The tomographic section shows that the grain size of deposits gets coarser downward.

The tomographic section "Cava Civita Est" (Fig. 3b) shows a range of resistivity values similar to that of "Cava Civita West" (from 70 Ohm·m to more than 4000 Ohm·m) with slightly different values close to the surface, probably due to anthropogenic reworking. In the northern part of the section, the bedrock is much closer to the surface than in the "Cava Civita West": this is probably due to a steeper slope, not allowing a thick deposition of slope deposits. Both sections crosscut the Pollino fault trace. In particular, two discontinuity planes (F1 and F2) are inferred by two steps of the high resistive area due to lowering of bedrocks and consequent increase of thickness of the deposits. The F2 interpretation in the "Cava Civita Est" section is questionable and the fault plane is traced as uncertain.

Based on the interpreted sections we identify a normal fault zone with N°120 direction and metric offset. This is consistent with the estimates in another site along the Pollino fault (5 km apart from Civita site), where 6 m of offset, deduced from topographic measurements of the fault scarp, are reported (Ferreli *et al.*, 1994; Michetti *et al.*, 1997).

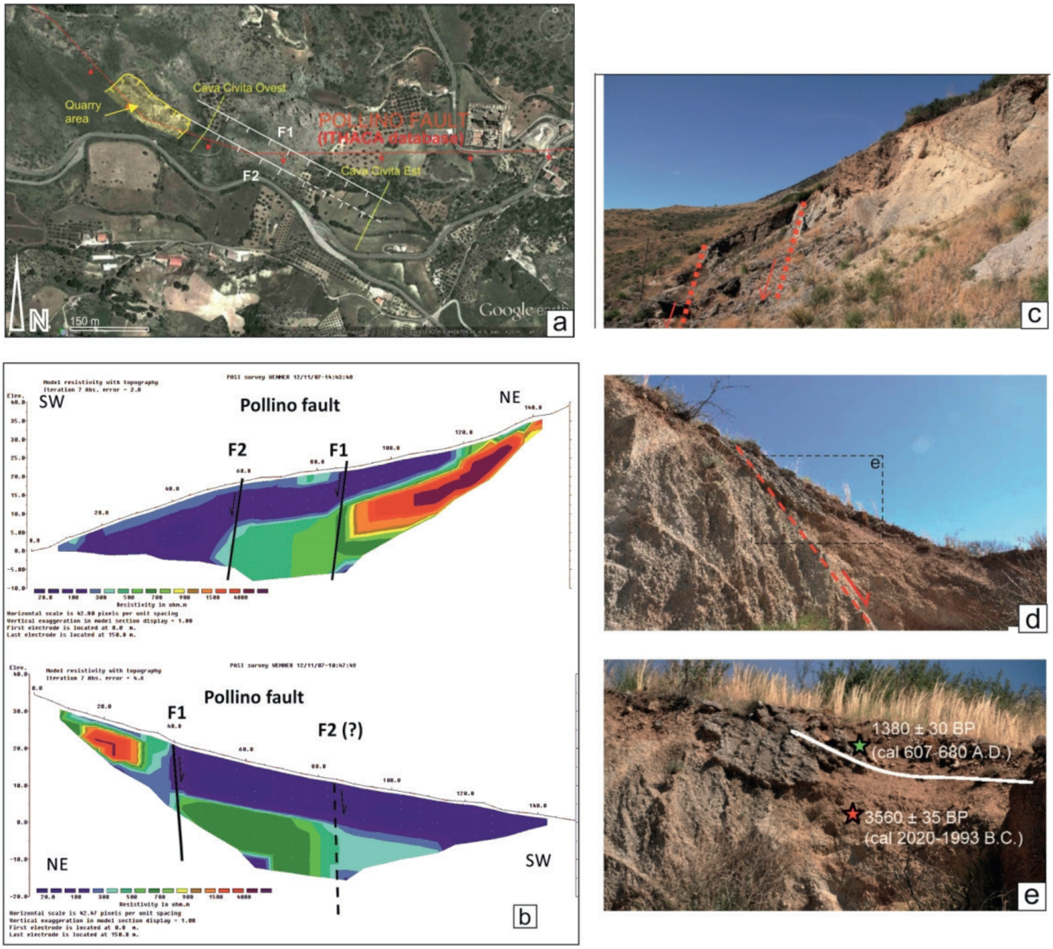

Fig. 3 – Geophysical and paleoseismological data acquired across the Pollino fault: a) GOOGLE™ image of the Cava Civita site: tomographic line traces in yellow, the quarry area is highlighted; b) the two ERT acquired at Cava Civita site; c) the western quarry wall; d) the eastern quarry wall, where samples for datings have been taken (see detail in inset "e").

The southeastern wall of the dismissed quarry was cleaned up and the outcropping fault was detected to display recent colluviums. The fault line appears capped by a shallow deposit. Dating of two samples from the faulted colluvium and from the post deformation deposit resulted in 2020-1993 B.C. and 607-680 A.D. respectively. A preliminary interpretation point to a reactivation of the fault right before the 607 A.D. Consistent evidence for a paleoevent around this age were previously assessed by Michetti *et al.* (1997) on the western section of the Pollino fault.

Conclusions. In summary from above, we draw the following conclusions from this study:

- trenching, performed on the Castrovillari and Pollino fault, shows evidence of historical paleoearthquakes on both the structures and confirms previous paleoseismological observations (Cinti *et al.*, 1997; Michetti *et al.*, 1997);
- both the structures show evidence of paleoearthquakes, associated with surface faulting, whose time window is overlapping;
- the observed fault displacement per event are consistent with paleoearthquakes equal or greater than M 6.5, as indicated also by the small displacement recorded during moderate earthquakes nearby (i.e. the M 5.6, 1998 Lauria earthquake; Michetti *et al.*, 2000b);
- ERT survey is still a poorly exploited technique in paleoseismological studies, even if quick and cost effective: in this case electric tomography allowed to correctly locate trenching sites and imaged the deep geometry of the faults, suggesting the presence of tectonic offset also in areas where subtle geomorphologic evidence are present (i.e. Cozzo S. Elia site);
- our observations confirm that the Pollino region has to be considered as active as other intramountain-basins in the Apennines, where Mw 6.5 to 7.0 earthquakes have been documented in the last 2000 years. The long-lasting historical seismic gap of the area, probably due to the incompleteness of the present-day catalogue, can be considerably filled took advantage by by the acquisition of punctual paleoseismological data.

Acknowledgement. This study has benefited from funding provided by the Italian Presidenza del Consiglio dei Ministri - Dipartimento della Protezione Civile (DPC). This paper does not necessarily represent DPC official opinion and policies.

References

Caputo, R., Piscitelli S., Oliveto A., Rizzo E. and Lapenna V.; 2003: The use of electrical resistivity tomographies in active tectonics: examples from the Tyrnavos Basin, Greece. Journal of Geodynamics **36** (1), pp. 19-35.

Cinti F.R., Cucci L., Pantosti D., D'Addezio G. and Meghraoui M.; 1997: A Major seismogenic fault in a 'silent area': the Castrovillari fault (southern Apennines, Italy). Geophys. J. Int. **130**, pp. 595–605.

Cinti F.R., Moro M., Pantosti D., Cucci L. and D'Addezio G.; 2002: New constraints on the seismic history of the Castrovillari fault in the Pollino gap (Calabria, southern Italy). J. Seismology, 6, pp. 199-217.

Ferreli L., Michetti A. M., Serva L. and Vittori E.; 1994: Terremoti olocenici lungo la Faglia del Pollino (Calabria Settentrionale): nota preliminare. In Paleosismologia e pericolosità sismica: stato delle conoscenze ed ipotesi di sviluppo. (ed. A. M. Michetti), CNR-GNDT (Gruppo Nazionale per la Difesa dai Terremoti) Rendiconti 2, pp. 65-88.

ISIDe Working Group INGV; 2012: Italian Seismological Instrumental and parametric database

Michetti A. M., Ferreli L., Serva L. and Vittori E.; 1997: Geological evidence for strong historical earthquakes in an "aseismic" region: the Pollino case (Southern Italy). J. Geodynamics, **24** (1-4), pp. 61-86.

Michetti, A. M., L. Serva and E. Vittori.; 2000a: ITHACA Italy Hazard from Capable Faults: a database of active faults of the Italian onshore territory. CD-Rom and explicative notes, ANPA (copies available from E. Vittori: vittori@ anpa. it).

Michetti A.M., Ferreli L., Esposito E., Porfido S., Blumetti A.M., Vittori E., Serva L. and Roberts G.P.; 2000b: Ground Effects during the 9 September 1998, Mw= 5.6 Lauria Earthquake and the Seismic Potential of the "Aseismic" Pollino Region in Southern Italy. Seismological Research Letters **71** (1), pp. 31-46.

Rovida A., Camassi R., Gasperini P. and Stucchi M. (eds.); 2011: CPTI11, the 2011 version of the Parametric Catalogue of Italian Earthquakes. Milano, Bologna, http://emidius.mi.ingv.it/CPTI. DOI: 10.6092/INGV.IT CPTI11.

THE WOOD ANDERSON MAGNITUDE OF THE TRIESTE STATION (TRI - NE ITALY): A NEW DATASET

D. Sandron, G.F. Gentile, S. Gentili, A. Rebez, M. Santulin, D. Slejko
National Institute of Oceanography and Experimental Geophysics – OGS, Trieste and Udine, Italy

Introduction. The standard torsion Wood Anderson (WA) seismograph owes its fame to the fact that historically it has been used for the definition of the magnitude of an earthquake (Richter, 1935). With the progress of the technology, digital broadband (BB) seismographs replaced it. However, for historical consistency and homogeneity with the old seismic catalogues, it is still important continuing to compute the so called Wood Anderson magnitude. It has been proven that synthetic seismograms WA equivalent can be simulated convolving the waveforms recorded by a BB instrument with a suitable transfer function.

The seismological station of Trieste (TRI), belonging to the World-Wide Standardized Seismographic Station Network (WWSSN) and sited in Borgo Grotta Gigante, about 12 km out of town, and managed by the National Institute of Oceanography and Experimental Geophysics (OGS), was equipped on September 1971 with two horizontal WA seismometers Lehner-Griffith TS-220 for the computation of local magnitude (Finetti and Morelli, 1972).

However, the start of the WWSS Trieste (code TRI-117 of the global WWSS network) recordings dates back to July 29, 1963. The short-period seismograph comprised three Benioff seismometers, while Ewing-Press seismometers were employed for the teleseismic detection. The recording room was located at the surface (268 m above the sea level) while the seismometers were installed at the bottom (161 m above the sea level) of the Grotta Gigante: a giant cave of the Trieste Karst with its central cavern 107 m high, 65 m wide and 130 m long. The WA instrument was located at the surface in a darkroom. The daily development of the photographic paper required a lot of time, not to mention that the photo paper procedure itself was very expensive. This uncomfortable configuration, along with the progress of the technology, contributed over the time to the abandonment of the WA recording, which occurred in April 1992. In 1995 the station was enhanced by the installation of a very BB Streckeisen STS-1 seismometer at the bottom of the cave.

The WA seismograph, after a period of inactivity, was recovered and modernized by replacing the recording on photographic paper with an electronic device. From December 17, 2002 to the present, with a period of interruption due to the property renovation of the building where it is located (May 2005 - March 2010), the instrument is fully operational and has recorded 783 events till August 9, 2012. Since 2004, next to the WA (few decimeters apart), a Guralp 40-T BB seismometer was installed, with a proper period extended to 60 s. Since then, the following signals have been acquired at the same time: i) the data of the digitized original WA, ii) the data of WA simulated by the BB close to it, and iii) those of the broad band installed at the bottom of the cave.

From April 1992, the WA magnitude (*MAW*) estimates, regularly reported in the seismic station bulletins up to 1992, had no more official publication.

Aim of the present work is twofold: from one side to recover the whole data set of *MAW* values recorded until 2012, and from the other side to verify the WA static magnification *GS*, so that to apply it in the WA simulation from waveforms recorded by broadband (BB) seismometers.

The Wood-Anderson instrument. The WA torsion seismograph, with its natural period of 0.8 s, 0.8 damping and *GS* value equal to 2800, was the instrument with which Richter (1935) defined the local magnitude as:

$$M_L = \log A - \log A_0 + dM \qquad (1)$$

where A is the maximum excursion (mm) of the WA seismograph, A_0 is an empirical function that depends on the epicentral distance of the station, dM is the station-specific corrections factor. The magnitude of an earthquake is the average value of the magnitude calculated separately on each of the two horizontal components (Richter, 1958). Among the different types of magnitude developed afterwards, this magnitude is still a solid reference both for its simple definition and widespread usage worldwide.

The sensor is formed by a copper cylinder with a diameter of 0.2 cm, 3.5 cm long and 0.944 g of weight suspended from a tungsten wire with a diameter of 0.02 mm (Anderson *et al.*, 1925) and immersed in an adjustable magnetic field. A small moving mirror adherent to the cylinder (with an angle of 22.5° respect to the front wall of the frame) reflected incident light, generated by an external bulb lamp, on a fixed spherical mirror (100 cm focal length), fixed on the instrument frame. The light was reflected back by the spherical mirror to the moving one that sent it to sheet of photosensitive paper placed over a rotating drum at one-meter physical distance from the sensor. The optical distance, because the double reflection, was four times greater (4 m). The damping is obtained through the magnetic field in which the cylinder is immersed: when the system is energized, the cylinder moves and generates Foucault currents proportional to its velocity, the resulting magnetic field contrasts that of the permanent magnet and the system is damped. It is possible to set period and idle position of the instrument bending it by the regulation screws situated on the base (changing the gravity component acting on the mass). The construction mechanics of the TS-220 instrument make the assessment of its static magnification very difficult simply from its mechanical characteristics (Uhrhammer *et al.*, 1990). In 1957 Gutenberg obtained, using a vibrating table, a value of 2800 +/- 500 (Gutenberg, 1957; Uhrhammer *et al.*, 1990).

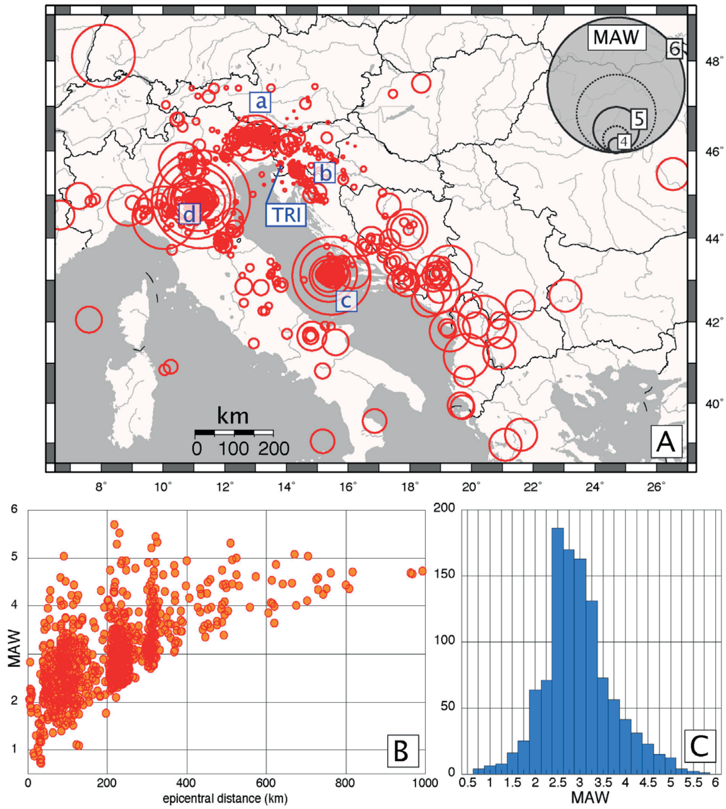

Fig. 1 – Overall data set of 1020 MAWs (circles proportional to the magnitude) recorded by the WA seismograph of the TRI station: A) (a) Friuli region, (b) Dinaric region, (c) Adriatic Sea, (d) Emilia region; B) distribution as function of epicentral distance; C) distribution as magnitude classes (bins equal to 0.25).

The Wood-Anderson instrument digitization and recalibration. The modernization of the instrument consisted in the removal of the fixed cylindrical mirror and its support creating a small side window; through this window a red laser visible beam (Flexpoint model FP-65/5 AE-AW-SD5-GL47, 650 nm wavelength, Power 5 mW) hits the moving mirror and then, once reflected, a Sitek 1L20 position-sensing detector (PSD) few centimeters far from the instrument. By removing the cylindrical mirror the ray undergoes a single reflection changing the optical leverage from 4 to 2 times. The PSD is a 1D semiconductor device sensitive to visible radiation. The sensor has two anodes (Y1 and Y2) and a cathode (bias) and provides an analogue output directly proportional to the position of the spotlight on its surface (20x3 mm of active area). It offers high resolution and linearity: it is enough to stay inside the 80% of his surface to preserve a 0.1% of linearity. The *y* centroid position measured from the center of the sensor surface is calculated by:

$$y = \frac{y_1 - y_2}{y_1 + y_2} \cdot \frac{L}{2} \tag{2}$$

where L is the length of the PSD and y_1 and y_2 are the distances of the beam spot from Y_1 and Y_2 respectively. An ON-TRAK OT-301SL amplifier, that provides in output a voltage directly proportional to the beam spot centroid position, drives the PSD. Presently, after an antialiasing filtering, the traces are recorded by a 16 bit system at 100 sps.

The two Lehner Griffith-TS-220 (N-S and E-W oriented respectively) were disassembled and cleaned, and then they were completely recalibrated. On the base of the two instruments there are two reference marks. Once the period and damping are correctly settled, moving the relative index over one of the two marks, a displacement of 50 mm over the photographic paper is produced. Dividing this value by the resulting number of counts, the sensitivity of the instruments is determined and has to be set in the data acquisition code. In this way we will have in output directly the width in mm of the tracks, equivalent to that we would have on the photographic paper. Tab. 1 reports the parameters for the first calibration operated. A few comments about it are reported in a devoted paragraph in the following.

Tab. 1 – The first calibration results after the new assemblage.

Component	Period (s)	Damping
N-S	0.792	0.787
E-W	0.796	0.818

Data available. First period: 1971-1992. During the period of operation of the original WA (1971-1992), the calculation of the local magnitude was performed following the Richter's formula (Richter, 1935), using the table of corrections factor unmodified from those calibrated for California and without station correction applied (Finetti, 1972). However the WA amplitudes were computed as vector sum (at the same instant of time) rather than as arithmetic average of the horizontal components, resulting in a systematic overestimation.

The TRI monthly paper bulletins reported only the phases recorded, the local magnitude and epicentral distance estimated by the time lag between P and S arrivals. On May 6, 1977 (exactly one year after the Friuli earthquake, whose TRI was the nearest station) OGS activated a stable network of 4 permanent stations that later expanded to cover a large part of Friuli first and north-eastern Italy later. Since 1977, then, OGS has been producing the seismological bulletin of its network. The bulletin locations have also undergone one major revision (Renner, 1995) and a number of minor revisions aimed at correcting the errors and maintaining, as possible, the homogeneity of the data over the years. At present, this bulletin is published in electronic format only, and it is accessible at the INTERNET address "http://www.crs.inogs.it/bollettino/RSFVG/" (complete access data from 1977 to the present).

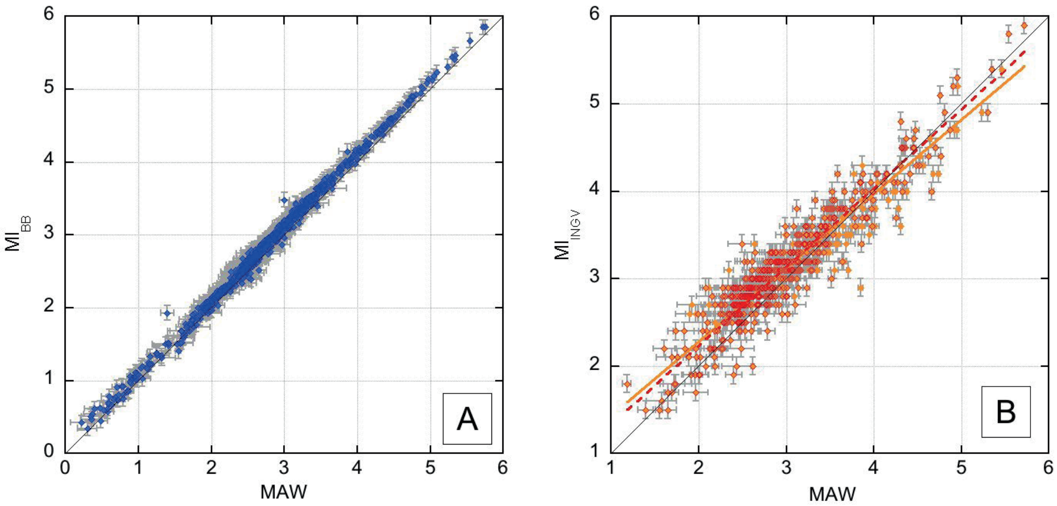

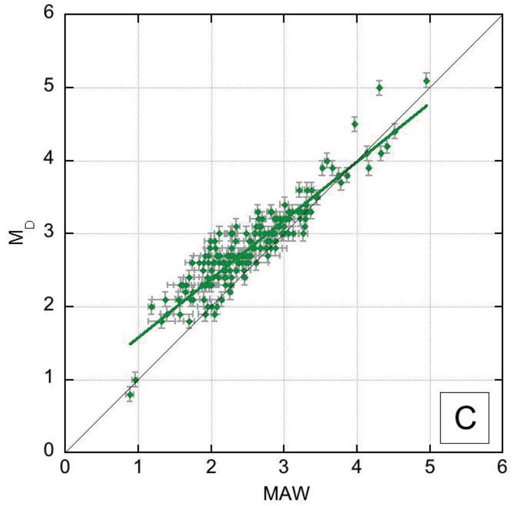

Fig. 2 – Orthogonal regression between *MAW*s and other quantities: a) the *MAW* simulated on the BB via the WA filter *MLBB*; b) M_L published by INGV (*MLINGV*). The earthquakes before April 16, 2005 are reported as red empty diamonds, the next as orange filled diamonds dots; c) M_D provided by OGS from October 31, 2004.

Crossing the TRI catalog with the localized events by the network, we retrieved a data set of 319 instrumentally located events with their *MAW*. As that the discrepancy between a vector length and the arithmetic mean of its projections strongly depends on azimuth, we have retrieved the E-W and N-S components of the original recordings. In fact, knowing the azimuth of the single event with respect to the Trieste station, the *MAW* vector has been resolved with respect to the horizontal (N-S and E-W) directions and then the correct *MAW* has been calculated, as the arithmetic mean of the two values estimated independently for the two horizontal components. The average overestimation of the *MAW* reported in the bulletins with respect to the actual *MAW* is equal to 0.25. The recovered earthquakes are mainly spatially concentrated in two regions: Friuli (a in Fig. 1a), with azimuth centered in the range 300°–330° N, and Dinarides (b in Fig. 1a), with a predominance of less clustered events with azimuth around 120° N. Overall, 56% of the data is placed in azimuthal bands where the two horizontal components have similar amplitude and, consequently, a minimal discrepancy (equal to 0.15) in magnitude computation (mean vs. vectorial composition) is theoretically expected.

To check the validity of the operation done, we selected 30 events of this data set, trying to cover the whole range of magnitudes, we recovered the original photographic sheets with the traces of the earthquakes, and we asked to three experts that were part of the seismological team from the 1970s to the 1990s to re-read the amplitudes of the WA waveforms. Apart from isolated cases, there was substantial agreement among the three specialists confirming a small but noticeable tendency to underestimate the obtained magnitude compared to the original one obtained wrongly by vectorial composition. This little exercise corroborated the opinion that the azimuthally operated recovery of the original WA amplitudes was satisfactory and that the past WA magnitude overestimation of the Trieste station was due to the incorrect method of its calculation (vectorial composition instead of arithmetic mean).

Second period: December 17, 2002 – August 09, 2004. December 17, 2002 marks the beginning of the recordings of the WA digitized seismograph. In this first stage 202 events has been recorded, however, only the magnitude and the epicentral distance have been catalogued. We have considered three location databases to associate to each event their hypocentral coordinates: that of OGS (www, preferred choice), that of the European-Mediterranean Seismological Centre (EMSC; www, second choice), and that of the National Institute of Geophysics and Volcanology [INGV; ISIDe Working Group (2010), last choice].

Moreover, we reported in the working data set the local magnitude provided by INGV, when available. If the difference in magnitude between the computed *MAW* and the *ML* provided by INGV was larger than 1, or the epicentral distances between the locations of the same event presented large discrepancies (greater than 50 km), the records were singularly double-checked, in order to avoid wrong earthquake associations. A total amount of 74 localized events has been retrieved for the time interval December 17, 2002 to August 9, 2004 and are largely clustered in the central Adriatic Sea (c in Fig. 1a).

Third period: October 22, 2004 to May 24, 2005 and March 6, 2010 to August 6, 2012. From October 22, 2004, the WA is placed side by side (at a distance of a few decimeters) to a Guralp 40-T BB seismometer with a period extended to 60 s. The *MAW* list was integrated with the hypocentral coordinates taken from the EMSC and INGV catalogues with the same approach adopted for the previous period. A total amount of 709 earthquakes have been recorded with an interruption in the recordings motivated by the renovation of the building where it is located. The instrument was temporarily moved from its historical site, and the recordings of this time period were discarded because the quality of the data in the temporary location was poor due to the high noise level.

The final catalogue. Putting together the events recorded in the three periods analyzed, a final catalogue of 1102 earthquakes, whose geographical distribution is shown in Fig. 1a, has been assembled. Three main clusters are clearly recognizable also in Fig. 1a and 1b, where the distribution of the earthquakes as a function of epicentral distance is plotted. The events of the first period and recovered from the historical paper bulletins are mostly local, with nearly half of the events in the range between 60 and 100 km, corresponding to the already mentioned area of Friuli (a in Fig. 1a). The cluster of events in central Adriatic Sea (c in Fig. 1a) refers to 80% of the localized events recorded in the second period (digitized WA). Most of the events recorded in the third period (50% in the range between 200 and 240 km) refer to the Emilia seismic sequence, started after the two strong earthquakes on May 20 and 29, 2012 (d in Fig. 1a). As regards the *MAW* distribution (Fig. 1c), the most represented bins are in the range 2.5 - 3.5. There are 14 events with magnitude greater than, or equal to 5, with the maximum value up to 5.7.

Comparative analysis of MAW values. As we have already stated, since 2004, the WA seismometer is placed side by side to a BB seismometer just with the intention to verify the goodness of the WA simulation on it. The WA magnification factor on the BB is set equal to 2800. Orthogonal regression has been performed on the data (Fig. 2a). This kind of approach, allows us taking into account the uncertainties of both magnitude values and achieving more reliable results (Castellaro *et al.*, 2006). The fitting equation is:

$$M_{LBB} = (1.016 \pm 0.004)\, MAW + (0.066 \pm 0.013) \quad R^2 = 0.9961 \qquad (3)$$

where M_{LBB} stands for the local magnitude simulated on the BB via the WA filter. The local magnitudes calculated by the BB seismometer are slightly higher than the actual *MAW*s. For the 833 events considered, on average, the M_{LBB} overestimation is equal to 0.11.

We compared the *MAW*s with the local magnitude provided by INGV M_{LINGV}, the institute that is responsible for the official magnitude publication in Italy (Fig. 2b). There were considered two different data sets and thus two corresponding fitting curves: the data until April 16, 2005 (red empty diamonds in Fig. 2b) are taken from Italian Seismic Bulletin (INGV, 2010), the following data (orange filled diamonds in Fig. 2a) are taken from the Italian Seismological Instrumental and parametric database ISIDe (INGV, 2010). Unfortunately the two data set of magnitudes are not entirely compatible because a mix of duration magnitude *MD* and local magnitude M_L is reported in the first data set while an *ML* simulated from BB recordings is available in the second data set. Considering only the earthquakes recorded after April 16, 2005 (538 events) the fit is:

$$M_{LINGV} = (0.930 \pm 0.007)\,MAW + (0.356 \pm 0.024) \quad R^2 = 0.8874 \qquad (4)$$

Taking into account also the events before April 16, 2005 (680 earthquakes), the fit is:

$$M_{LINGV} = (0.872 \pm 0.006)\,MAW + (0.511 \pm 0.021) \quad R^2 = 0.8743 \qquad (5)$$

The M_{LINGV} are on average higher compared to the MAW. In particular the overestimation (on average equal to 0.17) is more accentuated for events with a magnitude smaller than 3, while for higher magnitudes the difference is slightly reduced (on average it is equal to 0.13.)

As further analysis, we have compared *MAW*s and *MD*s provided by OGS in the time window October 22, 2004 to May 20, 2012, the day of the first strong event of the Emilia seismic sequence (Fig. 2c). The two catalogues have 187 events in common. A fixed uncertainty equal to 0.1 has been assumed on OGS *MD*s (Gentili *et al.*, 2011). The uncertainty on *MAW* was, however, obtained from the amplitude measurements as described in the next paragraph.

The equation of the fit is:

$$M_D = (0.84 \pm 0.01)\,MAW + (0.67 \pm 0.03) \qquad R^2 = 0.8874 \qquad (6)$$

It can be seen that *MD* overestimates *MAW* for low magnitudes, while it tends to underestimate it for high magnitudes. The result is qualitatively similar to that obtained in Gentili *et al.* (2011) comparing the local magnitude with that of duration comparing a set of local magnitude from Bragato and Tento (2005) and Garbin (2009) with the duration magnitude of the OGS bulletin.

Considerations on the WA magnification factor. The WA transfer function, determined empirically, is equivalent to an inertial pendulum with a free period of 0.8 s and damping of 0.8. Regarding the magnification, Anderson and Wood (1925) proposed a static magnification of 2800, which was commonly used since then. Uhrhammer and Collins (1990) and Uhrhammer *et al.* (1996) report a static magnification equal to 2080. According to Uhrhammer and Collins (2011), the difference derives from the wrong assumption by Anderson and Wood (1925) that the wire stretched in suspension used in the sensor WA does not deviate from a straight line. The deformation is actually sufficient to increase the moment of inertia and reduce the static magnification of about 30%. The difference in estimated magnification does not affect the measure of the amplitudes recorded by the original WA sensors, but it becomes crucial when synthetic seismograms are simulated. Using 2800 instead of 2080 in *MAW* estimation may cause an increase of magnitude of 0.129 (Uhrhammer *et al.*, 2011).

We tried to verify the static magnification factor of our WA with two different methods.

The first method involves a direct action on the instrument. According to Wood and Anderson (1925), *GS* is determined by:

$$G_S = A/a = L/l = \frac{A4\pi^2}{gbT_0^2} \qquad (7)$$

where *A* is the seismogram trace amplitude, *a* is the amplitude of the ground motion component normal to the equilibrium plane, *l* is the mass swinging center distance from the rotation axis, *L* is the optical lever length, *g* is the gravity acceleration (981 cm/s^2), acceleration, *b* is the instrument tilt angle (in radiants), and T_0 is its period of oscillation (0.8 s).

Tilting the instruments of a known angle *b* and measuring the output voltage from the PSD, which is proportional to *A*, and applying Eq. (7) we can calculate *GS* (Tab. 2).

Tab. 2 – Parameters used for the WA *GS* computation. *I* = WA seismograph component; *O* = PSD controller output (V); *A* = equivalent trace amplitude on paper (mm).

I	*O* (V)	*A* (mm)	*GS*
N-S	2.00±0.07	45.8 ± 1.6	2092 ± 73
E-W	2.31±0.07	52.9 ± 1.8	2339 ± 82

We must emphasize that the measure made on the N-S component of the instrument is more reliable than the E-W one because the latter was damaged. The moving mirror was partially detached and it was repaired at best with the tools and skills of the OGS technical staff. The total error associated to the estimate is evaluated as an amplifier error, equal to 1%, on the linearity of the response, plus the uncertainty on the voltmeter, equal to 0.05 V.

In order to assess the actual WA *GS*, the second method is based upon a comparative analysis of the data, in particular on the maximum amplitudes (peak to peak) of the seismograms traces, recorded by the two instruments placed side by side. On the BB seismometer we fixed *GS* equal to 2800.

Sliding a window of 50 WA samples on the values of the amplitudes recorded by the BB seismometer, the *GS* values have been calculated as the weighted average of the corresponding ratios (i.e. WA/BB×2800; see Fig. 3a). The uncertainty on the individual measurements was obtained by perturbing the error on the gain of the instrument. We simulated a series of test measurements moving the needle between two notches on the instrument from time to time, which correspond to one theoretical shift of 10 cm on the paper. We therefore measured the average number of counts of the test measures: the gain is the ratio between mm and counts. The standard deviation of the distribution of the test measurements is the error on the gain due to the imprecision in making the movement of the needle. To this, we added a further 1% error on the mean value of the measures of the test due to the amplifier.

The *GS* values decrease with increasing amplitude (Fig. 3a), reaching a value approximately constant in correspondence of 0.2 mm and close to that determined by Uhrhammer and Collins (1990) and equal to 2080. For amplitude values in the range 0.05-0.07 mm it is close to the original 2800 value. The asymptotic values in the two cases are very similar to those obtained with the first method (see Tab. 2). The magnitude estimation is slightly but clearly affected by adopting the theoretical magnification value equal to 2800 (Fig. 3b). If we simulate the WA through a BB seismometer fixing the magnification factor equal to 2800, instead of the real values of Fig. 3 A and B, we introduce an error that depends on the amplitude measured by the instrument, ranging between 0 and 0.13.

Conclusions. The Trieste Wood Anderson seismograph, officially discontinued in 1992, was recovered, modernized and after a decade of interruption, it continues presently to record earthquakes. We recovered the amplitudes of the two components of the past events (319 earthquakes retrieved from the TRI official paper bulletins) and re-computed *MAW* according to the original Richter (1935) formula obtaining a catalogue of 1102 events. The *MAW*s reported in the TRI paper bulletins are, on average, higher than the re-computed ones by 0.25. It has been asked to three experts to re-read the WA waveforms on the original photographic sheets, and we had the confirmation that the past WA magnitude overestimation was due to the wrong method of its calculation: the WA amplitudes were computed as vector sum rather than arithmetic average of the horizontal components.

For comparative purpose, we considered 833 common events recorded also by a Guralp 40-T BB seismometer installed close to the WA instrument. The WA transfer function, according to Anderson and Wood (1925) should have a *GS* value of 2800. As first result the *MAW*s calculated by the BB seismometer are higher than the WA *MAW*s on average 0.11. In order to check the actual WA *GS* value, we considered also a method involving a direct action on the instrument. The result suggests that the *GS* value depends on the waveform amplitude recorded: decreases with increasing amplitude, reaching a value approximately constant in

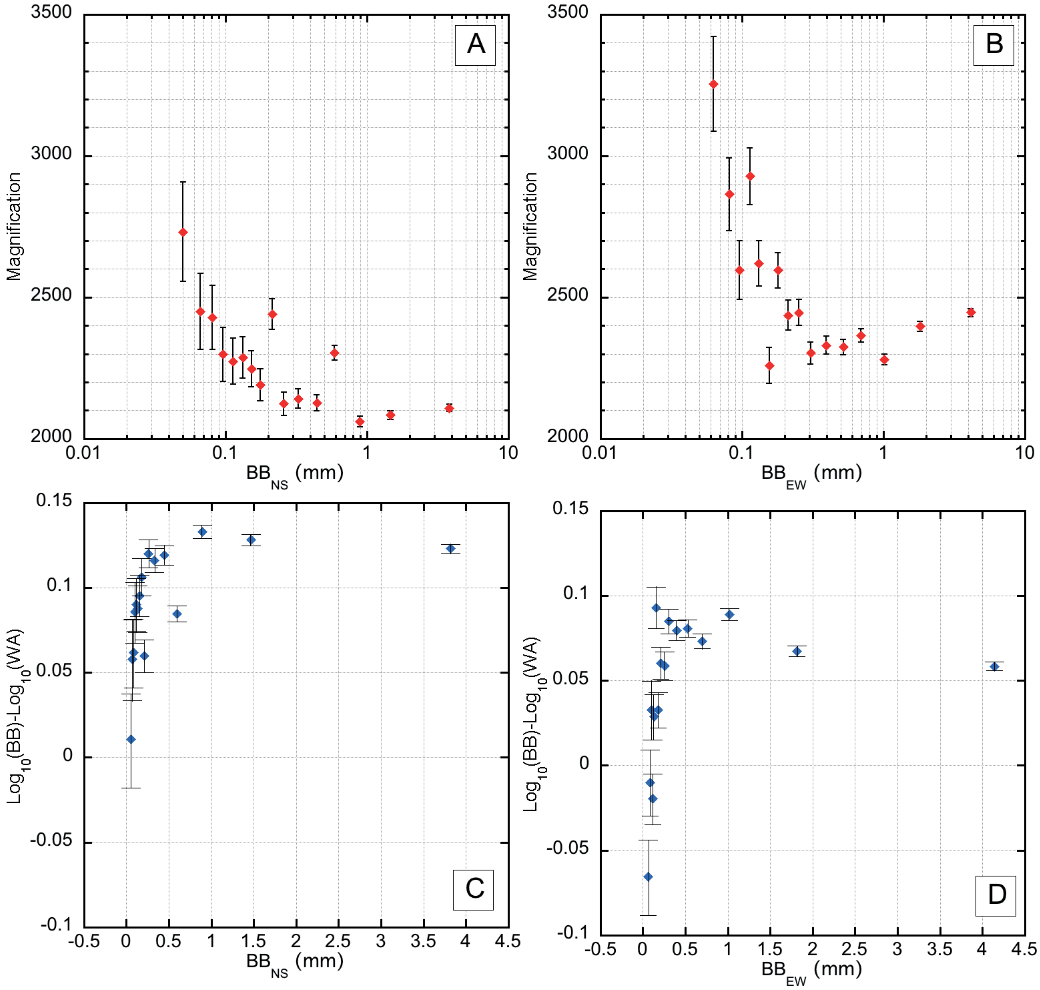

Fig. 3 – Actual WA *GS* as function of the amplitude of the seismograms recorded by the BB seismometer for: A) the N-S and B) the E-W components; uncertainty in the magnitude estimation applying a *GS* equal to 2800 as function of the amplitude of the waveform recorded on C) the N-S and D) the E-W component of the WA.

correspondence of 0.2 mm and close to 2080, i.e. the value determined by Uhrhammer and Collins (1990). For amplitude values in the range 0.05-0.07 mm the *GS* value is close to the original 2800 value proposed by Anderson and Wood (1925).

Our *MAW* values have been compared with the recent *ML* estimates provided by INGV and a good agreement has been obtained. Moreover, a comparison with the *MD* values provided by OGS for its regional network, that was originally calibrated on the TRI *MAW*, has shown an overestimation in agreement with previous a work (Gentili *et al.*, 2011), which reaches values up to 30% for magnitude less than 4.

Acknowledgements. All WA recordings are available at OGS. All the other magnitude and locations data used in this paper came from published sources listed in the references. Fig. 1a was made using the Generic Mapping Tools version 4.5.7 (www.soest.hawaii.edu/gmt; Wessel and Smith, 1998).

References

Anderson J.A. and Wood H.O.; 1925: *Description and Theory of the Torsion Seismometer*. Bull. Seism. Soc. Am., pp. **15** 1-72.

Bragato, P.L. and Tento, A.; 2005: *Local magnitude in northeastern Italy*. Bull. Seism. Soc. Am. 95, 579-591.

Castellaro S., Mulargia F. and Kagan Y. Y.; 2006: *Regression problems for magnitudes*. Geophys. J. Int. **165**, pp. 913-930.

EMSC/CSEM - European-Mediterranean Seismological Centre website: http://www.emsc-csem.org/

Finetti I. and Morelli C.; 1972: *Earthquake magnitude determination for Trieste WWSS station*. Boll. Geof. Teor. Appl. **14**, pp. 67-83.

Garbin, M.; 2009: *Predisposizione, riordino e archiviazione delle elaborazioni dati sismometrici relativi alle stazioni temporanee delle reti Ravedis e Firb*. Internal Report, 2009/64 CRS 6 APSES 94 pp.

Gasperini P.; 2002: *Local magnitude revaluation for recent Italian earthquakes (1981-1996)*. Journal of Seismology, **6**, pp. 503-524.

Gentile G. F.; 2002: *Digitalizzazione dei sismometro Lhener-Griffith TS-220 (Wood-Anderson)*. Rel. n. /47/2002/OGA-18, 39 pp.

Gentili S., Sugan M., Peruzza L. and Schorlemmer D.; 2011: *Probabilistic completeness assessment of the past 30 years of seismic monitoring in Northeastern Italy*. Phys. Earth planet. Inter. **186,** pp. 81-96.

ISIDe Working Group; 2010: *Italian Seismological Instrumental and parametric database*. <http://iside.rm.ingv.it>

Italian Seismic Bulletin (INGV, 2010) website: http://legacy.ingv.it/roma/reti/rms/bollettino/

OGS official bulletin website: http://www.crs.inogs.it/bollettino/RSFVG/RSFVG.en.html

Richter C.F.; 1958: *Elementary Seismology*. W. H. Freeman and Company, San Francisco, 768 pp.

Richter C. F.; 1935: *An instrumental earthquake magnitude scale*. Bull. Seism. Soc. Am., **25**, pp. 1-32

Uhrhammer R.A. and Collins E.R.; 1990: *Synthesis of Wood-Anderson seismograms from broadband digital records*. Bull. Seism. Soc. Am., **80** pp. 702-716.

Uhrhammer R.A., Loper S.J. and Romanowicz B.; 1996: *Determination of Local Magnitude Using BDSN Broadband Records*. Bull. Seism. Soc. Am., **86** pp. 1314-1330.

Uhrhammer R.A., Hellweg M., Hutton K., Lombard P., Walters A.W., Hauksson E. and Oppenheimer D.; 2011: *California Integrated Seismic Network (CISN) Local Magnitude Determination in California and Vicinity*. Bull. Seism. Soc. Am., **101**, pp. 2685-2693.

SOURCE INVERSION OF THE M6.3 1927 JERICHO EARTHQUAKE, POSSIBLE REPETITION OF THE BIBLICAL EARTHQUAKE OF 1473 B.C.

L. Sirovich, F. Pettenati
Istituto Nazionale di Oceanografia e di Geofisica Sperimentale, OGS, Trieste, Italy

Introduction. According to the Bible and the Torah (Joshua [Giosuè] 6:1-21), God made the walls of Jericho fall down, perhaps with an earthquake, to help Joshua to conquer the city. The battle would have taken place in 1473 B.C.. This hypothesis found some archaeological confirmations (e.g., Garstang and Garstang, 1940; Keller, 1956), but it is still controversial.

However, the M6.25 earthquake of 11 July 1927 (Ben-Menahem *et al.*, 1976) heavily hit also the area of Jericho and could perhaps be the repetition of the hypothetic biblical event. Vivid descriptions of earthquakes in the region are found in the Bible. In particular, as regards the area of study, Ambraseys (2009) pointed out that the descriptions by prophets Amos and Zacharias allow the interpretation of an earthquake about in 766 B.C.; the Zacharias' words even comply with a sinistral strike-slip movement.

The epicentre and causative faults of the 1927 destructive earthquake is still very controversial (see Tab. 1). Ben-Menahem *et al.* (1976) located it north of Jericho. According to Avni *et al.* (2002), however, the location north of the city was also based upon some secondary macroseismic evidence by Garstang (1931) and became one of the most accepted facts. In particular, this author reported the collapse of the banks of Jordan River about 20 km north of Jericho, damming thereby the Jordan for twenty-one hours. This damming became a crucial evidence for locating the epicentre by Ben-Menahem *et al.* (1976). However, upon close examination of the daily reports of the British Police of the time, Avni *et al.* (2002) concluded that: i) these detailed reports registered all happenings but did not even mention an important happening such as a one-day damming of the river (and the following flooding); ii) Garstang was not a witness of the phenomenon because, at the time of the 1927 earthquake, he went already back to Great Britain and iii) he had a personal religious interest «to relate natural disasters to miraculous biblical events» (Avni *et al.*, 2002; p. 471).

Then, Shapira *et al.* (1993) noticed that many authors reported the (32.0°; 35.5°) epicentre of Tab. 1 without re-evaluating it and thinks that that approximate location was not obtained using the many recordings collected by the International Seismological Summary, ISS, but was estimated by the Ksara, Lebanon, station using only the Ksara data. Instead, Shapira *et al.* (1993) used the ISS data and applied standard location procedures. But there is a question that puts some doubts on the Shapira *et al.* (1993) epicentre itself: the difficulties associated with synchronization of the mechanical clocks in 1927 and the relatively low sensitivity of the seismic stations at the time, which produces high residuals (they omitted those greater than ±10 s).

More recently, Zohar and Marco (2012) used the intensities, *I*, provided by Avni (1999) to relocate the 1927 epicentre. To find their best solution, they corrected the data for the site effects and, then, correlated the intensities spatially with a logarithmic variant of the epicentral distance. They explain that the optimum site corrections had the effect of moving their first epicentre some 25 km west, on the Dead Sea transform DST. Instead, exagerated corrections moved the epicentre 60 km east of DST. Their epicentre is close to that by Shapira *et al.* (1993). We comment that, in our opinion, an objective criterion for evaluation of all the sites is required. We avoid situations where only selected data are examined or where part of the data are modified, because this could drive the inversion results. It should also be kept in mind that deamplifications, if any, usually do not attract the same attention as cases of amplification, even though they have the same importance as far as inversion is concerned (Pettenati and Sirovich, 2007; pp. 1591). For these reasons, we do not correct single *I* values following local site studies, if any. In California and in Italy, we attempted to search for site effects by splitting the logarithms of the epicentral distances of each observed *I*, according to the prevailing soil condition at each site, studying their distributions (Sirovich and Pettenati, 2001, 2004; Pettenati and Sirovich, 2003, 2004). To this end different lithological and geophysical large-scale classifications were used, but none worked (Pettenati and Sirovich, 2007). No objective criteria for all the used sites were available in the present case, however.

In this context, some Israeli colleagues, who read our studies on two Italian earthquakes in 1570 and 1694 (Sirovich *et al.*, 2013a, b), suggested us to attempt the intensity-based source inversion also of the event of 1927 using our *KF* technique.

Tab. 1 – Epicentres of the 1927 earthquake proposed by various authors (and one secondary macroseismic effect supposedly connected to the epicentre).

Reference	Latitude [°]	Longitude [°]
Ben-Menahem *et al.* (1976)	32.2	35.5
Shapira *et al.* (1993)	31.6	35.4
many references [a]	32.0	35.5
Zohar and Marco (2012) [b]	31.8	35.5
Avni *et al.* (2002)	31.6	35.4
Doubtful Jordan damming [c] (Garstang, 1931)	32.0 [d]	35.5 [d]

[a]) 30 km north of Jericho, interpreted -on a qualitative basis- as a strike-slip rupture along the Dead Sea transform DST; according to Avni *et al.* (2002), most of these references relied on the recording of one only station (Ksara, Lebanon) and on the unreliable Jordan damming 'evidence' by Garstang (1931); [b]) using only intensities; [c]) unreliable, according to Avni *et al.* (2002); [d]) approximate values.

Tectonic context. The area of study is on the contact between the African and the Arabian plates, north of the Sinai sub-plate, along the Dead Sea Transform Fault extending Nward to the Amanos-Zagros section of the Eurasia-Africa-Arabia convergence zone. The tectonic interpretation of the area is not easy, also for political reasons, because the two sides of the Jordan Valley are for long not freely accessible. The pull-apart nature of the Dead Sea depression still is an unresolved questions. In short, as noticed by Devès *et al.* (2011), although most agree that the Dead Sea valleys are tectonic in origin, no one agrees on the processes that have led to its formation. The same authors notice a striking feature of the Red Sea-Galilee Lake allignement: there is an ~11.5° change of direction between the Jordan Valley (south of the Dead Sea) and the Araba Valley (north of it). This: i) precludes a uniform stress distribution in the region (as if the principal transform structure would be rectilinear); ii) causes still unknown stress distribution and, consequently, rupture mechanisms in the region. However, Devès *et al.* (2011) find that 65% of the deformation in the Dead Sea region can localise on kinematically stable through-going strike-slip faults (the DST; our comment) while the remaining ~35% has to remain distributed. If this holds, our preliminary source (Model 1 in Tab. 2) would belong to the remaining 35%. On the one hand, these authors specify that there are no clear normal faults along the valley flanks (unlike Carmel fault), such as in true rifts like Corinth or East Africa, but, on the other one, they comment on that there are no normal faults along the valleys flanks that could account for the 600 m depression of the Dead Sea.

The work by Shamir (2006) is more encouraging for us, because it lets hope that our source be more compatible with the tectonics of the region from the Dead Sea to the area north of Jericho. He thinks that the late-phase (late Pliocene-early Pleistocene) asymmetrical shear zone of the DST is characterized also by a penetrative, bimodal (NW and NE) structural orientation pattern, reflected in earthquake focal mechanisms. Regarding the NE-oriented

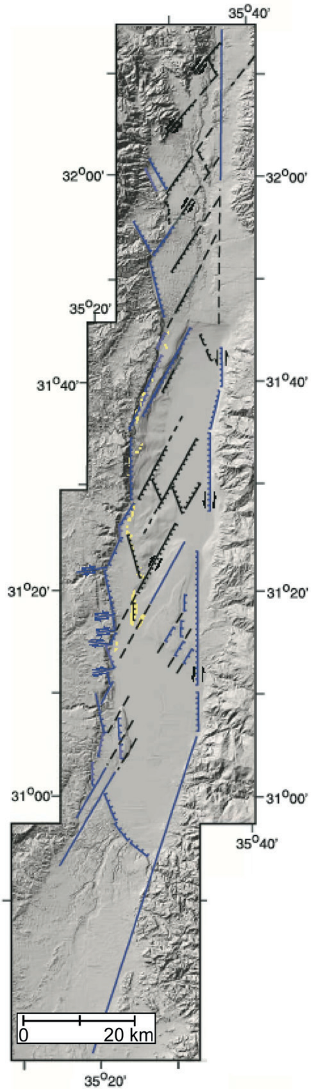

Fig. 1 – Tectonic interpretation of the Dead Sea region by Shamir (2006; his Fig. n. 9).

faults, Shamir (2006) thinks that they extend northeastward and produce subsided, fault-bounded depocentres within the Dead Sea basin. More studies and, possibly, also the use of some seismograms of the time are needed, however, before we can confirm our very prelimary results of a dip-slip source NNE oriented in 1927 (see Tab. 2 and Fig. 2).

The hypothesis of the Dead Sea as a pull-apart basin had been proposed by Garfunkel *et al.* (1981). We comment on, that such a basin, or a rhomboidal-shaped basin, needs bordering normal faults also north and south of the depression. In Fig. 1, we reproduce the interpretative fault map of the active late phase structure of the Dead Sea Depression by Shamir (2006; his Fig. n. 9). He used blue lines for previously mapped faults (we refer to his original caption for the fault references) and in black the newly mapped faults based on seismicity (Shamir, 2006) and seismic data of other authors (we refer again to the original caption of the figure).

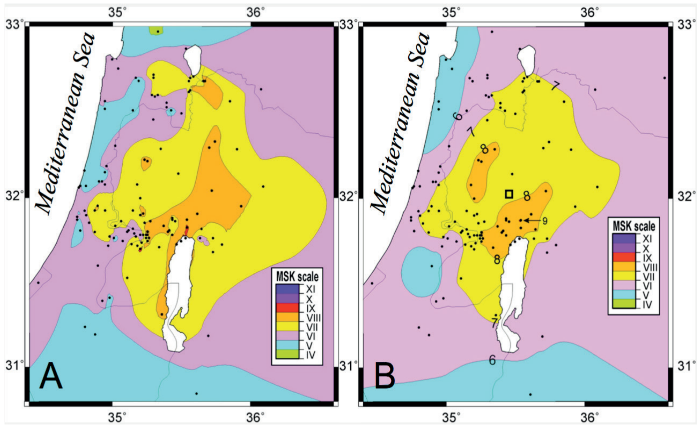

Fig. 2 – A: point intensities of the 1927 earthquake by Avni (1999) contoured with the n-n algorithm (see text); B: synthetic intensities produced by our inverted source of Tab. 2; the only point of degree 9 is marked by an arrow.

The intensity data used. We treated the 133 point intensities, *I*, provided by Avni (1999; and written communication, 2013). Following our procedure, which applies the Chauvenet method (Pettenati and Sirovich, 2007), we looked for statistical outliers. We found that, in this case, the epicentral location was crucial; thus, with a Dead Sea epicentre there were some outliers of high intensities to the north (Yarmuch-Fall *I* =8.5; Reyneh *I* =8), whilst an epicentre more Nward produced few outliers with low intensitiy to the south. In this preliminary experiment, we used the whole dataset, which is shown in Fig. 2A using the natural-neighbor n-n contour algorithm (Sirovich *et al.*, 2002); there are four points of degree 9. Remember that the n-n isoseismals strictly honour the data. You can see the dots corresponding to Yarmuch-Fall and Reyneh in the small brownish island of degree VIII in the upper part of Fig. 2A. We treated half-degrees as real numbers.

Tab. 2 - Ranges of the parametres explored by the genetic algorithm of the KF inversion.

Parametres	Range from:	to:	Step
Latitude N [°]	31.20	32.70	0.01
Longitude E [°]	35.20	35.80	0.01
H [Km]	5	35.0	0.1
Mach N. +	0.50	0.99	0.01
Mach N. -	0.50	0.99	0.01
Vs [Km/s]	3.50	3.95	0.01
Mo [N m) 10^{18}	1.0	5.0	0.01

Parametres	Model 1 (DEME 1)	Model2 (DEME 2)
Latitude N [°]	32.02	31.98
Longitude E [°]	35.45	35.36
Strike [°]	37	22
Dip [°]	41	34
Rake [°]	83	86
H [Km]	30.5	32.8
Mach N. +	0.91	0.99
Mach N. -	0.93	0.99
Vs [Km/s]	3.58	3.51
Mo [N m) 10^{18}	3.69	2.0
L+ [Km]	17.2	14.4
L - [Km]	2.2	0.8
Fitness	73.75	77.75

Intensity-based (preliminary) source inversion of the 1927 earthquake. The prelimary results of the KF source inversion are in Tab. 2 and Fig. 2B. The upper part of Tab. 2 shows the ranges of the parametres explored by the genetic algorithm of the KF inversion (the fault-plane solution was let free); values with "+" and "-" indicate values in the along-strike and anti-strike directions.

The lower part of Tab. 2 (please add ±180° to the rake angles) shows the best solution (striking 37°) and the second-choice one. They are not far from each other, indicating an almost flat area in the topography of residuals in the 11-parametre hyperspace. Remember the intrinsic ambiguity of ±180° in the rake angles of our solutions. Thus, the rake angle of Model is 83° or 263°, which could be compatible with the normal faults drawn by Shamir (2006), in the upper part of Fig. 1.

Discussion. In the case of earthquakes of the early instrumental era, using also the instrumental recordings is compulsory. For example, the polarities even of few P onsets, in the right geographical positions, could solve the intrinsic ambiguity of ±180° of our solutions. The work is in progress.

Acknowledgements. We thank Amotz Agnon of the Hebrew University of Jerusalem for providing selected bibliography and for helpful discussion. Ron Avni from Ben Gurion University for having provided his intensities in the format we needed. Moti Zohar for the conversion of the kilometric coordinates of intensities of the so-called black net to UTM geographical coordinates. We thank the Italian Embassy in Israel for having funded the 1st Italy-Israel Bi-National Symposium (September 2013) on «Earthquakes in Ancient Lands: The Apennines and the Levant», which gave us the opportunity to confront with several Israeli colleagues. The research was partly funded by OGS.

References

Ambraseys N.; 2009: *Earthquakes in the Mediterranean and Middle East, a Multidisciplinary Study of Seismicity up to 1900*. Cambridge University Press, UK, xx + 947 pp..

Avni R.; 1999: *The 1927 Jericho Earthquake, comprehensive macroseismic analysis based on contemporary Sources*. Ph.D. thesis, Ben-Gurion University of the Negev. Vol. 1, 64 pp., vol. 2, 139 pp. (in Hebrew).
Avni R., Bowman D., Shapira A. and Nur A.; 2002: *Erroneous interpretation of historical documents related to the epicenter of the 1927 Jericho earthquake in the Holy Land*. Journal of Seismology, **6**, 469-476.
Ben-Menahem A., Nur A. and Vered M.; 1976: *Tectonics, seismicity and structure of the Afro-Eurasian junction, the breaking of an incoherent plate*. Phys Earth Planet. Inter., **12**, 1-50.
Devès M., King G.C.P., Klinger Y. and Agnon A.; 2011: *Localised and distributed deformation in the lithosphere: Modelling the Dead Sea region in 3 dimensions*. Earth Pl. Sc. Letters, **308**, 172-184.
Garfunkel Z., Zak I. and Freund R.; 1981: *Active faulting in the Dead Sea rift*. Tectonophysics **80**, 1-26.
Garstang J.; 1931: *Joshua Judges*. Constable and Co. LTD London, pp. 134-139.
Garstang J. and Garstang, J.B.E.; 1940: *The Story of Jericho*, Hodder & Stoughton, 200 pp..
Keller W.; 1956: *The Bible as History*. William Morrow, New York, N.Y., 452 pp..
Pettenati F., and L. Sirovich; 2003: *Tests of source-parameter inversion of the U.S. Geological Survey intensities of the Whittier narrows 1987 earthquake*, Bull. Seismol. Soc. Am. 93, 47-60.
Pettenati F., and L. Sirovich; 2007: *Validation of the Intensity-Based Source Inversions of Three Destructive California Earthquakes*, Bull. Seismol. Soc. Am., **97**, 1587-1606, doi: 10.1785/0120060169.
Shamir G.; 2006: *The active structure of the Dead Sea Depression*. Geological Society of America Special Paper 401-02, 15-32.
Sirovich L., and F. Pettenati; 2001: *Test of source parameters inversion of the intensities of a 54,000-death shock of the seventeenth century in southeast Sicily*, Bull. Seismol. Soc. Am. 91, no. 4, 792-811.
Sirovich L., and F. Pettenati; 2004: *Source inversion of intensity patterns of earthquakes: A destructive shock in 1936 in northeast Italy*, J. Geophys. Res. 109, B10309, doi 10.1029/2003JB002919, 16 pp.
Sirovich L., Pettenati F., and F. Cavallini; 2013a: *Intensity-Based Source Inversion of the Destructive Earthquake of 1694 in the Southern Apennines, Italy*, J. Geophys. Res., in press.
Sirovich L., Pettenati F., and F. Cavallini; 2013b: *Fault planes obtained from macroseismic inversion of selected earthquakes of the Montello and Po Plain*. Deliverable D21/b3, Project S1 DPC-INGV, 5 pp..

RIVALUTAZIONE DEL TERREMOTO DELL'8 GENNAIO 1693 NELL'AREA DEL POLLINO

A. Tertulliani, L. Cucci
Istituto Nazionale di Geofisica e Vulcanologia, Roma

Alcune note sulla sismicità storica. L'area del Massiccio del Pollino, al confine calabro-lucano, è considerata una zona di gap sismico a causa della sua scarsa sismicità, come risulta dal Catalogo sismico (CPTI11- Rovida *et al.*, 2011).

I primi studi sul gap sismico del Pollino risalgono alla metà degli anni '80 (Valensise *et al.*, 1994; SGA, 1994; Cinti *et al.*, 1997; Guidoboni e Mariotti, 1997; Michetti *et al.*, 1997), mentre gli sviluppi più recenti sono di SGA (2000), Camassi e Castelli (2004), e Castelli e Camassi (2005). Le storie sismiche (DBMI11) delle località dell'area non riportano terremoti avvenuti prima del 1600 che possano aver interessato tali centri abitati. Le tracce più antiche di eventi sismici si riferiscono a danni prodotti a Castrovillari dal terremoto del 1638 (con epicentro in Calabria Centrale, a circa 100 km di distanza dall'area di studio), mentre il terremoto documentato più antico nell'area del Pollino è quello avvenuto nel 1693. Questo evento è stato inserito per la prima volta in un catalogo nel 2007 (CFTI4Med: Guidoboni *et al.*, 2007). La mancanza di terremoti (e risentimenti) nella Calabria settentrionale può però esser dovuta anche ad un gap documentale, cioè alla assenza di informazioni relative ad eventi sismici già noti ed avvenuti relativamente vicino (Scionti *et al.*, 2006).

Il terremoto del Pollino dell'8 gennaio 1693 rientra nel novero degli eventi che sono stati 'oscurati' da altri eventi sismici ben maggiori ed avvenuti molto vicino ai primi sia come distanza che come tempo; nel nostro caso il 9 gennaio 1693 ebbe inizio la sequenza sismica della Sicilia Orientale, uno dei più forti eventi sismici della storia italiana, che destò una vasta impressione e colpì anche buona parte del territorio calabrese, restando incisa a lungo nell'immaginario collettivo. La vicinanza spazio-temporale dei due eventi è la più probabile ragione della tardiva identificazione dell'evento del Pollino. La coincidenza temporale in un primo tempo ha confuso le notizie e le informazioni provenienti dalla *Calabria Citra* (l'odierna Calabria settentrionale), rendendole in un secondo momento invisibili alla letteratura sismologica.

Il fine di questo studio è la rivalutazione della storia sismica dell'area, ed in particolare l'aggiornamento delle conoscenze sull'evento del 1693, cercando di risolvere le questioni irrisolte attraverso una nuova lettura di tutte le fonti, note ed inedite. Qui di seguito descriviamo tutto il percorso della ricerca, dalle indagini svolte negli archivi alla valutazione dell'intensità macrosismica in ciascuna località.

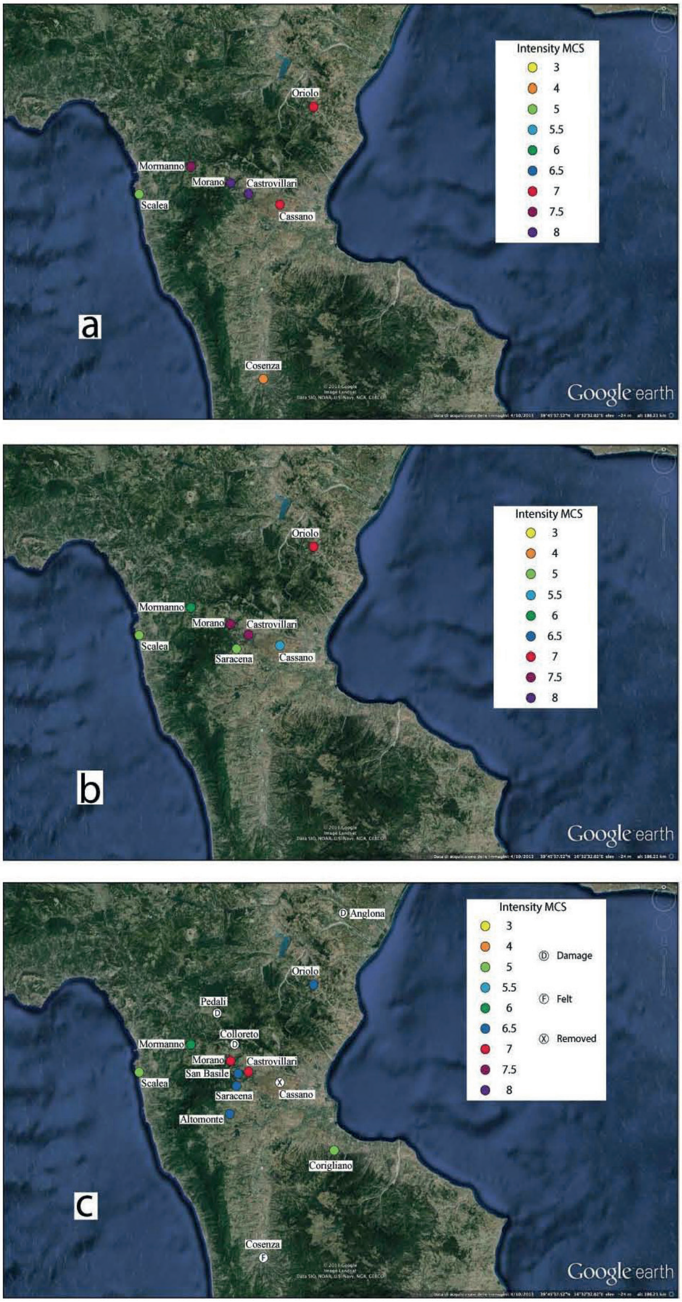

Fig. 1 – Mappa delle intensità del terremoto del 1693 da a) Guidoboni *et al.* (2007); b) Camassi *et al.* (2011); c) questo studio. La località Monteleone (odierna Vibo Valentia) è fuori dei limiti della mappa.

Archivi e fonti. La ricerca di nuove fonti documentali sul terremoto del Pollino dell'8 Gennaio 1693 non poteva prescindere da una dettagliata indagine sullo stato dell'arte della letteratura precedente, con particolare riferimento ai Rapporti Tecnici SGA (1994 e 2000), al Catalogo CFTI4Med (Guidoboni *et al.*, 2007), ed alla bibliografia in essi contenuta.

I Rapporti Tecnici (SGA, 1994; SGA, 2000) riportano testi ed altre fonti coeve relative alle località di Castrovillari, Mormanno, Morano Calabro e Oriolo. Altri documenti sono citati in CFTI4Med (Guidoboni *et al.*, 2007), che aggiunge altre quattro località al campo macrosismico (Cassano, Cosenza, Monteleone – l'odierna Vibo Valentia – e Scalea). Sfortunatamente le trascrizioni dei testi di CFTI4Med non sono state rese disponibili, e si è dovuto procedere a recuperare i documenti originali negli archivi dove erano conservati.

La ricerca ha interessato fonti d'archivio, in special modo corrispondenze diplomatiche o amministrative, ed anche lettere private, ed è stata eseguita in diversi luoghi di conservazione come l'Archivio Segreto Vaticano, gli Archivi di Stato di Firenze, Venezia, Napoli e Cosenza, ed in numerosi archivi locali e parrocchiali. Un altro gruppo di documenti è costituito da fonti giornalistiche originali, gazzette e notizie (vedi Gazzette in bibliografia) che, come moderne agenzie di stampa, divulgavano resoconti e notizie dalle principali città europee (Castelli e Camassi, 2005). Tuttavia, le notizie riportate in tali giornali erano in generale piuttosto vaghe e non approfondite.

Dalle fonti alle intensità. L'accurata ricerca storica ha consentito di recuperare molti documenti coevi, non considerati prima dagli autori. La lettura di tutti il materiale documentale, pubblicato e non, ha permesso di rivalutare con cura lo scenario del terremoto, assegnando valori di intensità macrosismica MCS (Fig. 1).

Danni sono stati riconosciuti e documentati a Castrovillari, Morano Calabro e Oriolo, dove alcune chiese e alcune abitazioni hanno sofferto un considerevole danneggiamento. In altri paesi come Altomonte, Mormanno, San Basile e Saracena le fonti riportano ("...*Né in luoghi convicini sta minore il danno havendo patito Altomonte* ..."), ma non descrivono il danno: per queste ultime località è stato valutato un grado di intensità incerto. Le informazioni raccolte sono relative alla sequenza sismica, certamente documentata dall'8 gennaio alla fine di marzo 1693, cosicché l'intensità è valutata necessariamente sulla base degli effetti cumulati delle repliche.

Castrovillari. È il vero centro documentale del terremoto. Gran parte dei documenti e delle fonti citano questa località, che era anche la reale sede episcopale della Diocesi di Cassano (Russo, 1967). Nei dispacci dai corrispondenti di Venezia, Firenze e Roma residenti nel Regno di Napoli Castrovillari è descritta come il paese più colpito. In particolare, dopo le scosse dell'8 gennaio, viene documentata la rovina di due chiese parrocchiali e di due monasteri, nonché di alcuni altri edifici. Durante la sequenza furono anche danneggiate la chiesa di S. Maria del Castello (ASFi, 1693; Russo 1982; Trombetti, 2012). In altri documenti sono descritti come completamente rovinati e collassati due edifici rurali (ASCs) di proprietà del monastero di San Francesco, nonché il danno sofferto dal chiostro di S. Chiara e dal Palazzo Vescovile. Intensità assegnata 7 MCS.

Morano Calabro. Insieme ad altre località Morano è citata da Toscano (1695) e da numerosi altri documenti come uno dei paesi più colpiti, senza alcuna descrizione del danno. Tuttavia, in alcuni documenti d'archivio (ASFi, 1693; APS, 1694; AGS) sono state ritrovate alcune informazioni contestuali, in particolare quella del collasso del campanile della chiesa dei Padri Zoccolanti (Minori Osservanti) e dei molti danni subiti nel territorio comunale. Intensità assegnata 7 MCS.

Altomonte, San Basile e Saracena. Queste sono nuove località nella lista dei paesi colpiti, e sono citate insieme in un paio di dispacci diretti da Castrovillari e Napoli a Firenze (ASFi, 1693). Le tre località sono descritte come molto sofferenti a seguito del terremoto, ma senza alcuna descrizione del danno (Fig. 2). Intensità assegnata 6-7 MCS.

Oriolo. Consideriamo come unica fonte affidabile il manoscritto di Giorgio Toscano (1695), che cita qualche danno provocato dai terremoti occorsi durante la notte fra l'8 ed il 9 gennaio. Qualche danno ai camini e il collasso parziale della torre del castello rappresentano l'immagine del danno ad Oriolo. Intensità assegnata 6-7 MCS.

Mormanno. Non abbiamo recuperato informazioni specifiche sul danneggiamento a Mormanno, al di là della generica descrizione del Toscano (1695) e di una lettera da Napoli a Firenze (ASFi, 1693). Ciononostante a Mormanno sono ben

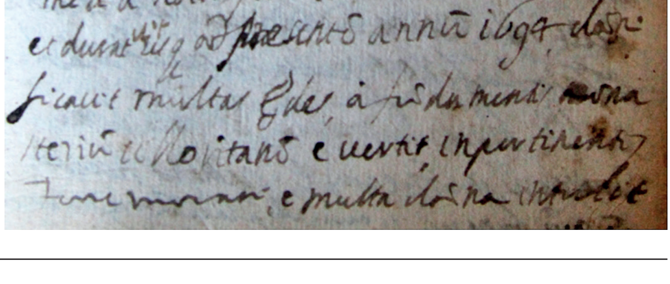

Fig. 2 – Stralcio della notizia dell'*immanis terremotus* nel Libro dei Morti della Chiesa delle Armi di Saracene conservato nell'Archivio Parrocchiale di Santa Maria del Gamio.

documentate cerimonie e pratiche religiose svolte per rendere grazie della sopravvivenza al terremoto del 1693, a rimarcare l'assenza di danno significativo. Intensità assegnata 6 MCS.

Colloreto (Morano C.). Il monastero di S. Maria di Colloreto è citato in documenti coevi (Libro seu Platea del Venerabile convento di Colorito, ADC, 1722) come pesantemente danneggiato dal terremoto del 1693. In questo caso, trattandosi di un singolo edificio, è più appropriata l'assegnazione di D (danno ad edificio singolo).

Pedali (Viggianello). Il monastero di San Nicola da Tolentino a Pedali, presso Viggianello, avrebbe sofferto "*…per il grandissimo danno patito dal terremoto…"*, cosicché i frati dovettero vendere due casali di loro proprietà per ripararlo. Poiché il documento è datato 1700, è ragionevole ipotizzare che il terremoto del 1693 sia il più probabile evento sismico causa del danno. Assegnazione di D (danno ad edificio singolo).

Anglona. Nella relazione del vescovo datata 19 agosto 1700 (ASV, 1700) la Cattedrale di Anglona "*dopo essere stata gravemente colpita dai recentissimi terremoti minacciava di rovinare".* Anche in questo caso, considerando il tempo trascorso e l'ubicazione, è ragionevole ritenere che il terremoto del 1693 sia il più probabile evento sismico causa del danno. Assegnazione di D (danno ad edificio singolo).

Corigliano. Nella sua cronistoria di Corigliano Amato racconta, citando il forte terremoto Siciliano (e confondendo le date) *"Corigliano ne fu potentemente scosso, le sue fabbriche vacillarono, ma fu immune da danni".* Si ritiene che, data la notevole differenza nella distanza epicentrale fra i due eventi, il terremoto cui si fa riferimento sia quello del Pollino. Intensità assegnata 5 MCS.

Scalea. In alcune lettere private spedite da Scalea in data 5 marzo 1693 si riporta un continuo avvertire di eventi sismici che generano qualche apprensione. Riteniamo che possa trattarsi di repliche dell'evento del Pollino dell'8 gennaio. Intensità assegnata 5 MCS.

Monteleone (odierna Vibo Valentia). In una lettera al Segretario di Stato di Spagna (AGS, 1693) viene riportata con dettaglio la descrizione delle scosse risentite a Monteleone a partire dall'8 gennaio 1693. Intensità assegnata 3 MCS.

Cassano sullo Ionio. Nessuna delle fonti consultate cita Cassano come interessata all'evento del Pollino, pertanto è stata rimossa dalla lista delle località coinvolte dal terremoto del 1693.

Tab. 1 – Lista delle località colpite dalla sequenza sismica del Pollino secondo gli studi precedenti ed a seguito del presente lavoro.

Località	Lat	Lon	Guidoboni *et al.*, 2007	Camassi *et al.*, 2011	**Tertulliani e Cucci**
Altomonte	39.698	16.131			**6.5**
Anglona	40.249	16.560			**D**
Cassano			7.0	5.5	
Castrovillari	39.814	16.202	8.0	7.5	**7**
Colloreto (Morano)	39.889	16.151			**D**
Corigliano	39.596	16.520			**5**
Cosenza	39.303	16.252	4.0		**F**
Monteleone (Vibo Valentia)	38.675	16.102	3.0		**3**
Morano Calabro	39.844	16.136	8.0	7.5	**7**
Mormanno	39.889	15.989	7.5	6.0	**6**
Oriolo	40.052	16.447	7.0	7.0	**6.5**
San Basile	39.809	16.164			**6.5**
Saracena	39.775	16.157		5.0	**6.5**
Scalea	39.814	15.792	5.0	5.0	**5**
Pedali (Viggianello)	39.997	16.060			**D**

Conclusioni. È stata condotta una approfondita revisione del terremoto del Pollino del 1693, con il recupero di una notevole mole di nuove fonti documentali che hanno permesso di incrementarne il livello di conoscenza. Su questo evento esistevano finora due studi differenti di Guidoboni *et al.* (2007), citato in CFTI4Med, e di Camassi *et al.* (2011). La sintesi di tali studi è mostrata in Fig. 1 ed in Tab. 2. La ricerca storica ha contribuito a) alla rivalutazione dei valori di intensità di alcune località; b) alla scoperta di altre località interessate dall'evento sismico; c) più in generale, ad aggiornare l'intero scenario dell'evento. Il numero delle località per cui esistono informazioni utili sale dalle 7-8 dei lavori precedenti a 14. La massima intensità scende da 8-7.5 a 7. Abbiamo calcolato la magnitudo macrosismica e l'epicentro macrosismico dell'evento con il codice Boxer 4.0 (Gasperini *et al.*, 2010). I risultati sono mostrati Tab. 2.

Tab. 2 – Parametri epicentrali del terremoto dell'8 gennaio 1693 secondo gli studi precedenti ed a seguito del presente lavoro. I parametri epicentrali di Camassi *et al.* sono stati calcolati in questo lavoro usando Boxer 4.0 poichè gli Autori non avevano elaborato questo dato nel loro lavoro.

Autori	latitudine	longitudine	Intensità epicentrale	Magnitudo Mw
Guidoboni *et al.* (2007)	39.850	16.217	8	5.7
Camassi *et al.* (2011)	*39.903*	*16.262*	7-8	*5.35*
Presente studio	**39.826**	**16.158**	**7**	**5.1**

Come si può notare in Tab. 2 la magnitudo macrosismica Mw dell'evento del 1693 è sensibilmente diminuita, ed è confrontabile con quella dell'ultimo evento sismico avvenuto nell'area il 26 ottobre 2012, Mw 5.0, I max 6.

Ringraziamenti. Vogliamo ringraziare le molte persone che ci hanno aiutato durante la ricerca, contribuendo al successo del lavoro. Prima di tutti Viviana Castelli per la traduzione dal latino – lingua in cui sono scritti molti documenti – e Beatriz Brizuela e Jaume Dinares Turrell per la traduzione dallo spagnolo e la corrispondenza con gli archivi spagnoli a Valladolid. Grazie per la pazienza e la gentilezza agli archivisti, ai parroci e a tutti coloro che sono stati consultati in cerca di materiale originale. Un ringraziamento speciale al Prof. Vincenzo Toscani che ha autorizzato la lettura di un manoscritto originale rivelatosi prezioso per i nostri risultati.

Bibliografia

Letteratura scientifica

Camassi R. and Castelli V.; 2004: *Looking for new earthquake data in the 17th-18th century European "newssellers" network*, Jou. Earth. Eng., **3**, 335-359.

Camassi R., Castelli V., Molin D., Bernardini F., Caracciolo C. H., Ercolani E., Postpischl L.; 2011: *Materiali per un catalogo dei terremoti italiani: eventi sconosciuti, rivalutati o riscoperti*, Quaderni di Geofisica n. **96**.

Castelli V. and Camassi R.; 2005: *The shadow-zone of large Italian earthquakes. Early journalistic sources and their perception of 17th-18th centuries seismicity*, Jou. Earth. Eng., **9**, 333-348

Cinti F. R., Cucci L., Pantosti D., D'Addezio G. and Meghraoui M.; 1997: *A major seismogenic fault in a 'silent area': the Castrovillari fault (southern Apennines, Italy)*, Geophys. Jou. Int., **130**, 595-605.

Gasperini, P., G. Vannucci, D. Tripone and E. Boschi ; 2010: *The location and sizing of historical earthquakes using the attenuation of macroseismic intensity with distance*, Bull. Seismol. Soc. Am., **100**, 2035-2066; doi: 10.1785/0120090330.

Guidoboni E. e Mariotti D.; 1997: *I terremoti sconosciuti: Appunti per un catalogo*, in Boschi, E., Guidoboni, E., Ferrari, G., Gasperini, P. and Valensise, G., Catalogo dei Forti Terremoti in Italia dal 461 a.C. al 1990, ING-SGA, Bologna, pp. 80-90.

Guidoboni E., G. Ferrari, D.Mariotti, A.Comastri, G.Tarabusi and G.Valensise; 2007: *CFTI4Med, Catalogue of Strong Earthquakes in Italy (461 B.C.-1997) and Mediterranean Area (760 B.C.-1500).* INGV-SGA. Available from http://storing.ingv.it/cfti4med/

Locati M., Camassi R. e Stucchi M. (a cura di); 2011: *DBMI11, la versione 2011 del Database Macrosismico Italiano.* Milano, Bologna, Available from http://emidius.mi.ingv.it/DBMI11.

Michetti A. M., Ferreli L., Serva L. and Vittori E.; 1997: *Geological evidence for strong historical earthquakes in an "aseismic" region: the Pollino case (Southern Italy)*, J. Geodynamics, **24**, Nos 1-4, 61-86, Rovida A., Camassi R., Gasperini P. e Stucchi M. (a cura di); 2011: *CPTI11, la versione 2011 del Catalogo Parametrico dei Terremoti Italiani*. Milano, Bologna, http://emidius.mi.ingv.it/CPTI. DOI: 10.6092/INGV.IT-CPTI11.

Scionti V., Galli P., Chiodo G.; 2006: *The Calabrian seismicity durint the Viceroyalty of Naples: sources silence or silent sources? The case of the strong 1744 earthquake*, Boll. Geof. Teor. Appl., **47**, 1-2, 53-72.

SGA RPT ; 2000: *Recupero ed integrazione di informazioni sui terremoti attualmente sconosciuti ai cataloghi*, Report 227/00, presso INGV.

SGA RPT; 1994: *Ricerche sulla sismicità storica dell'Italia Centrale e sul Massiccio del Pollino*, Report 115/94, presso INGV.

Valensise G., Pantosti D., D'Addezio G., Cinti F. R. e Cucci L.; 1994: *L'identificazione e la caratterizzazione di faglie sismogenetiche nell'Appennino Centro-Meridionale e nell'Arco Calabro: nuovi risultati e ipotesi interpretative.* In Atti XII Convegno GNGTS, Roma, 1993, 331-342. Esagrafica, Roma.

Fonti storiche

Essendo impossibile fornire qui la lista completa di tutte le fonti, presentiamo solo quelle ritenute essenziali per la comprensione del testo.

AAM, Archivio Arcipretale di S.Maria del Colle di Mormanno, Registro delli Beni Stabili dell'Arcipretale Chiesa di S.Maria del Colle della Città di Mormanno, Settembre 1742.

ADC, Archivio Diocesano di Cassano allo Ionio, Relazioni ad limina Mons. De Magistris anno 1701.

Amato G.; 1884: *Crono-istoria di Corigliano Calabro*, Forni Rist. anast., Bologna, 1980.

ASCs, Archivio di Stato di Cosenza, sez. Castrovillari, Fondo Corporazioni religiose, b. 32

ASFi, Archivio di Stato di Firenze, Fondo Mediceo del Principato, filza 1601 Napoli regno e isole 1691-1694.

ASNa, Archivio di Stato di Napoli, Corporazioni religiose soppresse, Monasteri soppressi, Colloreto b. 6090

ASVe, Archivio di Stato di Venezia, Senato, Dispacci degli ambasciatori e residenti, Napoli, filza 102 (1692-93).

AGS, Archivo General de Simancas, Secretaria de Estado, Negociacion de Sicilia, legajo 3507, Consultas decretos y notas, n. 3, Monteleone 15 gennaio 1693.

AGS, Archivo General de Simancas, Secretarias Provinciales, Napoles, legajo 61, Consultas originales, Napoli 11 febbraio 1693.

APS, Archivio Parrocchiale di Santa Maria del Gamio (Saracena), Libro dei morti (registro della Chiesa delle Armi), appunto manoscritto del 1694.

ASV, Archivio Segreto Vaticano, Congregatio Concilii, Relationes dioecesium, vol. 49 A, Relazione del vescovo di Anglona Matteo Cosentino, Napoli 19 agosto 1700.

ASV, Archivio Segreto Vaticano, Congregatio Concilii, Relationes dioecesium, vol. 198 A, Relazione del vescovo di Cassano allo Ionio, De Magistris, 15 dicembre 1704.

ASV, Archivio Segreto Vaticano, Segreteria di Stato, Napoli, vol. 114, avviso Napoli.

ASV, Archivio Segreto Vaticano, Segreteria di Stato, Avvisi vol. 56.

Basile P. (a cura di); 1978: *Toscano G. - La storia di Oriolo. Testo del XVII secolo,* Fasano editore Cosenza, pp. 298.

[Gazette d'] Amsterdam, 1693.02.23, n. 16.

[Gazette d'] Amsterdam, 1693.03.02, n. 18.

[Gazette d'] Amsterdam, 1693.03.02, n. 18 Nouvelles Extraordinaires.

[Gazzetta di] Bologna, 1693 gennaio-febbraio

[Gazzetta di] Mantova, 1693.02.12, n. 7.

[Gazzetta di] Napoli, 1693.01.28, n. 5.

Russo F.; 1967: *Storia della Diocesi di Cassano*, 4 voll., Napoli.

Russo F.; 1982: *Il Santuario di S. Maria del Castello in Castrovillari*, Castrovillari, 131 pp.

Toscano G.,: *Manoscritto senza titolo del 1695*, Archivio Famiglia Dr. Giorgio Toscani, Roma

Trombetti G.; 2012: *"Castrovillari è città antichissima…" memoria inedita del XVII secolo.* ed. Il Coscile, Castrovillari, 127 pp.

SCIENCEQUAKE: A SURVEY ON THE ITALIAN SEISMOLOGISTS COMMUNITY ABOUT THE CASE OF THE ITALIAN SCIENTISTS CONVICTION FOR THE EARTHQUAKE IN L'AQUILA

G. Tipaldo[1], R. Carriero[1], A. Pizzo[1,2]
[1]*Department of Culture, Politics and Society, University of Turin, Italy*
[2]*Centro Interuniversitario Agorà Scienza, Turin, Italy*

Introduction. On 22 October 2012 the court of L'Aquila (Italy) sentenced to six years in prison six members of the "Commissione Grandi Rischi" (CGR, National Commission for the Forecast and Prevention of Major Risks, an official government body), founding them guilty of multiple manslaughter for having falsely reassured citizens five days before the devastating earthquake of 2009, which claimed more than 300 lives.

This paper, as part of a wider study on Italian researchers' science communication practices initiated in 2012 by the University of Turin (ISAAC - *Italian Scientists multi-technique Auditing and Analysis on science Communication*), will take the story of L'Aquila as a "revelatory" case study (Yin, 2003), uncovering the complex communicative interactions that today increasingly bind Science, Politics, Media and Society in risk assessment and uncertainty management. After proposing a theoretical model of interaction between the components mentioned above, the paper focuses mostly on the first of it – Science – presenting the main results of a CAWI (computer assisted web interview) survey on a sample of the Italian seismologists community from INGV and GNGTS.

The L'Aquila earthquake trial as a 'revelatory' case. We aim to use the L'Aquila earthquake trial – which lasted from September 2011 until October 2012 – as a 'revelatory case' of the deep and intricate relationships between Science (SC), Pseudoscience (PS), Politics (PO), Mass Media (MM) and Society (SO).

Fig. 1 shows a sketchy representation of the general framework within which we placed our work: the model is inspired by the so called «mediatization» model of political communication (Mazzoleni and Schulz, 1999). The «mediatization» model recognizes that the media have become «the most salient arena» (Dahlgren, 1995) for discussing relevant issues in contemporary democracies, providing a stage for «political plays» and simultaneously interacting with both politics and society, not rarely offering contents deeply affected by populism (Mazzoleni *et al.*, 2003).

According to our case study, we introduced two extra elements, Science (SC) and Pseudoscience (PS), the latter being conceived of as an endemic component of the social or the political system or both (depending on circumstances), that acquires public visibility and a certain degree of legitimacy whenever it enters the media arena.

Due to space limits, this work will be focusing only on one of the five components leaving the others – and their reciprocal interactions – to forthcoming updates. At least five reasons can be adduced to justify the choice.

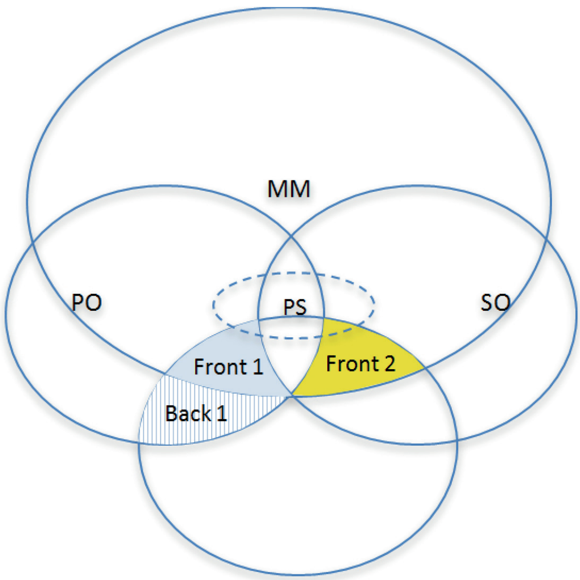

Fig. 1 – A model of mutual relationships between Science, Politics, Media and Society.

Firstly, the idea that a scientist could be prosecuted because of his/her scientific work, in advanced democracies, was something more suitable for history books than today's life. Not by chance, at least in the immediacy of the sentence, the media and not a few members of the Italian and international scientific communities spread the idea that the Italian scientists conviction was an attack on science, following the then Minister of Environment Corrado Clini, who claimed that the sentence had a sole precedent in trial held by the Catholic Church against Galileo Galilei in 1633.

This case – to move to the second reason – perfectly fits into the STS international debate on scientists' competencies when engaging with the public, pushing the discussion forward on key-points still not developed as much as it should be: how scientists think of their own role in risk assessment and emergency management, not excluding possible ethical implications; and how they represent the unavoidable – but sometimes "dangerous" – liaisons with politics in relevant decision-making processes. This is a crucial point in contemporary democracies, as Nature (2012) put down founding the verdict "perverse" and the sentence "ludicrous", worried about the serious implications «about the chilling effect on (scientists') ability to serve in public risk assessments».

A third point is about science, media and pseudoscience: an increasingly relevant twist of interests and communication strategies, which in the L'Aquila case is so sharp to be almost paradigmatic, gives the opportunity, for example, to explore whether and how Italian seismologists cope with a media logic (i.e. spectacularization and trivialization of information) keen on giving equal space to scientists and pseudoscientists (as defined just beyond), in a sort of «*par condicio*» or «equalization of positions» strategy of communication.

Lastly, we think it may argue for the sociological relevance of the study to survey for the first time the Italian seismologist community, the most directly affected scientific body by the quake in L'Aquila and what ensued.

Before moving to methods and results, it is important to underline that the five spheres composing our model are not to be intended as abstract categories. On the contrary, they precisely enclose specific social actors directly involved in the L'Aquila case. When we talk about MM, we refer to the huge video-textual documentation newspapers and televisions have produced over these years at a local, national and – not rarely – international level. By PO, we firstly and mostly intend the Italian Civil Protection and the CGR, whose members played a major role in assessing risk and managing the emergency in L'Aquila before, during and after the tragic earthquake of 6 April 2009. With SO we both refer to the Italian public opinion in general and to the citizens of L'Aquila, who more than everyone else have suffered the heavy consequences of the earthquake and a part of whom constituted as offended party kicking off trial against PO and SC. The "umbrella term" SC has in this paper quite a delimited semantic domain: it's the Italian seismologists community, where the six scientists sentenced came from. And PS is for us represented by the key-figure of Gioacchino Giuliani, a former technician of the Institute of Physics of Interplanetary Space detached to the National Laboratories of Gran Sasso. Giuliani made headlines by claiming to have predicted the disaster of April 6, 2009 with a radon detector. Yet, his profile is unfit to be represented as «experts» or «scientists» in seismology under many points of view: not appropriate CV, nor adequate academic qualifications, not belong to relevant research programs, list of publications without relevant peer-reviewed material.

Data and methods. Our data come from an online survey of 379 Italian researchers (from University, CNR, INGV and other research institutes) conducted in June 2013.[1] To reach the target population of Italian seismologists we used two email lists: GNGTS and INGV. From the former we deleted all the email addresses with an INGV account in order to avoid

1 This case study is part of a larger project (ISAAC) about science communication coordinated by prof. Sergio Scamuzzi at the Department of Cultures, Politics and Society, University of Torino.

overlaps with the latter. However we did not have direct access to the INGV list and emails were sent by staff of the Institute. After one invitation and two reminders, we received 241 valid questionnaires from the GNGTS list (response rate = 16.4%) and 138 from the INGV list (response rate unavailable)[2]. The low response rate from GNGTS is quite common in online survey: our previous questionnaire on science communication, addressed to a large sample of Italian academic scientists (ISAAC wave 1), registered a response rate of 17.4%. Unlike this case, however, we don't have *a priori* information about the target population of Italian seismologists, so we are not able to evaluate the representativeness of our sample. The latter can be characterized as follows:

- mean age is 46.1
- 64.9% are men
- 12.9% are university professors, 52.3% are research officers (at university and/or research institutes), 12.1% are technicians and 22.7% have other roles/positions (PhD students, post-docs, professionals, etc.)
- 62.1% belongs to academic/scientific associations or did so in the past

Moreover, based on reported main research interest, about 60% can be unambiguously classified as seismologists, while the rest are spread in other research fields (applied geophysics, volcanology, environmental geophysics, other).

The questionnaire included 19 closed-ended questions (52 items) focused on 4 topics: communication activities, attitudes toward the public of science, politics and the role of scientists, the case of l'Aquila (opinions on the sentence, its consequences, media coverage and media treatment of the case, the role of Giampaolo Giuliani). Twelve final questions provide information on the respondent.

Most opinion questions are Likert-type and require respondents to rate sentences on a 1-5 scale with labels only at extreme points (1=completely disagree; 5=completely agree). Principal component analysis and homogeneity analysis (Cronbach's alpha) revealed that the answers to three sets of questions can be summarized with summative scales. After appropriate reverse scoring, item ratings were averaged and three synthetic variables were created: attitude toward the sentence (6 items, alpha=0.83), attitude toward the media (5 items, alpha=0.65) and attitudes toward the role of Giuliani (5 items, alpha=0.70). All the resulting variables were re-scaled 0-10 where 10 means the most negative and 0 the least negative attitude toward the object probed (sentence, media, Giuliani).

Results. In this section, we comment upon the distributions of the most relevant items proposed in our survey. Particular attention will be devoted to any differences between INGV and GNGTS sub-samples.[3]

Topic 1: communication practices and attitudes. The answers to the question about involvement in communication activities during the last 5 years show that INGV researchers are more involved in such activities than GNGTS researchers, both during seismic events (35.8% vs. 23.9%) and during non-seismic periods or in low-risk areas (60.9% vs. 52.7%). INGV researchers, indeed, feel more prepared for public speaking during seismic events than GNGTS researchers (43.7% vs. 39.1%) and are more likely to have attended at least one specific course of risk communication (24,6% vs. 14.6% *). Consistently, a higher percentage of INGV researchers thinks that is important to attend courses on risk communication, public speaking and media analysis. The necessity of a specific formation, as opposed to a generic communication experience, is acknowledged more by INGV than by GNGTS researchers (76% vs. 63%*). However, data on participation in specific communication courses show that this research community (and/or their research institutions) pay more attention to the

2 It should be noted that the GNGTS email list includes also a number of people not directly involved in seismology. Thus, the response rate could be higher than actually calculated.

3 Statistically significant differences (p value < 0.05) are marked with an asterisk.

issue of scientific communication than the average of Italian researchers (only 6.1% attended a course; source: ISAAC wave 1).

More than half of the researchers surveyed (59.9% from INGV and 54.3% from GNGTS sample) have never been contacted by the media for interviews or comments about seismic risk, public safety and seismic risk prevention. Similar results have been found in the survey addressed to all kinds of scientists (ISAAC wave 1), suggesting that perhaps the media do not consider issues of seismic risk more important than other scientific issues.

Topic 2: representations and attitudes toward the public of science among scientists. Using semantic differential technique, we explored the image of public in scientists' mind. Researchers in both sub-samples think that their public is quite conditionable (about 75%), more biased than impartial, and more irrational than rational but, at the same time, quite open to dialogue. Moreover, the public is perceived to be older rather than younger. About 40% of INGV researchers (compared to only 19% of GNGTS researchers) think the public is "unable to learn".

GNGTS researchers believe that it is more important to transfer the scientific message rather than to engage with the public (51% vs. 42.8%*): this result could suggest different communication aims between INGV and other researchers. The former, as reported above, have more direct contacts with the public, especially in those critical situations such as during seismic sequences, when engagement and a more empathetic interaction with the public could be more necessary in order to establish a good communicative relationship.

Topic 3: politics, ethics and the role of scientists. The vast majority of researchers think that their research activities have relevant ethic implications (over 80% in both sub-samples). At the same time, 73.2% of INGV (vs. 58.6% of GNGTS*) researchers agreed that scientists should provide only technical evaluations when asked to cooperate with politics in decision-making about what to do during an earthquake sequence. Yet, according to 67.4% of GNGTS members (vs. only 38% INGV*) researchers are also required to provide an opinion on *how to manage* the risk situation. When we asked whether scientists have the duty to *publicly express* their disagreement with the operational decisions taken by governmental institutions, their answers were quite uniformly distributed along the scale, with a slight predominance of agreement scores, more marked among researchers from GNGTS.

Topic 4: the scientists facing the L'Aquila judgment. There are significant differences between INGV and GNGTS researchers about their (dis)agreement with the judgment of the court: 79.7% of the former disagreed completely or almost completely (scores 4-5) compared to 56.9% of the latter. However, when we asked their opinion on the idea that the ruling was a serious act of censorship of science like the process of the Church to Galileo, most of them disagreed (58.9%). We probed their opinion on the ruling by means of other items too. The index that summarizes their answers measures scientists' degree of hostility toward the ruling. INGV researchers scored significantly and substantially higher than GNGTS researchers (5.8 vs. 4.7 on a 0-10 scale).

With regard to the media coverage, the majority of researchers believe that information given by the media during the earthquake and about the judgment has been trivialized, dramatized and communicated superficially, and little room was available for scientists to explain the scientific points of view on the seismic events. In particular, most of them (70.9% GNGTS vs. 83.6% INGV*) accuse the media of having led the population to believe the radon thesis (as a reliable precursor for quakes) enjoys credibility from a scientific point of view, and of having given too much credit and visibility to Giuliani (92,6% INGV; 69.2% GNGTS*). About Giuliani, 89,7% of the researchers from INGV believe that he has no credibility in the scientific community but only 51,5% from GNGTS agree with this statement[4]. Researchers of both groups showed great uncertainty in judging whether Giuliani is credible or not in the eyes

4 However, 22.4% of GNGTS vs. only 1.5% of INGV has no opinion about scientific credibility of Giuliani.

of citizens. Overall researchers' attitudes toward the media and the role of Giuliani are more negative among INGV than GNGTS, as testified by significant differences in the scores on the synthetic indexes.

Scientists also believe that the ruling for the events in L'Aquila has negatively affected the availability of scientists to provide scientific opinions in institutional forums (82.4% GNGTS and 93.4% INGV*) and to communicate with the citizenship (about 70%). 45.4% GNGTS and 63.5% INGV* researchers believe that public's confidence in their research field decreased following the case of L'Aquila.

Conclusions. There are several significant and relevant differences between the two groups of scientists in various issues that our questionnaire touched upon. Generally speaking, INGV researchers seem to be more critical about the sentence, the media, and the role of Giuliani than their GNGTS colleagues. They also show greater sensitivity to communication issues, perhaps as consequence of their dramatic direct experience during the earthquake and the following months.

Both the INGV and the GNGTS groups recognize the earthquake coverage was affected by typical signs of the so called 'media logic' (trivialization and dramatization of information, deep emphasis, etc.). More, by claiming not to have had enough space to explain their point of view, they implicitly testify how still problematically they can cope with the media rules.

In fact, driven by a relentless research for emphasis and spectacularization in covering technoscientific issues (particularly those concerning controversies and conflicts) and with a strong propensity to alarmism, the media implicitly give the green light to pseudoscientists, social actors (e.g. Giuliani) whose profile is unfit to be represented as «experts» or «scientists» under many points of view, as briefly mentioned above. Yet, they claim to be admitted as fully qualified specialists in the public debate on Science and Technology, resulting not infrequently more appealing and understandable than the institutionalized scientists. The most evident media strategy that allows pseudoscience to enter the public arena in the case of the earthquake in L'Aquila – as somehow noticed by our interviews – consists in a sort of «par condicio» or «equalization of positions» approach. It refers to the media tendency, very strong in the Italian press and television, to provide public with bipolar representations of controversial issues. To those of the public less equipped to critically interpret media messages, science would therefore appear as perfectly divided into two parties, even in cases – e.g. the climate change, creationism vs. evolutionism, etc. – where the internal equilibriums of the scientific community are distributed in a very different way. The case of L'Aquila is a further radicalization of this strategy: not able to replicate any division within the community of seismologists (since scientists agree almost unanimously about the impossibility to predict seismic events), the Italian media have brought into the public debate a former technician of the Institute of Physics of Interplanetary Space detached to the National Laboratories of Gran Sasso, Giampaolo Giuliani, who claimed to have predicted the disaster of April 6, 2009 with a radon detector, without having any scientific trustworthiness in the field of seismology.

As new updates are needed to complete the in-depth exploration of what happened among the five components we briefly put in our model (fig. 1), what has been discussed so far seems to show that – while there is still much work to do to bridge science and society – such a desirable process can not be accomplished without the scientific community itself acquire communication skills and tools to effectively be on the media arena, also competing with social actors (i.e. pseudoscientists and other opinion leaders) that in an 'ideal' (as now utopian) context would not be considered competitors.

Acknowledgements. The authors want to thank Dr. Cesare Comina (University of Turin), Dr. Sergio Vinciguerra (University of Leicester), Dr. Lucia Montanari and Dr. Alessandro Amato (INGV), for their fundamental help in revising and dealing out the survey.

References

Dahlgren, P., 1995, Television and the Public Sphere. Citizenship, Democracy and the Media, London, Thousand Oaks & New Delhi, Sage.

Goffman, E., 1959, The presentation of self in everyday life Garden City, Doubleday.

Habermas, J., 1962, Strukturwandel der Öffentlichkheit, Darmstadt - Neuwied, Hermann LuchterhanhVerlag; en. The Structural Transformation of the Public Sphere: An Inquiry into a Category of Bourgeois Society, Cambridge, MA, MIT Press, 1989.

Mazzoleni, G., 1995, Towards a 'videocracy'? Italian political communication at a turning point, in «European Journal of Communication», 10, pp. 291-319.

Mazzoleni, G. e Schulz, W., 1999, "Mediatization" of politics: A challenge for democracy?, in «Political Communication.», 16, pp. 247-261.

Mazzoleni, G., Stewart, J. e Horsfield, B. (a cura di), 2003, The media and neo-populism. A contemporary comparative analysis, Westport, CT., Praeger Publishers.

Nature, 2012, Shock and law, in «Nature», 490.

Thompson, J.B., 1995 Media and Modernity: A Social Theory of the Media Cambridge, Polity Press; trad. it. Mezzi di comunicazione e modernità. Una teoria sociale dei media, Bologna, Il Mulino, 1998.

BODY WAVE ATTENUATION OF KUMAUN HIMALAYA

M.S. Chauhan[1], A.R. Bansal[2]

[1] *University of Naples "Federico II", Naples, Italy*

[2] *CSIR-National Geophysical Research Institute, Hyderabad, India*

Introduction. The Himalayan belt is formed due to the collision of Indian and Eurasian plates in the period 50-55 million years ago. This belt is seismically active and earthquake of varying magnitude are being observed. Most of these earthquakes are associated with great loss of life and destruction of property. For understanding of the nature of earthquakes and for reliable assessment of seismic risk in the Himalayan belt, knowledge and understanding of seismicity and the attenuation of strong ground motion are essential. Due to the vast natural resources in the Himalayan region, development of the region is being planned. For utilization of its resources major projects such as Tehri dam, Tunnels projects have been proposed. People living in this region are concerned about their survival due to the active seismicity of the region. In the light of the higher seismicity, an appraisal of the relation of earthquake occurrences with geology and tectonics of the region is very essential to make an assessment of the seismic potentialities, for survival of the lives and natural resources, and in designing of the major structures. The designing of earthquake resistant structures is a major challenge to the Civil Engineers. This challenge can be met if we develop ability to predict ground motion due to future earthquakes. The important structure such as nuclear power plants, dams, and high-rise buildings require estimate of ground motion for earthquake resistant designing. In the present work, we have made effort to understand the Body wave attenuation in Kumaun Himalaya using strong ground motion data (Kayal, 2008).

Geology of the Kumaun Himalaya. Himalaya is a large geodynamic laboratory of nature where orogeny is still in youth to early mature phases of evolution. It is one of the most active orogens of the world and is the consequence of the collision of the Indian plate with the collage of previously sutured micro continental plates of central Asia during mid to late Eocene. The Kumaun region of the Himalaya lies near the center of the Himalayan fold-and-thrust belt and is situated between the Kali River in the east and Sutlej in the west, including a 320 km stretch of mountainous terrain. This part of Himalaya exposes all the four major litho-tectonic subdivisions of the Himalaya from South to North. They are Sub-Himalaya, Lesser Himalaya, Great Himalaya and Tethys Himalaya. All the litho-tectonic zones are bound on either side by longitudinally continuous tectonic surfaces such as Main Boundary Thrust (MBT), Main Central Thrust (MCT), South Tibetan Detachment (STD) system and Indus Tsangpo Suture Zone (ITSZ). The Sub-Himalaya includes the molassic Siwalik super group of Mio-

Pliocene ages. The lesser Kumaun Himalaya exposes a thick pile of highly folded Proterozoic sedimentary strata together with a few outcrops of older crystalline rocks. It is bounded by the MBT to the south and the MCT to the north. The Great Himalaya exposes a massive pile of high grade metamorphic rocks and the Tethys Himalaya includes a thick pile of sedimentary rocks of Cambrian to Lower Eocene ages. The extension of Aravalli structures into the Himalayan regions has played a role in the tectonics of the Kumaun Himalaya, and probably is the cause of the complex nature of seismicity of the region. In Kumaun Himalaya region the groups of rocks are known as Vaikriti group (Valdiya, 1980). According to the model of Srivastava and Mitra (1994), the Kumaun Himalaya evolved by an overall forelandward progression of thrusting, with some reactivation along the Munsiari thrust (MT), the Main Boundary thrust (MBT), and the Main Central thrust (MCT). In this part the maximum strain-energy release is related to the Main Central Thrust (MCT). It is among the least understood parts of the Himalayan fold-and-thrust belt. Valdiya (1980) gives the most comprehensive account yet published on the geology of the region. It has been found that the large scale thrusts recognized in the Kumaun lesser Himalaya are boundary thrusts defining the limit of the various litho-tectonic units. There are large numbers of local thrusts less than 50 km in length, which have severed the tightly folded rock formations along the axial plane and brought the older rocks over the younger. This sector evidenced reactivation of some of the faults and thrusts during Quaternary times. This is amply evident by the recurrent seismicity patterns, geomorphic developments and by geodetic surveys (Valdiya, 1999). A generalized tectonic sequence for the Lesser Kumaun Himalaya (Valdiya, 1978) is tabulated below and shown in the Fig. 1 (after Célérier *et al.*, 2009).

Vaikrita Group
......................Vaikrita Thrust.....................
Munsiari Formation
...............................Main Central Thrust..............................
Almora-Dudhatoli Nappe
(with Askot, Baijnath, Chiplakot and Satpuli Klinne)
.......................Almora Thrust.........................
Outer Sedimentary Belt
Inner sedimentary Belt
..........................Main Boundary Fault............................
Siwalik Group

Methodology. In this work we used coda normalization method which provides a reliable way to estimate the frequency dependence of important parameters quantifying the seismic source radiation and receiver site amplification, both of which are used in seismic risk assessment. It also allows the investigation of propagation effects. Most of seismology is focused on characterizing one of these three influences, (1) source radiation propagation, (2) site amplification, on seismograms and (3) propagation effect. The coda normalization method is based on the idea that at lapse time, the seismic energy is uniformly distributed in some volume surrounding the source (Sato and Fehler, 1998).

In this method spectral amplitude of the earthquake source is normalized by coda waves at a fixed lapse time. It is based on the idea that coda waves consist of scattered S waves from random heterogeneities in the Earth (Aki, 1969; Aki and Chouet, 1975; Sato, 1977). Roughly lapse time is taken twice of the direct S-wave travel time and spectral amplitude of coda at a lapse time t_c, $A_c(f, t_c)$is independent of hypocentral distance r in the regional distance range, and can be described (Aki, 1980)

$$A_c(f,t_c) = S_s(f)P(f,t_c)G(f)I(f)$$

Where f is the frequency, $S_s(f)$ is the spectral amplitude of S waves, $P(f, t_c)$ is the coda-excitation factor and $I(f)$ is the instrument response. The code excitation factor $P(f, t_c)$ represents how the spectral amplitude of coda waves decays with lapse time. After solving mathematically, we get following equation (Aki, 1980):

$$<\ln\left[\frac{A_s(f,r)r^\gamma}{A_c(f,t_c)}\right]>_{r\pm\Delta r} = -\frac{\pi f}{Q_s(f)V_s}r + const(f) \qquad (1)$$

where $A_s(f, r)$ is the spectral amplitude of the direct P-wave, $Q_s(f)$ is the quality factor of S wave and V_s is the average S-wave velocity.

Eq. (1) was first proposed by Aki (1980). Yoshimoto *et al.* (1993) extended this method for the measurement of Q_P by assuming that earthquakes within a small range of magnitude have the same spectral ratio of P- to S-wave radiation within a narrow frequency range $f \pm \Delta f$ for different spectral shapes of P and Swaves (Molnar *et al.*, 1973; Rautian *et al.*, 1978). We are writing same symbol as Yoshimoto *et al.* (1993) used.

$$<\ln\left[\frac{A_p(f,r)r^\gamma}{A_c(f,t_c)}\right]>_{r\pm\Delta r} = -\frac{\pi f}{Q_p(f)V_p}r + const(f) \qquad (2)$$

where $A_p(f, r)$ is the spectral amplitude of the direct P-wave, $Q_p(f)$ is the quality factor of P wave and V_p is the average P-wave velocity. In our study we used Eqs. (1) and (2).

Data. A network of nine strong motion accelerographs of Kinemetrics, USA, have been installed in the Kumaun Himalaya under the major research project sponsored by Department of Science and Technology/MOES, Government of India, in March 2006. Location of the stations are shown in Tab. 1.

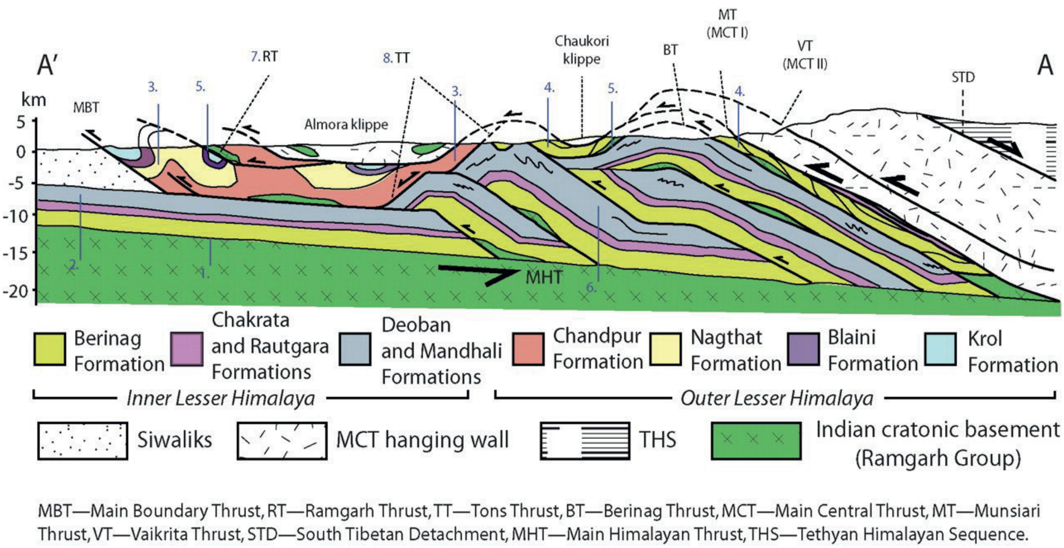

Fig. 1 – Generalized tectonic sequence for the Lesser Kumaun Himalaya (from Valdiya, 1978).

Tab. 1 – Location of the stations.

Name of Station	Latitude	Longitude	Elevation
Dharchula	**29.845**	**80.532**	**929**
Didihat	**29.801**	**80.252**	**1644**
Lohaghat	**29.404**	**80.083**	**1640**
Munsiari	**30.066**	**80.293**	**2105**
Narayan Ashram	**29.970**	**80.655**	**2535**
Pithoragarh	**29.584**	**80.212**	**1576**
Thal	**29.841**	**80.173**	**1576**
Sobla	**30.068**	**80.293**	**2105**
Tejam	**29.950**	**80.120**	**951**

Result and discussion. By using extended coda normalization method of Yoshimoto *et al.* (1993) as described in previous section. Frequency dependent Q_P and Q_S are estimated for the Kumaun Himalaya which can be obtained from the slope of the linear fitted lines for different frequencies. The estimated values of Q_P and Q_S with coefficient of determination are presented in Tab. 2 and Fig. 2.

Tab. 2 – Average value of Q_P and Q_S at different central frequencies.

Frequency (Hz)	Q_P	Q_S	R_p^2 (%)	R_s^2 (%)
1.5	34.09	87.00	95	69
3	61.00	173.92	91	63
6	105.77	379.76	78	57
12	126.07	416.63	66	76
24	205.44	530.39	72	79
$Q = Q_0 f^n$	$Q_p = (24 \pm 3) f^{(0.9 \pm 0.3)}$	$Q_s = (64 \pm 3) f^{(1.04 \pm 0.07)}$		

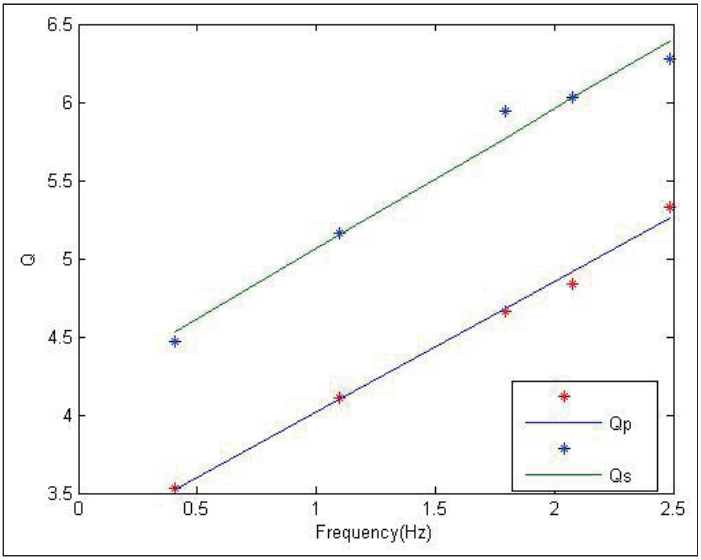

Fig. 2 – Q_P and Q_S fits.

The Q values increase from about 34 (P waves) and 87 (S waves) at 1.5 Hz to 205 (P waves) and 530 (S waves) at 24 Hz respectively. The frequency dependence is comparable to those obtained in other tectonic areas such as Kanto (Japan) (Yoshimoto *et al.*, 1993), Bhuj (India) (Padhy, 2009), Koyna (India) (Sharma *et al.*, 2007), NE India (Padhy and Subhadra, 2010) and Cairo Metropolitan area (Egypt) (Abdel-Fattah, 2009). To obtain the frequency-dependent relations, the estimated average Q values as a function of frequency are fitted by a power law in the form $Q = Q_0 f^{\,n}$ (where Q_0 is Q_c at 1 Hz and n is the frequency relation parameter) (Fig. 2). The power law forms of $Q_P = (24 \pm 3)\, f^{\,(0.9 \pm 0.3)}$ and $Q_S = (64 \pm 3)\, f^{\,(1.04 \pm 0.07)}$ for the Kumaun Himalaya region. The low Q_P and Q_s correspond to those of the seismically active areas in the world. The values of Q obtained for the S-waves in this study agree with the coda Q estimated in previous studies (Paul *et al.*, 2003; Singh *et al.*, 2011) for this region. We find that P waves attenuate more strongly than S waves) for the entire frequency ranges. The obtained is observed in the upper crust of many other regions with a high degree of lateral heterogeneity (Bianco *et al.*, 1999; Sato and Fehler, 1998). High degree of structural heterogeneities may be expected in the crust of Kumaun Himalaya as revealed by travel time tomography result of Sharma (2008) and by Mukhopadhyay *et al.* (2008) for the adjoining Garwhal Himalaya region (western part of our study area). According to Paul *et al.* (2003) Kumaun Himalaya is more heterogeneous and less stable compared to Garwhal Himalaya. So this underlying heterogeneity may have brought notable changes in seismic attenuation properties in the crust of Kumaun Himalaya.

On the other hand from MLTW (multiple lapse time window) analysis by Mukhopadhyay *et al.* (2010), it is revealed that dominating attenuation mechanism for the Garwhal Himalaya is scattering attenuation. The crustal level folding and faulting in this region are also evident from tomography results (Mukhopadhyay and Sharma, 2010). Therefore it may suggest that the scattering is likely to be an important factor contributing to the attenuation of body waves in the Kumaun region. Hough and Anderson (1988) pointed out that is expected for most kinds of scattering. Padhy (2009) suggested that a high value in is expected to be due to scattering from shallow heterogeneities in the crust. The observed high value in is anticipated to be due to scattering from shallow heterogeneities in the crust beneath the study area.

Conclusion. The strong motion data of digital network in Kumaun Himalaya is analyzed from 2006 to 2008 in this study.

- The modified coda normalization method (Yoshimoto *et al.*, 1993) is used for estimating of Q_P and Q_S.
- Q_P and Q_S in the Kumaun Himalaya region are found to be strongly frequency dependent.
- The Q_P and Q_S increase with frequency.
- The $Q_S / Q_P \geq 1$ is found for all frequency range.
- The low values of Q_P and Q_S correspond to seismically active areas with tectonic complexity due to the ongoing convergence between Indian and Eurasian plate.
- It is found that the attenuation is stronger for P wave than S waves for the entire frequency range and this probably reflects the high degree of heterogeneity presence in the crust of Kumaun Himalaya. Our results are well comparable to the other tectonically active regions characterized by high degree of heterogeneity reported globally.

Acknowledgement. First of all I, Mahak Singh Chauhan, would like to express my sincere gratitude to Dr. Dinesh Kumar, Chairman, Department of Geophysics, Kurukshetra University for allowing me to take up my dissertation at CSIR-National Geophysical Research Institute (NGRI), Hyderabad and cultivating my interest in Computational Seismology, which culminated in this humble effort. I am highly indebted to Dr. Abhey Ram Bansal, Senior Scientist, CSIR-NGRI, my dissertation supervisor, for his invaluable guidance, overwhelming enthusiasm and affection. I am grateful to Prof. Mrinal K. Sen, Director, CSIR-NGRI, for his kind permission to work with Non Linear Processing in Geophysics Group and for providing a conductive environment. I am also very grateful to Prof. V.P. Dimri, Distinguished Scientist and former Director, CSIR-NGRI for his kind encouragement and fruitful discussion at various stages of the work. His philosophy of merging enjoyment with work is very much inspiring and need to be followed in life.

References

Abdel-Fattah, A.K., 2009, Attenuation of body waves in the crust beneath the vicinity of Cairo Metropolitan area (Egypt) using coda normalization method, Geophysical Journal International, 176, 126–134.

Aki, K., 1969, Analysis of the seismic coda of local earthquakes as scattered waves, Journal of Geophysical Research 74, 615–631.

Aki, K., 1980, Attenuation of shear waves in the lithosphere for frequencies from 0.05 to 25 Hz, Physics of the Earth and Planetary Interiors, 21, 50–60.

Aki, K., Chouet, B., 1975, Origin of the coda waves: source, attenuation, and scattering effects, Journal of Geophysical Research, 80, 3322–3342.

Bianco, F., Castellano, M., Del Pezzo, E., Ibañez, J.M., 1999, Attenuation of short-period seismic waves at Mt. Vesuvius, Italy, Geophysical Journal International, 138, 67–76.

Célérier, J., Harrison, T.M., Webb, A.A.G., Yin, A., 2009, The Kumaun and Garwhal Lesser Himalaya, India: Part 1.Structure and stratigraphy, Geological Society of America, 1262- 1280.

Hough, S.E., Anderson, J.G., 1988, High-frequency spectra observed at Anza, California: implications for Q structure, Bulletin of the Seismological Society of America, 78, 692–707.

Kayal, J.R., 2008, Microearthquake seismology and seismotectonics of South Asia, Capital Publishing Company, pp.503

Mukhopadhyay, S., Sharma, J., 2010, Attenuation characteristics of Garwhal–Kumaun Himalayas from analysis of coda of local earthquakes. Journal of Seismology, 14, 693–713.

Mukhopadhyay, S., Sharma, J., Del-Pezzo, E., Kumar, N., 2010, Study of attenuation mechanism for Garwhal–Kumaun Himalayas from analysis of coda of local earthquakes, Physics of the Earth and Planetary Interiors, 180, 7–15.

Mukhopadhyay, S., Sharma, J., Massey, R., Kayal, J.R., 2008, Lapse time dependence of coda Q in the source region of the 1999 chamoli earthquake, Bulletin of the Seismological Society of America, 98, 2080–2086.

Padhy, S., 2009, Characteristics of body wave attenuations in the Bhuj crust, Bulletin of the Seismological Society of America, 99, 3300–3313.

Padhy, S., Subhadra, N., 2010, Attenuation of high-frequency seismic waves in northeast India. Geophysical Journal International, 181, 453–467.

Paul, A., Gupta, S.C., Pant, C., 2003, Coda Q estimates for Kumaun Himalaya, Proceedings of the Indian National Science Academy (Earth and Planetary Science), 112, 569–576.

Sato, H., 1977, Energy propagation including scattering effect: single isotropic scattering approximation, Journal of Physics of the Earth, 25, 27–41.

Sato, H., Fehler, M.C., 1998, Seismic Wave Propagation and Scattering in the Heterogeneous Earth, Springer-Verlag, New York. 308 pp.

Sharma, J., 2008, Crustal Investigations in Garwhal–Kumaun Himalayas: Velocity Tomography and Qc, Unpublished Ph.D. Thesis, IIT Roorkee, 249 pp.

Sharma, B., Teotia, S.S., Kumar, D., 2007, Attenuation of P, S, and coda waves in Koyna region, India. Journal of Seismology, 11, 327–334.

Singh, C., Singh, A., Mukhopadhyay, S., Sekhar, M., Chadha, R.K., 2011, Lg attenuation characteristics across the Indian Shield. Bulletin of the Seismological Society of America, 101, 2561–2567. 40

Srivastava, P., Mitra, G., 1994, Thrust geometries and deep structure of the outer and lesser Himalaya, Kumaon and Garhwal (India): implications for evolution of the Himalayan foldand- thrust belt, Tectonics, 13, 89–109.

Valdiya, K.S., 1978, The extension and analogue of the Chail Nappe in the Kumaun Himalaya, Indian Journal of Earth Sciences, 5, 1–19.

Valdiya, K.S., 1980, Geology of Kumaun Lesser Himalaya. Wadia Institute of Himalayan Geology, Dehradun. 291 pp.

Valdiya, K.S., 1999, Fast uplift and geomorphic development of the western Himalaya in quaternary period. In Geodynamics of NW Himalaya Gondwana Research Group Memoir(eds) A.K. Jain and Manickavasagam, 179–187.

Yoshimoto, K., Sato, H., Ito, Y., Ito, H., Ohminato, T., Ohtake, M., 1998, Frequency dependent attenuation of high-frequency P and S waves in the upper crust in western Nagano, Japan, Pure and Applied Geophysics, 153, 489–502.

Yoshimoto, K., Sato, H., Ohtake, M., 1993, Frequency-dependent attenuation of P and S waves in the Kanto area, Japan, based on the coda normalization method. Geophysical Journal International, 114, 165–174.

sessione 1.2

Dinamica e cinematica: processi tettonici attivi nell'area italiana

Convenor: A. Argnani e E. Serpelloni

KINEMATIC MODEL OF ACTIVE EXTENSION ACROSS THE UMBRIA-MARCHE APENNINES FROM GPS MEASUREMENTS: FAULT SLIP-RATES AND INTERSEISMIC COUPLING OF THE ALTO TIBERINA LOW-ANGLE NORMAL FAULT

L. Anderlini[1,2], E. Serpelloni[3], M.E. Belardinelli[1]
[1]*Istituto Nazionale di Geofisica e Vulcanologia, Sezione di Bologna, Italy*
[2]*Dipartimento di Fisica, Settore di Geofisica, Università di Bologna, Italy*
[3]*Istituto Nazionale di Geofisica e Vulcanologia, Centro Nazionale Terremoti, Roma, Italy*

Introduction. The growing number of continuously recording GPS stations over Italy, particularly during last 5 years, gives the possibility to detect, with higher accuracies and precisions than in the past, gradients of ground deformation rates across major fault structures. Using a kinematic block-modeling approach it is possible to model the observed gradients in order to estimate fault parameters and long-term slip-rates, inferring new information useful to evaluate the seismic potential of a region.

The Umbria-Marche Apennines are characterized mainly by SW-NE oriented extensional deformation (see Fig. 1), as documented by geodetic (D'Agostino *et al.*, 2009), geologic (Tondi, 2000; Boncio and Lavecchia, 2000a) and seismological (Pondrelli *et al.*, 2006) data. Most of major historical and instrumental earthquakes occurred mainly on the western side of chain,

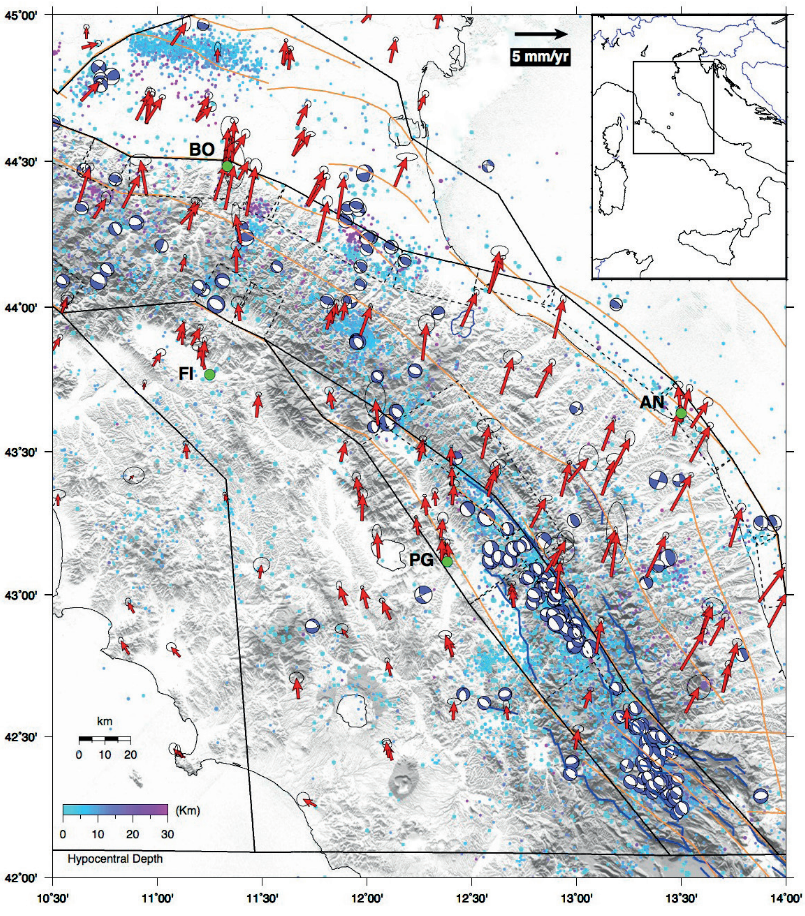

Fig. 1 – Seismotectonic framework of central Italy, red arrows show observed GPS velocities, black lines indicate bounds of the elastic blocks, blue dots represent instrumental seismicity, and also available focal mechanisms are shown; orange lines are DISS fault sources and blue lines are fault boxes from Lavecchia *et al.* (2002).

bounded by west-dipping buried high-angle normal faults (Boncio and Lavecchia, 2000b; DISS working group, 2010; Rovida *et al.*, 2011). Nevertheless which of the known fault systems play a major role in accommodating the extension, and which are the modes (seismic VS aseismic deformation) this extension is taken up, is still a debated topic. In particular recent studies about the northernmost part of Umbria-Marche region show seismic and tectonic activity (Chiaraluce *et al.*, 2007, Hreinsdóttir and Bennet, 2012, Mirabella *et al.*, 2011) on correspondence of Alto Tiberina (AT) low-angle normal fault (LANF), which is widely documented by geological data (Brozzetti, 1995; Boncio *et al.*, 2000; Collettini, 2000) and deep seismic reflection profiles (CROP03, Barchi *et al.*, 1998). The supposed detachment of AT fault is an interesting case in which crustal extension could be driven by a LANF, considered by "Andersonian" theory as averse to faulting.

During last years on Umbria-Marche Apennines close to Gubbio fault (GuF) a dense network of continuous GPS stations, belonging to the RING-INGV network, has been installed, improving significantly the spatial resolution of the detectable geodetic gradients. Using kinematic block models to reproduce GPS velocity field, we define the optimal fault boundaries accommodating the tectonic extension.

GPS data processing. To estimate the present-day deformation on Northern Apennines, we analyzed data from a dense network of continuous and survey-mode GPS stations. Survey-mode stations are those installed in the framework of the RETREAT project (Bennett *et al.*, 2012). The processing follows a three-step approach, as described on Serpelloni *et al.* (2006), which includes: 1) raw phase data reduction, 2) combination of loosely-constrained solutions and reference frame definition, and 3) time series analysis.

In the first step, we use the GAMIT (V10.4) software (Herring *et al.*, 2010) on daily GPS phase observations to estimate geodetic parameters applying loose constraints. We apply the ocean-loading and pole-tide correction model FES2004, and use the parameterized version of the VMF1 mapping function, the GMF for both hydrostatic and non-hydrostatic components of the tropospheric delay model. We use the IGS absolute antenna phase center model for both satellite and ground-based antennas. Continuous GPS data are divided into several subnets and processed independently; each subnet share a set of high quality IGS stations, which are subsequently used as tie-stations in step 2. Survey-mode GPS networks are processed separately, adding a larger number of high quality cGPS stations, in order to reduce the average baseline lengths.

In the second step we use the ST_FILTER program of the QOCA software (Dong *et al.*, 2002) to combine all the daily loosely constrained solutions, for both cGPS and sGPS subnets, with the global and regional solutions made available by SOPAC (http://sopac.ucsd.edu), and simultaneously realize a global reference frame by applying generalized constraints (Dong *et al.*, 1998). Specifically, we define the reference frame by minimizing the horizontal velocities of the IGS core stations (http://igscb.jpl.nasa.gov), while estimating a seven-parameter transformation with respect to the IGS08 realization of the ITRF2008 frame (Altamimi *et al.*, 2011).

In the third step we analyze the position time series in order to estimate velocities and uncertainties. For the cGPS and sGPS stations we estimate a constant velocity term together with annual and semi-annual seasonal components and, if present, offsets at specific epochs, and adopt a white + flicker noise model, following Williams *et al.* (2004). We incorporate data from cGPS and sGPS stations with an observation period longer than 2.5 years, as shorter intervals may result in biased estimates of linear velocities (Blewitt and Lavallée, 2002).

We use velocities and uncertainties of cGPS stations located on tectonically stable domains of the Eurasian and Nubian plates in order to estimate their Euler rotation poles. The final GPS velocity field is calculated w.r.t. Eurasia fixed frame and in this study we use overall 594 velocities (from continuous and survey-mode stations), located on Italian peninsula and European region.

Block modeling setting and analysis. The final geodetic interseismic velocity field provides information on both crustal blocks and microplate rotations and elastic responses of the major fault systems. The so called elastic block modeling method is a kinematic approach with which geodetic velocities are modeled considering the crust subdivided on discrete rigid and elastic blocks, bounded by faults embedded in an homogeneous and isotropic half-space (Okada, 1985). This kind of approach follows the *back-slip* concept (Savage, 1983), where the surface velocity field is decomposed into a rotational component of blocks and an elastic component, representing a coseismic slip-deficit on the block-bounding faults boundaries. In our analysis we use the block model formulation implemented in the Matlab code of Meade and Loveless (2009), which performs a linear inversion of geodetic data to determine rotational poles for each block and the corresponding fault slip-rates.

Since this approach requires defining the blocks geometry *a-priori* apriori, we set the block-boundary positions and fault parameters (dip angle and locking depth, i.e. seismogenic thickness of fault) using geological (DISS working group, 2010; Lavecchia *et al.*, 2002) information, taking into account also information from the available instrumental seismic catalogs. The whole model consists on 16 blocks related to Alps, Dinarides and Central Apennines, in order to consider a self-consistent kinematic scenario of the northern Apennines and Adriatic region. In particular we define the AT fault segment as a ~70 km long, 15° east-dipping fault, with a locking depth of 12 km, as shown by relocated microseismicity of Chiaraluce *et al.* (2007) and the isobaths obtained by Mirabella *et al.* (2011). Moreover we define the antithetic GuF as west-dipping plane of 40° with 6 km of locking depth, as a mean of the values proposed in the literature (Lavecchia *et al.*, 2002; Collettini *et al.*, 2003; Pucci *et al.*, 2003).

Focusing our analysis on the northern sector of the Umbria-Marche Apennines, we perform different tests to verify which of the fault boundaries proposed accommodates the tectonic

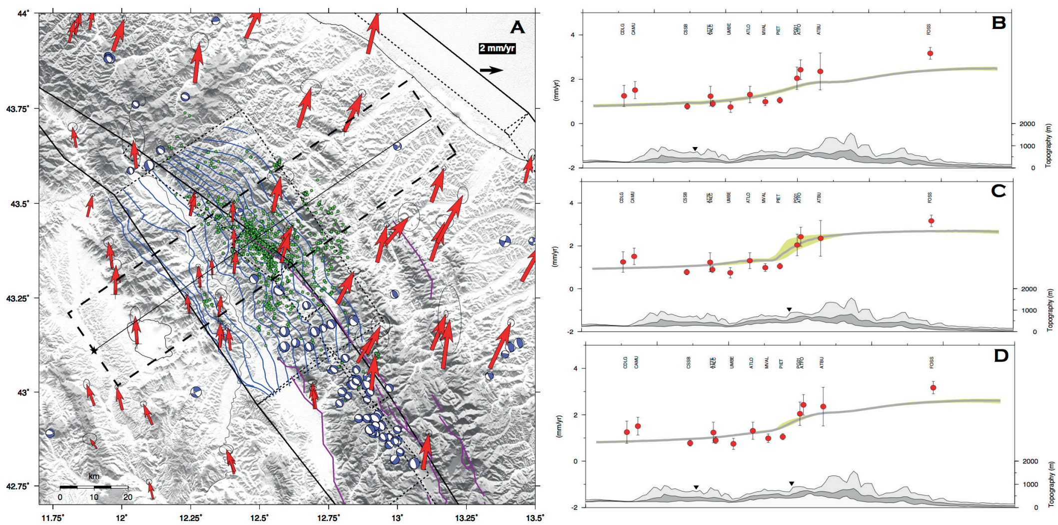

Fig. 2 – A) Near-field observed GPS velocities (red arrows) with block boundaries (black lines) and dipping planes (small dashed lines); blue lines are the ATF isobaths from Mirabella *et al.* (2011), violet ones represent fault boxes from Lavecchia *et al.* (2002) and green dots are the relocated microseismicity from Chiaraluce *et al.* (2007); large dashed box indicates the area interested by profiles shown on B-C-D; profile elements – red dots indicate observed velocities projected on the 55°N direction, with one standard deviation error bars and gray line represents the projected mean value of modeled velocities computed on a dense grid, yellow envelope indicates the variability of the modeled velocities within the swath profile and black triangle shows emerging faults tracves; B) modeling profile considering as fault boundary only the ATF fault; C) only antithetic faults as fault boundary; D)both fault systems.

extension-rate measured by geodetic data, which is of the order of ~2-3mm/yr oriented NE-SW (see Fig. 1). In particular we test three different scenarios in which we consider as fault boundary: 1) the Alto Tiberina LANF, 2) the antithetic high-angle normal faults and 3) both faults. To estimate the best model solution we compute for each inversion the reduced chi squared of data and we use the Fisher test (Stein and Gordon, 1984) to evaluate the acceptance between *n* and *n+1* plate models, i.e. to asses if more complex models are justified by the data.

Tab. 1 reports the results of our tests, together with the corresponding slip-rates obtained in each inversion. As we can see from Tab. 1, the reduced chi-squared values are lower assuming geometry 3, for which also the F-test is positive. The corresponding fault slip-rates obtained from each inversion are representative of the attempt of inversions to reproduce the horizontal tectonic extension by mean elevated slip-rates on faults, which are higher than those proposed on literature (Collettini *et al.*, 2003; Pucci *et al.*, 2003), but on geometry 1 we obtain the same slip-rate as on Hreinsdóttir and Bennett (2010). Using two fault systems as plate boundary we obtain lower down-dip slip-rates more in agreement with geological information, giving a total horizontal extension comparable with geodetic signal. Considering thus the result here obtained with the numerous information proving a very likely activity of both faults, we could infer that the tectonic extension on this sector of Apennines should be accommodated by at least these two major fault systems.

Tab. 1 – Reduced chi-squared values computed for the whole GPS dataset (tot) and for a selected set of stations (sel) located close to the northern sector of Umbria-Marche Apennines, for each inversion, performed with different setting geometries: 1 – only AT fault as block boundary; 2 – only antithetic faults as block boundary; 3 – considering both fault systems; the sixth and seventh columns report inferred down-dip fault slip-rates from elastic block modeling and in the last one is computed the corresponding horizontal slip-rate on extensional direction.

Geometry	Chi2rid (tot)	Chi2rid (sel)	ATF S.R. (mm/yr)	GuF S.R. (mm/yr)	Hor. S.R. (mm/yr)
1 - ATF	9.49	8.46	-2.4	-	-2.3
2 - GuF	9.51	7.89	-	-2.8	-2.1
3 - ATF + GuF	9.36	7.29	-1.5	-1.3	-2.4

Discussion and interseismic coupling on the ATF plane. Our block-modeling analysis suggests that on northern sector of the Umbria-Marche Apennines both the Alto Tiberina LANF and the antithetic, west-dipping, high-angle normal fault, here defined by the Gubbio fault, accommodate the tectonic extension measured by GPS stations. Nevertheless looking a velocity cross section about normal to the strike of major faults (see Fig. 2), we observe that a group of GPS sites, located between the two fault systems, show a systematic “flattening” of the velocity gradient, which is not well modeled by the three inversions discussed above. We tried to understand if the gradient can be better explained using different fault parameters for ATF and for this purpose we performed a series of inversions varying systematically locking depth and dip of the fault (Mastrolembo Ventura, 2012). Evaluating for each inversion the corresponding reduced chi-squared, we found a minimum for the ATF parameters that are close to the initial values (10 km of locking depth instead of 12 km). This result suggests that the ATF could have a significant elastic contribution on the observed geodetic gradient.

The approach used so far considers faults as rectangular planes. To evaluate a model including variable, non-uniform slip-deficit on the ATF, we generate a curved surface, meshed with triangular patches, using the GMSH software (Geuzaine and Remacle, 2009), and following the depth contour lines provided by faults isobaths from Mirabella *et al.* (2011). Moreover we modified the original code to invert for the slip-deficit distribution using a linear least-square

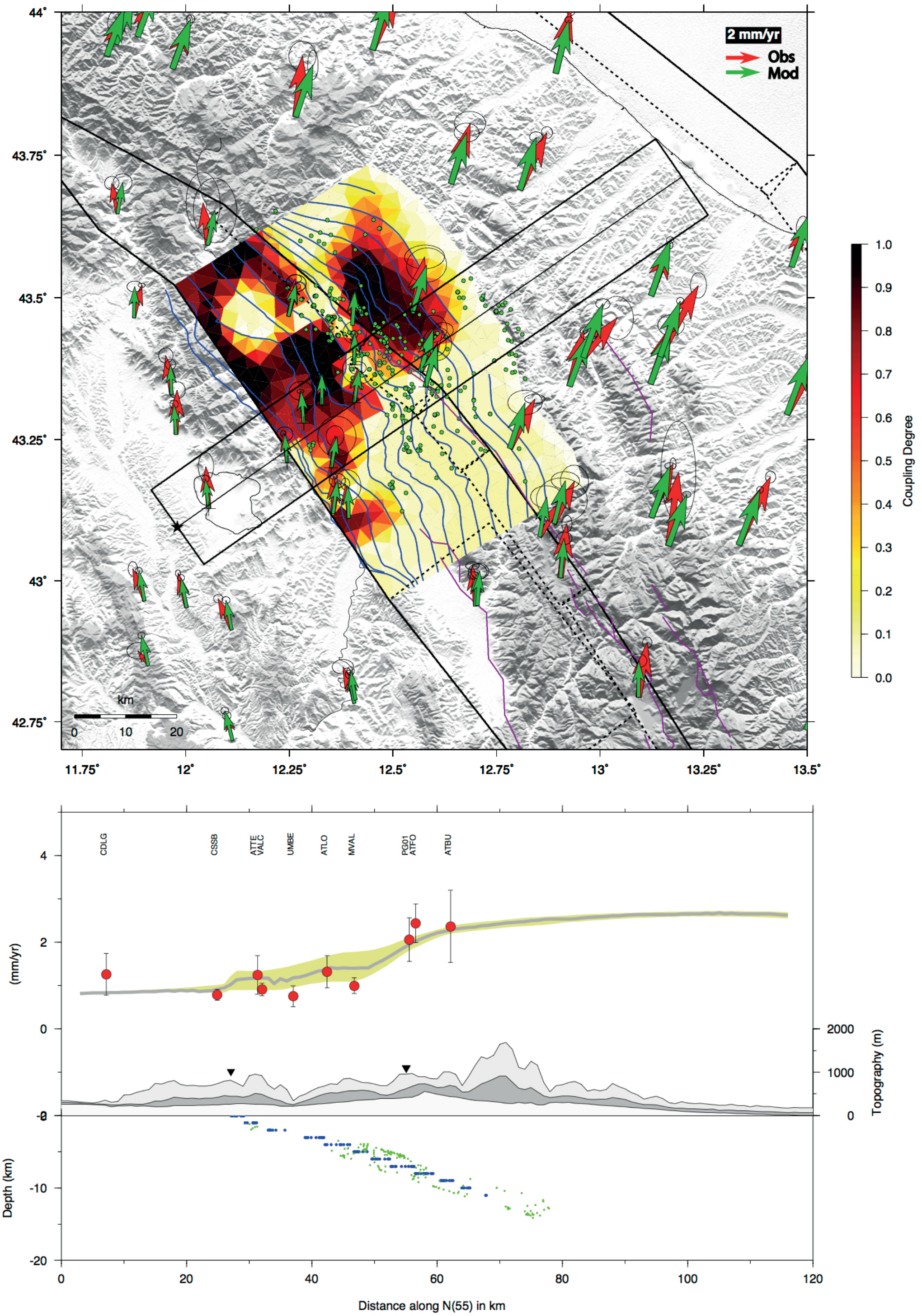

Fig. 3 – Modeling of GPS data inverting for ATF interseismic coupling: blue, violet and black lines are the same as on Fig. 2, green arrows are modeled velocities; on section below we present the same kind of profile as on Fig. 2, showing on depth the microseismicity and isobaths falling inside the box profile.

algorithm, while constraining the slip-rate of each fault patch to be equal or less than the long-term slip-rate estimated from the uniform-slip block model (see Tab. 1). This approach allows us to highlight portions of the fault surface that are characterized by low coupling (i.e., creeping patches) or elastic coupling (i.e. elastic slip-deficit). However, in this way the number of model parameters is greater than the number of data, and we perform a regularization of the inversion adding a smoothing constraint to the solution. The regularization is weighted by a factor β which controls the relative importance of minimizing the reduced chi-squared versus minimizing the roughness of the slip. We choose the optimal value of β equal to 0.7, following a trade-off curve approach (Harris and Segall, 1987). We applied a further constraint to the slip-deficit, forcing it to tape to zero at the bottom edge, at depth of ~13 km, a depth roughly corresponding to the brittle-ductile transition, expected for depth below of 11 km (Boncio *et al.*, 2004).

The final slip-deficit distribution gives a total (the whole model) reduced chi-squared value that is close to that obtained in the uniform slip inversion, but the reduced chi-squared statistics, computed on local stations, drops to 5.27. We represent the slip-deficit distribution as Interseismic Coupling (IC), defined as the ratio between slip-deficit on each patch and the long-term velocity slip-rate (considered in this study -1.5 mm/yr from Tab. 1). The IC ranges between 0 and 1, where 0 means fully uncoupled fault patches (i.e. aseismic creeping) and 1 means fully coupled fault patches (i.e. elastic asperities). Fig. 3 shows the final IC distribution, which shows two main asperities on northern part of the curved surface, and the relocated microseismicity recorded between October 2000 and May 2001 from Chiaraluce *et al.* (2007), selected within +-1.5 km from the ATF surface. The IC distribution shows a correlation between the selected microseismicity and a narrow uncoupled area, located between the two asperities, which position corresponds exactly of bottom edge of Gubbio fault. We perform a resolution test, adopting a checkerboard approach, in order to evaluate the reliability of our IC distribution. These tests show that the transition zone between two asperities is resolved by our data.

Conclusions. Using a self-consistent kinematic block modeling we study the northern sector of the Umbria-Marche Apennines, where several GPS stations show SW-NE oriented extensional deformation. We tested different block model geometries in order to understand which fault system is accommodating the tectonic extension. We found that the best model is the one considering two fault systems, i.e. the Alto Tiberina LANF and the antithetic high-angle Gubbio normal fault, since we obtain lower residuals on data and kinematic agreement with geological slip-rates (Collettini *et al.*, 2003; Pucci *et al.*, 2003). Nevertheless obtaining systematic residuals at a group of GPS sites located between the two fault systems, we parameterized the ATF fault as a, more realistic, curved surface to infer the distribution of interseismic coupling, which is validated by numerous resolution tests. The obtained IC distribution shows a correlation between relocated microseismicity and uncoupled patches attributed to aseismic creeping behavior (Vergne *et al.*, 2001; Schmidt *et al.*, 2005; Rolandone *et al.*, 2008), which could be explained by the presence of fluid overpressure, as was hypothesized by Collettini (2002). Otherwise this correlation has been verified with a very small quantity of events (almost 400) and it might be of interest to evaluate this correlation with future available data.

References

Altamimi, Z., X. Collilieux, and L. Métivier (2011), ITRF2008: an improved solution of the international terrestrial reference frame, *J Geodesy*, 85(8), 457-473, doi:10.1007/s00190-011-0444-4.

Boncio, P., & Lavecchia, G. (2000). A structural model for active extension in Central Italy. Journal of Geodynamics, 29, 233-244.

Bennett, R. A. *et al.* (2012), Syn-convergent extension observed using the RETREAT GPS network, northern Apennines, Italy, *J Geophys Res*, *117*(B4), doi:10.1029/2011JB008744.

Blewitt, G., and D. Lavallée (2002), Effect of annual signals on geodetic velocity, *J. Geophys. Res.*, 107(B7), 2145, doi:10.1029/2001JB000570.

Boncio, P., Lavecchia, G., (2000a), A structural model for active extension in Central Italy. *Journal of Geodynamics* 29, 233-244.

Boncio, P., Lavecchia, G., (2000b), A geological model for the Colfiorito earthquakes (September–October 1997, central Italy). *Journal of Seismology* 4, 345-356

Boncio, P., Brozzetti, F., and Lavecchia, G., 2000, Architecture and seismotectonics of a regional low-angle normal fault zone in central Italy: *Tectonics*, v. 19, p. 1038-1055.

Boncio, P., G. Lavecchia, and B. Pace (2004), Defining a model of 3D seismogenic sources for Seismic Hazard Assessment applications: The case of central Apennines (Italy), *J. Seismol.,* 8, 407-425, doi:10.1023/ B:JOSE.0000038449.78801.05.

Brozzetti, F. (1995): Stile deformativo della tettonica distensiva nell'Umbria Occidentale: l'esempio dei Massicci Massicci Mesozoici Perugini, *Studi Geologici Camerti*, 1, 105-119.

Chiaraluce L., Chiarabba C., Collettini C., Piccinini D., Cocco O M.; 2007: Architecture and mechanics o fan active low-angle normal faults: Alto Tiberina Faults, Northern Apennines, Italy. J. Geophys. Res., 112, B10310, doi:10.1029/2007JB005015.

Collettini, C., Barchi, M., Pauselli, C., Federico, C. and Pialli, G., 2000, Seismic expression of active extensional faults in northern Umbria (central Italy), J. Geodyn. 29, 309-321.

Collettini, C., L. Chiaraluce, F. Mirabella, S. Pucci and M.R. Barchi (2003): The Gubbio seismogenic normal fault: can different methods picture the same object?, J. Geodyn.

D'Agostino, N., S. Mantenuto, and E. D'Anastasio (2009), Contemporary crustal extension in the Umbria-Marche Apennines from regional CGPS networks and comparison between geodetic and seismic deformation, Tectonophysics, 476,3-12, doi:10.1016/j.tecto.2008.09.033.

DISS Working Group (2010). Database of Individual Seismogenic Sources (DISS), Version 3.1.1: A compilation of potential sources for earthquakes larger than M 5.5 in Italy and surrounding areas. http://diss.rm.ingv.it/diss/, © INGV 2010 - Istituto Nazionale di Geofisica e Vulcanologia - All rights reserved; DOI:10.6092/INGV.IT-DISS3.1.1

Dong, D., T. A. Herring, and R. W. King (1998), Estimating regional deformation from a combination of space and terrestrial geodetic data, *J. Geod*., 72, 200-211, doi:10.1007/s001900050161.

Dong, D., P. Fang, Y. Bock, M. Cheng, and S. Miyazaki (2002), Anatomy of apparent seasonal variations from GPS-derived site position time series, *J Geophys Res-Sol Ea*, 107, –, doi:10.1029/2001JB000573.

Geuzaine, C. and J.-F. Remacle, (2009), Gmsh: a three-dimensional finite element mesh generator with built-in pre- and post-processing facilities. *International Journal for Numerical Methods in Engineering* 79 (11), pp. 1309-1331

Harris, R.A. & Segall, P., 1987. Detection of a locked zone at depth on the Parkfield, California, segment of the San Andreas Fault, *J. geophys. Res*., 92, 7945-7962.

Herring, T., King, R.W. & McClusky, S., (2010), GAMIT Reference Manual, Release 10.4, Massachussetts Institute of Technology, Cambridge, MA.

Hreinsdóttir, S., and R. Bennett (2009), Active aseismic creep on the Alto Tiberina low-angle normal fault, Italy, Geology, 37, 683-686, doi:10.1130/G30194A.1.

Lavecchia, G., Boncio, P., Brozzetti, F., Stucchi, M., Leschiutta, I., 2002. New criteria for seismotectonic zoning in Central Italy; insights from the Umbria – Marche Apennines. Boll. Soc. Geol. It., Vol. Spec. 1, 881-891.

Mastrolembo Ventura, B., (2012), Kinematics of the Sicily and Calabria subduction system from elastic block modeling of GPS data, Ph.D. Thesis, University of Bologna, Italy

Meade, B. J., and J. P. Loveless (2009), Block modeling with connected fault-network geometries and a linear elastic coupling estimator in spherical coordinates, Bull. Seismol. Soc. Am., 99, 3124-3139, doi:10.1785/0120090088.

Mirabella, F., F. Brozzetti, A. Lupattelli, and M. R. Barchi (2011), Tectonic evolution of a low-0angle extensional fault system from restored cross-sections in the Northern Apennines (Italy), Tectonics, 30, TC6002, doi:10.1029/2011TC002890.

Okada, Y. (1985), Surface deformation to shear and tensile faults in a halfspace, Bull. Seismol. Soc. Am., 75, 1135-1154.

Pondrelli, S., S. Salimbeni, G. Ekstrom, A. Morelli, P. Gasperini and G. Vannucci (2006), The Italian CMT dataset from 1977 to the present, *Phys. Earth Planet. Inter*., 159, 286-303, doi:10.1016/j. pepi.2006.07.008, 159/3-4

Pucci, S., P. M. De Martini, D. Pantosti, G. Valensise (2003): Geomorphology of the Gubbio Basin (Central Italy): understanding the active tectonics and earthquake potential, Ann. Geophysics, 46 (5), 837-864

Rovida, A., Camassi, R., Gasperini, P. & Stucchi, M. (eds), (2011), CPTI 11, the 2011 Version of the Parametric Catalogue of Italian Earthquakes, Milano, Bologna, Available at http://emidius.mi.ingv.it/CPTI

Savage, J.C., 1983, A dislocation model of strain accumulation and release at a subduction zone: Journal of Geophysical Research, v. 88, p. 4984-4996, doi: 10.1029/JB088iB06p04984

Stein, S., Gordon, R. (1984): Statistical test of additional plate boundaries from plate motion inversion. *Earth Planet. Sci. Lett*, 69, 401-412.

Tondi, E. (2000), Geological analysis and seismic hazard in the central Apennines (Italy), J. Geodyn., 29, 517-533, doi:10.1016/S0264- 3707(99)00048-4.

Williams, S.D.P., Bock, Y., Fang, P., Jamason, P., Nikolaidis, R.M., Prawirodirdjo, L., Miller, M., Johnson, D.J., (2004), Error analysis of continuous GPS position time series. *J. Geophys. Res*.

NEW SEISMOLOGICAL, STRUCTURAL AND MARINE GEOLOGY CONSTRAINTS FOR A SEISMOTECTONIC MODEL OF THE HINGE ZONE BETWEEN NORTHERN SICILY AND SOUTHERN TYRRHENIAN

P. Capizzi, A. Giorgianni, G. Giunta, D. Luzio, R. Martorana, S. Orioli, A. Sulli
DiSTeM Department, University of Palermo, Italy

Northern Sicily and its Tyrrhenian off-shore are located in a very complex geodynamic context, where both the Sicilian-Maghrebian belt, associated to the collision between African and European Plates, and the more recent opening Tyrrhenian Basin coexist (Scandone *et al.*, 1979; Finetti and Del Ben, 1986; Malinverno and Ryan, 1986; Patacca *et al.*, 1990; Faccenna *et al.*, 1996; Monaco *et al.*, 1998; Giunta *et al.*, 2000b; Pepe *et al.*, 2000; Lo Iacono *et al.* 2011). This area represents therefore an important hinge zone between the two previous geodynamic elements evolving together since late Pliocene, which is part of a wider W–E trending right-lateral regional shear zone, extending for about 300 km from the Ustica-Eolie alignment to the Pantelleria rift.

The Northern Sicilian-Maghrebian chain courses WE from Trapani Mts to the Peloritani Mts and is composed by a set of tectonic units deriving from the deformation of the Northern African Continental Margin.

The architecture of the tectonic edifice, from the Late Oligocene, is the result of three main tectonic phases, characterized by compressional, extensional, and transcurrent tectonics (Giunta *et al.*, 2000b).

The first compressional phase, responsible for the building of the thrust belt, is represented by fold associations, cleavage and foliation, thrust and contraction, which shortened the original paleo-tectonic domains forming flat-ramp, duplex, enveloping, and breaching geometries.

This deformational style persisted, in the most internal sector of the thrust belt, until the Late Miocene. At that time the activation of low-angle top-to-the-north extensional faults produced a general stretching of the belt by re-orientation and inversion of pre-existing structures.

The recent pattern of the Sicilian Maghrebides has been interpreted as an effect of a complicated grid of neotectonic high-angle strike-slip faults, which have been affecting the tectonic edifice since the Pliocene (Boccaletti *et al.*, 1990a; Nigro, 1998; Giunta *et al.*, 2000a; Renda *et al.*, 2000), identifying a hinge zone between emerged Sicilian orogen, with a moderate thickened crust, and the southern Tyrrhenian, characterized by crustal thinning. Starting from the Pleistocene is also active a Tyrrhenian verging extensional net and dip slip system, over imposed to previous transcurrent one, which accommodates the recent uplift of the emerged sectors of the chain.

The brittle neotectonic pattern has been reconstructed on detail in the northern emerged areas of the Sicilian chain, where two main high-angle strike-slip systems occur, respectively NNW-SSE to W-E mainly right-lateral, and N-S to NW-SE left-lateral one (Fig. 1).

The structures occur from the kilometer to the meter scales and seem to control the recent evolution of the northern Sicilian coastline, determining the formation of either uplifting restraining zones, coinciding with the main morphostructural highs, and the interposed coastal plains located in the tectonic depressions along the subsiding releasing areas.

The interpretation of recent morphobatymetric maps allows to infer the neotectonic pattern also in the submerged areas, which highlights the continuity of the main morphostructural element between the emerged and submerged sectors, and the general coherence of the structural lineament trends controlling the genesis and the evolution of the main plio-pleistocenic clastic sedimentation areas (Giunta *et al.*, 2004).

In the hinge zone between the Northern Sicily chain and the Tyrrhenian basin the earthquake hypocenters distribution highlights the presence of two main types of seismicity (Giunta *et al.*, 2002b, 2004, 2008; Gueguen *et al.*, 2002): the first one, characterized by deep hypocenters (down to about 600 km) affecting the easternmost sector of the area, is associated

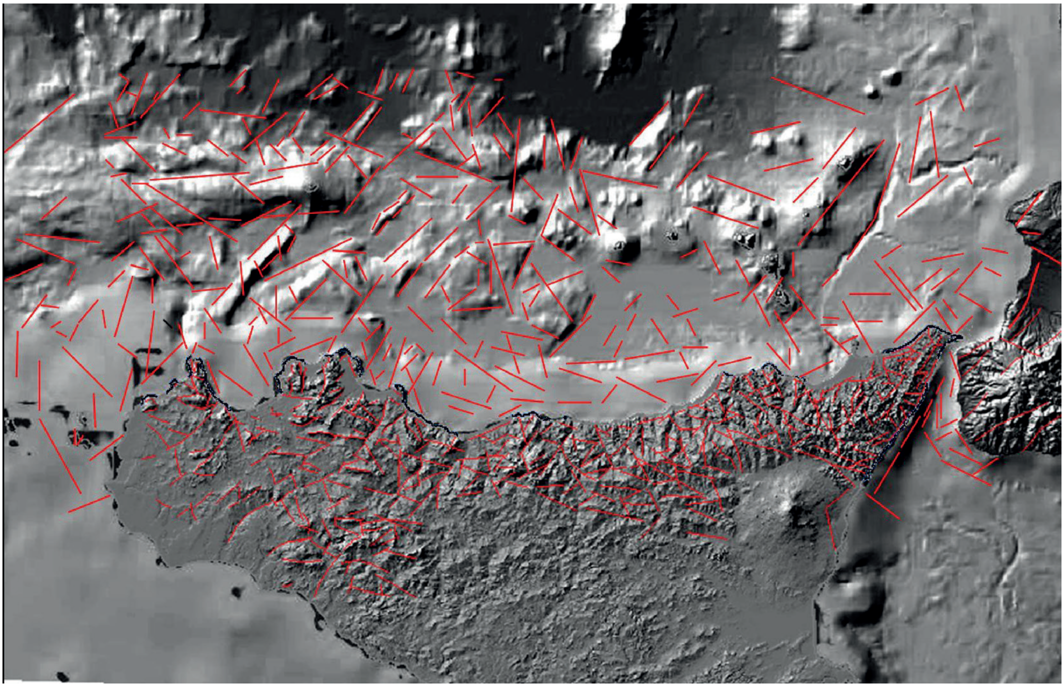

Fig. 1 – The brittle neotectonic pattern in the onshore and offshore sectors of the chain.

with the subduction of the Ionian lithospheric slab beneath the Calabrian arc the second one characterized by shallower hypocenters (down to about 30 km) is expression of the brittle strain crossing the whole orogen (Neri *et al.*, 1995). This latter seismogenic zone is strictly connected to the deformation field active within the hinge zone (Fig. 2).

Statistical analysis allows to extract from the overall distribution of seismicity some clusters of events that belong to individual sequences of aftershocks. This analysis highlights that the hypocenters tend to concentrate around high-angle dipping surfaces; moreover, the elongation axes of the clusters are mainly oriented between WNW and NE, well fitting the orientation of the main fault bands (Giunta *et al.*, 2008).

The analysis of the collected fault-plane solutions of the major events of the latter 30 years (DBMI11, Locati *et al.*, 2011; Pondrelli, 2004) shows transpressional and transtensional mechanisms likely related to NW-SE and NE-SW fault lineaments, and compressional and

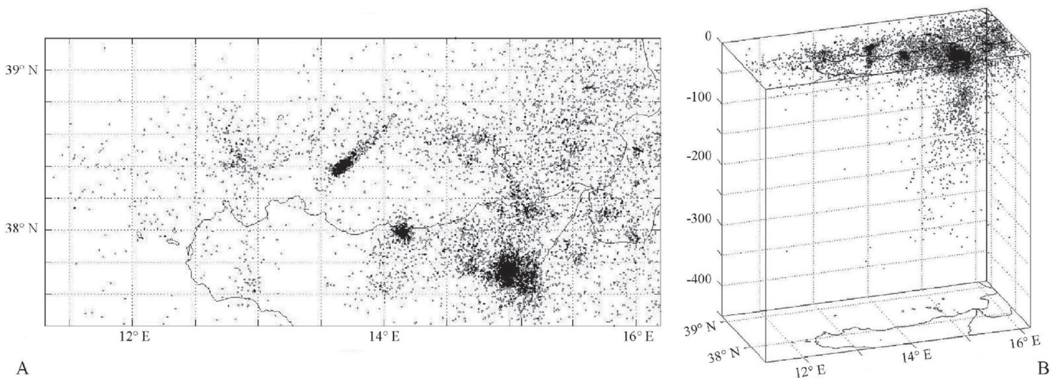

Fig. 2 – Epicenter (A) and hypocenter (B) distribution in the area.

transpressional mechanisms, mainly oriented from ENE to NW, either generally high-angle dipping and only in few cases low-angle. This evidence well fit the geological-structural data collected in the on-shore areas.

The structural setting sketched by the integration of above mentioned geological and seismological data underlines an intense mechanical heterogeneity of the rock volumes where the strain is accommodated by fault arrays also superimposed on inherited geometries such as flat-ramp, thrusts and/or low-angle normal faults.

The geometric characters of the rocks volumes seems to confirm the occurrence of a simple-shear deformational style according with a neotectonic model related to NW-SE trending maximum compressional stress axis producing a non-coaxial strain, even if in particular areas different seismogenic conditions are possible, due to the accommodation of the deformation leading a marked mechanical heterogeneity (Neri *et al.*, 2003, 2005).

Recently some seismological data of the main seismic sequences affecting the Northern Sicilian sector and its offshore has been checked with the aim to improve the above mentioned seismotectonic model. Particularly, the 1992-1993 Pollina, 1998 S. Vito high, 2002 Palermo, 2009-2012 Caprileone seismic sequences have been analyzed.

More events of the above mentioned seismic sequences were relocated using a process based on the HYPODD program (Waldhauser, 2001) and an eight layers velocity model optimized relocating some thousands events of the Southern Tyrrhenian (Chironi *et al.*, 2000). Moreover, new focal mechanisms were calculated using the FPFIT code (Reasenberg and Oppenheimer, 1985).

The hypocentral relocation allowed well defining the seismogenic volume geometries involved in the analyzed seismic sequences. The new focal mechanisms confirm a large structural heterogeneity of seismogenic volumes as observed in the structural analysis in the onshore sector of the chain (Fig. 3).

These new analysis of seismological data seems to confirm the congruence of the seismo-tectonic model of the hinge zone, where a main NW-SE stress field is still active, which induce a non-coaxial deformation expressed by a complex strike slip system: NE-SW/N-S trending antithetic, and WNW-ESE/W-E trending synthetic, both transpressional or transtensional.

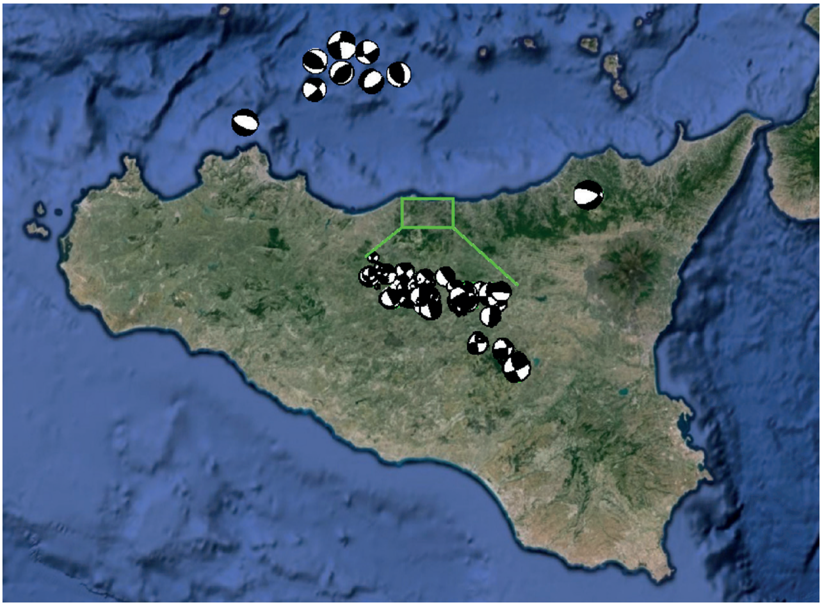

Fig. 3 – Focal mechanisms of the main events of the seismic sequences calculated by the FPFIT code.

The analyzed seismic activity also highlights the activation of rock volumes with a high degree of mechanical anisotropy, where variously oriented seismogenic structures can be active.

References

Adelfio, G., Chiodi, M., De Luca, L., Luzio, D., Vitale, M.; 2006. *Southern-Tyrrhenian seismicity in space-time-magnitude domain*. Annals of Geophysics **49** (6), 1245-1257.

Boccaletti, M., Nicolich, R., Tortorici, L.; 1990. *New data and hypothesis on the development of the Tyrrhenian Basin. Paleogeo*. Paleoclim. Paleoecol., **77**, 15-40.

Facenna, C., Davy, P., Brun, J.P., Funiciello, R., Giardini, D., Mattei, M., Nalpas, T.; 1996. *The dynamics of back-arc extension: an experimental approach to the opening of the Tyrrhenian Sea*. Geophysical Journal International **126**, 781-795.

Finetti, I., Del Ben, A.; 1986. *Geophysical study of the Tyrrhenian opening*. Bollettino di Geofisica Teorica ed Applicata **28**, 75-155.

Giunta, G., Nigro, F., Renda, P.; 2000a. *Extensional tectonics during Maghrebides chain building since Late Miocene: examples from Northern Sicily*. Ann. Soc. Geol. Poloniae **70**, 81-89.

Giunta, G., Nigro, F., Renda, P., Giorgianni, A.; 2000b. *The Sicilian-Maghrebides Tyrrhenian Margin: a neotectonic evolutionary model*. Memorie Società Geologica Italiana **119**, 553-565.

Giunta G., Nigro F., Renda P., Andaloro F., Giorgianni A., Sparacino V.; 2002a. *The structural and morphotectonic framework of the NW Sicilian Maghrebides, in a seismotectonic perspective*. Studi geologici Camerti, special number 103-107.

Giunta G., Nigro F., Luzio D., D'Anna G., Tondi E., Renda P., Cello G., Giorgianni A., De Luca L., Vitale M.; 2002b. *Sismicità e tettonica recente in Sicilia nord-occidentale e nel Tirreno meridionale per un modello sismotettonico preliminare*. Acts of 21° Convegno Annuale del Gruppo Nazionale di Geofisica Terra Solida (GNGTS), CNR, Roma (CD-ROM).

Giunta G., Luzio D., Tondi E., De Luca L., Giorgianni A., D'Anna G., Renda P., Cello G., Nigro, F., Vitale M.; 2004. *The Palermo (Sicily) seismic cluster of September 2002, in the seismotectonic framework of the Tyrrhenian Sea-Sicily border area*. Annals of Geophysics **47** (6), 1755-1770.

Giunta G., Luzio D., Agosta F., Calò M., Di Trapani F., Giorgianni A., Oliveri E., Orioli S., Perniciaro M., Vitale M., Chiodi M. & Adelfio G.; 2008. *An integrated approach to investigate the seismotectonics of northern Sicily and southern Tyrrhenian*. Tectonophysics, **476**, 12-21.

Gueguen E., Tavarnelli E., Renda P., Tramutoli M.; 2002. The geodynamics of the southern Tyrrhenian Sea margin as revealed by integrated geological, geophysical and geodetic data. Bollettino Società Geologica Italiana, sp. **1**, 77-85.

Lo Iacono C., Sulli A., Agate M., Lo Presti V., Pepe F., Catalano R.; 2011. *Submarine canyon morphologies in the Gulf of Palermo (Southern Tyrrhenian Sea) and possible implications for geo-hazard*. Mar. Geophys. Res. **32**, 127-138.

Locati M., Camassi R. and Stucchi M.; 2011. *DBMI11, la versione 2011 del Database Macrosismico Italiano*. Milano, Bologna, http://emidius.mi.ingv.it/DBMI11.

Malinverno A., Ryan W.B.F.; 1986. *Extension in the Tyrrhenian Sea and shortening in the Apennines as result of arc migration driven by sinking of the lithosphere*. Tectonics **5**, 227-54.

Monaco C., Tortorici L., Catalano S.; 1998. *Lateral extrusion in the Sicanian Mountains (Western Sicily)*. Proc. 79° Congresso Nazionale della Società Geologica Italiana, 599-600.

Neri G., Caccamo D., Cocina O., Montalto A.; 1996. *Geodynamic implications of recent earthquake data in the Southern Tyrrhenian Sea*. Tectonophysics **258**, 233-249.

Neri G., Barberi G., Orecchio B., Mostaccio A.; 2003. *Seismic strain and seismogenic stress regimes in the crust of the southern Tyrrhenian region*. Earth Planetary Science Letter **213**, 97-112.

Neri G., Barberi G., Oliva G., Orecchio B.; 2005 a. *Spatial variation of seismogenic stress orientations in Sicily, South Italy*. Physical Earth Planetary International **148**, 175-191.

Nigro F.; 1998. *Neotectonic events and kinematic of rhegmatic-like basins in Sicily and adjacent areas. Implications for a structural model of the Tyrrhenian opening*. Ann. Soc. Geol. Poloniae **68**, 1-21.

Patacca E., Sartori R., Scandone P.; 1990. *Tyrrhenian Basin and Appenninic Arcs: kinematics rotations since Late Tortonian Times*. Memorie Società Geologica Italiana **45**, 425-451.

Pepe F., Bertotti R., Marsella E.; 2000. *Rifted margin formation in the South Tyrrnenian Sea: a high-resolution seismic profile across the North Sicily passive continental margin*. Tectonics **19**, 241-257.

Pondrelli S., Morelli A., Ekström G.; 2004. *European-Mediterranean Regional Centroid Moment Tensor catalog: solutions for years 2001 and 2002*. Phys. Earth Planet. Int., **145**, 127-147.

Reasenberg P.A., Oppenheimer D.; 1985. *FPFIT, FPPLOT and FPPAGE: Fortran computer programs for calculating and displaying earthquake fault-plain solutions*. U.S. Geological Survey Open-file Rep, 85-739.

Renda P., Tavarnelli E., Tramutoli M., Gueguen E., 2000. *Neogene deformations of Northern Sicily, and their implications for the geodynamics of the Southern Tyrrhenian Sea margin*. Memorie Società Geologica Italiana **55**, 53-59.

Scandone, P.; 1979. *Origin of the Tyrrhenian Sea and Calabrian Arc*. Bollettino Società Geologica Italiana **98**, 27-34.

Waldhauser F.; 2001. *HypoDD: a program to compute double difference hypocenter locations*. U.S. Geological Survey Open-file, Menlo Park, California report, 01-113.

MODELING SURFACE GPS VELOCITIES IN THE SOUTHERN AND EASTERN ALPS BY FINITE DISLOCATIONS AT CRUSTAL DEPTHS

A. Caporali[1], F. Neubauer[2], L. Ostini[1], G. Stangl[3], D. Zuliani[4]
[1]*Department of Geosciences, University of Padova, Padova, Italy*
[2]*Department of Geography and Geology, University of Salzburg, Austria*
[3]*Austrian Academy of Sciences and BEV, Graz, Austria*
[4]*Istituto Nazionale di Oceanografia e Geofisica Sperimentale, Centro Ricerche Sismologiche, Udine, Italy*

In the Eastern and Southern Alps a complex fault geometry accommodates the northward indentation of the Adria plate, the uplift of the Tauern Window, and a lateral extrusion towards the Pannonian Basin. The northeastern edge of the Adria is associated with the seismically active Friuli (Anderson and Jackson, 1987; Bressan *et al.*, 1998, 2006; Schmid *et al.*, 2004, 2008). The compressive M_w=6.5 earthquake of May 6, 1976 is the largest recorded event in Friuli. The area of the Southern and Eastern Alps is characterized by significant crustal thickness variations (Brückl *et al.*, 2007, 2010). Seismic profiles show that the Eurasian and Adriatic plates interact with a thinner Pannonian unit as a structurally separated entity (Brückl *et al.*, 2007, 2010). Late Oligocene-Middle Miocene indentation tectonics is considered as the primary agent driving substantial lateral material transfer, or "lateral extrusion" (Ratschbacher *et al.*, 1991a; Neubauer *et al.*, 2000; Willingshofer and Cloetingh, 2003; Wölfler *et al.*, 2011). The indentation tectonics and resulting lateral extrusion is driven by a free boundary in the east due to subduction of a remnant land-locked basin within the present-day Carpathians (e.g., Wortel and Spakman, 2000). From the structural point of view, increasing evidence demonstrates inversion of the entire Alpine-Carpathian-Pannonian system at ca. Miocene/Pliocene boundary (ca. at 5 Myr before present, e.g., Peresson and Decker, 1997) and the sudden onset of surface uplift (e.g., Genser *et al.*, 2007; Hergarten *et al.*, 2010; Wagner *et al.*, 2010). Extension and related normal and transtensional faults as well as subsidence in sectors of the Eastern Alps including the Pannonian basin were replaced by E-W shortening structures and related surface uplift.

Using the analytic model of finite dislocation in an elastic half space of Okada (1985) and a dense set of GPS velocities, we present in this paper a first map of slip at depth. Based on structural surface data we identify a number of rectangular faults, which approximate the largest geological structures and which have the potential to accommodate the slip required to fit the GPS data (Fig. 1). We show that the GPS velocities, of the order of a few mm/yr, are consistent

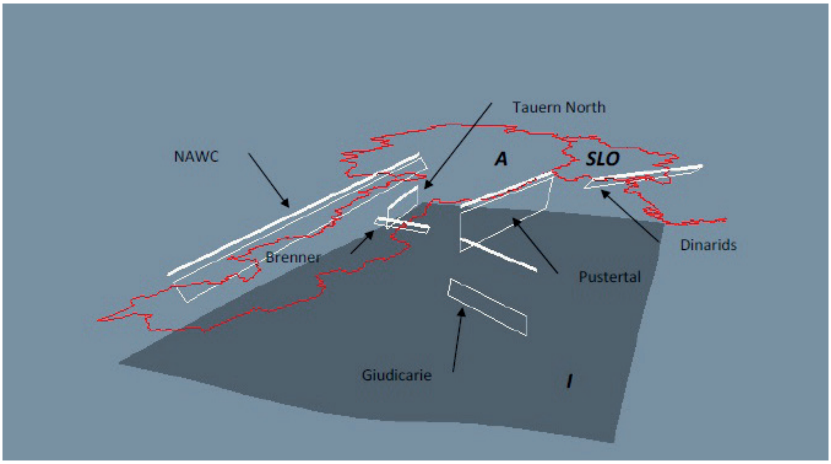

Fig. 1 – Three dimensional view of the model, seen from west. The rectangular faults are white rectangles, and a thicker white line on the surface represents the intersection of the prolongation of the fault with the Earth surface. A=Austria, I=Italy, SLO=Slovenia. The grey surface on the bottom is a smoothed approximation of the Moho, to emphasize that the rectangular faults are within the crust.

with a dynamic process where indentation and lateral extrusion involve slips at crustal depths ranging between 10 and 30 mm/yr. The available velocity data are consistent with slip taking place on at least six rectangular faults located in the upper crust: we associate them primarily with the Giudicarie Fault, the North Alpine Wrench Corridor, the Brenner fault, the SEMP fault along the northern part of the Tauern window, the Pustertal-Gailtal fault and the Dinarides, e.g., the Idrija and the eastern segments of the Fella-Save faults (Fig. 2). Whereas most of these zones represent well defined fault zones, the North Alpine Wrench Corridor corresponds to a zone of distributed seismicity close to the northern margin of Eastern Alps (Reinecker and Lenhardt, 1999; Lenhardt *et al.*, 2007) and consequently a zone of distributed deformation. Using the root mean square (r.m.s.) of the (observed-minus-modeled) velocities as an indicator of the goodness of the fit, we constrain the geometrical parameters of the rectangular faults and slip rates. There are nine parameters for each fault: three dimensional coordinates of an origin, length and width of the fault, two-dimensional slip vector, strike and dip angles. The least squares adjustment is done on a neighborhood of a priori values of these parameters, which come from independent information such as structural geology, average direction of P/T axes of fault plane solutions, and regional strain rate field from GPS velocities.

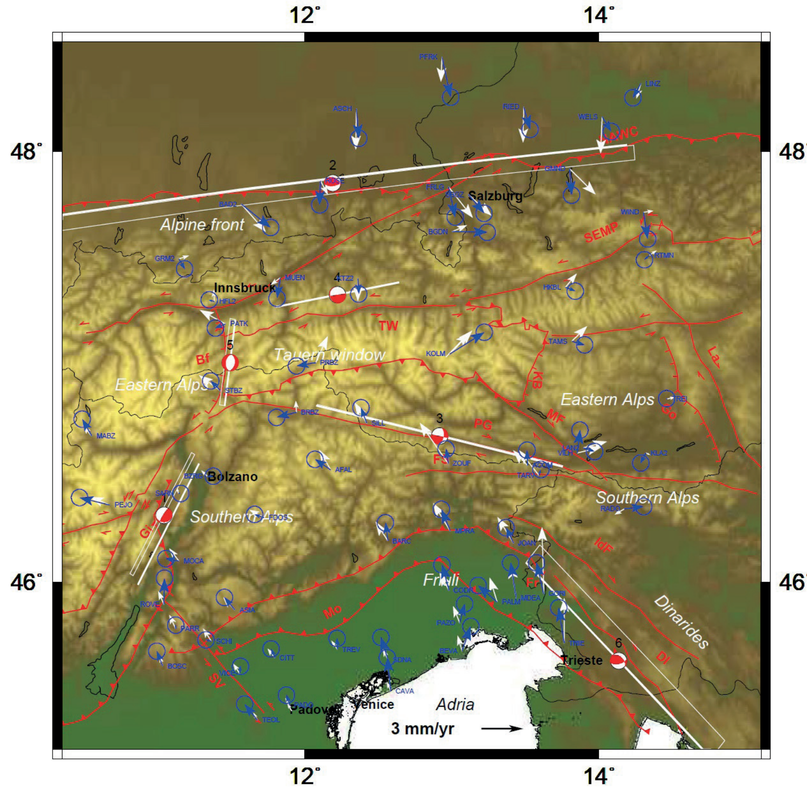

Fig. 2 – Geometry of the six rectangular slip planes (grey rectangles) projected onto the topographic surface. The grey line parallel to one of the sides of each rectangle represents the intersection of the fault plane with the topographic surface. The 'beach balls' give a pictorial view of the data in Tab. 1. The number in black above each beach ball refers to the indexing in Tab. 1. The blue arrows represent the measured velocities with 1σ error ellipse, and the white arrows the predicted model velocities based on Tab. 1. To = Tonale fault, PG = Pustertal-Gailtal, Gi = Giudicarie fault, TW = Tauern Window, NAWC = North Alpine Wrench Corridor, La = Lavant Fault, MF = Möll Valley-Hochstuhl fault, Di = Dinarides, Mo = Montello, Fr = Friuli, SEMP = Salzachtal-Ennstal–Mariazell–Puchberg fault, Go= Görtschitztal fault, IdF= Idrjia fault, KF= Katschberg Fault. Vergence and faults style are from the Structural Model of Italy (CNR, 1990).

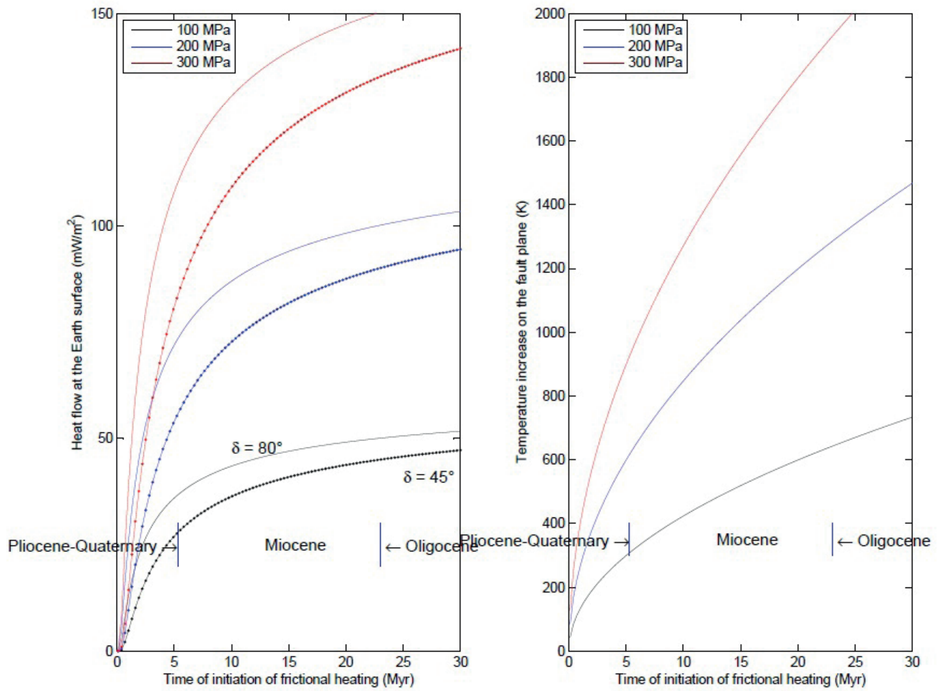

Fig. 3 – (Left) Heat flux on the Earth surface due to shear heating on a rectangular fault at depth. The continuous curves correspond to a dip of 80°, and the dotted curves to a dip of 45°. Different colors are assigned to different shear stresses. (Right) Temperature increase on the fault surface, due to shear heating, for various values of the shear stress.

Shear heating is likely to increase the temperature on the fault planes. The resulting heat flow adds to that generated by radiogenic sources in the upper continental crust. The available data (Della Vedova *et al.*, 2001; Viganò *et al.*, 2008, 2011; Clark, 1961) indicate that the total heat flow observed on the surface does not exceed 60 to 80 mW/m^2, although in middle Jurassic values as high as 85 to 105 mW/m^2 have been reported by Carminati *et al.* (2010) using organic matter maturity data from outcropping sediments.

Following Turcotte and Schubert (2002) we model the surface heat flow and temperature increase on the fault planes as due to a sudden increase of heat flow caused by shear heating on the fault plane. It is reasonable to assume that the total temperature (for a nominal thermal gradient plus shear heating) on the fault plane is in the range 600-800 °C (Vosteen *et al.*, 2006, for the TRANSALP profile), and that the heat flow on the Earth surface, when added to the radiogenic heat (of the order of 50 mW/m^2), does not exceed 60-80 mW/m^2. The model then implies that the time of initiation of heat production by shear in the half space must be relatively recent, for shear stresses in the range 100-300 MPa. We infer that such epoch should be somewhere in the Plio-Pleistocene, hence more recent than the late Oligocene to Miocene collision of the Adria indenter with the stable European foreland. According to the analog models of Ratschbacher *et al.* (1991), this collision is responsible the fold and fault structure. Hence it can be concluded that the collision was ‘head on’ in the first 15-18 Myr, and has been accommodated by slip on inclined fault planes only in the past 5-7 Myr, since a longer slipping phase would imply an exceedingly large amount of frictionally generated heat to reach the Earth surface (Fig.3). Specific assumptions on the local geotherm are clearly needed to make these concepts more quantitative.

Tab. 1 – The nine parameters of each rectangular faults used in the analysis. The first three columns (Lat, Long, depth) identify the center of the rectangular fault. The last column gives the product of the previous three columns (slip area x slip rate) times the shear modulus μ = 30 GPa. Uncertainties (1σ), in the sense of square root of the corresponding element in the variance covariance matrix scaled by the r.m.s. of the post fit residuals, are: 0.05 deg for Longitude and Latitude, 2 km for depth, 3 degrees for strike and dip, 0.005 m/yr for slip, 5 km and 2 km for Length and respectively Width of the fault.

Fault id.	Name	Long. (deg)	Lat. (deg)	depth (km)	strike (deg)	dip (deg)	right lat. (m/yr)	reverse (m/yr)	Length (km)	Width (km)	Moment rate 10^{18} J/yr
1	Giudicarie	11.04	46.31	30	211	80	-0.01	0.03	58	10	0.56
2	NAWC	12.18	47.85	10	84	60	-0.01	0.02	297	12	2.02
3	Pustertal	12.91	46.68	20	282	89	0.01	0.01	123	30	1.41
4	TW north	12.22	47.34	8	261	89	0.00	0.02	61	20	0.55
5	Brenner fault	11.49	47.02	2	188	45	0.00	-0.02	35	4	0.08
6	Dinarids	14.13	45.62	5	312	45	0.01	0.01	122	14	0.73

References

Anderson, H., Jackson, J. (1987. Active tectonics of the Adriatic region. Geophys. J. R. Astron. Soc. 91, 937-983.

Bressan, G., Snidarcig, A., Venturini, C., 1998. Present state of tectonic stress of the Friuli Area (Eastern Southern Alps), Tectonophysics 292, 211-227.

Bressan, G., Kravanja, S., Franceschina, G., 2006. Source parameters and stress release of seismic sequences occurred in the Friuli – Venezia Giulia region (NorthEastern Italy) and in Western Slovenia. Phys. Earth Planet. Int., http://hdl.handle.net/2122/2513.

Brückl, E., Bleibinhaus, F., Gosar, A., Grad, M., Guterch, A., Hrubcovà, P., Randy Keller, G., Majdanski, M., Sumanovac, M., Tiira, T., Yliniemi, J., Hegedus, E., Thybo, H., 2007. Crustal structure due to collisional and escape tectonics in the Eastern Alps region based on profiles Alp01 and Alp02 from the ALP 2002 seismic experiment. J. Geophys. Res. 112, B06308. doi:10.1029/2006JB004687.

Brückl, E., Behm, M., Decker, K., Grad, M., Guterch, A., Keller, G. R., Thybo, H., 2010. Crustal structure and active tectonics in the Eastern Alps. Tectonics 29, TC2011, doi:10.1029/2009TC002491.

Carminati, E., Cavazza, D. Scrocca, D. Fantoni, R. Doglioni, C., 2010. Thermal and tectonic evolution of the southern Alps (northern Italy) rifting: Coupled organic matter maturity analysis and thermokinematic modeling. AAPG Bulletin, 94 (3), 369-397.

Clark, S., 1961. Heat flow in the Austrian Alps. Geophys. J. of the Royal Astron. Soc. 6, 54-63.

CNR, 1990. Structural model of Italy. Ed. by F. Barberi, SELCA editions, Firenze 1990.

Della Vedova, B., Bellani, S., Pellis, G., Squarci, P., 2001. Deep temperatures and surface heat flow distribution. G.B. Vai, I.P. Martini (Eds.), Anatomy of an Orogen, The Apennines and Adjacent Mediterranean Basins, Kluwer Ac. Publ., Great Britain, pp. 65-76.

Ratschbacher, L., Frisch,W., Linzer, H.-G., Merle, O., 1991. Lateral extrusion in the Eastern Alps, part 2. Structural analysis. Tectonics 10, 257-271.

Reinecker, J., Lenhardt, W.A., 1999. Present-day stress field and deformation in eastern Austria. International Journal of Earth Sciences 88, 532–550.

Schmid, S.M., Fügenschuh, B., Kissling, E., Schuster, R., 2004. Tectonic map and overall architecture of the Alpine orogen. Eclogae Geol. Helv., 97, 93-117.

Schmid, S.M., Bernoulli, D., Fuegenscuh, B., Matenco, L., Schefer, S., Schuster, R., Tischler, M., Ustaszewski, K., 2008. The Alpine–Carpathian–Dinaric orogenic system: correlation and evolution of tectonic units. Swiss J. Geosci. 101, 139-183.

TRANSALP Working Group, 2002. First deep seismic reflection images of the Eastern Alps reveal giant crustal wedges and transcrustal ramps. Geophys. Res. Lett. 29 (10), 1452, doi :10.1029 /2002GL014911.

Viganò, A., G. Bressan, G. Ranalli, S. Martin, 2008. Focal mechanism inversion in the Giudicarie Lessini seismotectonic region (Southern Alps, Italy): insights on tectonic stress and strain. Tectonophysics 460, 106-115.

Viganò, A., Della Vedova, B., Ranalli, G., Martin, S., Scafidi, D., 2011. Geothermal and rheological regime in the Po Plain sector of Adria (Northern Italy). Ital. J. Geosci., 131 (2), 228-240, doi: 10.3301/IJG.2012.09.

Vosteen, H.D., Rath, V., Clauser, C. Lammerer, B., 2006. A review of the thermal regime of the Eastern Alps with respect tothe effects of paleoclimate and exhumation. Tectonophysics 414, 157-167, doi:10.1016/j.tecto.2005.10.022.

Wagner, T., Fabel, D., Fiebig, M., Häuselmann, P., Sahy, D., Xu, S., Stüwe, K., 2010. Young uplift in the non-glaciated parts of the Eastern Alps. Earth and Planetary Science Letters 295, 159-169.
Willingshofer, E., Cloetingh, S., 2003. Present-day lithospheric strength of the Eastern Alps and its relationship to neotectonics. Tectonics 22, 1075, doi:10.1029/2002TC001463.
Wölfler, A., Kurz, W., Fritz, H., Stüwe, K., 2011. Lateral extrusion in the Eastern Alps revisited: Refining the model by thermochronological, sedimentary, and seismic data, Tectonics, 30, TC4006, doi:10.1029/2010TC002782
Wortel, M.J.R., Spakman, W., 2000. Subduction and slab detachment in the Mediterranean-Carpathian region. Science 290, 1910-1017.

PRESENT-DAY VERTICAL KINEMATIC PATTERN IN THE CENTRAL AND NORTHERN ITALY FORM PERMANENT GPS STATIONS

N. Cenni[1,2], P. Baldi[1], F. Loddo[3], G. Casula[3], M. Bacchetti[1]
[1]*Dipartimento di Fisica ed Astronomia – Università degli Studi di Bologna, Bologna, Italy*
[2]*Dipartimento Scienze Biologiche, Geologiche ed Ambientali – Università degli Studi di Bologna, Bologna, Italy*
[3]*Istituto Nazionale di Geofisica e Vulcanologia, Sezione di Bologna, Bologna, Italy*

Introduction. The aim of this work is to describe the results of the analysis of observational GPS data of permanent stations located in the Northern Italy and surroundings in order to estimate the present-day vertical kinematic pattern. The high density GPS network distributed on the area can provide a detailed spatial description of the movements.

The area considered includes regions with different kinematic style: Alps, Apennines and Po river alluvial basin. The Po valley has been affected in the last sixty years by a strong anthropogenic land subsidence due to groundwater pumping from a shallow well-developed multi-aquifer system and gas production from a number of onshore and offshore gas reservoirs; its vertical movements in the last years are well known from repeated precise leveling spanning nearly hundred years and more recently from DinSAR measurements and GPS permanent stations observations. The long observation period of several GPS permanent sites can allow us to investigate about actual vertical rates and their possible time variations.

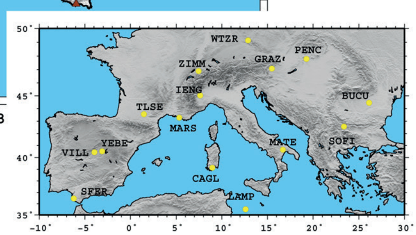

Fig. 1 – Locations of the permanent GPS stations used in this work. Circles and triangles respectively indicate scientific and commercial permanent stations, given in the legend. The inset shows the 16 IGS stations we have used to align the above regional network to the ITRF2005 reference frame.

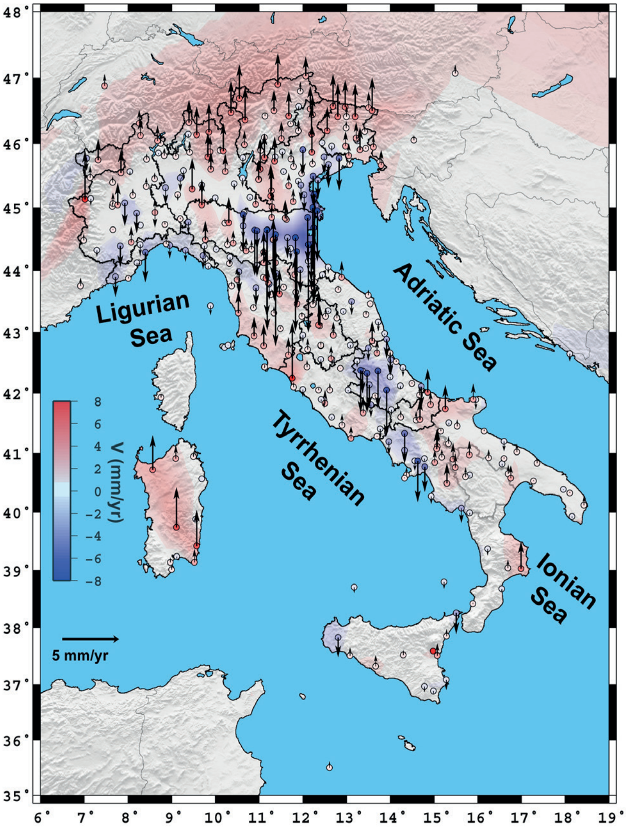

Fig. 2 – Vertical velocities and contour map obtained considering the stations with an observation time span longer than 2 years. The interpolation pattern has been estimated using the kriging geostatistical method over a regular spaced grid (0.1°x0.1°).

GPS data analysis. In order to update the knowledge of present day vertical movements in the Italian peninsula, we have analyzed the observation data of 450 permanent GPS stations (Fig. 1), managed by scientific agencies and commercial network (e.g. Baldi *et al.*, 2009, 2011; Bennett *et al.*, 2012; Cenni *et al.*, 2012, 2013; Devoti *et al.* 2008; 2011). The observation periods of the sites are comprised between January 1, 2001 and July 19, 2013. Observations have been carried out with a 30 s sampling rate. The position of each continuous GPS sites (CGPS) has been estimated with the scientific GAMIT software (Herring *et al.*, 2010a), adopting a distributed procedure (Dong *et al.*, 1998). The network is divided into 30 sub-networks (clusters), each including at least the following six common stations; BRAS, CAGL, GRAZ, MATE; WTZR and ZIMM. The IGS precise ephemerides are included in the processing with tight constraints, such as the Earth Orientation Parameter (EOP). The Phase Centre Variation (PCV) absolute corrections for both ground and satellite antennas are included. Loose constraints are assigned to the daily position coordinates of stations.

The daily loosely constrained solutions of the 30 clusters obtained after GAMIT processing are combined into a unique solution by the GLOBK software (Herring *et al.*, 2010b) and aligned into the ITRF2005 reference frame (Altamimi *et al.*, 2007) by a weighted six parameters transformation (three translation and three rotation), using the ITRF2005 coordinates and velocities of the following 16 high quality common IGS stations: BUCU, CAGL, GRAZ, IENG, LAMP, MARS, MATE, PENC, SFER, SOFI, TLSE, VILL, WTZR,YEBE and ZIMM (inset in Fig. 1). At the end of this procedure, the daily time series of the north, east and vertical geographical position components of each site included in the analysis are estimated. In order to estimate the velocity values the time series of each site with a time span greater than 2 years, are analyzed with the following procedure:

1. Data cleaning: time series have been preliminarily analyzed in order to detect and remove outliers, defined as the data with value or associated uncertainties greater than 3 times the weighted root mean square (wrms) of the series. The outlier epochs have been identified separately in each coordinate direction and then applied to all three components.
2. Preliminary processing: the time pattern of the daily position component $y_{1k}(t)$ (k=1,2,3, for the North, East and Vertical component) has been modelled by the following relation:

$$y_{1k}(t_i) = A_{1k} + v_{1k}t_i + \sum_{j=1}^{N} g_{1kj} H(t_i - T_j) \qquad (1)$$

where A_{1k} and v_{1k} are, respectively, the intercept and trend of the best fitting straight line, the g_{1kj} terms are the N instrumental or seismic steps eventually occurred at the Tj epochs, H is the Heaviside step function. These parameters are estimated with a weighted least square method, using as weight the uncertainties associated to the components estimated in the GAMIT processing.

3. Spectral analysis: the residual time series obtained modeling the linear motion by mean of the parameter estimated in the previous step (Eq. 1), are analyzed with a nonlinear least squares technique to estimate spectra following the Lomb (1976) – Scargle (1982) approach. The spectrum of each component is analyzed in order to estimate the period P of the principal signal, in the interval between the seven days to half of the observation time span.

4. Parameter estimation: the daily position component $y_{1k}(t)$ (k=1,2,3, for the North, East and Vertical component) has been modelled only with the contribution of the principal periodic signal estimated in the spectral analysis phase. The daily time pattern of each component $y_{2k}(t)$ can be re-written as:

$$y_{2k}(t_i) = A_{2k} + v_{2k}t_i + \sum_{j=1}^{N} g_{2kj} H(t_i - T_j) + B_{1k}\sin(2\pi t_i / P) + B_{2k}\cos(2\pi t_i / P) + \varepsilon_k(t_i) \qquad (2)$$

where A_{2k} and v_{2k} are the re-estimated intercept and constant velocity, the B_k ($B_k = \sqrt{B_{1k}^2 + B_{2k}^2}$) is the amplitude of the principal periodic signal P. The g_{2kj} terms are the re-estimated offset magnitudes for the N identified discontinuities due to instrumental changes or seismic events eventually occurred at the T_j epochs, H is the Heaviside step function. As argued in several papers (e.g. Hackl *et al.* 2011, Bos *et al.* 2008; 2010), the noise $\int_k(t_i)$ in time series can be described as a power law process (Agnew, 1992). Different methods have been developed to characterize noise in GPS time series and its impact on velocity uncertainties (Dixon *et al.*, 2000; King and Williams 2009; Hackl *et al.* 2011; Santamaria-Gomez *et al.* 2011; Williams 2004, 2008). We have used the Allan Variance of the Rate (AVR) method introduced by Hackl *et al.* (2011), which is based on the Allan variance, an analysis often used as a measurement of frequency stability in clock and oscillators (Allan 1966). The method provides the velocity uncertainties after an analysis in the time domain, without any assumption about the noise characteristics of the series. As the calculation is done in the time domain, the method is not too sensitive to gaps in the series and it is computationally cheap.

Vertical kinematic pattern. The present-day vertical kinematic pattern in the Italian peninsula is showed in Fig. 2. This pattern presents some significant features; in particular the sites located in the Alps and Apennine domains are characterized by a slow uplift velocity, while the Po plan and some Central Apennine basins are affected by subsidence phenomena.

In the Alps, the rates are of the order of a few mm/yr, in agreement with previous estimates carried out by repeated leveling in the last century. At present, the uplift of that zone is attributed to the combined effects of tectonic shortening (e.g., Schlunegger and Hinderer, 2001; Persaud and Pfiffner, 2004; Lardeaux *et al.*, 2006), postglacial isostatic rebound (e.g. Gudmundsson, 1994; Stocchi *et al.*, 2005, 2009; Barletta *et al.*, 2006), flexural response to climate-driven denudation and rapid glacier shrinkage. (e.g., Champagnac *et al.*, 2007, 2009; Korup and Schlunegger, 2009).

The observed uplift in the Northern Apennines, with rates mostly lower than 2 mm/yr, is consistent with the results obtained by repeated leveling surveys carried out over 129 years by the Istituto Geografico Militare Italiano (IGMI). This last investigation, performed along several lines crossing the chain from the Tyrrhenian to the Adriatic coasts, indicates maximum uplift rates in the range of 1-3 mm/yr (under the assumption that most of the Tyrrhenian side of the Central-Northern Apennines is essentially stable). The uplift of the Northern Apennines is consistent with the effects expected from the longitudinal shortening of the belt suggested by Mantovani *et al.* (2009) and Cenni *et al.* (2012, 2013).

The part of Central Apennines centered on the L'Aquila area and the corresponding Adriatic side is characterized by small negative rates.

Significant subsidence, with velocities up to 5-10 mm/y, occurs in the eastern Po basin zone, while minor (or positive) vertical movements are recognized in the western Po Valley. This considerable difference between vertical movements in the two parts of the basin cannot be simply imputed to different anthropogenic effects or to ground settlement (Teatini *et al.*, 2011; Bonsignore, 2008). The same pattern was highlighted by the results of repeated levelling measurements from 1897 to 1957 (Arca and Beretta, 1985), a period that preceded the strong increase of economic activities in the second half of the XX century. They found a mean uplift velocity of about 2-3 mm/y in the central-western part of the Alpine chain, reducing rapidly moving toward the Po plain and in eastern direction; the study pointed out that the eastern Po Valley were affected by subsidence, with rates increasing from west (1-2 mm/y) to east (5-7 mm/y), whereas the western part (Lombard plain) mainly undergoes uplift, generally lower than 2 mm/y, except a narrow EW belt in the Monferrato zone, where uplift rates even reach 3.5 mm/y. The effects of a complex interaction of different tectonic structures of the area clearly influences the vertical movements, masking the anthropogenic subsidence.

The comparison between the high density GPS network and the results obtained previously (up to 2006) with different techniques (Baldi *et al.*, 2009; Bonsignore 2007) indicates that the rates

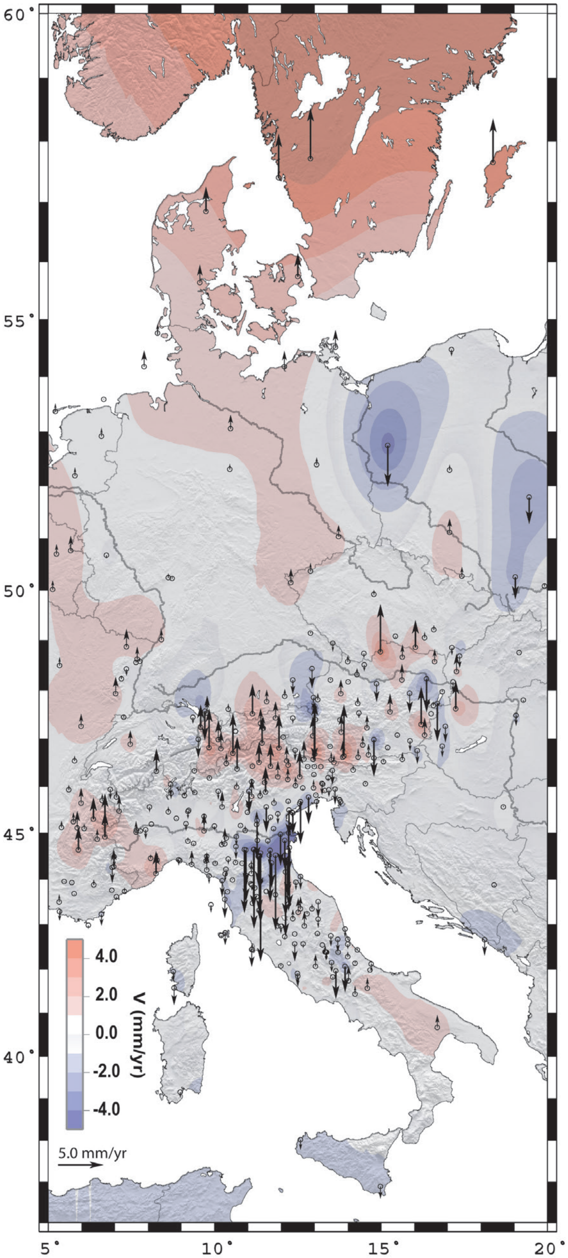

Fig. 3 – The vertical kinematic pattern obtained after the combination of our solution and Euref, Amon and Regal solutions.

are stable or in some cases are decreasing, as a consequence of the drastic reduction of water withdrawal. In particular the data of two regions (the industrial area north of Bologna town and Po Delta, east of Rovigo), which were involved in a very strong subsidence in the past, with maximum rate of 60-70 mm/y, confirm the decrease of the subsidence velocity.

European Vertical Reference frame. In order to investigate if the absolute values of the computed vertical velocities of the CGPS sites located in the Italian region have a real geophysical significance, some careful considerations have to be made: the vertical velocities estimated are obtained in the International Terrestrial Reference Frame (ITRF2005) realized by the combination of different space techniques (Altamini *et al.*, 2007). Considering that the central part of Europe lying north of the Alps is generally seen as a relatively tectonically stable area of Eurasia (Campbell and Nothnagel, 2010), we analyze the vertical velocity field of this area obtained by aligning our data to the EUREF Permanent Network solution at 1600 (2010/09/06) GPS week (Bruyninx and Kenyeres, 2008). Additional information about the present vertical velocity field in the Alps and the European area can also be inferred from the Regal permanent GPS array (Calais *et al.*, 2000, 2002), and from the AMON network (Austrian Monitoring Network; Höggerl *et al.*, 2011), whose solutions are given in the International Terrestrial Reference Frame (ITRF2005) realized by the combination of different space techniques (Altamini *et al.*, 2007). In order to evaluate eventual bias due to different procedures for aligning the four networks in the ITRF frame, we performed a seven Helmert transformation assuming as reference the EUREF solution at 1600 GPS week (2010/09/06). The Helmert transformation parameters are listed in Tab. 1. These parameter have been estimated using the velocity of the common sites included in the EUREF and in the other solution (AMON, Regal, our) included in the analysis. So the AMON, Regal and our solution Have been aligned to the EUREF - ITRF2005 ones using the values listed in Tab. 1.

Moreover, the number of the common stations included in EUREF and of the other networks, along with their characteristics (mean and root mean square RMS of the velocity differences), are listed in Tab. 2. The four networks considered are all aligned in the ITRF2005 reference frame; the mean of the difference are lower than 1 mm/yr with a distribution (RMS) of about the same value (Tab.1).

The vertical velocities obtained after the 7 parameter Helmert transformations are shown in Fig. 3. It can be noted that the global vertical velocities field obtained in this Reference Frame is in good agreement with the vertical displacements measured by the tide gauges network (e.g. Bouin and Wopplelmann, 2010), and shows also an overall agreement with the Glacial Isostatic Adjustment (GIA); this process could affect the Europe south of Fennoscandia, inducing a prevalent uplift north of the 48th parallel. The small subsiding areas shown in figure and located almost above the 48th parallel of latitude, are generally inferred by one or few velocity data that do not seem to be consistent with nearby stations, and may be connected with regional and local tectonic structures (LODZ and CATO stations, Mid Polish Trough and its sedimentary infill) and oil/gas production (GWWL station, western Poland).

Tab. 1 – Helmert transformation parameters in Cartesian coordinate system estimated assuming as reference the EUREF solution at 1600 GPS week (2010/09/06). T and R are respectively the translation and rotation velocity vector, S is the velocity scale factor.

Source	Tx (m/yr)	Ty(m/yr)	Tz(m/yr)	Rx(mas/yr)	Ry(mas/yr)	Rz(mas/yr)	S (x10-9)
Amon	(-0.010 ± 0.017)	(-0.004 ± 0.004)	(0.018 ± 0.004)	(0.3 ± 0.1)	(-0.594 ± 0.001)	(0.055 ± 0.007)	(-0.84 ± 0.03)
Regal	(-0.004 ± 0.001)	(-0.002 ± 0.001)	(0.002 ± 0.001)	(0.06 ± 0.02)	(-0.127 ± 0.003)	(-0.007 ± 0.003)	(0.22 ± 0.01)
This paper	(-0.004 ± 0.04)	(-0.001 ± 0.03)	(-0.020 ± 0.020)	(-0.01 ± 0.08)	(-0.035 ± 0.003)	(-0.035 ± 0.003)	(0.19 ± 0.02)

Tab. 2 – Mean value and root mean square of the differences between the velocities of the Euref solution (1600 GPS week, 2010/09/06, Bruyninx and Kenyeres, 2008) and the velocities obtained by the GPS network here considered: the Austrian Monitoring Network (AMON, Höggerl *et al.*, 2011), the REGAL (Réseau GPS Permanent dans les Alpes) permanent GPS network located in the Western Alps and their surroundings (Calais *et al.*, 2000, 2002) and the network analyzed in this paper. N is the number of sites in common with the Euref network.

Source	N	North	East	Vertical
Amon	6	0.11 ± 0.25	0.01 ± 0.43	0.39 ± 0.71
Regal	28	0.05 ± 0.29	-0.21 ± 0.40	-0.33 ± 0.80
This paper	21	0.11 ± 0.29	-0.34 ± 0.38	-0.80 ± 0.76

Acknowledgements. We are grateful the following Institutions: ASI, ARPA Piemonte, FOGER (Fondazione dei Geometri e Geometri Laureati dell'Emilia Romagna), FREDNET (OGS), LABTOPO (University of Perugia), LEICA-Italpos, Regione Abruzzo, Regione Friuli Venezia Giulia, Regione Liguria, Regione Lombardia, Regione Piemonte, Regione Veneto, RING-INGV, Provincia Autonoma di Bolzano (STPOS), Provincia Autonoma di Trento (TPOS), STONEX, which have kindly made available GPS recordings. We are grateful to Settore - Coordinamento Regionale Prevenzione Sismica Dir. Gen. Politiche Territoriali e Ambientali Regione Toscana and Servizio Geologico, Sismico e dei Suoli Regione Emilia Romagna for the economic and logistic support. The figures have been carried out by the Generic Mapping Tools (Wessel and Smith, 1998).

References

Agnew, D. C., 1992. *The time domain behavior of power law noises*. Geophys. Res. Lett. 19 (4), 333–336.

Allan, D. W., 1966. Statistics of atomic frequency standards. Proc. IEEE, 54 (2), 221-230.

Arca S. and Beretta G.P.; 1985: *Prima sintesi geodetica-geologica sui movimenti verticali del suolo nell'Italia Settentrionale*. Boll. Geod. Sci. Aff., 44, 125-156.

Altamimi Z., Collilieux X., Legrand J., Garayt B. and Boucher C.; 2007: *ITRF2005: a new release of the International Terrestrial Reference Frame based on time series of station positions and Earth Orientation Parameters*. J. Geophys. Res., 112, B09401. doi:10.1029/2007JB004949.

Bennett, R.A., Serpelloni E., Hreinsdóttir S., Brandon M.T., Buble G., Basic T., Casale G., Cavaliere A., Anzidei M., Marjonovic M., Minelli G., Molli G., and Montanari A., 2012: *Syn-convergent extension observed using the RETREAT GPS network, northern Apennines, Italy*. J. Geophys. Res., 117, B04408, doi:10.1029/2011JB008744.

Barletta, V.R., Ferrari, C., Diolaiuti, G., Carnielli, T., Sabadini, R., Smiraglia C.; 2006: *Glacier shrinkage and modeled uplift of the Alps*. Geophys. Res. Lett. 33, L14307, doi:10.1029/2006GL026490.

Baldi P., Casula G., Cenni N., Loddo F. and Pesci, A.; 2009: *GPS-based monitoring of land subsidence in the Po Plain (Northern Italy)*. Earth Planet. Science Letts., 288, 204-212, doi:10.1016/j.epsl.2009.09.023.

Baldi, P., Casula, G., Cenni, N., Loddo, F., Pesci, A., Bacchetti, M., 2011. *Vertical ad horizontal crustal movements in Central and Northern Italy*. Boll.Soc.Geol.It. (Ital. J. Geosci.) 52, 4, 667-685.

Bonsignore, F., 2007. *Il monitoraggio della subsidenza a scala regionale in Emilia-Romagna*. Proceedings of the meeting La subsidenza in Emilia-Romagna: Il monitoraggio tramite interferometria satellitare, esperienze a confronto. ARPA, Bologna, Italy. 3 dicembre 2007.

Bonsignore F.; 2008: *Il monitoraggio della subsidenza a scala regionale in Emilia-Romagna*. Arpa Rivista, 1, 16-17.

Bos M.S., Fernandes R.M.S., Williams S. D. P. and Bastos L., 2008: *Fast error analysis of continuous GPS observations*. J. Geod., 82 (3), 157-166, doi:10.1007/s00190-007-0165-x.

Bos M.S., Bastos L. and Fernandes R.M.S.; 2010: *The influence of seasonal signals on the estimation of the tectonic motion in short continuous GPS time-series*. J. Geodyn., 49: 205-209.

Bouin M.N. and Woppelmann G.; 2010: *Land motion estimates from GPS at tide gauges: a geophysical evaluation*. Geophys. J. Int, 180, 193-209, doi: 10.1111/j.1365-246X.2009.04411.x

Bruyninx, C., Kenyeres, A., 2008: EUREF densification of the ITRF2005, EUREF-mail 4142, http://www.epncb.oma.be/ftp/mail/eurefmail.4142.

Calais, E., Galisson, L., Stéphan, J.F., Delteil, J., Deverchère, J., Larroque, C., Mercier de Lépinay, B., Popoff, M., Sosson, M., 2000. Crustal strain in the Southern Alps, France, 1948–1998, Tectonophysics 319, 1-17.

Calais, E., Nocquet, J.M., Jouanne, F., Tardy, M., 2002. Current strain regime in the western Alps from continuous GPS measurements, 1996-2001, Geology 30, 651-654.

Campbell J., Nothnagel A. (2010) *Intra-plate deformation in west-central Europe,* J. of Geodyn., 49, 130-140, DOI: 10.1016/j.jog.2009.10.004.

Champagnac, J.D., Molnar, P., Anderson, R.S., Sue, C., Delacou, B.; 2007: *Quaternary erosion-induced isostatic rebound in the Western Alps*. Geology 35 (3), 195-198, doi: 10.1130/G23053A.1.

Champagnac, J.D., Schlunegger, F., Norton, K., von Blanckenburg, F., Abbühl, L.M., Schwab, M.; 2009: *Erosion-driven uplift of the modern Central Alp*s. Tectonophysics 474, 236–249

Cenni N., Mantovani E., Baldi P. and Viti M.; 2012: *Present kinematics of Central and Northern Italy from continuous GPS measurements*. J. Geodyn., 58, 62-72.

Cenni, N., Viti, M., Baldi, P., Mantovani, E., Bacchetti, M.,Vannucchi, A., 2013. *Present vertical movements in central and northern Italy from GPS data: possible role of natural and anthropogenic causes*. Journal of Geodynamics, 71, 74-85. http://dx.doi.org/10.1016/j.jog.2013.07.004.

Devoti, R., Riguzzi, F., Cuffaro, M., Doglioni, C.; 2008: *New GPS constraints on the kinematics of the Apennines subduction*. Earth Planet. Sci. Lett. 273, 163-174.

Devoti, R., Esposito, A., Pietrantonio, G., Pisani, A.R., Riguzzi, F.; 2011. Evidence of large scale deformation patterns from GPS data in the Italian subduction boundary. Earth Planet. Sci. Lett. 311, 230-241, doi:10.1016/j.epsl.2011.09.034.

Dixon T.H., Miller M., Farina F., Wang H. and Johnson D.; 2000: *Present-day motion of the Sierra Nevada block and some tectonic implications for the Basin and Range province, North American Cordillera*. Tectonics, 19, 1-24.

Dong D., Herring T.A. and King R.W.; 1998: *Estimating regional deformation from a combination of space and terrestrial geodetic data*. J. Geod., 72, 200-214.

Feigl K.L., King R.W. and Jordan T.H., 1990: *Geodetic measurement of tectonic deformation in the Santa Maria fold and thrust belt, California*. J. Geophys. Res., 95, 2679–2699.

Gudmundsson, G.H.: 1994. *An order-of-magnitude estimate of the current uplift-rates in Switzerland caused by the Wurm Alpine deglaciation*. Eclogae Geol. Helv. 87, 545-557.

Guidoboni E. and Comastri A.; 2005: *Catalogue of earthquakes and tsunamis in the Mediterranean area from the 11th to the 15th century.* Istituto Nazionale di Geofisica e Vulcanologia, Roma, pagg. 1037.

Hackl M., Malservisi R., Hugentobler U. and Wonnacott R., 2011: *Estimation of velocity uncertainties from GPS time series: Examples from the analysis of the South African TrigNet network*. J. Geophys. Res., 116, B11404, doi:10.1029/2010JB008142.

Herring T.A., King R.W. and McClusky S.C.; 2010a: *GAMIT Reference Manual, GPS Analysis at MIT, Release 10.4*. Department of Earth, Atmospheric and Planetary Sciences, Massachusset Institute of Technology, Cambridge MA.

Herring T.A., King R.W. and McClusky S.C.; 2010b: *Global Kalman filter VLBI and GPS analysis program,* GLOBK Reference Manual, Release 10.4. Department of Earth, Atmospheric and Planetary Sciences, Massachusset Institute of Technology, Cambridge MA.

Höggerl, N., Stangl, G., Imrek, E., Ruess, D., Zahn, E., Krauss, S.,2012. EUREF 12: National Report of Austria. http://www.bev.gv.at/

King, M.A., Williams, S.D.P., 2009. Apparent stability of GPS monumentation from short-baseline time series, J. Geophys. Res. 114, B10403, doi:10.1029/2009JB006319.

Korup, O., Schlunegger, F., 2009: *Rock-type control on erosion-induced uplift, eastern Swiss Alps.* Earth Planet. Sc. Lett. 278, 278-285.

Lardeaux, J.M., Schwartz, S., Tricart, P., Paul, A., Guillot, S., Béthoux, N., Masson, F.; 2006: *A crustal-scale cross-section of the south-western Alps combining geophysical and geological imagery.* Terra Nova 18, 412-422, doi: 10.1111/j.1365-3121.2006.00706.x.

Lomb N.R., 1976: *Least-Squares Frequency Analysis of Unevenly Spaced Data*. Astrophysical and Space Science, 39, pp. 447-462.

Mantovani E., Viti M., Babbucci D. and Tamburelli C; 2009: *A review on the driving mechanism of the Tyrrhenian-Apennines system: implications for the present seismotectonic setting in the Central-Northern Apennines.* Tectonophysics, 476, 22-40.

Persaud, M., and Pfiffner, O.A.; 2004. *Active deformation in the eastern Swiss Alps: post-glacial faults, seismicity and surface uplift*. Tectonophysics 385, 59-84.

Santamaría-Gómez, A., Bouin, M.N., Collilieux, X., Wöppelmann, G., 2011. Correlated errors in GPS position time series: Implications for velocity estimates, J. Geophys. Res. 116, B01405, doi:10.1029/2010JB007701.

Scargle J.D., 1982: *Studies in Astronomical Time Series Analysis II. Statistical Aspects of Spectral Analysis of Unevenly Sampled Data*. Astrophysical Journal, 263, 835-853.

Schlunegger, F., Hinderer, M.; 2001: *Crustal uplift in the Alps: why the drainage pattern matters.* Terra Nova 13, 425-432.

Stocchi, P., Spada, G., Cianetti, S.; 2005: *Isostatic rebound following the Alpine deglaciation: impact on the sea level variations and vertical movements in the Mediterranean region*. Geophys. J. Int.162, 137-147, doi: 10.1111/j.1365-246X.2005.02653.x.

Stocchi, P., Girometti, L., Spada, G., Anzidei, M., Colleoni, F.; 2009: *Post-Glacial Readjustment, Sea-Level Variations, Subsidence And Erosion Along Italian Coasts*. Boll. Geof. Teor. Appl. 50, 2, 129-144.

Teatini, P., Tosi L. and Strozzi T.; 2011: *Quantitative evidence that compaction of Holocene sediments drives the present land subsidence of the Po Delta, Italy.* J. Geophys. Res., 116, B08407, doi:10.1029/2010JB008122.

Wessel P. and Smith W.H.F.; 1998: *New, improved version of the Generic Mapping Tools released*. Eos Trans. AGU, 79, 579.
Williams, S.D.P., Bock, Y., Fang, P., Jamason, P., Nikolaidis, R-M., Prawirodirdjo, L., Miller, M., Johnson J., 2004. Error analysis of continuous GPS position time series, J. Geophys. Res. 109, B03412, doi:10.1029/2003JB002741.
Williams, S.D.P., 2008. CATS: GPS coordinate time series analysis software, GPS Solutions 12(2), 147-153, doi:10.1007/s10291-007-0086-4.

2D-3D GPR ACROSS THE MT. POLLINO AND CASTROVILLARI FAULTS (SOUTHERN CALABRIA): DRIVING PALEO-SEISMOLOGY RESEARCHES IN A COMPLEX SITE TO INFER QUATERNARY EARTHQUAKES

M. Ercoli[1], C. Pauselli[1], E. Forte[2]
[1]Dipartimento di Scienze della Terra, Università di Perugia, Italy
[2]Dept. of Mathematics and Geosciences, Università di Trieste, Italy

Introduction. The definition of the seismic hazard of major seismogenic fault zones is often reached with the support of geophysical investigations to the geological and paleoseismological studies. Over the last years, paleoseismology investigates the subsurface through trenches realized across the fault branches (Galli *et al.*, 2008) and employing geophysical techniques like 2D-3D Ground Penetrating Radar (GPR) (Liner and Liner, 1997; Mc Clymont *et al.*, 2008; Pauselli *et al.*, 2010, Ercoli *et al.*, 2013). A multidisciplinary approach is particularly recommended on areas classified seismically "***silent***" from relatively long time and representing "seismic gaps". On the other hand, these structures have morphological, geological and structural evidences compatible with the occurrence of past strong earthquakes, therefore any faults inside these "gaps" can be particular interesting for geoscientists in order to assess the seismic hazard. The knowledge of the characteristics and of the seismic behavior of the single fault segments, is fundamental to infer their evolution in the Quaternary age, to delineate which portion shows the highest probability of generate strong events, and to plan mitigation efforts for the area. The Mt. Pollino region can be classified as one of the most apparent "seismic gaps" along the central and southern Apennines seismogenic fault zone (Cinti *et al.*, 1997; Michetti *et al.*, 1997; Valensise and Pantosti, 2001), due to the historical seismicity and the poor "recent" instrumental activity consisting in small/moderate magnitude earthquakes (Ferreli *et al.*, 1994). Anyway, a recent paroxystic seismic activity, characterized by about 3400 seismic events of M>1, including an earthquake of M = 5.0 (2012/10/26, Mormanno) have been recorded during the last two years on the area surrounding Castrovillari, (ISIDe Working Group, INGV, 2010). The Project S1 "Miglioramento delle conoscenze per la definizione del potenziale sismogenetico" (Agreement INGV-DPC 2012-2013, https://sites.google.com/site/progettisismologici/progetto-s1) is a recent integrated project started with two main aims: 1) to improve the base-knowledge for assessing the seismogenic potential of some areas considered of significant interest by the Project Board. 2) to develop innovative methodologies for the study of active faults, with a quantitative approach. The Pollino area, due to these uncertainties in the definition of the seismic hazard, is one of the zones studied during the last year. Among a broad spectrum of research topics and units, the project includes the GPR fault imaging on several sites close to Castrovillari, having different purposes: 1) to define the location and the geologic characteristics of the Quaternary faults in well-know sites; 2) to detect evidences of a geophysical signature interpretable with recent faulting extending the GPR surveys to new study sites; 3) to map these geological structures on thematic maps; 4) to support and drive new paleoseismological surveys.

We collected 2D-3D GPR data on the Mt. Pollino and the Castrovillari Faults (Fig. 1) in several sites. A first 2D-GPR survey was done at the "Grotta Carbone" site in order to calibrate the data with available trench logs (Michetti *et al.*, 1997). The surveys have been extended to other places, like the eastward fault termination close to Civita, finally making an extensive 2D-3D GPR survey to a Southern branch of the Castrovillari fault. In particular the acquisition of 3D data was done to analyze a wider area with a dense recording grids (Grasmueck *et al.*, 2005), in order to provide a data volume suitable to study the geological structure in their actual geometry. We obtained suitable a-priori information then used by the paleoseismologists to efficiently plan and drive the trench excavation.

Geological outline. Geologists and seismologists consider both the Mt. Pollino and the Castrovillari faults as two active, but "silent" structures, anyway capable to potentially generate strong earthquakes. Thanks to geomorphological field observations, paleoseismological analysis and comparison with surface faulting events in the Apennines and nearby regions, the estimated Mmax could be about 6.5-7 degrees. The Pollino area is located in the Calabria region (Southern Italy) and divides the NW-SE trending Southern Apennines from the Calabrian Arc. A crustal extension during the Quaternary age affected the area, generating tectonic basins like the Northest Mercure Basin and the southern Morano – Castrovillari Basin. The area represents the most significant seismicity gap within the southern Apennines (Michetti *et al.*, 1997; Cinti *et al.*, 2002), like analogous "silent" structures in the Central Apennines (Galli *et al.*, 2008) because seismological data don't show historical record of seismic events of M > 5. The W-NW "Pollino fault" and the N-S trending Frascineto/Castrovillari faults (Fig. 1), bound the hangingwall hosts named Morano – Castrovillari basin, filled by about 900 m of sedimentary units like marine rocks (upper Pliocene-lower Pleistocene) and continental deposits (middle Pleistocene to Holocene). These two faults are among the major Quaternary normal faults of the area showing paleoseismological evidences of late Quaternary activity (Michetti *et al.*, 1997; Cinti *et al.*, 1997, 2002). Recently, a seismic sequence including an earthquake of M = 5.0 (2012/10/26) struck in particular the western part of the region (ISIDe Working Group, INGV, 2010).

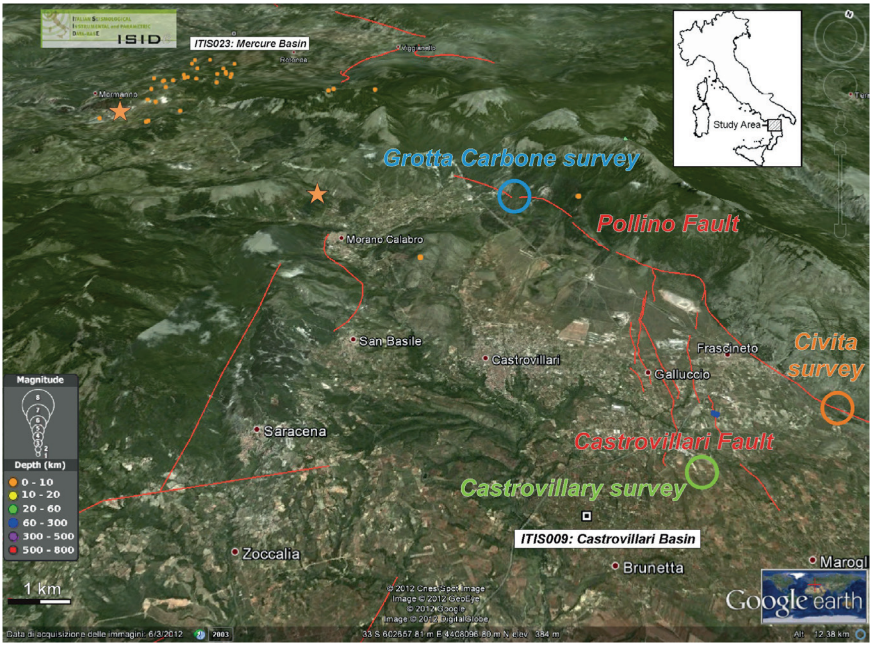

Fig. 1 – View of the study area. The Castrovillari basin shows the main faults alignments with the red lines, highlighted by morphologic fault scarps. The orange points indicate the earthquake locations and magnitude (M > 2.5) occurred between 2011-2013, whilst the two orange stars represent two events with M > 4 (Mormanno, M = 5.0, Morano Calabro, M = 4.3), extracted by the Iside Database. The circles highlight the three principal survey sites on which GPR data were recorded during the project.

2D GPR Survey across the Mt. Pollino Fault (Grotta Carbone site). The "Grotta Carbone" site was chosen for a first 2D-GPR survey across a sector of the Mt. Pollino Fault, due to the availability of past paleoseismological analysis (Fig. 1, Ferreli *et al.*, 1994; Michetti *et al.*, 1997), used to validate the GPR data. More than 10 high-resolution 2D GPR profiles were recorded using a Zond 12e radar system; the profiles have been recorded parallel and very close to the two original trench tracks. 300 and 500 MHz shielded antennas guaranteed an optimal imaging of the fault zone, showing the best trade-off between resolution and investigation depth. The GPR lines were recorded intercepting transversally the fault and to check the lateral extension and other possible branches. The used acquisition parameters are summarized on Tab. 1. A Topcon GR-5 GNSS receiver, connected directly to the GPR system has been employed for the positioning with a centimetric accuracy. The data processing was done using a commercial software (Tab. 1). A recovery function was applied to compensate for the attenuation losses, preserving both lateral and vertical amplitude contrasts. A frequency bandpass filter and 2D average filter were used to reduce noise components and a background removal just on the 500 MHz profiles to remove horizontal ringing. After an accurate topographic correction, a time-depth conversion was done using a constant velocity of 0.08 m/ns, estimated by diffraction hyperbola analysis and tying the radar units with the stratigraphic logs. Finally, we calculated the "Envelope" attribute (Chopra and Marfurt, 2005; Forte *et al.*, 2012), then plotted over the same processed radargram, to provides additional information for data analysis and interpretation, enhancing the high-resolution imaging of the fault zone and sedimentary structures.

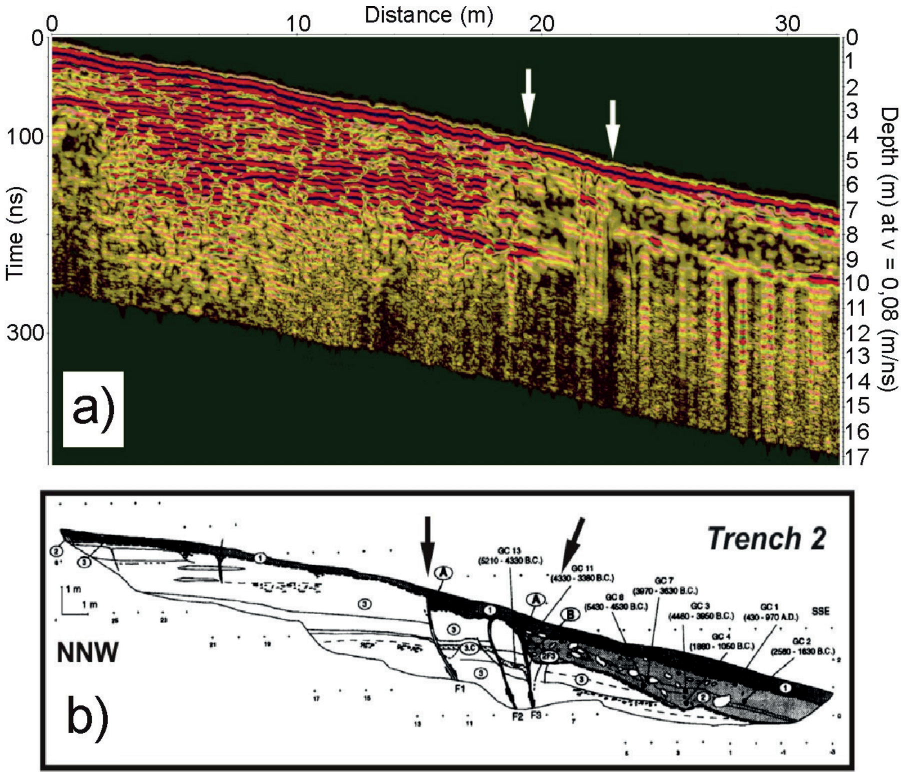

Fig. 2 – a) Envelope attribute calculated for the Grotta Carbone profile and plotted under the processed profile after the time-depth conversion. The discontinuities are enhanced by the combination of different amplitudes and layers bedding, simplifying and improving the overall accuracy in the radargram interpretation. b) log of the trench T2 (from Michetti *et al.*, 1997) is here re-proposed for direct comparison with the radar data.

2D-3D GPR survey across the Castrovillari Fault. A wide number of 2D GPR profiles and a 3D GPR volume were acquired during the last field survey across the Castrovillari fault (Fig. 1). The survey site has been identified by the UR of Dr. Francesca Cinti (INGV), after an accurate geological survey on the area. The same was employed for the data recording. In the present paper only some main results on the preliminary 2D 300 MHz profiles are reported. The 2D profile in Fig. 3a was recorded close to an outcrop showing the studied fault and close to the area on which the 3D GPR acquisition grid was materialized. An inter-trace distance of 0.01 m (Δx) has been used for data recording with both the used antennas. The data have been first processed with a basic flow. The velocity estimation has been defined through an hyperbola diffraction analysis ("hyperbola fitting"): a resulting average velocity value of 0,095 m/ns has been estimated for the investigated subsoil, and then used for the final time to depth conversion. A static ("topographic") correction and a f-k migration algorithm has been applied to the data employing the same velocity, in order to restore the true dips to the reflectors and collapse the hyperbolic diffractions. The fault zone has been better focused in a narrow line at about 22 m, providing reliable information on its geometric characteristics. Fig. 3a illustrates the processed un-migrated profile, more suitable to highlight the fault zone even using the diffractions. Then, a 3D GPR volume has been acquired employing a 300 MHz antenna, employing a distance of 0.1 m between profiles and an inter-trace distance of 0.01 m. The size of the acquisition grid was 5,5 x 20 m, respectively in NW-SE and NE-SW directions, consisting in 56 2D GPR profiles each of 2000 (Fig. 3). The flow used for the data processing was analogous to the one already described for the 2D lines.

Tab. 1 – Table summarizing the main acquisition parameters used for the 2D/3D GPR survey done on the Castrovillary area.

<table>
<tr><th>Acquisition parameter</th><th rowspan="2">Time window (ns)</th><th rowspan="2">Estimated RelativeDielectric Permittivity (ε_r)</th><th rowspan="2">Total number of samples for trace (n°)</th><th rowspan="2">Inter-trace distance (m)</th><th rowspan="2">Profile distance (3D data) (m)</th></tr>
<tr><th>Antenna Central Frequency</th></tr>
<tr><td>300 MHz</td><td>200/300</td><td>14 (Pollino)</td><td>512/1024</td><td>0.05/0.01</td><td>0.10 (Castrovillari)</td></tr>
<tr><td>500 MHz</td><td>100/200</td><td>10 (Castrovillari)</td><td>512/1024</td><td>0.01</td><td>/</td></tr>
</table>

Integrated interpretation of the 2D/3D data. The available trench data in Fig. 2b across the Mt. Pollino fault (Grotta Carbone site) have been extended in length as well as in depth by the GPR profiles, imaging the geological structures and the fault zone with high-resolution. The original stratigraphic information about the units described by Michetti *et al.* (1997) as alluvial fan deposits (Pleistocene) were highlighted in depth by a discontinuity dividing gentle inclined bedding on underlying dipper layers (Fig. 2a, 100 ns): these can be interpreted as an older unit belonging to the alluvial fan deposits, like a seismic "bedrock", compatible with the high probing depth investigated. The attribute analysis helps the visual interpretation of the tectonic discontinuities and the sedimentary units, which can be accurately deduced and easily followed. The fault offset can be estimated from some steps separating the colluvial materials on the fault hanging wall, that looks like "transparent" to the radar energy due to the strong reflection of the continuous basal reflector, comparable with the one of the foot wall units (Fig. 2a,b). Some geophysical signatures already observed in literature by some authors (Liner and Liner, 1997; Bano *et al.*, 2002; Pauselli *et al.*, 2010; Ercoli *et al.*, 2013) were identified, like relative differences in signal amplitude, attenuation of the radar units, interruptions of the lateral continuity and dip of the reflectors, diffraction hyperbolas (in un-migrated data) and also a different character of the direct arrivals. The different geological units can be therefore interpreted and mapped, and some parameters can be extracted by the radargrams, like the layers thickness, bedding and the fault offset, of about 1 meter at 23 m along the profile (white arrow on the right in Fig. 2a).

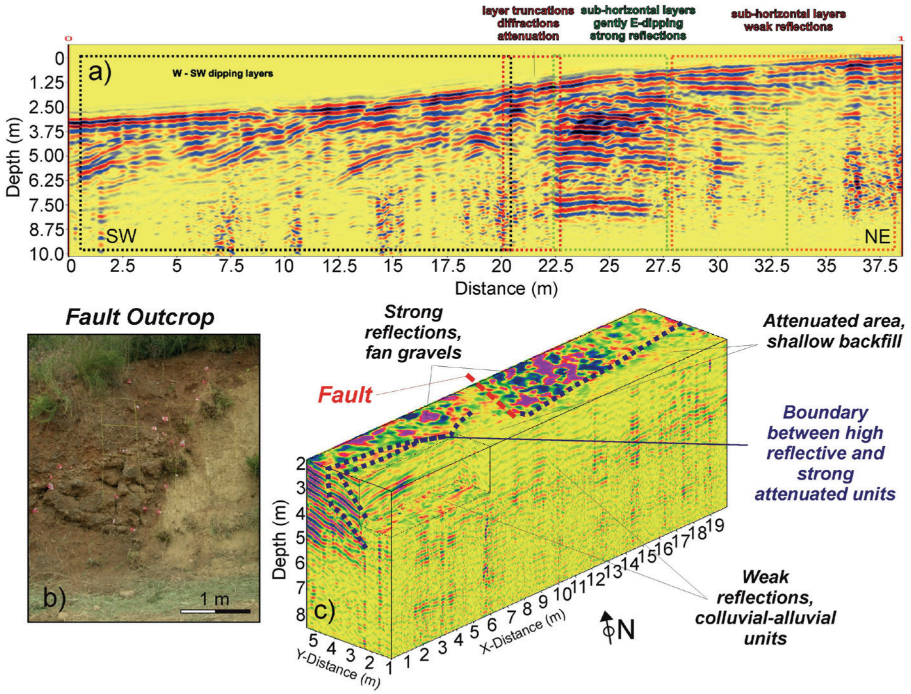

Fig. 3 – 2D and 3D GPR data recorded on the Castrovillari site. a) Un-migrated 2D profile shows different areas within the dashed boxes, where the fault zone, characterized by a well defined signature, has been highlighted by the red one. b) Field picture reporting the fault on the outcrop. c) The 3D data show both the fault located at about 10 m along the GPR volume (X axis), and the different units detected in this complex site, like the shallow backfill layers and the colluvial/alluvial deposits corresponding with the attenuated side.

The 300 MHz radargram here reported for the Castrovillari survey shows a good S/N ratio and signals suitable for an efficient geological interpretation (Fig. 3a). This can be ideally divided in four sectors, having different characteristics: in the SW sector between 0-20 m (black box) some W-SW dipping reflectors are visible over a sub-horizontal unit at about 2 m of depth from the topographic surface. That geometry is compatible with a transversal section of the lentiform sedimentary bodies belonging to N-S alluvial fan: such layers are also well-visible on outcrops close to the survey site. The red box highlights an area characterized by the presence of some diffractions (in unmigrated data) and an interruption of the lateral continuity among the reflectors, which represents a peculiar geophysical signature of a fault. The diffractions are probably generated by the high dipping "fault plane" and the lateral stratigraphic contact between two materials having different dielectric properties, probably including cemented filling and/or cemented "blocks" within the faulted units (like in the outcrop picture in Fig. 3b).The fault is highlighted also by the different electrical response of the subsurface within the foot-wall and hanging-wall sectors, and by the stronger signal attenuation compared with the surrounding areas. The unit enclosed in the green box (Fig. 3a) is high reflecting with sub-horizontal layers, gently NE-dipping: this is interpretable as a sort of "bedrock", probably related to a cemented unit. Finally, some weak reflecting reflectors are imaged in the Eastern sector of the radargram (fault hanging-wall, orange box about between

28-38 m, Fig. 3a). These are layered over the high reflective unit and can be correlated with the ochre sands mapped on the nearby outcrop (Fig. 3b). The combined analysis of the 3D GPR volume on vertical sections and depth slices provide an optimal visualization and imaging of the structures, highlighting a sector of the volume between the interval 2.5-5.5 m in the NW-SE direction (Y axes), where the geological structures are clearly defined (limited by a blue dashed line in fig. 3). In the area ranging from 0-3 m, with the exception of the shallower layers (0-40 ns), the structures are not well defined in depth due to a strong attenuation of the GPR signal. The boundary between the two zones in the 3D volume is sharp and easily detectable, and it separates two units showing very different electric properties. The North sector of the volume, located close to the scarp in field, highlights the discontinuity between the reflectors interpretable with the fault zone at about 10 m along the profiles (along the SW-NE direction, from SW to NE). In addition to this discontinuity, some diffractions already described in the 2D profile, represent features defining a characteristic geophysical signature of the fault zone. Fig. 3c reports a close-up obtained trough a depth-slice at about 2 m. Though the management and the interpretation of the whole volume at different depth, the fault zone visible also in the nearby outcrop was localized with high-resolution, extending in depth the morphological and geological surface data and providing new data useful for further paleoseismological analysis. Some quantitative and geometrical characteristics of the fault zone and others considerations about the sedimentary units can be done: a mean dip-direction has been estimated in about 235°, whilst the dip angle was close to 70°. These values are in agree with ones provided after the further ground-truth done on the site by the INGV research group of paleo-seismologists (UR Cinti). The new trench was focused across the two areas showing different GPR signature, intercepting both the fault and the sharp boundary highlighted by the 3D GPR volume, ensuring a successful data validation about the geometric characteristic of the fault. The blue dashed boundary therefore actually represents the separation between the natural subsoil nearby the scarp (fan deposits) and progressively thicker backfill layers located above the road on the survey site. The latter resulted stratified above a colluvial-fluvial unit originated by the erosion and re-sedimentation of a NE-SW stream, which generated the small NE-SW valley where the 3D data were acquired.

Discussion and conclusions. The 2D/3D GPR "Grotta Carbone" and "Castrovillari" datasets highlighted characteristic geophysical signature of fault zones, efficiently defining the tectonic structure through some features like lateral truncations of layers, different dip of the reflectors on the two sides of the fault, presence of diffraction hyperbolas (un-migrated data) and a narrow strong attenuated zone. Some others considerations can be done on the areas surrounding the fault zone. The survey site shows reflectors having a W-dipping direction trend, excepted for the NE sector of the radargrams, where the layers are gently E-dipping. The 3D GPR analysis highlights how the S-SE sector of the acquisition is characterized by electrical properties of the investigated materials, which prevent to image geological structures in the S-SE side due to strong signal attenuation. Close to the outcrop (scarp), already from about half of the survey grid, both the fault zone and the sedimentary layers are well imaged by the data. The subsoil between the scarp and about 3 m towards South, is characterized in the first 3 m of depth by strong E-dipping reflectors. Some vertical sections and the depth-slices illustrate this unit is laterally extending in depth but then abruptly interrupted, probably due to the erosion / re-sedimentation operated by a pre-existent stream. In the shallow part a boundary with some backfill layers filling the valley, probably produce high attenuation and low amplitude reflections, reducing the investigation depth and complicating the visualization/interpretation within this sector. The structures interpreted in the 2D GPR sections and 3D GPR volume, like the fault zone, some important layers and stratigraphic units have been successively validated by the trench excavation. The trench revealed a correct geophysical interpretation not only of the geometrical characteristic of the fault (strike, dip direction, dip angle), but also of the lateral boundary visible in the depth-slices (backfill, alluvial deposits…etc). The survey represents an effective case history of GPR application on the study of geological discontinuity as faults and fractures, but also efficient in the characterization of the related sedimentary structures: the technique is fundamental to provide both suitable "a-priori" information to plan and optimize a further paleoseismological survey and to potentially extend the data on a wider area. This work therefore represents a successful example of how a GPR survey can be for paleoseismological studies, providing a detailed geological model of the subsurface by the interpretation of high-resolution 3D GPR volume and 2D sections, also improved by a basic attributes calculation like in the "Grotta Carbone" case. It represents a valuable tool to detect, though the interpretation of typical radar signature, a Quaternary fault zone and the sedimentary structures, both to define in a non invasive way, the optimal area for future trenches, and to extrapolate complementary information to derive an improved geological model. These detailed results provided on tectonic and stratigraphic information are comparable and complementary with the ones provided by the trenches stratigraphies, therefore suitable to the paleoseismologists to efficiently plan and drive a new trench excavation on the studied Castrovillari site. GPR data can be extensively used where there is a lack of geological information and the results of data interpretation can improve the definition of the seismic hazard of an area, proving a base suitable to plan valid actions for the prevention and the mitigation of the earthquake risks. The interpreted faults can be then potentially added to detailed structural and geological maps thanks to the centimetric accuracy of the geographic coordinates provided by the GNSS receiver linked to a NRTK correction.

Acknowledgements. We wish to thank Leonardo Speziali, for his indispensable contribution during the field surveys, Alessandro Maria Michetti and Livio Franz for the preliminary field trip on the study site and for the geological framework provided, the whole Cinti UR for sharing the trench excavation data and Roberto Volpe for the help provided in data acquisition and processing.

References

Bano M., Edel J.-B., Herquel G. and EPGS class 2001-2002; 2002. *Geophysical investigation of a recent shallow fault,* The Leading Edge, 21:7, 648-650.

Chopra S. and Marfurt K. J.; 2005: *Seismic attributes - A historical perspective*. Geophysics, **70**:5, 3SO-28SO.

Cinti F. R., Cucci L., Pantosti D., D'Addezio G. and Meghraoui M.; 1997: *A major seismogenic fault in a 'silent area': the Castrovillari fault (southern Apennines, Italy)*, Geophysical Journal International, **130**:3, 595-605.

Cinti F. R., Moro M., Pantosti D., Cucci L. and D'Addezio G.; 2002: *New constraints on the seismic history of the Castrovillari fault in the Pollino gap (Calabria, southern Italy)*, Journal of Seismology, **6**, 199-217.

Ferreli L., Michetti A. M., Serva L, Vittori E. and Zambonelli E.; 1994: *Terremoti olocenici lungo la Faglia de1 Pollino (Calabria Settentrionale): nota preliminare*, Paleosismologia e pericolosità sismica: stato delle conoscenze ed ipotesi di sviluppo, ed. A. M. Michetti, CNR-GNDT (Gruppo Nazionale per la Difesa dai Terremoti) Rendiconti **2**, 65-88.

Galli P., Galadini F. and Pantosti D.; 2008: *Twenty years of paleoseismology in Italy.* Earth-Science Reviews, **88**:1-2, 89-117.

Grasmueck M., Weger R., Horstmeyer H.; 2005: *Full-resolution 3D GPR imaging*. Geophysics, **70**:1, K12-K19.

Ercoli M., Pauselli C., Frigeri A., Forte E., Federico C., 2013. "*Geophysical paleoseismology" through high resolution GPR data: A case of shallow faulting imaging in Central Italy*, Journal of Applied Geophysics, **90**, 27-40.

Forte E., Pipan M., Casabianca D., Di Cuia R. and Riva A.; 2012: *Imaging and characterization of a carbonate hydrocarbon reservoir analogue using GPR attributes*, Journal of Applied Geophysics, Special Issue: Recent, Relevant and advanced GPR studies in Applied Geophysics, **81**, 76-87.

ISIDe Working Group INGV; 2010: *Italian Seismological Instrumental and parametric database*: http://iside.rm.ingv.it

Liner C. L. and Liner J. L.; 1997: *Application of GPR to a site investigation involving shallow faults*, The Leading Edge, **16:11**, 1649-1651.

McClymont A. F., Green A. G., Villamor P., Horstmeyer H., Grass C., and Nobes D. C.; 2008: *Characterization of the shallow structures of active fault zones using 3-D ground-penetrating radar data*, J. Geophys. Res., **113**.

Michetti A. M., Ferreli L., Serva L. and Vittori E.; 1997: *Geological evidence for strong historical earthquakes in an "aseismic" region: The Pollino case (Southern Italy)*, Journal of Geodynamics, **24**:1-4, 67-86.

Pauselli C., Federico C., Frigeri A., Orosei R., Barchi M.R. and Basile G.; 2010: *Ground Penetrating Radar investigations to study active faults in the Norcia Basin (Central Italy)*. Journal of Applied Geophysics, **72**:1, 39-45.

Valensise, G. and Pantosti D.; 2001: *Seismogenic faulting, moment release patterns and seismic hazard along the central and southern Apennines and the Calabrian Arc*, G.B. Vai & I.P. Martini (editors), Anatomy of an orogen: the Apennines and adjacent Mediterranean basins. Kluwer Academic Publishers, Dordrecht, 495-512.

MORPHOLOGICAL EVIDENCES OF TECTONIC TILTING IN NE SICILY

F. Pavano
Dipartimento di Scienze Biologiche, Geologiche ed Ambientali, Università degli Studi di Catania, Italy

Introduction. The NE-Sicily, the southern termination of the Calabrian arc, represents a discrete crustal mobile block (**PMB -** Peloritani Mobile Block; inset in Fig. 1a) diverging towards the NNE from the rest of the Sicilian collision zone and moving independently from rest of the Calabrian arc (Hollenstein *et al.*, 2003; D'Agostino and Selvaggi, 2004). The marine terraces analysis suggests that this crustal block, since the Middle-Pleistocene (~600 ka) experienced a homogeneous uplift constraining a long-term uplift-rate of about 1.1 ± 0.13mm/a, respect to the 0.76 ± 0.05 mm/a measured for the surrounding areas. This change in uplift-rate is accommodated, to the SW, by several NW-SE-oriented normal fault segments, showing rejuvenated fault scarps and providing a short-term vertical displacement-rate of about 0.4-0.5 mm/a. In correspondence of the south-western portion of the **PMB** a drainage system analysis has been carried out in order to recognized the morphological effects due to local tectonic deformation occurred along the NW-SE oriented faulted belt. Several morphometric features of fluvial network and drainage basins, like basins lateral asymmetry, fluvial hierarchical anomalies and drainage system arranging, have been analyzed. The results of these analysis, show that, since the Middle-Pleistocene, the southwestern portion of **PMB**, underwent a NE-ward tectonic tilting, complying and geomorphometrically confirming the NW-SE oriented, SW-dipping, normal faults activity.

Tectonic and seismotectonic setting. The NE Sicily is located at the southern termination of the Calabrian Arc, at the intersection between the Neogene Sicilian collision belt and the incipient Siculo-Calabrian Rift Zone (**SCRZ** – Catalano *et al.*, 2008) (Fig. 1a). The NE Sicily represents an orocline that during the Neogene-Quaternary age has been involved in two main stages of deformation. During the first one, the Calabrian Arc experienced a lateral extrusion towards to the south-east (Boccaletti *et al.*, 1990), accommodating the hinge retreat of the Ionian slab. This process caused the development of a wide system of NW-SE and WNW-

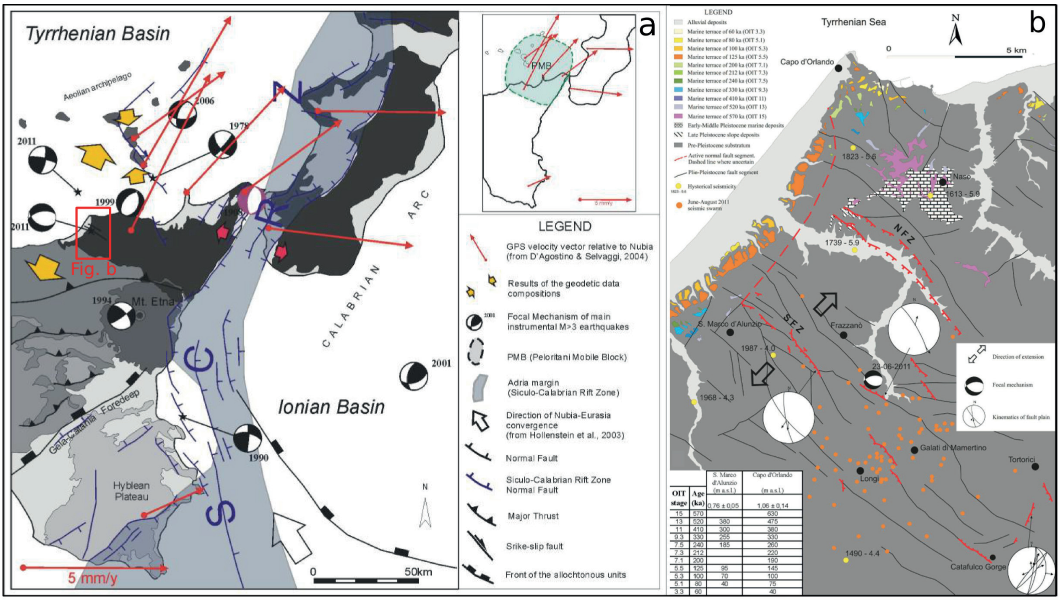

OIT stage	Age (ka)	S. Marco d'Alunzio (m a.s.l.)	Capo d'Orlando (m a.s.l.)
		0,76 ± 0,05	1,06 ± 0,14
15	570		630
13	520	380	475
11	410	300	380
9.3	330	255	330
7.5	240	185	260
7.3	212		220
7.1	200		190
5.5	125	95	145
5.3	100	70	100
5.1	80	40	75
3.3	60		40

Fig. 1 – a) Seismotectonic sketch map of Sicily and southern Calabria, displaying the main Quaternary tectonic features and their relationships with plate boundary. The inset shows the location of the PMB (Peloritani Mobile Block); b) Active tectonics and Pleistocene deposits at the SW margin of PMB. The inset shows the absolute elevation (m a.s.l.) of the marine terraces recognised in this area.

ESE oriented right-lateral shear zones that disjointed the SE-verging orogenic belt (Finetti *et al.*, 1996; Lentini *et al.*, 1996). These processes have been linked to the differential roll back between continental crust of the northern termination of the Nubia plate, facing the Sicilian collision zone, and the adjacent less resistant oceanic crust of the Ionian slab, sub-ducting beneath the Calabrian Arc.

Starting from about 600 ka B.P. the whole NE Sicily has been characterized by a huge tectonic uplift, disengaging from the surrounding domains. The main fault systems that define the **PMB** have been partially identified, someone of which has been thoroughly studied. To the east, the **PMB** is bordered by a relevant off-shore NE-SW oriented faults (Taormina Fault) belonging to the **SCRZ** (Catalano *et al.*, 2008), the whose effects of activity are already recognizable along the near Ionian on-shore. The south-western margin of **PMB**, as also evidenced by geodetic data (Hollenstein *et al.*, 2003; D'Agostino and Selvaggi, 2004) (Fig. 1a), corresponds to a narrow NW-SE oriented fault belt at the Nebrodi-Peloritani boundary (Fig. 1b), represented by a set of normal fault segments showing morpho-structural evidences of Holocene activity (Pavano *et al.*, 2012). Except for some seismic profile, carried out in the Tyrrhenian off-shore, and some seismological data, the location of the north-eastern and north-western edges of the mobile block is quite uncertain.

Recently (June-September 2011) the area around Longi and Galati Mamertino villages has been affected by a swarm of medium-low magnitude seismic events. The main event (M = 4.1 – ISIDe Working Group, 2011) provided a focal mechanism showing a NNE-SSW oriented extension (Fig. 1b), according to the geodetic data. The linkage between this seismic swarm and the fault-controlled south-western border of the mobile block, has been hypothesized.

A meso-scale structural field investigation has been carried out in order to analyse and kinematically define several normal fault segments. The segments located to the south of Naso village, near Capo d'Orlando (**NFZ** in Fig. 1b), are characterised by a 2 m high scarp, clearly displacing the Recent (Holocene) talus. Further well defined rejuvenated fault scarps have been recognized between S. Marco d'Alunzio and Galati Mamertino villages (Fig. 1b), belonging to a 8.5 km-long fault zone (San Marco d'Alunzio Fault Zone – **SFZ**, Fig. 1b; Pavano *et al.*, 2012). These are charcterized by 3-5 m high, SW facing fresh bedrock scarp, marked by a basal light coloured strip as an evidence of their Holocene activity (Benedetti *et al.*, 2002; Palumbo *et al.*, 2004). Kinematic markers with pitch of 80° observed on the fault plane, constrain a normal sense of motion. Normal movement indicators (pitch 80°), superimposing on ancient dextral kinematic striations (Pitch 160°), has been found along the fault plane of an associated 3 m-high, 2 km-long antithetic segment.

More to the southeast, further fault segments, showing 2-3 m-high fresh bedrock scarps, have been recognised (Fig. 1b). In the surrounding area of Tortorici, an antithetic 1600 m long, N140° oriented, rejuvenated fault scarp shows clear rests of welded fault breccias along its 3 m high fault plane, as a further evidence of recent activity. Kinematic indicators measured along this latter indicate a normal sense of the deformation (pitch 90°).

Finally, in the same area two measurement sites have been located along a N10 directed, E-dipping, more than 1500 m long fresh bedrock scarp. On these sites striations and accretion and fracture steps indicate both dextral (pitch= 30°) and more recent normal (70-80°) motions.

Morphostructural analysis. The tectonic uplift involving the **PMB** is evidenced in NE Sicily by the presence, around the coastal area, of a marine terraces flight assigned to the Oxygen Isotope Stage (OIS) from 15 (570 ka) to 3 (60 ka) (Catalano and Di Stefano, 1997). Along the Tyrrhenian coast, from Capo d'Orlando to Capo Rasocolmo (Catalano and Cinque, 1995; Catalano and Di Stefano, 1997), the ancient NW-SE and NNW-SSE oriented dextral faults are crossed without interruption, strongly indicating an almost uniform elevation of strandlines around the **PMB**. In contrast, along the Ionian side of **PMB** the elevation of the Late Quaternary marine terraces is extremely variable, due to the huge faulting-related deformation at the footwall of the Taormina Fault.

The marine terraces analysis enables to determine an evaluation of the long-term uplift-rate involving the region since the Middle-Pleistocene (~600 ka). Along the Ionian coast, starting from the Alcantara River mouth the values of uplift-rate switch from 0.9 to 1.1 mm/a towards the NE, near Messina area (Catalano and De Guidi, 2003). Between this two localities the uplift-rate values reach a maximum value of about 1.7 mm/y, ascribable to the Taormina fault activity.

Along the western side of the Tyrrhenian coast of the **PMB** a sharp variation of the long-term uplift-rate has been found between the Capo d'Orlando and San Marco d'Alunzio areas. In particular, in correspondence of the **PBM** side has been calculated an uplift-rate of 1.1 ± 0.13 mm/a switching to 0.76 ± 0.05 mm/a to the south (inset in Fig. 1b). This 0.3-0.4 mm/y gap is significantly in accordance with the short-term deformation rate (0.4-0.5 mm/a) calculated on the basis of the above discussed structural analysis.

In addition has been calculate the variation of the uplift-rate between the **PMB** and the southern area, getting a reconstruction of the trend in time of the deformation-rate along the studied faulted zone. As constrained by the obtained data, after an early decrease, lasted until OIS 7.1 (200 ka), starting from the period elapsing between this latter and the OIT stage 3 (125 ka) the deformation-rate along the faulted zone increased from 0.15 to 0.45 mm/a.

Morphometric analysis. A morphometric analysis regarding the drainage system of the south-western sector of the **PMB** has been carried out. This analysis firstly consisted of a semi-quantitative study of the fluvial network of main drainage basins, roughly NW-SE oriented and flowing to the NW. In addition to defining the relationships between fluvial network and both the faults of the region and the rejuvenated Holocene fault segments, a morphometric characterization of basins has been performed, based on appropriate morphometric indexes generally exploited for tectonic geomorphology studies. The obtained data, as a whole, enable to understand how the Late Quaternary tectonic deformation has driven the landscape evolution and the fluvial network arrangement.

Basins asymmetry. Since the studied area is affected by a NW-SE oriented SW-dipping normal faults system, defining several faulted blocks, it was reasonable expecting a tectonic tilting towards the north-east. In order to detect and numerically evaluate the tectonic tilting of the region, it was applied an useful index employed in region involved in neo-tectonic processes (Hare and Gardner, 1985; Cox, 1994); it is represented by the Asymmetry Factor (**AF**) of the drainage basins (Hare and Gardner, 1985). In the studied sector of the **PMB**, regardless of hierarchical order, were analysed 10 basins in order to cover as much as possible the investigated area. The results (<50%) suggest an almost significant asymmetry of basins to the right (facing downstream) constraining a NE-ward tectonic tilting (Fig. 2a). Only a small basin shows an AF value slightly more than 50%. The valleys asymmetry, associated with the NE-ward tilting of the faulted-blocks, testifies the tectonic deformation cumulated along the NW-SE oriented, SW-dipping, normal faults. Another asymmetry index is represented by the Transverse Topographic Symmetry Factor (**T**) (Cox, 1994), whose obtained values confirm the AF data, providing a more detailed distribution of asymmetry along the basins (Fig. 2a).

Across the faulted belt several NE-directed swath profiles have been realized (Fig. 2b). It is possible to firstly appreciate the NE-ward tilted summit surfaces of the landscape, dislocated by SW-dipping faults, and the clear NE-ward asymmetry of the transverse subsequent valley, showing their northern flank steeper than the southern one.

Fluvial network arrangement analysis. The fluvial network analysis has been performed for the main basins lying on the south-western side of the **PMB** and flowing towards to the Tyrrhenian sea. After the reconstruction of the fluvial network, the stream system has been hierarchized as proposed by Strahler (1958). Afterwards sectioning the streams in several trunks, each fluvial hierarchical order, from 1 to 7, has been separately processed. The same procedure has been followed for the tectonic structure that lie inside the studied area and for the Holocene fault scarps recognized within the aforementioned faulted zone. Firstly, the analysis has focused on the rivers azimuthal distribution, in order to understand the relationships between faults and drainage system arrangement.

The data show that the overall faults and active faults segments have the same NW-SE preferential orientation, at about N140-150° (Fig. 2c). This means that the fresh bedrock scarps are the result of the reactivation of previous faults, in accordance with the collected kinematics data measured along the fault planes. The azimuthal distribution of the subsequent IV-VII orders streams, show a clear main direction of about N130-150° (Fig. 2c), coincident with the azimuthal orientation of the overall faults. In contrast, this analysis indicates that the I-III order streams are widely distributed, with a slightly marked main direction focused between 30° and 50° (Fig. 2c), perpendicularly to the main faults. This group of streams would include both relicts of the heads of basins of the ancient drainage system and the new tributary channels flanking the NW-pointed subsequent streams.

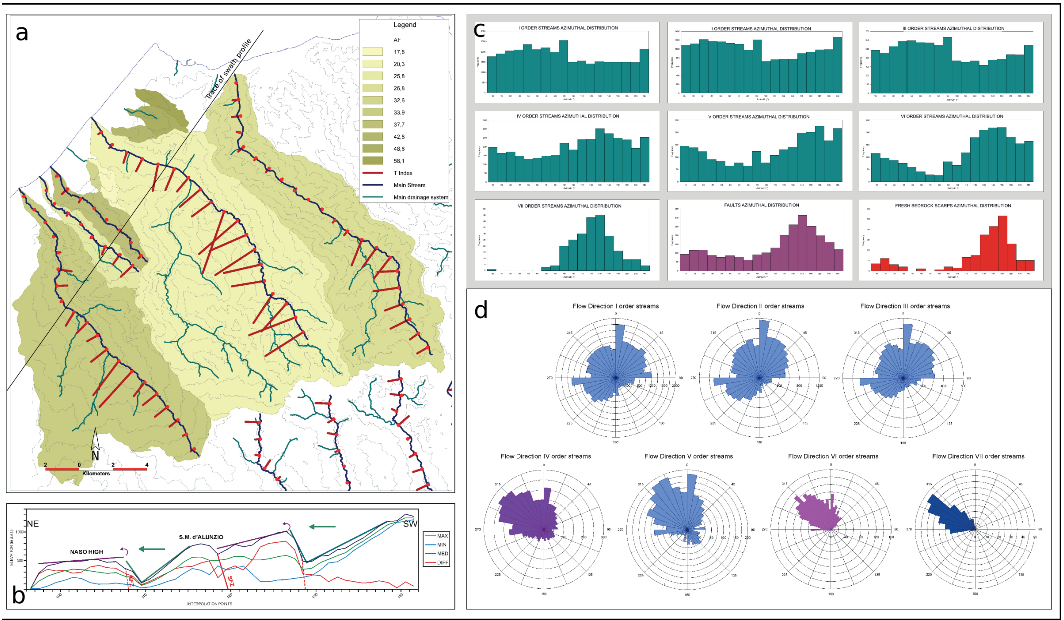

Fig. 2 – a) AF map of the main drainage basins in the SW sector of the PMB. The map also shows the results of the T index. b) NE-SW oriented swath profile across the faulted belt; the trace of the profile is showed in Panel a. c) Azimuthal distribution of fluvial streams distinguished by hierarchical order (green bars), azimuthal distribution of faults (violet bars) and active faults recognized in the studied area (red bars). d) Flow directions of streams calculated for different hierarchical orders.

In order to thoroughly understand the relationships between the faults activity, the behaviour of the drainage system and the fluvial network arrangement, a more detailed analysis has regarded the evaluation of the streams flow-directions (rose diagrams in Fig. 2d). The results, obtained for several streams of different hierarchical orders, show that the IV-VII order subsequent streams flow towards the north-west. In contrast, the flow-direction orientations of the I-III order channels show anomalous differences between the streams flowing towards the northern sector and those flowing towards the southern one. The first group covers a 180° wide range of directions, without a clear main value, while the channels flowing to the opposite sense are mostly confined in a narrow azimuthal range, focusing between 200° and 270° (Fig. 2d).

These anomalous distributions has been explained considering that the streams pointing towards the northern sector are represented by both sub-sequent and re-sequent channels belonging to an inherited drainage system. In addition, they result from fluvial captures of previous smaller basins that complied in time the NE-ward tilting of the faulted blocks.

In contrast, the channels pointing towards the southern sector are channels developed on the steeper cumulative SW-dipping fault slope, locally coincident with the right hillside of the valleys.

Furthermore, a morphological local effects of the Late Quaternary tectonic deformation along the studied sector of the **PMB** is represented by a well defined distribution of the basins extent values (Fig. 3a). In order to carry out this analysis, the III order basins has been taken into account, due to their more homogeneous spatial coverage. In particular, the smaller basins are concentrated close to the faults, in correspondence of their SW-dipping cumulative slope, while the larger III order basins lie on wider and flatter surfaces of the opposite flank of the valleys. These evidences highlight a different significance and evolution history between the two group of basins with the same hierarchical order.

The landscape of the studied area, as well as being dominated by the effects of the regional deformation (marine terracing, river entrenching), is characterized by local fault-controlled morphological features connected to the tilting of faulted blocks, such as the diffuse and wide N/NNE-ward fluvial captures. Each captured fluvial channel, flowing from the uplifted sector towards the depressed areas of the tilted blocks, caused a rearrangement of the drainage system. The main effects of this geomorphological processes are represented by an increase in terms of hierarchical orders of the subsequent valleys and the consequent decrease in order of the hosting streams. As a consequence, the forced phase of the drainage system reorganization determined the development of fluvial network anomalies through the tilted blocks, as showed by the distribution of the Hierarchical Anomaly Index (**Da**) (Avena *et al.*, 1967) calculated for the III order basins (Fig. 3b).

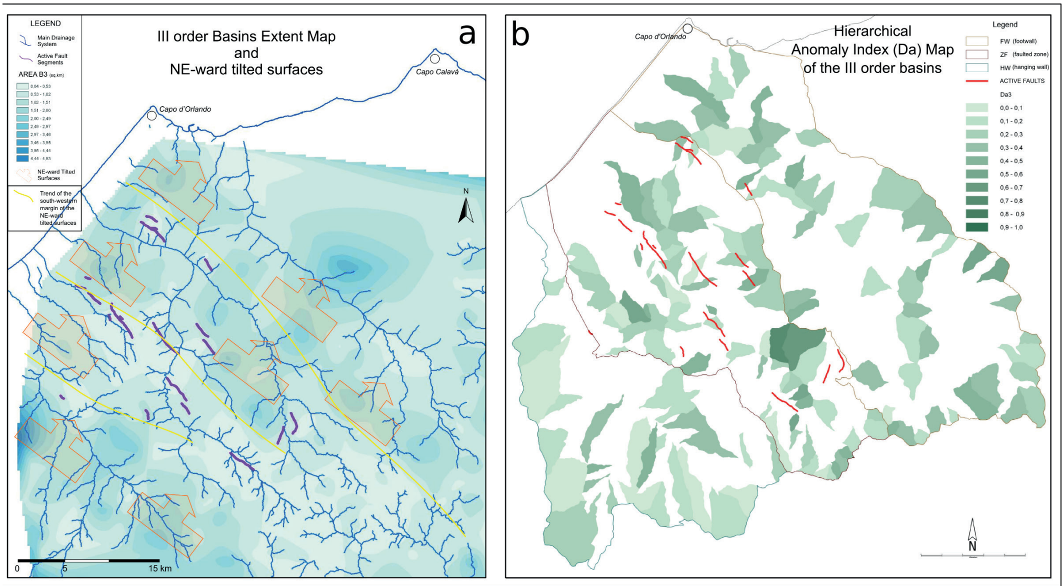

Fig. 3 – a) Map of the distribution of the III order basins extent displaying the NE-ward tilted surfaces. b) Hierarchical Anomaly Index (Da) Map calculated for the III order basins.

Discussion and conclusions. The NE Sicily can be designed as a crustal mobile block (**PMB**) diverging towards the NNE respect to the rest of the Sicilian collision belt (Hollenstein, 2003), disengaging from the rest of the Calabrian Arc. As suggested by the analysis of the marine terraces carved along both the Tyrrhenian and Ionian coasts of NE Sicily, starting to the Middle-Pleistocene the **PMB** has experienced a huge uplift inferring a difference in uplift-rate of about 0.3-0.4 mm/y between the **PMB** (~1.1 mm/a) and the surrounding area (~0.75 mm/a).

Along the south-western margin of the **PMB** this divergence in uplift is accommodated by a 10 km wide normal fault zone, represented by several NW-SE oriented, SW dipping fault segments that show clear evidences of Holocene activity, such as 2-5 m high fresh bedrock scarps (Pavano *et al.*, 2012), that recently was home of a low magnitude (M = 4.1, INGV) seismic swarm (June-September 2011). The tectonic deformation inferred a NE-ward tilting of several faulted blocks, imprinting the main features of the landscape, such as the drainage system.

The morphometric analysis reveals evidences of huge fluvial captures, picturing a rearrangement of the fluvial network as a consequence of the tectonic tilting. The inherited main sub-sequent rivers, identified as the IV-VII order streams and flowing to the NW, maintained their orientation pushing to the NE the earlier symmetry of their basins. As regarding the I-III order streams, they should be considered as two main groups, distinguished on the basis of the flow direction data. The first group regards the streams pointing to the northern sectors, that, in addition to including streams inherited from the heads of previous basins, have complied the NE-ward tectonic tilting. This resulted in an increase in terms of length and basin extension. The second group is represented by steeper and shorter streams, flowing towards the SW as ob-sequent side streams, developing, as also evidenced by the NE-SW oriented swath profile, in correspondence of cumulative SW-dipping fault slope.

The rightward basins asymmetry, the N-pointed fluvial captures, the NE-ward tilting of the summit surfaces and the general rearrangement of the fluvial network through the faulted block represent the morphological response of Late Quaternary tectonic activity occurred along the NW-SE oriented, SW-dipping normal faults, that bound the south-western margin of the **PMB**. These evidences enable to conclude that the active tectonic processes affecting the NE-Sicily since the Middle Pleistocene, strongly influenced the landscape evolution of the region, and in particular the drainage system.

References

Avena G.C., Giuliano G. and Lupia Palmieri E.; 1967: *Sulla valutazione quantitative della gerarchizzazione ed evoluzione dei reticoli fluviali*. In: Boll. Soc. Geol. It., 86.

Benedetti L., Finkel R., Papanastassiou D., King G., Armijo R., Ryerson F.J., Farber D. and Flerit F.; 2002: *Post-glacial slip history of the Sparta fault /Greece) determined by 36Cl cosmogenic dating: evidence for non-periodic earthquakes*. In: Geophys. Res. Lett., 27.

Boccaletti M., Nicolich R. and Tortorici L.; 1990: *New data and hypothesis on the development of the Tyrrhenian basin*. In: Paleogeog. Paleoclimat. Paleoecol., 77, 15-40.

Catalano S. and Cinque A.; 1995: *L'evoluzione neotettonica dei Peloritani settentrionali (Sicilia nord-orientale): il contributo di una analisi geomorfologica preliminare*. In: Studi Geologici Camerti, Vol. Spec. 1995/2, 113-123.

Catalano S. and De Guidi G.; 2003: *Late Quaternary uplift of northeastern Sicily: relation with the active normal faulting deformation*. In: Journal of Geodynamic, 36, 445-467.

Catalano S., De Guidi G., Monaco C., Tortorici G. and Tortorici L.; 2008: *Active faulting and seismicity along the Siculo-Calabrian rift zone*. In: Tectonophysics, 453, 177-192.

Catalano S. and Di Stefano A.; 1997: *Sollevamento e tettogenesi Pleistocenica lungo il margine tirrenico dei Monti Peloritani: integrazione dei dati geomorfologici, strutturali e biostratigrafici*. In: Il Quaternario, 10, 337-342.

Cox R.T.; 1994: *Analysis of drainage basin symmetry as a rapid technique to identify areas of possible Quaternary tilt-block tectonics: an example from the Mississippi Embayment*. In: Geological Society of America Bulletin, 106: 571-581.

D'agostino N. and Selvaggi G.; 2004: *Crustal motion along the Eurasia-Nubia plate boundary in the Calabrian arc and Sicily and active extension in the Messina Straits from GPS measurements*. In: J. Geophys. Res., 109, B11402.

Finetti I.R. and Del Ben A.; 1996: *Crustal Tectono-Stratigraphic setting of the Pelagian Foreland from new CROP seismic data*. In: Finetti, I.R. (eds). CROP PROJECT: deep seismic exploration of the central Mediterranean and Italy. Chapter 26, 581-595.

Hare P.W. and Gardener T.W.; 1985: *Geomorphic indicators of vertical neotectonism along converging plate margin, Nicoya Peninsula, Costa Rica*. In: Tectonic Geomorphology: Proceedings of the 15th Annual Binghamton Geomorphology Symposium, September 1984. Allen & Unwin: Boston.

Hollestein Ch., Kahle H.-G., Geiger A., Jenny S., Geos S. and Giardini D.; 2003: *New gps constraints on the Africa-Europe plate boundary zone in southern Italy*. In: Geophysical Research Letters, 30, NO.18, 1935.

ISIDEe Working Group (Ingv, 2010) – *Italian seismological Instrumental and parametric database:* http://iside.rm.ingv.it.

Lentini F., Carbone S., Catalano S. and Grasso M.; 1996: *Elementi per la ricostruzione del quadro strutturale della Sicilia orientale*. In: Mem. Soc. Geol. Ital. 51, 179-195.
Pavano F., Catalano S., Romagnoli G. and Tortorici G.; 2012: *Dynamics and seismotectonics of NE Sicily*. In: Rend. Online Soc. Geol. It., 21, 241-243.
Palumbo L., Benedetti L., Bourles D., Cinque A. and Finkel R.; 2004: *Slip history of the Magnola fault (Appennines, Central Italy) from 36Cl surface exposure dating: evidence for strong earthquakes over the Holocene*. In: Earth Planetary Science Letters, 225, pp. 163-176.
Strahler A. N.; 1958: *Dimensional analysis applied to fluvially eroded landforms*. Bull. Geol. Soc. Amer, 69.

CONTRIBUTO PER LA SISMOTETTONICA DELLA PIANURA PADANA, DAI TERREMOTI DEL 1570 E DEL 2012

F. Pettenati, L. Sirovich, F. Cavallini
Istituto Nazionale di Oceanografia e di Geofisica Sperimentale OGS, Trieste

Introduzione. Nell'ambito del Progetto Sismologico S1 DPC-INGV, abbiamo condotto due studi per capire meglio la sismotettonica della Piana del Po. Abbiamo infatti: a) invertito le intensità del terremoto di Ferrara del 1570 (M5.8), per recuperare informazioni sulla sorgente; b) operato il calcolo di tutte le possibili disorientazioni γ (rotazioni 3D necessarie per far coincidere una doppia coppia, DC, con un'altra) delle doppie coppie calcolate nella sequenza sismica del maggio – giugno 2012 dell'Emilia.

Inversione del "Ferrara 1570". Abbiamo usato le intensità del data-base di Guidoboni *et al*. (2007), che sono riportate nel catalogo DBMI11 (2011). Ci siamo serviti della nostra tecnica che usa la funzione KF (Sirovich and Pettenati, 2004; Pettenati and Sirovich, 2007) procedendo con il protocollo standard: controllo degli outliers statistici, uso di quattro demi (popolazioni di sorgenti, che esplorano l'iperspazio dei residui) nell'algoritmo genetico con la variante niching (Gentile *et al*., 2004). Nella presente inversione, è stato assegnato il grado V a tre siti classificati "felt" (San Giovanni in Persiceto 44.638°, 11.187°; Novellara 44.845°, 10.731°; Padova 45.407°, 11.876°). In totale, sono stati quindi trattati 51 dati; dei quali, un consistente numero (25) con gradi intermedi (es.: VI-VII); motivo per cui abbiamo trattato due data-sets: il primo con i gradi intermedi usati come "mezzi gradi" (es.: 6.5), e l'altro con i gradi intermedi arrotondati al valore più alto.

La Tab. 1 mostra le due migliori soluzioni per i due data-sets; notare la forte similitudine dei due risultati. I valori con il "+" si intendono calcolati nel verso dello strike, quelli con il "-" nel verso opposto. Sono da rilevare le opposte direzioni delle due propagazioni di rottura (vedere i valori di L+ e L- nella Tab. 1). Concludiamo che l'affidabilità di questa informazione è bassa. Come sempre, segnaliamo che anche la profondità ottenuta non è molto attendibile, perchè viene usato nell'inversione un semispazio elastico e forse anche perché la taratura empirica dei valori KF è ottenuta da una correlazione su dati californiani (in altre parole, è importante l'attenuazione delle intensità). Nella nostra esperienza, entrambe le soluzioni sono interessanti. La magnitudo derivata da Mo in Tab. 1 è M5.8.

La Fig. 1 mostra la soluzione del meccanismo focale e la proiezione in superficie della box della soluzione centrale (in verde) ricavata dall'inversione di Tab 1, poco a nord della città di Ferrara. Attorno a questa soluzione centrale, abbiamo rappresentato in grigio quattro box, che fanno intendere l'entità degli errori di inversione in latitudine, longitudine e angolo di strike. In altre parole, la nostra sorgente potrebbe trovarsi in un'area abbastanza vasta. La Fig. 1 riassume inoltre la nostra interpretazione tettonica della sequenza 1570-2012, come una sequenza molto irregolare nel tempo (una scossa nel 1570, due nel 2012) disposta in echelon ad interessare, da nord a sud (dal più al meno giovane), tre settori consecutivi del fronte appenninico esterno sepolto.

Tab. 1 – Parametri di sorgente (± errori di inversione) delle due migliori soluzioni ottenute dai due data set del terremoto di Ferrara del 1570.

Parametro	Data-set con "mezzi gradi"	Data-set da arrotondamento
Latitudine N [°]	44.97±0.07	44.97±0.07
Longitudine E [°]	11.55±0.10	11.63±0.09
Strike [°]	121±16	127±16
Dip [°]	26±6	28±7
Rake [°]	(73±18) ±180	(77±16) ±180
Depth [km]	35.3±4.8	34.9±5.4
Vs [km/sec]	3.96±0.06	3.90±0.09
Mach+	0.71±0.10	0.63±0.10
Mach -	0.53±0.05	0.60±0.06
L+ [km]	1.8	8.9
L- [km]	5.8	0.0
Mo [N m] 10^{17}	3.21±1.7	4.95±1.05
Fitness [$\sum r^2$]	11	13

Sequenza dell'Emilia, 2012. Il nostro algoritmo (Sirovich *et al.*, 2013), che usa l'algebra lineare, per calcolare le disorientazioni γ fra doppie coppie DC, è stato applicato alle DC disponibili della sequenza maggio-giugno 2012. Sono stati presi in considerazione i tre database degli esperti del progetto S1: Malagnini *et al.* (2012; sigla MA in Fig. 2), Pondrelli *et al.* (2012; Pondrelli, comunicazione scritta 2013; sigla PO in Fig. 2), Saraò e Peruzza (2012; Saraò, comunicazione scritta 2013; SA in Fig. 2). Purtroppo, il controllo di compatibilità tra i tre database, mediante confronti delle rispettive determinazioni ipocentrali, ha dato esito insufficiente per un uso congiunto. In Fig. 2 (centro e destra), si vede che le profondità determinate dai tre gruppi sono poco correlate.

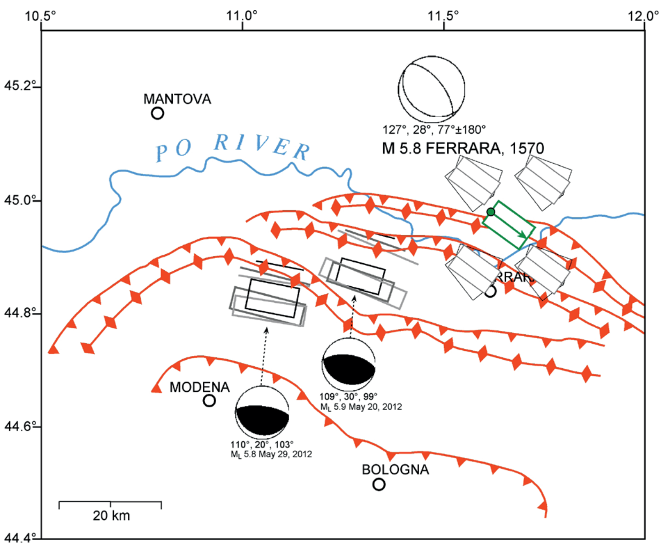

Fig. 1 – Proiezione (verde) della nostra sorgente per il terremoto M 5.8 di Ferrara del 1570 (freccia verde: propagazione unilaterale della rottura verso SE [*non attendibile*]); per gli errori di inversione, vedi il testo. In rosso con losanghe: assi delle anticlinali; con triangoli: principali fronti dei thrust appenninici sepolti (da Boccaletti *et al.*, 2010; Picotti, 2012; Pezzo *et al.*, 2013). Rettangoli grigi e neri: sorgenti dei principali eventi del 20 maggio, 2012 (destra) e del 29 maggio, 2012 (sinistra) ottenute da tre gruppi indipendenti dell'INGV, che hanno modellato le deformazioni cosismiche (da Serpelloni *et al.*, 2012).

Per quanto concerne le γ, avevamo a disposizione solo le orientazioni degli assi T, P, N dei data-base MA e PO; abbiamo calcolato le γ fra tutte le possibili coppie di DC del solo data-base MA perché era il più numeroso (27 DC). In Fig. 2, a sinistra, è riportato l'istogramma tra coppie di DC del data-base Malagnini *et al.* (2012). Si notano due picchi, a 15º e 45º. Il primo riguarda le combinazioni delle 16 DC giudicate molto simili (γ <20º) alla scossa principale (11DC) ed a una replica (4DC); il secondo picco (γ <50º) sarebbe al limite della somiglianza fra DC (vedi Sirovich *et al.*, 2013); l'elevato numero di coppie con γ >50º indica che vi sono parecchie scosse con DC non somiglianti ad altre, indicando quindi una rottura complessa.

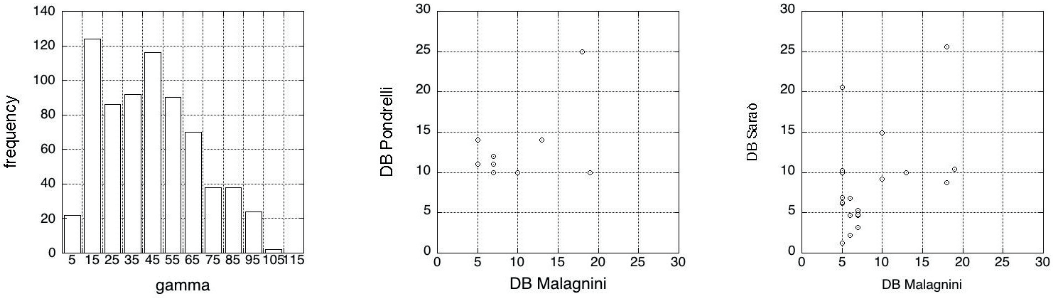

Fig. 2 – Sinistra: distribuzione di tutte le disorientazioni γ fra doppie coppie, DC, γ nel data-base Malagnini *et al.*, 2012 (MA) (ascisse: γ in gradi; ordinate: conteggio delle γ fra tutte le possibili coppie di DC del data-base). Centro e destra (profondità in km su entrambi gli assi): confronto fra profondità ipocentrali dei tre gruppi di esperti del progetto S1 (centrale: set PO su set MA; destra: SA su MA).

La Fig. 3 rappresenta spazialmente la sequenza in questione (DC da Malagnini *et al.*, 2012), con il meccanismo dell'evento principale del 20 maggio 2012, delle ore 02:03:53 (M 5.7) associato al punto epicentrale marcato dal numero "0" in rosso); sono anche rappresentati gli 11 meccanismi ad esso molto simili (γ <20º; criterio molto stringente; abbiamo infatti indicazione che il limite di somiglianza sia attorno a 40°: Pettenati *et al.*, 2011; Sirovich *et al.*, 2013). Come noto, le nostre soluzioni hanno un'ambiguità di 180° nel rake; in figura abbiamo risolto tale

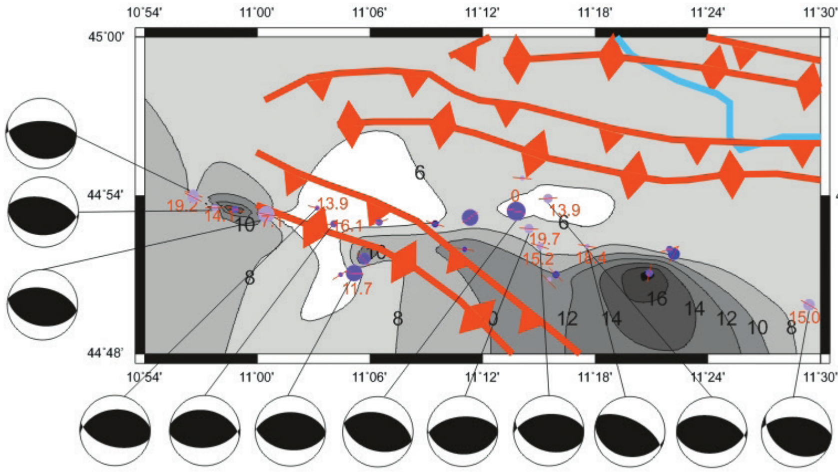

Fig. 3 – Le 11 doppie coppie DC simili alla DC dell'evento principale del 20.05.2012, 02:03:53 (pallino viola in zona centrale, con uno "0" in rosso). I numeri rossi sono i valori delle disorientazioni γ<20º rispetto all'evento principale. La mappa di contour rappresenta le profondità ipocentrali delle 27 soluzioni del set Malagnini *et al.*, 2012 (MA); le dimensioni dei pallini sono proporzionali alla M ed il loro colore quantifica il dip, da viola pallido (30º) a viola scuro (90º). Linee rosse con losanghe: assi degli anticlinali; linee rosse con triangoli: fronti dei thrust apenninici principali (da Boccaletti *et al.*, 2010; Picotti, 2012; Pezzo *et al.*, 2013)

ambiguità per analogia con le soluzioni strumentali. La Fig 3 si presterebbe ad un'animazione (che verrà presentata al convegno) che mostra la distribuzione spazio-temporale, in cui si identificano due gruppi di DC simili: il primo attorno all'evento principale, il secondo è un allineamento parallelo ai thrust, più a O ed OSO.

Discussione. Il nostro principale risultato è riassunto dalla Fig. 1. Ci pare che l'ipotesi di un processo in echelon, altamente irregolare nel tempo, ma plausibile nello spazio, con propagazione delle rotture dal fronte più giovane ed esterno verso settori di fronte disposti più a SO, sia abbastanza convincente. Le nostre stime di profondità ipocentale non sono attendibili per l'evento del 1570 (abbiamo però visto quanto delicata sia questa determinazione anche con gli strumenti). Se tuttavia proiettiamo la sorgente della Tab. 1 (destra) sulla sezione di Picotti e Pazzaglia, 2008 (loro Fig. 11) integrata da Picotti (2012) ad una profondità di 10 km, od un po' superiore, e consideriamo anche gli errori di inversione in latitudine e angolo di dip, notiamo (figura qui non riprodotta) la compatibilità della nostra soluzione per il 1570 sia con il fronte più esterno e giovane, sepolto, sia eventualmente con il detachment profondo ("blind crustal-scale thrust", Picotti e Pazzaglia, 2008).

Per quanto riguarda i tre eventi: 1570, 20 e 29 maggio 2012, concludiamo quindi che essi ci sembrano appartenere alla complessa rottura del sistema di thrust esterni sepolti, con propagazione retrograda della rottura nel corso del tempo.

Nella sequenza del 2012, 11 eventi su 27 del data-base Malagnini *et al.* (2012) sono associabili direttamente alla scossa più forte di M5.7 e quindi ai thrust Appenninici. Sono identificati due gruppi di doppie coppie DC simili, il primo attorno all'evento principale, il secondo trasferito verso ovest a fine maggio e giugno. Sono presenti molte rotture minori non ad orientamento apenninico. Purtroppo, le determinazioni ipocentrali sono troppo poche e poco accurate per consentire di seguire in dettaglio la cinematica della propagazione delle rotture utilizzando le disorientazioni γ.

Bibliografia

Boccaletti M., G. Corti and Martelli L.; 2010: *Recent and active tectonics of the external zone of the Northern Apennines (Italy).* Int. J. Earth Sci. (Geol Rundsch) DOI 10.1007/a00531-010-0545-y

Burrato P., Ciucci F. and Valensise G.; 2003: *An inventory of river anomalies in the Po Plain, northern Italy: Evidence for blind thrust faulting.* Ann Geophys., **48**, 865-882

Cassano, E., Anelli L., Fichera R. and Cappelli V.; 1986: *Pianura Padana. Interpretazione integrata di dati geofisici e geologici*. 73° Congr Soc Geol It, 29 sett-4 ott, Roma, 27.

DBMI11 (2011) http://emidius.mi.ingv.it/DBMI11.

Guidoboni E., Ferrari G., Mariotti D., Comastri A., Tarabusi G., and Valensise G.; 2007: *CFTI4Med, Catalogue of Strong Earthquakes in Italy (461 B.C.-1997) and Mediterranean Area (760 B.C.-1500).* INGV-SGA. http://storing.ingv.it/cfti4med ©

Malagnini L., Herrmann R. B., Munafò I., Buttinelli M., Anselmi M., Akinci A. and Boschi E.; 2012: *The 2012 Ferrara Seismic Sequence: Regional Crustal Structure, Earthquake Sources, and Seismic Hazard*. G.R.L. In stampa.

Pettenati F., Sirovich L.; 2007: *Validation of the Intensity-Based Source Inversions of Three Destructive California Earthquakes*. Bull. Seism. Soc. Am., **97**, 5, 1587-1606, doi:10.1785/0120060169.

Pezzo, G, Merryman Boncori, J.P., Tolomei C., Salvi, S. Atzori, S. Antonioli, A. Trasatti, E. Novali, F., Serpelloni, E., Candela, L. and Giuliani, R.; 2013: *Coseismic deformation and Source Modellino of the May 2012 Emilia (Northern Italy) earthquakes*. 84, 4, 645-655

Pondrelli S.; 2013. Quick RCMT, http://autorcmt.bo.ingv.it/quicks.html.

Pondrelli S., Salimbeni S., Perfetti P., and Danecek P; 2012: *Quick regional centroid moment tensor solutions for the Emilia 2012 (northern Italy) seismic sequence.* Annals of Geoph., spec. issue "The Emilia (northern Italy) seismic sequence of May-June, 2012: preliminary data and results" edited by Marco Anzidei, Alessandra Maramai and Paola Montone, **55**, 4, 615-621, doi:10.4401/ag-6146.

Pettenati F., Cavallini F., and Sirovich L.; 2011: *Confronto tra meccanismi focali tramite le loro disorientazioni*. 30° Convegno Nazionale Gruppo Nazionale di Geofisica della Terra Solida GNGTS. Trieste, 14-17 Novembre. 2011. Abstract, 104-106.

Picotti V.; 2012: *La crisi sismica Emiliana del maggio – giugno 2012 e la tettonica attiva in Appennino Settentrionale*. Il Geologo dell'Emila-Romagna. **45**, 7-11.

Saraò A., and Peruzza L.; 2012: *Fault-plane solutions from moment-tensor inversion and preliminary Coulomb stress analysis for the Emilia Plain*. Annals of Geoph., spec. issue "The Emilia (northern Italy) seismic sequence of May-

June, 2012: preliminary data and results" edited by Marco Anzidei, Alessandra Maramai and Paola Montone, **55**, 4, 647-654, doi:10.4401/ag-6134.

Serpelloni E., and 21 more authors; 2012: *GPS observations of coseismic deformation following the May 20 and 29, 2012, Emilia seismic events (northern Italy): data, analysis and preliminary models.* Annals of Geoph., spec. issue "The Emilia (northern Italy) seismic sequence of May-June, 2012: preliminary data and results" edited by Marco Anzidei, Alessandra Maramai and Paola Montone, **55**, 4, 759-766, doi:10.4401/ag-6168.

Sirovich L. and Pettenati F.; 2004: *A new Automatic Source Inversion Technique of Intensity Patterns of Earthquakes; Validation on a Destructive Shock of 1936 in NE Italy.* Journal of Geophysical Research, **109**, B10309, doi: 10.1029/2003JB002919, 2004, pp. 16.

Sirovich, L., Pettenati, F., and Cavallini, F.; 2013: *Intensity-Based Source Inversion of the Destructive Earthquake of 1694 in the Southern Apennines, Italy.* J. Geophis. Res. In stampa

SEISMIC ANALYSIS OF THE WESTERN MARGIN OF THE EASTERN SOUTHERN ALPS FOREDEEP

M. Pola[1], A. Ricciato[2], R. Fantoni[3], P. Fabbri[1], D. Zampieri[1]

[1]*Dipartimento di Geoscienze, Università degli Studi di Padova, Italy*
[2]*GEPlan consulting, Ferrara, Italy*
[3]*Eni E&P, San Donato Milanese, Italy*

Introduction. The Veneto-Friuli area (NE Italy) represents the foreland of three orogenic belts, which are currently active although at different rates: the Dinarides to the E, the Eastern Southern Alps to the N and the Apennines to the SW (Massari *et al*., 1986; Fantoni *et al*., 2002). Since the Mesozoic time this area has been affected by several phases of tectonic deformation (Mesozoic extensional cycle and Cenozoic compressional cycle; Fantoni and Franciosi, 2009, 2010) resulting in a fragmented architecture buried beneath the Quaternary Veneto-Friuli alluvial plain. With the aim of unravelling the architecture and the evolution of the western margin of the Veneto-Friuli foredeep, marked by the Schio-Vicenza Fault, about 1000 km of 2D seismic sections and more than 10 deep wells acquired by ENI for hydrocarbon exploration were interpreted.

The Schio-Vicenza fault marks also the eastern boundary of the structural high of the Lessini and Berici mountains and Euganei hills (LBE), which constitutes a foreland block only weakly affected by the Alpine shortening separating the Western from the Eastern Southern Alps and their forelands (Bigi *et al*., 1990; Laubscher, 1996). The northern part of the Schio-Vicenza fault is well exposed in the Veneto Pre-Alps to the north of Schio (Fig. 1) and has been the subject of many studies (*e.g*., De Boer, 1963; Semenza, 1974; Zanferrari *et al.,* 1982; Zampieri, 1995; Castellarin and Cantelli 2000; Zampieri and Massironi, 2007; Fondriest *et al*., 2012). In contrast, the southern part of the fault is buried beneath the Veneto alluvial plain and its occurrence is only highlighted to the south of the Euganei Hills near Conselve (Finetti, 1972; Fig. 1).

The Veneto-Friuli foreland was affected by different flexural cycles related to the diachronous build up of the three surrounding chains (Fantoni *et al*., 2002). The flexuring started during the Paleocene-Eocene with an eastward faint inflection affecting mainly its eastern sector (Friuli Plain) and linked to the build up of SW-vergent Dinaric thrust belt (Doglioni and Bosellini, 1987; Fantoni *et al*., 2002). After the Lower Oligocene regional emersion, two main depositional/flexuring cycles occurred in the foredeep (Fantoni *et al.,* 2002): i) the Chattian-Langhian cycle, characterised by a weak north-ward inflection (bending angle below 1°) and producing an accommodation space filled by clastic supply mainly from the uplifted sector of the South Alpine chain; ii) the Serravallian-Lower Messinian cycle, affected by a prominent bending towards NNW due to the quick uplift of the Southern Alps belt (Zattin *et al*., 2006). The end of the Serravallian-Lower Messinian cycle is attested by a prominent sub-aerial erosion (intra-Messinian Unconformity) controlled by a combination of factors like dropdown of the eustatic level, differential subsidence and regional uplift (Ghielmi *et al*., 2013). During the Pliocene-

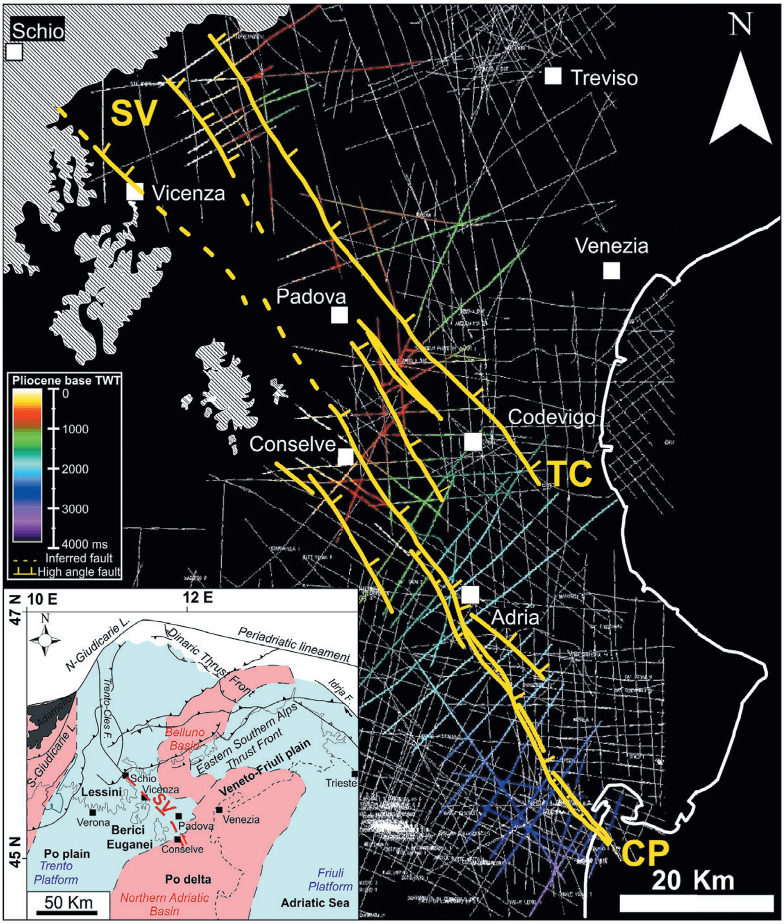

Fig. 1 – Map of the Upper Messinian unconformity (Pliocene base) performed using the seismic sections database and carried on in the time domain (TWT). A sharp colour transition evidence a TWT/depth variation of the horizon interpreted as linked to a fault. Three main faults composing the Schio-Vicenza fault system are evidenced: the Schio–Vicenza fault (SV) to the NW, the Travettore–Codevigo fault (TC) to the E and the Conselve–Pomposa fault (CP) to the SW. Inset: simplified structural map of the eastern Southern Alps (modified from Zampieri *et al.*, 2003).

Pleistocene, only the south-westernmost part of the Veneto-Friuli foredeep (southern part of the Veneto Basin) bent towards SW due to the Northern Apennines build up (Fantoni *et al.*, 2002).

Seismic interpretation. The Landmark software was used to digitise the seismic horizon of the intra-Messinian Unconformity (corresponding to the Pliocene base) in Two Way Travel time (TWT) domain (Fig. 1). This horizon records the last deformational phase (Pliocene-Pleistocene) affecting the Veneto-Friuli foredeep. Several TWT variations are observed and interpreted as related to faults that accommodated the Pliocene-Pleistocene flexural phase. The depicted network of fault segments was subsequently imported and analysed by a GIS software to map the whole system.

Seven seismic sections (Tab. 1; Fig. 2) sub-orthogonal to the western margin of the Veneto-Friuli foredeep were depth converted. Stratigraphic horizons from the Upper Trias to the Pleistocene were recognised (Fig. 2) and deep exploration wells, located close to the lines (Tab. 1), were used to calibrate the interpretation. The use of a GIS software has allowed conversion of the seismic section from the time-domain to the depth-domain.

Tab. 1 – Interpreted seismic sections and related calibration wells used for the depth conversion processes. The seismic lines, wells location and interpreted sections are shown in Fig. 2.

Seismic Section	Section Length (km)	Calibration Well
AA’	28	Vicenza 1 = Vi1
AA-AA’	36.5	Ballan 1 = Ba1
BB’	27.8	S. Angelo Piove di Sacco 1 = Sa1
		Legnaro 1 = Le1
CC-CC’	30.9	Villadose 1 = Vd1
		Codevigo 1 = Co1
CC’	28	-
DD’	24	Corte Vittoria 1 = Cv1
EE’	24	Pomposa 1 = Po1

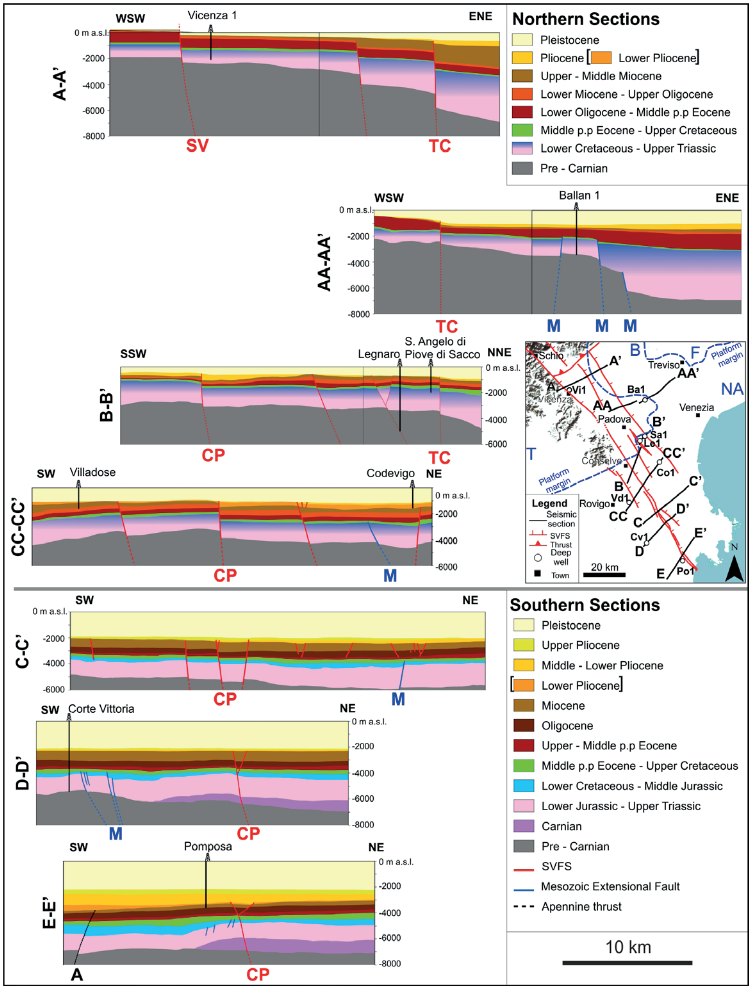

Fig. 2 – Cross-sections sub–orthogonal to the SVFS obtained through the seismic sections interpretation and the subsequent depth conversion process. Different stratigraphic horizons were recognised leading to a subdivision between the southern sections, located close the Po delta, and the northern ones, located close to the relief. Fault traces associated to the Schio-Vicenza fault system are recognised (SV: Schio–Vicenza fault; CP: Conselve–Pomposa fault; TV: Travettore–Codevigo fault). Mesozoic extensional faults (M) and an Apennine reverse fault (A) are also depicted. The faults divide the subsurface in a mosaic of blocks deepening towards NE. The map evidences also the border of the basins and swells representing the Mesozoic architecture of the study area (T: Trento platform-plateau, B: Belluno basin, NA: Northern Adriatic basin, F: Friuli platform-plateau; see also Fig. 1).

Results. A deepening of the Pliocene base is observed along all seismic sections moving from the western to the eastern side (Fig. 1). Such variation mainly occurs as a sharp TWT increment (up to 250 ms in the northern part of the study area) within a small distance (200-300 m) and is interpreted as an offset related to fault activity. The faults traces in adjacent seismic sections were joined showing a complex fault system with a NW-SE or NNW-SSE trend. The faults are parallel to the Schio-Vicenza fault and collectively compose the so-called Schio-Vicenza fault system (SVFS) made by three main faults: i) the Schio-Vicenza fault to the NW, extending for about 45 km from the foot of the pre-Alps (Schio) to the north of the Euganei Hill (north of Padova) with a main NW-SE trend (SV in Fig. 1); ii) the Travettore-Codevigo fault to the E, extending for about 70 km from the foot of the pre-Alps to the to the south of the Venezia Lagoon (Codevigo) with a main NNW-SSE trend (TC in Fig. 1); iii) the Conselve-Pomposa fault to the SW, extending for about 80 km from the East of the Euganei Hill (south of Padova) to the south of the Po delta with a main NNW-SSE trend (CP in Fig. 1).

The depth-converted sections (Fig. 2) show a general deepening from west to east and from north to south of all the recognised horizons (from Upper Triassic to Pleistocene). The W-E deepening is mainly related to faults with variable dip that are associated to the SVFS. These faults usually dip at high angle to ENE or NE and cut the horizons from Upper Triassic to Pliocene displaying a variable throw both in space and time (Tab. 2; Fig. 2). The geometric characteristics of the main faults of the SVFS are also depicted: i) the Schio-Vicenza fault dips 85° to ENE (section A-A'); ii) the Travettore-Codevigo faults dips 85° to 88° to ENE (section

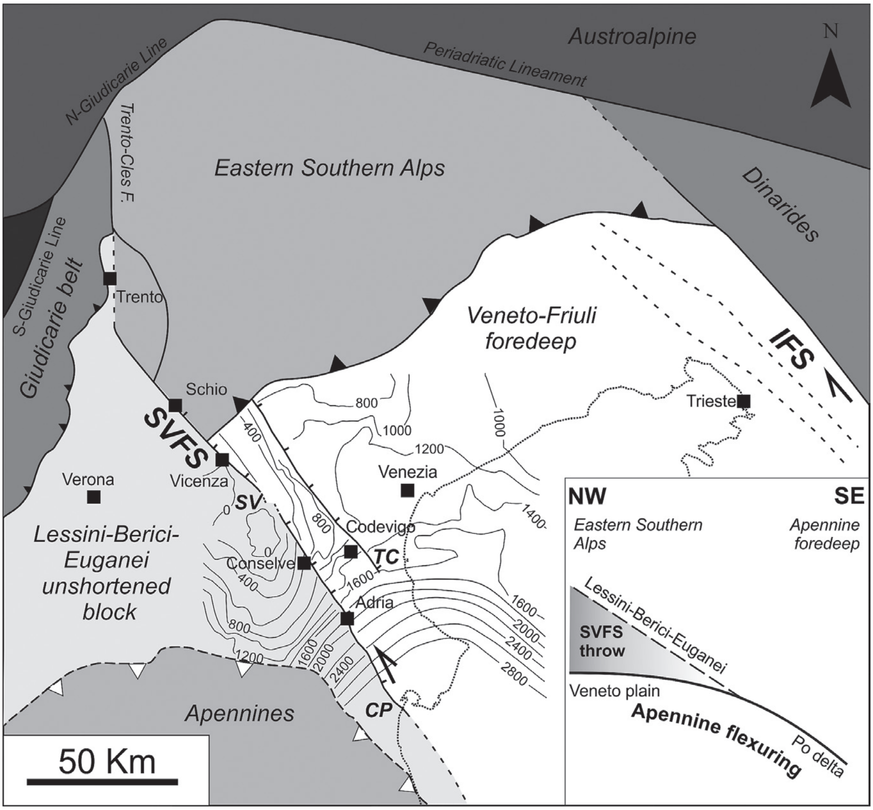

Fig. 3 – Map of the depth of the Pliocene base along the Schio-Vicenza fault system (SV: Schio-Vicenza fault; TC: Travettore-Codevigo fault; CP: Conselve-Pomposa fault). The contour lines (black solid lines; the depth is in metres below the ground level) show a deepening towards the S related to the Apennines Pliocene-Pleistocene flexuring. Conversely, the faults throw increase towards the NW (sketch in the inset).

A-A', AA-AA', B-B'); iii) the Conselve-Pomposa fault dips 70° to 87° to ENE or NE (sections B-B', CC-CC', C-C', D-D', E-E'). In addition, faults cutting only Mesozoic horizons, dipping at high angle to ENE/NE or to WSW/SW (sections AA-AA', CC-CC', C-C', D-D', E-E'), and an high angle reverse fault dipping at high angle to SW (section E-E'), probably associated to the Apennines activity, are observed. The throw of the Upper Triassic base and the Pliocene base along the main segments of the SVFS depicted in the depth-converted sections is also measured (Tab. 2).

The data obtained through the fault mapping and depth conversion were used to perform a map of the depth of the Pliocene base along the SVFS. The collected data were merged with available data provided by ENI in the whole Veneto plain gaining a broader regional view (Fig. 3). This map shows a general deepening towards the S, clearly related to the Apennines subduction and the subsequent flexuring of the north Adriatic (Fantoni *et al.*, 2002). In addition, a different behaviour in the deepening of the Pliocene base is observed crossing the SVFS. The LBE block, to the west of the SVFS, shows a regular slope starting from 0 m near the reliefs and reaching about 2800 m of depth near the Apennines thrust front (about 2.8 km of deepening in 90 km; dip ~3% = 1.7°). The Veneto-Friuli foredeep, to the east of the SVFS, shows a gentle slope in its northern part close to the reliefs and the Eastern Southern Alps thrust front (about 0.6 km of deepening in 60 km; dip ~1% = 0.6°), followed by a steeper slope in the southern part (about 1.4 km of deepening in 40 km; dip ~3% = 1.7°) similar to the LBE block slope. These results are in accordance with the dip of the Apennines monocline (1.5°) calculated by Cuffaro *et al.* (2009).

Tab. 2 – Throw of the base of Dolomia Principale (Upper Triassic base) and the Upper Messinian Unconformity (Pliocene base) measured in the depth-converted sections and related to the Conselve-Pomposa and Schio-Vicenza faults and the Travettore-Codevigo fault. The throw marked by * in AA' section is inferred using the Upper-Middle Miocene throw.

Conselve-Pomposa fault + Schio-Vicenza fault				Travettore-Codevigo fault		
Section	X (Km)	Upper Triassic Base throw (m)	Pliocene Base throw (m)	X (Km)	Upper Triassic Base throw (m)	Pliocene Base throw (m)
E-E'	14	60	70	-	-	-
D-D'	31	50	10	-	-	-
C-C'	37	200	30	-	-	-
CC-CC'	52	550	320	-	-	-
B-B'	61	240	260	33	190	60
AA-AA'	-	-	-	50	150	170
A-A'	112	430	430(*)	71	1070	200

Discussion and conclusions. The throw analysis of the Upper Triassic base and the Pliocene base (Tab. 2) allows to elucidate the role of the fault system in the accommodation of the two main deformational events of the foredeep, i.e. the Mesozoic extensional phase and the Cenozoic flexural phase. A clear separation between the cumulative throw of the two horizons is depicted. The Upper Triassic base throw is usually greater than the Pliocene base throw and their separation increases towards the N (from 170 m near Adria to 870 m near Vicenza), with a main supplying of the Travettore-Codevigo fault. Therefore, the SVFS, or some segments of the fault system, seems to be active during the Mesozoic when the extension was controlled by synsedimentary normal faults (Masetti and Bianchin, 1987). Such control is clearly detected in the northernmost sections crossing the eastern margin of the Jurassic Trento Platform-Plateau and it is testified by the abrupt increasing thickness of the Mesozoic units across the high-angle normal faults, mostly dipping towards the E (i.e., an increase of about 2500 m is depicted in AA-AA' section moving from the hanging wall to the footwall of Mesozoic faults; an increase of about 1800 m is depicted in A-A' section moving from the hanging wall of the fault trace in the middle part of the section to the footwall of the Travettore-Codevigo fault; Fig. 2). The other sections don't allow unravel the Mesozoic extension because they parallel the platform margin (B-B' section) or fall within the Northern Adriatic Basin (CC-CC', C-C', D-D' and E-E' section). The SVFS partially accommodates also some phases of the Cenozoic flexuring as attested by the thickness variations of the Paleogene to Neogene units, while a control of the eustatism could not be totally neglected (Massari *et al.,* 1986; Mellere *et al*., 2000). The Paleocene-Eocene flexuring, linked to the growth of the Dinarides, is recorded only in the eastern side of the foredeep and doesn't influence the western part (Fantoni *et al.,* 2002). The Chattian-Langhian flexuring of the Veneto-Friuli foredeep is less pronounced and related to the Sothern Alps loading. On the other hand, the subsequent Serravallian-Lower Messinian cycle testifies a prominent flexuring linked to the build up of the Eastern Southern Alps with the development of a deep sedimentary basin (up to 1460 m deep; Fantoni *et al*., 2002). Such flexuring is recorded mainly in the central and eastern part of the foredeep and marginally in the study area: an increase of the Upper-Middle Miocene thickness (about 1500 m) is observed only in the A-A' section moving from W to E with a sharp variation near the faults (*e.g*., the fault depicted in the middle part of the section and the Travettore-Codevigo fault; Fig. 2). The Pliocene-Pleistocene flexural cycle affected only the southern and western part of the foredeep with a bending towards SW linked to the Northern Apennines build up (Fantoni *et al*., 2002). The map of the Pliocene base depth (Fig. 3) clearly shows the general deepening of the horizon towards the S, even though a differential slope is observed in the foredeep and between the hanging wall and the footwall of the SVFS. On the other hand, the throw of the Pliocene base along SVFS show a general increase towards NW (from 70 to 430 m along the Conselve-Pomposa and Schio-Vicenza faults; from 60 m to 200 m along the Travettore-Codevigo fault; Tab. 2) with only a small local irregular trend (from 70 m in E-E' section to 10 m in DD' section and to 30 m in C-C'; Tab. 1). The two apparently-conflicting results, i.e. the general deepening of the Pliocene base towards the S versus increasing gradient of the post-Miocene fault throws towards the NW, can be reconciled considering the different response of LBE block and the Veneto-Friuli foredeep to the Apennines subduction and the SVFS as a structural boundary between the two domains (inset of Fig. 3). During the Pliocene-Pleistocene, the LBE block was affected by a strong uplift in its northern sector (Zanferrari *et al*., 1982) and a deepening in its southern part, as depicted by the Pliocene base map (Fig. 3). Indeed, the area constituted an inherited structural high separating the central-western from the Eastern Southern Alps foredeeps and was free to tilt due to the Apennines subduction. In contrast, the Veneto-Friuli foredeep was already a low area because of the Serravallian-Upper Messinian flexuring associated to the Eastern Southern Alps load (Barbieri *et al*., 2004). During the Pliocene-Pleistocene, the foredeep suffered a supplemental southward flexuring with the development of accommodation space filled by Pliocene shallow water sandstones (Eraclea sandstone), grading southward into fine-grained hemipelagic sediments (Santerno group) locally covered by Flysch (Porto Corsini and Porto Garibaldi Formations), and by Pleistocene-Holocene shallow marine sand and sandstone (Asti group) (Mancin *et al*., 2009). A differential response of the Veneto foredeep to the Apennines subduction is observed: the southern part was free to bend showing a slope similar to the one of the LBE block (ca. 3%; Fig. 3), while the northern part was unable to uplift due to load of the Eastern Southern Alps margin and was less affected by the bending (slope ca. 1%; Fig. 3). This different Pliocene-Pleistocene behaviour between the two structural domains (LBE block versus Veneto-Friuli foredeep) is recorded along the boundary of the blocks marked by the SVFS. A vertical scissor movement took place on the fault system testified by the increasing throw of the Pliocene base towards NW (Fig. 3).

The results of the throw analysis show that the SVFS developed during the Mesozoic regional extension. Subsequently, it was reactivated during the Pliocene-Pleistocene flexuring, accommodating with a scissor movement the differential bending between the Lessini-Berici-Euganei block to the W and the Veneto-Friuli foredeep to the E. The results of this study don't allow to recognize the most probably sinistral strike-slip component of the SVFS displacement, suggested by the GPS data (D'Agostino *et al.*, 2005; Grenerckzy *et al.*, 2005; Serpelloni *et al.*, 2005) and geodynamic reconstructions (Semenza, 1974; Castellarin and Cantelli, 2000; Massironi *et al.*, 2006). The fault system seems to be active at least until 20 ka as suggested by the U/Th dating carried out on a travertine deposit (Montirone Hill; Abano Terme) located in the hanging wall of the SVF (Pola *et al.*, in press).

Acknowledgements. The authors are grateful to M. Zattin and A. Argnani for helpful reviews.

References

Barbieri C., Bertotti G., Di Giulio A., Fantoni R. and Zoetemeijer R.; 2004: *Flexural response of the Venetian foreland to the South-Alpine tectonics along the TRANSALP profile*. Terra Nova, **16**, 273-280.

Bigi G., Cosentino D., Parotto M., Sartori, R. and Scandone P.; 1990: *Structural model of Italy. Sheet n. 1*. In: Castellarin A., Coli M., Dal Piaz G.V., Sartori R., Scandone P., Vai G.B. (Eds.), Progetto Finalizzato Geodinamica. CNR, Roma.

Castellarin A. and Cantelli L.; 2000: *Neo-Alpine evolution of the Southern Eastern Alps*. Journal of Geodynamics, **30**, 251-274.

Cuffaro M., Doglioni C. and Riguzzi F.; 2009: *Present geodynamics of the northern Adriatic plate*. Rendiconti Online Società Geologica Italiana, **9**, 21-24.

D'Agostino N., Cheloni D., Mantenuto S., Selvaggi G., Michelini A. and Zuliani D.; 2005: *Strain accumulation in the southern Alps (NE Italy) and deformation at the northeastern boundary of Adria observed by CGPS measurements*. Geophysical Research. Letters, **32**, 19.

De Boer J.; 1963: The geology of the Vicentinian Alps (NE Italy) (With special reference to their paleomagnetic history). Geologica Ultraiectina, **11**.

Doglioni C. and Bosellini A.; 1987: *Eoalpine and Mesoalpine tectonics in the Southern Alps*. Geologische Rundschau, **76**, 735-754.

Fantoni R., Cattelani D., Merlini S., Rogledi S. and Venturini S.; 2002: *La registrazione degli eventi deformativi cenozoici nell'avampaese Veneto-Friuliano*. Memorie della Società Geologica Italiana, **57**, 301-313.

Fantoni R. and Franciosi R.; 2009: *Mesozoic extension and Cenozoic compression* in *Po Plain and Adriatic foreland.* Rendiconti online della Società Geologica Italiana, **9**, 28-31.

Fantoni R. and Franciosi R.; 2010: *Tectono-sedimentary setting of the Po Plain and Adriatic foreland*. Rendiconti Lincei, **21**, 197-209.

Finetti I.; 1972: *Le condizioni geologiche della regione di Venezia alla luce di recenti indagini sismiche*. Bollettino di Geofisica Teorica ed Applicata, **14**, 275-290.

Fondriest M., Smith S.A.F., Di Toro G., Zampieri D. and Mittempergher S.; 2012: *Fault zone structure and seismic slip localisation in dolostone, an example from Southern Alps, Italy*. Journal of Structural Geology, **45**, 52-67.

Ghielmi M., Minervini M., Nini C., Rogledi S. and Rossi M.; 2013: *Late Miocene-Middle Pleistocene sequences in the Po-Plain - Northern Adriatic Sea (Italy): The stratigraphic record of modification phases affecting a complex foreland basin*. Marine and Petroleum Geology, **42**, 50-81.

Grenerczy G., Sella G., Stein S. and Kenyeres A.; 2005: *Tectonic implications of the GPS velocity field in the northern Adriatic region*. Geophysical Research Letters, **32**, 16.

Laubscher, H.P.; 1996: *Shallow and deep rotations in the Miocene Alps*. Tectonics, **15**, 1022-1035.

Mancin N., Di Giulio A. and Cobianchi M.; 2009: *Tectonic vs. climate forcing in the Cenozoic sedimentary evolution of a foreland basin (Eastern Southalpine system, Italy)*. Basin Research, **21**, 799-823.

Masetti D. and Bianchin G.; 1987: *Geologia del Gruppo dello Schiara (Dolomiti Bellunesi): Suo inquadramento nell'evoluzione giurassica del margine orientale della piattaforma di Trento*. Memorie di Scienze Geologiche, **39**, 187-212.

Massari F., Grandesso P., Stefani C. and Jobstraibizer P. G; 1986: *A Small Polyhistory Foreland Basin Evolving in a Context of Oblique Convergence: The Venetian Basin (Chattian to Recent, Southern Alps, Italy)*. Foreland Basin, Special Publication International Association of Sedimentologists, **8**, 141-168.

Massironi, M., Zampieri, D. and Caporali, A.; 2006: *Miocene to present major fault linkages through the Adriatic indenter and the Austroalpine-Penninic collisional wedge (Alps of NE Italy)*. Geological Society London Special Publications, **262**, 245-258.

Mellere D., Stefani C. and Angevine C.; 2000: *Polyphase tectonics through subsidence analysis: the Oligo-Miocene Venetian and Friuli Basin, north-east Italy*. Basin research, **12**, 159-182.

Pola M., Gandin A., Tuccimei P., Soligo M., Deiana R., Fabbri P. and Zampieri D.; (in press): *A multidisciplinary approach to understanding carbonate deposition under tectonically controlled hydrothermal circulation: A case study from*

a recent travertine mound in the Euganean Hydrothermal System, northern Italy. Sedimentology, doi: 10.1111/sed.12069.
Semenza E.; 1974: *La fase giudicariense, nel quadro di una nuova ipotesi sull'orogenesi alpine nell'area italo-dinarica*. Memorie della Società Geologica Italiana, **13**, 187-226.
Serpelloni E., Anzidei M., Baldi P., Casula G. and Galvani A.; 2005: *Crustal velocity and strain-rate fields in Italy and surrounding regions: new results from the analysis of permanent and non-permanent GPS networks*. Geophysical Journal International, **161**, 861-880.
Zampieri D.; 1995: *Tertiary extension in the southern Trento Platform, Southern Alps, Italy*. Tectonics, **14**, 645-657.
Zampieri D., Massironi M., Sedea R. and Sparacino V.; 2003: *Strike-slip contractional stepovers in the Southern Alps (northeastern Italy)*. Eclogae Geologicae Helvetiae, **96**, 115-123.
Zampieri D. and Massironi M.; 2007: *Evolution of a poly-deformed relay zone between fault segments in the eastern Southern Alps, Italy*. Geological Society London Special Publications, **290**, 351-366.
Zanferrari, A., Bollettinari, G., Carobene, L., Carton, A., Carulli, G.B., Castaldini, D., Cavallin, A., Panizza, M., Pellegrini, G.B., Pianetti, F. and Sauro, U.; 1982: *Evoluzione neotettonica dell'Italia nordorientale*. Memorie di Scienze Geologiche, **35**, 355-376.
Zattin M., Cuman A., Fantoni R. Martin S., Scotti P. and Stefani C.; 2006: *From Middle Jurassic to Neogene cooling: the thermochronological evolution of the Southern Alps*. Tectonophysics, **414**, 191-202.

UPPER PLEISTOCENE - HOLOCENE TECTONIC ACTIVITY OF THE M. JOUF-MANIAGO THRUST-SYSTEM (CARNIC PREALPS, NE ITALY)

M.E. Poli[1], G. Monegato[2]
[1]*Dept. of Chemistry, Physics and Environment, University of Udine, Italy*
[2]*Institute of Geosciences and Earth Resources, C.N.R. Torino, Italy*

Introduction. The study area belongs to the Plio-Quaternary front of the eastern Southalpine Chain (ESC), a SSE verging, WSW-ENE striking fold and thrust belt in evolution from the Middle Miocene to the Present (Fig.1).

Up to now the ESC thrust-system accommodates the present 2 mm/y shortening (Serpelloni *et al.*, 2005) and crustal thickening and propagates towards the Friulian piedmont Plain.

The Venetian-Friulian prealpine area is characterized by medium/high seismicity both instrumental and historical. According the DBMI11 (Locati *et al.*, 2011) many M>6 historical earthquakes hit the Prealpine area: 1117 (Verona), 1348 (Carnia), 1695 (Asolo), 1873 (Belluno), 1936 (Bosco del Cansiglio) and 1976 (Friuli). The DISS3 Catalogue (http://diss.rm.ingv.it/dissNet/) shows three seismogenetic sources in the investigated area: the Maniago source that is considered responsible for the 07/10/1776 Tramonti earthquake; the Tramonti source linked to the 07/06/1794 earthquake and the Sequals source that is considered a silent source because of no historical earthquakes can be referred to this fault until now (Burrato *et al.*, 2008).

In order to define the upper Pleistocene – Holocene tectonic activity of Southalpine chain in the Carnic Prealps we carried out a morphotectonic analysis of the terraced succession and the related sedimentary units in the lower reach of the Meduna valley.

Stratigraphic and structural framework. The structural framework of the investigated area is characterized by the M. Jouf-Maniago thrust-system (JM in Fig. 1) dealing with two arched WSW-ENE striking, SSE-verging thrusts (the Maniago and Mt. Jouf respectively), bordering the prealpine area between Maniago and Forgaria del Friuli, south the Periadriatic thrust (PE in Fig. 1).

The JM strongly involves the pre-Quaternary succession that in the study area starts with the Upper Jurassic–Upper Cretaceous Friulian Carbonate Platform that drowned during the Paleogene because of the westward propagation of the front of the External Dinarides. The platform was buried by the Scaglia Rossa Friulana hemipelagic unit and by the thick turbiditic sequence of the Clauzetto Flysch during the Lower Eocene. Starting from the Aquitanian, the Cretaceous and Paleogene formations were unconformably covered by the thick (about 3000 m) Miocene clastic wedge of the eastern Southalpine Chain foredeep (Massari *et al.*, 1986; Zanferrari *et al.*, 2008 and references therein).

The Quaternary successions within the Meduna valley are discontinuous and lacking in chronological data. Better preserved successions are located in the lower reach of the valley, at Ponte Racli with the occurrence of lacustrine bodies interbedded with deltaic or fluvial deposits, ascribed to downstream damming by moraines (Venturini, 1985) and at Del Bianco village, where fluvial conglomerates, glacial and glaciolacustrine sediments were described by Feruglio (1929). However, no specific studies are so far available for the terraces at the outlet of the valley. On the contrary, the geological surveys for the CARG-FVG Project (Zanferrari *et al.*, 2008) let the reconstruction of the late Quaternary evolution of the Meduna alluvial fan (Avigliano *et al.*, 2002).

From a structural point of view, the JM gives rise to a km WSW-ENE striking, S-vergent M. Ciaurlec anticline that involves both the Upper Jurassic-Upper Cretaceous Friulian Carbonate Platform and its Tertiary siliciclastic roofing. Moreover the prevailing siliciclastic Tertiary succession (Scaglia Rossa, Clauzetto Flysch and Miocene succession) gives rise to a WSW-ENE anticlines-synclines tight fold-system. East of Meduno locality, this structural framework shows a noticeable ondulation, probably reflecting a Cretaceous or Eocene paleostructure and causing a NW-SE striking transpressive transfer zone.

Evidence of JM Quaternary activity is shown near Maniago locality, where the terraced Middle-upper Pleistocene units (respectively Maniago gravels and Maniago conglomerates: Zanferrari *et al.*, 2008) are uplifted and suspended on the present piedmont plain by the activity of the M. Jouf thrust; moreover, along the Colvera creek lacustrine deposits (9090 ± 90 years 14C BP) are gently folded and fractured (Zanferrari *et al.*, 2008).

South of the JM, the Miocene succession is thrust and folded by the Arba-Ragogna thrust-system (AR in Fig. 1). It shows evidence of Quaternary activity, as testifies the angular unconformity between the Lower Messinian (Montello conglomerate) and the Early Quaternary

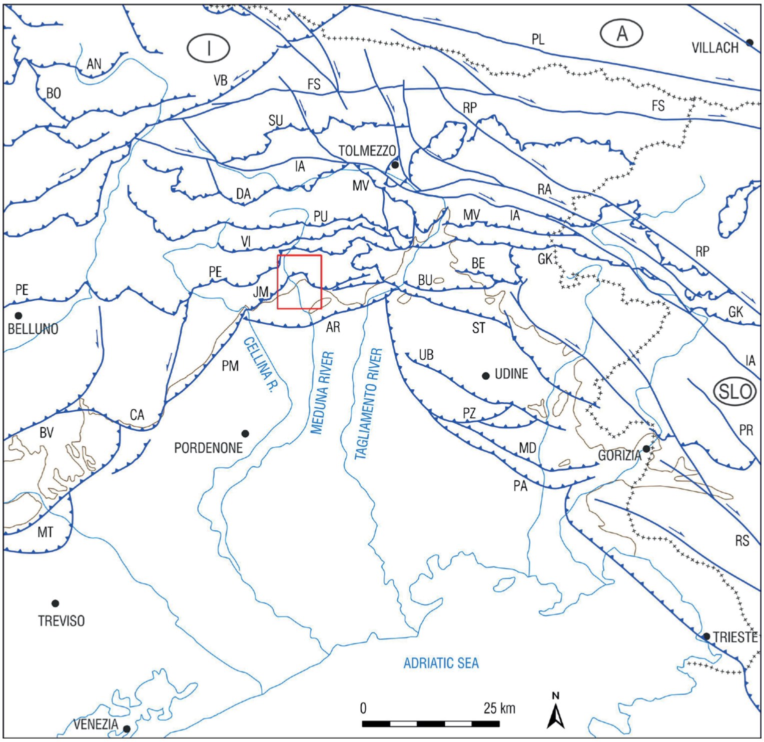

Fig. 1 – Structural sketch of NE Italy and W-Slovenia. In the red rectangle the study area. JM: M. Jouf-Maniago thrust-system; AR: Arba Ragogna; PE: Periadriatic thrust (mod. after Zanferrari *et al.*, 2013).

(San Pietro di Ragogna conglomerate) (Zanferrari *et al.*, 2008; Poli *et al.*, 2009). The recent tectonic activity of the Arba-Ragogna thrust system is also testified by drainage anomalies and gentle scarps connecting uplifted paleolandscapes of Quaternary age (Galadini *et al.*, 2005; Monegato *et al.*, 2010). A vertical slip-rate of about 0.19 mm/y has been calculated during the last 21 kys (Poli *et al.*, 2009).

The sedimentary units and terraced staircase at the outlet of the Meduna valley. Detailed stratigraphical and morphotectonic studies of the terraced surfaces at the outlet of the Meduna valley (south of Ponte Racli locality) allow to detect 9 depositional units (Q1 - Q9 in Fig. 2) linked to alluvial (Q1, Q2, Q3, Q5, Q6, Q7, Q8, Q9) or glacial (Q4) paleo-enviroinments. Starting from the available chronological data for the Meduna alluvial fan (Avigliano *et al.*, 2002; Zanferrari *et al.*, 2008), the geometric relationships between the observed units and the terraced surfaces pinpointed to a succession of depositional events from the Early Pleistocene to the Holocene (Fig. 2). Q4, Q5, Q7, Q8 e Q9 units are terraced but the thickness of the deposits is not steady, for which a distinction between "strath terrace" and "fill terrace" (*sensu* Bull, 1991) can be adopted. A "strath terrace" is characterized by thin deposits (<3m) above an erosion surface on the bedrock; whereas the "fill terrace" is characterized by thicker preserved deposits. According Wegmann and Pazzaglia (2009) this subdivision is a key parameter for discussing the genesis of the terrace staircase in tectonically active areas.

Deformational events. The reconstruction of the deformative events is based both on morphological (piracy and valley deepening) and tectonic evidence. Starting from the older we identified four deformative events (Fig. 2).

1. Early Pleistocene (Gelasian). This event can be morphologically recognized by the main changes in the valley drainage that took place in the Meduna catchment: from the path across the present Forchia di

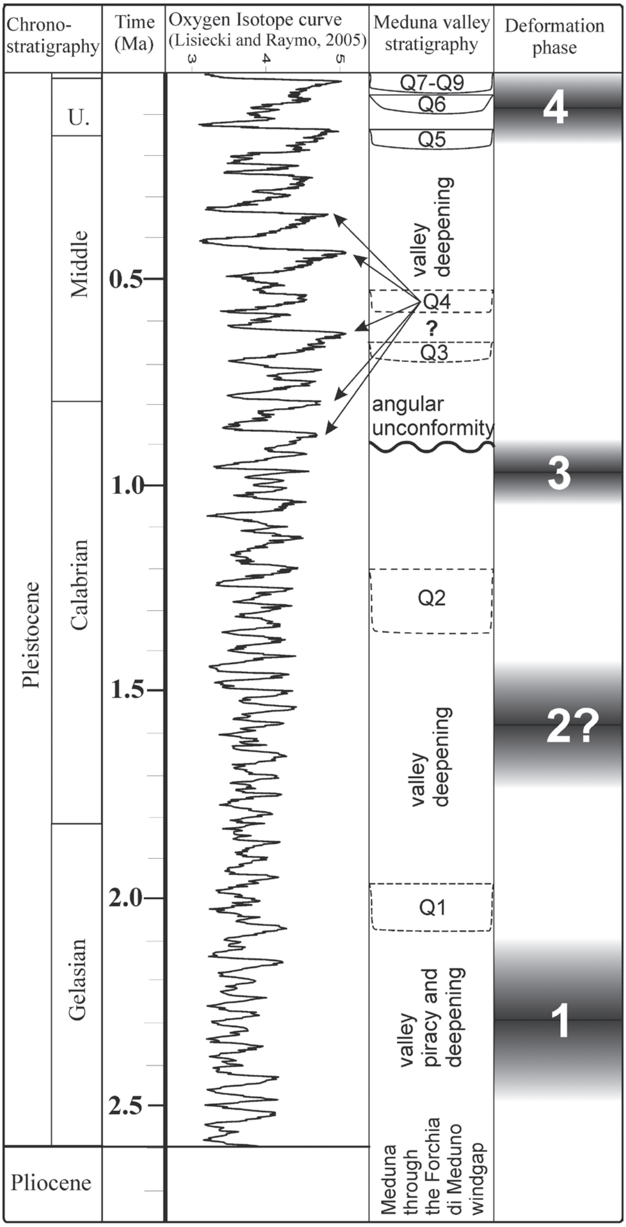

Fig. 2 – Chrono-stratigraphical sketch of sedimentary units (Q1-Q9) and tectonic events (1-4) recognized at the outlet of Meduna Valley. Unit Q4 is not dated and can be ascribed to only one of the glacial maxima linked with arrows.

Meduno windgap (Fig. 2), the river shifted towards the west deepening the valley of about 200 m. This change was tentatively correlated to the deformation phase well recognized in the foothills (Caputo *et al*., 2010). The new Meduna valley crossed the Periadriatic thrust (PE in Fig. 1) whose activity may have driven the geomorphological change. In addition, the thick Q1 conglomerate, exceeding 40 m, suggests a local subsidence at the footwall of the Periadriatic thrust itself.

2. Calabrian (?). A second important deepening of the valley, of about 150 m, with a westward shifting, occurred between Q1 and Q2 aggradation phases. However, the lack of chronological data for these two units makes speculative the age attribution of this phase. It is likely that a tectonic uplift drove this deepening, but it needs more investigations.

3. Calabrian-Middle Pleistocene. This event is recognizable at the boundary between Q2 and Q3 units. Here the Q2 conglomeratic unit presents a crude bedding, gentle folding (dip ca. 10-15°, from 340° to 45°). The Q2 unit is unconformable cut by another conglomerate (Q3) horizontally bedded. Both can be ascribed to alluvial sedimentation of the Meduna Stream within a valley reach, while the angular unconformity suggests a relative time-span occurred between their deposition. Moreover, Q4 is related to a glacial advance during the late Calabrian – middle Pleistocene (Fig. 2), suggesting a similar age for the deformation. An angular unconformity ascribed to the same time span is visible in the conglomerate succession of the Tagliamento valley (Monegato and Stefani, 2011).

4. Middle-upper Pleistocene-Holocene. This tectonic event involves both the M. Jouf thrust and the Maniago one, showing a clear shifting of the tectonic activity from the inner thrust (M. Jouf th.) to the external one (Maniago th.). It is the better constrained tectonic event.

On the terrace near Meduno, the Q5 unit (Middle Pleistocene, upper portion, Fig. 2) give rise a transition from "strath terrace" located in the hangingwall of the M. Jouf thrust to "fill terrace" in the footwall of the thrust. Therefore according to Wegman and Pazzaglia (2009) a broad tectonic control on the formation of this terrace can be hypothesized.

Moreover, Q1 unit (Del Bianco conglomerate, probably Early Pleistocene in age) is crosscut by the M. Jouf thrust. Here the conglomerate is strongly fractured and tilted back of about 20°.

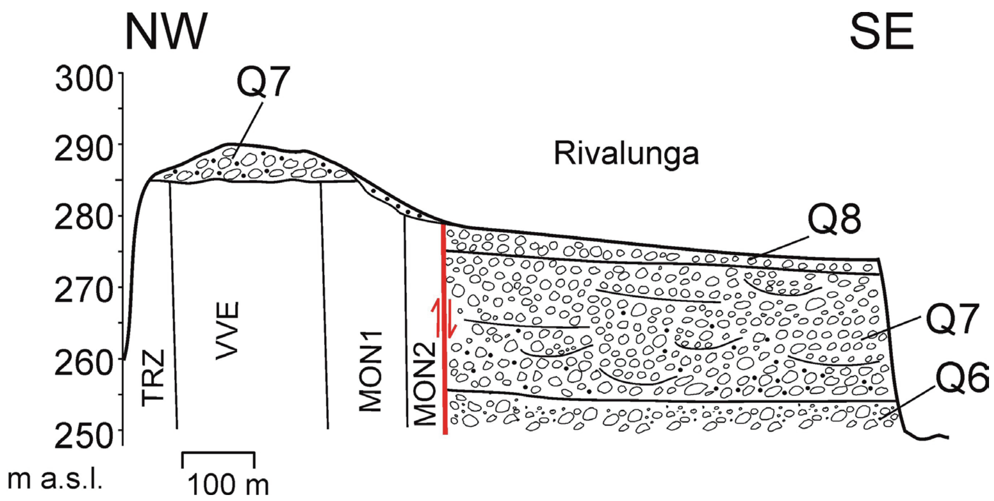

Fig. 3 – NW-SE geological profile across the LGM terrace on left side of Meduna Stream near Ponte Maraldi. Q6: Ponte di Pietra sedimentary unit (upper Pleistocene); Q7: Sequals syntem (Travesio lobe, upper Pleistocene – 22-23 ka cal. BP); Q8: Sequals syntem (Arba lobe upper Pleistocene-Holocene). TRZ: Tarzo Marl (Lower Serravallian-Lower Tortonian); VVE: (Vittorio Veneto Sandstone, Tortonian); MON1 and MON2: Montello Conglomerate members (Upper Tortonian-Lower Messinian).

On the left side of the Meduna river near Ponte Maraldi, the Q7 unit (Sequals syntem, Travesio lobe, upper Pleistocene according to Zanferrari *et al*., 2008) presents a throw of about 25 m on the Maniago thrust (Fig. 3). On these bases an uplift rate of about 1.1. mm/y can be evaluated. Moreover the terrace surface on the Q7 unit near Maraldi presents a fault scarp of about 7-8 m. Instead on the hanginwall of the Maniago fault the thickness of the Q7 unit is very thin (close to the "strath terrace"definition), on the contrary in the footwall of the thrust the alluvial deposits are more than 20 meters in thickness ("fill terrace").

References

Avigliano R., Calderoni G., Monegato G. and Mozzi P.; 2002: *The late Pleistocene-Holocene evolution of the Cellina and Meduna alluvial fans (Friuli NE Italy)*. Memorie Società Geologica Italiana, **57**, 133-139.

Bull W.B.; 1991: *Geomorphic Response to Climatic Change*. Oxford University Press, New York.

Burrato P., Poli M.E., Vannoli P., Zanferrari A. and Basili R., Galadini F.; 2008: *Sources of Mw 5+ earthquakes in northeastern Italy and western Slovenia: An updated view based on geological and seismological evidence*. Tectonophysics, **453**, 157-176.

Caputo R., Poli M.E. and Zanferrari A.; 2010: *Neogene-Quaternary tectonic stratigraphy of the eastern Southern Alps, NE Italy*. Journal of Structural Geology **32**, 1009-1027.

DISS Working Group; 2010: *Database of Individual Seismogenic Sources (DISS), Version 3.1.1: A compilation of potential sources for earthquakes larger than M 5.5 in Italy and surrounding areas*. http://diss.rm.ingv.it/diss/, © INGV 2010 - Istituto Nazionale di Geofisica e Vulcanologia - All rights reserved; DOI:10.6092/INGV.IT-DISS3.1.1.

Feruglio E.; 1929: *Nuove ricerche sul Quaternario del Friuli*. Giornale di Geologia, **4**, 1-36.

Galadini F., Poli M.E. and Zanferrari A.; 2005: *Seismogenic sources potentially responsible for earthquakes with M≥6 in the eastern Southern Alps (Thiene-Udine sector, NE Italy)*. Geophysical Journal International **161**, 739-762.

Lisiecki L E. and Raymo, M. E; 2005: *A Pliocene-Pleistocene stack of 57 globally distributed benthic d18O records*. Paleoceanography, **20**, PA1003, doi:10.1029/2004PA001071 Locati M., Camassi R., Stucchi M. (eds.); 2011: *DBMI11, the 2011 version of the Italian Macroseismic Database*. Milano, Bologna, http://emidius.mi.ingv.it/DBMI11.

Massari F., Grandesso P., Stefani C. and Zanferrari A.; 1986: *The Oligo-Miocene Molasse of the Veneto-Friuli region, Southern Alps*. Giornale di Geologia, **48**, 235-255.

Monegato G. and Stefani C.; 2011: *Preservation of a long-lived fluvial system in a mountain chain: the Tagliamento Valley (Southeastern Italian Alps)*. In: Davidson S.K., Leleu S., North C.P. (eds.): From river to rock record: The preservation of fluvial sediments and their subsequent interpretation. Society for Sedimentary Geology, Special Publication, **97**: 359-374.

Monegato G., Lowick S.E., Ravazzi C., Banino R., Donegana M. and Preusser F.; 2010: *Middle to Late Pleistocene chronology and palaeoenvironmental evolution of the south-eastern Alpine Foreland: the Valeriano Creek succession (NE Italy)*. Journal of Quaternary Science, **25**, 617-632.

Poli M.E., Zanferrari A. and Monegato G.; 2009: *Geometria, cinematica e attività pliocenico-quaternaria del sistema di sovrascorrimenti Arba-Ragogna (Alpi Meridionali orientali, Italia NE)*. Rendiconti online Società Geologica Italiana, **5**, 172-175.

Serpelloni E., Anzidei M., Baldi P., Casula G. and Galvani A.; 2005: *Crustal velocity and strain-rate fields in Italy and surrounding regions: new results from the analysis of permanent and non-permanent GPS networks*. Geophys. J. Int. **161**, 861-880.

Venturini C.; 1985: *I depositi quaternari di Ponte Racli (PN, Prealpi Friulane)*. Gortania, Atti Museo Friulano di Storia Naturale, Udine, **7**, 37-58

Wegmann K.W. and Pazzaglia F.J.; 2009: *Late Quaternary fluvial terraces of the Romagna and Marche Apennines, Italy: Climatic, lithologic, and tectonic controls on terrace genesis in an active orogen*. Quaternary Science Reviews, **28**, 137-165.

Zanferrari A., Avigliano R., Grandesso P., Monegato G., Paiero G., Poli M.E. and Stefani C.; 2008: *Note illustrative della Carta Geologica d'Italia alla scala 1:50.000: Foglio 065 "Maniago"*. APAT-Servizio Geologico d'Italia – Regione Autonoma Friuli Venezia Giulia.

Zanferrari A., Masetti D., Monegato G. and Poli M.E.; 2013: *Note illustrative della Carta Geologica d'Italia alla scala 1:50.000; Foglio 049 "Gemona del Friuli"*. ISPRA-Servizio Geologico d'Italia - Regione Autonoma Friuli-Venezia Giulia, 262 pp. http://www.isprambiente.gov.it/Media/carg/friuli.html

SLOW TRANSIENT RECORDED BY THE CGPS FREDNET NETWORK AT THE ADRIA NORTHERN TIP (NE ITALY)

G. Rossi, D. Zuliani, P. Fabris
OGS (Istituto nazionale di Oceanografia e di Geofisica Sperimentale), Trieste, Italy

Introduction. In the last years the attention to GPS measurements increased enormously, for the capability of reconstructing plate boundaries and their movements, as well as faults activity at a more local scale. This implied also a continuous effort in increasing the reliability and accuracy of the measurements and of the calculus of the relative linear trends. Nowadays, having at disposal time series long enough (more than ten years) it is possible to begin to distinguish other terms that are superimposed to the linear trend, and hence to the rigid plate motion. In fact, Dong *et al.* (2002) and Blewitt and Lavallee (2002) identified annual and seasonal effects, while Smalley *et al.* (2005), Calais *et al.* (2005) evidenced some characters of the North-American plate movements that differ from the simple linear motion, and the interpretation of which is vividly debated. Also in our regions, Devoti *et al.* (2008; 2011) evidenced slow varying patterns in Italy at long-scale length (> 100 km) that cannot be explained by simple block models, and Nocquet (2012) interprets the observed velocity field in the whole Mediterranean region as a combination of localized and distributed deformation.

These considerations are at the basis of the research here presented. Having a disposal a data set of continuous GPS measurements, of decadal average length, in an area of intense and complex tectonic phenomena, we tried to inquire whether deviations from the linear trend are present, and the possible physical origin.

The data. The northern tip of the Adria microplate (NE-Italy) is continuously monitored by the Friuli Regional Deformation Network (FReDNet) of OGS (Istituto Nazionale di Oceanografia e Geofisica Sperimentale), consisting of 15 GPS/GNNS stations, the first 8 of which were installed between 2002 and 2004. The 10 stations of the Marussi network of the Friuli-Venezia Giulia regional council, some of which record continuously since 1999, provide additional information on the strain field in the region.

Fig. 1 – Vectors of the yearly horizontal velocities for the sites of the two networks (yellow, FReDNet stations, green, Marussi network stations), calculated from the linear trend. Dashed: the vectors calculated on the shortest time series.

We considered the GPS data of the longest time series from both networks, starting from 2002 till present. The resulting data set is composed by the data of: ZOUF, AFAL, ACOM, MPRA, UDI1, MDEA, TRIE from FReDNet, and AMP0, MOG0, POR0, PAL0 and TRI0 from the Marussi network.

We processed the data using GAMIT/GLOBK, eliminated the outliers, and filled the eventual short gaps in the data through linear interpolation. A strong annual component is present, as expected, due to seasonal variations of hydro-meteorological parameters (e.g., Blewitt and Lavallee, 2002). We tested, however, whether this annual term is affected by the so-called draconitic term, i.e. the time between two passages of the object through its ascending node, or the point of its orbit where it crosses the ecliptic from the southern to the northern hemisphere. From an accurate spectral analysis of the time series, it resulted that only a couple of station show, on one of the components, relevant amplitude associated to the draconitic term. A low-band pass filter allowed obtaining the time-series cleaned from the components with frequencies higher than 1.5 year, so to eliminate the annual and quasi-annual terms, and the highest frequencies. The so-obtained time-series for the two horizontal components are dominated by a linear trend, as expected, to which clear oscillations of apparent period of a few years (2-4) are superimposed. Oscillations are present also in the vertical component.

The data are shown in European plate reference frame, obtained from ITRF08 after rotation using the Euler vectors of Altamimi *et al.* (2012). The resulting velocity field from the analysis of the linear trend suggest crustal shortening, with values ranging between 0.6 and 2.8 mm/year, decreasing from South to North and, less pronounced, from East to West. This is in agreement with preceding observations and with the geodynamic character of the region, located in the area of convergence between Adria microplate and Eurasia (Fig. 1).

Deviations from the linear trend: characteristics and analysis. A said above, in the various sites, superimposed on the linear trend, 2-4 year period oscillations are present, and show higher amplitude with respect to the annual terms (Fig. 2).

To better analyse the oscillations, we first applied a band-pass filter (1.5–3 years) to the data, and then calculated the signal component along directions, spaced 15°, from N to N165E. This procedure allowed to evidence a sort of transient, of "period" of roughly 2.0 years, causing a bending in all the stations considered, distributed over the whole region, mainly along a direction about coincident with the Dinaric trend, N120E. Only in a few cases, the transient causes a bending toward an anti-dinaric direction which is also a dominant tectonic direction in the region (e.g. Bressan *et al.*, 2003, 2007). Fig. 3 shows the curves relative to the signal along the direction in which the maximum is recorded at each station, as well as the correspondent vertical GPS signal.

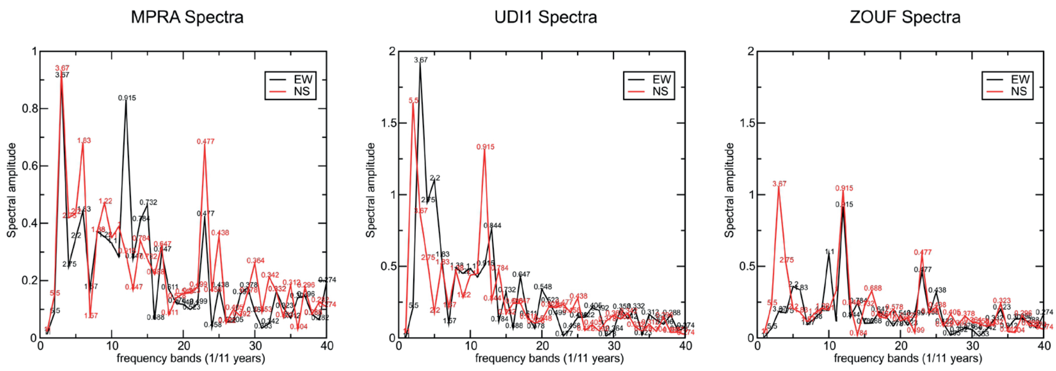

Fig. 2 – Three of the amplitude spectra of the longest time series from the FReDNet and Marussi networks: the numbers on the peaks are indicative of the periods in years and fractions of year.

As it may be seen, the transient causes positive displacement up-wards and along the directions indicated in the legend between 2007 and 2008, and opposite trend in 2009.

In order to state, whether the transient is due to tectonic phenomena or, vice versa, has an hydrologic origin, as found by Zerbini *et al.* (2010) in a neighboring area, we calculated the seismic energy released in the region in the same periods (e.g. Franceschina *et al.*, 2006), as well as the hydrological balance.

The first is defined as:

$$\log(E) = 1.94 M_D + 2.26$$

where E is the seismic energy and MD is the earthquake duration magnitude.

For the calculus of the hydrological balance, we started from the meteorological stations of the regional council networks nearest to each of the GPS stations and corrected the de-trended cumulative curves for the estimated evapo-transpiration, using the Thornthwaite (1948) formula:

$$PET = 16\left(\frac{L}{12}\right)\left(\frac{N}{30}\right)\left(\frac{10T_a}{l}\right)$$

where

$$l = \sum_{1}^{12}\left(\frac{T_{ai}}{S}\right)^{1.514}$$

and

$$a = \left(6.75\cdot 10^{-7}\right)l^3 - \left(7.71\cdot 10^{-5}\right)l^2 + \left(1.792\cdot 10^{-2}\right)l + 0.49239$$

with PET = estimated potential evapotranspiration (mm/month), Ta is the average daily temperature, N is the number of days in the month, L is the average length of the day, and l is the heat index. We compared GPS displacements, seismic energy, and hydrological balance in time, at time interval of about two months, starting from 2005 to 2010. There is a certain correlation between the time variations of the seismic energy distribution in the region and the ones of the deformation field induced by the transient. On the contrary, the variations in time of the hydrological balance distribution appear less in agreement, varying more slowly.

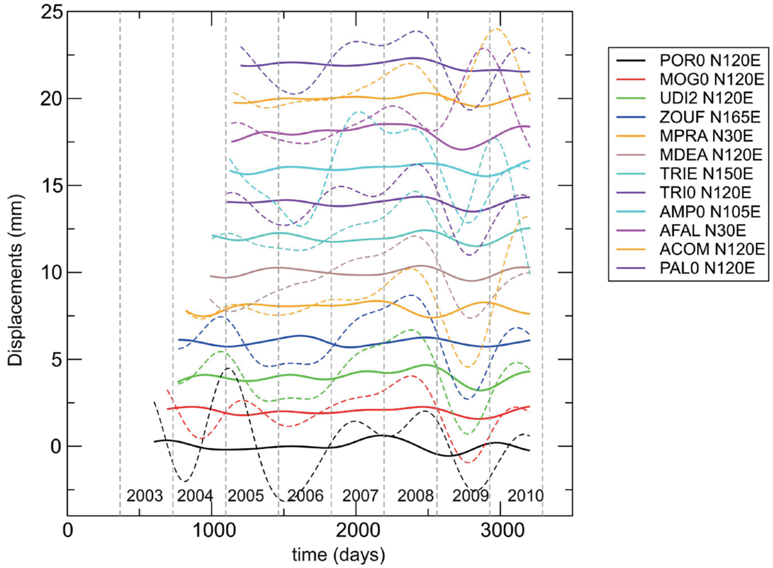

Fig. 3 – Solid lines: horizontal displacements along the directions shown in the legend box, along which the displacement is maximum for each station; dashed lines: vertical components. Constant values are applied to the curves to enable the comparison between the various sites. Grey dashed, vertical lines indicate the years.

Discussion and conclusions. In other parts of the world GPS networks recorded creep phenomena or silent or slow earthquakes (rupturing over a period of hours or days instead of seconds), in some cases accompanied by tremors, as observed, e.g., by Dragert *et al.* (2001), Lowry *et al.* (2001). In the region under study, after the tremors recorded by the horizontal pendulums of Grotta Gigante in the three years preceding the Friuli earthquake (Chiaruttini and Zadro, 1976), interpreted a-posteriori as slow earthquakes (Dragoni *et al*., 1984/5), tiltmeters and strainmeters evidenced the presence of quasi-periodic signals of longer-term (9 years and 33 years) with respect to the ones here analysed, and acting along directions about N70°E and N-S oriented respectively, hence, normal to the two main tectonic systems present in the region (the Alpine and the Dinaric ones) (Rossi and Zadro, 1996; Braitenberg and Zadro, 1999).

The present study focused on short period variations, recognizable on all the time-series considered, and causing bending from the linear trend mainly in the Dinaric direction. The data were compared both with the seismic energy released in the region and with the distribution of the hydrological balance, as representing possible hydrological effect. The results of the comparison are slightly more in favour of a tectonic origin of the transient, but to come to a definitive conclusion requires more analyses in the next future.

References

Altamimi, Z., L. Metivier, and X. Collilieux; 2012): ITRF2008 plate motion model, J. Geophys. Res., 117, B07402, doi:10.1029/2011JB008930.

Blewitt, G., and Lavallee D.; 2002: *Effect of annual signals on geodetic velocity*, J. Geophys. Res., 107(B7), 10.1029/2001JB000570.

Braitenberg C. and Zadro M.; 1999: *The Grotta Gigante horizontal pendulums – instrumentation and observations*. Boll. Geof. Teor. Appl., 40, 3/4, 577-582.

Bressan G., Bragato P.L. and Venturini C.; 2003: *Stress and Strain Tensors Based on Focal Mechanisms in the Seismotectonic Framework of the Friuli–Venezia Giulia Region (Northeastern Italy)*, Bulletin of the Seismological Society of America, 93, 3, 1280–1297.

Bressan G., Kravanja S., Franceschina G.; 2007: *Source parameters and stress release of seismic sequences occurred in the Friuli-Venezia Giulia (Northeastern Italy) and in Western Slovenia*, Phys. Earth Planet. Inter., 160, 192-214.

Calais, E., Mattioli G., DeMets C., Nocquet J.-M., Stein S., Newman A., Rydelek P.; 2005: *Tectonic strain in plate interiors?* Nature 438, doi: 10.1038/nature04428.

Chiaruttini C., Zadro M.;1976: *Horizontal pendulum observations at Trieste. Udine Meeting on the Friuli Earthquake, 1976*. Boll. di Geof. Teorica ed Applicata, Vol.XIX, n.72, 441-455.

Devoti R., Riguzzi F., Cuffaro M. and Doglioni C.; 2008: *New GPS constraints on the kinematics of the Apennines subduction*. Earth Planet. Sci. Lett. 273, 163-174, doi:10.1016/j.epsl.2008.06.031.

Devoti R., Riguzzi F., Cuffaro M. and Doglioni, C.; 2011: *New GPS constraints on the kinematics of the Apennines subduction*, Earth and Planetary Science Letters, 273, 163-174.

Dong, D., Fang P., Bock Y., Cheng M. K., and Miyazaki S.; 2002: *Anatomy of apparent seasonal variations from GPS-derived site position time series*, J. Geophys. Res., 107(B4), doi:10.1029/2001JB000573.

Dragert, H., Wang, K., James T.S.; 2001: *A Silent Slip Event on the Deeper Cascadia Subduction Interface*, Science, 292, 1525-1528, DOI: 10.1126/science.1060152.

Dragoni M., Bonafede M., Boschi E.; 1984/85: *On the interpretation of slow ground deformation precursory to the 1976 Friuli earthquake*, Pure Appl. Geophys., 122, 781-792.

Franceschina, G., Kravanja S.and Bressan G.; 2006: *Source parameters and scaling relationships in the Friuli-Venezia Giulia (Northeastern Italy) region*, Phys. Earth. Planet. Int., 154, 2, pp. 148-167.

Nocquet J-M.; 2012: *Present-day kinematics of the Mediterranean: A comprehensive overview of GPS results*, Tectonophysics, 579, 220-242.

Rossi G. and Zadro M.; 1996: *Long-term crustal deformations in NE-Italy revealed by tilt-strain gauges*, Phys. of the Earth and Plan. Int., 97, 55-70.

Smalley, R. Jr, Ellis M. A., Paul J. and Van Arsdale R. B.: 2005: *Space geodetic evidence for rapid strain rates in the New Madrid region, central USA*, Nature 435, pp. 1088-1090.

Thornthwaite, C.W.; 1948: An Approach toward a Rational Classification of Climate, Geogr. Rev., 38, 1., pp. 55-94.

Zerbini, S., Raicich F., Richter B., Gorini V. and Errico M.; 2010: *Hydrological signals in height and gravity in Northeastern Italy inferred from Principal Components analysis*, J. Geodyn., 49, 3-4, pp. 190-204.

INSAR-MEASURED CRUSTAL DEFORMATION TRANSIENTS ASSOCIATED TO THE EMILIA AND POLLINO SEISMIC SEQUENCES, 2011-2012

C.O. Tolomei, S. Salvi, G. Pezzo
Centro Nazionale Terremoti - INGV, Roma, Italy

Introduction. The occurrence and significance of crustal deformation transients in the seismic cycle is still a debated issue. The presence of mid- or short-term transient crustal deformation signals, has been fragmentarily reported for over a century, with different levels of quality and reliability (Roeloffs, 2006). Most of the reports deal with anomalies in the assumed steady inter-seismic deformation rates, often occurring in the temporal and spatial vicinity of large earthquakes (Rikitake, 1976; Wyss, 1991).

More recently, observations have also focused on the observation of transients occurring during the post-seismic phase, when the stress changes imparted by the earthquake are relaxed, stimulating significantly faster crustal and lithospheric deformation than during the inter-seismic phase (Wright *et al.*, 2013).

Thanks to the improved quality of GPS and InSAR data and analysis methods, new observations of long-term and short-term deformation transients are increasingly reported (Salvi *et al.*, 2012; Calais *et al.*, 2008; Furuya and Satyabala, 2008; Pritchard and Simons, 2006; Cakir *et al.*, 2005; Bernard *et al.*, 2004; Larson *et al.*, 2004; Dragert *et al.*, 2004; Miyazaki *et al.*, 2003; Ozawa *et al.*, 2002; Peltzer *et al.*, 2001). Some of these events are associated with post-seismic deformation, while others occur during the inter-seismic phase. Their duration ranges from weeks to years, with detected movements from mm/yr to cm/yr; their intensity can be large: the geodetic moment magnitude can exceed Mw=7 in subduction zones.

Modeling and theoretical developments (Peng and Gomberg, 2010; Liu and Rice, 2007) suggest that most of these events can be generated by aseismic slip or slow-slip events, often located in the deeper parts of a larger fault which later release seismic slip (Miyazaki *et al.*, 2011; Roeloffs, 2006).

This work, carried out within the 2012-2013 S3 INGV-DPC project *Measurement and analysis of crustal deformation transients during the Emilia and Pollino seismic sequences,* was aimed at the investigation of deformation transients using SAR Interferometry techniques in two test cases: the Emilia 2012, and the Pollino 2011-2012 seismic sequences. While Continuous GPS data are certainly the best suited for the detection of such transients (especially

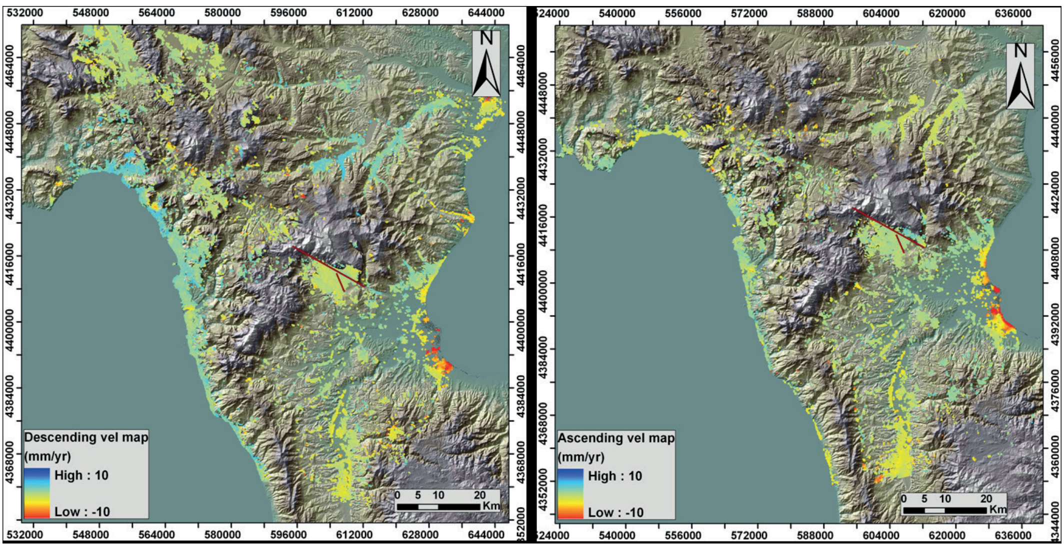

Fig. 1 – Envisat descending and ascending mean ground velocity map retrieved from SBAS approach.

the short-term ones), the two test areas were not well monitored by CGPS stations. ASAR and COSMO-SkyMed InSAR data sets allowed instead to investigate the presence of mid-term transients occurring at the scale of few days to months, giving at the same time the high spatial coverage and resolution needed to distinguish between tectonic and non-tectonic effects.

Deformation transients associated to the Pollino seismic sequence. We investigated the presence of deformation transients associated to the area surrounding the Pollino massif, where a seismic swarm is occurring since September 2010. This is an active but slow extensional deforming zone, affected by shallow, normal fault earthquakes, within the diffuse plate boundary between Africa and Eurasia (Sabadini *et al.*, 2009). In this area the most geologically evident structure is the long-lasting Castrovillari normal fault (Cinti *et al.*, 1997; Monaco *et al.*, 2000).

Ground deformation occurred before September 2010. We consider both the period preceding the inception of the seismic sequence (September 2010), as well as the period preceding the M 5.2 earthquake occurred in October 2012.

For the period before September 2010, we had three InSAR data sets. Two ENVISAT data set of 38 ascending and 32 descending ASAR images and a COSMO-SkyMed descending data set of 36 images.

A time-series for 38 ascending and 32 descending ASAR Envisat acquisitions respectively, was calculated using the Small Baseline Subset (SBAS) technique of [Berardino *et al.*, 2002]. The acquisitions span from May, 2003 to September, 2010.

The mean-velocity maps derived by SBAS in ascending and descending geometries are shown in Fig.1. Both maps show very low deformation velocities within the noise floor at about +/- 1.5 mm/yr, highlighting a generally low deformation rate for the entire Pollino area.

We have validated our results comparing the SAR mean velocities with the corresponding GPS benchmarks velocities (kindly provided by Dr. E. Serpelloni, INGV-Bologna) projected onto the ascending and descending satellite Line of Sights.

Due to the characteristics of the Pollino range, showing steep slopes, vegetated areas and presence of snow during the winter season, large decorrelated areas are present in the maps.

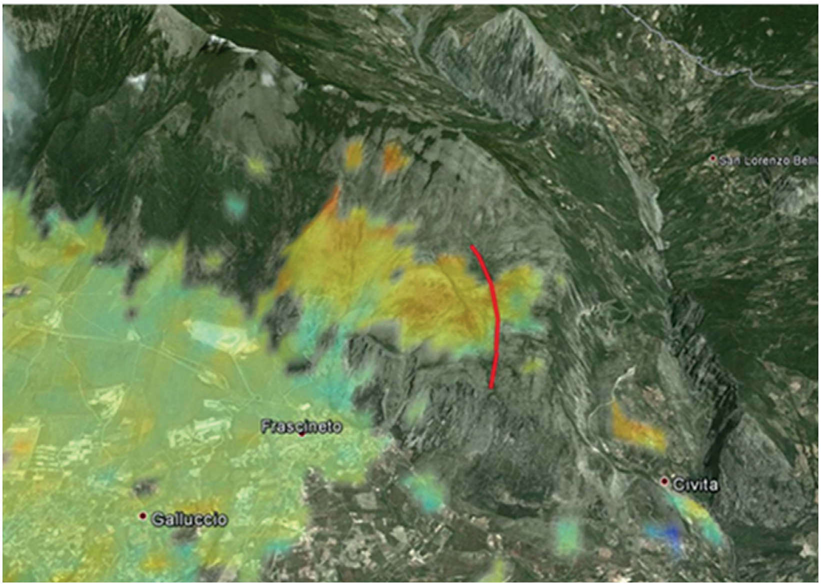

Fig. 2 – East velocity along the Southern Pollino range slope (red values), preliminary interpreted as due to mainly horizontal downslope sliding of the mid slope part, probably driven by the sliding surface whose main outcropping scarp is indicated with a red line.

In fact, over the areas affected by the ongoing seismic sequence few ground velocity values could be measured. The relative time series show clear atmospheric seasonal signals which are however filtered out given the length of the covered period. In the larger epicentral area we could not evidence relative ground velocity variations higher than the noise level. No medium-term transients are therefore detected. However, an interesting local signal is present along the SW front of the Pollino range.

In the ascending map, we observe a ground velocity gradient of ~1.5 mm/yr across the Pollino fault. A less evident gradient is observed in the descending map. Since a dense GPS network was not available across the fault at the same time of image acquisitions, we cannot validate this specific feature using independent data.

However a qualitative validation can be obtained comparing our results with the velocities obtained by Sabadini *et al.*, 2009 using an independents stack of ERS SAR images. These authors find a ~1.5 cm/yr vertical velocity difference in the same area, i.e along the SE slope of the Pollino range, between Frascineto and Civita, with the same sense of movement of our observations.

Apart from the differences in the deformation rates, the similarity of the two results suggests that the presence of artifacts in the DEM (two different DEMs were used in the two studies) or layered atmosphere can be discarded.

If we discard a tectonic origin, which seems not supported by the local scale of the signal, the only remaining possibility is that the deformation pattern is due to gravitational deformation. We have investigated the presence of long-term evidences of such movements, and have identified many clear ones: old detachment zones, slope-parallel fractures, a large mid-slope valley flanked by sliding “fault” scarps, and a general bulge of the slope. All these evidences suggest that the entire slope facing Frascineto is affected by slow, possibly episodic surface movements due to deep-seated gravitational deformation, were the dominating mechanism seems to be the lateral spreading.

To check the consistency of this interpretation, we used the ascending and descending velocity maps to derive the Up and East components for the common pixels in the entire area.

The considered part of the Pollino slope shows a clear eastward component of movement with respect to the stable Castrovillari plain, and this is in good agreement with the geometrical arrangements of the lateral spreading mechanism driven by the visible sliding surface. In fact, deep-seated gravitational deformation on the mountain ranges forming the footwall of normal faults has been observed at several sites in the Apennines (Moro *et al.*, 2012, 2009, 2007; Galadini, 2006; Salvi *et al.*, 2003).

Our preliminary interpretation will be followed by detailed field and geophysical studies of the slope. These footwall, slow moving, gravitational deformations can be excited by earthquake ground shaking up to complete collapse, and their mapping should be an important step of the seismic hazard assessment.

The COSMO-SkyMed time series acquired between October 2009 and October 2010 was processed using the SBAS algorithm. Unfortunately the short period of the time series does not allow to separate the seasonal contributions from the possible tectonic signals, and the data show no convincing evidences of the presence of deformation transients before the inception of the seismic sequence in September 2010.

Ground deformation occurred before October 26th, 2012. The only SAR data acquired across the October 26, 2012, Mw=5.2 event, is a COSMO data set from an ascending orbit. Unfortunately, for this data set the strong temporal decorrelation (mainly due to the high canopy vegetation cover, and to the limits of the X-band) and the presence of some temporal gaps in the image acquisition, prevented us to obtain an accurate and continuous measure of ground velocities in the epicentral area. In fact, a gap of image acquisitions of about 1.5 months precedes the mainshock, and we could not measure any deformation transient occurred in this period.

The Emilia area. In this case study, we processed COSMO-SkyMed ascending and descending data to monitor the deformation occurred in the areas affected by the May, 2012 earthquakes. We also considered an Envisat-ASAR descending dataset spanning from September, 1992 to June, 1999.

The aim was to investigate the possible presence of transient deformation signals occurring before any possible seismic activity in the area, i.e. before the mainshock and any following aftershocks. Thus the analysis included the measurement of the deformation occurring in the post-seismic period of the 2012 sequence.

Ground deformation occurred during the May-June, 2012 seismic sequence. The detection of possible transients associated to the largest aftershocks of the sequence (those occurred up to June 4th 2012) was not possible using time-series InSAR, since there were not enough COSMO images acquired before May 20th (Salvi *et al.*, 2012).

Using the classical two-pass InSAR technique on COSMO and Radarsat-1 data (Pezzo *et al.*, 2013), the coseismic ground displacement due to the main shocks of the sequence from May 20th to June 4th was mapped. InSAR, GPS, geological and seismological data were then used to constrain a source model for the May 20th and May 29th events, which suggested that the activated structures were the Ferrara and Mirandola thrusts, respectively (Pezzo *et al.*, 2013).

The results of the coseismic deformation analysis, source modeling, and interpretation allowed to estimate a 6-bar stress increase caused by the May 20th mainshock on the fault of the May, 29th event, which suggests a possible triggering (or clock-advancing) of the dislocation on the Mirandola thrust by the Ferrara thrust dislocation.

The InSAR analyses revealed also that during the 9-day period separating the two largest earthquakes, a ~7-8 cm aseismic deformation transient occurred in the area between the two dislocations. Unfortunately, as mentioned above, there were not enough pre-event images to investigate in detail this transient, but its closeness in space and time with the May 29th aftershock might imply a cause-effect relationship. This pattern is not associated with any significant (Ml ≥5) aftershock or foreshock of the May 20th event, and it can be modeled as slip occurring before the May, 29th aftershock fault plane (Pezzo *et al.*, 2013) or it could represent a slowslip event with no seismic signature.

Ground deformation occurred in the post-seismic phase. The temporal evolution of the ground deformation in this area could be investigated in detail only for the post-seismic time period following May 30th.

To this aim, we processed 2 ascending and 1 descending 9-month COSMO data sets covering the epicentral zone and the adjoining areas to the East and to the West (Tab. 1).

We obtained the mean ground velocity maps and the displacement time series for the frames listed in Tab. 1, using the SBAS (B3 asc and B10h asc) and the Persistent Scatterer (for the B4 asc North, Hooper, 2007) techniques.

The SRTM-1 DEM (30m) was used to remove the topographic component during the processing.

Tab. 1 – The 3 COSMO-SkyMed frames processed.

Orbit type	Beam	Number of images	Number of pairs	Temporal span	Resolution	Incidence angle
Ascending	B4North	18	17	11/6/2012 26/3/2013	180m	32.2
Ascending	B10h	17	24	04/07/2012 27/4/2013	180m	41.3
Descending	B3	13	26	23/5/2012 8/4/2013	180m	29.3

Since at the time of writing no reliable GPS time series were available for the post-seismic period, we validated the InSAR results by comparing the velocities in the overlapping areas. This procedure is possible because each velocity map is obtained using independent data from different orbits, but it is only qualitative, since the satellite-to-ground line of sights (LoS) are also different for each map.

Frame B4 North. The map shows a post-seismic uplift pattern (in the LoS direction) of up to ~20 mm/yr in the area of the May 20th, Mw=5.9 mainshock, corresponding to the top of the Ferrara thrust fold.

We tentatively attribute the uplift observed in the area 5 km North of Finale Emilia to afterslip over the May 20th fault plane, since: a) the displacement time series here show a nearly exponential trend typical of such local post-seismic signals; b) although decorrelation and noise are larger in the postseismic map, the similarity between the post-seismic mean velocity and the co-seismic displacement map (Pezzo *et al.*, 2013), is evident.

Lower uplift rates are observed in the frontal part of the Ferrara arc (to the North of the mainshock), while to the South negative ground velocities are present in the Finale Emilia and the Reno paleo-channel areas. The latter is an area where widespread co-seismic liquefaction effects were observed after the May 20th mainshock (Emergeo Working Group, 2013). The spatial correlation with these local co-seismic effects suggests that the high post-seismic

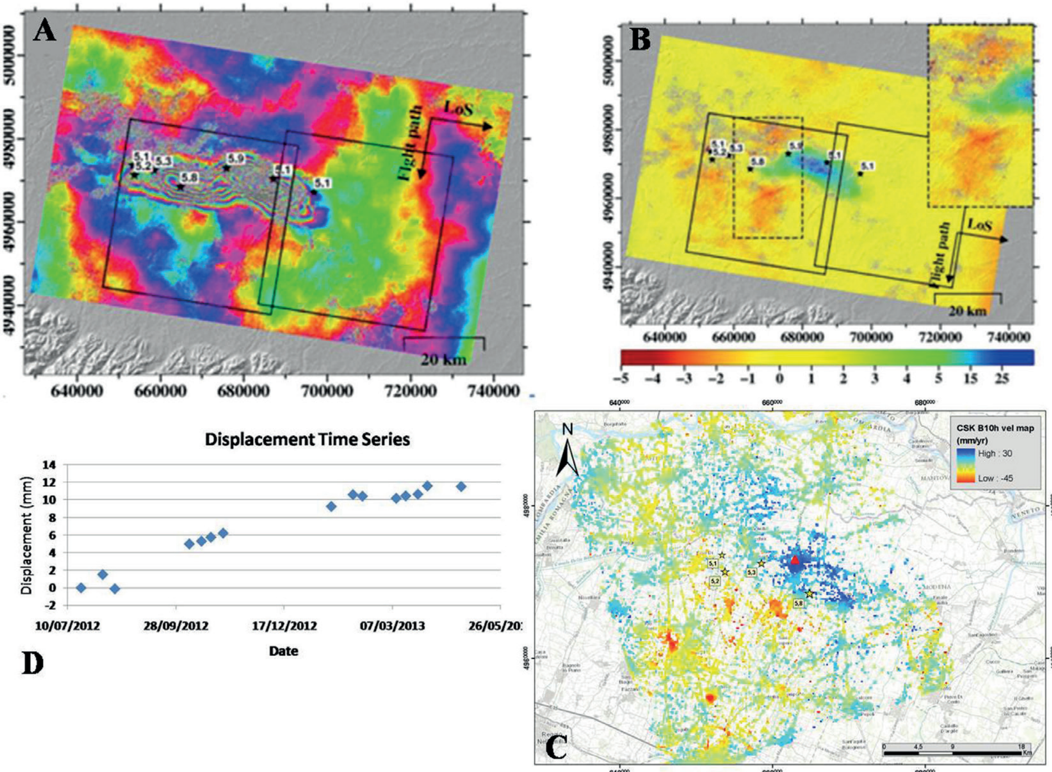

Fig. 3 – (A): Wrapped Radarsat-1 interferogram spanning from May, 12th to June, 5th. The black rectangles represent the COSMO-SkyMed footprints; (B): Displacement map obtained by subtracting COSMO-SkyMed and Radarsat deformation fields. In the top-right corner a zoom of the area enclosing the aseismic transient occurred between the two largest shocks of the sequence (Pezzo *et al.*, 2013); (C): Post-seismic ascending COSMO-SkyMed ground velocity map (Beam 10h); (D): Displacement COSMO-SkyMed time series (red triangle in (C)).

deformation rates observed along the Reno paleo-channel, and at least partially also in Finale Emilia, could be related to the readjustment of the shallow acquifer level.

Finally, an minor uplift of ~4 mm/yr is observed SE of Ferrara. This deformation shows a different sign in the frame B3 descending velocity map thus it may indicate the presence of a small component of horizontal displacement. In this case the movement would be W-directed, since the signals are positive in the ascending LoS and negative in the descending LoS.

Frame B10h. This map shows also interesting mean velocity patterns. LoS uplift velocities up to ~18 mm/yr are evident in the surroundings of the Mw= 5.8 Mirandola aftershock, as well as minor negative velocities immediately to the South. This pattern follows approximately the extent of the coseismic deformation (Pezzo *et al.*, 2013) and can likely be attributed to afterslip along the same fault.

In this map too we observe minor uplift North of the Mirandola thrust front. Moreover, few large, but very local subsidence patterns are also visible to the South (e.g. in Carpi); these patterns are not related to post-seismic deformation, and are due to long term ground movements caused by local acquifer depletion and/or shallow sediment compaction.

Frame B03 descending. In this map we notice again the LoS uplift in the area of co-seismic uplift (East of Bondeno), and the strong negative velocities along the Reno paleo-channel, with similar values observed in the ascending Beam 4 North and Beam 4 center (not shown).

The fact that in this area the ground velocities are similar on both the ascending and descending maps, indicates that most of the ground deformation here is occurring along the vertical direction.

The time series in the area of maximum subsidence shows that most of the deformation occurred within 4-5 months from the mainshock.

Ground deformation occurred before the start of the Emilia sequence. To investigate the inter-seismic phase in the area an Envisat-ASAR (C-Band) descending dataset of 37 images (10/02/2003-06/09/2010) has been processed using the SBAS algorithm.

The obtained mean ground velocity map shows a maximum negative value of ~35 mm/yr around the cities of Bologna and Forlì. These patterns depend on well-known urban subsidence phenomena due to hydro-geological reasons and are not related to tectonic movements. Moreover, a positive (towards the satellite) ground velocity signal is visible close the area affected by the May, 2012 mainshocks.

Discussion and conclusions. We analysed several different InSAR datasets of COSMO-SkyMed and ENVISAT images encompassing the Pollino and Emilia sequences of moderate seismicity.

From a methodological point of view, the two test cases were very challenging. In the premises, the inherent difficulties of these test cases where: low deformation rates, probable presence of spatially and temporally complex deformation patterns, probable fast InSAR decorrelation between successive images due to vegetation and agriculture developments, short monitoring periods and limited size of the data sets (for COSMO), limited availability of the CGPS time series to be used for the correction of InSAR orbital artifacts.

Eventually, we demonstrated the good capacities of time series InSAR techniques for the measurement of ground deformation patterns in these areas. Local, non tectonic deformation patterns were easily detected, as well as subtle patterns extended over larger spatial wavelengths.

Quantitative validation by independent data could not be performed using CGPS, but qualitative validation using overlapping InSAR results gave in general good results.

The COSMO-SkyMed coverage was temporally very discontinuous before the start of the Emilia sequence, and no good data set was available for possible pre-seismic deformation studies. However, an ENVISAT dataset of 37 images covering the temporal span 10/02/2003-06/09/2010 and an ERS1/2 dataset of 36 images (30/09/1992-05/06/1999) were analyzed, and they did not show particular long-term deformation transients in the area interested by the 2012 Emilia sequence.

During the seismic sequence we detected a rapid deformation transient which likely occurred between the two events, and which could be attributed to an aseismic dislocation (perhaps triggered by the first event) occurred on the fault plane of the second event. Unfortunately this deformation event is mapped on only two images, and its temporal behaviour is not known (Pezzo *et al*., 2013).

In the post-seismic phase of the Emilia sequence, our results did allow to detect deformation transients in the areas of the largest shocks of the sequence, with progressively decreasing ground velocities during a period of few months. The temporal (and spatial) characteristics of these signals suggest that they are related to afterslip along the same faults activated during the sequence. The amount of total postseismic surface displacement is about 5-10% of the coseismic one. Modeling is under way to determine in which parts of the sources this afterslip was released.

A methodological consideration stemming from our work is that time series InSAR is certainly able to measure small ground velocity transients, with temporal wavelengths of several days, but to this purpose an ad hoc monitoring strategy must be put in place and strictly followed.

In particular, for X-band imagery as COSMO-SkyMed, a very high repeat pass frequency is required (1-4 days), and temporal acquisition gaps must be avoided, to prevent loss of coherence and signal degradation.

In both the Emilia and Pollino cases the image sampling was well below these requirements and we were only able to detect the post-seismic transient signals.

Finally, we stress that the search for possible preseismic ground deformation anomalies should not be abandoned based on the results of this study, but should be approached isolating test cases involving larger earthquakes than those considered here, and integrating Continuous GPS networks with a 10-km spacing, with InSAR time series with a very high sampling rate (1-4 days).

Acknowledgements. The COSMO-SkyMed SAR data are copyright of ASI. We thank all public and private institutions that manage and distribute the GPS data. We thank FOGER for providing the Emilia-Romagna GNSS network, the Dept. of Earth Science of the University of Siena and the Dept. of Physics of the University of Bologna for providing data of the GPS station in Finale Emilia. A particular thanks is addressed to Dr. Paolo Riccardi (Sarmap) for his fruitful support during the SAR data processing.

References

Berardino, P., Fornaro, G., Lanari, R. & Sansosti, E.; 2002: *A new algorithm for surface deformation monitoring based on small baseline differential SAR interferograms*. IEEE Trans. Geosci. Remote Sens., 40 (11), 2375-2383.

Bernard P., Boudin F., Sacks S., Linde A., Blum P.-A., Courteille C., Esnoult M.-F, Castarede H., Felekis S. and Billiris H.; 2004*: Continuous strain and tilt monitoring on the Trizonia Island, Rift of Corinth, Greece*. Compt. Rend. Geosci., 336, 313-323.

Bigi, G., G. Bonardi, R. Catalano, D. Cosentino, F. Lentini, M. Parotto, R. Sartori, P. Scandone and E. Turco (Eds.); 1983: *Structural Model of Italy 1:500,000*. CNR Progetto Finalizzato Geodinamica.

Cakir Z., A.M. Akoglu, S. Belabbes, S. Ergintav, M. Meghraoui; 2005: *Creeping along the Ismetpasa section of the North Anatolian fault (Western Turkey): rate and extent from InSAR*. Earth. Planet. Sci. Lett., 238, pp. 225-234

Calais E., N. d Oreye, J. Albaric, A. Deschamps, D. Delvaux, J. Deverchere, C. Ebinger, R.W. Ferdinand, F. Kervyn, A.S. Macheyeki, A. Oyen, J. Perrot, E. Saria, B. Smets, D.S. Stamps, C. Wauthier; 2008*: Aseismic strain accommodation by slow slip and dyking in a youthful continental rift.*. East Africa Nature, 456.

F. R. Cinti, L. Cucci, D. Pantosti, G. D'Addezio, M. Meghraoui; 1997: *A major seismogenic fault in a 'silent area': the Castrovillari fault (southern Apennines, Italy*, Geophysical Journal International, 130, 3, 595-605.

Dragert, H., Wang, K. & Rogers, G.; 2004: *Geodetic and seismic signatures of episodic tremor and slip in the northern Cascadia subduction zone*. Earth Planets Space 56, 1143-1150

Emergeo Working Group: Alessio, G., L. Alfonsi, C. A. Brunori, P. Burrato, G. Casula, F. R. Cinti, R. Civico, L. Colini, L. Cucci, P. M. De Martini, E. Falcucci, F. Galadini, G. Gaudiosi, S. Gori, M. T. Mariucci, P. Montone, M. Moro, R. Nappi, A. Nardi, R. Nave, D. Pantosti, A. Patera, A. Pesci, G. Pezzo, M. Pignone, S. Pinzi, S. Pucci, S. Salvi, C. Tolomei, P. Vannoli, A. Venuti, and F. Villani; 2013: *Coseismic geological effects associated with the Emilia earthquake sequence of May-June 2012 (Northern Italy)*. Nat. Hazards Earth Syst. Sci. 13, 1-13.

Furuya M., S.P. Satyabala; 2008: *Slow earthquake in Afghanistan detected by InSAR*. Geophys. Res. Lett., 35.

Galadini, F.; 2006: *Quaternary tectonics and large-scale gravitational deformations with evidence of rock-slide displacements in the Central Apennines (central Italy).* Geomorphology, 82(3), 201-228.
Hooper, A., P. Segall, and H. Zebker; 2007: *Persistent scatterer interferometric synthetic aperture radar for crustal deformation analysis, with application to Volca′n Alcedo, Gala′pagos*. J. Geophys. Res., 112, B07407, doi:10.1029/2006JB004763.
Larson, K. M., A. R. Lowry, V. Kostoglodov, W. Hutton, O. Sánchez, K. Hudnut, and G. Suárez; 2004: *Crustal deformation measurements in Guerrero, Mexico*. J. Geophys. Res., 109, B04409.
Liu, Y. & Rice, J. R.; 2007*: Spontaneous and triggered aseismic deformation transients in a subduction fault model.* J. Geophys. Res. 112, B09404.
Miyazaki, S., J. J. McGuire, and P. Segall; 2003: *A transient subduction zone slip episode in southwest Japan observed by the nationwide GPS array.* J. Geophys. Res., 108(B2), 2087.
Miyazaki S., J. J. McGuire, P. Segall; 2011: *Seismic and aseismic fault slip before and during the 2011 off the Pacific coast of Tohoku earthquake*. Earth Planets Space 63, 637.
Monaco C., Tortorici L.; 2000; *Active faulting in the Calabrian arc and eastern Sicily.* Journal of Geodynamics, 29, 3-3, 407-424.
Moro, M., Saroli, M., Gori, S., Falcucci, E., Galadini, F., & Messina, P.; 2012: *The interaction between active normal faulting and large scale gravitational mass movements revealed by paleoseismological techniques: A case study from central Italy.* Geomorphology, 151, 164-174.
Moro, M., Saroli, M., Tolomei, C., & Salvi, S.; 2009: *Insights on the kinematics of deep-seated gravitational slope deformations along the 1915 Avezzano earthquake fault (Central Italy), from time-series DInSAR*. *Geomorphology*, *112*(3), 261-276.
Moro, M., Saroli, M., Salvi, S., Stramondo, S., & Doumaz, F.; 2007: *The relationship between seismic deformation and deep-seated gravitational movements during the 1997 Umbria–Marche (Central Italy) earthquakes*. Geomorphology, 89(3), 297-307.
Ozawa S., Murakami M., Kaidzu M., Tada T., Sagiya T., Hatanaka Y., Yarai H., Nishimura T.; 2002: *Detection and monitoring of ongoing aseismic slip in the Tokai region, central Japan*. Science298, 1009–1012.
Peltzer, G., Crampé, F., Hensley, S. & Rosen, P.; 2001: *Transient strain accumulation and fault interaction in the Eastern California shear zone*. Geol. Soc. Am., 29(11), 975–978.
Peng, Z. & Gomberg, J.; 2010: *An integrated perspective of the continuum between earthquakes and slow-slip phenomena.* Nature Geosci. 3, 599–607
Pezzo G., Merryman Boncori J.P, Tolomei C., Salvi S., Atzori A., Antonioli A., Trasatti E., Novali F., Serpelloni E., Candela L., Giuliani R.; 2013: *Coseismic deformation, and source modeling of the May 2012 Emilia (Northern Italy) earthquakes.* Seismol. Res. Lett..
Pritchard, M. E., Ji, C., & Simons, M.; 2006: *Distribution of slip from 11Mw >6 earthquakes in the northern Chile subduction zone*. Journal of Geophysical Research, 111, doi:10.1029/2005JB004013.
Pritchard, M. E., and M. Simons; 2006: *An aseismic slip pulse in northern Chile and along-strike variations in seismogenic behavior.* J. Geophys. Res., 111, B08405.
Rikitake, T.; 1976: *Earthquake Prediction*. xvi, 357 p., Elsevier, Amsterdam.
Roeloffs, E. A.; 2006: *Evidence for aseismic deformation rate changes prior to earthquakes*. Annu.Rev. Earth Planet. Sci., 34, 591–627.
Sabadini R, Aoudia A, Barzaghi R, Crippa B, Marotta AM, Borghi A, Cannizzaro L, Calcagni L, Dalla Via G, Rossi G, Splendore R, Crosetto M.; 2009: *First evidences of fast creeping on a long-lasting quiescent earthquake normal-fault in the Mediterranean.* Geophys J Int., 179, 720-732.
Salvi, S., Cinti, F. R., Colini, L., D'addezio, G., Doumaz, F., & Pettinelli, E.; 2003: *Investigation of the active Celano–L'Aquila fault system, Abruzzi (central Apennines, Italy) with combined ground-penetrating radar and palaeoseismic trenching.* Geophysical Journal International, 155(3), 805-818.
Salvi, S., Tolomei, C., Merryman Boncori, J. P., Pezzo, G., Atzori, S., Antonioli, A. & Coletta, A.; 2012: *Activation of the SIGRIS monitoring system for ground deformation mapping during the Emilia 2012 seismic sequence, using COSMO-SkyMed InSAR data.* Annals of Geophysics, 55(4).
C. Tansi, A. Tallarico, G. Iovine, M. Folino Gallo, G. Falcone; 2005: *Interpretation of radon anomalies in seismotectonic and tectonic-gravitational settings: the south-eastern Crati graben (Northern Calabria, Italy.,* Tectonophysics, vol.396, doi:10.1016/j.tecto.2004.11.008
Wright T.J., John R. Elliott, Hua Wang, Isabelle Ryder; 2013: *Earthquake cycle deformation and the Moho: Implications for the rheology of continental lithosphere*. Tectonophysics, ISSN 0040-1951, http://dx.doi.org/10.1016/j.tecto.2013.07.029.
Wyss, M.; 1991: *Evaluation of proposed earthquake precursors, in IASPEI Sub-commission on Earthquake Prediction*. American Geophysical Union, Washington, D.C., 94 pp.

SEISMIC STRAIN RATE VARIATION IN THE AREA SHOCKED BY THE 2012 EMILIA SEISMIC SEQUENCE

S. Barani[1,2], R. De Ferrari[1,2]
[1]*DISTAV, Università degli Studi di Genova, Italy*
[2]*GEAmb S.r.l., spin-off dell'Università di Genova, Italy*

Foreword and scope of work. This work draws inspiration from the discussion, taken during the final meeting of the DPC-INGV 2012-2013 projects (https://sites.google.com/site/progettisismologici/), about seismic strain rate variations in the area shocked by the 2012 Emilia seismic sequence. A further motivation for this work is the evident anomaly (with respect to the neighboring areas) shown in that area by the seismic strain rate map published by Barani *et al.* (2010), map which is presented also here (Fig. 1). The map clearly shows a deficit in the release of seismic deformation or, more precisely, a deficit in the distribution of the strain rate values in the area between Modena and Ferrara. This pattern is very similar to that observed by Chen *et al.* (2009) analyzing the distribution of the total amount of seismic moment in the Taiwan region before and after the 1999 Chi-chi earthquake (M_w = 7.6) and to that found by Barani and Eva (2011) in the area stricken by the 2009 L'Aquila earthquake (M_w = 6.3). Both studies have evidenced clear deficits in the total amount of seismic moment, deficits which were then filled following the occurrence of strong earthquakes. The major conclusion from both studies was that, for domains with similar tectonic settings, the analysis of deficit-then-fill patterns may be useful for the inference of future disastrous earthquakes.

In this study, the approach for seismic strain rate calculation proposed by Barani *et al.* (2010) is applied to the area of the 2012 Emilia sequence in order to investigate, in a retrospective way, the anomaly observed in the map in Fig. 1. The study is also important to further test the reliability of the method of Barani *et al.* (2010) to study seismicity patterns, such as seismic gaps and quiescence periods.

Seismotectonic framework. The area struck by the Emilia 2012 seismic sequence is located in the outermost portion of the northern Apennines. The Apennine chain is a post-collisional

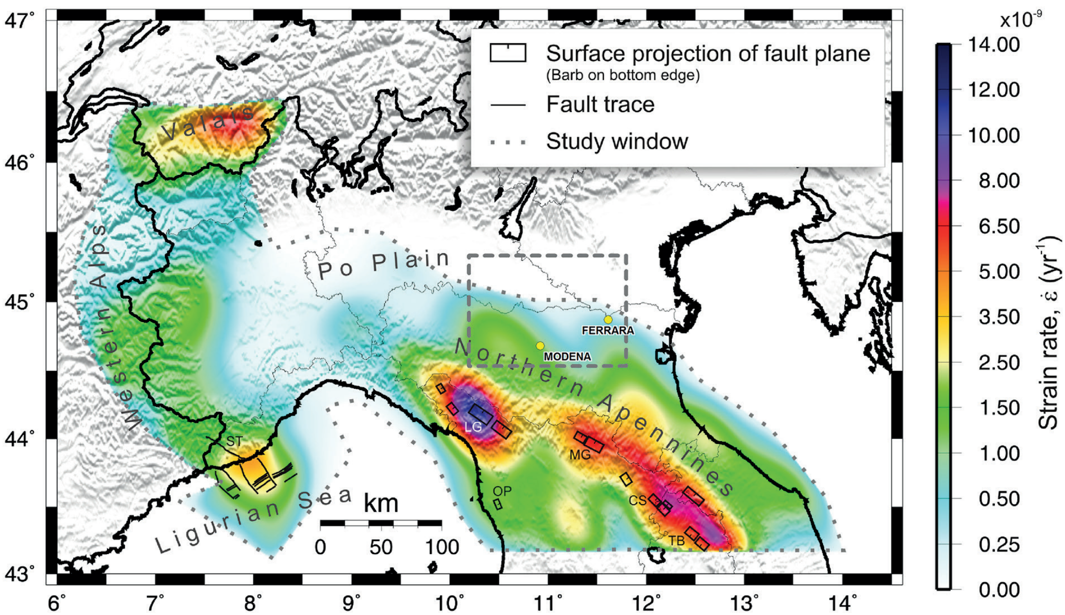

Fig. 1 – Seismic strain rate map for Northwestern Italy (after Barani *et al.*, 2010). The map accounts for the contribution of earthquakes occurred between year 1350 and 2006. The dashed square indicates the interpolation area Fig. 2.

belt, the formation of which is related to the tectonic interaction between the African and European plates. Compressional deformation results from the westward subduction of the Adriatic lithosphere, causing the formation of compressional fronts migrating towards E and NE, thus progressively affecting the Adriatic foreland (Patacca *et al.*, 1990; Chiarabba *et al.* 2005; Molli *et al.* 2010; Bignami *et al.*, 2012).

The May-June 2012 seismic sequence was characterized by two strong events of M_w 6.1 and 6.0 occurred on May 20 and 29, respectively. Both events were located close to the buried front of the Ferrara northward-verging active thrust belt. The two main earthquakes were then followed by six $M_w \geq 5.0$ events and by many weaker shocks. The aftershock distribution covers an area of 800 km^2 extending in the E-W direction for a total length of approximately 55km (Mirandola Earthquake Working Group, 2012). Compared to the May 20 event, the earthquake occurred on May 29 is located westward and the related aftershocks cover the western and central parts of the thrust front (Mirandola Earthquake Working Group, 2012).

As argued by some authors, the 2012 Emilia seismic sequence activated a portion of the buried outer thrust fronts of the northern Apennines (Bignami *et al.*, 2012). More specifically, two N-NNE-verging segments of the blind thrust of the external Ferrara-Romagna Arc were activated (Serpelloni *et al.*, 2012). Focal mechanisms indicate a prevalent compression (Pondrelli *et al.*, 2012), which is in agreement with the regional compressional tectonics characterizing the Apennine structures buried below the Po Plain sediments (Boccaletti *et al.*, 2004, Boccaletti *et al.*, 2011, Pondrelli *et al.*, 2012). Only in a few rare cases, a strike-slip component was observed. Of note is the rotation of the axis of maximum compression (P-axis). The major events show pure, low angle, thrust mechanisms with P-axis pointing towards north. Some aftershocks clearly present a rotation with respect to this dominant northward direction. In particular, those pointing towards NW are located close to the NE-striking part of the buried thrust front (Pondrelli *et al.*, 2012).

Concerning past earthquakes, the seismicity was mostly concentrated along northeastern sector of the Apennine chain, at the border with the Po Plain. However, strong earthquakes also occurred in the blind thrust zone in the outer sector of the Apennines, such as the 1346 Ferrara (M_w = 5.8), 1570 Ferrara (M_w = 5.5), and 1688 Romagna (M_w = 5.9) earthquakes.

Methodology. The calculation method proposed by Barani *et al.* (2010) is based on the zone-less, smoothed seismicity approach used by Frankel (1995) for the seismic hazard assessment of the Central and Eastern United States. The method of Barani *et al.* (2010) consists of calculating moment rates, $\dot{M}_o$, for each cell of a homogeneous grid covering the entire study area. Then, an elliptical kernel (here applied with smoothing parameters τ_1 = 30km and τ_2 = 20 km) with the major axis (τ_1 is the major semi-axis) oriented parallel to the prevalent direction of compression characterizing the outer Apennines is applied on them to determine smoothed $\dot{M}_o$ values. Based on this approach, the elliptical smoothing function allows for both the epicentral location error (quantified by τ_1 and τ_2) and the prevalent orientation of active faults within a region. $\dot{M}_o$ values are then converted into strain rates, $\dot{\varepsilon}$, by applying the Anderson formula (Anderson, 1979):

$$\dot{\varepsilon} = \frac{\dot{M}_o}{(2/k)\mu V} \qquad (1)$$

where k (= 0.66) is an empirical constant that depends on the regional stress field, μ is the shear modulus (taken as $3.6 \cdot 10^{10}$ N/m^2), and $V = Ah$ is the seismogenic volume (A indicates the area of a grid cell and h is the thickness of the seimogenic layer).

In this application, $\dot{M}_o$ values are calculated by summing the moments M_o of all events with $M_w \geq 4.0$ (and then dividing the cumulative moment by the observation period to obtain the rate per year) included in the catalog used by Barani *et al.* (2010) updated to year 2013 (to this end, the ISIDE database is used; http://iside.rm.ingv.it). The catalog collects both historical [the CPTI04 catalog is used (Gruppo di Lavoro CPTI, 2004)] and instrumental earthquake data. Note, finally, that a Monte Carlo simulation procedure is adopted to allow for the uncertainty affecting earthquake magnitude and seismogenic thickness. Strain rate maps presented here display average results from 500 randomizations. For further details regarding the overall procedure, the reader can refer to the article of Barani *et al.* (2010).

Results and discussion. Fig. 2 shows the distribution of the seismic strain rate values before (Fig. 2a) and after (Figs. 2b and 2c) the 2012 sequence. While the maps in Figs. 2a and 2b are based on earthquake data sets collecting independent events [analogously to Barani *et al.* (2010)], Fig. 2c includes also the contribution of aftershocks and foreshocks recorded between year 2007 and 2013. Compared to the map in Fig. 1, the maps in Fig. 2 are computed using a finer grid, of 0.025° spacing in latitude and longitude. Comparing the three maps not only seems to confirm our suspicion about the presence of a seismicity gap (precisely, a spatial gap) between Modena and Ferrara but would also indicate that this gap was completely filled in by 2012 crisis. Note the non-negligible contribution from the stronger aftershocks following

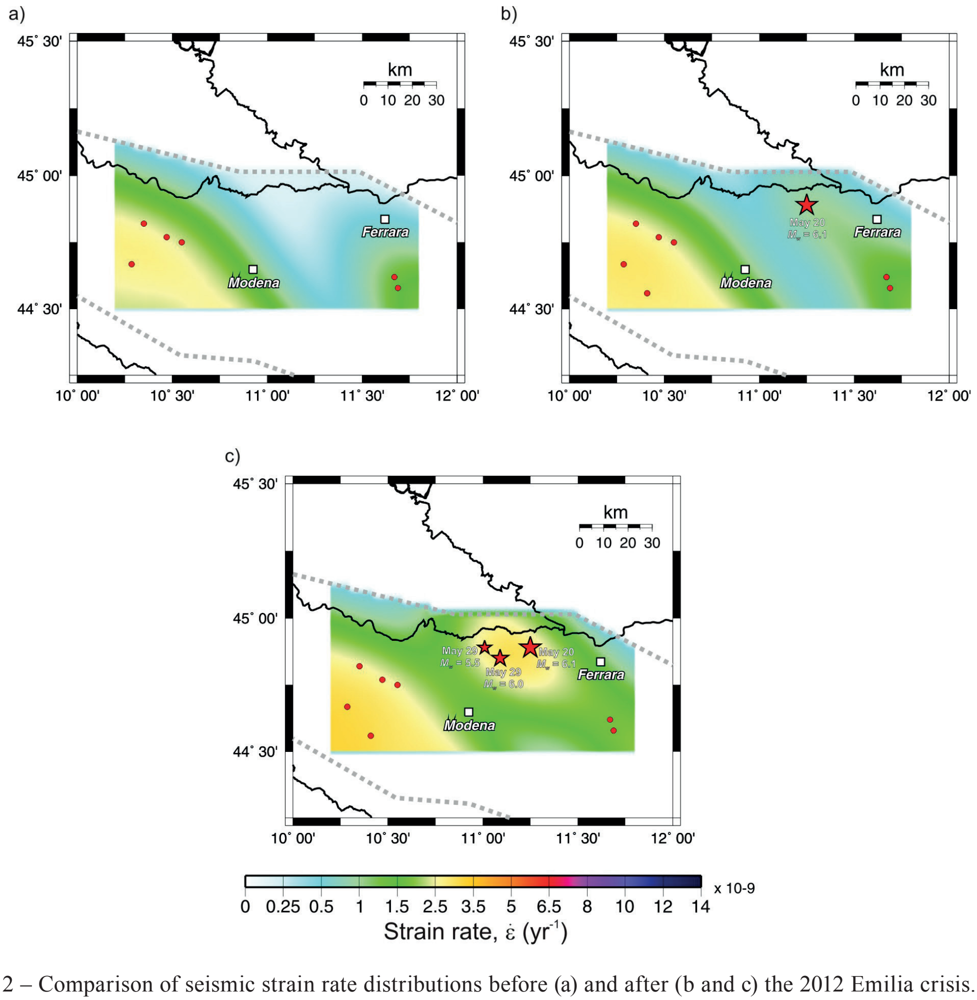

Fig. 2 – Comparison of seismic strain rate distributions before (a) and after (b and c) the 2012 Emilia crisis. The maps in Figs. 2a and 2b use declustered catalogs. Clusters from year 2007 to 2013 are retained to produce the map in Fig. 3c. Red circles indicate M5.5+ earthquakes occurred since 1740 (year of completeness for M5.5+ events). The major events belonging to the 2012 sequence are indicated by red stars.

the May 20 shock, which produce an increase in the strain rate from about 1-1.5 yr[1] (Fig. 2b) to 2.5-3.5 yr[1] (Fig. 2c).

In order to identify a possible quiescence period (often named as temporal gap or gap of 2nd kind) preceding the May 20 earthquake, we have analyzed the variation of the seismic moment release rate with time. More specifically, we plot 50-year running averages of the (smoothed) seismic moment release rate as a function of time (Fig. 3a) accounting for the contribution of earthquakes with magnitude $M_w \geq 5.0$ since 1825 [which corresponds to the year of catalog completeness for M5+ events as determined by Barani *et al.* (2010)]. In such a way, quiescence periods are identified by minima in the $\dot{M}_o$ curve which are attributable to seismic inactivity (particularly concerning the occurrence of moderate to large earthquakes). The temporal variation of the cumulative seismic moment (again calculated using the smoothed seismicity approach) is also shown (Fig. 3b). In this latter plot, quiescence periods are identified by "plateau" in the cumulative curve. In this study, we compare the curves for two sites, one (site S1) located close to the May 20 event and one (site S2) between the two larger aftershocks occurred on May 29 (see Fig. 2c).

Similarly to the case study of the 2009 L'Aquila earthquake, Fig. 3a evidences that the occurrence of the main shock is preceded by a minimum in the running average of $\dot{M}_o$. The minimum in the $\dot{M}_o$ curve, which presents a rise in the latter stages (last 15 years) before the occurrence of the main shock, corresponds to a period of time during which the seismic activity in the region surrounding the seismic gap is sporadic (i.e., earthquakes of $M_w \geq 5.0$ are almost absent). Only five events of M_w greater than or equal to 5.0 occurred in the study region (dashed square in Fig. 1) from year 1923 to 2012, at distances greater than 30 km from the gap area.

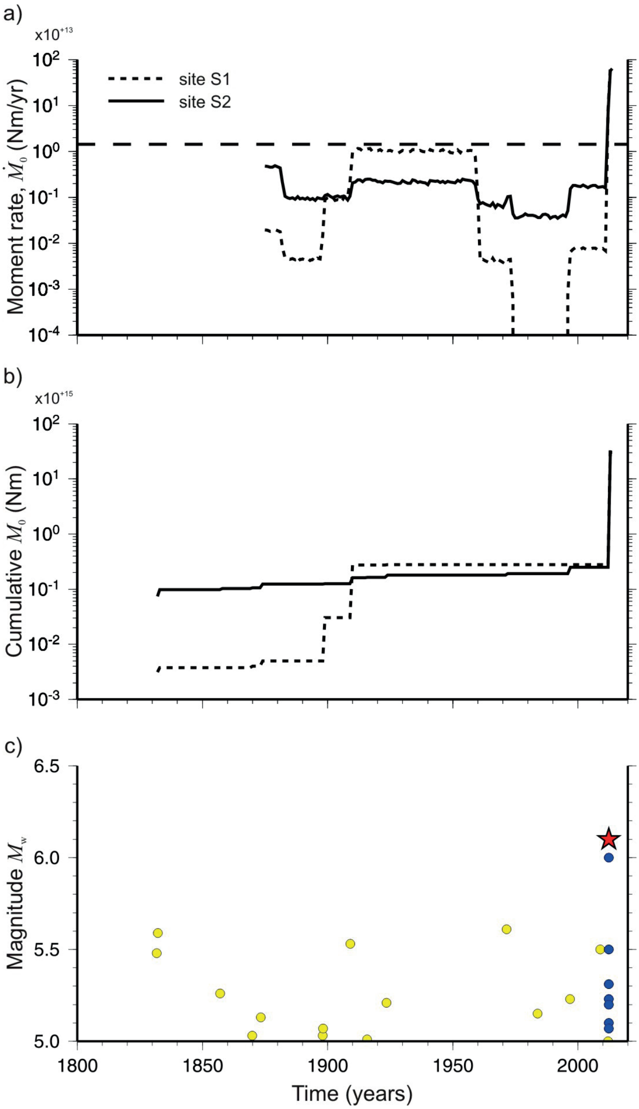

Fig. 3 – Evolution of seismic activity ($M_w \geq 5.0$) in the area shocked by the Emilia 2012 seismic sequence from 1825 to 2013: 50-year running averages of the seismic moment release rate versus time (data points in the running average curve are plotted at the end of each time interval) (a); cumulative seismic moment versus time (b); distribution of earthquake magnitude versus time (c). The horizontal dashed line in Fig. 3a indicates the average moment rate calculated in the seismicity gap area. Blue circles in Fig. 3c indicate the earthquakes belonging to the 2012 sequence; the May 20 main shock is displayed by a red star.

They concentrated in a period of time of about 30 years close to the 2012 sequence, from July 1971 to January 2012. As such, this pattern may be an index of preseismic quiescence (e.g., Kanamori, 1981, Ellsworth, 1981, Scholz, 1988). Defining the length of the preseismic quiescence stage is not an easy task. One could assume the time frame going from year 1909 (occurrence of the Bassa Padana earthquake, M_w 5.5) to 2012, corresponding to the “plateau” in Fig. 3b (dashed line). However, considering the average moment rate for the area under study (horizontal dashed line in Fig. 3a), it is not unreasonable to assume a wider period of time (which is not considered in the calculation due to catalog incompleteness), possibly extending from the 1570 Ferrara (M_w = 5.5) or 1688 Romagna (M_w = 5.9) earthquakes to 2012. To verify this second hypothesis, one should analyze the variation of the seismic moment release rate with time taking into consideration the contribution of the seismic activity since 1500 (despite the possible incompleteness of the catalog). Finally, comparing the results for site S1 and site S2, it is evident that the curves relevant at site S2 in Figs. 3a and 3b are influenced by the higher seismic activity characterizing the northeastern sector of the Apennine chain, at the border with the Po Plain.

Concluding, this study has revealed that the 2012 Emilia seismic crisis occurred in an area characterized by a seismicity gap and was preceded by a quiescence period of at least 100 years (or possibly wider, going back to 1570) during which the moment rate and the cumulative moment trends indicate a deficit in the release of seismic deformation. Furthermore, the study has confirmed the effectiveness of the smoothed seismicity method of Barani *et al.* (2011) for the detection and analysis of peculiar seismicity patterns, such as seismic gaps and quiescence periods. This makes the method useful for the monitoring of the evolution of the seismic activity in a region, as it may help in inferring the areas of occurrence of future disastrous earthquakes.

References

Anderson, J. G.; 1979: *Estimate the seismicity from geological structure for seismic-risk studies*. Bull. Seism. Soc. Am., **69**, pp. 135-158.

Barani. S. and Eva C.; 2011: *Did the April 6, 2009 L’Aquila earthquake fill a seismic gap?* J. Geophys. Res., **82**, pp. 645-653.

Barani. S., Scafidi D. and Eva C.; 2010: *Strain rates in northwestern Italy from spatially smoothed seismicity*. J. Geophys. Res., **115**, B07302, doi: 10.1029/2009JB006637.

Bignami C., Burrato P., Cannelli V., Chini M., Falcucci E., Ferretti A., Gori S., Kyriakopoulos C., Melini D., Moro M., Novali F., Saroli M., Stramondo S., Valensise G. and Vannoli P.; 2012: *Coseismic deformation pattern of the Emilia 2012 seismic sequence imaged by Radarsat-1 interferometry*. Annals Of Geophysics, **55**, pp. 789-795.

Boccaletti M., Bonini M., Corti G., Gasperini P., Martelli L., Piccardi L., Tanini C. and Vannucci G.; 2004: *Seismotectonic Map of the Emilia-Romagna Region, 1:250000*. Regione Emilia-Romagna – CNR.

Boccaletti M., Corti G. and Martelli L.; 2011: *Recent and active tectonics of the external zone of the northern Apennines (Italy)*. Int. J. Earth Sci., **100**, pp. 1331-1348.

Chen R.-Y., Kao H., Liang W.-T., Shin T.-C., Tsai Y.-B. and Huang B.-S.; 2009: *Three-dimensional patterns of seismic deformation in the Taiwan region with special application from the 1999 Chi-Chi earthquake sequence*. Tectonophysics, **466**, pp. 140-151.

Chiarabba C., Jovane L. and Di Stefano R.; 2005: *A new view of Italian seismicity using 20 years of instrumental recording*. Tectonophysics, **395**, pp. 251-268.

Ellsworth W. L., Lindh A. G., Prescott W. H. and Herd D. G.; 1981: *The 1960 San Francisco earthquake and the seismic cycle*. In: Simpson J. D. and Richards P. G. (ed), Earthquake Prediction: An International Review, Maurice Ewing Series 4, AGU, Washington, D.C., pp. 126-140.

Frankel A.; 1995: *Mapping seismic hazard in the Central and Eastern United States*. Seism. Res. Lett., **66**, pp. 8-21.

Gruppo di Lavoro CPTI; 2004: *Catalogo Parametrico dei Terremoti Italiani, versione 2004 (CPTI04)*. INGV, Bologna, http://emidius.mi.ingv.it/CPTI/.

Kanamori H.; 1981: *The nature of seismicity patterns before large earthquakes*. In: Simpson J. D. and Richards P. G. (ed), Earthquake Prediction: An International Review, Maurice Ewing Series 4, AGU, Washington, D.C., pp. 1-19.

Mirandola Earthquake Working Group (DPC, UniChieti, Uni Trieste, Regione Umbria); 2012: *Report 2* (http://www.protezionecivile.gov.it/jcms/it/ran.wp).

Molli G., Crispini L., Mosca P., Piana F. and Federico L.; 2010: *Geology of the western Alps-northern Apennine junction area: a regional review*. In: M. Beltrando, A. Peccerillo, M. Mattei, S. Conticelli and C. Doglioni (eds.), The Geology of Italy, J. Virt. Explor., 36, paper 9

Patacca E., Sartori R. and Scandone P.; 1990: *Tyrrhenian basin and Apenninic arcs: kinematic relation since Late Tortonian times*. Memorie della Società Geologica Italiana, **45**, pp. 425-451.

Pondrelli S., Salimbeni S., Perfetti P. and Danecek P.; 2012: *Quick regional centroid moment tensor solutions for the Emilia 2012 (northern Italy) seismic sequence*. Annals of Geophysics, **55**, pp. 615-621.
Scholz C. H.; 1988: *The mechanisms of seismic quiescences*. Pure Appl. Geophys., **126**, pp. 701-718.
Serpelloni E., Anderlini L., Avallone A., Cannelli V., Cavaliere A., Cheloni D., D'Ambrosio C., D'Anastasio E., Esposito A., Pietrantonio G., Pisani A., Anzidei M., Cecere G., D'Agostino N., Del Mese S., Devoti R., Galvani A., Massucci A., Melini D., Riguzzi F., Selvaggi G. and Sepe V.; 2012: *GPS observations of coseismic deformation following the May 20 and 29, 2012, Emilia seismic events (northern Italy): data, analysis and preliminary models*. Annals Of Geophysics, **55**, pp. 759-765.

ACTIVE TECTONICS OF SOUTH-EASTERN SICILY AS DEPICTED BY SEISMOLOGICAL AND GEODETIC OBSERVATIONS

C. Musumeci, M. Palano, D. Patanè, L. Scarfì
Istituto Nazionale di Geofisica e Vulcanologia, Osservatorio Etneo - Sezione di Catania, Italy

Introduction. Southeastern Sicily, one of the most seismically hazardous zones in central Mediterranean area, experienced several historical destructive events such as the 1169 and 1693 earthquakes (MCS intensities of XI with estimated magnitudes of about 7 or higher; Boschi *et al.*, 2000), and more recently, a M_L = 5.4 earthquake occurred on December 13, 1990 about 10 km offshore (Amato *et al.*, 1995).

From a geological point of view, southeastern Sicily must be considered in the frame of the complex tectonic features of the Mediterranean basin, which is dominated by the ~N20°W Neogene-Quaternary convergence between Nubian plate (the African plate west of the East African Rift) and Eurasia, occurred in the last 100 million years (Faccenna *et al.*, 2001). It is mostly formed by the foreland domain (the Hyblean Plateau; Fig. 1a), a crustal unit located at the northeastern end of the mostly submerged Pelagian Block extending up to Sicily Channel, the Maltese islands and Tunisia (*e.g.* Malinverno and Ryan, 1986; Boccaletti *et al.*, 1990; Patacca *et al.*, 1990). The Sicilian foreland consists of a thick Meso-Cenozoic sequence of carbonate sediments which are underlain by a continental basement of unknown age (Yellin-Dror *et al.*, 1997). Eastward, the foreland is bounded by the NNW-SSE-striking Hybleo-Maltese Escarpment Fault System (HMEFS; see Fig. 1a), a Mesozoic lithospheric boundary separating the Ionian oceanic basin from the thick Pelagian Block continental crust (Nicolich *et al.*, 2000). The northern and western margins of the Hyblean Plateau are characterized by an older extensional belt (named Gela-Catania Foredeep), that is downbent by a NE-SW fault system under the front of the northern imbricate mountain chain (Appennine-Maghrebian Chain or Maghrebian Thrust Belt; Yellin-Dror *et al.*, 1997). The frontal thrust belt was considered locked since the Middle Pleistocene (Butler *et al.*, 1992; Lickorish *et al.*, 1999; Tortorici *et al.*, 2001), but recent studies, based on geological (Bousquet and Lanzafame, 2004; Catalano *et al.*, 2008), seismolological (Lavecchia *et al.*, 2007; Visini *et al.*, 2009) and geodetic (see Palano *et al.*, 2012 for an overview) observations have detected the occurrence of active contraction. Another main tectonic alignment is a 70 km long fault system (named as Scicli line or Scicli-Ragusa Fault System, SRFS in Fig. 1b: Ghisetti and Vezzani, 1980, Grasso and Reuther, 1988) extending along the main direction striking about N-S and the conjugated structures NE-SW from northeast to southwest of the western district of the foreland.

Despite the recent advances achieved through geological, seismological and geodetic studies (among others Scarfì *et al.*, 2007; Catalano *et al.*, 2008; Palano *et al.*, 2012), the geodynamic processes and the tectonic regime of southern Sicily are far from being unanimously described. Several aspects related to the geometry, type and contributions of each fault and its seismogenic role have still not been satisfactorily explored and there is little consensus regarding the location and geometry of the faults causing major earthquakes.

In this work, exploiting local monitoring network high-quality data, we performed an in-depth analysis of the ongoing tectonics of southeastern Sicily, between the outermost front of the chain and the Ionian offshore, through the integration of seismic and GPS-based geodetic observations, collected in nearly two decades. In particular, we carried out a simultaneous inversion of both the three-dimensional velocity structure and the distribution of seismic foci to define the geometry of seismogenic structures responsible of this seismicity. The computation of fault plane solution for the major and best recorded earthquakes was of great importance for the characterization of seismogenic sources and the orientation of the crustal stress field acting in the area. The comparison of these findings with the GPS-based ground deformation will help to improve the knowledge of the investigated area.

Seismic data. About 1020 small-to moderate-magnitude earthquakes ($1.0 \leq M_L \leq 4.6$), recorded between 1994 and 2013 by a local network, were selected from the "Catalogo dei terremoti della Sicilia Orientale - Calabria Meridionale. INGV, Catania" (Gruppo Analisi Dati Sismici, 2013).

In particular, the events have been employed as data source for simultaneous inversion of both a 3-D velocity structure and the hypocentre parameters by the code tomoDDPS (Zhang *et al.*, 2009). With respect to more simple algorithms, this code has the ability to improve the accuracy of event locations and to sharpen the velocity images near the source region because of the combination of absolute and differential arrival times.

For the tomography, we filtered the initial dataset according to the quality criteria of location. In particular, we selected only well located events, i.e. those with at least nine observations (P- and S-phases), root-mean-square (RMS) residuals smaller than 0.35 s and horizontal and vertical location errors lower than 2.5 km and 4.5 km, respectively. Finally, about 880 earthquakes with

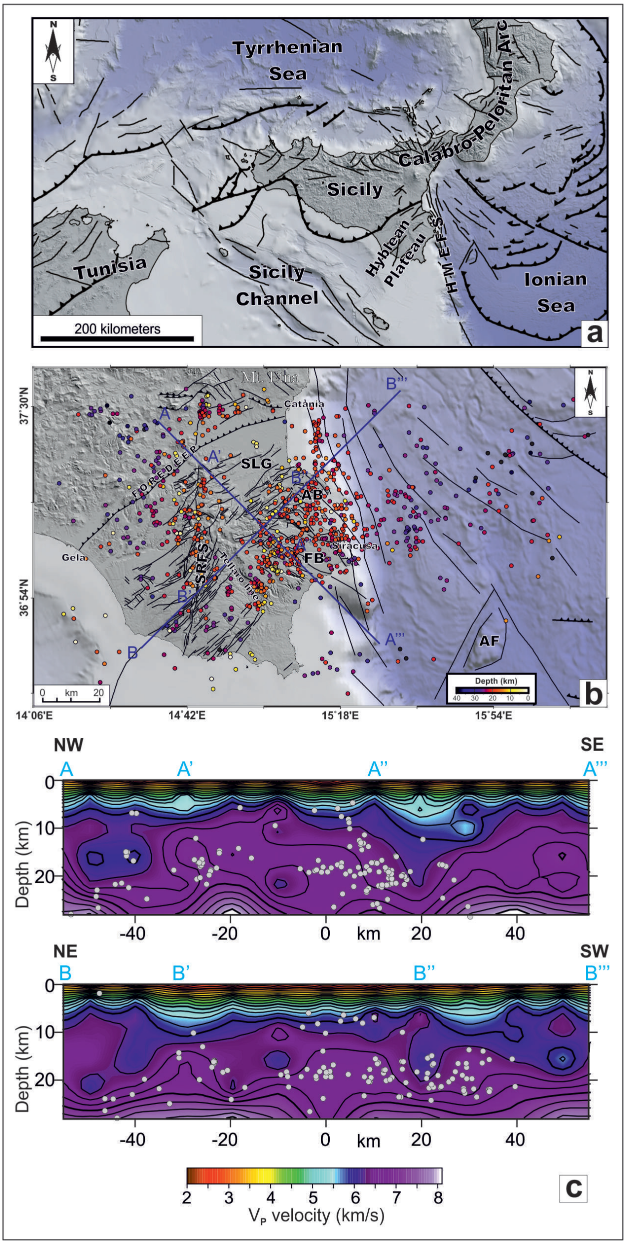

Fig. 1 – a) Simplified tectonic map of Sicily. b) Relocated seismicity (see text for further details). c) Vertical sections through the VP model. The traces of sections are reported in the map (b) with blue lines. Contour lines are at an interval of 0.25 km/s and the relocated earthquakes, within ±10 km from the sections are plotted as grey circles. HMEFS, Hybleo-Maltese Escarpment Fault System; SLG, Scordia-Lentini Graben; AB, Augusta basin; FB, Floridia basin; SRFS, Scicli-Ragusa Fault System; AF, Alfeo seamount.

a total of 6131 P and 3668 S absolute arrival times and 52980 P and 30138 S catalogue-derived differential times. We performed the data inversion with an horizontal grid of 7x7 km node spacing, covering an area of 110 x 110 km, and a vertical step varying between 3 and 6 km, from the surface to 28 km of depth, following the one-dimensional reference velocity model of Musumeci *et al.* (2003). This mesh configuration allows to achieve a better spatial resolution with respect the other tomographic studies carried out in the area, also ensuring a good over-determination factor (i.e. the ratio between known and unknown parameters). The finely tuned velocity distribution was used to relocate by TomoDDPS the whole dataset of events recorded in the studied region. This provided an improvement in the quality of the final locations and an higher clustering of the earthquakes, which emphasizes some lineaments (Fig. 1b).

As we can observe, tomographic images (Fig. 1c) reveal several sharp lateral velocity perturbations pointing out meaningful discontinuities in the crust which can be related to major tectonic structures. In particular, a low velocity anomaly was detected in the northwestern sector (profile A), about corresponding with the Gela-Catania Foredeep. Location and geometry of this feature suggest that it may be related with the Hyblean Foreland crust bending beneath the outermost edifice of the Maghrebian Chain. Coastal and offshore zones (from Catania to Siracusa) and the western sector are also accompanied by a considerable velocity contrasts. These anomalies likely mark the known fault systems, striking about NW-SE, such as the HMEFS and those bounding the Augusta basin and the Scicli-Ragusa Fault System, respectively. Current results, compared to the previous tomographic inversion of Scarfì *et al.* (2007), obtained with a similar calculation code (TomoADD: Zhang and Thurber, 2005), maintain the fundamental characteristics but at the same time show a greater detail, this thanks to the larger amount of available data, which results in an higher density of seismic rays sampling the spatial mesh.

Looking at the 3D event locations, to the north and northwest, earthquakes are distributed along the edge between the foreland and the chain, with depth increasing towards NW, down to about 40 km, to outline the flexure of the Hyblean crust below the thin-skinned outermost chain. Towards south, in the western district, the epicentres finely overlap to the Scicli-Ragusa

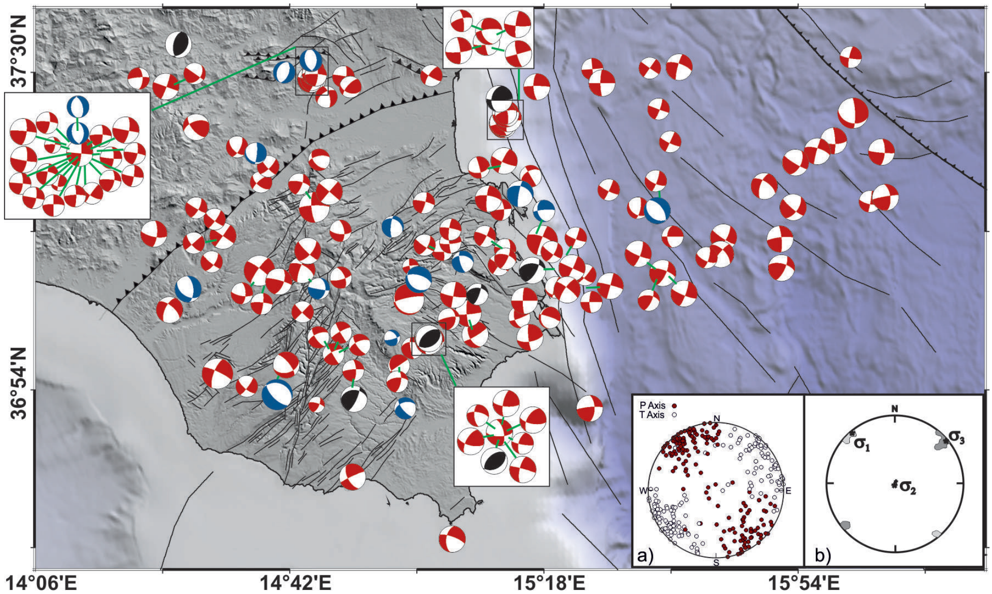

Fig. 2 – Computed focal mechanisms. Red, strike-slip fault; blue, normal fault; black, inverse fault. Insets show the stereonets of the P and T-axes (a) and the orientations (stars) of the principal stress axes (b), with the 95% confidence limits (grey areas).

Fault System, along the main direction striking about N-S and the conjugated structures NE-SW. Moving eastward, events are concentrated in the area of the Hyblean Plateau. They become sparse or lacking beyond its edges, namely to the south, to the north (in the Scordia-Lentini Graben area) and between the Scicli-Ragusa Fault System and the Tellaro Line (Fig. 1b). Several earthquakes occurred instead along the coastal area, matching quite well the faults that border the Augusta and Floridia basins (Fig. 1b). In the plateau, the geometry of several clusters seems indicate the NW-SE direction as the main direction of the seismogenic structures. In the nearby Ionian offshore, earthquakes lie along the HMEFS, between Catania Gulf and Siracusa, while a cluster is detectable at the Alfeo Seamount (AF). Eastward, other events are more scattered, although some NW-SE lineaments could be traced. Here the seismogenic depths is between 20 and 40 km, but this last finding must be read with caution as the geometrical gap of the network could create artefacts.

The following step was to analyze the stress pattern acting on southeastern Sicily. We calculated the fault-plane solutions (FPSs) of a selected subset of earthquakes by using the FPFIT algorithm (Reasenberg and Oppenheimer, 1985), with rays traced through the computed 3D velocity model. From the initial dataset 195 earthquakes with M_L>1.0 and at least 8 clear first-motion picks (71% of the 195 shocks had 10 or more first-motion readings, 15 on average) have been selected. We discarded FPSs if they met any one of the following criteria: i) ratio NDisc/NPol (NDisc is the number of discrepant observations and NPol is the number of first readings used in the solution) greater than 0.2; ii) large uncertainty in P- and T-axes orientation and regions overlapped; iii) averaged uncertainties in strike, dip and rake greater than 20° and iv) the number of multiple solutions greater than 2. These selection criteria yielded 165 well-constrained FPSs (Fig. 2).

Uncertainties in fault parameters (strike, dip, and rake) range mostly between 10° and 15°. All types of mechanisms are represented in this dataset although strike-slip solutions outweigh normal and reverse ones. A plot of all P and T axes obtained (inset (a) of Fig. 2) shows that the tensional axes have an average trend that is nearly horizontal and in the NE-SW direction, while the average compressive stress axis is nearly horizontal and in the NW-SE direction. Although some vertical compressive axes were observed, they are less numerous in comparison to the horizontal ones.

To determine stress directions from the 165 selected focal mechanisms we applied the focal mechanism stress inversion (FMSI) computer program developed by Gephart and Forsyth (1984). The parameters obtained from the inversion algorithm are the directions of the maximum (σ_1), intermediate (σ_2), and minimum (σ_3) principal stress axes, and a measure of their relative magnitudes $R = (\sigma_2 - \sigma_1)/(\sigma_3 - \sigma_1)$. Moreover, a variable misfit (F) is introduced in order to define discrepancies between the stress tensor and the observed fault plane solutions. The main findings for the whole dataset (165 fault-plane solutions) can be summarized as follows: F= 6.598°; R=0.6; s1= N320° dip 0°; s2=N203°E dip 89°; s3=N50°E dip 1° (inset (b) of Fig. 2). The average misfit of 6.598° suggests that the dataset may be affected by some heterogeneity.

GPS data. Geodetic GPS-based monitoring of the Hyblean area is currently carried out by INGV through the set-up of a permanent GPS network in the framework of the "Rete Integrata Nazionale GPS (http://ring.gm.ingv.it)" project, since 2005. In addition, a network comprising a local trilateration network and a levelling route managed by the International Institute of Volcanology (merged into INGV in 2001) and the Istituto Geografico Militare Italiano (www.igmi.org) respectively, was surveyed in 1998, 2000, 2005 and 2006. All available GPS data were processed by using the GAMIT/GLOBK software (Herring *et al.*, 2010). To adequately show the crustal deformation pattern over the investigated area, estimated GPS velocities (Fig. 3a) were aligned to a fixed Eurasian reference frame (Palano *et al.*, 2012).

By taking into account the observed horizontal velocity field and associated covariance information we derived a continuous velocity gradient tensor on a regular 0.1° x 0.1° grid (whose nodes do not coincide with any of the GPS stations) using a "spline in tension" technique

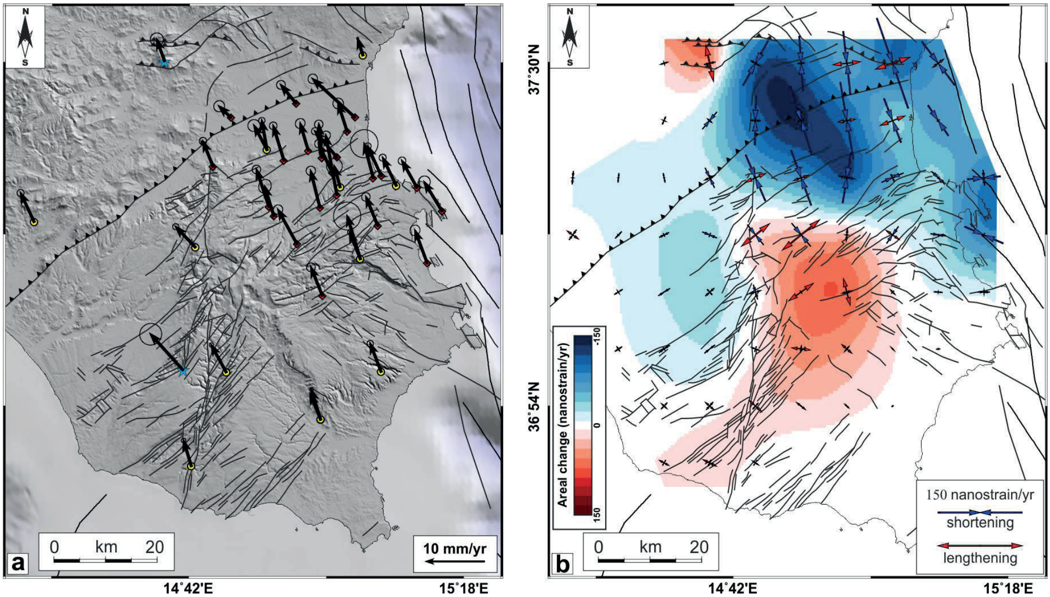

Fig. 3 – a) GPS velocities and 95% confidence ellipses in a fixed Eurasian reference frame; red diamonds for survey GPS sites, yellow circles for continuous GPS stations and light-blue stars for solutions coming from Ferranti *et al.* (2008). b) Geodetic strain-rate parameters: the colour in background shows the rate of areal change, while arrows represent the greatest extensional (red) and contractional (blue) horizontal strain-rates.

(Wessel and Bercovici, 1998). Sites showing large uncertainties have not been used into the velocity gradient tensor computation. As a final step, we computed the average 2D strain-rate tensor as derivative of the velocities at the nodes of each grid cell. The estimated strain-rates are shown in Fig. 3b.

The geodetic velocity field, referred to a fixed Eurasian reference frame depicts a general NNW-directed motion with an N-S decreasing gradient across the Scordia-Lentini Graben, passing from values of ca. 5.5 mm/yr, along the southern-central sector of the Hyblean Plateau, to values of ca. 3.0 mm/yr on the northern rim of the plateau itself (Fig. 3a). The strain-rate field (Fig. 3b) clearly evidences as Scordia-Lentini Graben is dominated by a ~140 nanostrain/yr contractional belt with shortening axis oriented along the prevailing N-S direction. The southern-central sector of the plateau is characterized by a positive areal change of ~90 nanostrain/yr; westward this area seems delimited by the Scicli-Ragusa Fault System. Westward the Scicli-Ragusa Fault System, the plateau shows a gentle negative areal change (~30 nanostrain/yr).

Discussion and conclusions. This study is mainly devoted to investigate the current tectonic setting of a large sector of southern Sicily, most including the Hyblean Foreland and the front of the Appennine-Maghrebian Chain, as well as the Ionian Sea offshore, by using an extensive GPS-based and a seismological dataset. In detail, GPS velocity field depicts a general NNW-directed motion in good agreement with the horizontal stress direction inferred from the inversion of focal mechanism solutions. Also, these results well map some interesting features related to the different deformation patterns observed on the investigated area. In particular, a fine-scale analysis of seismic and GPS data indicate that Hyblean Foreland wedge is separate in two crustal blocks (western and eastern) by the Scicli-Ragusa Fault System. Earthquakes distribution, as well as the Vp anomalies, depict the geometry of this important structural lineament, while the focal mechanisms clearly indicate its kinematics, which is mainly left-lateral strike-slip. The left-lateral strike-slip behavior is also confirmed by GPS data, which show a tensile and a strike-slip component of 3 mm/yr and 1 mm/yr (positive for left-lateral shear) between the two blocks, respectively. In addition, while the western foreland crustal block is limited by the front of the chain to the west and north and its seismic activity is mostly related to the Scicli-Ragusa Fault System, the eastern part moves bounded by two main regional tectonic structures, the Scicli-Ragusa Fault System and the Hybleo-Maltese Escarpment Fault System. The activity of the latter is well evidenced by the distribution of hypocenters along the Ionian coast, from the Gulf of Catania up to several kilometres south of Siracusa, with prevailing trastensive kinematics. The brittle deformation of the eastern block seems to be confined inside the Plateau, where most of the seismic events occur. Focal mechanisms computed for this area, are characterized by prevailing transtensive solutions with a nodal plane prevalently oriented WNW-ESE to NW-SE, fitting with the direction emphasized by the location of some event clusters (Fig. 1b) and in agreement with the main geological features (*e.g.* Catalano *et al.*, 2008). Moreover, the transtensive nature of this area is well depicted also by GPS measurements (i.e. the horizontal strain-rate axes have comparable magnitude). Southward, the earthquakes are confined to the edge of the Plateau, where the tomography shows a discontinuity, down to 15 km of depth. From the morphological point of view, this area exhibits an escarpment (100-400 m) delimiting the Hyblean Plateau from the southern coastal plain, which several authors relate to a fault NE-SW oriented (i.e. the Avola Fault, see Catalano *et al.*, 2008).

GPS data reveal also that a contractional belt is the overriding feature of the the Foredeep-Chain edge zone. In particular, an higher shortening, with respect the western side of the Scicli-Ragusa Fault System, was found along an area extending from the Scordia-Lentini Graben to the lower southern slope of Mt. Etna. There, several geological studies have shown that normal faults controlling the graben have been reactivated by reverse motion during the last 0.85 Myr (e.g. Bousquet and Lanzafame, 2004; Catalano *et al.*, 2008). We showed that the earthquakes deepen below the chain, down to 40 km, moving from the plateau towards NW; a clear signal of an active foredeep. On the other hand, however, very few events occurred in the Scordia-Lentini Graben area. This raises the question whether the lacking of seismic energy release, compared to the pronounced shallow deformation, can be correlated to a seismic gap, which would result in a very high seismic hazard for the area. Nevertheless, an hypothesis can be advanced to explain the different deformation pattern, between the western and eastern sectors of the foredeep-chain edge zone, discussed above. This hypothesis implies that the phenomenon can be connected with the thick and ductile layer of alluvial sediments that fill the graben and deform more rapidly than the western area with more strength and brittle crust. This hypothesis could better reconcile both the higher strain rate and the low occurrence of earthquakes.

References

Amato A., Azzara R., Basili A., Chiarabba C., Cocco M., Di Bona M. and Selvaggi G.; 1995: Main shock and aftershocks of the December 13, 1990, Eastern Sicily earthquake. Ann. Geofis., 38, 255-266.

Boccaletti M., Cello G. and Tortorici L.; 1990: Strike-slip deformation as a fundamental process during the Neogene-Quaternary evolution of the Tunisian-Pelagian area. Ann. Tecton., 4, 104-119.

Boschi E., Guidoboni E., Ferrari G., Mariotti D. and Valensise G.; 2000: Catalogue of strong Italian earthquakes. Ann. Geofis., 43, 268 pp.

Bousquet J.C. and Lanzafame G.; 2004: Compression and Quaternary tectonic inversion on the Northern edge of the Hyblean Mountains, foreland of the Appenine-Maghrebian chain in Eastern Sicily (Italy): geodynamic implications for Mt. Etna. GeoActa, 3, 165-177.

Butler R.W.H., Grasso M. and La Manna F.; 1992: Origin and deformation of the Neogene-Recent Maghrebian foredeep at the Gela Nappe, SE Sicily. J. Geol. Soc. London, 149, 547-556.

Catalano S., De Guidi G., Romagnoli G., Torrisi S., Tortorici G. and Tortorici L.; 2008: The migration of plate boundaries in SE Sicily: influence on the large-scale kinematic model of the African promontory in southern Italy. Tectonophysics, 449, 41-62, doi:10.1016/j.tecto.2007.12.003.

Faccenna C., Becker T.W., Lucente F.P., Jolivet L. and Rossetti F.; 2001: History of subduction and back-arc extension in the central Mediterranean. Geophys. J. Int., 145, 809-820, doi:10.1046/j.0956-540X.2001.01435.x.

Ferranti L., Oldow J.S., D’argenio B., Catalano R., Lewis D., Marsella E., Avellone G., Maschio L., Pappone G., Pepe F. and Sulli A.; 2008: Active deformation in southern Italy, Sicily and southern Sardinia from GPS velocities of the Peri-Tyrrhenian Geodetic Array (PTGA). Boll. Soc. Geol. Ital, 127(2), 299-316.

Gephart J.W. and Forsyth D.W.; 1984: An improved method for determining the regional stress tensor using earthquake focal mechanism data: application to the San Fernando earthquake sequence. J. Geophys. Res., 89, 9305-9320.

Ghisetti F. and Vezzani L.; 1980: The structural features of the Iblean plateau and of the Monte Iudica area (South Eastern Sicily). A microtectonic contribution to the deformational history of the Calabrian Arc. Boll. Soc. Geol. It., 99, 57–102.

Grasso M. and Reuther C.D.; 1988: The western margin of Hyblean plateau: a neotectonic transform system on the SE Sicilian foreland. Ann. Tectonicae, 2, 107–120.

Gruppo Analisi Dati Sismici; 2013: Catalogo dei terremoti della Sicilia Orientale - Calabria Meridionale (1999-2011). INGV, Catania http://www.ct.ingv.it/ufs/analisti/catalogolist.php

Herring T.A., King R.W. and McClusky S.C.; 2010: Introduction to GAMIT/GLOBK, Release 10.4. Massachusetts Institute of Technology, Cambridge MA, 1-48.

Lavecchia G., Ferrarini F., De Nardis R., Visini F. and Barbano M.S.; 2007: Active thrusting as a possible seismogenic source in Sicily (southern Italy): Some insights from integrated structural-kinematic and seismological data. Tectonophysics, 445, 145-167, doi:10.1016/j.tecto.2007.07.007.

Lickorish W.H., Grasso M., Butler R.W.H., Argnani A. and Maniscalco R.; 1999: Structural styles and regional tectonic setting of the ‘‘Gela Nappe’’ and frontal part of the Maghrebian thrust belt in Sicily. Tectonics, 18, 655-668, doi:10.1029/1999TC900013.

Malinverno A. and Ryan W.B.F.; 1986: Extension in the Tyrrhenian Sea and shortening in the Apennines as result of arc migration driven by sinking of the lithosphere. Tectonics, 5(2), 227-245, doi:10.1029/TC005i002p00227.

Musumeci C., Di Grazia G. and Gresta S.; 2003: Minimum 1-D velocity model in Southeastern Sicily (Italy) from local earthquake data. J. Seism., 7, 469–478.

Nicolich R., Laigle M., Hirn A., Cernobori L. and Gallard J.; 2000: Crustal structure of the Ionian margin of Sicily: Etna volcano in the frame of regional evolution. Tectonophysics, 329, 121-139, doi:10.1016/S0040-1951(00)00192-X.

Palano M., Ferranti L., Monaco C., Mattia M., Aloisi M., Bruno V., Cannavò F. and Siligato G.; 2012: GPS velocity and strain fields in Sicily and southern Calabria, Italy: Updated geodetic constraints on tectonic block interaction in the central Mediterranean. J. Geophys. Res., 117, B07401, doi:10.1029/2012JB009254.

Patacca E., Sartori R. and Scandone P.; 1990: Tyrrhenian basin and Apenninic arcs. Kinematic relations since late Tortonian times. Mem. Soc. Geol. It., 45, 425-451.

Reasenberg P.A. and Oppenheimer D.; 1985: Fortran computer programs for calculating and displaying earthquake fault-plane solutions. U.S. Geol. Surv., Open File Rept. 85-379, 109 pp.

Scarfì L., Giampiccolo E., Musumeci C., Patanè D. and Zhang H.; 2007: New insights on 3D crustal structure in Southeastern Sicily (Italy) and tectonic implications from an adaptive mesh seismic tomography. Phys. Earth Planet. Int., 161, 74-85.

Tortorici L., Monaco C., Mazzoli S. and Bianca M.; 2001: Timing and modes of deformation in the western Sicilian thrust system, Southern Italy. J. Pet. Geol., 24(2), 191-211, doi:10.1111/j.1747-5457.2001.tb00667.x.

Visini F., De Nardis R., Barbano M.S. and Lavecchia G.; 2009: Testing the seismogenic sources of the January 11th 1693 Sicilian earthquake (Io X/XI): insights from macroseismic field simulations. Ital. J. Geosci. (Boll. Soc. Geol. It.), 128(1), 147-156.

Wessel P. and Bercovici D.; 1998: Interpolation with splines in tension: a Green’s function approach. Mathematical Geology, 30, 77-93.

Yellin-Dror A., Grasso M., Ben-Avraham Z. and Tibor G.; 1997: The subsidence history of the northern Hyblean Plateau margin, Eastern Sicily. Tectonophysics, 282, 277-289.

Zhang H. and Thurber C.H.; 2005: Adaptive mesh seismic tomography based on tetrahedral and Voronoi diagrams: application to Parkfield, California. J. Geophys. Res., 110, B04303, doi:10.1029/2004JB003186.

Zhang H., Thurber C. and Bedrosian P.; 2009: Joint inversion for Vp, Vs, and Vp/Vs at SAFOD, Parkfield, California. Geochem. Geophys. Geosyst., 10:Q110032, doi:10.1029/2009GC002709.

sessione 1.3

Vulcani e campi Geotermici

Convenor: E. Del Pezzo e R. Petrini

NEW MORPHOBATHYMETRIC AND SEISMOSTRATIGRAPHIC RESULTS ON THE NORTH-WESTERN ISCHIA OFFSHORE (NAPLES BAY, SOUTHERN TYRRHENIAN SEA, ITALY) AND THE EMPLACEMENT OF SUBMARINE SLIDES IN A VOLCANIC SETTING

G. Aiello, E. Marsella, S. Passaro
Istituto per l'Ambiente Marino Costiero (IAMC), Consiglio Nazionale delle Ricerche (CNR), Napoli, Italy

Introduction. New morphobathymetric and seismostratigraphic results on the north-western Ischia offshore (Naples Bay, Southern Tyrrhenian sea) are here discussed based on high resolution Multibeam bathymetry and Sparker seismic profiles recently collected in the frame of research programmes on marine geological mapping (Aiello *et al.*, 2012a; 2012b).

The Phlegrean islands (Ischia, Procida and Vivara) represents a physiographic domain occurring among the Gaeta Gulf to the north and the Naples Bay to the south. This can be seen with the use of large-scale bathymetric maps, obtained by satellite data (Amante and Eakins, 2008).

An elevation versus average slope plot (Moore and Mark, 1993), highlighting where steep and flat areas occur in terms of elevation (Fig. 1) has been constructed in order to describe the main morphological features of Ischia, including both the onshore volcanic edifice and the offshore surrounding the island. This plot, derived by the marine Digital Elevation Model of Ischia (DEM) and the related slope map, constructed through an opportunely built routine, helped to identify Ischia morphological macro-areas, since they individuate groups of elevation/slope pairs related to specific physiographic and morphologic settings.

Geologic setting. Systematic studies carried out on the sea bottoms around the Ischia island (Naples Bay, Southern Tyrrhenian sea) having a notable, up to date scientific content have been recently carried out and are, in any case, mainly geophysical. The first marine geological study concealing the whole Neapolitan area has been carried out by Walther (1886) and has furnished, with the old methods available at that times, an overall framework on the trending, constitution and structure of the sea bottoms between the Capri island and the Naples town (Aiello *et al.*, 2001).

The Ischia island represents an alkali-trachytic volcanic complex, whose eruptive activity lasted from the Late Pleistocene up to historical times (Vezzoli, 1988). The activity of the island is characterized by the occurrence of a resurgent caldera, where volcanic eruptions coupled to tectonic activity gave rise to the Mount Epomeo block (Orsi *et al.*, 1991). Five eruptive cycles have characterized the magmatic system of Ischia-Procida-Phlegrean Fields, ranging in age from 135 ky B.P. up to prehistorical and historical times. Several volcanic edifices, both dismantled and preserved or buried below Quaternary deposits crop out onshore at Ischia (Forcella *et al.*, 1981; Gillot *et al.*, 1982; Luongo *et al.*, 1987; Vezzoli, 1988). Landslide deposits, cropping out onshore and deriving from the accumulation and fragmentation of pre-existing volcanic rocks, extensively crop out (Guadagno and Mele, 1995; Mele and Del Prete, 1998; Calcaterra *et al.*, 2003; De Vita *et al.*, 2006, 2007; Di Maio *et al.*, 2007; Di Nocera *et al.*, 2007).

Many geo-volcanologic studies have been carried out on the island, starting from the syntheses of Rittmann (1930, 1948) and then on the specific aspects of the eruptive activity of the island and related geological processes (Forcella *et al.*, 1981; Gillot *et al.*, 1982; Chiesa *et al.*, 1985, 1987; Poli *et al.*, 1987, 1989; Civetta *et al.*, 1991; Orsi *et al.*, 1991; Luongo *et al.*, 1997). A particular meaning is accomplished by the aspects concerning the geochronology of the volcanic deposits in the island (Orsi *et al.*, 1996) and the time evolution of the magmatic system (Luongo *et al.*, 1997).

The geologic and volcanologic history of the Ischia island has been characterized by a main event, represented by the eruption of the Green Tuff of the Epomeo Mt, which verified 55 ky B.P. ago, allowing for the down throwing of the central sector of the island consequent to a caldera formation (Orsi *et al.*, 1991; Acocella *et al.*, 1997; Acocella and Funiciello, 1999). Consequently, the volcanic activity of the island has been conditioned by a complex phenomenon of calderic resurgence, started from 30 ky B.P., allowing for the gradual uplift and emersion of the rocks deposited in the caldera, initially submerged under the sea level. The rate of uplift, indicating the caldera resurgence, has been evaluated in about 800-1100 m (Barra *et al.*, 1992).

The tectonic activity is characterized by systems of extensional faults, NW-SE and NE-SW trending, Plio-Quaternary in age (Acocella and Funiciello, 1999; Acocella *et al.*, 2004). NW-SE and NE-SW systems of extensional fractures predominate in all the island and around the resurgent caldera block, suggesting a close relationship with the regional extensional structures. N-S and E-W trending normal faults have been found along the rims of the Epomeo block and interpreted as controlled by the caldera resurgence. The process of resurgence has locally substituted the volcanic activity during the last 33 ky, since the most of the pyroclastic products coeval with the resurgence has been erupted out of the uplifted area.

Marine geological studies already showed that the Ischia island lies on a E-W trending volcanic ridge (Bruno *et al.*, 2002; Passaro, 2005; de Alteriis *et al.*, 2006; Aiello *et al.*, 2009a, 2009b, 2012a, 2012b). The continental slope off the south-western Ischia island is incised by a dense network of canyons and tributary channels, starting from a retreating shelf break, parallel to the coastline and located at varying depths. Large scars characterize the platform margin off south-western Ischia island, in particular the scar of the southern flank of the island, corresponding onshore to the Mount Epomeo block and probably at the origin of the Ischia Debris Avalanche (Chiocci and de Alteriis, 2006). Volcanic banks, having irregular morphologies, have been identified on the south-western flank of the island, as the "Banco di Capo Grosso" and the banks "G. Buchner" and "P. Buchner" (Passaro, 2005; de Alteriis *et al.*, 2006). A large field of hummocky deposits, named the Ischia Debris Avalanche has put in evidence by swath bathymetric surveys coupled with Sidescan Sonar imagery and

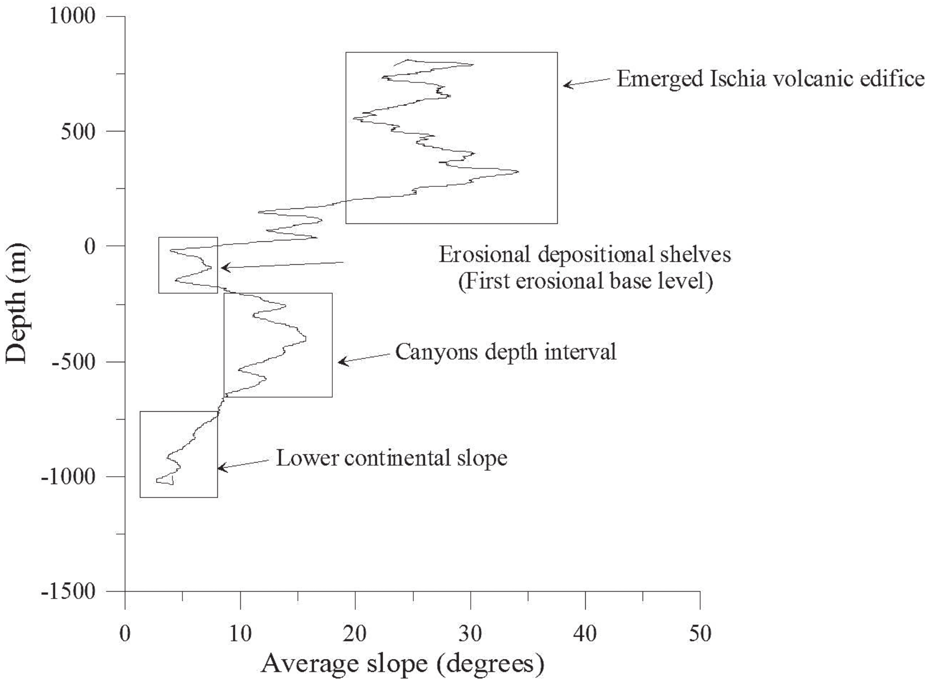

Fig. 1 – Sketch diagram showing the elevation intervals versus average slopes offshore the Ischia island (modified after Aiello *et al.*, 2012b).

seismic profiles. Detailed piston coring and tephrostratigraphy suggested that the volcano-tectonic collapse originating the avalanche occurred during prehistorical times (Chiocci and de Alteriis, 2006). A stratigraphic framework for the last 23 ky marine record in the southern Ischia offshore has been recently constructed based on AMS ^{14}C dating and tephrostratigraphic analysis (de Alteriis *et al.*, 2010).

Data and methods. The Multibeam bathymetry here presented was recorded from September to November 2001, using a Reson Seabat 8111 Multibeam system, which works properly in the 50-600 m depth range, onboard the Thetis R/V (Aiello *et al.*, 2012a). The Multibeam system, interfaced with a Differential Global Positioning System (DGPS) was composed of a ping source of 100 kHz, 150° for the whole opening of the transmitted pulse and a 101 beams receiver, with a beam opening of 1.5°. Sound velocity profiles (CTD) were regularly recorded and applied every 8 hours.

The data were processed using the PDS2000 software (Reson-Thales), according to the IHO standards (IHO, 1998), with a real time acquisition control and partial beam exclusion filtering. Offline swath editing and despiking were also carried out. The DTM generation and rendering of the whole dataset were reorganized in a MXN matrix having a grid cell of 20x20m.

The meaning of morphometric indicators is explained, necessary for a correct comprehension of the data presented in this paper (Figs. 1 and 2). The elevation versus slope plot was used as a morphometric tool for an objective description of the DTM. The elevation distribution provides a standard tool to highlight the relative elevation distribution of topography and bathymetry, thus allowing to describe or compare different DEM's (Passaro *et al.*, 2010, 2011).

Seismic acquisition was carried out using a multielectrode sparker system (SAM96 model). Its technical characteristics include shorter pulse lengths for an equivalent energy discharge, as well as an increase in peak pressure. The seismic sections were recorded graphically on continuous paper sheets with a vertical recording scale of 0.25 s. The best vertical resolution was approximately 1 m for the sparker data. The seismic grid surrounding the Ischia island facilitated the stratigraphic correlations between the seismic sections and revealed structural and stratigraphic variations along the seismic lines.

The morpho-depositional environments of Ischia island. Marine geological survey and morpho-bathymetric analyses carried out in the frame of the CARG research project (Ispra, 2010; Geological map n. 464 "Isola d'Ischia") have evidenced in the Ischia island such a geomorphological characters allowing to distinguish different physiographic and depositional environments. A strong control of the lithostratigraphic and structural setting on the sea bottom evolution and on the present-day or inherited morphological processes can be singled out.

A first control on the physiography, structure and evolution of the sea bottoms is furnished by the coastal types which characterize the Ischia littorals, characterized by both coastal cliffs (high relief coasts) and beaches (low relief coasts).

The morpho-depositional environment of low relief coasts individuates the sectors of littoral environment mainly characterized by the occurrence of coastal plains joining onshore through reliefs having an average to low energy, more or less close to the coast. In this way, coastal cliffs do not realize and the submerged beach and adjacent continental shelf may be considered as the physical prolongation along a homogeneous and continuous profile.

In some cases the continental shelf is characterized by the occurrence of detritic deposits having a chaotic internal structure and a hummocky topography, articulating on the sea bottom both with a longitudinal and transversal trending (Ispra, 2010).

The morpho-depositional environment of high relief coasts includes the sectors of littoral characterized by slopes directly joining the sea with high steepness, not depending from the lithology of the units forming the slopes themselves. This condition, mainly morphometric, of the sector of the emerged coastal slope (emerged coastal cliff) is connected to a sector of submerged slope (submerged coastal cliff), developing with similar characteristics up to 20-30 m of water depth.

The eastern Ischia island: from Casamicciola to Punta della Signora. The eastern Ischia coastal sector between the Casamicciola harbour (northern Ischia) to Punta della Signora (south-western Ischia) is mostly constituted by rocky outcrops, mainly nearshore, having a lavic and/or pyroclastic composition (Ispra, 2010). These outcrops are formed mainly of blocks having also great dimensions (more than 1 m^3), or by the seaward prosecution of lava flows or pyroclastic deposits. The remaining portions of sea bottom are formed by a wide cover of middle to fine-grained sandy sediments grading into gravels having a varying nature (lavic, pyroclastic and sometimes anthropic; Ispra, 2010). The sea bottoms from the east of Casamicciola to the Spiaggia degli Inglesi, to the west of Ischia harbour are characterized by artificial blocks having a varying nature and, in correspondence to the beach of Spiaggia degli Inglesi, by gravels grading into sands and gravels. At 2.5 m of water depth it occurs a volcanic dyke, N-S trending.

The sea bottoms from the Ischia harbour to Ischia Ponte are characterized by artificial blocks in correspondence to the harbour and by wide outcrops of sands, often colonized by *Posidonia oceanica* (Gambi and Buia, 2003; Gambi *et al.*, 2003). From Ischia Ponte to the lavic coastal cliff of the Ischia Castle the sea bottom is formed of pelitic sands up to – 4 m, followed by sands colonized by mattes of *Posidonia oceanica*. From the Ischia Castle to Punta della Pisciazza, mainly sands occur at the sea bottom, at water depths among – 2 m and – 25 m, often colonized by mattes of *Posidonia oceanica*. In the coastal area surrounding Punta della Pisciazza lava blocks occur up to – 6 m of water depth, grading seawards into sands with mattes of *Posidonia oceanica*.

The western Ischia island: from Lacco Ameno to the Maronti littoral. The western coastal sector of the Ischia island, from Lacco Ameno to the Maronti beach is characterized by two main morphologic types: high relief coasts, conditioned by the occurrence of rocky formations, directly adjoining the sea or separated by narrow beaches of gravels and pebbles; low relief coasts, in correspondence to reliefs retreated with respect to the present-day shoreline, allowing for the formation of coastal cliffs with sandy littorals, sites of an intense touristic activity.

From the Lacco Ameno harbour to the Casamicciola harbour the sea bottom is characterized by a lowered area, developed up to 30 m of water depth, where an abrupt slope occurs. The sea bottom shows the occurrence of coarse-grained heterometric deposits, composed of blocks pertaining to the Epomeo Green Tuffs (Gillot *et al.*, 1982; Vezzoli, 1988; Ispra, 2010), often organized as sedimentary wedges having a variable extension.

The M.te Vico and Zaro promontories face directly the sea with active rocky coastal cliffs. The submerged cliff represents the physical continuity of the Zaro lava flow along all the coastal belt, covered by detritic deposits at the toe of slope. The sea bottoms are characterized by large detritic accumulations composed of heterometric blocks and representing landslide deposits.

From Punta Imperatore to Punta del Chiarito high relief coasts occur due to the outcrop of coherent lavic and pyroclastic successions. The sea bottom follows the articulated physiography of the emerged sector, characterized by rocky promontories. The base of the submerged slope is aligned with the structure of the continental slope and results close to some canyons' heads, draining the coastal sediment supply. The Maronti littoral is characterized by a narrow beach of sands and gravels located at the foot of a partly inactive coastal cliff, whose elevated portion shows the outcropping of the Epomeo Green Tuffs.

Physiographic and morphologic settings of the Ischia island. The study area includes several morphological ranges, each one characterized by a well defined elevation interval versus average slope (Fig. 1).

The domain A1 includes the Ischia outcropping volcanic edifice at depth more than 0, characterized by an average slope range of about 20°-40°. The domain A2 represents an intermediate stage, acting as an according layer towards the continental shelf. The domain B is the continental shelf, between the coastline and the 140-150 m (200 m in some cases) isobaths. The domain C includes the upper continental slope, located between the platform margin and the 650 m isobaths. The domain D is the lower continental slope, deeper than 650 m in depth.

These physiographic domains include several morphological elements, each representing tectonic or sedimentary processes or volcanic events. On the continental shelf, as well as at greater depths, abrasional and/or depositional terraces, relict volcanic edifices, canyons and gullies can be recognized. The increase of dip angles in the lower portion of the A physiographic unit is due to basal normal faulting of the Epomeo resurgent block. The submarine canyons occur on the A and C physiographic units, acting as morphological and depositional links between physiographic ranges.

The slope instability on the flanks of the volcanoes is a well-known geological process, mainly controlled by mechanisms of volcanic emplacement, hydrothermal vents, fast accretion of volcanic edifices and different erosional rates, as controlled by different lithologies of slope deposits (Thouret, 1999). Classical morpho-tectonic studies include the statistical analysis of the geometry of drainage patterns and stream direction controlled by tectonics and the identification of morpho-tectonic features. The main morphological characters of volcanic complexes of Latium in Italy are strongly controlled by four prevailing tectonic directions for Vulsini and three for Sabatini and Colli Albani volcanoes (Buonasorte *et al.*, 1993; Trigila, 1995). The structural setting of sedimentary units and the recent tectonic activity strongly controlled the location and the shape of the calderas.

The influence of structural framework on the shape and the formation of large caldera complexes has been inferred from remote sensing and ground-based structural analyses.

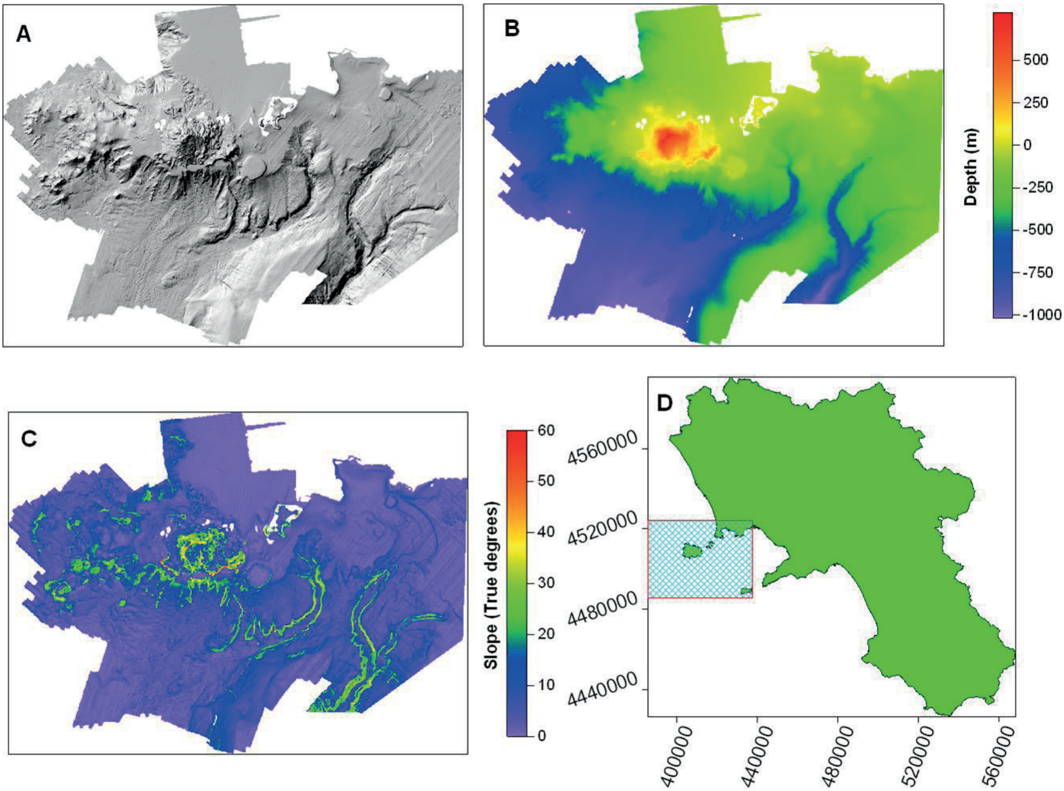

Fig. 2 – Composite map, respectively showing the DEM of the Naples Bay and Ischia island (A), the shaded relief map of the Naples Bay and Ischia island (B), the slope map of the Naples Bay and Ischia island (C) and the location map of the study area (D).

In particular, the main morphological and structural features on the submerged portions of volcanic edifices, such as Panarea and Stromboli in the Aeolian Arc (Sicily, Southern Italy) have been identified through high resolution seismic profiles and seismic tomography in the south-eastern Tyrrhenian sea (Gabbianelli *et al*., 1996; Castellano *et al*., 2008).

Conclusions. The Ischia island is encircled by several lava outcrops, interpreted as megadykes, whose formation seems to be linked to the calderic nature of the volcanic complex. These megadykes are located in correspondence to the Punta Cornacchia, Punta dello Zaro, S. Angelo and Punta del Soccorso promontories (Rittmann, 1930). Debris avalanche detachments develop between these volcanic lineaments, both in the southern and in northern sides of the island. This is not verified for the eastern side. Here, the lateral collapses occur within morphological protrusions, coincident with lava outcrops. The debris deposits systematically originate inside the A and C morphological units, whereas the marine deposits are detected within the C and D physiographic units. Slow mass movements and borders of detachments are detected only into the D unit area. We have interpreted this evidence as it follows. The A morphological unit is mainly related to the rising up of the Epomeo block. The B morphological unit is related to the presence of the upper shelf, strongly eroded at its upper border. The C morphological unit individuates the upper scarp, which is to be retained as tectonically-controlled, since it exhibits an average slope value with respect to the expected one and a strong gradient at its foot. Finally, the D morphological unit outlines the lower escarpment, which is characterized by the presence of hemipelagic drapes.

References

Acocella V. and Funiciello R.; 1999: *The interaction between regional and local tectonics during resurgent doming: the case of island of Ischia, Italy*: Journ. Volcanol. Geoth. Res., 88, pp. 109-123.

Acocella V., Funiciello R. and Lombardi S.; 1997: *Active tectonics and resurgence in Ischia island (southern Italy).* Il Quaternario, 10, pp. 427-432.

Acocella V., Funiciello R., Marotta E., Orsi G. and De Vita S.; 2004: *The role of extensional structures on experimental caldera and resurgence.* Journ. Volcanol. Geoth. Res., 129, pp. 199-217.

Aiello G., Budillon F., Cristofalo G., D'Argenio B., de Alteriis G., De Lauro M., Ferraro L., Marsella E., Pelosi N., Sacchi M. and Tonielli R.; 2001: *Marine geology and morpho-bathymetry in the Bay of Naples.* In: Faranda F.M., Guglielmo L. and Spezie G. (Eds.) *Structures and Processes of the Mediterranean Ecosystems*, Springer-Verlag Italy, Chapter 1, pp. 1-8.

Aiello G., Marsella E. and Passaro S.; 2009a: *Submarine instability processes on the continental slopes off the Campania Region (Southern Tyrrhenian sea, Italy): the case history of Ischia island (Naples Bay).* Boll. Geof. Teor. Appl., 50 (2), pp. 193-207.

Aiello G., Budillon F., Conforti A., D'Argenio B., Putignano M.L. and Toccaceli R.M.; 2009b: *Progetto per la realizzazione di cartografia geologica marina secondo le modalità CARG. Note illustrative alla cartografia geologica marina. Foglio geologico n. 464 "Ischia".* Preprints, 25 May 2009, III SAL Geologia Marina, IAMC, Istituto per l'Ambiente Marino Costiero, Geomare Sud, CNR, Napoli.

Aiello G., Marsella E. and Passaro S.; 2012a: *Stratigraphic and structural setting of the Ischia volcanic complex (Naples Bay, southern Italy) revealed by submarine seismic reflection data.* Rend. Lincei, 23 (4), pp. 387-408.

Aiello G., Giordano L., Marsella E. and Passaro S.; (2012b): *Seismic stratigraphy and marine magnetics of the Naples Bay (Southern Tyrrhenian sea, Italy): the onset of new technologies in marine data acquisition, processing and interpretation.* In: Elitok O. (Ed.) *Stratigraphic Analysis of Layered Deposits*, Intech, Chapter 2, pp. 21-60.

Amante C. and Eakins B.W; 2008: *ETOPO1 Arc-Minute Global Relief Model: Procedures, Data Sources and Analysis.* 1st Edition, NOOA, National Geophysical Data Center, Boulder, Colorado.

Barra D., Cinque A., Italiano A. and Scorziello R. (1992): *Il Pleistocene superiore marino di Ischia; paleoecologia e rapporti con l'evoluzione tettonica recente.* Studi Geologici Camerti, Suppl. 1, pp. 231-243.

Bruno P.P.G., de Alteriis G. And Florio G.; (2002): *The western undersea section of the Ischia volcanic complex (Italy, southern Tyrrhenian sea) inferred from marine geophysical data.* Geophys. Res. Lett., 29 (9), 1343, doi: 10.1029/2001GL013904.

Buonasorte G., Ciccacci S., De Rita D., Fredi P. and Lupia Palmieri E.; (1993): *Some relations between morphological characteristics and geological structure in the Vulsini Volcanic Complex.* Zeitsch fur Geomorph., Suppl. BD 82, pp. 59-71.

Calcaterra D., De Riso R., Evangelista R., Nicotera A., Santo A. and Scotto di Santolo A.; (2003): *Slope instabilities in the pyroclastic deposits of the Phlegrean district and the carbonate Apennine (Campania, Italy).* Int. Workshop on Occurrence and Mechanisms in Natural Slopes and Earthfills, IW Flows 2003, Sorrento, May 14-16, 2003.

Castellano M., Augusti V., De Cesare W., Favali P., Frugoni F., Montuori C., Sgroi T., De Gori P., Govoni A., Moretti M., Patanè D., Cocina O., Zuccarello L., Marsella E., Aiello G., Di Fiore V., Ligi M., Bortoluzzi G., Ferrante V., Marchetti E., Lacanna G. and Ulivieri G.; (2008): *Seismic tomography experiment at Italy's Stromboli volcano*. Eos Transactions AGU, 89 (30), pp. 269-276.

Chiesa S., Cornette Y., Forcella F., Gillot P.Y., Pasquarè G. and Vezzoli L.; (1985): *Carta geologica dell'isola d'Ischia*. CNR, Progetto Finalizzato Geodinamica, Roma, Italy.

Chiesa S., Civetta L., De Lucia M., Orsi G. and Poli S.; (1987): *Volcanological evolution of the island of Ischia*. In: De Girolamo P. (Ed.) *The volcanoclastic rocks of Campania (southern Italy)*. Rend. Acc. Sc. Fis. e Mat. in Napoli, Special Issue: pp. 69-83.

Chiocci F.L. and de Alteriis G.; (2006): *The Ischia Debris Avalanche: first clear submarine evidence in the Mediterranean of a volcanic island prehistorical collapse*. Terra Nova, 18 (3), pp. 202-209.

Civetta L., Gallo G. and Orsi G.; (1991): *Sr and Nd isotope and trace elements constraints on the chemical evolution of the magmatic system of Ischia (Italy) in the last 55 ky*. Journ. Volcanol. Geoth. Res., 46, pp. 213-230.

de Alteriis G., Tonielli R., Passaro S. and De Lauro M.; (2006): *Isole flegree (Ischia e Procida). Batimetria dei fondali marini della Campania. Scala 1:30.000*. Liguori Editore, Napoli.

de Alteriis G., Insinga D.D., Morabito S., Morra V., Chiocci F.L., Terrasi F., Lubritto C., Di Benedetto C. and Pazzanese M.; (2010): *Age of submarine debris avalanches and tephrostratigraphy offshore Ischia island, Tyrrhenian sea*. Marine Geology, 278, pp. 1-18.

De Vita P., Agrello D. and Ambrosino F.; (2006): *Landslide susceptibility assessment in the ash-fall pyroclastic deposits surrounding Mount Somma-Vesuvius. Application of geophysical surveys for soil thickness mapping*. Journ. of Appl. Geophys., 59, pp. 126-139.

De Vita P., Celico P., Di Clemente E. and Rolandi M.; (2007): *Engineering geological models in the initial landslides occurred on 30 April 2006 at the Mount of Vezzi (Ischia island)*. Ital. Journ. of Engineering Geology and Environment, University of Rome La Sapienza, Research Center Ceri, 2.

Di Maio R., Piegari E., Scotellaro C. and Soldovieri M.G.; (2007): *Tomografie di resistività per la definizione dello spessore e del contenuto d'acqua delle coperture piroclastiche a M.te di Vezzi (Isola d'Ischia)*. Ital. Journ. of Engineering Geology and Environment, University of Rome La Sapienza, Research Center Ceri, 2.

Di Nocera S., Matano F., Rolandi G. and Rolandi R.; (2007): *Contributo agli aspetti geologici e vulcanologici del M.te di Vezzi (Isola d'Ischia) per lo studio degli eventi franosi dell'Aprile 2006*. Ital. Journ. of Engineering Geology and Environment University of Rome La Sapienza, Research Center Ceri, 2.

Forcella F., Gnaccolini M. and Vezzoli L.; (1981): *I depositi piroclastici del settore sud-orientale dell'isola d'Ischia*. Riv. Ital. Paleont. Strat., 89, pp. 1-35.

Gabbianelli G., Romagnoli C., Rossi P.L. and Calanchi N.; (1993): *Marine geology of the Panarea-Stromboli area (Aeolian Arcipelago, Southeastern Tyrrhenian sea)*. Acta Vulcanologica, 3, pp. 11-20.

Gambi M.C. and Buia M.C.; (2003): *Sintesi delle conoscenze floro-faunistiche ed ecologiche sui popolamenti marini delle isole flegree (Ischia, Procida e Vivara – Golfo di Napoli)*. In: Gambi M.C., De Lauro M., Iannuzzi F. (Eds.) *Ambiente marino costiero e territorio delle isole flegree (Ischia, Procida e Vivara – Golfo di Napoli). Risultati di uno studio multidisciplinare*. Mem. Acc. Sc. Fis. e Mat. in Napoli, 5, pp. 133-161.

Gambi M.C., Dappiano M. and Lanera P.; (2003): *Popolamenti bentonici di alcuni fondi selezionati dell'Isola d'Ischia*. In: Gambi M.C., De Lauro M., Iannuzzi F. (Eds.) *Ambiente marino costiero e territorio delle isole flegree (Ischia, Procida e Vivara – Golfo di Napoli). Risultati di uno studio multidisciplinare*. Mem. Acc. Sc. Fis. e Mat. in Napoli, 5, pp. 187-200.

Gillot P.Y., Chiesa S., Pasquarè G. and Vezzoli L.; (1982): *K/Ar dating of the volcano-tectonic horst of the isle of Ischia*. Nature, 229, 242-245.

Guadagno F.M. and Mele R.; (1995): *La fragile isola d'Ischia*. Geol. Appl. e Idrogeol., 30 (1), pp. 177-187.

IHO Special Publication n. 44; (1998): *Standards for hydrographic surveys*. 4th Edition International Hydrographic Bureau, Munchen.

Ispra (2010); *Geological map n. 464 "Isola d'Ischia"*. Systemcart, Roma, Italy.

Luongo G., Cubellis E. and Obrizzo F.; (1987): *Ischia: storia di un'isola vulcanica*. Liguori Editore, Napoli.

Luongo G., Cubellis E. and Obrizzo F.; (1997): *Storia e strumenti per un Museo Vulcanologico*. In: Luongo G. (Ed.) *Mons Vesuvius,* Fiorentino Ed., Napoli.

Mele R. and Del Prete S.; (1998): *Fenomeni di instabilità dei versanti in Tufo Verde del Monte Epomeo (Isola d'Ischia, Campania)*. Boll. Soc. Geol. Ital., 117 (1), pp. 93-112.

Moore J.G. and Mark R.K.; (1992): *Morphology of the island of Hawaii*. GSA Today, 2, pp. 257-262.

Orsi G., Gallo G. and Zanchi A.; (1991): *Simple-shearing block resurgence in caldera depressions. A model from Pantelleria and Ischia*. Journ. Volcanol. Geoth. Res., 47, pp. 1-11.

Passaro S.; (2005): *Integrazione di dati magnetici e batimetrici in aree vulcaniche e non vulcaniche: esempi dall'isola d'Ischia e dal Banco di Gorringe (Oceano Atlantico)*. PhD Thesis, University of Naples "Federico II", Naples, Italy.

Passaro S., Ferranti L. and de Alteriis G.; (2011): *The use of high resolution elevation histograms for mapping submerged terraces: a test from the Eastern Tyrrhenian sea and the Eastern Atlantic Ocean*. Quaternary International, 232 (1-2), pp. 238-249.

Passaro S., Milano G., D'Isanto C., Ruggieri S., Tonielli R., Bruno P.P.G., Sprovieri M. and Marsella E.; (2010): *DTM-based morphometry of the Palinuro seamount (Italy, Eastern Tyrrhenian sea):geomorphological and volcanological implication*. Geomorphology, 115 (1-2), pp. 129-140.
Poli S., Chiesa S., Gillot P.Y., Gregnanin A. and Guichard F.; (1987): *Chemistry versus time in the volcanic complex of Ischia (Gulf of Naples, Italy).* Contr. to Mineral. and Petrol., 95 (3), pp. 322-335.
Poli S., Chiesa S., Gillot P.Y., Guichard F. and Vezzoli L.; (1989): *Time dimension in the geochemical approach and hazard estimation of a volcanic area: the isle of Ischia case (Italy).* Journ. of Volcanol. and Geoth.Res., 36, pp. 327-335.
Thouret J.C.; (1999): *Volcanic geomorphology – an overview.* Earth Science Reviews, 47, pp. 95-131.
Trigila R., Agosta E., Currado C., De Benedetti A., Freda C., Gaeta M., Palladino D.M. and Rosa C.; (1995): *The Volcano of the Alban hills – IV – Petrology.* In: *The Volcano of the Alban Hills.*, pp. 95-165.
Walther J.; (1886): *I vulcani sottomarini del Golfo di Napoli.* Estratto dal Bollettino del Real Comitato Geologico, 9-10, 12 pp.
Vezzoli L.; (1988): *Island of Ischia.* CNR, Quaderni De La Ricerca Scientifica, 114 (10), 122 pp.

EVIDENZE GEODETICHE SULLA PRESENZA DI DUE SORGENTI DI DEFORMAZIONE AI CAMPI FLEGREI

A. Amoruso, L. Crescentini, I. Sabbetta
Dipartimento di Fisica, Università di Salerno

Abbiamo analizzato gli spostamenti del suolo registrati ai Campi Flegrei dal 1980 al 2010, con lo scopo di evidenziare somiglianze o differenze tra i periodi di bradisismo positivo e negativo e mettere in luce possibili anomalie deformative in aree particolari. A questo scopo, abbiamo usato misure di livellazione dal 1980 al 1994, misure topografiche (angoli e distanze) eseguite nel giugno 1980 e giugno 1983 (Barbarella *et al.*, 1983), e dati SAR dal 1993 al 2010.

In un primo momento abbiamo confrontato tra di loro gli spostamenti verticali relativi ai periodi di maggiore deformazione, caratterizzati da velocità di sollevamento o abbassamento del suolo pressoché costanti. In particolare, abbiamo considerato i periodi giugno 1980 - giugno 1983, giugno 1983 - ottobre 1984, gennaio 1985 - dicembre 1988, giugno 1989 - dicembre 1992, marzo 1995 - dicembre 1999. Nel caso dell'ultimo periodo abbiamo ricostruito gli spostamenti verticali in prossimità dei caposaldi di livellazione usando i dati SAR. Opportunamente scalati, gli spostamenti coincidono all'interno degli errori, con l'eccezione dei caposaldi situati nella Solfatara e in prossimità di essa.

Il confronto tra la componente est degli spostamenti orizzontali del 1980-1983 e quella del 1995-2000 ha fornito risultati analoghi.

Quanto sopra suggerisce la costanza del campo di deformazione durante tutti i periodi summenzionati, a parte la zona prossima alla Solfatara.

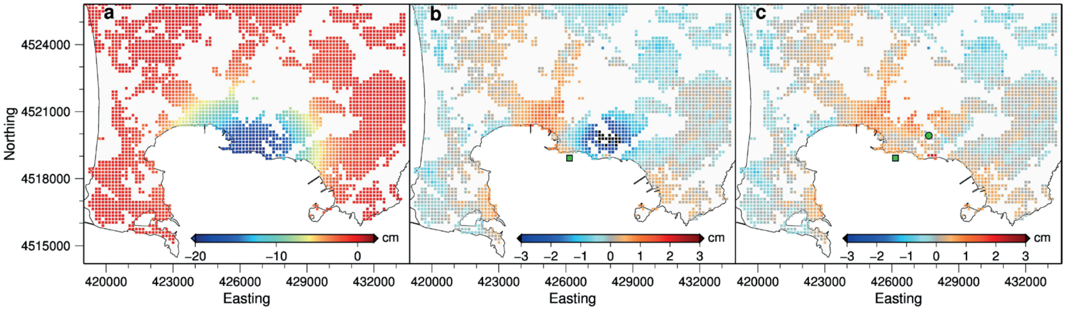

Fig. 1 – a) Spostamenti verticali nel periodo 1995-2000, da dati SAR. b) Deformazione residua dopo aver sottratto l'effetto della sorgente della deformazione su larga scala; il quadrato verde rappresenta il centro della sorgente. c) Deformazione residua dopo aver sottratto anche il contributo della sorgente localizzata sotto la Solfatara; il cerchio verde rappresenta il centro della sorgente.

Come è noto, il periodo 1980-1983 è caratterizzato da un forte sollevamento (circa 60 cm) e dalla disponibilità di dati relativi sia agli spostamenti verticali (misure di livellazione) che ad entrambe le componenti degli spostamenti orizzontali (Barbarella *et al.*, 1983). La disponibilità di questi dati permette di cercare le caratteristiche della sorgente responsabile del sollevamento alla scala dei Campi Flegrei nel loro complesso. Poiché la zona della Solfatara non è coperta da dati, l'inversione non è influenzata apprezzabilmente dall'anomalia locale precedentemente riscontrata. Abbiamo utilizzato un semispazio elastico stratificato, le cui caratteristiche sono state ottenute dalla tomografia sismica. Si è così dimostrato che la deformazione su larga scala è spiegabile, durante tutto il periodo analizzato, con una singola sorgente deformativa stazionaria, di cui cambia nel tempo solo l'intensità. Sulla base dell'accordo tra previsioni e misure e di criteri informativi, la sorgente favorita è un crack ellittico sub-orizzontale orientato NO-SE posto tra 3500 e 4000 m di profondità, indicato con CE in quanto segue.

Una volta sottratto l'effetto della sorgente della deformazione su larga scala (CE) dai dati SAR relativi al periodo 1995-2000, rimane un'evidente deformazione residua nell'area della Solfatara (Fig. 1). Da un punto di vista matematico, la sorgente favorita per la deformazione nella Solfatara è una piccola (rispetto alla profondità) sorgente sferoidale con asse verticale, immersa a circa 1900 metri di profondità nel semispazio elastico stratificato di cui sopra. È presente un'evidente correlazione tra profondità e rapporto tra i semiassi.

Abbiamo quindi verificato l'ipotesi che la deformazione a larga scala, con l'esclusione quindi della Solfatara, sia sempre dovuta alla sorgente responsabile del sollevamento del 1980-1983 (CE), ma con intensità variabile nel tempo in ampiezza e segno (fasi di bradisismo positivo e negativo).

L'andamento temporale dell'intensità della sorgente è ottenuto dalla media spaziale degli spostamenti da dati SAR, relativi a pixel contenuti all'interno di un'area di riferimento nella zona di massimo spostamento verticale (cerchio nero nelle mappe di sinistra e centrale in Fig. 2).

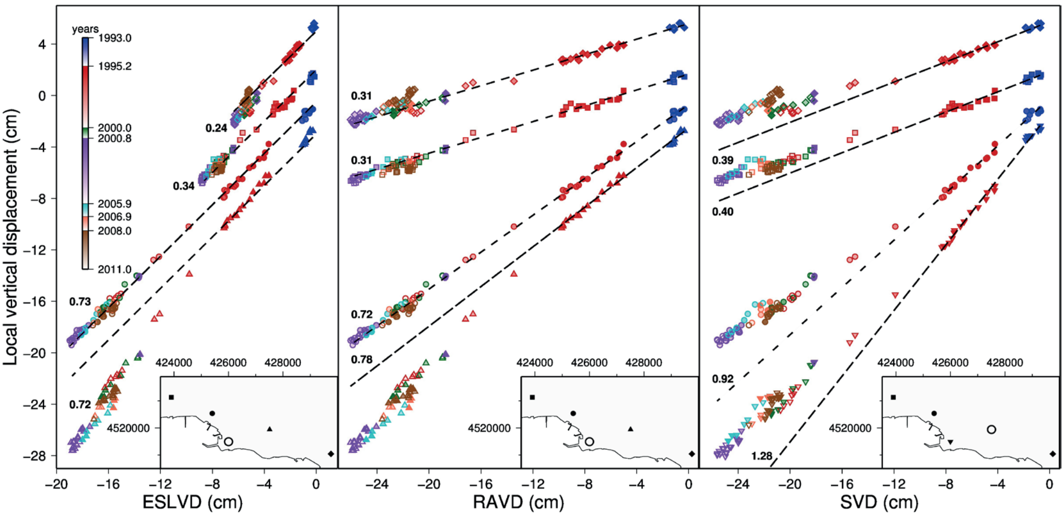

Fig. 2 – Grafici di correlazione tra spostamenti verticali. Pannello sinistro: spostamenti verticali locali (Local vertical displacements) nei punti indicati con simboli pieni nella mappa e spostamenti previsti sulla base del CE (Ellipsoidal Source Local Vertical Displacements, ESLVD), ottenuti tramite i rapporti LRDR (v. testo); gli LRDR sono esplicitamente riportati a sinistra di ciascuna sequenza; la linea tratteggiata rappresenta la bisettrice degli assi. Pannello centrale: spostamenti verticali locali nei punti indicati con simboli pieni nella mappa e spostamenti verticali nell'area di riferimento (Reference Area Vertical Displacements, RAVD, cerchio vuoto nella mappa); i numeri indicano la pendenza delle rette di regressione relative al periodo 1993-1997. Pannello destro: spostamenti verticali locali nei punti indicati con simboli pieni nella mappa e spostamenti verticali nella Solfatara (Solfatara Vertical Displacements, SVD, cerchio vuoto nella mappa); i numeri indicano la pendenza delle rette di regressione relative al periodo 1993-1997. I colori forniscono la scala temporale.

Gli spostamenti in altre posizioni vengono quindi calcolati dal campo di deformazione dovuto al CE attraverso il rapporto tra lo spostamento locale e quello dell'area di riferimento (local-to-reference displacement ratio, LRDR) e confrontati con quelli osservati, mediante grafici di correlazione. Per brevità e facilità di interpretazione visiva, qui si mostrano solo alcuni grafici relativi a spostamenti verticali.

Il pannello di sinistra nella Fig. 2 mostra esempi di tipici grafici di correlazione relativi agli spostamenti verticali all'esterno e all'interno della Solfatara. Se gli spostamenti fossero dovuti esclusivamente al CE, i punti si disporrebbero approssimativamente lungo la bisettrice degli assi, così come effettivamente osservato per le posizioni esterne alla Solfatara. All'interno della Solfatara, le deviazioni dalla bisettrice degli assi sono evidenti e non casuali dal 1997 in poi.

Il diverso comportamento dei punti interni ed esterni alla Solfatara non è un artefatto prodotto dall'uso del CE come riferimento. Il pannello centrale mostra i grafici di correlazione tra gli spostamenti verticali misurati sugli stessi punti mostrati nel pannello di sinistra e quelli misurati nell'area di riferimento. I punti all'esterno della Solfatara sono sempre molto vicini alla retta di regressione relativa al periodo 1993-1997, indicando quindi una correlazione lineare temporalmente invariante. I punti all'esterno della Solfatara si discostano sensibilmente e in maniera non casuale dalla stessa retta di regressione. Il confronto tra i valori degli LRDR (Fig. 2, pannello sinistro) e la pendenza delle rette di regressione relative al periodo 1993-1997 (Fig. 2, pannello centrale) conferma ulteriormente la similitudine tra il campo di deformazione a larga scala e quello generato dal CE.

Ulteriore conferma del comportamento anomalo della Solfatara (rispetto a quello dei Campi Flegrei nel loro complesso) è fornita dal pannello destro della stessa Fig. 2, dove vengono confrontati gli spostamenti verticali negli stessi punti dei pannelli di sinistra e centrale, con l'esclusione di quelli nella Solfatara, con gli spostamenti verticali nella Solfatara (cerchio nero nella mappa dello stesso pannello destro). Le rette di regressione relative al periodo 1993-1997 mostrano l'assenza di una correlazione lineare temporalmente invariante tra punti esterni e interni alla Solfatara.

Abbiamo anche dimostrato che la deformazione residua alla Solfatara è spiegabile, durante tutto il periodo analizzato, con una singola sorgente deformativa stazionaria, di cui ancora una volta cambia nel tempo solo l'intensità.

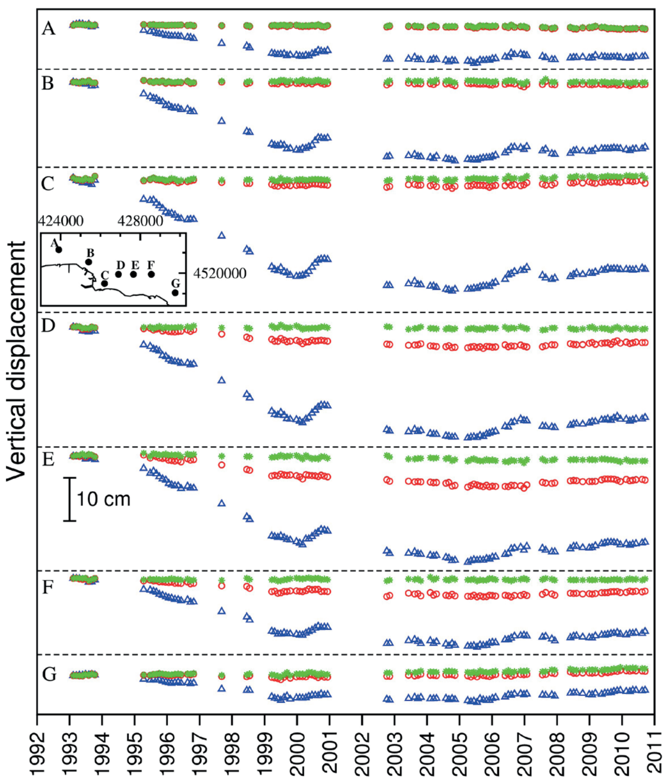

Fig. 3 – Andamenti temporali dello spostamento verticale rispetto al 1993 da dati SAR per sette diversi punti nei Campi Flegrei. I triangoli blu rappresentano lo spostamento misurato, i cerchi rossi il residuo dopo aver sottratto il contributo della sorgente della deformazione su larga scala, gli asterischi verdi quanto rimane dopo aver sottratto anche il contributo della sorgente posta sotto la Solfatara.

L'evoluzione temporale delle intensità delle due sorgenti (CE e sorgente locale sotto la Solfatara) è simile, ma tutt'altro che uguale. Le differenze confermano che la sorgente locale sotto la Solfatara è reale e non un semplice artefatto dovuto alla distorsione locale del campo di deformazione su larga scala, indotta da particolari caratteristiche reologiche. L'efficacia delle due sorgenti nel rendere conto della deformazione complessiva ai Campi Flegrei dal 1993 a fine 2010 è mostrata in Fig. 3.

Ovviamente, il fatto che una sorgente sferoidale renda conto della deformazione locale nella Solfatara non implica l'esistenza di una vera cavità pressurizzata. Come recentemente mostrato da Fournier e Chardot (2012), quando la deformazione del suolo è legata a processi idrotermali e spiegabile con semplici sorgenti puntiformi o finite, la deformazione stessa è probabilmente controllata dalla risposta poroelastica del substrato all'aumento della pressione di poro nei pressi del punto di iniezione dei fluidi magmatici nel sistema idrotermale. La profondità della sorgente, ottenuta invertendo i dati di deformazione, è molto prossima a quella dell'area di iniezione.

La posizione delle due sorgenti (quella responsabile del campo di deformazione su larga scala e quella responsabile della deformazione locale nella Solfatara) è pienamente consistente con la probabile presenza di fuso tra i 3000 e 4000 metri sotto Pozzuoli, messa in luce da recenti studi di attenuazione sismica (De Siena *et al.*, 2010), con modelli concettuali geochimici della Solfatara (Chiodini *et al.*, 2010), e con le misure geochimiche (Chiodini *et al.*, 2012).

Riconoscimenti. I dati di livellazione sono stati gentilmente concessi da G. Berrino e F. Obrizzo. I dati SAR sono stati gentilmente concessi da R. Lanari.

Bibliografia

Barbarella M., Gubellini A., e Russo P.; 1983: *Rilievo ed analisi dei recenti movimenti orizzontali del suolo nell'area flegrea*, Atti 2° Convegno GNGTS, Roma, 12-14 dicembre.

Chiodini G., Caliro S., Cardellini C., Granieri D., Avino R., Baldini A., Donnini M., and Minopoli C.; 2010: *Long-term variations of the Campi Flegrei, Italy, volcanic system as revealed by the monitoring of hydrothermal activity*. J. Geophys. Res., 115, B03205, doi: 10.1029/2008JB006258.

Chiodini G., Caliro S., De Martino P., Avino R., and Gherardi F.; 2012: *Early signals of new volcanic unrest at Campi Flegrei caldera? Insights from geochemical data and physical simulations*. Geology, 40, 943-946, doi:10.1130/G33251.1

De Siena L., Del Pezzo E., and Bianco F.; 2010: *Seismic attenuation imaging of Campi Flegrei: Evidence of gas reservoirs, hydrothermal basins, and feeding systems*. J. Geophys. Res., 115, B09312, doi:10.1029/2009JB006938.

Fournier N., and Chardot L.; 2012: *Understanding volcano hydrothermal unrest from geodetic observations: Insights from numerical modeling and application to White Island volcano, New Zealand*. J. Geophys. Res., 117, B11208, doi:10.1029/2012JB009469.

VALUTAZIONE STATISTICA DELLA POTENZIALITÀ GEOTERMICA DELL'ACQUIFERO SUPERFICIALE NEL SETTORE SUDORIENTALE DELLA PIANURA PADANA PIEMONTESE

D. Barbero[1], M.G. Forno[2], L. Magnea[1]

[1]*Dipartimento di Fisica, Università di Torino*

[2]*Dipartimento di Scienze della Terra, Università di Torino*

Introduzione. Nella valutazione del potenziale geotermico di un'area concorrono diversi fattori. Gli aspetti geologici e geofisici sono quelli che per primi vengono presi in considerazione per poter esprimere un parere favorevole alla fattibilità di un progetto per sfruttamento ed estrazione della risorsa geotermica. Tra i fattori geologici e geofisici, si ricordano la distribuzione della temperatura nel sottosuolo, il calore specifico, la permeabilità, la porosità (totale ed effettiva), e la profondità del serbatoio.

In questa ricerca viene presa in esame la distribuzione della temperatura nell'immediato sottosuolo, in relazione alla profondità, valutando il potenziale geotermico dell'acquifero superficiale di un'area campione corrispondente al settore sudorientale della Pianura Padana piemontese. Obiettivo del lavoro è una determinazione statisticamente consistente del valore della temperatura del sottosuolo, e dell'incertezza ad esso associata: un dato che contribuisce in modo significativo a stabilire se una determinata area possa essere considerata promettente per lo sfruttamento per scopi geotermici.

Nell'ambito di un progetto finalizzato allo sfruttamento della falda superficiale per mezzo di impianti a circuito aperto, in cui viene utilizzata l'acqua di falda superficiale a mezzo di pozzi, il metodo proposto offre la possibilità di prevedere, in senso statistico, i valori della temperatura del sottosuolo, con un prescelto intervallo di confidenza. Questo consente, in linea di principio, un controllo della variabilità della temperatura, fondamentale per il dimensionamento di un impianto, senza la necessità procedere per ogni impianto ad esplorazioni dirette "in situ".

Le misure termometriche a disposizione sono state raccolte da ARPA Piemonte (Balsotti, 2009) a seguito dell'installazione di piezometri di controllo per scopi di monitoraggio ambientale.

I 18 piezometri utilizzati, distribuiti per lo più nella Provincia di Alessandria, hanno fornito 80 misure primaverili e 86 misure autunnali, raccolte a varie profondità mediante l'introduzione di una sonda multiparametrica dotata di vari sensori, tra cui quello relativo alla temperatura e alla profondità della misurazione. I piezometri, la cui ubicazione è stata georiferita tramite GIS (Fig. 1), hanno una lunghezza media di circa 20 metri e, in alcuni settori della pianura, si spingono fino a una profondità di circa 30 metri.

Il quadro geologico e idrogeologico dell'area. Il settore piemontese della Pianura Padana è stato oggetto di numerose indagini che hanno evidenziato l'esistenza di almeno due tipi principali di *reservoir* geotermici. Il primo serbatoio, più superficiale, è impostato nei depositi terrigeni terziari e quaternari, essenzialmente incoerenti e caratterizzati da una permeabilità primaria per porosità; il secondo, più profondo, è invece impostato nelle rocce carbonatiche di età mesozoica, prevalentemente coerenti e caratterizzate da una permeabilità secondaria per fessurazione (Bortolami *et al.*, 1982).

Studi più recenti (Balsotti, 2009; Stringari *et al.*, 2010) hanno fornito una mappatura termica della falda superficiale a scala regionale, nell'ottica di un possibile sfruttamento mediante impianti geotermici a bassa entalpia. Nell'ambito degli stessi studi gli autori hanno riconosciuto la cosiddetta "superficie di omeotermia", in corrispondenza della quale i valori di temperatura rimangono costanti tutto l'anno; tale superficie ripropone nel sottosuolo, a una profondità di circa 20 metri, l'andamento della superficie topografica. Studi ancora successivi dimostrano come al di sotto di questa superficie la temperatura cresca gradualmente e lentamente e indipendentemente dalle condizioni climatiche esterne, per poi crescere più rapidamente per profondità maggiori di 100 metri in accordo al gradiente geotermico locale (Lo Russo e Civita, 2010).

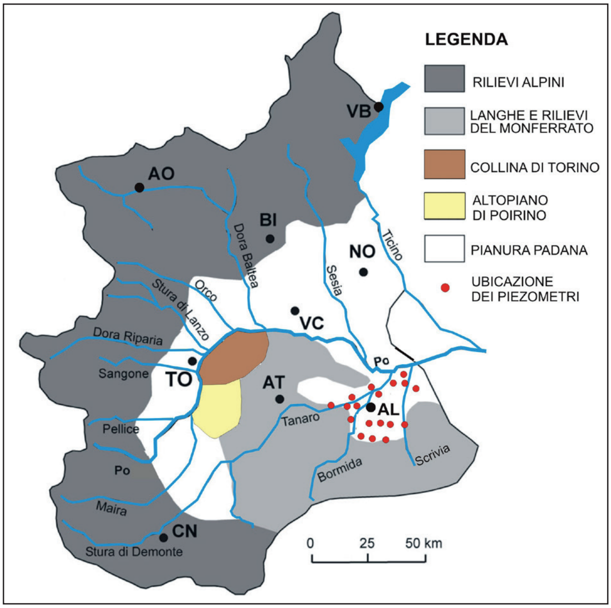

Fig. 1 – Ubicazione di dettaglio dei piezometri nel settore sudorientale della Pianura Padana piemontese.

Analisi geostatistiche effettuate su un campione significativo di misure termometriche relative a piezometri distribuiti nel settore nordorientale della Pianura Padana piemontese hanno consentito, non solo di individuare il *range* di profondità in corrispondenza della quale si situerebbe la "superficie di omeotermia" sopracitata, ma anche di determinare, per profondità comprese tra 20 e 50 metri, un valore di temperatura costante di 14,0 °C, con una precisione di 0,6 ±0,1°C, estrapolabile ad una vasta area (Barbero *et al.*, 2012).

L'area campione presa in esame, corrispondente al settore sudorientale della Pianura Padana piemontese, con debole inclinazione verso NE, presenta uno sviluppo altimetrico variabile tra 300 m, al margine sudoccidentale in prossimità al limite con i rilievi collinari delle Langhe, e 70 m, nel settore nordorientale in corrispondenza della confluenza fra il fiume Po e il torrente Scrivia.

Dal punto di vista idrografico, l'area è drenata dal fiume Tanaro, che costituisce l'elemento drenante principale, e dai suoi principali affluenti rappresentati dal torrente Belbo, il torrente Bormida e il torrente Scrivia.

L'area è caratterizzata nel sottosuolo da numerosi assi drenanti e spartiacque sotterranei: particolarmente significativo è lo spartiacque sotterraneo ricostruibile a SW di Alessandria, che separa le acque di falda drenanti nel fiume Tanaro, da quelle che drenanti nel fiume Bormida. I flussi idrici sotterranei mostrano un andamento centripeto verso l'area di Alessandria. I valori di soggiacenza della falda superficiale diminuiscono progressivamente dai settori prossimi ai rilievi delle Langhe e del Monferrato, dove raggiungono i 20 metri, al settore assiale della pianura, presso l'alveo del fiume Tanaro, dove le soggiacenze hanno valori inferiori ai 2 metri (Canavese *et al.*, 2004).

Il sottosuolo appare costituito da una potente successione di sedimenti prevalentemente incoerenti, connessi ad un ambiente marino, deltizio e fluviale, individuabili nelle stratigrafie dei sondaggi (Boni e Casnedi, 1970; Bortolami *et al.*, 1976; Canavese *et al.*, 2004). La successione stratigrafica è intercettata nella sua completezza nel settore meridionale, dove lo spessore dei termini superiori risulta relativamente modesto; nel settore settentrionale, invece, lo spessore rilevante dei termini fluviali e la ridotta profondità dei pozzi per approvvigionamento idrico non consentono di individuare la parte inferiore della successione, marina e deltizia.

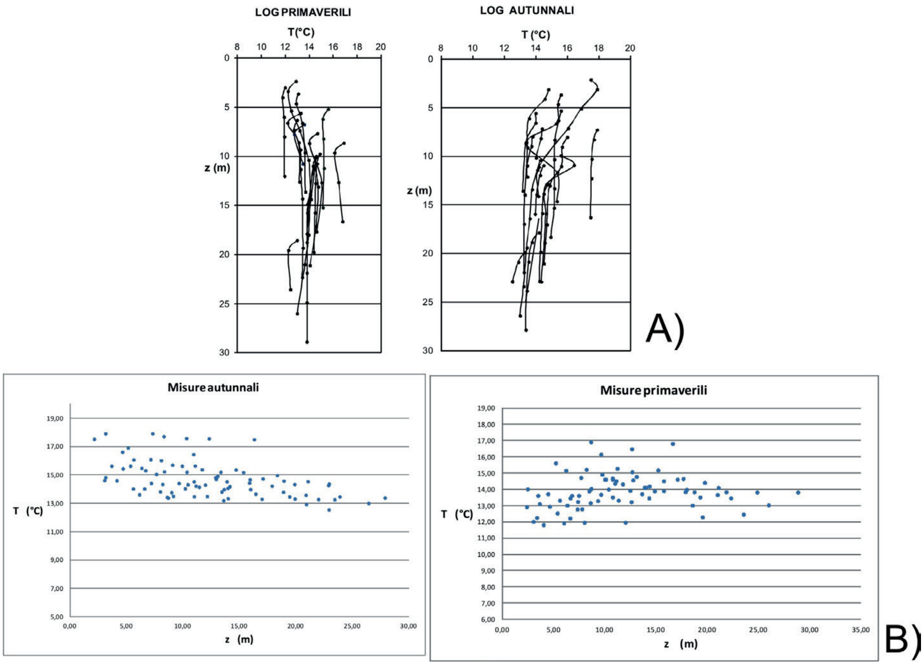

Fig. 2 – Log di temperatura (A) e diagrammi di dispersione delle misure termometriche (B).

Il termine inferiore della successione marina osservabile nelle stratigrafie è rappresentato dalle "Argille di Lugagnano", corrispondenti a silt argillosi e marne sabbiose di colore grigio-azzurro, ricchi di microfossili, deposti in ambiente marino profondo. Al di sopra si sviluppano le "Sabbie di Asti", corrispondenti a sabbie fini di colore giallastro con stratificazione piano-parallela, ricche di macrofossili, deposte in ambiente marino litorale (Boni e Casnedi, 1970). Questi due corpi sedimentari, alla luce delle interpretazioni più recenti, sono riferibili rispettivamente al Pliocene inferiore e al Pliocene inferiore-medio (Dela Pierre *et al.*, 2003). Nell'area alessandrina la successione pliocenica marina mostra spessori variabili: nel settore più settentrionale le stratigrafie di pozzi profondi intercettano tali sedimenti già a partire da 50 metri di profondità dal piano campagna, fino a profondità del centinaio di metri. Nel settore meridionale invece le stratigrafie non raggiungono i termini della successione marina: ciò suggerisce che tale successione sia presente a profondità superiori al centinaio di metri (Bortolami *et al.*, 1976; Bove *et al.*, 2005).

Al di sopra dei termini marini si sviluppa la successione villafranchiana, costituita a sua volta da due complessi sedimentari sovrapposti (Carraro, 1996; Boano e Forno, 1999). Il Complesso Inferiore, di ambiente deltizio ed età pliocenica media, è formato nella parte basale da sabbie grossolane, con stratificazione incrociata concava e locali intercalazioni siltose, indicate come Unità di Ferrere. Nella parte media e superiore questo complesso è invece formato da ripetute alternanze di sedimenti siltosi, con laminazione piano-parallela, ricchi di macroresti vegetali, e sedimenti sabbiosi, con stratificazione incrociata concava, contenenti numerosi vertebrati continentali. All'interno di questi sedimenti si riconoscono localmente livelli con resti vegetali lignitizzati e minori intercalazioni di ghiaie minute. Il Complesso Superiore, di ambiente fluviale ed età pleistocenica inferiore, è formato nella parte basale da sabbie grossolane e sabbie ghiaiose, con stratificazione incrociata concava, e nella parte superiore da silt argillosi privi di stratificazione, estremamente pedogenizzati. Nell'area alessandrina la successione villafranchiana mostra spessori variabili: nel settore settentrionale ha uno spessore inferiore come suggerito dal rinvenimento di sedimenti riferibili alla successione pliocenica già a partire da circa 50 metri di profondità dal piano campagna; nel settore meridionale invece, la successione villafranchiana raggiunge spessori di alcune centinaia di metri (Bortolami *et al.,* 1976; Bove *et al.,* 2005).

I depositi più superficiali, corrispondenti ai sedimenti affioranti, sono costituiti prevalentemente da ghiaie grossolane, ghiaie sabbiose e sabbie, deposte in ambiente fluviale e di età pleistocenica media-olocenica. I termini più antichi risultano intensamente pedogenizzati, costituendo superfici terrazzate ai margini della pianura alluvionale attuale. Questi sedimenti, nel loro insieme, hanno prevalentemente uno spessore di alcune decine di metri, fino a raggiungere spessori più cospicui dell'ordine di un centinaio di metri nel settore meridionale della pianura (Boni e Casnedi, 1970).

La locale presenza di depositi fluviali pedogenizzati ricchi della componente argillosa, affioranti nel settore sudorientale, consente una separazione netta tra l'acquifero superficiale, ospitato nei depositi fluviali, e gli acquiferi profondi, ospitati prevalentemente nei livelli permeabili marini e nella successione villafranchiana (Canavese *et al.,* 2004; Bove *et al.,* 2005). La base dell'acquifero superficiale è generalmente ben evidenziata grazie alla variabilità tessiturale dei depositi (Canavese *et. al.,* 2004; Bove *et. al.,* 2005): nell'area alessandrina lo spessore dei depositi in cui è impostato l'acquifero superficiale raggiungono profondità di circa 50 metri (Stringari *et al.*, 2010). Il comportamento termico dell'acquifero superficiale, come già descritto da diversi autori, è in accordo con il quadro geologico e idrogeologico del settore in esame, in cui si sviluppano l'acquifero superficiale e gli acquiferi profondi (Boni e Casnedi, 1970; Bortolami *et al.,* 1976; Canavese *et al.,* 2004).

Infine, nell'area in esame, considerata la ridotta profondità interessata dai piezometri di monitoraggio, si escludono manifestazioni superficiali di gradienti geotermici anomali connessi a motivi strutturali profondi in grado di determinare un trasferimento di calore in superficie attraverso moti convettivi.

Metodi. Aspetti teorici della conduzione del calore nel sottosuolo ed Analisi dei dati termometrici Come già osservato in precedenza (Barbero *et al.*, 2012), nell'analisi dei flussi termici alle limitate profondità considerate nel nostro lavoro, non è necessario prendere in considerazione il gradiente geotermico profondo. Si può quindi utilizzare l'equazione di propagazione del calore nella forma che essa assume in assenza di sorgenti endogene di calore, e prendendo in considerazione le variazioni di temperatura nella sola direzione verticale. L'equazione differenziale così ottenuta (1), alle derivate parziali del secondo ordine, fornisce, tra le altre, soluzioni oscillanti rappresentative delle oscillazioni stagionali (2), in cui la temperatura, per via del termine esponenziale, tende progressivamente a smorzarsi in profondità fino a raggiungere un andamento asintotico, con valore di temperatura circa costante: tale valore è riconducibile alla cosiddetta "superficie di omeotermia".

$$\frac{\partial T}{\partial t} = \frac{1}{\alpha}\frac{\partial^2 T}{\partial z^2} \qquad (1)$$

$$T(z,t) = T_0 + Ae^{-\gamma z}\cos(\omega t - \gamma z) \qquad (2)$$

In particolare, se si considera una condizione al contorno per $z = 0$ della forma $T = \mathrm{f}\,(t)$, si trovano soluzioni oscillanti smorzate, rappresentative delle variazioni stagionali, della forma (2). Quando poi si prendono in esame profondità significative, $z > 1/\gamma$, ovvero profondità in cui le fluttuazioni stagionali sono trascurabili, si osserva il comportamento asintotico (3).

$$T(z > 1/\gamma, t) \cong T_0$$

Lo scopo del lavoro è pertanto quello di determinare il valore di T_0 e la sua relativa incertezza attraverso un'analisi statistica su un campione di misure ritenuto statisticamente significativo.

Lo studio statistico, in analogia alla metodologia già adottata per il settore nordorientale (Barbero *et al.*, 2012), è stato preceduto da un'analisi per via grafica dei dati di temperatura (Fig. 2A). L'analisi dei dati di temperatura, congruentemente a quanto già riscontrato nell'area limitrofa, ha mostrato un andamento comune per tutti i profili termici dei singoli piezometri: le variazioni verticali e orizzontali di temperatura, già a partire dai 10 metri di profondità tendono sensibilmente a ridursi fino ad registrare una situazione di sostanziale stabilità termica per profondità maggiori di 15 metri. Tale aspetto, in accordo a studi precedenti effettuati a scala regionale (Stringari *et al.*, 2010), è riconducibile sia alla presenza della colonna d'aria presente alla testa del tubo piezometrico, che alle capacità termiche del terreno. Infatti, proprio per motivi connessi all'immagazzinamento nel terreno del calore durante la stagione estiva e al calore ceduto dal terreno durante quella invernale, in autunno si registra una temperatura maggiore nei primi 5 metri di profondità (a partire dal pelo libero dell'acqua), che poi si stabilizza attorno ad un valore medio procedendo in profondità. Al contrario, in primavera, si osserva una temperatura che è inferiore nei primi metri (a partire dal pelo libero dell'acqua) per poi aumentare fino a stabilizzarsi procedendo a profondità maggiori.

Un riscontro analogo è emerso dall'analisi dei grafici di dispersione (Fig. 2B) riportanti le misure di temperatura e di profondità sia per le misure autunnali che primaverili. La proiezione dei dati suggerisce che nell'intervallo di profondità compreso tra 15 e 20 metri si raggiunga una situazione di stabilità termica, mentre per profondità superiori ai 20 metri la temperatura assuma un valore costante compatibile con il comportamento asintotico connesso alle oscillazioni termiche stagionali riscontrabili nell'immediato sottosuolo.

Analisi statistica delle misure termometriche. Per poter determinare il valore della temperatura T_0 in corrispondenza alla "superficie di omeotermia" è stata effettuata un'analisi statistica su un campione di misure registrate a profondità maggiori di 20 metri, valore in corrispondenza del quale i grafici di dispersione e i dati termometrici evidenziano una situazione di stabilità termica.

Per poter valutare il valore di T_0 (così come definita nella 3), occorre verificare che la relazione funzionale che lega la temperatura e la profondità, non solo sia di tipo lineare ma anche che si abbia $\vec{\nabla} T = 0$, ovvero che la pendenza della retta sia prossima a zero.

Com'è noto, il procedimento analitico più semplice per poter verificare l'adattamento di un'equazione fisica ai dati sperimentali (*fit*), e viceversa, è il "metodo dei minimi quadrati". Avendo a disposizione due grandezze x e y, nel nostro caso le misure di profondità e di temperatura, in generale si ipotizza un legame funzionale tra y e x, della forma y = f*(x)*. Nel nostro caso naturalmente sarà sufficiente una forma lineare, $y = a + b\,x$. Assumendo inoltre che la misura di ogni valore y_i sia governata da una distribuzione Gaussiana con la stessa larghezza σ_y, in generale dipendente dal valore di y, al fine di determinare la retta dei minimi quadrati che meglio interpola le misure, occorre rendere minima la distanza tra la retta e le singole misure: tale quantità rappresenta la variabile χ^2, definita come

$$\chi^2 = \sum \left[\frac{(y_i - a - bx_i)}{\sigma_i} \right]^2$$

essendo $(x_i\,,\,y_i)$ le coppie di misure a disposizione, per le quali si ipotizza che i valori di x_i abbiano incertezza trascurabile, e gli y_i abbiano incertezza σ_i.

In questo caso il valore atteso è che y_i sia f(x_i); pertanto il χ^2 fornisce una stima di quanto bene y si adatti a f*(x)*. Con il metodo dei minimi si determina inoltre il valore dei parametri a e

RETTA DI REGRESSIONE MISURE PRIMAVERILI

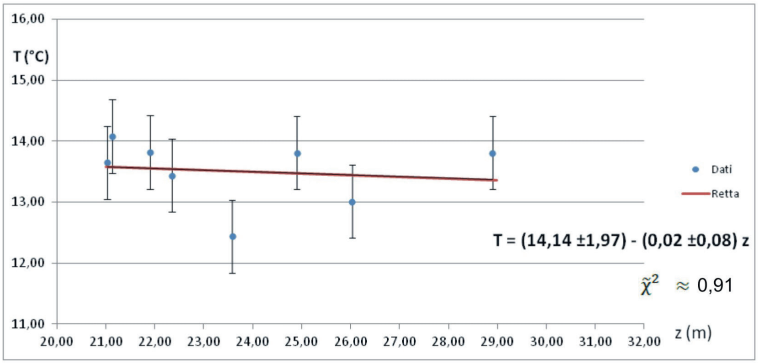

RETTA DI REGRESSIONE MISURE AUTUNNALI

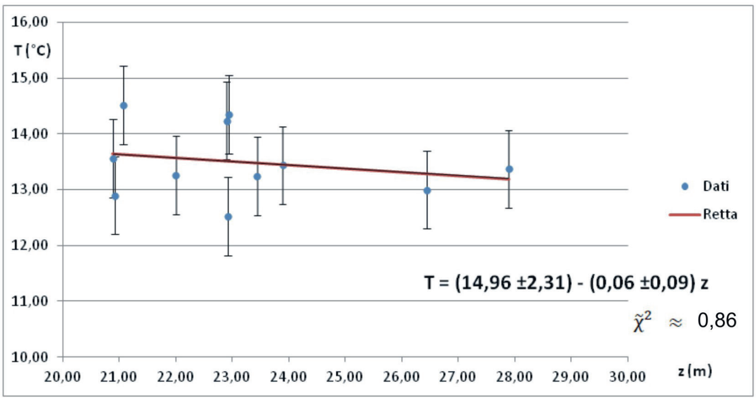

Fig. 3 – *Fit* lineare delle misure termometriche con relativa incertezza.

b che compaiono nell'equazione. Si può poi calcolare il valore del χ^2, tenendo conto del numero dei gradi di libertà ν del sistema dato dal numero N di variabili indipendenti diminuito del numero *c* di parametri calcolati, ovvero d = *N* – *c*. Precisamente, noto il valore di χ^2 è possibile calcolare il valore del "Chi quadro ridotto" $\tilde{\chi}^2$ definito come

$$\tilde{\chi}^2 = \frac{\chi^2}{d}$$

Calcolando dapprima il valore di chi quadro χ^2 e poi il valore del chi quadro ridotto $\tilde{\chi}^2$ si può dedurre se le misure si accordano soddisfacentemente con la distribuzione attesa.

Come già osservato nell'analisi statistica effettuata per le misure relative all'area nordorientale della Pianura Padana piemontese, anche in questo caso, è stato appurato che, associando alle misure di temperatura un valore incertezza dato da ±0,1°C, pari alla sensibilità del termometro utilizzato, l'analisi statistica restituisce valori di $\tilde{\chi}^2$ decisamente elevati, indicativi del fatto che le misure termometriche appaiono difficilmente comparabili tra loro. Pertanto, è stata condotta un'analisi inversa, ovvero è stato ipotizzato che le misure sposassero un *fit* lineare, dal quale dedurre un valore d'incertezza sperimentale ragionevole da associare ai dati. L'ipotesi formulata viene accettata se il valore del $\tilde{\chi}^2$ è dell'ordine di uno.

Associando rispettivamente alle misure primaverili un'incertezza sulla temperatura $\sigma_{T=}$ 0,6 °C e alle misure autunnali un'incertezza $\sigma_{T=}$ 0,7 °C si ottiene un valore di $\tilde{\chi}^2$ ragionevole per poter affermare che i dati in questione si adattano ad un *fit* lineare.

Le equazioni delle rette trovate sono le seguenti (Fig. 3). Per i dati autunnali

$$T = (14{,}96 \pm 2{,}31) - (0{,}06 \pm 0{,}09)\, z$$

mentre per i dati primaverili si ha

$$T = (14{,}14 \pm 1{,}97) - (0{,}02 \pm 0{,}08)\, z$$

La verifica dell'andamento orizzontale delle rette, a cui corrisponderebbe il valore costante di temperatura, T_0, effettuata con il metodo statistico detto "test normale", ha mostrato che il coefficiente angolare delle rette trovate è confrontabile con lo zero a un livello di significatività del 5%, il che indica che il valore di T_0 può essere ritenuto costante entro un ampio livello di probabilità.

Infine, poiché i valori di temperatura medi ottenuti per le misure primaverili e autunnali appaiono a prima vista leggermente differenti, $\langle T\rangle_{\text{autunnale}} = 14{,}96$ e $\langle T\rangle_{\text{primaverile}} = 14{,}14$, si è proceduto alla verifica della consistenza dei valori medi ottenuti attraverso il "Test di ipotesi" mediante la distribuzione di Student. Si è assunto che i campioni di misure appartengano a popolazioni distribuite normalmente aventi lo stesso valore aspettato, E, in modo che la variabile $< T >$ autunnale – $< T >$ primaverile abbia come valore aspettato E = [($< T >$ autunnale – $< T >$ primaverile] = 0, e stessa varianza σ.

Definendo quindi la variabile *t* di Student come

$$t = \frac{\left(< T > autunnale - < T > primaverile\right) - 0}{\sigma\left(< T > autunnale - < T > primaverile\right)}$$

si è proceduto alla verifica con un "test a due code". In conclusione, dal momento che il valore della variabile osservata *t* cade ben dentro gli intervalli, a essa è associata una probabilità ben superire al 5%; in altre parole, la differenza dei valori medi di temperatura autunnale e primaverile in corrispondenza della superficie di omeotermia non è significativa ma è connessa solo a fluttuazioni statistiche, dunque i dati osservati sono consistenti

Conclusioni. L'analisi inversa ha consentito di determinare i valori medi di temperatura stagionali con relativa incertezza e i test statistici hanno appurato la consistenza dei risultati ottenuti con una confidenza di probabilità del 97,5% che il valore vero della variabile *T* (temperatura) sia compreso entro l'intervello di fiducia.

Avendo stabilito che la temperatura è costante per profondità maggiori di 20 metri, ne possiamo calcolare il valor medio e la deviazione standard accorpando tutti i dati a disposizione. Il risultato è che il valor medio della temperatura, valutato a una profondità media di 24 metri, è pari a 13,60 °C, mentre l'incertezza sulla temperatura è $\sigma_{T\,=}$ 0,65 ± 0,05°C.

$$< T >_{z\,=\,24\,\mathrm{m}} = (13{,}60 \pm (0{,}65 \pm 0{,}05))\ °\mathrm{C}$$

Le fluttuazioni statistiche osservate per profondità superiori a 20 m sono compatibili con un valore di temperatura costante, compatibile a sua volta con il valore nullo dalla pendenza della retta d'interpolazione. Il valore di temperatura è inoltre congruente con il comportamento asintotico dell'andamento sinusoidale connesso alle oscillazioni termiche stagionali riscontrabili nell'immediato sottosuolo, ovvero in accordo con le soluzioni dell'equazione differenziale del calore con condizioni al contorno stazionarie (3).

Data la distribuzione territoriale dei dati raccolti, è ragionevole estrapolare il risultato ottenuto a tutta l'area interessata dal campionamento e alle zone limitrofe, purché non interessate da sostanziali differenziazioni geologiche di facile identificazione.

La metodologia sperimentale proposta può essere adottata come semplice metodo statistico per la valutazione del potenziale geotermico di una determinata area ospitante un acquifero superficiale, nella quale sia necessaria la conoscenza della temperatura nell'ottica di valutazioni di sfruttamento della risorsa idrica per scopi geotermici a bassa entalpia con impianti a circuito aperto. La metodologia inoltre evidentemente consente di limitare in modo significativo la necessità di misure dirette, diffuse e ripetute, e quindi dispendiose.

Bibliografia

Balsotti R.; 2009: *Indagine piezometrica sui piezometri della rete di monitoraggio quantitativa regionale*. Resoconto delle attività svolte, Arpa Piemonte.

Barbero D., Forno M.G. and Magnea L.; 2012: *Geotermia a bassa entalpia: determinazione della temperatura della superficie di omeotermia e della relativa incertezza. Un'applicazione all'acquifero superficiale del Piemonte nordorientale*. Ed. Mosetti Tecniche Grafiche, Vol. 31, pag. 194-200. Atti del 31° Convegno Nazionale GNTS. Potenza, 20-22 novembre 2012.

Boano P. and Forno M.G.; 1999: *La successione "villafranchiana" nell'area di Castelnuovo Don Bosco (Asti)*. Il Quaternario 12 (2), pag. 161-194.

Boni A. and Casnedi R.; 1970: *Note illustrative della Carta Geologica d'Italia alla scala 1:100.000, Fogli 69 e 70 "Asti e Alessandria",* II[a] ed., Serv. Geol. It., Roma.

Bortolami G.C., Maffeo B., Maradei V., Ricci B., Sorzana F.; 1976. *Lineamenti di litologia e geoidrologia del settore piemontese della Pianura Padana*. Quaderni dell'Istituto di Ricerca sulle Acque, 28 (1), 3-37, Roma.

Bove A., Destefanis E., De Luca A.D., Masciocco L., Ossella L. and Tunossi M.; 2005: *Assetto geoidrologico della regione Piemonte. (Cd Rom). Idrogeologia della Pianura Piemontese*, Regione Piemonte.

Canavese P. A., De Luca A.D. and Masciocco L.; 2004: *La rete di monitoraggio delle acque sotterranee delle aree di pianura della Regione Piemonte: quadro idrogeologico. PRISMAS: Il monitoraggio delle acque sotterranee nella Regione Piemonte*, Regione Piemonte, II.

Dela Pierre F., Piana F., Fioraso G., Boano P., Bicchi E., Forno M. G., Violanti D., Clari P., Polino R., Balestro G. and D'atri A.; 2003: *Foglio 157 "Trino" della Carta Geologica d'Italia alla scala 1: 50.000*. APAT, Dipartimento Difesa del Suolo, Roma.

Lo Russo S. and Civita M.V.; 2010: *Hydrogeological and thermal characterization of shallow aquifers in the plain sector of Piemonte region (NW Italy): implications for groundwater heat pumps diffusion*. Environ Earth Sci, 60, 703-713.

Stringari M., Balsotti R. and De Luca A.D.; 2010: *Le caratteristiche termiche dell'acquifero superficiale della Regione Piemonte*. Acque Sotterranee, 121, 29-42.

CAMPI FLEGREI CALDERA UNREST: A POSSIBLE SCENARIO FOR THE NEXT ERUPTION

S. Carlino[1], A. Troiano[1], M.G. Di Giuseppe[1], R. Somma[1], C. Kilburn[2], A. Tramelli[1], C. Troise[1], G. De Natale[1]
[1]*Istituto Nazionale di Geofisica e Vulcanologia, Osservatorio Vesuviano, Italy*
[2]*Dept of Earth Sciences, Aon Benfield UCL Hazard Centre, UK*

The eruption of calderas is among the most intense and variable volcanic phenomena in the world, spanning from quite lava dome emplacement to large eruptions (VEI>5). Caldera dynamic has been widely studied by many authors to understand the mechanisms of eruption, resurgence and subsidence using either numerical than analogue methods (Lipman, 1997; Acocella, 2007 and reference therein). Magma withdrawal and related under-pressurization of magma chamber is the most common mechanism to explain the caldera collapse. Subsequent to large ignimbrite eruptions, the activity within calderas is frequently characterized by recurrent period of uplift and subsidence. This behavior is generally explained in terms of magma intrusion and/or disturbance of geothermal fluids in the shallow crust, which in turn are both source of ground deformations and seismicity (Troiano *et al.*, 2010). A major goal is, therefore, to determine the relative contribution of each process, since the potential for eruptions significantly enhanced if magma movements represents the primary component. An important case study is represented by the Campi Flegrei caldera, CFc, (west to Naples city) where the volcanic risk is very high due to 350,000 people living inside the caldera and neighboring. This volcanic area is characterized, since Holocene, by regional tectonic extension as a consequence of Tyrrhenian basin spreading. Geophysical, geological and archeological data have shown an area of background subsidence across the caldera, which arose at least since Roman time, with average rate of 1.7 cmy^{-1} (Woo and Kilburn, 2010). This process in periodically spaced out by uplift phases which, during historic time, can be recognized before the last eruption (1538 A.D., Monte Nuovo) with more than 10 m of uplift, during 1970-72 with maximum uplift of 1.7m, and during 1982-84 with 1.8 m of uplift (the deformation pattern of the two latest episodes is the same and centered in Pozzuoli harbor). The last episode of unrest indicated the possibility of an imminent eruption, forcing the authorities to evacuate Pozzuoli town, which was also damaged by the continuous seismic activity and ground deformation; however, the unrest essentially ended in December 1984, without any eruption occurring (De Natale *et al.*, 2001). The unrest observed at CFc can be explained both in terms of magma and/or fluids migration, but the controversy relating to what is the source (magma, hydrothermal, or hybrid) is still a matter of debate. The non-uniqueness of the physical models adopted in the literature is provided by the different interpretations of the available geophysical data (Carlino and Somma, 2010). For instance, the inversion of both gravity and deformation data from the 1982-1984 unrest fits well with sources of different natures and shapes: magmatic or hydrothermal spherical sources in a viscoelastic or plas-

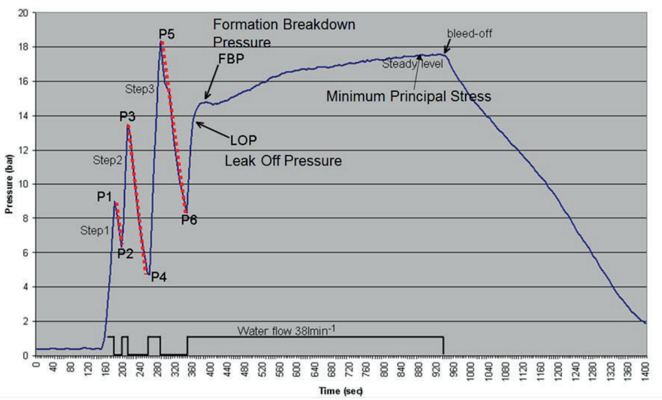

Fig. 1 – Adapted Leak Off Test for in situ permeability assessment. The ateps 1-2-3 correspond to stop (P1-P3-P5) and start (P2-P4-P6) of the pump. The drop of pressure (P1-P2-P3-P4-P5-P6) corresponds to the fluid migration through the wall rock.The pressure drop rate was utilized to assess the in-situ permeability. During the test, was also evaluated the minimum principal stress with standard test.

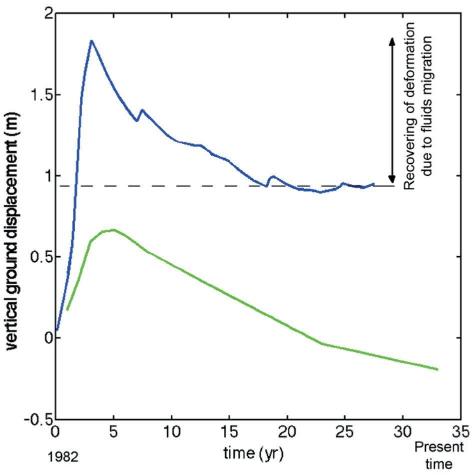

Fig. 2 – Compartson between experimental (blue) and calculated (green) curves for 1982-84 unrest at Campi Flegrei caldera using code TOUGH2.

tic medium; penny-shaped hydrothermal sources in an elastic halfspace; and penny-shaped magma intrusions in a layered elastic half-space. Geophysical investigations have also excluded the presence of significant melt formations down to about 7.5 km in depth (Vanorio *et al.*, 2005; Zollo *et al.*, 2008), although the methods used in these investigations did not allow the defining of a shallow magma body with a volume less than 1 km^3. The phases of rapid inflation have been well-explained by different models (Carlino and Somma, 2010 and references therein), while the subsidence phases that follow the uplift, at rates greater than the secular subsidence, cannot be explained in terms of magma migration. Otherwise, this process is well modeled in terms of the radial outwards migration of hydrothermal fluids. Hybrid model sources have also been proposed, in which magma intrusion occurs at the beginning of each period of unrest and produces perturbations of the geothermal system (De Natale *et al.*, 2001; Battaglia *et al.*, 2006). The main problem related to these fluid-dynamic modeling is the constrain of a fundamental physical parameter, namely the permeability (k). In recent time, new data related to the permeability of shallow CFc crust, at 500 m of depth, was inferred during the drilling of the pilot hole performed in the framework of the Campi Flegrei Deep Drilling Project (CFDDP). An adapted Leak Off Test allows us to infer the average value of k at a depth of 500 m (bottom hole) (Fig. 1). The depth permeability variation (>500 m) is then extrapolated by using the empirical formula of Manning and Ingebritsen (1999). This new fundamental data has been applied to the previous fluid-dynamic model published by Troiano *et al.* (2010) in order to obtain a more reliable picture of the process generating the unrest. The simulations have been carried out by the numerical code TOUGH2, considering an injection of fluids (H_2O+-CO_2) with inflow rate inferred from literature (Chiodini *et al.*, 2012) during 1982-84 unrest. The code TOUGH2 allows to compute the mass and heat exchange related to multidimensional flows of multiphase (gas and liquid) mixtures of many components within a porous medium of assigned permeability. It assumes local equilibrium between fluid and rock matrix, through the direct discretization of the balance equations for mass and energy describing the thermodynamic conditions of the system in their integral form, in a scheme called integral finite difference method. The comparison between the experimental curve of 1982-84 uplift, including the subsequent phase of subsidence, and the calculated curve is shown in Fig. 2. It is clear that the fluid-injection supplies only a partial contribution (about 0.7 m) to the total uplift for both the solutions, which, besides, are quite equivalents. Furthermore, this partial uplift is totally recovered after about 30 years due to radial fluids migration and inflow rate decrease. Considering the total uplift in the period 1982-1984 amounted to about 1.8 m, we can conclude about 1.0 m of uplift, interestingly corresponding to the remaining uplift after the partial recovering, should be ascribed to the contribution of magma injection in a shallow reservoir. This result is very important in evaluating the potential eruptible magma, to assess the possible energy of future eruptions, which is crucial in such extremely densely populated area.

References

Acocella V., 2007, Understanding caldera structure and development; an overview of analog models compared to natural calderas, Earth-Science Reviews, v. 85, 125-160.

Battaglia M., Troise C., Obrizzo F., Pingue F., De Natale G., 2006, Evidence for fluid migration as the source of deformation at Campi Flegrei caldera (Italy). Geophys Res Lett 33:01307. doi:10.1029/2005GL024904

Carlino S., Somma R., 2010, Eruptive versus non-eriptive behaviour of large calderas: the example of Campi Flegrei caldera (southernItaly), Bull Volcanol 72:871-886. doi:10.1007/s00445-010-0370-y.
Chiodini G., Caliro S., De Martino P., Avino R., Gherardi F., 2012, Early signals of new volcanic unrest at Campi Flegrei caldera? Isights from geochemical data abd physical simulation, Geology, doi: 10.1130/G33251.1
De Natale G., Troise C., Pingue F., 2001, A mechanical fluid-dynamical model for ground movements at Campi Flegrei caldera. J Geodynam., 32, 487-517.
Lipman P.W., 1997, Subsidence of ash-flow calderas: relation to caldera size and magma-chamber geometry, Bull. Volcanol., 59,198-218.
Manning C.E., and Ingebritsen S.E., 1999, Permeability of the continental crust: Implications of geothermal data and metamorphic systems: Reviews of Geophysics, v. v. 37 pp. 127-150.
Troiano A., Di Giuseppe M.G., Petrillo Z., Troise C., De Natale G., 2011, Ground deformation at calderas driven by fluid injection: modeling unrest episodes at Campi Flegrei (Italy). Geophys J. Int., 187:833-847. doi:10.111/j.1365-246X.2011.05149.x
Vanorio T., Virieux J., Capuano P., Russo G., 2005, Three-dimensional seismic tomography from P wave and S wave micro earthquake travel times and rock physics characterisation of the Campi Flegrei caldera. J Geophys Res 110:B03201. doi:10.1029/ 2004JB003102
Woo J.Y.L., and Kilburn C.R.J., 2010, Intrusion and deformation at Campi Flegrei, southern Italy: Sills, dikes and regional extension, J. Geophys. Res. doi: 10.1029/2009JB006913.
Zollo A., Maercklin N., Vassallo M., Dello Iacono D., Virieux J., Gasparini P., 2008, Seismic reflections reveal a massive melt layer feeling Campi Flegrei caldera. Geophys Res Lett 35: L12306. doi:10.1029/2008GL034242

CONTINUOUS GEOCHEMICAL MONITORING BY MASS-SPECTROMETER IN THE CAMPI FLEGREI GEOTHERMAL AREA. AN APPLICATION AT PISCIARELLI-SOLFATARA (DIFFUSE AND FUMAROLIC GASES)

A. Fedele[1], R. Somma[1], T. Wiersberg[2], M.G. Di Giuseppe[1], A. Troiano[1], C. Troise[1], G. De Natale[1]
[1] *INGV-Osservatorio Vesuviano, Naples, Italy*
[2] *Deutsches GeoForschungsZentrum GFZ, Potsdam, Germany*

Introduction. The Campi Flegrei (Southern Italy) is a restless, nested caldera structure resulting from two main collapses related to the two most powerful eruptions of the volcanic system (Orsi *et al.*, 1992, 1995, 1996.): the Campanian Ignimbrite CI. eruption 37 ka (Deino *et al.*, 1992, 1994; Armienti *et al.*, 1983; Rosi and Sbrana, 1987; Rosi *et al.*, 1983, 1996; Barberi *et al.*, 1991; Fisher *et al.*, 1993; Civetta *et al.*, 1997) and the Neapolitan Yellow Tuff (NYT) eruption 12 ka (Alessio *et al.*, 1971; Orsi and Scarpati, 1989; Orsi *et al.*, 1992, 1995, 1996). The structural boundaries of both CI and NYT calderas result from partial reactivation of earlier regional faults (Orsi *et al.*, 1996.). The central part of the younger NYT caldera is uplifting since its formation, likely as a consequence of the arrival of new magma in the system (Orsi *et al.*, 1996).

The uplift occurs through a complex simple-shearing block resurgence mechanism (Orsi *et al.*, 1991). Because of this mechanism, the conditions for magmas to rise to the surface were established only in those parts of the caldera floor subject to extensional stress (Orsi *et al.*, 1996). Thus, the caldera structure strongly constrains the areal distribution of volcanism active during the past 12 ka. Volcanism in the Campi Flegrei began more than 60 ka ago and was essentially explosive and subordinately effusive (Orsi *et al.*, 1996; Pappalardo *et al.*, 1999). The sedimentological characteristics of deposits erupted before the CI eruption indicate that volcanism was highly explosive and that vents were located also outside the Campi Flegrei depression (Orsi *et al.*, 1996). The products erupted before the CI eruption range in composition from latite to phono-trachyte. The CI is the largest pyroclastic flow deposit of the Campanian area. The products range in composition from trachyte to phono-trachyte. They covered an area of 30,000 km^2 with an estimate volume of erupted magma of 150 km^3 DRE (Fisher *et al.*, 1993; Civetta *et al.*, 1997).

After the Neapolitan Yellow Tuff eruption and related caldera collapse that occurred within the 39 ka-caldera, at least 70 eruptions, took place in three epochs of intense activity (15.0÷9.5, 8.6÷8.2 and 4.8÷3.8 ka) and followed one to another at mean time intervals of a few tens of years. The last event was in 1538 AD, after about 3.0 ka of quiescence, and formed the Mt. Nuovo tuff cone (Di Vito *et al.*, 1987; Piochi *et al.*, 2005a). Sixty-four of these eruptions were phreato-magmatic to magmatic explosive events, and 76% of these eruptions occurred from vents active in the central-eastern sector of the caldera (Mormone *et al.*, 2011).

Solfatara geological setting. The Solfatara volcano, about 2 km east-northeast of Pozzuoli, is a tuff cone (180 m above sea level) characterized by a sub rectangular (0.5x0.6 km) crater, shaped by NW-SE and SW-NE trending faults along which the vegetation lacks. The volcano generated a low-magnitude explosive eruption that deposited a tephra over a small area (<1 km^2), named Solfatara Tephra, during phreatomagmatic and subordinate magmatic explosions (Di Vito *et al.*, 1999). This tephra overlies the Monte Olibano and Accademia lavas, both younger than Agnano-Monte Spina Tephra (4.1 ka), and underlies the Astroni Tephras (3.8 ka), from which it is separated by a thin paleosoil containing many charcoal fragments.

The Solfatara Tephra comprises a phreato-magmatic coarse breccias overlain by a sequence of stratified, dune-bedded deposits composed of accretionary lapilli-bearing ash surge layers, alternating with thin, well sorted, rounded pumiceous lapilli beds pyroclastic pumiceous fallout beds. The breccia contains large blocks of green tuff, altered lavas and dark scoriaceous bombs engulfed in a hydrothermally altered matrix. The scoriae of the basal breccia are porphyritic containing crystals of sanidine, plagioclase, clinopyroxene, biotite and Fe-Ti oxides, in order of decreasing abundance. Rare crystals of leucite converted to analcime are also present. The late erupted pumice fragments are alkali-trachytic in composition, crystal-poor to subaphyric pumice (upper sequence), and contain rare crystals of plagioclase. A thin massive fallout layer, grey to yellowish in color, consisting of fine-to-coarse ash with scattered pumice clasts and interbedded pumice beds represents the distal counterpart of the Solfatara Tephra. It is a deposit dispersed towards the north-east with a minimum measured thickness of 5 cm at Verdolino, at about 7 km from vent. The crater of the Solfatara has been the site of an intense hydrothermal activity since Greek times. It is the most impressive manifestation of the present hydrothermal activity of the caldera, which includes both focused vents, with a maximum temperature of about 160°C (Bocca Grande fumarole), and large areas of hot steaming ground. The average molar composition of the fluids is H_2O about 82 %, CO_2 17.5%, H_2S 0.13% and minor amounts of N_2, H_2, CH_4 and CO. Systematic measurements of the gas fluxes from the soil evidenced up to 1500 tonnes/day of CO_2 emission (Chiodini *et al.*, 2011) through the main fault system, coinciding with temperature up to 95°C (Granieri *et al.*, 2010); the degassing area is enlarging since the first analytical campaign. The isotopic compositions of H_2O, CO_2 and He suggest the involvement of magmatic gases in the feeding system of the fumaroles. Subsequently the original magmatic gases are condensed by an aquifer system as suggested by the absence of the soluble acid gases SO_2, HCl and HF, typical of the high-temperature volcanic gas emissions. Boiling of this heated aquifer(s) generates the Solfatara fumaroles. Based on geochemical data, the hydrothermal system at the Solfatara crater consists of a heat source, possibly represented by a relatively shallow (few kilometres deep) magma batch, a geothermal system located above the magma, and the shallow hydrothermal system.

During the last 24 years of monitoring of the geochemical composition of the fumaroles the ratio of the concentration of CO_2/H_2O showed three clear peaks in 1985, 1990 and 1995 which was followed a few months later, a lifting of the ground. According with Caliro *et al.* (2007) these peaks reflecting the composition of the fumaroles rich component of magmatic, probably due to episodes of degassing of the magma in depth during periods of lifting the soil.

Other physical and numerical simulations have shown that periods of intense degassing of fluids rich in CO_2 can explain other relevant characteristics of the crisis of 1984, 1990 and 1995, such as ground deformation and gravity anomalies (Todesco *et al.*, 2004; Todesco and Berrino, 2005). After 2000, the ratio of the concentration of CO_2/H_2O fumaroles showed no peaks but a slow upward trend still underway. This different behaviour of the composition of fumarolic reflect a change in the style of degassing at depth. If this growing trend is the ascending portion of fluids rich in CO_2 then this is easily relatable to an episode of out-gassing from the deepest portion of the magmatic system. Alternatively, this behaviour could be related to a magmatic source that degas constantly compared to isolated periods as previously thought. In particular a slow lifting of the soil is started in 2004 and continues to this day and is characterized by a deformation longer and slower than previous episodes of lifting (Troise *et al.*, 2007).

Cioni *et al.* (1989) suggest that the relationship CO_2/H_2O behave like a true precursor of the crisis of 1984 as it was thought that a geochemical indicator for monitoring the boiling hydrothermal confined aquifer.

In this first interpretation, the decrease in the ratio CO_2/H_2O observed before the crisis of 1984 and even before the smaller crisis that followed, it could indicate an increase in the boiling process and overpressure of the aquifer due to an increase in the flow of heat from magmatic body. Unlike Caliro *et al.* (2007) show that the ratio CO_2/H_2O is controlled by the mixing zone of magmatic gases and liquid of meteoric origin. The decrease of the ratio CO_2/H_2O corresponds to periods in which there is a low flow of magmatic component and underpressure of hydrothermal plume in agreement with the subsidence of the soil always accompanied by periods of decrease of the ratio gas/vapor.

Pisciarelli geological setting. The Pisciarelli area is located slightly outside the caldera rim of the Solfatara with NO direction. This area is characterized by the presence of fractures and is affected by phenomena of emission of gases and fluids.

The main component of the fumaroles is H_2O followed by CO_2 and H_2S and with a range of temperature between 100-110 °C (Chiodini, 2009).

During field surveys in the Pisciarelli made during the year 2006 were observed, compared to similar surveys conducted in the past (the year 2005), changes in the most affected by the

Fig. 1 – Gases and fluids in Pisciarelli area.

phenomena of gases and fluids. Particularly in the first characterized by several point sources of emission of fluids. In addition, along the eastern side of the small hill to the east of this place pool have increased the points of greenhouse gas emissions. Fractures are mostly trending N110-120E and the area is dominated by two main features NW-SE and NE-SW. Also were not observed accumulations of material from surface gravitational movements of recent formation. 24.10.06 The day the area has been the subject of an initial investigation with camera portable thermal, both for carrying out a first thermal relief that identify a favourable area for the installation of a thermal fixing station. On 30 October, the station has been installed TIR Mobile (TITANO: Thermal Infrared Transportable Apparatus for Nearby Observation). The average distance is about 150m field of view which shows an average resolution of pixels of about 15cm. From that date shall be acquired and the control unit of the network TIIMNet 6 images at night.

Construction of the gas-line monitoring station (May 16-30 2012, June 1-5, 16-23 2012). The on-line gas monitoring station is localized close to the fumaroles field (100 m). The equipment used for on-line monitoring consists of a Quadrupole Mass Spectrometer (Pfeiffer Omnistar©) for on-line gas analysis, a field computer and a data logger for data storage.

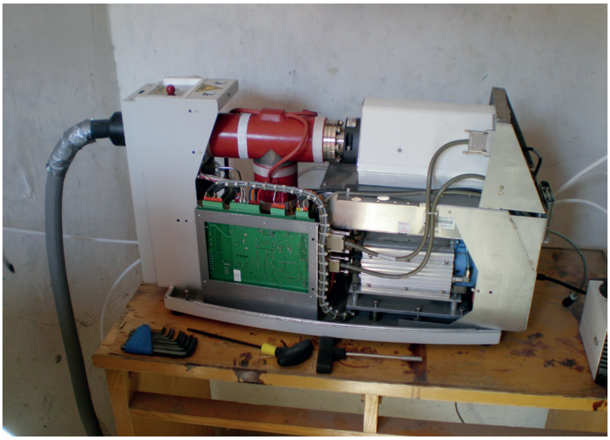

Fig. 2 – Quadrupole Mass Spectrometer in the monitoring station.

Air condition was used to stabilize the temperature of the station and an UPS (Uninterrupted Power Supply) was used for buffering in case of short power cut offs. Silicon tubings, a temperature probe, a gas plastic trap and some additional devices (eg., water trap, connection plastics, metal rings) were also used during the construction of the gas line between the station and the bubbling pool.

Construction of the gas line: different experimental test

Test 1. For the construction of the gas line, a Teflon tube with 6 mm diameter was placed in the main fumaroles (T=114 °C) where gas was discharged. The gas was pumped by a membrane pump located in the monitoring station. Few meters away from the fumaroles, a water trap was installed to condense water vapour, so that only dry gas was admitted to the gas line. Nevertheless, in this test the temperature of the fumaroles was too high and condensation starts already before the water trap and blocked the gas flow.

Test 2. In the second test we sampled in a bubbling pool close the main fumaroles. Here we used an inverted gas trap inserted in the pool to collect gas. Gas was pumped by the membrane pump but the problem we had was that the pressure in the gas trap became too low and in this case the gas line was blocked by the rise of mud along the Teflon tube.

Test 3. In the third and last test we sampled in a fumaroles situated at a height greater than the other sampling points. This is because its lower temperature allows to have a lower condensation inside the Teflon tube. In fact the best results were obtained by considering this point of sampling.

Calibration of the QMS. For quantitative analysis, the QMS was calibrated with air, pure CO_2, and certified gas mixtures, the composition of which are selected according to the expected nature of gas. With calibration, the measured ion currents are put to a solution matrix with the individual concentrations of the components in the gas to be analyzed to determine sensitivity factors. For calculating the gas concentrations from ion currents, the mass spectrometer sensitivity for the individual gas components must be known (Suer, 2010). Those relative mass spectrometer sensitivities are determined by the measurement and stored as calibration factors.

Calibration gas files were prepared via the Quadstar software. After the preparation of the calibration files, the QMS was calibrated with air and the calibration gas. With these calibrations, a table containing the gases and their respective calibration factors was generated.

During air calibration, the capillary of the QMS was disconnected from the gas line and exposed to air. Air was used to calibrate for Oxygen, Nitrogen, and Argon. As internal standard, Argon was used. During calibration with gas standards, the QMS was disconnected from the gas line and then connected to the calibration gas flask. After establishing the connection, the "dead volume", i.e. the space between the inlet capillary of the QMS and the calibration flask was evacuated by using the QMS for some time until a pressure inside the chamber of $<10^{-7}$ mbar was achieved. Then the calibration gas flask was opened to the QMS for measuring. Once calibrated, the QMS was ready to proceed with the quantitative analysis.

Geochemical evidence from data set May-June 2010. The best result obtained during the development of the continuous monitoring system has occurred during the months of May-June 2012. In particular from 16th May to 5th June have occurred the best conditions for performing the continuous extraction of gas 24 hours a day. In the following it will be discussed the geochemical composition trends from the Pisciarelli degassing field as well as the main relationships of good tracer of magmatic fluids injection such us CO_2/CH_4 and H_2S/CO_2.

Methane is a gas species which differentiates in hydrothermal systems, where it is present in relatively high concentrations, from high temperature volcanic magmatic fluids where it is normally absent or present in very low concentrations.

Measured CO_2/CH_4 in fumaroles from 23 hydrothermal systems on the world range from 10 to 10^4 roughly in agreement with the theoretical values expected for a gas phase in chemical equilibrium at temperatures from 200°C to 400°C and redox conditions fixed by hydrothermal buffers (Chiodini and Marini, 1998).

The CO_2/CH_4 is a good tracer of magmatic fluids injection because CO_2 concentration increased, due to its higher content of the magmatic component, and CH_4, a gas species formed within the hydrothermal system, is lowered both by dilution and by the more oxidizing, transient conditions caused by the arrival of SO_2 into the hydrothermal system (Chiodini, 2009, 2012). This opposite behaviour causes rapid increases of the CO_2/CH_4 ratio in fumarolic fluids like it showed by the following figure.

This trend seems to be confirmed by the data of GPS ground deformation that show a general tendency to uplift with an acceleration of the phenomenon in the period spanning from June to August 2012 (25 mm/month in average) and increasing during the last month beginning on December 2012 (10 mm/month).

The total lifting from January 2012 is about 8 cm. In general systematically every ground inflation corresponds to an increase of CO_2/CH_4, and systematically a decrease of the ratio accompanies any deflation for each of the four minor bradyseisms in the last 25 years (Chiodini, 2009).

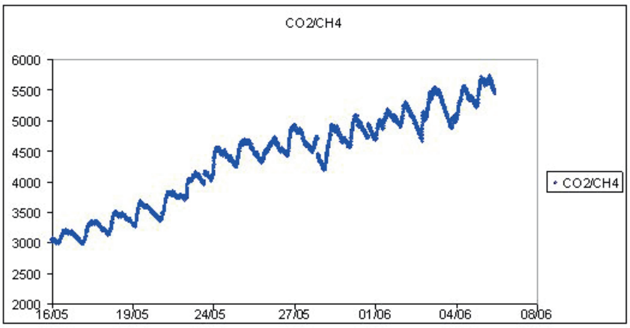

Fig. 3 – The CO_2/CH_4 ratio from 16/05/2012 to 05/06/2012 measured by QMS.

Therefore, the numerous CO_2/CH_4 peaks observed at Solfatara fumaroles can be interpreted as the result of the injection of new magmatic fluids into the hydrothermal system, a process that occurs some time before the geochemical signal is observed at the surface.

Conclusion and discussion. A new unrest phase started in 2004 and is followed by our measurements since 2009. It involves large geochemical signatures, with increase of several volcanic gases, with relatively minor ground deformation and seismicity.

It is consistent with an extensive fracturing of the caldera volume, caused by past unrests, with a consequent increase of the connection between deep fluids and shallow aquifers. This implies we should expect, in the future, less prominent uplift and seismic events, and more marked geochemical indicators as eruption precursors. A continuous, multi-gas geochemical monitoring as the one we developed, is then even more crucial for volcano monitoring, interpretation and forecast.

This innovative methodology of continuous monitoring, which does not replace the traditional sampling using vial, allowed us to acquire more frequent data of gas composition in the fumarolic and degassing area of Pisciarelli. Taking into account some interruption in the time series of data it was possible to compare the behaviour of the shallow hydrothermal system. The period May-June 2012, in agreement with the recent changes in the activity of the Campi Flegrei also recorded by other geophysical parameters, shows that a rapid decrease in methane concentration in fumarolic composition and values of He progressively increasing. This behaviour confirms a greater contribution of magmatic fluids in the hydrothermal system, resulting in alteration of the composition of the fumaroles that characterize the overhead Solfatara and Pisciarelli, earthquake swarms more frequent and raising the ground level.

References

Armienti P., Barberi F., Bizouard H., Clocchiatti R., Innocenti F., Metrich N., Rosi M. and Sbrana, A.; 1983: The Phlegraean Fields: magma evolution within a shallow chamber. J. Volcanol. Geotherm. Res., **17**: pp. 289-311.

Barberi F., Corrado G., Innocenti F. and Luongo G.;1984: Phlegrean Fields 1982-1984: brief chronicle of the volcano emergency in a densely popolated area Bull. Volcanol. **47**, pp. 175-185.

Caliro S., Chiodini G., Moretti R., Avino R., Granieri D., Russo M., Fiebig J. (2007) - The origin of the fumaroles of La Solfatara (Campi Flegrei, South Italy) Geochim Cosmochim Acta **71**, pp. 3040-3055.

Chiodini G. and Marini L.;1998: Hydrothermal gas equilibria: The H2O-H2-CO2-CO-CH4 system. Geochim. Cosmochim. Acta, **62.**

Chiodini G.; 2009: CO2/CH4 ratio in fumaroles a powerful tool to detect magma degassing episodes at quiescent volcanoes: Geophysical Research Letters, v. **36**, L02302, doi:10.1029/2008GL036347.

Chiodini G., Avino R., Caliro S. and Minopoli C.;2011: Temperature and pressure gas geoindicators at the Solfatara fumaroles (Campi Flegrei) Annals Geophysics, **54**, 2 doi: 10.4401/ag-5002.

Chiodini G., Caliro S., De Martino P., Avino R., and Gherardi F.;2012: Early signals of a new volcanic unrest at Campi Flegrei caldera? Insights from geochemical data and physical simulations (Geology pp. 943-945).

Cioni R., Corazza E., Fratta M., Guidi M., Magro G. and Marini L.;1989: Geochimical precursors at Solfatara Volcano, Pozzuoli (Italy) In Volcanic Hazard (ed. J. H. Latter). Sprinter Verlag, Berlin, pp. 384-398.

Civetta L., Orsi G., Pappalardo L., Fisher R.V., Heiken G. and Ort M.; 1997: Geochemical zoning, minling, eruptive dynamics and depositional processes - The Campanian Ignimbrite, Campi Flegrei, Italy. J.Volcanol. Geotherm. Res., **75**, pp. 183-219.

Deino A.L., Southon J., Terrasi F., Campajola L. and Orsi G.;1994: 14C and 40Ar/39Ar dating of the Campanian Ignimbrite, Phlegrean Fields, Italy. Abstract ICOG, Berkley California USA.

Di Vito M.A., Lirer L., Mastrolorenzo G. and Rolandi G.; 1987: The Monte Nuovo eruption (Campi Flegrei, Italy). Bull. Volcanol., **49**, pp. 608-615.

Granieri D., R. Avino and Chiodini G.; 2010: Carbon dioxide diffuse emission from the soil: ten years of observations at Vesuvio and Campi Flegrei (Pozzuoli), and linkages with volcanic activityBull Volcanol **72**, pp. 103-118, DOI 10.1007/s00445-009-0304-8.

Mormone A., Piochi M., Bellatreccia F., De Astis G., Della Ventura G., Moretti R., Cavallo A., Mangiacapra A.;2011: A CO2-rich magma source beneath the Phlegraean Volcanic District (Southern Italy): Evidence from a melt inclusion study; Chemical Geology **287**, pp. 66-80, doi: 10.1016/j.chemgeo.2011.05.019.

Orsi G., de Vita S. and Di Vito M.;1996: The restless, resurgent Campi Flegrei nested caldera (Italy): constraints on its evolution and configuration; J. Volcanol. Geotherm. Res., **74**, pp.179-214.

Pappalardo L., de Vita S., Orsi G., Civetta L., Carandente A., D'Antonio M., Deino A., di Cesare T., Di Vito M., Fisher R.V., Isaia R., Marotta E., Necco A., Ort M., Piochi M. and Southon J.; 1999: The Agnano - Monte Spina eruption (4100 years BP) in the restless Campi Flegrei caldera (Italy). J. Volcanol. Geotherm. Res., Special Issue "Volcanism in the Campi Flegrei" Orsi G.,Civetta L., Valentine G.A. (Eds), **91** (2-4), pp. 269-301.

Piochi M., Mastrolorenzo G., Pappalardo L.; 2005a :Evidence of magma rising eruptive processes from textural and compositional features of Monte Nuovo (Campi Flegrei,Italy) pyroclastic products. Bull Volcanol **67**, pp. 663-678, doi:10.1007/s00445-005-0410-1.

Suer S., 2010: Geochemical Monitoring of the seismic activities and noble gas characterization of the geothermal fields along the eastern segment of the Buyuk Menderes graben (Ph.D. Thesis).
Todesco M., Rutqvist J., Chiodini G., Pruess K., and Oldenburg C.M.; 2004: Modeling of recent volcanic episodes at Phlegrean Fields (Italy); geochemical variations and ground deformation. Geothermics **33**(4), pp. 531-547.
Troise C., De Natale G., Pingue F., Obrizzo F., De Martino P., Tammaro U., and Boschi E.; 2007: Renewed ground uplift at Campi Flegrei caldera (Italy): New insight on magmatic processes and forecast. Geophys. Res. Lett., **34** (3), L03301, doi: 10.1029/2006GL028545.

FRACTURE INFLUENCE ON THERMAL WATER CIRCULATION IN FOREDEEP BASIN: PRELIMINARY DATA FROM THE SOUTHERN MARCHE FOOTHILLS, ITALY

A. Fusari, C. Invernizzi
School of Science and Technology, University of Camerino, Italy

Introduction. Although the Adriatic side of Italy shows a low heat flow, due to a fast recent sedimentary deposition and meteoric water infiltration, that depresses the geothermal gradient (Della Vedova *et al.,* 2001), some interesting areas are present along this side, and one of these is Acquasanta thermal area (Central Italy, Fig. 1). Here, thermal springs rise along the Tronto river valley and their temperatures range between 27° and 44°C (Galdenzi *et al.,* 2010). Because the geothermal energy is one of the most promising resources for the forthcoming future, with low environmental impact and excellent sustainability, also from an economic point of view, it is important to perform geological and geochemical preliminary studies to evaluate the potential and sustainability of area such as Acquasanta for the development of the geothermal resource for low and medium enthalpy plants. In this frame, a quantitative structural analysis (i.e. Dezayes *et al.,* 2010, Agosta *et al.,* 2010) is important for the identification of preferential infiltration or rising paths of fluids and to assess the reservoir and the cap rock characteristics. In addition, chemical and isotopic analysis of water are important to define the origin and types of water (i.e. Minissale *et al.,* 2002; Armannsson and Fridriksson, 2009) and its deep circulation. Finally, hydrogeological studies are useful to reconstruct a correct water balance.

The aim of our work concern a possible modelling of water circulation at depth, in order to evaluate the geothermal potential in this part of the foredeep basin and its relations to important structural elements.

So our preliminary studies regard water chemical and stable isotopes analyses (Fusari *et al.,* 2013) and qualitative and semi-quantitative fracture analyses finalized to understand the hydrogeological pattern and the hot waters ascent path, and to produce a model of the possible thermal reservoir.

Geological background. The Acquasanta Anticline is one of the positive structures cropping out within the outer part of the Umbria–Marche Central Apennine. This periclinal structure emerges within the siliciclastic Laga Basin, it is a 25 km-long east-vergent fold, trending about N170°, and it is bounded to the east by a thrust with a displacement of few km (Koopman, 1988). The Umbria-Marche sedimentary succession records a regular sin- and post-rift succession which includes Triassic evaporites (Burano Anhydrites), late Triassic–Liassic platform carbonates (Calcare Massiccio), Jurassic to Mid-Miocene pelagic well bedded limestones and marls succession. The entire carbonatic sequence from Calcare Massiccio to Scaglia Rossa Formation, up to 1500–2000 m thick, host the most important aquifers in the area, which are separated by two main marly levels (Marne a Fucoidi and Rosso Ammonitico Formations). The following Oligocene Scaglia Cinerea Formation, a marly unit up to 200 m thick, together with the overlying Miocene marly units (Bisciaro, Marne con Cerrogna and Marne a Pteropodi Formations) constitute the most important regional aquiclude (Galdenzi *et al.,* 2010). Upward, the sin-tectonic siliciclastic Laga Formation fills the Early Messinian Laga foredeep basin (Bigi *et al.,* 2011 and references therein).

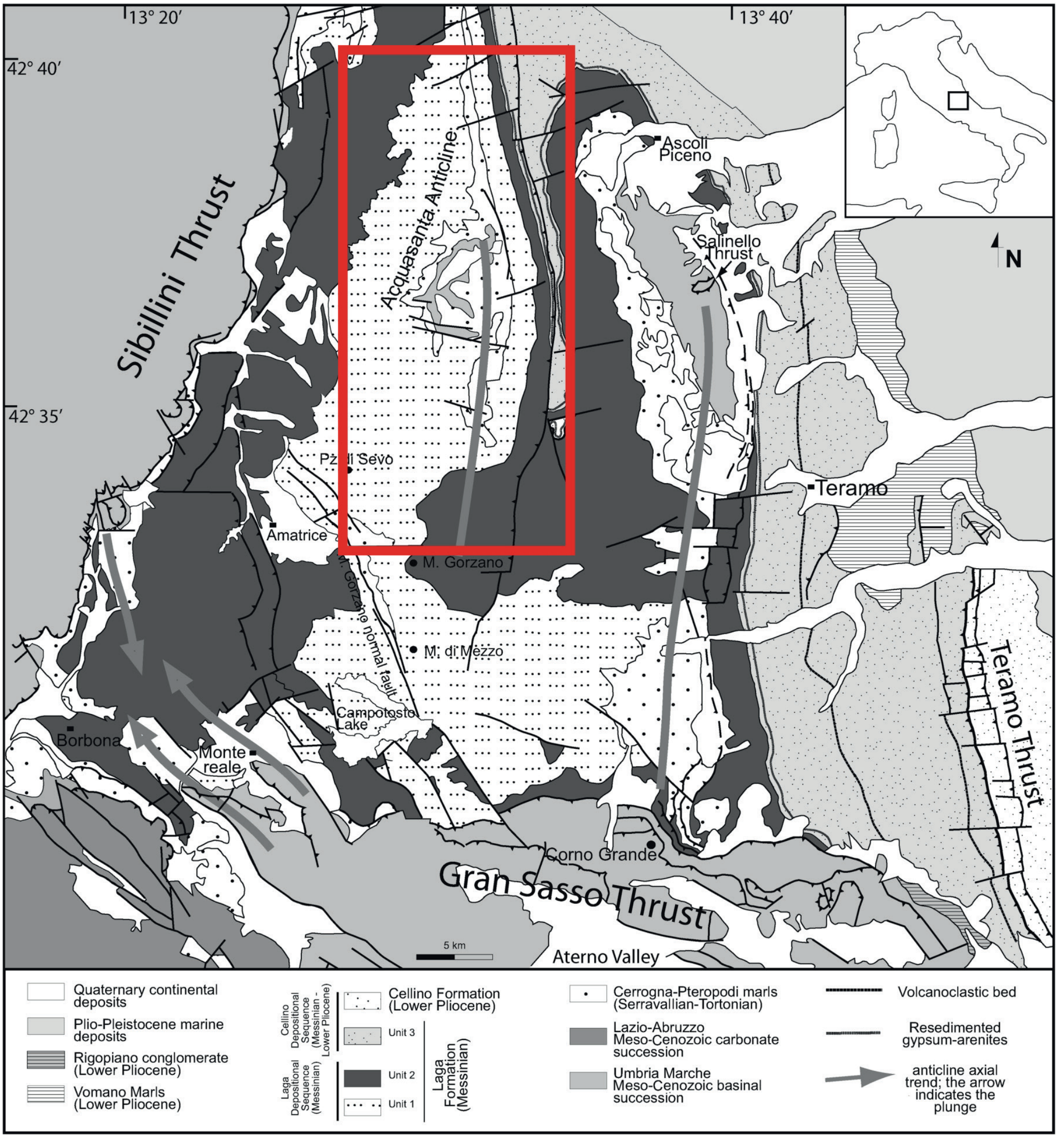

Fig. 1 – Geological and structural map of the Laga Basin (modified from Bigi *et al.*, 2011); red box identifies the study area.

Quaternary Travertine deposits represent the top part of the sedimentary succession and they constitute a peculiar feature of the area (Boni and Colacicchi, 1966). Travertine are hundreds of metres thick and they have several square kilometres of extension. These deposits are present only on the right side of the Tronto River and they have been associated to oversaturated thermal water rising up along deep fractures (Farabollini *et al.,* 2003).

Hydrogeological framework. The reference catchment area for our study consists of the Tronto River and its tributaries. These river and tributaries have an irregular discharge due to the low permeability of the bed rocks and to the contribution of snow thawing from the mountains. Groundwater mainly consists of thermal sulfidic water that rises from the capped aquifer hosted in the carbonate sequence. The most important hot spring in the area is in Acquasanta Terme town at the outflow of the Acquasanta Cave. This spring is located in the

Scaglia Cinerea Formation, near the core of the anticline, along the right bank of the Tronto River. It has an average discharge of about 180 l/s, and it is sensible to seasonal variations. Some further minor thermal springs are present downstream within the river bed and also at higher altitude, along the right side of the valley. The thermal groundwater can be reached also in the lower sections of the caves in the Rio Garrafo Valley. The groundwater flowpath is heavily influenced by the geologic setting. The prevailing low permeability formations that cap the thermal aquifer reduce its local recharge, and probably only in the Rio Garrafo gorge sinking stream water directly reaches the thermal water inside the caves, creating a fluid mixing and a dilution of the hot water (Galdenzi *et al.,* 2010).

The forecast weather conditions have been considered, in order to obtain preliminary information on the potential water recharge for this area. The average annual rainfall is 947 mm/yr over the period 1961-2000; in 2012 rainfall was 905 mm, consistent with the average historical trend, while in 2013 a slight increase was detected in the first eight months, 108 mm more than the historical mean.

Geochemical prospection. Chemical and isotopic analyses were carried out since October 2012 on seven selected springs. Four of these are thermal springs and represent almost all the thermal output of the area: T1 is a small outflow located 100 m above the Tronto River bed, T2 and T3 are located along the right side of the river, T4 is the big discharge of the Acquasanta Cave. The other three springs are cold waters, sampled near the hot springs, to be utilized as a comparison: C1 along a slope, C2 in the Rio Garrafo stream, C3 from a fountain at the base of the Laga Formation. First water sampling started at the end of October 2012, and was repeated in February 2013. Chemical results show that cold samples are bicarbonate-calcic, except for the C3 water that presents much higher quantities of SO_4 and Chlorine. Thermal waters show temperatures ranging from 26°C to 30.3°C, with seasonal variations lower than 10°C. They can be classified as chloride-sulphate rich in Na, K, Ca and Mg (Fig. 2a) and containing H_2S, with small variations between the two periods and with differences in electrical conductivity.

An important amount of Magnesium is present, suggesting further contributions in addition to the common water-clays interaction and, looking at minor elements of thermal waters, an anomalous

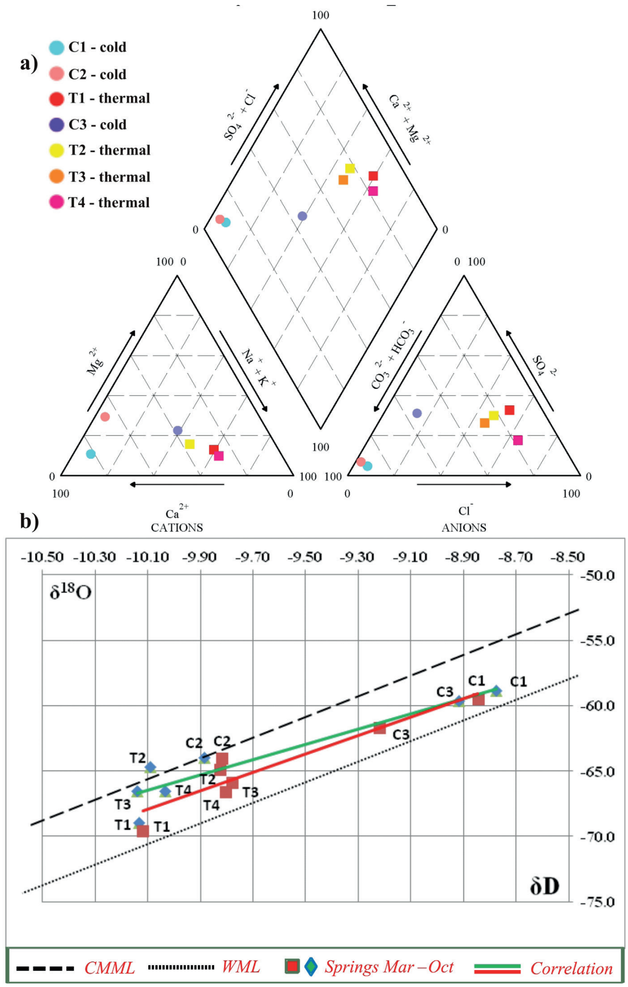

Fig. 2 – a) Piper's diagram of waters sampled in February 2013; b) relation between Oxygen and Deuterium isotopic ratio.

enrichment in Lithium, Strontium, Fluorine and Boron is evident. Considering the deep structure of the anticline as it has been reconstruct by previous works (Ghisetti and Vezzani, 2000; Mazzoli *et al.,* 2002; Tozer *et al.,* 2006; Scisciani, 2009), we believe that the high salt content and the minor elements mentioned above could be acquired by waters flowing through the underlying Triassic evaporites at the core of the anticline or through Messinian gypsum in the footwall of the Acquasanta thrust, while Madonna *et al.,* 2005 hypothesized a contribution from volcanic fluids. In this framework, isotopic analyses of oxygen and deuterium provide useful results. In Fig. 2b, isotopic results of October and February sampling are represented. In October, cold springs C1 and C3 show high isotopic values, thermal waters (T1-T4) have the lowest ones, while C2 samples, from Rio Garrafo stream, shows intermediate values, closer to thermal ones. In February an evident shift of T2, T3 and T4 to values similar to Garrafo ones happens, probably due to a greater mixing. All these data are compatible with a meteoric origin of deep waters (Craig, 1961; Longinelli and Selmo, 2003) and the variation in oxygen seem to outline C2 as cold end-member and T1 as hot end-member of a possible mixing. Comparing these values with a correlation line $\delta^{18}O$/altitude, we can estimate an altitude of water infiltration of approximately 1500 m a.s.l. (Zuppi *et al.,* 1974; Conversini and Tazioli, 1993). This allows identifying possible recharge areas both to the west and to the south of the Acquasanta anticline.

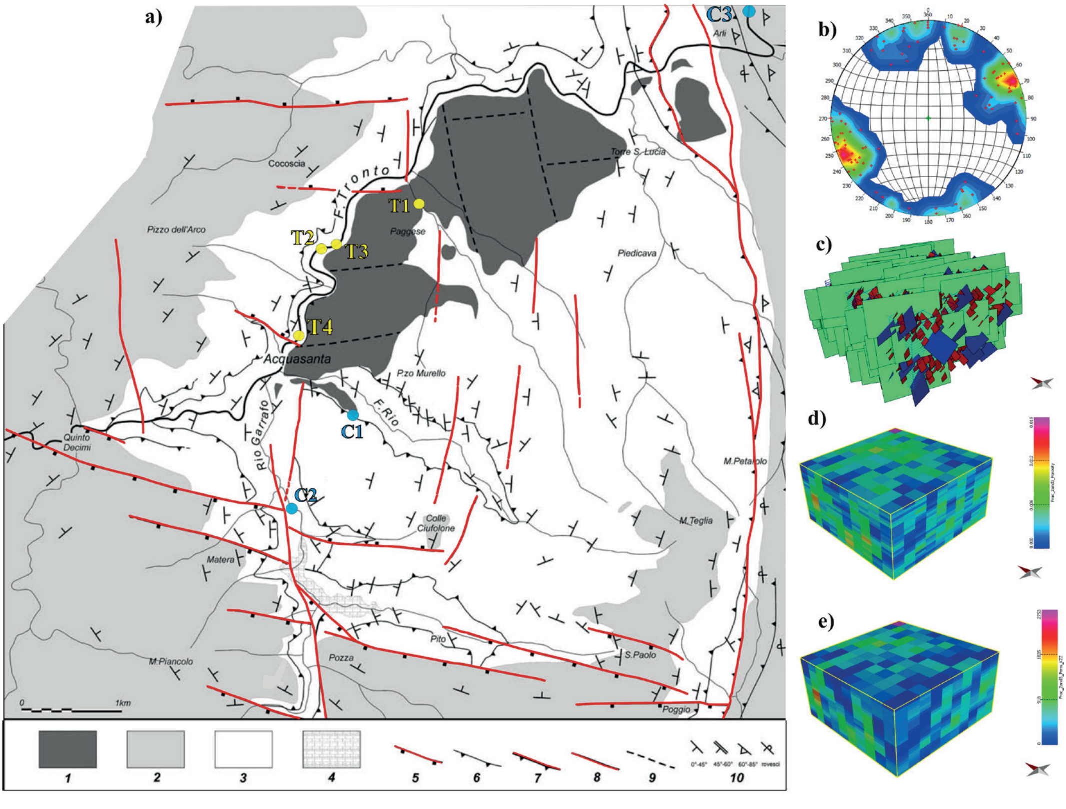

Fig. 3 – a) Schematic structural map of the Acquasanta area (modified from Menichetti, 2008); b) Contour plot from poles to fracture planes; c) DFN model; d) calculated porosity model; e) calculated permeability model. Legend: 1) Travertines; 2) Laga Formation; 3) Marly units, from Scaglia Variegata Formation to Marne a Pteropodi Formation; 4) Scaglia Rossa Formation; 5) Normal faults; 6) Detachment thrust; 7) Regional thrust; 8) Strike-slip fault; 9) Inferred fault; 10) Bedding attitude; C/T = Analyzed springs (C=cold, T=thermal).

Structural data. This area is structurally complex, and our structural analysis mainly considered data about bedding and fractures orientation. For the first step of the work, these data are especially referred to cap rock formations, because they diffusely crop out in the area, while outcrops of a possible reservoir, such as Scaglia Rossa Formation, are more difficult to reach and less extended. Furthermore, western side of the anticline can be easily investigated, due to the lower steepness of the limb. Bedding along the western side dips few tens of degrees to the west, with a main trend N175/20°W, while it becomes very steep, and subvertical to reverse in the eastern flank, with a main trend N155/90° (Fig. 3a). An anomalous dip direction of the strata is recognized in the particular area of the Garrafo Stream, with dip direction about N330/10°. The Marne con Cerrogna, Bisciaro and Scaglia Cinerea Formations are characterized by important detachment levels locally developing complex shear zones with doubles and elisions of the stratification, mainly affecting the Bisciaro Formation (Marsili and Tozzi, 1995). The first detailed meso-structural stations confirmed that mean directions of the shear planes range between N170/50°W and N10/30°W. Furthermore, some steeper planes are locally present (N50/70°W). These information will be important to better characterize the cap rock of our geothermal system and for the next implementation of a 3D model.

Further structural analyses carried out in the area reveal two important systems of open fractures, the first one from NNW–SSE to NW–SE oriented, and the second one trending about E-W (Fig. 3b). These fracture systems are related to the complex structural history of the area, and can affect the hydraulic conductivity of the rock mass, and favoring preferential paths for surface and deep water drainage, as shown by the karst corrosion in limestone layers and clay or calcite filling in marly levels. For this reason, a detailed meso-structural analysis has been planned to collect data from scan lines distributed across the main structure. Preliminary results from this survey confirm the general fracture trend mentioned above (N110/70°W). At this stage of the work, we have also elaborated small DFN (Fig. 3c) in order to calculate porosity (Fig. 3d) and permeability (Fig. 3e) values from fractures distribution in specific lithologies (Cerrogna Marls).

Many faults are also present (Fig. 3a). Their main orientations are N–S and WNW–ESE and they can also represent the preferential ascent path for deep hot waters and, on the other hand, can facilitate the mixing of superficial waters with the thermal ones.

Conclusions. A meso-structural analysis together with water isotopic analyses have been carried out along the Acquasanta positive structure (southern Marche region, Central Italy), in the surroundings of the thermal area.

First results allowed to: i) determine the origin of thermal water, ii) inferring a double water circulation path, iii) recognise the main fracture systems, their relationships with the main anticline structure and their possible relationships to fluid circulation. A double fluid circulation model is inferred: hot waters with a probable meteoric origin are involved in a deep circuit that rises to the surface and mixes with a shallower circuit of cold waters. Variations in conductivity among the four thermal springs, that present similar temperatures, let us think that these thermal waters dilute with a variable amount of cold water coming from the shallow circuit, probably from the Rio Garrafo stream. So we can also suppose that the shallow path could flow within Scaglia Rossa Formation due to its intense fracturing, with marly formations as cap rocks, while the deep one could flow within the underlying carbonate formations.

Finally, our first structural data allow us to make some observations. Shear zones and detachment levels present in the marly formations are related to the compressional history of the area, in particular to the thrusting phase. The main fracture systems instead are probably related to a more recent extensional event, and they have slightly increased porosity and permeability values of the rocks, especially in the ZZ direction.

Acknowledgements. We thank R. Giovannetti, S. Ferraro and the Water Chemistry Laboratory of Camerino University for their contribution during this stage of our work. We also thank Ing. M. Mussi and the Pisa CNR Laboratory for stable isotopes analyses, M. Carroll and P. Pierantoni for useful discussions.

References

Agosta F., Alessandroni M., Antonellini M., Tondi E., Giorgioni M.; 2010: From fractures to flow: A field-based quantitative analysis of an outcropping carbonate reservoir. Tectonophysics, 490, 197-213.

Armannsson H., Fridriksson T.; 2009: Application of geochemical methods in geothermal exploration. Short Course on Surface Exploration for Geothermal Resources, El Salvador.

Bigi S., Casero P., Ciotoli G.; 2011: Seismic interpretation of the Laga Basin; constraints on the structural setting and kinematics of the Central Apennines. Journal of the Geological Society, 168, 1-11.

Boni C., Colacicchi R.; 1966: I travertini della valle del Tronto. Memorie della Società Geologica Italiana, 5, 315-339.

Conversini P., Tazioli G. S.; 1993: Indagini idrogeologiche nella media e alta valle del fiume Menotre, Umbria orientale. Atti Ticinesi di Scienze della Terra, 36, 153-164.

Craig H.; 1961: Isotopic variation in meteoric waters. Science, 133, 1702-1703.

Della Vedova B., Bellani S., Pellis G., Squarci P.; 2001: Deep temperatures and surface heat flow distribution. Anatomy of an orogen: the Apennines and adjacent Mediterranean Basins, Vai, G. B. and Martini, P. (eds.), 65-76, Kluwer Academic Publishers, Dordrecht, Netherlands.

Dezayes C., Genter A., Valley B.; 2010: Structure of the low permeable naturally fractured geothermal reservoir at Soultz. Comptes Rendus Geoscience, 342, 517-530.

Farabollini P., Gentili B., Materazzi M., Pambianchi G.; 2005: Freshwater travertines in Central Apennine (Italy): genesis and climatic and neotectonic significante. Revista de geomorfologie, 7, 61-75.

Fusari A., Invernizzi C., Pierantoni P. P., Carroll M.; 2013: Preliminary insights from the Acquasanta thermal area (Marche, Italy). Proceedings of the European Geothermal Congress 2013, Pisa, Italy, 1-6.

Galdenzi S., Cocchioni F., Filipponi G., Morichetti L., Scuri S., Selvaggio R., Cocchioni M.; 2010: The sulfidic thermal caves of Acquasanta Terme (Central Italy). Journal of Cave and Karst Studies, 72, 43-58.

Ghisetti F., Vezzani L.; 2000: Detachments and normal faulting in the Marche fold-and-thrust belt (central Apennines, Italy): inferences on fluid migration paths. Journal of Geodynamics, 29, 345-369.

Koopman A.; 1988: Detachment tectonics in the central Apennines, Italy. Geol. Ultraiectina, 30, Utrecht, 1-155.

Longinelli A., Selmo E.; 2003: Isotopic composition of precipitation in Italy: a first overall map. Journal of Hydrology, 270, 75-88.

Madonna R., Signanini P., Crema G., Di Sabatino B., Rainone M.L., Di Nunzio A.; 2005: The Geothermal Area of Acquasanta Terme (Central Italy): Main Characteristics and an Attempt of Field Evaluation. Proceedings of the World Geothemal Congress 2005, Antalya, Turkey, 1-8.

Marsili P., Tozzi M.; 1995: Un livello di scollamento nella dorsale di Acquasanta (Ascoli Piceno). Bollettino della Società Geologica Italiana, 114, 177-194.

Mazzoli S., Deiana G., Galdenzi S., Cello G.; 2002: Miocene fault-controlled sedimentation and thrust propagation in the previously faulted external zones of the Umbria-Marche Apennines, Italy. EGU Stephan Mueller Special Publication Series, 1, Utrecht, 195-209.

Menichetti M.; 2008: Assetto strutturale del sistema geotermico di Acquasanta Terme (Ascoli Piceno). Rend. Online SGI, 1, 118-122.

Minissale A., Vaselli O., Tassi F., Magro G., Grechi G.P.; 2002: Fluid mixing in carbonate aquifers near Rapolano (central Italy): chemical and isotopic constraints. Applied Geochemistry, 17, 1329-1342.

Scisciani V.; 2009: Styles of positive inversion tectonics in the Central Apennines and in the Adriatic foreland: Implications for the evolution of the Apennine chain (Italy). Journal of Structural Geology, 31, 1276-1294.

Tozer R.S.J., Butler R. W. H., Chiappini M., Corrado S., Mazzoli S., Speranza F.; 2006: Testing thrust tectonic models at mountain fronts: where has the displacement gone?. Journal of Geological Society, 163, 1-14.

Zuppi G.M., Fontes J.C., Leotolle R.; 1974: Isotopes du milieu et circolations d'eaux sulfureès dans le Latium. Proceedings of the Symp. Isotope Techniques in Groundwater Hydrology, I.A.E.A, 1, Vienna, Austria, 341-361.

GEOCHEMICAL EXPLORATION AND GEOTHERMOMETRIC EVALUATION OF LAMEZIA TERME (CALABRIA) AND CONTURSI TERME (CAMPANIA) SITES, SOUTHERN APENNINES, ITALY

A. Garone[1], L. Pizzino[2], A. Sciarra[2], F. Quattrocchi[2]
[1]"Sapienza" Università di Roma, Italy
[2]Istituto Nazionale di Geofisica e Vulcanologia, Rome, Italy

Introduction. The areas of Lamezia Terme and Contursi Terme were chosen within the framework of the VIGOR project, started in 2011. The main goals of the project were define the different chemical water families and identify the water-rock interaction processes, study the relationships between fluid circulation and tectonic faults and evaluate the geothermal potential of the area.

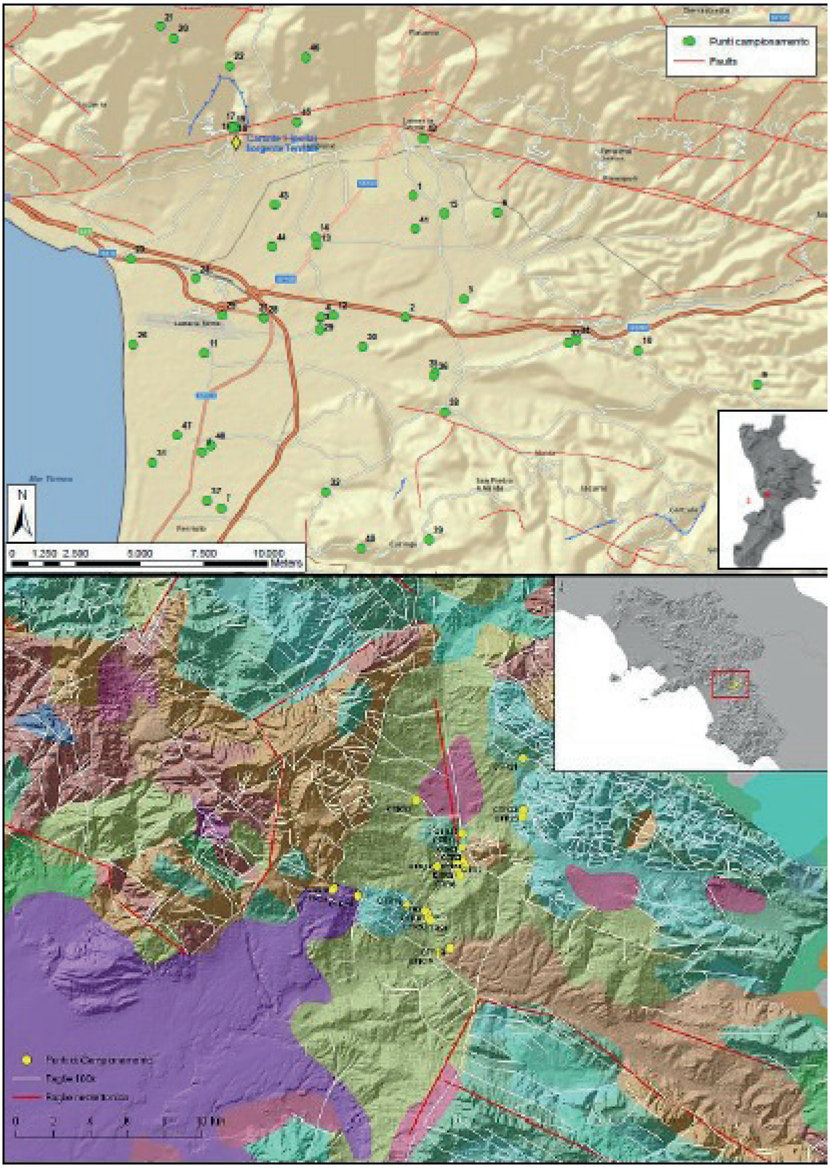

Fig.1 - Investigated areas and locations of the sampled water sites. Numbers refer to the samples ID.

A first geochemical survey was conducted in May 2012, in the area of Lamezia Terme (Calabria) for a total of 48 groundwaters sampled (Fig. 1) and then, in July 2012 the area of Contursi Terme (Campania) with a total of 24 sites (Fig. 1).

During this time, new geochemical data on groundwater were acquired, interpreted and modelled. These data provide an overview of the possible use of geothermal potential in the studied areas; in order to obtain useful information, thermal and cold waters were sampled in the last year.

Methods. Physical parameters (temperature, pH, Eh and electrical conductivity) and alkalinity (titration with 0.05 N HCl) were determined in situ. Water samples were filtered (0.45 µm) and stored in high-density polyethylene flacons for laboratory analysis. Major anions and cations were analyzed by ion-chromatography (analytical error was < 5); minor and trace elements were determined by ICP–MS (analytical error was 10%). The analysis of the chemical composition of dissolved gases (He, H_2, O_2, N_2, CH_4, CO_2) was carried out by using a gas chromatograph equipped with TCD, with argon as carrier gas (analytical error was < 5%).

Dissolved ^{222}Rn was stripped from water and adsorbed into the activated charcoal layer hosted in Active Charcoal Collectors (ACC) by using a Radon Degassing Unit; ACC were analyzed through γ-spectrometry (Mancini *et al.*, 2000). Analytical error was < 5%. The $^{18}O/^{16}O$ ad $^{2}H/^{1}H$ isotopic ratios (expressed as $\delta^{18}O$ and δD ‰ vs. VSMOW) were determined by a mass spectrometer. The analytical precision is 0.1 ‰ for $\delta^{18}O$ and 1 ‰ for δD. The carbon isotopic ratio of TDIC (Total Dissolved Inorganic Carbon), expressed as $\delta^{13}C$ ‰ vs. VPDB, was analyzed by mass spectrometry following the procedure described by Favara *et al.* (2002).

Geological setting. The following main tectonic-stratigraphic units crop out in the Lamezia Terme area, briefly described from bottom to top (Tansi *et al.*, 2007): *i*) *Slate and metapelite Unit*, made up by dominantly foliated slates, black metapelites and metasilts, interbedded with quartzite strata (Paleozoic); *ii*) *Orthogneiss Unit*, made of mylonitic augen-gneiss, micaschist, and subordinately thick granitoid sheets (Paleozoic); *iii*) *Paragneiss Unit* made of high-grade metamorphic rocks (biotite-sillimanite-garnet gneiss), intruded by plutonic bodies (Paleozoic); *iv*) *Mesozoic carbonate complex*, made up by dolostone and metalimestone Unit (Late Triassic-Liassic), locally outcropping in "tectonic windows" of the Apennine chain, as in the Caronte area.

A transgressive Late Miocene conglomerate-calcarenite-clay-evaporite succession, and an Early Pliocene conglomerate-sand-clay succession unconformably overlie the above-mentioned tectonic units. Middle Pliocene to Middle Pleistocene deposits, made of thick conglomerate-sand-sandstone-clay marine successions, represent the basin-fill deposits of the main tectonic depression (Catanzaro Trough). Locally, Late Pleistocene fluvial terraced deposits, marine terraces and Late Pleistocene-Holocene alluvial fans crop out.

The tectonic of the area in its northern sector is dominated by the Lamezia-Catanzaro Fault (LCF, Tansi *et al.*, 2007), a 50-60 km long left-lateral strike-slip fault, separating the Plio-quaternary Catanzaro Trough from the southern edge of the Sila Massif.

Contursi Terme area is a tectonic depression bounded by the Mt. Polveracchio – Mt. Cervialto to the north-west and the Mt. Marzano – Mt. Ogna to the south-east. In the study area, the following main stratigraphic-structural units crop out, briefly described from top to bottom (Celico *et al.*, 1979; Polselli, 2004): *i) Continental deposits* mainly consisting of pebbles and sand. This complex is characterized by a variable permeability in relation to the lithology and the grain size of the sediments; *ii) Irpinian Unit* outcropping in small patches in the northern part of the valley and consist of alternation of conglomerates, sandstones and clays unconformable on the limestone and clays of the Campania-Lucania platform; *iii) Varicolored shales* consist of alternations of clay, limestones, calcilutites, micaceous sandstones and marls; *iv) Apennine carbonate platform* consist of Triassic dolomite (with a thickness of about 1000-1200 m), typically tectonised. Follows, in stratigraphic continuity, a stretch of calcareous series (thickness equal to about 2500 m) which present, in the lower part, dolomite and limestone-dolomite. These units represent the most productive aquifers of the study area.

Results and discussion.

Lamezia Terme area. The chemical composition of the samples is described in terms of major ion contents, in the Langelier-Ludwig diagram.

Four geochemical families have been recognized, each one is characteristic of a different water-rock interaction processes: *i) Ca-HCO$_3$*, characterized by low salinity (EC < 600 µS/cm), temperature between 10 and 18°C and oxidizing condition. Both chemical and physical characteristics are typical of a fast interaction in circulating waters with both Plio-Quaternary sediments (filling the plain) and Paleozoic igneous rocks (cropping out in the main mountains of the area); *ii) Ca-SO$_4$*, characterizing the thermal water of Caronte and some hypothermal water of the plain. They have strong reducing conditions and high salinity (up to 2500 µS/cm). Sulphate concentrations derive from the gypsum contained in the Triassic carbonates in thermal waters and from gypsum lenses contained in sandy clays in hypothermal waters; *iii) Na-Cl* typical of marine sediments leaching; *iv) Na-SO$_4$*, represented by a salty artesian aquifer sampled in the plain, characterized by a slow hydraulic circuit interacting with evaporates in a clayey environment. Dissolved gases in the sampled waters show an average value of N_2, O_2 and CO_2 equal to 20.25, 5.04 and 16.42 cc/l, respectively. As in other areas of Calabria (Italiano *et al.*, 2010), the investigated area is characterized by the absence of a common degassing of CO_2 in groundwater. This feature is well highlighted by the absence of a clear positive correlation between the CO_2 and electrical conductivity. Moreover, the lack of a high flux of CO_2 in the water sampled is also pointed out by non-correlation between the concentration of CO_2 and radon content. Dissolved radon shows an average concentration of 8 Bq/l, with noticeable values found in thermal springs (100-130 Bq/l) and in one cold water discharging in the Serre mountains, with more than 1000 Bq/l. These values can be explained with the presence of a deep circulation into fractured carbonates driven by the LCF and the presence of uranium-bearing mineralization (already found in similar geological settings in Calabria: Calcara *et al.*, 1996).

Environmental isotopes minimizing the existence of high temperature (> 150°C) at depth due to the lack of any oxygen-shift, even in the thermal area of Caronte. O and H isotopes point out a common meteoric origin of the sampled waters. In fact, in the graph (Fig. 2) all waters sample are positioned between the Global Meteoric Water Line (that represent the isotopic compositions of the global rainfalls: Craig, 1961) and the Regional Meteoric Water Line (RMWL, that represent the isotopic composition of the meteoric precipitations in southern Italy, defined by Longinelli and Selmo, 2003). In order to individuate the elevation of the potential recharge area of the thermal waters, it has been calculated a regression line, based on the isotopic composition of cold waters discharging in the Caronte area.

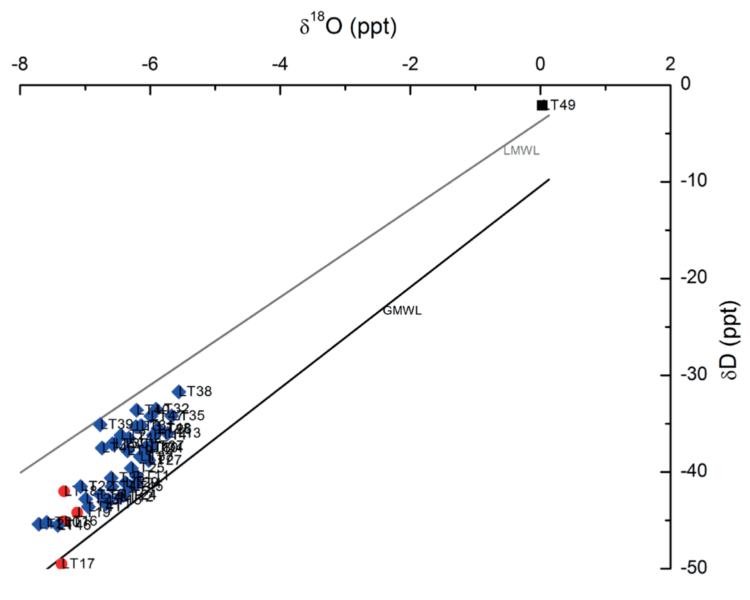

Fig. 2 – Environmental isotopes diagram of the water collected in the Lamezia Terme area.

Carbon isotopes point out a biogenic origin of the dissolved carbon for the bulk of the groundwaters (Cerling *et al.*, 1991), while a trend toward the equilibrium with deep carbonates was showed by thermal waters of Caronte. This process is possible only hypothesizing a slow deep circulation in the geothermal system, characterized by a prolonged WRI. Equilibrium with carbonates is favored by both the presence of well developed fracture network (Tansi *et al.*, 2007) in the Mesozoic complex and by the relatively high thermal condition existing at depth.

Geothermometric considerations on the collected waters were carried out with extreme care, due to the geological, lithological and mineralogical features of the Lamezia Terme area. The use of the classical Na/K and K/Mg ionic solute ratios (Giggenbach and Corrales, 1992) on collected waters evidenced their immaturity, emphasizing their unsuitability for any estimate of deep temperatures.

The evaluation of deep temperatures was carried out by applying selected geothermometer equation. Due to the geological, lithological and mineralogical features of the Lamezia Terme area, we selected and applied the SO_4/F_2 geothermometer (Marini *et al.*, 1986), mostly used in carbonate-evaporite environment in Italy that indicated a realistic deep temperature estimate of about 50-60°C, confirming the low enthalpy of the Caronte hydrologic system.

Contursi Terme area. Basing on their outlet temperature, waters were classified as *i)* thermal (Contursi Bagni, T > 35°C), *ii)* hypothermal (20 < T < 35°C) and *iii)* cold (T < 20°C), following the classification of Marotta and Sica (1933). The relative abundances of major elements allowed us to identify three geochemical families. Waters have the following chemical composition: *i) Ca-HCO$_3$*, characterizing the cold and hypothermal water and one thermal water (sample 1). Their chemical composition is typical of the interaction with the carbonate lithologies (that characterize the studied area) and surface sediments (that characterize local geology). These processes differ both in timing and intensity, justifying the different position of the samples in the Langelier-Ludwig diagram. Generally, the cold water seem to be characterized by a fast and shallow circulation and seem to have a limited interaction time with the lithologies. Hypothermal waters have lower ratios of HCO_3/Cl, HCO_3/SO_4 and (Ca+Mg)/(Na+K) than cold waters, feature most noticeable in thermal sample (sample 1). Probably, this water is characterized by a slower and deep circuit, with a more intense leaching of the Triassic evaporite rocks; *ii) Na (Ca-Mg) – HCO$_3$(Cl)*, represented by thermal spring (sample 10). This sample, together with sample 11, represents the end-member of the deep circulation of the study area. These waters circulate in deeper geological units (dolomites, limestones and evaporites) and acquiring their thermal character and salt content. These waters are more aggressive against the rocks because of the presence of dissolved carbon of deep origin and, consequently, the water-rock interaction processes are more intensive; *iii) Na (Ca) – Cl (HCO$_3$)*, represented by thermal spring (sample 11, for discussion on its chemical composition, please consult the *ii*)).

The investigate area is characterized by an intense and diffuse degassing of CO_2 in the groundwater, especially in the hypothermal and thermal waters. The measured values are extremely high (up to 650 cc/l) comparable with other geo-tectonic contexts in Italy (both in volcanic areas that not volcanic) and in adjacent areas (Telese, Mefite d'Ansante, Irpinia). There is a positive correlation between electrical conductance and CO_2; it means that the presence of CO_2 in solution (i.e., an acid environment) favors the leaching of rocks/sediments, increasing the salinity of water.

O and H isotopes (Fig. 3) point out a common meteoric origin of the sampled waters. All waters fall between the Global Meteoric Water Line (Craig, 1961) and the Regional Meteoric Water Line (RMWL, defined by Longinelli and Selmo, 2003). Environmental isotopes minimizing the existence of high temperature (> 150°C) at depth due to the lack of any oxygen-shift; however, there are clear isotopic exchange between CO_2 and groundwater (*negative oxygen shift*), especially in the gaseous bubbling springs. In order to individuate the elevation of the potential recharge area of the site, it has been calculated a regression line, based on the isotopic composition of cold waters.

Isotopic analysis of total carbon suggests a mixing between a biogenic source of CO_2 and carbonates in most cold waters; while, the measured values for the thermal waters suggest the tendency of these waters to isotopic equilibrium with the Mesozoic marine carbonates, favored by prolonged water-rock interaction and high temperatures.

A first geothermometric evaluation on the waters sampled can be introduced by analyzing the Mg-Na-K geothermometer (Gibbenbach, 1988). This geothermometer evidenced the immaturity of waters sampled, emphasizing their unsuitability for any estimate of deep temperatures. However, the evaluation of deep temperatures was carried out by applying selected geothermometer equation. We selected and applied the SO_4/F_2 geothermometer (Marini *et al.*, 1986), that indicated a realistic deep temperature estimate of about 50-60°C. This results is in accord with the normal geothermal gradient (30°C/km) estimated for Contursi Terme area (Cataldi *et al.*, 1995), leaving assume that the thermal waters reach depths of 2-3 km.

Conclusions.

Lamezia Terme. Considering all collected data three hydrological circulations were recognized in the area, each one is characterized by different WRI:

- A fast interaction of cold waters with Palaeozoic metamorphic units (cropping out in the Sila Massif and in the Serre mountains) and hypothermal waters with Plio-Quaternary shallow sediments (filling the plain). These waters have a limited WRI (i.e. low salinity, < 600 μS/cm) and a chemistry from $Ca\text{-}HCO_3$ to Na-Cl;
- A relatively deep circulation of the hypothermal waters in the Miocene-aged terrigenous sedimentary succession (conglomerates, sands, calcarenites and clays) of the Catanzaro Trough. Waters have low to medium salinity, that locally become high due to evaporite (mainly halite and gypsum) dissolution. As a result, chemistry varies from $Ca\text{-}HCO_3$ to Ca (Na)-SO_4;
- A deep and slow circulation of thermal waters belonging to the Caronte system in the fractured Mesozoic carbonate complex. Waters have relatively high salinity (up to 2500 μS/cm) and a $Ca\text{-}SO_4$ chemistry. Waters infiltrate in the southern edge of the Sila Massif, go through the fractured Palaeozoic units and circulate at depth in the Mesozoic carbonate complex.

The regional LCF plays a key role in permitting the existence of a dense fracture network and the maintenance of the geothermal system, throughout a continuous slip, as recognized in other sectors of Calabria (e.g. Gioia Tauro Fault: Pizzino *et al.*, 2004). Finally, waters ascent toward surface, discharging as thermal springs.

Considering the mineral assemblage of the carbonate complex, we selected and tentatively applied the SO_4/F_2 geothermometer, mostly used in other similar geological environments in Italy (Marini *et al.*, 1986), that indicated a realistic deep temperature estimate of about 50-60°C, confirming the low enthalpy of the Caronte hydrologic system, as emphasized by the use of environmental isotopes.

Contursi Terme. Considering all collected data, two main hydrological circuits have been recognized in the study area, each one is characterized by different water-rock interaction processes, depth circuits, residence time in the aquifer, temperature deep, composition of dissolved gases:

- A shallow and fast circulation of cold water ($T \leq 20$°C) that originate from rainwater infiltrating in the main massive area (Mt. Polveracchio, Mt. Marzano) and interact with limestone formations and/or with the clay-sandy conglomeratic of continental origin and Plio-Quaternary marine deposits. These waters have modest CO_2, alkaline pH, limited interaction with rocks and sediments and $Ca\text{-}HCO_3$ chemistry. Locally, the cold waters have a considerable gaseous contribution (CO_2, up to 400 cc/l as dissolved phase) with a consequent decrease in the pH value and a considerable increase of their salinity. These waters have been found mainly in the area of Contursi Terme, along the tectonic lines of the Sele Valley;

- A deep and probably slow circulation of hypothermal and thermal waters belong to Contursi Bagni circuit. These waters are recharged in/by carbonate massive outcrops in the area (Mt. Polveracchio, Mt. Marzano), infiltrate and reach the Mesozoic carbonatic and dolomitic deep complex (from -1000 to -3000 m). The waters, that become hot (50-70°C) for the normal geothermal gradient existing (30°C/km), are enriched in CO_2, acquire their salt concentration and go back along the main tectonic discontinuities in the emerging area of Contursi Bagni. These waters have an intensive interaction with carbonate rocks (limestone and dolomite) and evaporite deposits (anhydrite and gypsum), as consequence have a high salinity (electrical conductivity up to 7000 mS/cm) and a Na (Ca-Mg)-HCO_3 (Cl) e Na (Ca)-Cl (HCO_3) chemistry. These waters have high CO_2 concentration (up to 450 cc/l), acid pH, important concentration of Na, Cl, K, Mg and SO_4, are enriched in minor and trace elements (i.e. the thermal indicators, such as Li, B, As and Rb). Some thermal water during the ascent is mixed with cold water less saline and showing a geochemical composition between hot and cold water: they belong to the group of hypothermal water of Contursi Bagni area.

We selected and tentatively applied the SO_4/F_2 geothermometer, that indicated a realistic deep temperature estimate of about 50-60°C. This results is in accord with the normal geothermal gradient (30°C/km) estimated for Contursi Terme area (Cataldi *et al.*, 1995), leaving assume that the thermal waters reach depths of 2-3 km.

References

Calcara M., Guerra I., Moretti A., Pizzino L., Quattrocchi F.; 1996: Il gas radon nelle acque e nei suoli della Sila: implicazioni geotettoniche e rischio ambientale. Atti XV Convegno GNGTS 1996, Roma - CNR, 11-13 Novembre, 449-454.

Cataldi R., Mongelli F., Squarci P., Taffi L., Zito G., Calore C.; 1995: Geothermal ranking of Italian territory - Geothermics, 24, 115-129.

Celico P., De Gennaro M., Ghiara M. R., Stanzione D. (1979). Le sorgenti termominerali della Valle del Sele (Salerno): indagini strutturali, idrogeologiche e geochimiche. Rendiconti Società Italiana di Mineralogia e Petrologia, 35, 389-409.

Cerling T.E., Solomon D.K., Quade J., Bowman J.R.; 1991: On the isotopic composition of carbon in soil carbon dioxide. Geochimica et Cosmochimica Acta, 55, 3403-3405.

Craig, H.; 1961: Isotopic variations in meteoric waters. Science, 133: 1702-1703.

Favara R., Grassa F., Inguaggiato S., Pecoraino G., Capasso G.; 2002: A simple method to determine the ‰13C content of total dissolved inorganic carbon. Geofisica Internacional, 41, 313-320.

Giggenbach, W.F., 1988: *Geothermal gas equilibria. Derivation of Na-K-Mg-Ca geoindicators*. Geochim. Cosmochim. Acta 52, 2749-2765.

Giggenbach W.F., Corrales R.S.; 1992: *The isotopic and chemical compsition of waters and steam discharges from volcanicmagmatic-hydrothermal systems of the Guanacoste Geothermal Province, Costa Rica*. Applied Geochemistry, 7, 309-322.

Italiano F., Bonfanti P., Pizzino L., Quattrocchi F.; 2010: *Geochemistry of fluids discharged over the seismic area of Southern Apennines (Calabria region, Southern Italy): implications for Fluid-Fault relationships*. Applied Geochemistry, 25, 540-554.

Longinelli A., Selmo E.; 2003: *Isotopic composition of precipitation in Italy: a first overall map.* Journal of Hydrology, 270, 75-88.

Mancini C., Quattrocchi F., Guadoni C., Pizzino L., Porfidia B.; 2000: *222Rn study throughout different seismotectonical areas: comparison between different techniques for discrete monitoring.* Annali di Geofisica, 43, 1-28.

Marini L., Chiodini G., and Cioni R.; 1986: *New geothermometers for carbonate-evaporite geothermal reservoirs,* Geothermics, 15(1), 77-86.

Marotta and Sica; 1933: *Classificazione italiana delle acque minerali*. Annuali di Chimica applicata. Vol. 19 fasc. 12, 1929; Vol. 23 fasc. 6.

Polselli P. (2004): *Relazione tra fenomeni di sprofondamento, risalite di fluidi mineralizzati e sismicità in alcune aree di studio dell'Italia centro-meridionale*. Tesi di stage APAT 2004, 67 pp.

Tansi C., Muto F., Critelli S., Iovine G.; 2007: *Neogene-Quaternary strike-slip tectonics in the central Calabrian Arc (southern Italy).* Journal of Geodynamics 43 (2007) 393-414.

THE CFDDP PROJECT: PRELIMINARY RESULTS FROM THE 506 M PILOT HOLE DRILLING AT THE BAGNOLI PLAIN, EASTERN SECTOR OF THE CAMPI FLEGREI CALDERA (SOUTHERN ITALY)

A. Mormone[1], G. Aiello[2], D. Barra[1,2], T. Caputo[1], S. Carlino[1], S. de Vita[1], M.A. Di Vito[1], R. Isaia[1], M.J. Jurado[3], A. Marturano[1], F. Molisso[4], M. Piochi[1], M. Sacchi[4], R. Somma[1], A. Tramelli[1], T. Wiersberg[5], G. De Natale[1], C. Troise[1]

[1]Istituto Nazionale di Geofisica e Vulcanologia, sezione di Napoli, Osservatorio Vesuviano, Napoli, Italy
[2]Dipartimento di Scienze della Terra, dell'Ambiente e delle Risorse, Università Federico II, Napoli, Italy
[3] Instituto de Ciencias de la Tierra Jaume Almera - CSIC, Barcelona, Spain
[4] Istituto per l'Ambiente Marino Costiero-IAMC, Napoli, Italy
[5]Deutsches GeoForschungsZentrum GFZ, Telegrafenberg, Germany

Introduction. The Campi Flegrei caldera (Fig. 1) is one of the highest-risk volcanic areas on the Earth with more than 70 explosive eruptions that occurred in the past 14.9 ka (Smith *et al.*, 2011; Di Renzo *et al.*, 2011), the historical eruption in 1538 AD that followed tens of years of unrest, and alternating episodes of uplift and subsidence recorded since Roman Times (bradyseism: Parascandola, 1947; Del Gaudio *et al.*, 2010). The present state of the volcanic system is related to 7 m of net uplift and more than 16,000 earthquakes that took place between 1950 and 2013 in the Pozzuoli area (e.g., Del Gaudio *et al.*, 2010; D'Auria *et al.*, 2010), and huge gaseous emissions with about 1500 tonnes/day of CO_2 (Chiodini *et al.*, 2001). These phenomena are linked to a high-temperature, fluid-rich and saline geothermal system (e.g., Guglielminetti 1986; De Vivo *et al.*, 1989; Mormone *et al.*, 2011 and reference therein) supplied by magmatic fluids and heat (e.g., De Natale *et al.*, 1991; Todesco *et al.*, 2010; Troiano *et al.*, 2011).

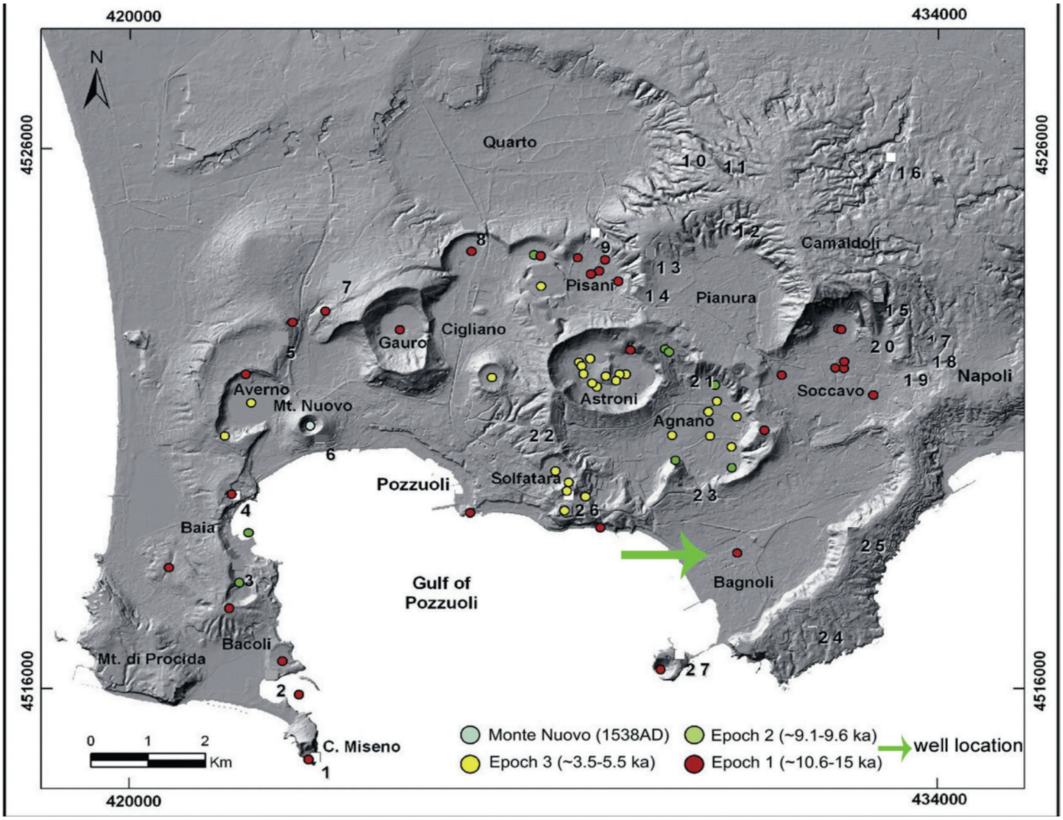

Fig. 1 – Map of the Campi Flegrei caldera with the eruptive vent locations for post 15 ka eruptions, and well location (modified from Smith *et al.*, 2011).

The Campi Flegrei volcanic system was investigated in the '40-'80 years by the Azienda Geologica Italiana Petroli (AGIP) and the Società Anonima Forze Endogene Napoletane (SAFEN) through deep holes at about 3050 m of depths (e.g, AGIP, 1987; Rosi and Sbrana, 1987) mostly in the western and north-central sectors of the caldera. The drilling exploiting activities have strongly contributed to the definition of the subsurface structure of the caldera (Rosi and Sbrana, 1987; Rosi *et al.*, 1983). However, since the AGIP and SAFEN programmes, a lot of geological, geochemical, and geophysical studies have been conducted at the Campi Flegrei, improving the knowledge of the volcano.

Nonetheless, the recent dynamics and history of the volcano are still affected by several uncertainties. Among the most important ones, there are: 1) the debated origin and shape of the caldera attributed to the Campanian Ignimbrite or the Neapolitan Yellow Tuff eruptions, or both (Rosi *et al.*, 1983; Orsi *et al.*, 1996; Perrotta *et al.*, 2006; De Vivo *et al.*, 2001), 2) the volcanism older than 14.9 ka that is buried by later volcanic products and lies mostly in the subsurface (Orsi *et al.*, 1996), 3) the 3D-distribution of the volcano-tectonic dislocations during collapse and resurgent phenomena, 4) the mechanisms of bradyseisms and their relation with magma dynamics, and 5) the relationships among caldera structure and chemico-physical features of the geothermal system. These questions determine doubts on the significance of the monitored phenomena, in particular with their relation to the dynamics of the caldera and the evolution of the magmatic system.

The eastern caldera coincides onshore with the Bagnoli Plain and its volcanic evolution is certainly among the least known in the area. A medium pilot well, 506 m deep, was realized in Bagnoli Plain with the scope to fill the gap of knowledge. The drilling activities was conducted in the frame of the Campi Flegrei Deep Drilling Project (CFDDP) that is principally aimed to the improvement of volcanic hazard mitigation and to the promoting the geothermal energy exploitation in the Campania Region. Here we present the preliminary results from analysis of the drilling mud and core samples, as well as from geophysical loggings.

Geological context and drilling site. The Campi Flegrei volcanic complex developed inside the Campanian graben (Piochi *et al.*, 2005 and reference therein). The oldest erupted products are dated at >60 ka and crop out in a quarry in the Quarto Plain (Pappalardo *et al.*, 1999), although the volcanism in the area dated back at least 1.5 Ma (Piochi *et al.*, 2005 for a review). At the Present, the Campi Flegrei volcanic field characterizes for a ~10km large caldera. According to several studies (Rosi and Sbrana, 1987; Orsi *et al.*, 1996), the caldera was originated at 39 ka BP (De Vivo *et al.*, 2001) during the catastrophic Campanian Ignimbrite eruption. Orsi *et al.* (1996) and Perrotta *et al.* (2006) suggested that a second collapse occurred within the primary caldera during the 14.9 ka Neapolitan Yellow Tuff eruption (Deino *et al.*, 2004). Few authors (De Vivo *et al.*, 2001) recognized the only Neapolitan Yellow Tuff caldera and indicated for the Campanian Ignimbrite an origin from faults located north of Campi Flegrei.

All the authors consider the Posillipo cliff as a volcano-tectonic structure that thus is possibly related to the eastern caldera margin of the only Neapolitan Yellow Tuff (Orsi *et al.*, 1996; Perrotta *et al.*, 2006) or also of the Campanian Ignimbrite (Rosi *et al.*, 1983; Isaia *et al.*, 2009). Orsi *et al.* (1996) suggested a larger 39 ka caldera that includes part of the city of Naples and the western portion of the Gulf of Naples. Along the Posillipo cliff, the Neapolitan Yellow Tuff (NYT) has a thickness of about 120 m; a level of scoriae with thickness of 10-20 meters has been also documented upper in the NYT sequence (Rittmann, 1950). The base of the NYT is exposed in the Cavalleggeri-Fuorigrotta area, just at the foothill.

The Bagnoli Plain lies at the foot of the cliff. It is characterized by two cones, Nisida and Santa Teresa that were active in the past 14.9 ka (Di Renzo *et al.*, 2011) and a complex depositional sequence recovered by few <223 m boreholes (Orsi *et al.*, 1996; Calderoni and Russo, 1998). The Neapolitan Yellow Tuff, with some exceptions, is not recovered in the boreholes, which, however, never reached its base. Fossils were described in the boreholes and are used to infer the subsidence of the Plain. The Bagnoli Plain (Fig. 1) was, thus, selected to perform the drilling activities for different reasons: a) it is the less investigated area, because the larger part of previous deep drillings were located in the eastern and central-northern sector of the caldera (AGIP, 1987; Mormone *et al.*, 2011; Carlino *et al.*, 2012 and references therein); b) the site is located about 1km west from the NYT volcano-tectonic structure (Posillipo cliff) and, therefore, new well stratigraphic data could represent a further constrain to understand the amount of sin-caldera collapse and post-caldera volcanic events; c) the site is less than 2 km from the eastern part of the La Starza marine terrace and from the most active Solfatara crater; and d) the site hosts the western part of the city of Naples, consequently it represents the highly exposed area to volcanic risk. Moreover, from technical point of view, the drilling site meets an important safety requirement, since it is located within an iron factory (ILVA), which is now dismissed, and therefore is far enough to residential buildings (>400 m) to guaranty the absence of risk straightforwardly related to the drilling activity. Finally, the borehole has been designed in order to be equipped with technologically advanced instruments for the seismic and geochemical monitoring the plain which houses part of the city of Naples, consequently it represents one of the highly exposed area to the volcanic risk in the caldera.

Drilling operations. The drilling of pilot hole was conducted in to two phases in late summer and late fall 2012, interrupted by three months of drill stop. Borehole diameters are 16 inch down to 33.5 m and 121/4" down to 222 m. In the second phase, the hole was deepened to 434 m (8 ¼ inch borehole diameter) and finally drilled to 506 m with 6 inch diameter (all depths are meter below Kelly Bushing). Almost the entire hole was drilled for cuttings, which were separated from the drilling mud at the shale shakers, analysed in a field laboratory and sampled for further studies. The drilling was carried out with circulating drilling mud having densities from 1.10 kgl^{-1} in the shallower part (222 m) to 1.20 kgl^{-1} at greater depth. In the last stage of drilling, from 423 m to 506 m the bentonite-based mud was replaced by a mud based on water and organic additives. At the bottom of the well, two cores were retrieved from the depth interval 438.0-438.9 m (0.9 m recovery) and 500-501 m (1 m recovery), respectively. The well is completely cased, with exception of the lowermost 80 m, where a slotted liner is installed. This will promote fluids and gases to flow into the well for future geochemical monitoring and sampling. At the end of the drilling, mud was replaced by water with anti-corrosion additive (Brineback).

The Baker Hughes Company provided all monitoring services during the drilling, including pressure, mud temperature, rate of penetration, environmental and drill mud gas concentration in the mud, etc. The drilling was also accompanied by geophysical downhole logging, performed by Schlumberger Company, from 0 m to 422 m of depth.

Analytical methods. We have analyzed mud samples from deep drilling exploiting of the 506 m pilot-borehole in the Bagnoli Plain. Cutting samples were collected every 3 m in the first 225 m and every 5 m down to 501 m. Samples were washed, sieved and dried at 80°C. Measurements were also performed on cored rocks collected at 438 m and 501 m of depths.

The different grain size fractions and the cores were observed under a binocular microscope to define type, texture, mineralogy and alteration of the drilled materials; single crystals or fragments were hand-picked for further investigations.

Thin sections of cored rocks were studied under a reflex-light-equipped optical microscope and by Scanning Electron Microscope (SEM) and Energy dispersed scanning microscopy (EDS).

SEM observations and semi-quantitative and quantitative EDS analysis were carried out at CISAG Laboratory (Università di Napoli Federico II), by using a JEOL-JSM 5310 SEM, equipped with a Link EDS and a Inca 4.08 software. Operating conditions were 15 kV accelerating voltage, 50-100 mA filament current, 5-10 µm spot size and 50 s net acquisition time.

X-Ray Diffraction (XRD) intensity data were collected on selected grains, minerals or whole-rocks. We have used a X' Pert Powder diffractometer by PANalytical, at the Istituto

Nazionale di Geofisica e Vulcanologia - Osservatorio Vesuviano, with a high speed PIXcel detector, Ni-filtered, CuKα radiation, at 40 kV and 40 mA in a 3-70 º2θ range, with 0.02º steps at 8 s/step. The samples were powdered in an agate mill immediately before analysis. Diffraction patterns were interpreted using the X'Pert HIGH Score Plus computer program.

Feldspars and glass shards were leached with cold and warm 2.5 N HCl for 10 minutes, then rinsed several times in pure sub-boiling distilled water, and finally dissolved with high-purity $HF–HNO_3–HCl$ mixtures. Sr and Nd were separated by standard cation-exchange methods. Their isotope ratios were measured statically by Thermal Ionization Mass-Spectrometer (TIMS, ThermoFinnigan™ Triton TI) at the Istituto Nazionale di Geofisica e Vulcanologia, Sezione Osservatorio Vesuviano di Napoli and were corrected for mass fractionation using $^{86}Sr/^{88}Sr$ = 0.1194. Replicate analysis of NIST NBS 987 Reference Standard gave average values of 0.710192 ± 0.000017 (2σ, n = 25); Sr blank was of the order of 0.1ng during the period of chemistry processing. The measurement of $^{143}Nd/^{144}Nd$ ratios is in progress.

Very pure feldspar crystals from cores and from selected drilled strata were also prepared for $^{40}Ar/^{39}Ar$ dating for the results of which we are waiting.

Drilling mud gas monitoring was carried out to gain new insights into the structure of the fluid regime at depth and to understand migration processes of deep circulating fluids. Gas was extracted mechanically from the circulating drilling mud in a separator tank equipped with a motor which drives an inside propeller. The separator was placed at the so-called "Possum

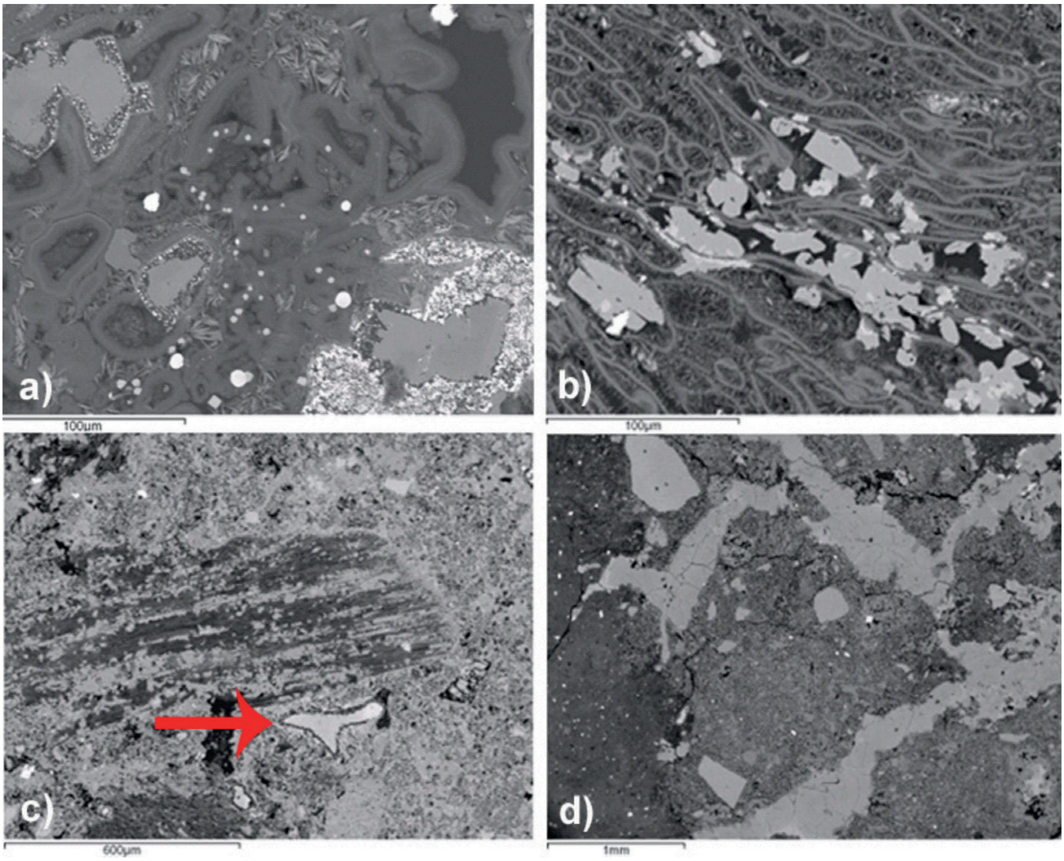

Fig. 2 – Back-scattered electron images (core at 500 m): a) widespread hydrothermal alteration in argillitic phases; b) Illite/montimorillonite and glauconite plats grown in pumice pipes; c) dolomite in isolated cuspate grains; d) within rocks fractures.

Belly" before the mud runs over the shale shakers. A slight vacuum was established to improve gas extraction and to pump the gas into a nearby container for real-time gas analysis. Delay time between gas extraction and analysis was determined with 2 minutes. All data were corrected for this delay.

In the container, condensed water was removed from the gas phase. The gas was then analyzed with a quadrupole mass spectrometer (QMS, Balzers OmniStar) for N_2, O_2, CH_4, CO_2, H_2, He and Ar.

Results and conclusions. The analyzed gas phases mainly consist of CO_2 with lower amounts of CH_4 and local outflow of H_2S. Highest gas concentrations were observed in the lowermost 30 m. The temperature at 410 m was ~60°C and the thermal gradient was ~0.1°C/m. The total gamma ray emission varies in the range of 80-220 gAPI, with an average at 162 gAPI. The Vp/Vs ratio is similar to the value at the surface and displays an evident reduction between 170 and 210 m reaching values close to 2 below 210 m. Compared to the mean value of Vp/Vs found by Battaglia *et al.* (2008) that is close to 1.8, the measured values in the hole are very high. The resistivity logs indicate a stratified subsurface.

Macroscopic and microscopic investigations together with diffraction data on mud samples allows: a) defining the primary sample lithology; 2) describing the relationships among texture, mineralogy and depth of the drilled rocks; 3) examining the character of the secondary minerals. SEM-EDS analyses of the two cored rocks showed a widespread hydrothermal alteration due circulation of thermal fluids. Sr-isotope data provide constraints to stratigraphic correlations. In particular, the drilled rocks are generally made of mostly pumices and subordinately scoriae with variable crystals and vesicles, and include dense lithic-type grains such as gray lavas and hydrothermal altered clasts. Crystals are up to several mm in size and include plagioclase, pyroxene, biotite, and rare magnetite.

We can, therefore, reconstruct a complex pyroclastic sequence emplaced during several episodes of explosive eruptions and through secondary sedimentation in both subaerial and submarine environments. The sequence includes (top downward) i) pyroclastic deposits composed of variably vesicular and porphyritic fragments, ii) a succession of pyroclastic and volcanoclastic beds made up of sub-rounded or rounded vesicular to dense, heterogeneous pyroclastic fragments containing a variable amount of siliceous fossils, carbon, wood fragments and peat, iii) a ~60 m-thick level dominated by brown dense to vesicular glass fragments, iv) a low crystalline greenish tuffs between -270 to -470 m, and v) a basal gray pumice- and -scoriae bearing tuff. The amount of primary crystals is higher in the shallow 260 m and very low porphyricity was detected in the 260-470 m depth range. The marine paleoenvironment is testified by exclusively siliceous fossil remains.

Secondary minerals appear and increase in abundance from 320 m; they include pyrite, carbonate and adularia. The secondary paragenesis of cores is more complicated consisting mostly of illite/montimorillonite and glauconite as replacement of primary volcanic glass (Fig. 2a) or dispersed within pumice pipes (Fig. 2b). The cement matrix is made of dolomite in isolated cuspate grains (Fig. 2c) and filling the veins (Fig. 2d). EDS analyses showed a pyrite mineralization surrounding rhombohedral carbonates. Albite is widespread, while sulphides and sulphates are generally rare (< 5% by area).

Sr-isotope data are in the range of values detected in Campi Flegrei rocks (Di Renzo *et al.*, 2011; Pabst *et al.*, 2011), allowing correlation with outcropping deposits.

Textural, mineralogical, petrographic and isotopic results will be corroborated by Ar-dating to reconstruct the stratigraphyic sequence and the history of caldera in this sector.

Acknowledgements. This work has been supported by ICDP-CFDDP and PON-MON.I.C.A. projects. The VULCAMED project provided funds to install the XRD laboratory at the Istituto Nazionale di Geofisica e Vulcanologia, in Naples. Thanks are due to key partner Bagnolifutura S.p.A.. We thank the staff of the Laboratorio of Mass Spectrometry at the Istituto Nazionale di Geofisica e Vulcanologia - Osservatorio Vesuviano and in particular I. Arienzo for the kindly laboratory assistance.

References

Agip; 1987: *Geologia e geofisica del sistema geotermico dei Campi Flegrei*. Unpublished Internal Report, 17 pp.

Battaglia J., Zollo A., Virieux J. and Dello Iacono D.; 2008: *Merging active and passive data sets in travel-time tomography: The case study of Campi Flegrei caldera (Southern Italy).* Geophys. Prosp., 56, 555-573, Doi:10.1111/j.1365-2478.2007.00687.x. 55.

Calderoni G. and Russo F.; 1998: *The geomorphological evolution of the outskirts of Naples during the Holocene: a case study of the Bagnoli-Fuorigrotta depression.* The Holocene, 8, 581 - 588.

Carlino S., Somma R., Troise C. and De Natale G.; 2012: *The geothermal exploration of Campanian volcanoes: Historical review and future development*. Renewable and Sustainable Energy Reviews, 16, I, 1004-1030, DOI:10.1016/j.rser.2011.09.023.

Chiodini G., Frondini F., Cardellini C., Granirei D., Marini L. and Ventura G.; 2001: *CO2 degassing and energy release at Solfatara volcano, Campi Flegrei, Italy.* J. Geophys. Res., 106, 213-221.

D'Auria L., Giudicepietro F., Aquino I., Borriello G., Del Gaudio C., Lo Bascio D., Martini M., Ricciardi G.P., Ricciolino P. and Ricco C.; 2011: *Repeated fluid-transfer episodes as a mechanism for the recent dynamics of Campi Flegrei caldera (1989- 2010).* J. Geophys. Res., 116, B04313, DOI:10.1029/2010JB007837.

Deino A.L., Orsi G., de Vita S. and Piochi M.; 2004: *The age of the Neapolitan Yellow Tuff caldera forming eruption (Campi Flegrei caldera - Italy) assessed by 40Ar/39Ar dating method*. J. Volcanol. Geotherm Res., 133, 157-170.

Del Gaudio C., Aquino I., Ricciardi G.P., Ricco C. and Scandone R.; 2010: *Unrest episodes at Campi Flegrei: A reconstruction of vertical ground movements during 1905-2009.* J. Volcanol. Geotherm Res., 195, 48-56.

De Natale G., Pingue F., Allard P. and Zollo A.; 1991: *Geophysical and geochemical modelling of the 1982-1984 unrest phenomena at Campi Flegrei Caldera, southern Italy.* J. Volcanol. Geotherm. Res., 48, 199-222.

De Vivo B., Belkin H.E., Barbieri M., Chelini W., Lattanzi P., Lima A. and Tolomeo L.; 1989: *The Campi Flegrei (Italy) geothermal system: A fluid inclusion study of the Mofete and San Vito fields.* J. Volcanol. Geotherm. Res., 36, 303-326.

De Vivo B., Rolandi G., Gans P.B., Calvert A., Bohrson W.A., Spera F.J. and Belkin H.E.; 2001: *New constraints on the pyroclastic eruption history of the Campanian volcanic Plain (Italy).* Min. Petr., 73, 47-65.

Di Renzo V., Arienzo I., Civetta L., D'Antonio M., Tonarini S., Di Vito M.A. and Orsi G.; 2011: *The magmatic feeding system of the Campi Flegrei caldera: architecture and temporal evolution*. Chem. Geo., 281, 227-241, DOI: 10.1016/j.chemgeo.2010.12.010.

Guglielminetti M.; 1986: *Mofete geothermal field. Geothermics,* 15, pp. 781-790.

Isaia R., Marianelli P. and Sbrana, A.; 2009: *Caldera unrest prior to intense volcanism in Campi Flegrei (Italy) at 4.0 ka B.P.: implications for caldera dynamics and future eruptive scenarios.* Geophys. Res. Lett., 36, L21303.

Mormone A., Tramelli A., Di Vito M.A., and Piochi M.; 2011: *Hydrothermal alteration minerals in buried rocks at the Campi Flegrei Caldera, Italia: a possible tool to understand the rock-physics and to assess the state of the volcanic system*. Per. Mineral., 80, 385-406, DOI: 10.2451/2011PM0027.

Orsi G., De Vita S. and Di Vito M.; 1996: *The restless, resurgent Campi Flegrei nested caldera (Italy): constraints on its evolution and configuration*. J. Volcanol. Geotherm Res., 74,179-214.

Pabst S., Wörner G., Civetta L., and Tesoro R.; 2008: *Magma chamber evolution prior to the Campanian Ignimbrite and Neapolitan Yellow Tuff eruptions (Campi Flegrei, Italy).* Bull. Volcanol., 70, 961-976, DOI 10.1007/s00445-007-0180-z.

Pappalardo L., Civetta L., D'Antonio M., Deino A., Di Vito M., Orsi G., Carandente A., de Vita S., Isaia R. and Piochi M.; 1999: *Chemical and Sr-isotopical evolution of the Phlegraean magmatic system before the Campanian Ignimbrite and the Neapolitan Yellow Tuff eruptions.* J. Volcanol. Geotherm. Res. 91, 141-166.

Parascandola A.; 1947*: I Fenomeni Bradisismici del Serapeo di Pozzuoli. Stabilimento Tipografico G. Genovese,* Naples, Italy.

Perrotta A., Scarpati C., Luongo G. and Morra V.; 2006: *The Campi Flegrei caldera boundary in the city of Naples. In Volcanism in the Campania Plain: Vesuvius, Campi Flegrei and Ignimbrites.* Elsevier, (ed. B. De Vivo), pp. 85-96.

Piochi M., Bruno P.P. and De Astis G.; 2005: *Relative roles of rifting tectonics and magma ascent processes: Inferences from geophysical, structural, volcanological, and geochemical data for the Neapolitan volcanic region (southern Italy).* Geochem. Geophys. Geosyst. 6, Q07005, DOI:10.1029/2004GC000885.

Rittmann A.; 1950: *Sintesi geologica dei Campi Flegrei.* Boll. Soc. Geol. It., 69, 117-28.

Rosi M., Sbrana A. and Principe C.; 1983: *The Phlegrean Fields: structural evolution, volcanic history and eruptive mechanism.* J. Volcanol. Geotherm Res., 17, 273- 288.

Rosi M. and Sbrana A.; 1987: *Phlegrean Fields: Petrography.* Quaderni de La Ricerca Scientifica 114, 9, 60-79.

Smith V.C., Isaia R. and Pearce N.J.G.; 2011: *Tephrostratigraphy and glass compositions of post-15 kyr Campi Flegrei eruptions*: *implications for eruption history and chronostratigraphic markers.* Qua. Sci. Rev., 30, 3638-3660, DOI: 10.1016/j.quascirev.2011.07.012.

Todesco M., Rinaldi A.P. and Bonafede M.; 2010: *Modelling of unrest signals in heterogeneous hydrothermal systems.* J. Geophys. Res., 115, B09213, 1-19, DOI:10.g29/ 2010JB007474.

Troiano A., Di Giuseppe M.G., Petrillo Z., Troise C. and De Natale G.; 2011: *Ground deformation at calderas driven by fluid injection: modelling unrest episodes at Campi Flegrei (Italy).* Geophys. J. Int., 187, 833-847, DOI: 10.1111/j.1365-246X.2011.05149.x.

GEOTHERMAL RESOURCES IN THE CARBONATE AQUIFERS OF THE FRIULI VENEZIA GIULIA COASTAL AREA: PRELIMINARY CONCEPTUAL MODEL

R. Petrini[1], F.F. Slejko[2], B. Della Vedova[3], U. Aviani[2], F. Iadarola[4], F. Italiano[5], M. Ponton[2], L. Zini[2]
[1] *Dipartimento di Scienze della Terra, Università di Pisa, Italy*
[2] *Dipartimento di Matematica e Geoscienze, Università di Trieste, Italy*
[3] *Dipartimento di Ingegneria e Architettura, Università di Trieste, Italy*
[4] *Ordine Regionale dei Geologi del Friuli-Venezia Giulia, Trieste, Italy*
[5] *INGV-Sezione Palermo, Italy*

Introduction. The high-temperature geothermal systems exploited for the generation of electric energy, are generally associated to areas of active volcanism or recent magmatism. In these systems heat is transferred from the deep source to the shallow reservoirs by magmatic intrusions and circulating fluids.

However, low enthalpy geothermal resources may be hosted in buried karsted or fractured carbonates of the foreland areas and adjacent sedimentary basins, mainly when they are structurally controlled. The geothermal fluids contained in these reservoirs are receiving much attention in recent years, for residential and commercial heating, balneology and recreational purposes and likely represent the most important type of shallow geothermal resources outside volcanic areas (Goldscheider *et al.*, 2010). A systematic assessment, evaluation and mapping of these resources, at regional scale, would hence provide a useful basis for their correct management and sustainable use to avoid overexploitation.

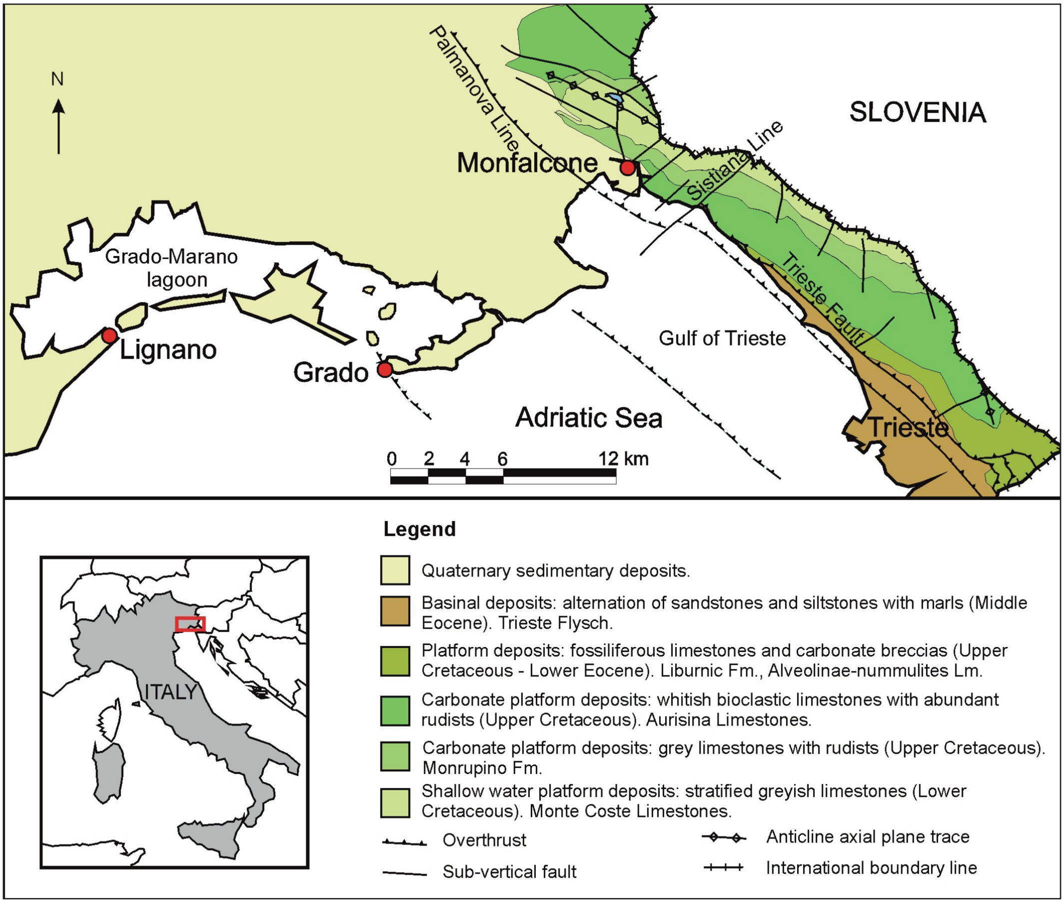

Fig. 1 – Geological sketch map showing the main lithologies and lineaments. The sites of the Monfalcone station, Grado-1 and Lignano deep well are indicated.

The geochemical fingerprints of thermal fluids contribute significantly in planning resources assessment, sustainable exploitation, and in mitigating possible environmental threats. In particular, the trace element geochemistry, the application of conservative and non-conservative isotopic systematics and the geochemistry of dissolved gas species can be used to investigate the fluid origin, the water-rock and water-gas interaction processes and in the reconstruction of the flowpaths at depth.

The present study is focused on a conceptual model for the geothermal water reservoirs hosted in the Mesozoic and Early Paleogene carbonates of the Friuli Venezia Giulia carbonatic platform buried beneath the north-Adriatic coastal plain, to understand formation hypothesis, evolutionary patterns through time and hydrothermal circulation paths, possibly enabling an improved assessment of the geothermal resources.

Geology and water sampling. The carbonatic reservoirs in the study area (Cesarolo-1 well) consist of Upper Jurassic-Lower Cretaceous well-stratified limestones with breccias, overlain by karstified limestones with abundant rudists and dolostones dated Upper Cretaceous and locally by grey bioclastic limestones dated Upper Cretaceous – lower Eocene. These sequences are buried beneath the Quaternary and Late Cenozoic (flysch and molasses) sediments which blanket the Adriatic Apulian foreland. Multi-channel seismic profiles and high-resolution single-channel profiles acquired by OGS and University of Trieste across the Grado-Marano lagoon and the Gulf of Trieste, in addition to the regional information obtained from ENI exploration wells and seismic profiles inland, indicate the occurrence of SW-verging Dinaric compressive structures, segmented by NE-SW-oriented faults with normal and transcurrent components (Cimolino *et al.*, 2010). During Neogene times the inherited Alpine NW-SE ramp-anticline of the thrust underwent a northward tilting and deformation, connected with the evolution of the South Alpine foreland. The paleogenic Dinaric thrusts (often reactivated in Neogene times) involve the carbonatic platform which is fractured, karstified and affected by intense deformational regimes, mainly in its upper portion.

Waters were collected from natural thermal springs, thermal baths and wells near the Monfalcone thermal springs (Petrini *et al.*, 2013); from the Grado-1 deep well (1100 m: Della Vedova, 2009) and from a deep well in Lignano Sabbiadoro (1505 m) (Fig. 1).

Experimental methods. Water physical-chemical parameters were measured in the field. Major ion chemistry was determined by conventional ion chromatography. Trace elements were determined by ICP-OES and ICP-MS spectroscopy. Oxygen and hydrogen isotopic data were determined by IRMS using a Delta Plus spectrometer: The isotopic data were expressed as per mil deviation from the V-SMOW standard (Vienna Standard Mean Ocean Water) using the conventional $\delta^{18}O$ and δD notation, where $\delta = [(R_{sample}/R_{standard}) - 1] \times 1000$ (‰) and R represent the $^{18}O/^{16}O$ or D/H isotopic ratios. The strontium isotopic composition was determined by thermal ionization mass-spectrometry (TIMS), after chemical extraction of the element by the matrix using ion-exchange chromatography. The measures of the $^{87}Sr/^{86}Sr$ ratio were fractionation-corrected using $^{86}Sr/^{88}Sr=0.1194$. Chemical analyses were carried out on the gas phase extracted after the attainment of equilibrium (at constant temperature) between the water sample and a known volume of host, high purity gas (argon), injected inside the sampling bottle. The analytical determinations were carried out by gas-chromatography.

Results and discussion. It is observed that waters with the highest electrical conductivity are characterized by the highest temperature, suggesting that the geothermal reservoir feeding all the sampling sites is constituted by saline waters. In the Monfalcone area, waters from springs, thermal baths and wells define a dilution series, indicating that in this site the uprising thermal waters mix with fresh and colder waters. The molar ratios between major and trace constituents which behave conservatively, such as chloride and bromide, indicate that the saline thermal end-member is seawater.

Using chloride as a marker of the marine component, it is noted that most major and trace ions are distributed along a simple binary mixing line between the seawater end-member, best represented by geothermal waters from the Lignano well, and a low-chloride term, which is consistent with karst-type waters. Waters from the Grado-1 well are in intermediate position, suggesting that also in this case a dilution process likely occurs at depth.

However, some elements deviate from these correlations. In particular, the spring and well waters collected at Monfalcone are characterized by sulfate excess with respect to the mixing trend. The sulfate *surplus* might represent the record of processes occurring at depth. In particular, high sulfate values with increasing temperature are found in thermal waters hosted in carbonate aquifers and are attributed to the reaction of sulfuric acid produced by oxidation of hydrogen sulfide generated by the microbial reduction of sulfates with the calcite of the hosting carbonates, providing that sufficient oxygen becomes available, according to reactions such as:

$$H_2S+2O_2=H_2SO_4$$

and

$$H_2SO_4+2CaCO_3=2Ca^{2+}+SO_4^{2-}+2HCO_3^-.$$

These reactions also contribute to the creation of secondary porosity. In this scenario, a deeper mixing process of the saline end-member with oxygenated waters would occur, at least in this sector eastern of the carbonatic platform.

In water samples from the Roman thermal baths, characterized by an increasing in dilution, the sulfate excess is not observed, possibly reflecting the additional admixing of shallow freshwaters from soils.

On the contrary, waters from the Grado-1 well are displaced towards lower sulfate content with respect to the mixing trend, likely reflecting the depletion of SO_4^{2-} due to reduction processes and sulfide production. Sulfate depletion is even larger in the Lignano well waters, suggesting that in this western sector of the aquifer reductive reactions were enhanced.

The Ca ion content in waters from the Monfalcone springs and wells, Grado-1 well and Lignano well also shows an excess in concentration with respect to a binary mixing, still assuming chloride as conservative. The Ca *surplus* is the highest in Lignano well waters. This is interpretable as the interaction of the waters with Cretaceous limestones of the carbonatic platform which provide a *surplus* of Ca, hence reflecting diagenetic reactions of the thermal waters with hosting lithologies.

The oxygen and hydrogen isotopic data also support the hypothesis of a thermal marine component that progressively mixes with low-salinity waters of meteoric origin; the effects of mixing are negligible or small for the Lignano well waters. This is consistent with the observation that these waters are the closest to the saline end-member.

The Sr isotopic composition ($^{87}Sr/^{86}Sr$ ratio) is significantly lower with respect either to the $^{87}Sr/^{86}Sr$ ratio of modern seawater standard (MSS, $^{87}Sr/^{86}Sr$ = 0.70918) or to the present-day seawater sampled offshore the Friuli coastline ($^{87}Sr/^{86}Sr$ ratio of 0.70917±0.00002). These data indicate that the saline end-member is likely represented by connate fluids. In addition, the Sr-isotope ratios are higher compared with those reported for the Upper Cretaceous limestone (average $^{87}Sr/^{86}Sr$=0.70760). It has also to be noted that in the Monfalcone dilution series, the Sr isotopic composition does not correlate with electrical conductivity, chloride content and, in general, with major and trace ion content. This suggests that the $^{87}Sr/^{86}Sr$ ratio is not significantly affected by the mixing of the saline thermal component with freshwaters, as expected on the basis of mass-balance considerations. Thus, the Sr-isotope ratio can be used to infer the pristine isotopic composition of the marine end-member. This has been obtained by mass balance calculations; the obtained results yield an $^{87}Sr/^{86}Sr$ ratio ranging between 0.7083 and 0.7088, corresponding to a Miocene "age". It is hence suggested that the deep saline reservoir in Mesozoic carbonates from the Friuli platform represents the remnant of paleo-seawater, entrapped in the deeper formations during the late Oligocene - Miocene sea transgression, connected with the northward tilting of the ramp anticlines.

The gases dissolved in groundwaters provide information on the gas-water interactions (GWI) occurring in the subsurface hydrologic systems, in order to distinguish a dissolved atmospheric component (air saturated water, ASW) and gas phases released from deeper sources. The waters from the Monfalcone site, and in particular Grado-1 and Lignano wells, lie far from the typical ASW composition, showing enrichments in both He and CO_2.

Since the ^4He abundance produced by the α decay of the parent uranium and thorium nuclides which are present in rocks and sediments increases with the rock-water-gas contact time, high ^4He concentrations are common in groundwaters characterized by long residence times. The $^3He/^4He$ helium isotope-ratio normalized to the atmosphere (R/Ra) is in the range 0.08-0.27 at Monfalcone, and has values of 0.04 and 0.02 in the waters from the Grado-1 and Lignano wells, respectively. ^3He values below the atmospheric $^3He/^4He$ ratio, with ^4He resulting from mixing of deep-derived and atmospheric-derived helium to various extents support the hypothesis of a significant input of gas from crustal sources, as highlighted by the correlation in the He/Ne vs. R/Ra diagram (Fig. 2), which indicate the mixing between a crustal end-member and a water component equilibrated with the atmosphere. This is mostly evident in the Lignano well waters. The dissolved gas data also indicate that samples are characterized by the interaction with a CO_2-rich gas phase, in particular at the Grado-1 well,

The temperature of the end-member seawater in the reservoir, modeling the evolutionary trends of seawater-carbonate interaction using PHREEQC and the observed correlations, is estimated between 65-70 °C. The various amount of mixing increasing from the Lignano end-member saline water, to the Grado and Monfalcone reservoirs is also consistent with the inverse trend of decreasing temperatures from Lignano-Cesarolo (58-65 °C), to Grado well (42-44 °C) and Monfalcone springs (32-41 °C).

Conclusions. The thermal waters hosted in the Mesozoic carbonatic platform of the Friuli Venezia Giulia coastal area have the nature of ancient, diagenetically modified seawater. Sr-isotopes indicate that the deep saline reservoir might represent remnants of seawater entrapped in the Cretaceous carbonate strata during the late Oligocene - Miocene sea transgression which followed the uplift of some portions of the carbonatic units during upper Eocene. The carbonatic aquifer has a complex geometry, is confined and interested by important fault systems which allow the development of hydrothermal cells and some local mixing with the shallower freshwater aquifers. The data indicate that the waters outflowing at Monfalcone and sampled by the deep wells of Grado-1 and Lignano likely fed by the same regional saline reservoir, which underwent interactions with more superficial aquifers at different extent in the different sites.

Acknowledgements. Società Imprese Lignano-SpA is acknowledged for allowing waters of the Lignano deep well to be sampled.

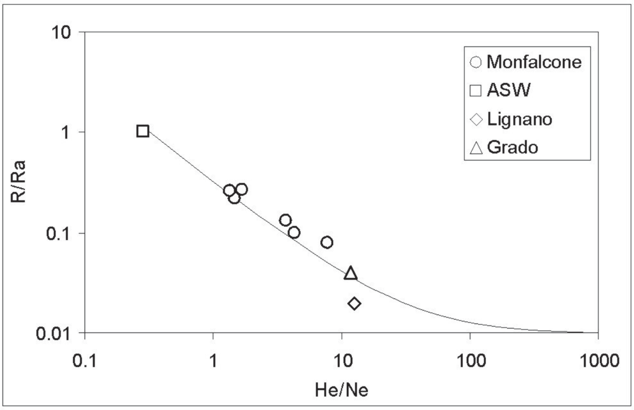

Fig. 2 – He/Ne vs. R/Ra ratios. Samples lie on a mixing line between ASW and a radiogenic-type end-member of crustal origin (solid line).

References

Cimolino A., Della Vedova B., Nicolich R., Barison E., Brancatelli G.; 2010: *New evidence of the outer Dinaric deformation front in the Grado area (NE-Italy).* Rend. Fis. Acc. Lincei, **21**, 167-179.

Della Vedova B.; 2009: *Geothermal potential of the carbonatic platform buried beneath the Veneto and Friuli coastal areas: results from the Grado-1 borehole.* FIST Congress, Rimini, September 9-11, E1-E8.

Goldscheider N., Mádl-Szónyi J., Eróss A., Schill E.; 2010: *Review: Thermal water resources in carbonate rock aquifers.* Hydrogeol. J., **18**, 1303-1328.

Petrini R., Italiano F., Ponton M., Slejko F.F., Aviani U., Zini L.; 2013: *Geochemistry and isotope geochemistry of the Monfalcone thermal waters (northern Italy): inference on the deep geothermal reservoir.* Hydrogeol. J., **21**, 1285-1287.

GEOCHEMICAL CHARACTERIZATION OF THE SAN CALOGERO THERMAL SPRING (LIPARI): INDICATIONS OF ACTIVE JUVENILE CONTRIBUTIONS

F. Picone[1], G. Bianchini[1], F. Italiano[2], M. Martelli[2], C. Marchina[1], N. Colombani[1], R. Tassinari[1]

[1]*Dipartimento di Fisica e Scienze della Terra, Università di Ferrara, Italy*

[2]*Istituto Nazionale di Geofisica e Vulcanologia (INGV), Sezione di Palermo, Italy*

Introduction. The San Calogero thermal spring is located in the Island of Lipari (Aeolian volcanic arc) and was known (and used) since Greek and Roman times, thus representing an important archeological and cultural site. In this contribution that will be presented at the GNGTS Conference, we report new geochemical and isotopic data that could be useful for a better understanding of the observed thermal components. Results are important taking into consideration the existing project of restoration and qualification of the investigated thermal resource.

Geological framework and background information. The Aeolian archipelago is located in the south-eastern margin of the Tyrrhenian sea and is interpreted as a volcanic arc located about 250 km above a subducting slab (Beccaluva *et al.*, 1985; Peccerillo *et al.*, 2005). The igneous processes are still effective and represented by active volcanoes: Stromboli, with persistent activity; Vulcano, which had numerous explosive eruptions during historic times, the last of which occurred in 1888-1890; and Lipari where the last eruption took place about 1400 y.b.p. in the northeastern part of the island (Tranne *et al.*, 2000).

Low-temperature fumaroles (80-90 C°) and hot springs are currently the only manifestations of volcanic heat in Lipari. The volcanic and structural evolution of Lipari is well known (Crisci *et al.*, 1991). The oldest Lipari products consist of 223-150 kyr-old basalt-andesitic lavas erupted from submarine vents and from subaerial volcanoes. The successive volcanism (from 127 to 92 kyr) occurred in the central sector of the island, where the activity of the Mt. S. Angelo and Costa d'Agosto volcanoes (high-K andesitic lavas and pyroclastics) developed within the Mt. S. Angelo depression. After a gap in volcanic activity of about 50 kyr, volcanism resumed in the southern sector of the island with the emplacement of rhyolitic–shoshonitic pyroclastics and of the N-S-aligned South Lipari and Mt. Guardia domes (42-20 kyr). This activity developed within a pre-existing volcanotectonic depression formed between 92 and 42 kyr. The last phase of activity on Lipari developed in the northeastern sector of the island where the 11.4-1.41 kyr-old N–S-aligned Gabellotto, Forgia Vecchia, and Pilato rhyolitic eruptive centers occur.

The structural setting of Lipari is defined by fault segments and associated fractures which can be grouped in two main sets striking NNW–SSE/NW– SE and from N–S to ENE–WSW. The results of previous geological, structural and geochemical prospecting performed in the study area suggest the possible presence of a high-enthalpy geothermal system on the Island (Bruno *et al.*, 2000). This system, similar to what was observed in analogous geological environments, is probably made up by a magmatic heat source and by a convective circulation of shallow waters that seep through the volcanic rocks. Consequently, these waters are heated by the source and rise back to the earth surface. All thermal emergencies discovered on the island seem connected with the tectonic structures cutting the western sector of Lipari. Along some of these structures, remarkable hydrothermal alteration phenomena that generated kaolin and alum deposits, which are known since ancient times, are present.

According to the geophysical study of Bruno *et al.* (2000) the investigated thermal spring of San Calogero is located close to a direct fault that juxtaposed two distinct lithologies characterized by different permeability, i.e. 1) an andesite lava flow and 2) a pyroclastic deposit. According to historical chronicles (Cavallaro, 1954) the temperature recorded at the spring decreased, as it was 93 °C in the year 1872, ca. 60 °C in the 1950. The temperature decrease has been coupled with a decrease in the discharge that is currently varying between 40 and 90 liters per hour.

Geochemical characterization of the thermal water of San Calogero. The waters have been sampled during a period of 2 years (August 2012 - April 2013) to evaluate the compositional variations. In situ measurements of samples (Sg) collected in the proximal point of emission of the spring showed that temperature and pH range between 40-50°C and 7.0-7.6, respectively, whereas the electric conductivity varies between 2.4 and 2.9 milliSiemens/cm. Slightly higher pH (7.6-7.9) and lower temperature are observed in samples (Th) collected in the old thermal building (named tholos) located 20 m far from the emission point, in relation to CO_2 escape and $CaCO_3$ precipitation that is observed as diffuse carbonate concretions.

The water samples were subsequently investigated in the laboratories of the Department of Physics and Earth Science of the University of Ferrara using an ion-chromatograph DIONEX ICS-1000 for the analysis of anions and an inductively coupled plasma mass spectrometer (ICP-MS; X Series, Thermo-Scientific) for the analysis of major cations and trace elements. Certificated standards were periodically used to calibrate measurements and to verify analytical precision and accuracy. Results, reported in Tab. 1 and Fig. 1, indicate that the TDS varies between 2050 and 2200 mg/l, with a hydrochemical facies characterized by sulphate as predominant anion, and sodium and magnesium dominating among cations.

Tab. 1 – Chemical composition (expressed in mg/l) of the San Calogero thermal water sampled during the period August 2012 – April 2013. The label *Sg* refers to the samples taken in the proximal point of emission of the spring, while the label *Th* refers to samples taken in the old thermal building named tholos. Note that arsenic concentration often exceeds the WHO standard for drinkable water.

sample	Sg	Th
Cl	250-282	263-283
Br	0.5-0.7	0.4-0.5
NO_3	18.1-23.6	15.7-29.3
SO_4	895-1110	932-1018
HCO_3	450-600	435-510
Ca	87.2-142	54.5-87.6
Mg	83.6-96.3	68.7-95.0
Na	240-283	240-272
K	23.4-27.2	21.8-29.3
Li	0.06-0.10	0.06-0.09
Rb	0.02-0.04	0.02-0.04
Sr	2.36-3.72	1.3-2.3
B	0.05-0.20	0.03-0.11
As	0.01-0.02	0.01

Noteworthy, the studied waters display a constant SO_4/Cl (3.4-3.6) ratio very similar to that recorded in the historical hydrochemical investigations carried out in the fifties (Cavallaro, 1954). This is probably an indication of a constant long term supply of juvenile fluids. The Cl^-/Br molar ratio with values near 1200 suggests a non marine origin of the groundwater,

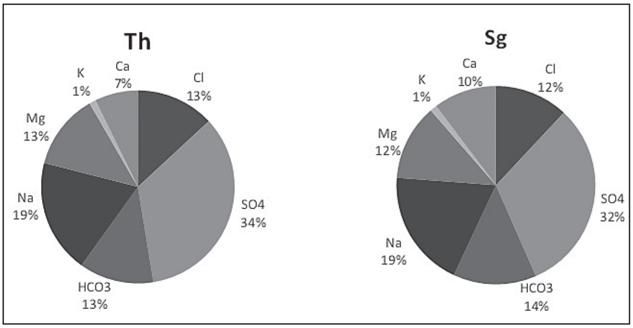

Fig. 1 – Pie chart showing the major elements relative abundance of San Calogero thermal waters (starting compositions expressed as milliequivalents per liter). The label *Sg* refers to the samples taken in the proximal point of emission of the spring, while the label *Th* refers to samples taken in the old thermal building named tholos.

since typical seawater values range around 655±4 (Alcalà and Custodio, 2008). This finding coupled with elevated dissolved CO_2 concentrations is consistent with the results of Custodio and Herrera (2000), suggesting a volcanic origin.

The $^{18}O/^{16}O$ and $^{2}H/^{1}H$ isotopic composition of the studied water were determined, by laser absorption spectrometry using the CRDS LOS GATOS LWIA 24d isotopic analyzer. Results were reported as $\delta^{18}O$ and δD (relative to SMOW) in Tab. 2 and Fig. 2.

Tab. 2 – Oxygen and hydrogen isotopic analyses of the San Calogero thermal water, expressed as δ units respect to SMOW (Standard Mean Oceanic Water). The label *Sg* refers to the samples taken in the proximal point of emission of the spring, while the label *Th* refers to samples taken in the old thermal building named tholos.

	δD‰	**δ18O‰**
sampling date	**Sg**	
08/08/2012	-24.4	-6.54
31/08/2012	-23.4	-6.57
29/03/2013	-28.0	-5.53
09/04/2013	-28.7	-5.58
	Th	
08/08/2012	-27.3	-5.03
31/08/2012	-26.2	-5.13
28/12/2012	-29.1	-4.45
30/12/2012	-28.6	-4.90

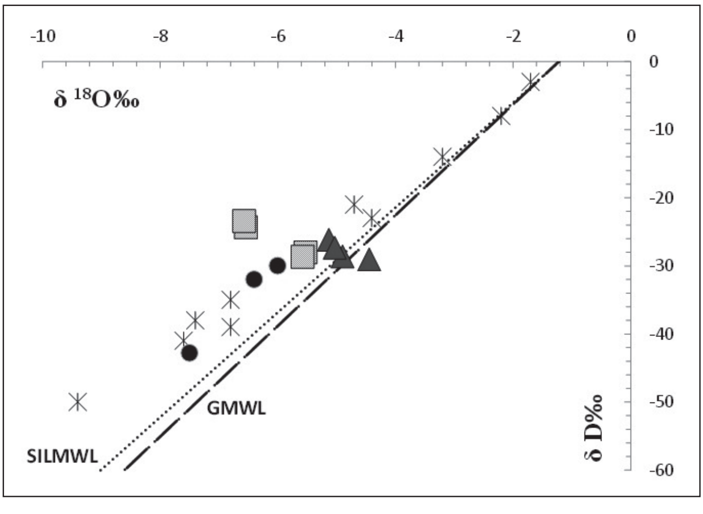

Fig. 2 – The isotopic ratios of oxygen and hydrogen show deviation from the global meteoric water line (GMWL; Craig, 1961), the Southern Italy Local Meteoric Line (SILMWL; Longinelli and Selmo 2003) and from the precipitations on Stromboli and Vulcano. *Sg* and *Th* waters from San Calogero are represented with grey squares and black triangles, respectively. Asterisks and black circles represent the rainfall in Stromboli and Vulcano, respectively (Cortecci *et al.*, 2001; Liotta M. *et al.* 2006; Federico *et al.*, 2010).

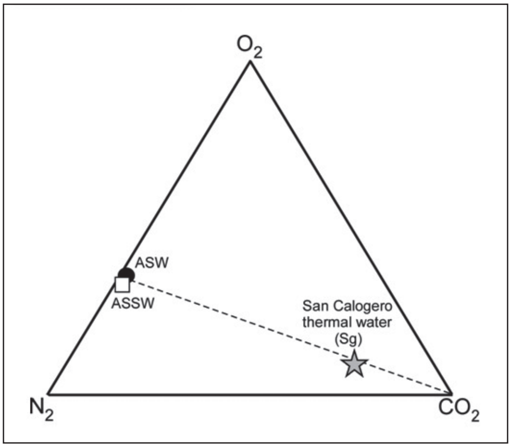

Fig. 3 – Gases dissolved in the San Calogero thermal water (Sg; star) compared with the composition of Air Saturated Water (ASW; black circle) and Air Saturated Sea Water (ASSW; white square). Note the predominance of CO_2 that characterize the studied thermal water.

Isotopic compositions of water sampled just at the spring (label Sg) diverge from the notional meteoric lines, further suggesting the possible involvement of deep juvenile fluids.

This hypothesis is corroborated by the investigation of the dissolved gases, carried out in the laboratories of the Istituto Nazionale di Geofisica e Vulcanologia (INGV, Palermo), according to the method described by Capasso and Inguaggiato (1998) and Liotta and Martelli (2012). Results reported in Tab. 3, indicate that the dissolved CO_2 appears nearly 100 times higher respect to that expected in water equilibrated with the atmosphere (see Fig. 3).

The delineated framework is compatible with the carbon isotopic signature (on DIC) measured according to the method of Capasso *et al.* (2005) that revealed a $\delta^{13}C$ (relative to PDB) of -4.2 ‰. Starting from this value, the carbon isotope composition of CO_2 gas phase in equilibrium with the sampled water can be calculated. According to the isotopic fractionations delineated by Grassa *et al.* (2006) the CO_2 equilibrated with this water at the sampling temperature should have a $\delta^{13}C$ of -10 ‰. This value is clearly lower than that expected for a carbon originated in mantle horizons in Mediterranean area ($\delta^{13}CO_2$ = -3 to 0 ‰, e.g. Capasso *et al.*, 1997) and testifies an addition of light carbon, probably of shallow organic origin. It is worth of notice that, in agreement with many other thermal spring of Sicily and surrounding islands, the S. Calogero carbon content and isotopic ratio fall into the two-endmember mixing proposed by Grassa *et al.* (2006) between a magmatic (-3 to 0 ‰) and an organic (lower than -20 ‰) term. Unfortunately, the $^3He/^4He$ and $^4He/^{20}Ne$ ratios measured in the gas phase dissolved into San Calogero waters (method of Inguaggiato e Rizzo, 2004) shows a clear atmospheric contamination that covers the eventual presence of deep helium and does not allow to gain significant information from noble gases. Even if effort has been made in the field to collect the samples as close as possible to the water emergence point, the presence of noble gases with atmospheric signature suggests that waters have the possibility to interact with air, possibly shortly before the emergence at surface.

Tab. 3 – Composition of gases dissolved in the thermal water of San Calogero (*Sg*), expressed in ml (at Standard Temperature and Pressure, STP) per liter.

He	O_2	N_2	CH_4	CO_2
6.93E-05	4.84	12.43	2.21E-04	43.9

Conclusions. The upraising of reactive juvenile fluids hypothesized observing the geochemical data is coherent with the pervasive alteration of the volcanic rocks surrounding the spring. The source is probably a magmatic chamber that is plausibly in a cooling stage. Therefore the studied water seems to reflect a mixing between meteoric water and volcanic fluids, whereas the involvement of sea water is not observed. The observed decrease in the spring temperature and discharge is plausibly related to variations on the fluid paths that can occur both for natural or anthropogenic processes. Further investigation is in progress in order to refine and constrain the mentioned hypothesis.

References

Beccaluva L., Gabbianelli G., Lucchini F., Rossi P.L. and Savelli C.; 1985: *Petrology and K/Ar ages of volcanic dredged from Eolian seamounts: implications for geodynamic evolution of the Southern Tyhrrenian basin.* Earth Planetary Sciences Letters, 74, 187-208.

Bruno P.P.G., Paoletti V., Grimaldi M. and Rapolla A.; 2000: *Geophysical exploration for geothermal low enthalpy resources in Lipari Island, Italy.* Journal of Volcanology and Geothermal Research, 98, 173-188.

Capasso G., Favara R., Grassa F, Inguaggiato S. and Longo M.; 2005: *On-line technique for preparing and measuring stable carbon isotope of total dissolved inorganic carbon in water samples (δ 13C TDIC).* Annals of Geophysics, 48, 159-166.

Capasso G., Favara R., and Inguaggiato S.; 1997*: Chemical features and isotopic composition of gaseous manifestations on Vulcano Island, Aeolian Islands, Italy: An interpretative model of fluid circulation*. Geochim. Cosmochim. Acta, 61, 3425-3440.

Capasso G. and Inguaggiato S.; 1998: *A simple method for the determination of dissolved gases in natural waters. An application to thermal waters from Vulcano Island.* Applied Geochemistry, 13, 631-642.

Cavallaro C.; 1954: *Le acque termo-minerali di S.Calogero di Lipari*. Grafiche La Sicilia (Messina).

Cortecci G., Dinelli E., Bolognesi L., Boschetti T. and Ferrara G.; 2001: *Chemical and isotopic compositions of waterand dissolved sulfate from shallow wells onVulcano Island, Aeolian Archipelago, Italy.* Geothermics, 30, 69-91.

Craig H., 1961: *Isotopic variations in meteoric waters*. Science, 133, 1702-1703.

Crisci G.M., De Rosa R., Esperanca S., Mazzuoli R. and Sonnino M.; 1991: *Temporal evolution of a three component system: the island of Lipari (Aeolian Arc, southern Italy).* Bulletin of Volcanology, 53, 207-221.

Custodio E. and Herrera C.; 2000: *Utilizacion de la relacion Cl/Br como trazador hidrogeoquımico en hidrologıa subterranea*. Boletın Geologico y Minero, 111 (4), 49-67.

Federico C., Capasso G., Paonita A. and Favara R.; 2010: *Effects of steam-heating processes on a stratified volcanic aquifer: Stable isotopes and dissolved gases in thermal waters of Vulcano Island (Aeolian archipelago).* Journal of Volcanology and Geothermal Research, 192, 178-190.

Fischer P, Giggenbach W.F., Sano Y. and Williams S.N.; 1998: *Fluxes and sources of volatiles discharged from Kudryavy,a subduction zone volcano, Kurile Islands*. Earth and Planetary Science Letters, 160, 81-96.

Grassa F., Capasso G., Favara R. and Inguaggiato S.; 2006: *Chemical and isotopic composition of waters and dissolved gases in some thermal springs of Sicily and adjacent volcanic islands, Italy.* Pure appl. Geophys., 163, 781-807.

Inguaggiato S. and Rizzo A.; 2004: *Dissolved helium isotope ratios in ground-waters: a new technique based on gas-water re-equilibration and its application to Stromboli volcanic system*. Applied Geochemistry, 19, 665-673.

Liotta M., Brusca L., Grassa F., Inguaggiato S., Longo M. and Madonia P.; 2006: *Geochemistry of rainfall at Stromboli volcano (Aeolian Islands): Isotopic composition and plume-rain interaction*. Geochemistry, Geophysics, Geosystems 7, 7.

Liotta M., Grassa F., D'Alessandro W., Favara R., Gagliano Candela E., Pisciotta A. and Scaletta C.; 2013: *Isotopic composition of precipitation and groundwater in Sicily, Italy.* Applied Geochemistry, 34,199-206.

Liotta M. and Martelli M.; 2012: *Dissolved gases in brackish thermal waters: an improved analytical method.* Geofluids, 12, 236-244.

Longinelli A. and Selmo E.; 2003: *Isotopic composition of precipitation in Italy: a first overall map.* Journal of Hydrology, 270, 75-88.

Peccerillo A.; 2005: *Plio-Quaternary Volcanism in Italy.* Editor Springer.

Tranne C.A, Calanchi N., Lucchi F. and Rossi P.L.; 2000: *Carta geologica schematica di Lipari, scale 1:10000.* Edited by Agip.

SPACE-TIME CHANGES OF SEISMIC ACTIVITY AT MT. ETNA VOLCANO (ITALY) OBSERVED THROUGH STATISTICAL APPROACHES

S. Sicali[1,2], M.S. Barbano [1], S. D'Amico [2], G. Lombardo[1], F. Panzera [1,2]

[1] *Dipartimento di Scienze Biologiche, Geologiche e Ambientali, Università di Catania, Italy*

[2] *Osservatorio Etneo, Istituto Nazionale di Geofisica e Vulcanologia, Sezione di Catania, Italy*

Introduction. Volcanic processes can locally modify the normal stress state of a volcano, which generally is connected to the regional stress field. Volcanic eruptions are often preceded by changes both in the rate and the location of local volcano-tectonic earthquakes so that a statistical approach can give a clue to investigate about precursors (Alparone *et al.*, 2011; Bell and Kilburn, 2012). The analysis of the space-time variations of the hypocentral distribution during pre-eruptive and inter-eruptive periods, could provide important constrains for a better understanding of the link between seismicity and eruptive processes (Lombardo and Cardaci, 1994; Vinciguerra *et al.*, 2001). Besides, some authors have pointed out that, in a volcano, the analysis of the inter-event times (IETs) distribution pattern could represent an important tool to distinguish among sectors affected by different stress fields (e.g. Bell and Kilburn, 2008; Traversa and Grasso, 2010). An IET is defined as the waiting time between two consecutive earthquakes, related to a specific interval of time and a particular threshold of magnitude. The waiting time distribution of global or national size catalogues is usually modelled using a gamma law (Corral, 2003). This single-peaked distribution, typical of tectonic areas, is clearly different from the IET distribution for regional or local catalogues that generally has a bimodal shape deriving from the combination of two distributions, one due to correlated events (which have short inter-event time) and the other due to independent events (which tend to be separated by longer gaps) (Naylor *et al.*, 2010). Therefore, for a small region, the bimodal shape of IET distribution is heavily influenced by the high percentage of correlated events (aftershocks). IET analysis in the Etnean area was already performed by Sicali *et al.* (2012) investigating the seismic events occurred during the time interval 1988-2011 (Patanè e*t al.*, 2004; Gruppo Analisi Dati Sismici, 2011). The authors, aimed to identify the existence of either a periodicity or a stationary behaviour of the seismic activity and tried to correlate it with the volcano-tectonic features of the region. As a result of this study, the presence of different volcano sectors showing specific behaviour was set into evidence. The comparison between the spatial variation of Etna IET distributions with those obtained for Sicily and Italy, showed that at a large scale the IETs are well-modelled by a gamma distribution, whereas at the local Etnean scale the IETs are characterized by a bimodal curve. The two peaks are related to: (i) the background regional stationary seismicity, (ii) the contribution of the local seismic swarms with very short inter-event times, which considerably modify the usual seismic rate. Sicali *et al.* (2012) concluded that the seismicity taking place at depth shallower than 5 km is almost entirely represented by short IETs and is mainly confined to the Etna summit area. On the other hand, earthquakes deeper than 5 km, appear mainly linked to the regional tectonic setting. In particular, the eastern flank seismicity is influenced by the extensional regional tectonics typical of the eastern Sicily, whereas the western flank seismicity seems consistent with the compressional processes observed at a regional scale. Such findings further support the evidences that Mt. Etna is located at the boundary of two different tectonic domains (Neri *et al.*, 2005; La Vecchia *et al.*, 2007; Palano *et al.*, 2012).

In the present study a more thorough analysis, at a scale of the sectors previously identified, is performed in order to investigate about possible correlations between the occurrence of Etnean eruptions and its seismicity. The dataset used is now extended back to the period 1976-1987, matching the date coming from the IIV, Poseidon and INGV-CT seismic networks (Gruppo Analisi Dati Sismici, 2011) with those recorded by the seismic network run by University of Catania. This allow us to analyze a longer and more significant range of time which spans from 1976 to 2011, evaluating both the space-time IET distributions and the earthquake cumulative patterns in different sectors of the volcano.

Seismic data and method. The used catalogue consists of 12,645 earthquakes occurred at Mt. Etna from January 1976 to December 2011, which were recorded through the permanent seismic networks run by the University of Catania (1976-1987) and by the IIV-CNR (Istituto Internazionale di Vulcanologia), Sistema Poseidon and INGV-CT (Istituto Nazionale di Geofisica e Vulcanologia, Sezione di Catania) from 1988 up to 2011 (Patanè *et al.*, 2004; Gruppo Analisi Dati Sismici, 2011). Moreover, in addition to the permanent network, data recorded by several temporary seismic networks, held by different institutions, were added when available in order to reduce the gap in the azimuthal distribution of the recording stations. With the aim of having an homogenous catalogue, all recorded earthquakes were relocated using the HypoEllipse algorithm (Lahr, 1989) and the velocity model proposed by Hirn *et al.* (1991). The sensitivity of the seismic monitoring network at Mt. Etna (gap, erh, erz, rms, etc.) was gradually enhanced several times between 1976 and 2011 so that, the minimum magnitude of earthquakes located in the study area, varied over the time following the network upgrade.

Tests have been performed to evaluate the completeness of the catalogue and consequently a completeness magnitude Md = 2.5 has been obtained. According to this result, all further analysis have been carried out by selecting the earthquakes having such magnitude threshold and an hypocentre location uncertainty lower than 2.5 km, therefore obtaining a revised final dataset consisting of 2,762 earthquakes (Fig. 1a). Three different patterns of hypocenter distributions can be observed (Fig. 1b), therefore in order to obtain information about the

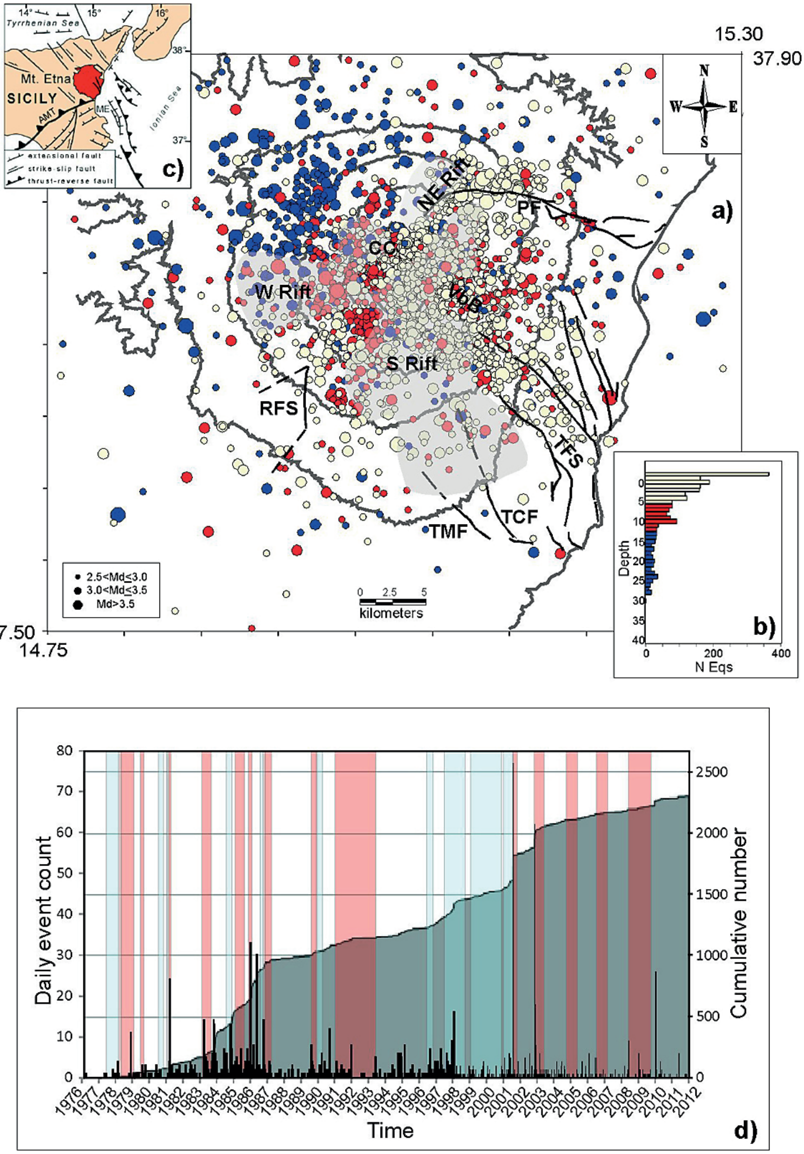

Fig. 1 – a) Epicentre location of earthquakes with magnitude Md > 2.5 occurring between 1976 and 2011 at Mt. Etna; circle size indicates magnitude classes; colours indicate the depth range (see inset b for details); black lines indicate the main faults: PF (Pernicana fault system), RFS (Ragalna fault system), TFS (Timpe fault system), TCF (Trecastagni fault), TMF (Tremestieri fault) (modified from Azzaro *et al.*, 2012); b) number of earthquakes vs. focal depth; c) structural settings of eastern Sicily; d) daily and cumulative number of earthquakes during the study period; the size of the red and blue bands indicates the duration of the flank and the summit eruptions, respectively (Andronico and Lodato, 2005; Bullettin data from http://www.ct.ingv.it/it/banca-dati-delle-eruzioni/eruzioni-etna.html).

seismic behaviour of different crustal volumes, a space-time analysis of the IETs has been performed by sub-grouping the earthquakes into three depth classes: 1) from the surface to 5 km b.s.l., 2) between 5 km and 12 km b.s.l. and 3) below 12 km b.s.l. We then have calculated the IET distributions and some associated statistical parameters (aperiodicity α, skewness S, kurtosis k) for all the earthquakes located within 3.5 km around each node, in a grid map having inter-node distance of 2 km. The statistical parameters allow quantifying the shape features of each IET distributions (Sicali *et al.*, 2012). The kurtosis k and the skewness S, provide a measure of the distribution "peakedness" and an indication of the peaks position with respect to high or low IET values. The aperiodicity α ($\alpha = \sigma/\mu$, where σ is the standard deviation and μ is the mean) represents a way to estimate the regularity of earthquake occurrence over time. In general the α value defines: (i) periodic regime, if $\alpha \sim 0$, $\sigma << \mu$; (ii) stationary regime, if $\alpha \sim 1$, $\sigma \sim \mu$; (iii) clusters regime, if $\alpha \geq 2$, $\sigma >> \mu$. The skewness is particularly suitable for our purposes since it gives information about the position of the dominant peak in the IET distribution (high or low IET values, in relation to negative or positive skewness).

Finally, in order to verify a possible correlation between the occurrence of eruptive phenomena and the activation of particular seismogenic volumes, following the results of IET analysis, we have analyzed the seismic rate - time variations of the seismic sectors characterized by different earthquake recurrence time.

Data analysis and discussion. In a recent study, Sicali *et al.* (2012) framed, through the analysis of spatial variation of IET distributions, the seismicity related to volcanic processes in the regional seismotectonic context highlighting the presence of sectors showing specific seismic behaviours. The statistical parameters suggest that the Mt. Etna is located at the boundary between two different regional domains. The IET distribution pattern, evaluated for depth z > 5 km, set indeed into evidence that the western sector of the volcano and north-western Sicily share similar recurrence times, whereas eastern sector of Mt. Etna shares similar

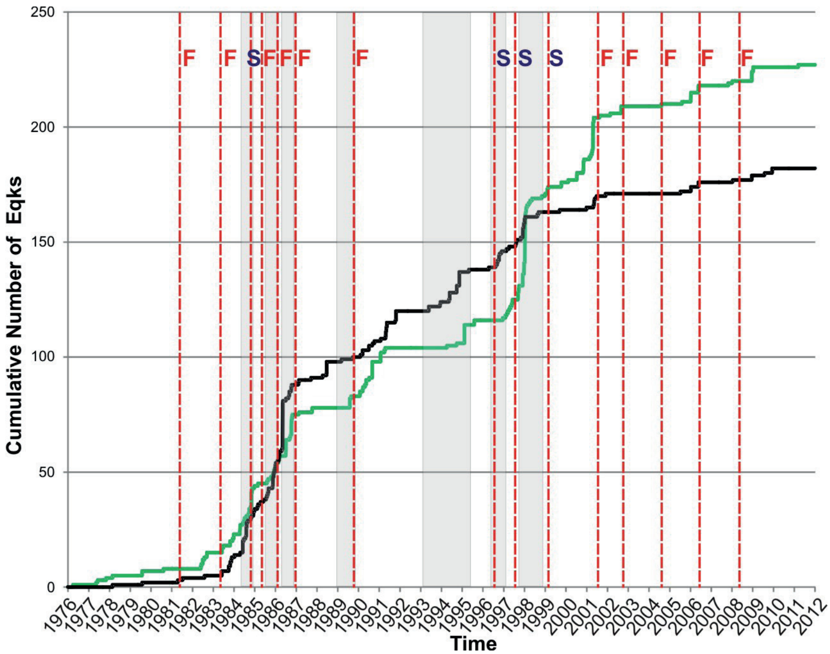

Fig. 2 – Cumulative number of earthquakes during 1976-2011 in the western flank of Mt. Etna. Black curve refers to earthquakes occurring at depth z > 12 km green curve refers to earthquakes occurring at depth 5 < z ≤ 12 km. The grey bands indicate the periods during which the increase of deeper crustal volume seismicity precede the shallower ones. Dashed lines indicate the beginning of either flank F or summit S main eruptions.

features with eastern Sicily. Present study aims to carry out a more detailed analysis about the seismic features of different sectors of Mt. Etna volcano and for this purpose a seismic catalogue covering a longer span time has been adopted.

Spatial Analysis of Seismicity. The IETs distributions within the main seismogenic depth intervals identified at Mt. Etna (Fig. 1b) have been computed, for the time interval 1976-2011, with the aim of obtain information about the seismic behaviour of different crustal volumes. The level $z \leq 5$ km appears to be quite active from the seismogenic point of view and very well defined by the statistical parameters. The high values of skewness ($S > 0$), observed in this depth interval, point out that most of the IETs are characterized by short recurrence times and are concentrated on the left of the distribution, therefore implying the existence of correlated events. In particular, in the north-eastern and south-eastern sectors of the volcano (Pernicana and Timpe fault systems respectively) IET distributions are characterized by bimodal shape, while a peaked curve at low IET values and therefore correlated events is observed close to the summit area. As concerns the aperiodicity values, we observe $\alpha > 1.5$ for the whole depth level that assume in particular values $\alpha > 3$ in proximity of the summit area, therefore indicating a strongly clustered seismic activity. In our opinion, the seismicity of the seismogenic volume with $z \leq 5$ km seems affected by both the regional stress field, which imply a background seismicity and the local stress connected to the magma rising processes. These latter activities, in the summit area in particular, usually with a very low background seismicity, is characterized by swarms that point out the beginning of some eruptions. The shallower seismogenic level can therefore be defined as the more typically "volcanic" volume since it appears activated as a consequence of magma induced stresses. In the 5-12 km depth interval, negative values of the skewness are found. This denotes a seismicity with a moderate number of correlated events and IET distributions inclined to be unimodal with high recurrence times, as well. Moreover a different seismic behaviour characterizes the eastern and western sectors of the volcano. The former being characterized by high IET values ($S \sim -1.5$, $k > 3$), indicating the prevalence of independent events, the latter being characterized by an higher percentage of correlated events ($S \sim -0.5$, $k \sim 2$). Finally, in the $z > 12$ km depth interval, two sectors can be discriminated: the first one located in the NW part of the volcano, with $S > 0$, which is affected by the occurrence in recent time (after the 2009) of several seismic swarms; the second, located towards the south-western portion of the summit area, with $\alpha \sim 1.5$, indicating quite homogeneously distributed seismicity recurrence times.

The cumulative number of earthquakes has been calculated for different sectors of the volcano at the afore-mentioned depth intervals. A different behaviour considering either $z \leq 5$ or $z > 5$ km depth is observed. In the first case, alternating periods of high and modest seismic activity are found; these periods are so relevant that the global cumulative rate depicted in Fig. 1d is strongly affected by them. The time interval 1991-2001 shows in particular a reduced seismic activity. This could be related to the lack of lateral eruptions at Mt. Etna and the prevalent summit activities occurred after the end of the flank eruption of 1991-1993 (Allard *et al.*, 2006). Such behaviour is particularly evident close to the summit area, where usually the moderate background seismic activity is interrupted by sudden increments of the seismic occurrence rate that point out the beginning of lateral eruptions whereas, summit eruptions are preceded and accompanied by a gradual increase of the seismic activity. These findings further support the tight relationship between volcanic activities and seismic rate inside the first 5 km beneath the volcano. When the cumulative number of earthquakes is calculated for depth $z > 5$ km no significant sharp increments of the seismic activity are observed during the whole considered time interval (1976-2011). Only in a few instances slight increments of the seismic activity in the western sector of the volcano precede the onset of some flank eruptions. Such behaviour continues to be observed at depth greater than 12 km, although seldom seismic swarms without a clear correlation with eruptive episodes are detected. A detailed analysis of the number of intermediate ($5 < z \leq 12$ km) and the deep ($z > 12$ km) earthquakes in the western sector of the volcano highlights that an increment of the occurrence frequency of the events precedes by some days (sometimes months) the unrest of several flank eruptions and some summit eruptions (Fig. 2). It is indeed quite clear that the increase of seismic activity starts in the deeper seismogenic level and continues in the shallower one. We are keen to interpret these results as a first sign of the deep ($z > 12$ km) recharging of the volcanic system that is soon after followed by the increment of the seismic rate at shallower levels which seems to mark a sort of magma migration ($5 < z \leq 12$ km). When the magma rising process keeps going it triggers shallow seismic swarms ($z \leq 5$ km) indicating the opening of eruptive fractures. It has however to be specified that such tendency towards a magma migration is not observed in some instances (i.e. before the 2002 and 2004 eruptions). In such cases it could be hypothesized (Andronico *et al.*, 2005; Collins *et al.*, 2013) that magma was already still standing in the shallower part of the volcano consequently to a previous uprising.

Temporal Analysis of Seismicity. Trying to describe the time evolution of the seismicity recorded on Mt. Etna in the study period, it appears clear (Fig. 1d) a change in the seismic style of the volcano. The cumulative curve shows indeed a significant difference in dip before and after 1987. Moreover it is noticeable that all summit eruptions, except the 1998 one, occur without significant increments of the seismic rate whereas most of the flank eruptions are marked by a sharp increase of the seismic activity. Inspection of Fig. 1d shows that the dataset 1976-2011 can be subdivided into four time intervals characterizing both periods of intense volcanic activity with lateral eruptions and periods with summit activities without flank episodes. The IET distributions was therefore carried out during the following periods: 1976-1987, 1988-2000, 2000-2003, 2003-2011. In Fig. 3 the values of skewness (S) for each period are reported since they better represent the different seismic styles and the IET distribution patterns. During the 1976-1987 time interval several eruptive events, both of lateral and summit kind, occurred. The chiefly active seismogenic level, as defined by the statistical parameters, is the one at depth $z \leq 5$ km. It shows high S values (Fig. 3a) pointing out that we deal with several correlated events especially in the summit area. At $z > 5$ km the skewness assume slightly negative values ($S < -0.5$) indicating seismicity characterized by independent events with relatively long recurrence times. During the second time interval (1988-2000) only summit eruptions occurred, except the 1991-1993 flank activity. In this case all the seismogenic levels appear equally affected by the seismic activity and the observed statistical parameters are those typical of time stationary activities represented by independent events ($S < 0$) linked to the background seismicity (Fig. 3b). It is in particular noticeable that, as already observed when the whole dataset has been analyzed (1976-2011), a marked difference between the seismic style of the western and eastern sectors of the volcano is set into evidence particularly at depths $z > 5$ km, the former showing some correlated events. The values of the statistical parameters calculated for the time interval 2000-2003, for the depth level $z \leq 5$ km are quite pronounced ($0.5 < S < 2.5$, Fig. 3c), pointing out in this way the tight relation existing between seismic and volcanic activities, relationship that is set into evidence by IET distributions with a lot of correlated events (seismic swarms preceding eruptive activities). Although the analyzed interval is particularly short, the small number of data anyway allows us to observe, similarly to the findings obtained when the whole dataset was analyzed, that below 5 km depth a distinct different behaviour of the western and eastern sectors of Mt. Etna is still detectable (Fig. 3c). The dataset concerning the period 2003-2011 is also formed by a few data so that information regarding only small sectors of the volcano can be inferred from the IET distributions. Similarly to the 1988-2000 period, low values of the statistical parameters are obtained for the depth interval $z \leq 5$ km, therefore indicating the presence of background seismicity only without earthquake swarms (Fig. 3d). Below 5 km depth, in the NW sector of the volcano high values of skewness ($S \sim 1.5$) are obtained, suggesting the occurrence of seismic swarms. Such seismic activity occurred in recent time (after 2009) and appears not linked to any eruptive phenomenon.

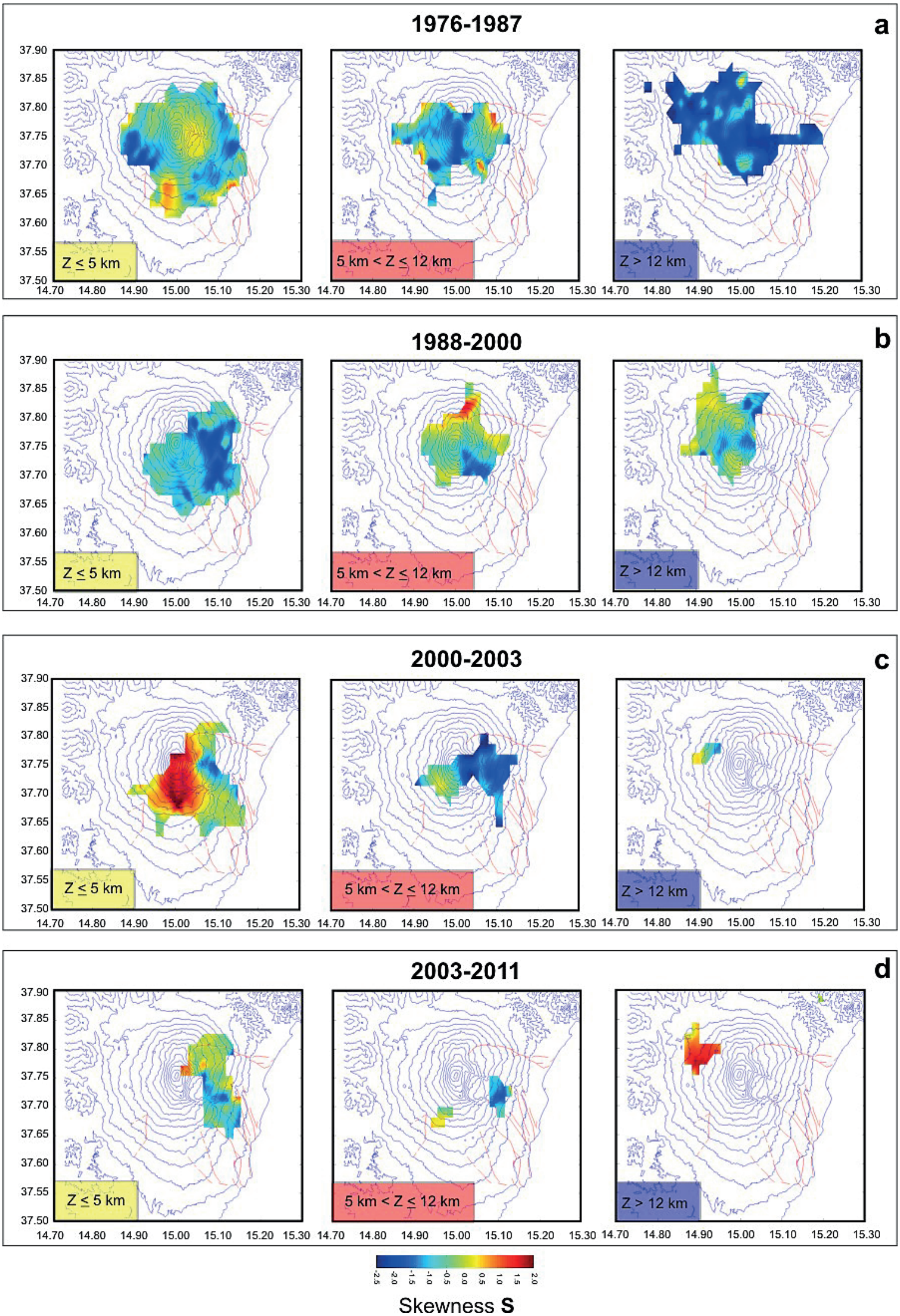

Fig. 3 – Areal distribution of skewness values during different time intervals.

Concluding remarks. The space-time IET distributions and the variation of the seismic rate, performed using a dataset collecting 25 years of instrumental earthquake records (1976-2011), allows us to draw the following considerations:

- The seismicity at Mt. Etna is not randomly located in time and space, but the hypocentral distribution of the earthquakes defines seismogenic volumes characterized by particular seismic patterns. Similar finding were obtained, through other methodologies (Cardaci *et al.*, 1993; Lombardo and Cardaci, 1994; Privitera *et al.*, 2001; Alparone *et al.*, 2010) that describe the relationships between different stages in the volcanic activity of Mt. Etna and the characteristics of recorded seismic activity.
- A detailed analysis of different sectors of the volcano indicates that seismogenic volumes at depth shallower than 5 km show a quite stationary background seismic activity that sometimes is interrupted by sudden increments of the seismic rate linked to eruptive phenomena. This result was already observed by Sicali *et al.* (2012) although the used dataset was concerned a shorter time interval.
- The temporal IET analysis highlights that during the periods with strong flank activities of the volcano, the occurrence of seismic swarms is mainly restricted within the seismogenic level at depth $z \leq 5$ km which in other words means that a great number of correlated events take place in this seismogenic volume. On the contrary, during periods without flank activities, only a moderate background seismicity is observed testified by unimodal IET patterns with uncorrelated events.
- The seismogenic volumes at depth $z > 5$ km do not show significant temporal variations keeping steady the observed differences between the eastern and western sectors of the volcano.
- Changes of the seismic rate underlines a tendency towards the migration of hypocenters from seismic volumes deeper than 12 km to shallower depth, especially in the western sector of the volcano, before the occurrence of the main flank eruptions. This result gives further support to similar observations of Lombardo and Cardaci (1994), Privitera *et al.* (2001), Bonaccorso *et al.* (2004) and Sicali *et al.* (2011) that describe the occurrence of shallow seismic swarms preceding the opening of eruptive fractures. These swarms follow sequences of deeper earthquakes which are interpreted as responsible for the refilling of the volcano feeding system. Such finding, at the same time, shows the soundness of present statistical approach.

Finally, we have to affirm that present analysis validate the results obtained by Sicali *et al.* (2012) adding significant details as a consequence of the larger number of data used. Moreover, we can after all assert that the time variation of statistical parameters, evaluated by splitting the dataset in several periods, emphasize different seismic behaviours linked to different typologies of the volcanic activity. Lateral eruptions imply the most evident variations in the space-time features of the seismicity, as confirmed by the activation of specific seismogenic volumes. On the other hand, summit eruptions follow and occur simultaneously to a regular increasing of the seismic rate.

References

Allard P., Behncke B., D'Amico S., Neri M. and Gambino S.; 2006: *Mount Etna 1993-2005: Anatomy of an evolving eruptive cycle*. Earth Science Review, **78**, 85-114.

Alparone S., D'Amico S., Maiolino V. and Ursino A.; 2010: *Sismicità all'Etna dal 1989 al 2010: evidenze sull'evoluzione spazio-temporale della attività sismica*. Proc. 29° GNGTS.

Alparone S., Barberi G., Bonforte A, Maiolino V. and Ursino A.; 2011: *Evidence of multiple strain fields beneath the eastern flank of Mt. Etna volcano (Sicily, Italy) deduced from seismic and geodetic data during 2003-2004*. Bull. Volcanol., **73** (7), 869-885.

Andronico D., Branca S., Calvari S., Burton M., Caltabiano T., Corsaro R.A., Del Carlo P., Garfì G., Lodato L., Miraglia L., Murè F., Neri M., Pecora E., Pompilio M., Salerno G. and Spampinato L.; 2005: *A multi-disciplinary study of the 2002-03 Etna eruption*: *insights into a complex plumbing system*. Bull. Volcanol., **67**, 314-330.

Andronico D. and Lodato L.; 2005: *Effusive Activity at Mount Etna Volcano (Italy) During the 20th Century: A Contribution to Volcanic Hazard Assessment.* Natural Hazards, **36**, 407-443.
Azzaro R., Branca S., Gwinner K. and Coltelli M.; 2012*: The volcano-tectonic map of Etna volcano, 1:100.000 scale: an integrated approach based on a morphotectonic analysis from high-resolution DEM constrained by geologic, active faulting and seismotectonic data.* Ital. J. Geosci. (Boll. Soc. Geol. It.), **131**, 153-170. Doi: 10.3301/IJG.2011.29.
Bell A. and Kilburn C.; 2008: *Patterns of accelerating rates of volcano-tectonic seismicity preceding basaltic flank eruptions*. EGU General Assembly, Geophys. Res. Abs., **10**, EGU2008-A-03752.
Bell A. F. and Kilburn C.R.J.; 2012: *Precursors to dyke-fed eruptions at basaltic volcanoes: insights from patterns of volcano-tectonic seismicity at Kilauea volcano, Hawaii.* Bull. Volcanol., **74**, 325-339.
Bonaccorso A., D'Amico S., Mattia M. and Patanè D.; 2004: *Intrusive mechanism at Mt Etna forerunning the July-August 2001 eruption*. Pure and Applied Geophysics, **161** (7), 1469-1487.
Cardaci C., Falsaperla S., Gasperini P., Lombardo G., Marzocchi W. and Mulargia F.; 1993: *Cross-correlation analysis of seismic and volcanic data at Mt. Etna volcano, Italy.* Bull. Volcanol., **55**, 596-603.
Collins S. J., Pyle D. M. and Maclennan J.; 2009: *Melt inclusions track pre-eruption storage and dehydration of magmas at Etna*. Geology, **37**(6),571-574.
Corral A.; 2003. *Local distributions and rate fluctuations in a unified scaling law for earthquakes.* Phys. Rev. E **68**, 035102.
Gruppo Analisi Dati Sismici; 2011: *Terremoti recenti localizzati con la rete sismica della Sicilia Orientale.* INGV, Catania, available from http://www.ct.ingv.it/Sismologia/analisti.
Hirn A., Nercessian A., Sapin M., Ferrucci F. and Wittlinger G.; 1991: *Seismic heterogeneity of Mt. Etna: Structure and activity.* Geophys. J. Int., **105**, 139-153.
Lavecchia G., Ferrarini F., De Nardis R., Visini F. and Barbano M.S.; 2007: *Active thrusting as a possible seismogenic source in Sicily (Southern Italy): some insights from integrated structural-kinematic and seismological data.* Tectonophysics, **445**, 145-167.
Lahr J. C.; 1989: *HYPOELLIPSE/VERSION 2.0*: A Computer Program for Determining Local*
Earthquake Hypocentral Parameters, Magnitude, and First-motion Pattern. U. S. Geol. Survey, Open-File Report 89/116, 81 pp.
Lombardo G. and Cardaci C.; 1994: *The seismicity of the Etnean area and different features of observed seismic sequences*. Acta Vulcanologica, **5**, 155-163.
Naylor M., Touati S., Main I. and Bell A.; 2010: *Earthquake interevent time distribution reflect the proportion of dependent and independent events pairs and are therefore not universal.* EGU General Assembly, Geophys. Res. Abs., **12**, EGU2009-8699.
Neri G., Barberi G., Oliva G. and Orecchio B.; 2005: *Spatial variation of seismogenic stress orientations in Sicily, South Italy.* Phys. Earth Planet. Inter., **148**, 175-191.
Palano M., Ferranti L., Monaco C., Mattia M., Aloisi M., Bruno V., Cannavò F. and Siligato G.; 2012: *GPS velocity and strain fields in Sicily and southern Calabria, Italy: Updated geodetic constraints on tectonic block interaction in the central Mediterranean*. J. Geophys. Res., **117**, B07401, doi:10.1029/2012JB009254.
Patanè D., Cocina O., Falsaperla S., Privitera E. and Spampinato S.; 2004: *Mt. Etna Volcano: A Seismological Framework*. In Mt. Etna: Volcano Laboratory, Geoph. Monograph Series **143**, 147-165.
Privitera E., Alparone S., D'Amico S., Gambino S., Maiolino V., Spampinato S. and Zuccarello L.; 2001: *Seismic evidences of magma intrusion at intermediate depth before the July-August 2001 Mt. Etna (Italy) eruption.* Assemblea Generale GNV.
Sicali S., Barberi G., Cocina O., Musumeci C. and Patanè D.; 2011: *Seismological constraints on the intrusive mechanism leading to the 2001 Etna eruption*. Annual workshop "S O S: Seismic & Other Signals", ESC Working Group and the IAVCEI-IASPEI. Abs. Vol. INGVCT2011-004.
Sicali S., Barbano M.S., D'Amico S. and Azzaro R.; 2012: *Characterization of Mt. Etna's Seismicity Inter-event Time Distribution*. Proc. 31st GNGTS, 243-248.
Traversa P. and Grasso J. R.; 2010: *How is Volcano Seismicity Different from Tectonic Seismicity?* Bull. Seism. Soc. Am., **100** (4), 1755-1769.
Vinciguerra S., Latora V., Bicciatod S. and Kamimura R.T.; 2001: *Identifying and discriminating seismic patterns* leading flank eruptions at Mt. Etna Volcano during 1981-1996. *J.* Volcanol. Geoth. Res., **106**, 211-228.

MODELLING RESERVOIR STIMULATION IN ENHANCED GEOTHERMAL SYSTEM

A. Troiano [1], M.G. Di Giuseppe [1], A. Monetti [2], D. Patella [2], C. Troise [1], G. De Natale [1]

[1] *Istituto Nazionale di Geofisica e Vulcanologia - Osservatorio Vesuviano, Napoli, Italy*
[2] *Dipartimento di Fisica. Università degli Studi di Napoli 'Federico II', Italy*

Introduction. Geothermal systems represent a large resource that can provide, with a reasonable investment, a very high and cost-competitive power generating capacity. Considering also the very low environmental impact, their development represents, in the next decades, an enormous perspective (MIT Report, 2006). Despite this unquestionable potential, geothermal exploitation has always been perceived as limited, mainly because of the dependance from strict site-related conditions, mainly correlated to the reservoir rock's permeability, the amount of fluid saturation and, first of all, a convenient temperature-depth relationship. However, many of such limitations are overcome with the Enhanced Geothermal System (EGS, Majer *et al.*, 2007), where massive fluid injection is performed to enlarge the natural fracture system of the basement rock. The permeability of the surrounding rocks results highly increased by pressurized fluids circulation and geothermal resource, in such way, become accessible in areas where exploitation, otherwise, could be not advantageous or even possible. Numerical procedures have already been presented in literature reproducing the thermodynamic evolution of the system where fluids are injected (Troiano *et al.*, 2013). In such a way, changes of Coulomb stress can be computed from Pressure and Temperature changes; the correlation between computed Coulomb stress changes and observed induced seismicity patterns has been shown to be very effective for the Soultz-sous-forets case (Troiano *et al.*, 2013) thus validating the procedure. We upgrade this kind of procedures to obtain an evaluation of the permeability enhancement obtained in the stimulation process. Assuming a conceptual model linking induced strain and permeability modification, we can estimate the induced permeability change during the water injection. In this way we adapt the medium behavior to mechanical changes and we could possibly evaluate the effectiveness of stimulation process in enhancing a geothermal reservoir permeability.

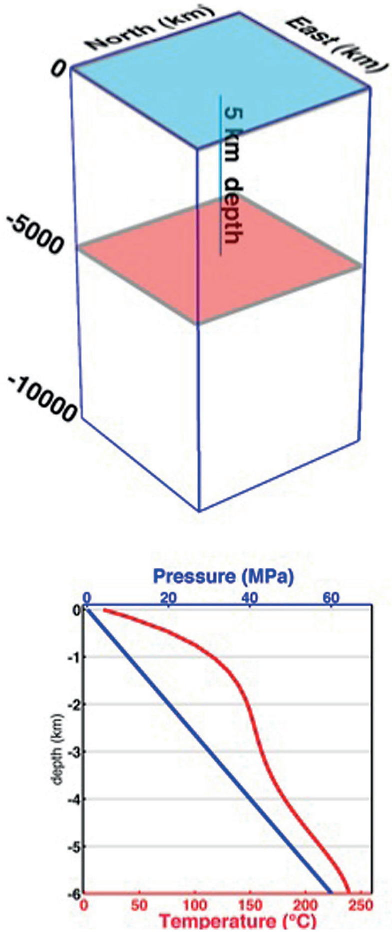

Fig. 1 – Top: sketch of the simulation volume. Blue plane, Earth surface; red plane, injection plane. Bottom: pressure and temperature initial conditions are indicated. Initial pressure (blue) and temperature (red) conditions as a function of depth.

In addition to the enhancement permeability with evaluation of induced seismicity, another kind of phenomena has been be studied. Stimulated fluid flow in geothermal reservoirs can produce surface Self-Potential (SP) anomalies of several mV. A commonly accepted interpretation involves the activation of electro-kinetic processes. SP anomalies observed above the Soultz-sous-Forets geothermal reservoir while injecting cold fresh water have been modeled, imposing a source related to the fluid flow induced by the well stimulation process. In particular, the retrieved changes of pressure due to well stimulation in the EGS system has been utilized as source term to evaluate the electric currents generating the potential anomalies, using Comsol Multiphysics.

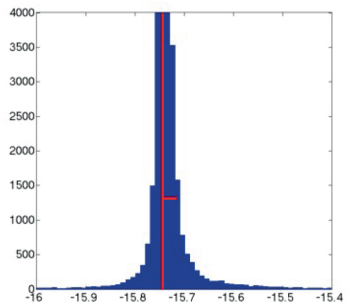

Fig. 2 – Histogram of *k'*, the new medium permeability after fluid stimulation. The histogram show a gaussian distribution of permeability values around the volume, centered around k_0, the initial permeability value. Mean value and standard deviation are represented with the red lines.

Being the induced seismicity risk correlated to fluid circulation stimulated in an area exceeding the well of several hundreds of meters, the wellbore pressure values are totally uncorrelated to seimic hazard. However, SP anomalies, being generated from pressure gradient in the whole area where fluids flow, has an interesting potential as induced earthquake precursor Detectability of changes in the SP values respect to the natural background values has been investigated in our study.

Method. Our method of analysis consists of a two-step procedure. In the first step, injection of water is simulated (Pruess, 1991) in a homogeneous medium, approximating a crystalline granite basement compatible with the deep structure of the Soultz-sous-Forets (France) EGS site. The modeled 3D physical domain and the imposed initial conditions are shown (Fig. 1). Water at ambient condition is injected at a 100 kg/s rate for 10 days in a point located at -5 km depth. In such a way we obtain the pressure and temperature changes at each point in the medium, at the final time. Such P and T changes at any point are subsequently considered as elementary sources, heterogeneously distributed in the whole discretized volume, which generate an incremental stress tensor field estimated by using the Comsol Multiphysics finite element code (Troiano *et al.*, 2011, Troiano *et al.*, 2013). Once the complete field of stress changes is computed, a conceptual model linking induced stress and permeability modification in orthogonally fractured media is adopted, incorporating the influences of both normal strain and shear dilation on the effect of fluid flow, in order to reconstruct *k'*, the new medium permeability after fluid stimulation. Histogram of *k'* show a gaussian distribution of permeability values around the volume (Fig. 2). The gaussian result centered around the k_0 value, with a standard deviation of about $k_0/3$.

To give an idea of the stimulation effects, it has to be considered that permeability at the injection point has been imposed as enhanced of two orders of magnitude. Furthermore, if values of *k'*, are selected exceeding the mean of the gaussian more than 1 standard deviation, the corresponding points in the stimulated volume can be considered as the zone where permeability is effectively enhanced due to fluid injection (Fig. 3). The mean value of *k'* in this zone results of $4.2 \cdot 10^{-16}$ m^2, leading to a permeability about three times greater than k_0 in a spheric volume of about 0.5 km^3.

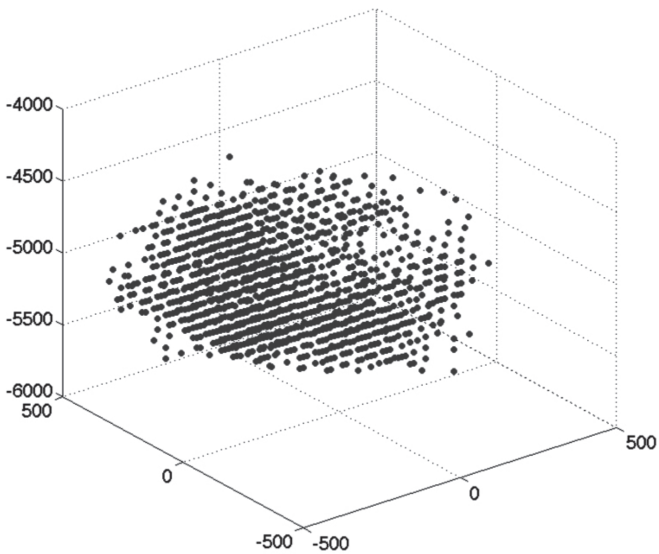

Fig. 3 – Points in the stimulated volume corresponding to values of *k'* exceeding the mean of this gaussian distribution more than 1 standard deviation. This area is considered as the zone where permeability is effectively enhanced due to fluid injection. The enhancement is estimated considering the mean value if this point.

Conclusion. Our procedure rely on a very affordable basis, being a very good reconstruction of induced seismicity already been obtained. The new step that we are calibrating involve an estimate of the permeability enhancement correlated to stimulation process of geothermal boreholes. The proposed procedure lead to promising results, being the permeability enhancement estimated distributed in the space in a coherent way. The magnitude of this enhancement too, result coherent with the experimental data, once the wellbore overpressure and fluid flow has been imposed. SP anomalies generated during the stimulation process has been reconstructed in order to evaluate the effectiveness of SP monitoring to mitigate the induced seismicity risk.

References

Bai M, Elsworth D. 1994: *Modeling of subsidence and stress-dependent hydraulic conductivity for intact and fractured porous media*. *Rock Mech Rock Eng*, **27**, 209-234.

Majer, E., Baria, R., Strak, M., Oates, S., Bommer, J., Smith, B. & Asanuma, H. 2007: *Induced seismicity associated with enhanced geothermal sys-tems*, *Geothermics*, **36**, 185-222.

Massachussetts Institute of Technology 2006: *The Future of Geothermal Energy: Impact of Enhanced Geothermal Systems (EGS) on the United States in the 21st Century: An Assessment*, MIT Press, MA, USA.

Peng, S., Zhang, J. 2007: *Engineering Geology for Underground Rocks*, 207-211. Springer.

Pruess, K., 1991: *TOUGH2-A General Purpose Numerical Simulator for Multiphase Fluid and Heat Flow,* L.B.L. Report, Berkeley, CA.

Troiano, A., Di Giuseppe, M.G., Petrillo, Z., Troise, C. and De Natale, G. 2011: *Ground deformation at calderas driven by fluid injection: modelling unrest episodes at Campi Flegrei (Italy). Geophys. J.,* **187**, 833-847.

Troiano, A., Di Giuseppe, M.G., Troise, C., Tramelli, A., and De Natale, G. 2013: *A Coulomb stress model for induced seismicity distribution due to fluid injection and withdrawal in deep boreholes. Geophys. J. Int.,* **195**, 504-512.

GEOPHYSICAL AND GEOCHEMICAL EVIDENCE OF THE SOLFATARA-PISCIARELLI SHALLOW HYDROTHERMAL SYSTEM

A. Troiano[1], M.G. Di Giuseppe[1], D. Patella[2], A. Fedele[1], R. Somma[1], C. Troise[1], G. De Natale[1]

[1]*Istituto Nazionale di Geofisica e Vulcanologia - Osservatorio Vesuviano, Napoli, Italy*

[1]*Dipartimento di Fisica - Università degli Studi di Napoli 'Federico II', Italy*

Solfatara and Pisciarelli settings. Campi Flegrei caldera (CFc) has been formed by huge eruptions, occurred 39000 and 15000 years ago, which have been the largest ones occurred in the Mediterranean since the beginning of mankind (Rosi and Sbrana, 1987). Up and down ground movements with rates from centimetres to meters per year characterize the dynamics of this area also during quiescent periods (Dvorak and Mastrolorenzo, 1991) Since 1969, the area started a new phase of uplift after several centuries of subsidence dating back to 1538 A.D., when the last eruption occurred in the area (Di Vito *et al*., 1987). Recent studies on the interpretation of such uplift episodes point out the important role played by the the geothermal system, which is characterized by hydrothermal manifestations such as distributed degassing zones and fumaroles (De Natale *et al*., 2001; Chiodini *et al*., 2003; De Natale *et al*., 2006).

The Solfatara-Pisciarelli area represents the most active zone within the CFc in terms of hydrothermal manifestations and nowdays local seismicity. The Solfatara volcano is located inside the CFc, about 2 km east-NE of the town of Pozzuoli. It is a tuff cone formed about 3,7-3,9 ky ago, which generated in 1198 AD a low-magnitude hydromagmatic explosive eruption that ejected tephra over a small area (<1 km^2) (Di Vito *et al*., 1999). The crater has a roughly elliptical shape with the two axes of 580 and 770 m, and a maximum elevation of 199 m asl.

The Solfatara crater is located very close to the area of maximum ground uplift, the benchmark 25A at Pozzuoli, during the last unrest crises. It hosts large and spectacular fumarole vents, with maximum temperatures in the range 150-160°C at the Bocca Grande (BG) and Bocca Nuova (BN) and about 100°C at Le Stufe (LS) and La Fangaia (LF) ones (Chiodini *et al*., 2001). Systematic measurements of the gas fluxes from the soil evidenced up to 1500 tonnes/day of CO_2 emission which are well aligned with the the main fault system and temperature up to 95°C far from the fumaroles (Granieri *et al.*, 2010).

During the first 16 years of systematic monitoring of the geochemical composition of the BG and BN fumaroles, from 1984 to 2000, the CO_2/H_2O has shown three clear anomalous ratios, in 1986, 1991 and 1995-96, respectively of 0.30, 0.26 and 0.34 over a background average value of 0.17, peaked about one year later from the corresponding unrest ground deformation. Since 2000 the CO_2/H_2O has progressively increased with a nearly linear trend from the background value of 0.17 up to about 0.32 (Chiodini *et al.*, 2010).

The Pisciarelli area is located outside the Solfatara crater. It extends from the eastern slopes of the Solfatara volcano to the western margin of the nearby Agnano crater. The Pisciarelli area is characterised by a fumarole field, which is affected by near-surface secondary processes of seasonal character that seem to mask the deeper signals related to the temperature-pressure changes occurring in the hydrothermal system, clearly observed, instead, inside the Solfatara crater at the BG and BN fumarole vents (Chiodini *et al.*, 2011).

Starting from 2003, the Pisciarelli field has experienced an evident increase of activity, which has been marked by a sequence of temperature peaks of the fumaroles above the average background temperature of 95°C, each lasting up to half a year until early 2011, and exceptionally about one year, from mid 2011 to mid 2012, the last recorded peak. Furthermore, a nearly linear trend of the peak temperatures, from about 97° C up to around 112°C, has been recorded from 2003 up to date. The increase of activity has also been marked by the opening of new vigorous vents and degassing pools, also accompanied by intense local seismic activity (D'Auria *et al.*, 2011).

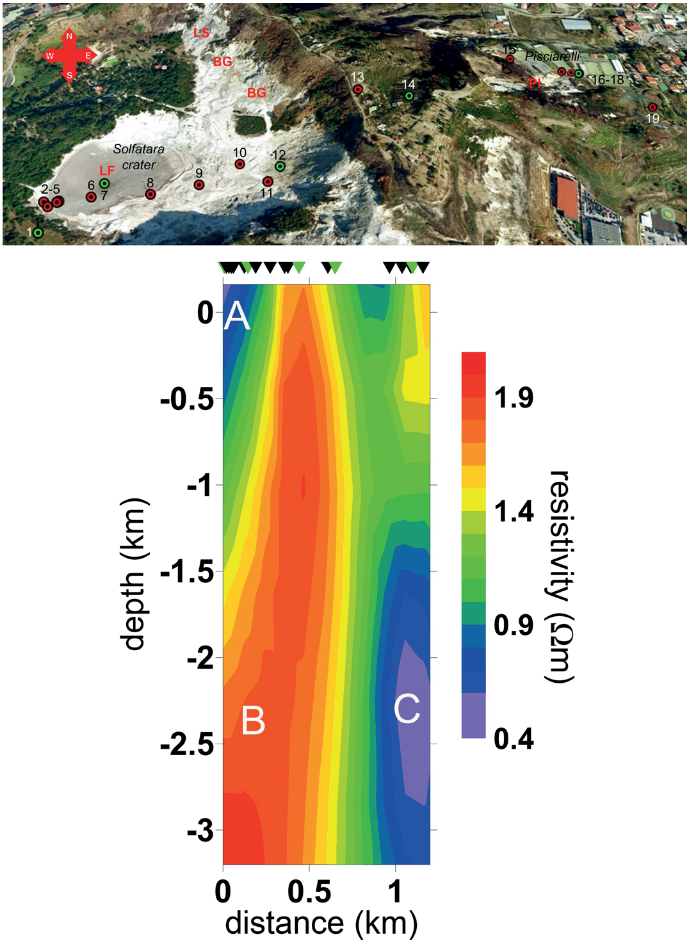

Fig. 1 – Top: aerial view of the Solfatara crater and surrounding urbanized areas. The white area inside the crater is the vegetation-free degassing area. BG, BN, LS and LF indicate the Bocca Grande, Bocca Nuova, Le Stufe and La Fangaia main fumaroles, respectively, located inside the Solfatara crater. PI indicates the Pisciarelli main fumaroles, located outside the crater. Red and green circles indicate the CSAMT and combined CSAMT-MT sounding stations, respectively. Bottom: resistivity model obtained from the 1D inversion of the MT data, along the Solfatara-Pisciarelli profile. A common logarithmic scale is used for the resistivity. Black and green triangles along the distance scale indicate the CSAMT and combined CSAMT-MT stations, respectively.

Continuous monitoring of such phenomena is on-going, by permanent networks for seismic, ground deformation and geochemical measurements. Geophysical surveys have so far allowed a quite good knowledge of the subsurface structure of the CFc volcanic system.

Electromagnetic evidence. A 1 km long, nearly W-E directed CSAMT-MT profile crossing the fumaroles field was realised (Troiano *et al.*, *submitted*), carried out with the aim of deducting an EM model of the structural setting of the hydrothermal system in the first 3 km depth of the Solfatara-Pisciarelli area. The results allow us to identify three EM zones (Fig. 1). The first EM zone (A) is characterized by a very shallow, electrically conductive body localized beneath the westernmost segment of the profile, which, within a short distance of about 100 m, dips westwards from near surface down to some hundred metres depth. This shallow zone has been ascribed to a water-saturated, high-pressurized geothermal reservoir. The second EM zone (B), which has been localized below the west-central portion of the EM transect, appears as a composite body made of a nearly vertical plume-like structure arising from about 2.25 km depth to the top edge of the east side of a presumably horizontal plate-like body. Such plume-like structure, centered in correspondence of the Solfatara fumaroles field, rises up to the free surface whereas the plate-like structure deepens at least down to the 3 km of maximum EM exploration depth. The plume-like portion is likely associated with a steam/gas-saturated column and the plate-like portion to a high temperature (>300°C), over-pressurized, gas-saturated reservoir. Finally, a third EM zone (C), which has been localized beneath the eastern half of the EM transect, corresponding to the Pisciarelli area, is also characterized by the lowest resistivity values (1-10 Ωm) from about 1.2 km down to about 3 km of depth. As it is known, in a volcano-geothermal coastal environment a highly conductive body can indicate either a hydrothermally mineralized, clay-rich layer (e.g. Keller and Frischknecht, 1966; Ward, 1990; Parasnis, 1997), or a cold seawater-bearing layer (e.g. Goldman *et al.*, 1991; Frohlich *et al.*, 1994; Di Maio *et al.*, 1997; Mauriello and Patella, 1999), or a highly hydrothermalized water-bearing rock (e.g. Patella *et al.*, 1979; Detwiler and Roberts, 2003).

In order to decide which of this hypothesis is the most reliable, we consider that in all of the deep wells drilled by AGIP at the west border (Mofete area) and north border (San Vito area) of the caldera, the effects of a strong hydrothermal paragenesis have been detected. Abundance of semiconducting minerals (*e.g.* pyrrhotite, pyrite, magnetite) and presence of thick argillitic layers, are, in fact, documented at temperatures ranging between 250°C and 350°C, in the depth range between 1 and 3 km, which was the maximum depth reached by the wells (Chelini and Sbrana, 1987; Mormone *et al.*, 2011). Therefore we are tentatively allowed to associate the very low resistivity zone (C), under the Pisciarelli area, with a hydrothermally mineralized, clay-rich body. Alternatively, we cannot exclude the presence of a deep hydrothermal aquifer, although we know from previous drillings that critical temperature is reached in the whole

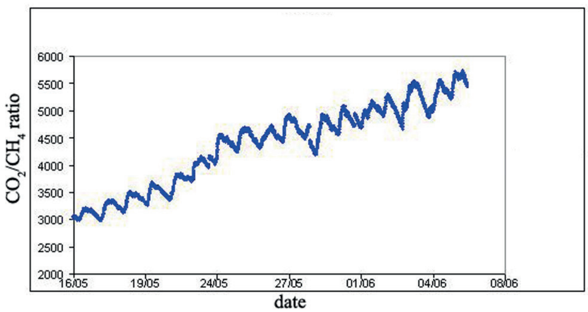

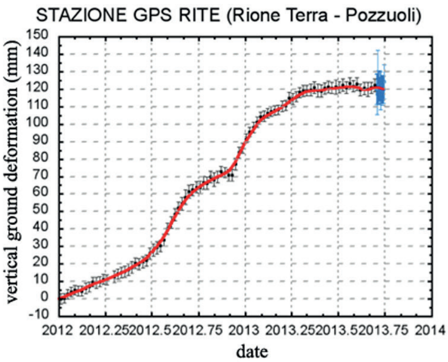

Fig. 2 – On the left CO2/CH4 ratio from 16/05/2012 to 05/06/2012 measured by Quadrupole Mass Spectometer. On the right ground deformation (from Osservatorio Vesuviamo website).

caldera at depths higher than 3 km (AGIP, 1987). Further consideration arise from the analysis of the seismic P-wave velocity (v_P) and the P-wave/S-wave velocity ratio (v_p/v_s) in the same zones (Battaglia *et al.* 2008). The conductive C-zone almost completely coincides with a low v_p/v_s area (v_p/v_s~1,73). The reason for assuming v_p and v_p/v_s as test parameters resides in the relationship existing between their variations and reservoir fluid phases. In detail, low v_p/v_s values are related to a decrease of v_p in areas with low pore pressure, high heat flow, fracturing and steam/gas saturation in reservoirs, while high v_p/v_s values are found in liquid-saturated high-pressure fields (e.g., Nakajima *et al.*, 2001; Simiyu, 2009; Jousset *et al.*, 2011; Mormone *et al.*, 2011; Gritto *et al.*, 2013). It is well established, in fact, that the presence of steam/gas in rocks generally changes the rock compressibility with a v_p decrease, whereas waters in rock voids do not sustain shear stress and decrease the v_s without any v_p variation (e.g., Vanorio *et al.*, 2002). It has also been ascertained that the v_p/v_s ratio increases with pressure increase and temperature decrease from vapour-saturated to liquid-saturated conditions (e.g., Ito *et al.*, 1979), and that v_P is affected by the degree of water saturation (e.g., O'Connell and Budiansky, 1974, 1977). The lowest resistivity values that characterize this zone, combined with the seismic evidences, allow us to exclude a water-saturated reservoir, but very likely to admit the presence of a dry and impermeable hydrothermally mineralized, clay-rich body.

Geochemical evidence. An important issue for further discussion is the implication that this EM model, correlated with the evidences emerging from geochemical analysis, can have on the understanding of the fluids uplift in the Solfatara-Pisciarelli area.

According to Caliro *et al.* (2007) the peaks of the CO_2/H_2O concentration ratio, occurred in 1986, 1991 and 1995-96 at the Solfatara crater a few months later an uplift of the ground (Chiodini *et al.*, 2010), reflect the increased component of magmatic gases in the composition of the fumaroles, probably due to episodes of intense degassing of magma at depth.

The Pisciarelli area is also characterized by emission of gases and fluids through fractures mostly trending N110-120E and mainly NWSE and NE-SW. The main component of the fumaroles is H_2O followed by CO_2 and H_2S and with a range of temperature between 100-110 °C (Chiodini, 2009; Fedele, 2013).

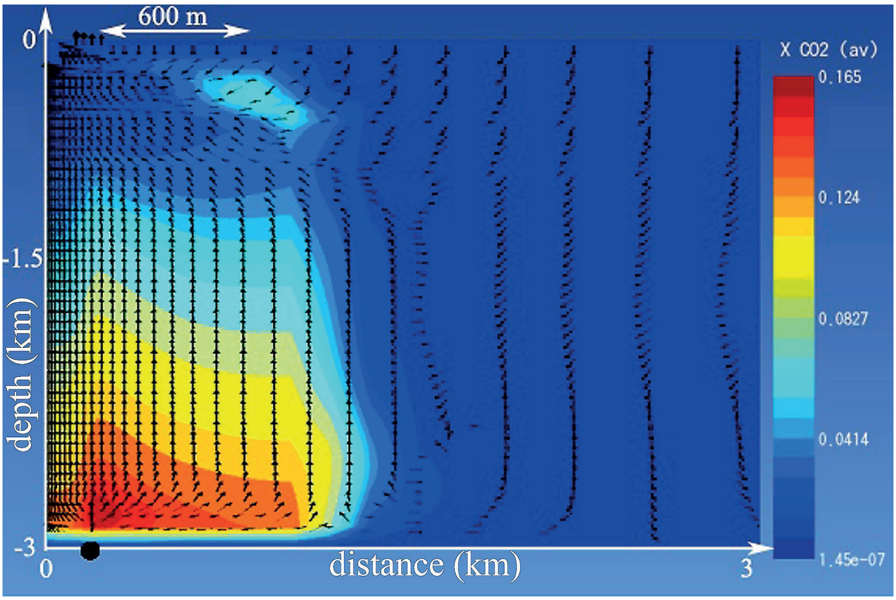

Fig. 3 – Fluid flows patterns as reconstructed by numerical simulation. Black arrows show the CO_2 fluxes migrating from the injection point, placed below the Solfatara crater, towards the surface, ending in the Pisciarelli area. Colour contours shows the CO_2 mass fraction.

During field surveys in the Pisciarelli made during the year 2006 were observed, compared to similar surveys conducted in the past (the year 2005), changes emission style of gases and fluids. Particularly the first are characterised by several point sources of emission while, along the eastern side of the small hill to the east, it is a mud boiling characterised by a diffuse and active degassing zone.

A on-line gas monitoring station was localised close the fumaroles field (100 m) during the period May 16-30th 2012, June 1st-5th, 2012. The main relationships of good tracer of magmatic fluids injection such us CO_2/CH_4 and H_2S/CO_2 was reconstructed due to this continuous monitoring (Fedele, 2013). In particular, the CO_2/CH_4 is a good tracer of magmatic fluids injection because CO_2 concentration increased, due to its the higher content of the magmatic component, and CH_4, a gas species formed within the hydrothermal system, is lowered both by dilution and by the more oxidizing, transient conditions caused by the arrival of SO_2 into the hydrothermal system (Chiodini, 2009, 2012). This opposite behaviour causes rapid increases of the CO_2/CH_4 ratio in fumarolic fluids like it showed by the Fig. 2.

This trend seems to be confirmed by the data of GPS ground deformation that show a general tendency to uplift with an acceleration of the phenomenon in the period spanning from June to August 2012 (25 mm/month in average) and increasing during the last month beginning on December 2012 (10 mm/month), as also shown in Fig. 2.

Discussion and conclusion. In effect, periodic injections of hot CO_2-rich fluids at the base of a relatively shallow hydrothermal system has been correlated to ground uplift in a wide range of numerical modelling of the CFc unrests, that highlight a strong correlation between chemical composition of the Solftara and Pisciarelli fumaroles, seismicity and ground movements (D'Auria *et al.*, 2011, Todesco *et al.*, 2004; Todesco and Berrino, 2005, Troiano *et al.*, 2011).

In particular, a new simulation has been realised via the coupling of TOUGH2® and Comsol Multiphysics®, (Troiano *et al.*, 2011). Recent uplift episodes in the in the centre of Pozzuoli Bay have been reconstructed imposing fluid flows in the system as experimentally recorded. The comparison between numerical simulation, geochemical data and EM survey highlight the main features of the shallower part of the hydrothermal system of the Pisciarelli area. The high CO_2/CH_4 ratio indicate a plausible magmatic component. For such magmatic origin, the plume identified in the MT imaging below the Solfatara crater seems to contribute also to fluid flow uplift below Piasciarelli. The low resistivity values under Pisciarelli, that indicate a strong local fluid circulation, support this kind of hypothesis. The fluid flow patterns reconstructed by our numerical simulations enforce this interpretation (Fig. 3). Fluids migrate, in the upper part of our model, from its central part, ideally placed below the Solfatara crater, toward an area localised some hundreds of meters away, fitting the Pisciarelli zone. The clear evidence that the thermodynamic condition of the system in the shallower part results compatible with the presence of convective cells enforce the idea that the degassing of the magma batch localised under the Solfatara crater contribute also to fluid circulation under Pisciarelli.

References

AGIP, 1987: *Geologia e geofisica del sistema geotermico dei Campi Flegrei*. Unpublished Internal Report, 1-17.

Battaglia, J., Zollo, A., Virieux, J., and Dello Jacono, D., 2008: *Merging active and passive data sets in travel-time tomography: The case study of Campi Flegrei caldera (Southern Italy),* Geophys. Prospect., 56, 555-573.

Caliro, S., Chiodini, G., Moretti, R., Avino, R., Granieri, D., Russo, M., and Fiebig, J., 2007: *The origin of the fumaroles of La Solfatara (Campi Flegrei, South Italy)*, Geochim. Cosmochim. Acta, 71, 3040-3055, doi: 10.1016/j.gca.2007.04.007.

Chelini, W., and Sbrana, A., 1987: *Phlegrean Fields. Subsurface geology*, Quad. Ric. Sci., CNR, 114, 94-103.

Chiodini G., Frondini, F., C. Cardellini, C., D. Granieri, D., Marini, D., and G. Ventura, G., 2001: *CO2 degassing and energy release at Solfatara volcano, Campi Flegre*i, Italy, J. Geophys. Res., 106, B8, 16213-16221.

Chiodini, G., Todesco, M., Caliro, S., Del Gaudio, C., Macedonio, G., and Russo, M., 2003: *Magma degassing as a trigger of bradyseismic events: The case of Phlegrean Fields (Italy),* Geophys. Res. Let., 30 (8), doi: 10.1029/2002GL016790.

Chiodini G.; 2009: *CO2/CH4 ratio in fumaroles a powerful tool to detect magma degassing episodes at quiescent volcanoes*. Geophysical Research Letters, v. 36, L02302, doi:10.1029/2008GL036347.

Chiodini, G., Caliro, S., Cardellini, C., Granieri, D., Avino, R., Baldini, A., Donnin, M., and Minopoli, C., 2010*: Long term variations of the Campi Flegrei (Italy) volcanic system as revealed by the monitoring of hydrothermal activity*, J. Geophys. Res., 115, B03205, doi: 10.1029/2008JB 006258.

Chiodini, G., Avino, R., Caliro, S., and Minopoli, C., 2011: *Temperature and pressure gas geoindicators at the Solfatara fumaroles (Campi Flegrei)* , Ann. Geophys., 54, 151-160, doi: 10.4401/ag-5002.

Chiodini G., Caliro S., De Martino P., Avino R., and Gherardi F.;2012: *Early signals of a new volcanic unrest at Campi Flegrei caldera? Insights from geochemical data and physical simulations*. Geology 943-945.

D'Auria, L., Giudicepietro, F., Aquino, I., Borriello, G., Del Gaudio, C., Lo Bascio, D., Martini, M., Ricciardi, G.P., Ricciolino, P., and Ricco, C., 2011*: Repeated fluid-transfer episodes as a mechanism for the recent dynamics of Campi Flegrei caldera (1989–2010),* J. Geoph. Res., 116, B04313, doi: 10.1029/2010JB007837.

De Natale, G., Pingue, F., Allard, P., and Zollo, A., 2001: *Geophysical and geochemical modeling of the Campi Flegrei caldera*, J. Volcanol. Geotherm. Res., 48, 199-222.

De Natale, G., Troise, C., Pingue, F., Mastrolorenzo, G., Pappalardo, L., Battaglia, M., and Boschi, E., 2006: *The Campi Flegrei caldera: unrest mechanisms and hazards*. In C. Troise, G. De Natale and C.R.J. Kilburn (eds.), Mechanics of Activity and Unrest at Large Calderas, Geological Society, London, Special publications, 269, 25-45.

Detwiler, R.L., and Roberts, J.J., 2003: *Electrical resistivity as an indicator of saturation in fractured geothermal reservoir rocks: experimental data and modeling*, Geothermal Resources Council 2003 Annual Meeting, Morelia, Mexico, October 12-15, 2003, 12 p.

Di Maio, R., Mauriello, P., Patella, D., Petrillo, Z., Piscitelli, S., Siniscalchi, A., and Veneruso, M., 1997: *Self-potential, geoelectric and magnetotelluric studies in Italian active volcanic areas*, Ann. Geophys., 40, 519-537.

Di Vito, M.A., Lirer, L., Mastrolorenzo, G. and Rolandi, G., 1987: *The Monte Nuovo eruption (Campi Flegrei, Italy),* Bull. Volcanol., 49, 608-615.

Di Vito, M.A., Isaia, R., Orsi, G., Southon, J., D'Antonio, M., De Vita, S., Pappalardo, L., and Piochi, M., 1999: *Volcanism and deformation since 12000 years at the Campi Flegrei caldera (Italy)*, J. Volcanol. Geotherm. Res., 91, 221-246.

Dvorak, J.J., and Mastrolorenzo, G., 1991: *The mechanisms of recent vertical crustal movements in Campi Flegrei caldera*, Southern Italy, Geol. Soc. Am., Special paper 263, 1-47.

Fedele, A., 2013: *Continuous geochemical monitoring by mass-spectometer in the Campi Flegrei geothermal area. An application at Pisciarelli-Solfatara (diffuse and fumarolic gases) and at the mud gases during drilling of the CFDDP pilot hole*, Ph.D. Thesis, Alma Mater Studiorum Università degli Studi di Bologna.

Frohlich, R.K., Urish, D., Fuller, J., and Reilly, M.O., 1994: *Use of geoelectrical methods in groundwater pollution surveys in a coastal environment*, J. Appl. Geophys., 32, 139-154.

Goldman, M., Gilad, D., Ronen, A., and Melloul, A., 1991: *Mapping of seawater intrusion into the coastal aquifer of Israel by the time domain electromagnetic method*, Geoexploration, 28, 153-174, doi: 10.1016/0016-7142(91)90046-F.

Granieri, D., Avino, R., and Chiodini, G., 2010: *Carbon dioxide diffuse emission from the soil: ten years of observations at Vesuvio and Campi Flegrei (Pozzuoli), and linkages with volcanic activity*, Bull. Volcanol., 72, 103–118, doi:10.1007/s00445-009-0304-8.

Gritto, R., Yoo, S.H., and Jarpe, S.P., 2013: *Three-dimensional seismic tomography at the Geysers Geothermal Field, CA, USA*, Proceedings 38th Workshop on Geothermal Reservoir Engineering, Stanford, California, February 11-13, 2013, SGP-TR-198.

Ito, H., De Vibriss, J., and Nur, A., 1979: *Compressional and Shear waves in saturated rock during water-steam transition*, J. Geophys. Res., 84, 4731-4735.

Jousset, P., Haberland, C., Bauer, K., and Arnason, K., 2011: *Hengill geothermal volcanic complex (Iceland) characterized by integrated geophysical observations*, Geothermics, 40, 1-24.

Keller, G.V., and Frischknecht, F.C., 1966: *Electrical Methods in Geophysical Prospecting*, Pergamon Press, Oxford.

Mauriello, P., and Patella, D., 1999: *Resistivity anomaly imaging by probability tomography*, Geophys. Prospect., 47, 411-429, doi: 10.1046/j.1365-2478. 1999.00137.x.

Mormone, A., Tramelli, A., Di Vito, M.A., Piochi, M., Troise, C., and De Natale, G., 2011: *Secondary hydrothermal minerals in buried rocks at the Campi Flegrei caldera, Italy: a possible tool to understand the rock-physics and to assess the state of the volcanic system*, Periodico di Mineralogia, 80, 385-406.

Nakajima, J., Matsuzawa, T., Hasegawa, A., and Zhao, D., 2001: *Three-dimensional structure of Vp, Vs, and Vp/Vs beneath northeastern Japan: Implications for arc magmatism and fluids*, J. Geophys. Res., 106, 843-857.

O'Connell, R.J., and Budiansky, B., 1974: *Seismic velocities in dry and saturated cracked solids*, J. Geophys. Res., 79, 5412-5426.

O'Connell, R.J., and Budiansky, B., 1977: *Viscoelastic properties of fluid-saturated cracked solids*, J. Geophys. Res., 82, 5719-5736.

Parasnis, D.S., 1997: *Principles of Applied Geophysics*, Chapman & Hall, London.

Patella, D., Rossi, A., and Tramacere, A., 1979: *First results of the application of the dipole electrical sounding method in the geothermal area of Travale-Radicondoli (Tuscany),* Geothermics, 8, 111-134.

Rosi, M., and Sbrana, A., 1987: *Phlegrean Fields. Introduction, geological setting of the area, stratigraphy, description of mapped products, petrography, tectonics*, Quad. Ric. Sci., CNR, 114, 9-93.

Simiyu, S.M., 2009: *Application of micro-seismic methods to geothermal exploration: examples from the Kenya rift*, Short Course IV on Exploration for Geothermal Resources, Lake Naivasha, Kenya, November 1-22, 2009, 27 p.
Todesco M., Rutqvist, J., Chiodini, G., Pruess, K., and Oldenburg, C.M., 2004: *Modeling of recent volcanic episodes at Phlegrean Fields (Italy): geochemical variations and ground deformation*. Geothermics, 33, 531-547.
Todesco, M., and Berrino, G., 2005: *Modeling hydrothermal fluid circulation and gravity signals at the Phlegraean Fields caldera*, Earth Plan. Sci. Lett., 240, 328-338.
Troiano, A., Di Giuseppe, M.G., Petrillo, Z., Troise, C., and De Natale, G., 2011: *Ground deformation at calderas driven by fluid injection: modelling unrest episodes at Campi Flegrei (Italy),* Geophys. J. Int., 187, 833-847, doi: 10.1111/j.1365-246X.2011.05149.x.
Troiano, A., Di Giuseppe, M.G., Patella, D., Troise, C., and De Natale, G., *Electromagnetic outline of the Solfatara-Pisciarelli hydrothermal system, Campi Flegrei (Southern Italy)*, submitted to J. Volcanol. Geotherm. Res.
Vanorio, T., Prasad, M., Nur, A., and Patella, D., 2002: *Ultrasonic velocity measurements in volcanic rocks: Correlation with microtexture*, Geophys. J. Int., 149, 22-36.
Ward, S.H., 1990: *Resistivity and induced polarization methods*, in S.H. Ward (ed.), Geotechnical and Environmental Geophysics, vol. 1: Review and Tutorial, Society of Exploration Geophysicists, Tulsa, OK, 147-189.

Indice degli autori

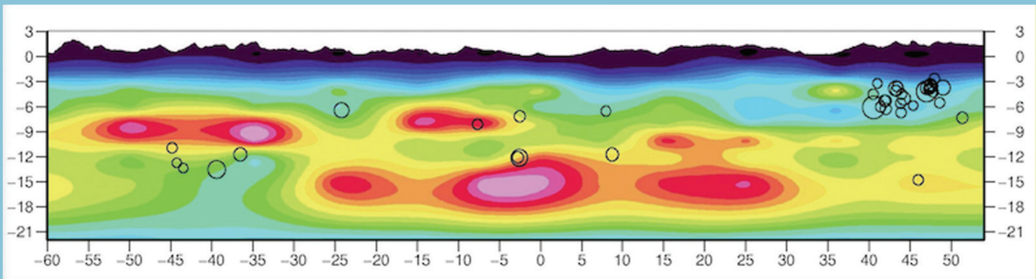

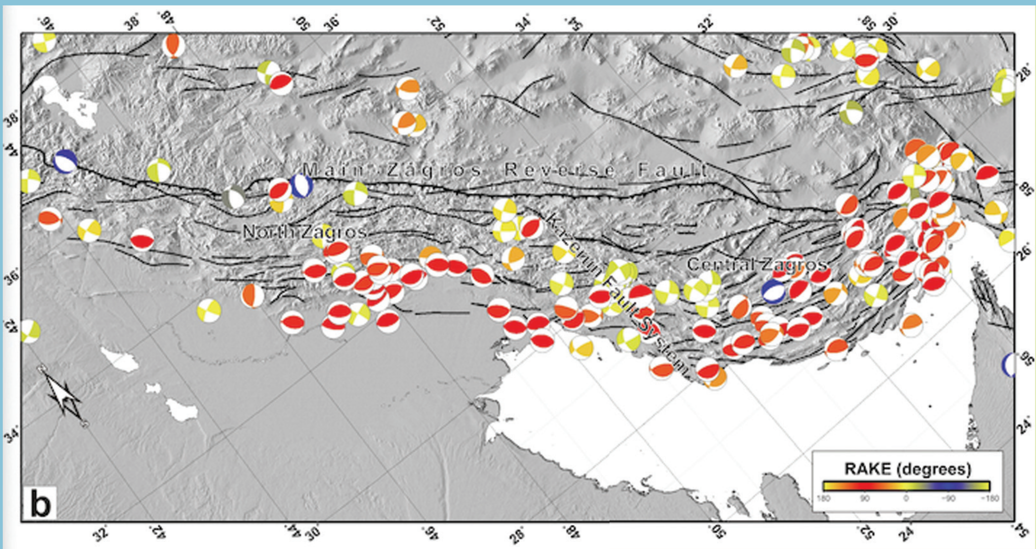

con la sponsorizzazione di:

EAGE
EUROPEAN ASSOCIATION OF GEOSCIENTISTS & ENGINEERS
SEG
SEZIONE ITALIANA

13° Convegno Nazionale

CODEVINTEC
Tecnologie per le Scienze della Terra

GNGTS

volume raccolta

ISBN 978-88-902101-6-7 ISBN 978-88-902101-9-8